APPENDIX A

Comparison of DOTs Design Requirements

A.1 Summary of DOTs design requirements

Table A.1 presents a summarized comparison of design requirements for different DOTs. Note that this Appendix has been prepared in collaboration with Mr. Muhammad Hassan, of NESPAK, Pakistan (Former MSc student at UB).

Table A.1. Comparison of DOTs design requirements

DOT/ Codes	Connection method for Type II/oversized shaft [See note 1]	Embedment length required [See note 2 and 10]	Casing contribution in strength	Minimum thickness and diameter of casing [See note 6]	Minimum concrete cover for drilled shaft
FHWA (Brown et al. 2010)	When non-contact splice must be used at top of drilled shafts, there are basically two methods for connecting oversized or Type II drilled shaft with column. Either: A column cage is extended into the shaft for some specific development length. A "splice cage" is used, and additional lap splices are provided into the column. [See note 1] (Brown et al. 2010)	Refer to Article 5.11.2.1 and 5.11.2.2 of AASHTO LRFD Specifications. For seismic zones 2, 3 and 4 multiply this length with 1.25 as per requirement of Section 5.10.11.4.3. [See note 2 and 3] (Brown et al. 2010)	Use AASHTO provisions for CFT columns, for calculating strength parameters. Refer AASHTO BDS Article 6.9.5:6.12.2.3.2:6.9.2.2- [See note 4] (Brown et al. 2010)	Minimum thickness of casing and diameter of drilled shaft is not specified. Typical diameter of shaft is 3 ft. [See note 7] (Brown et al. 2010)	• "3.0 inches for shafts ≤ 3'-0" diameter • 4.0 inches for > 3'-0" but < 5'-0" diameter • 6.0 inches for shafts ≥ 5'-0" diameter." (Brown et al. 2010)
AASHTO BDS (2012) and AASHTO SGS (2011)	Non-contact splice into top of drilled shaft.	• As per, AASHTO SGS (2011), "column longitudinal reinforcement should be extended into oversized shafts in a staggered manner with the minimum embedment lengths of $D_{c,max}+ l_d$ and $D_{c,max}+ 2l_d$, where $D_{c,max}$ is the larger cross-section dimension of the column and l_d is the development length in tension of the column longitudinal reinforcement bars determined in accordance with Article 5.11.2.1 of AASHTO BDS (2012) using	AASHTO BDS (2012) Article 10.8.3.9.3 specifies that, "minimum requirements to consider the steel shell to be load carrying shall be as in Article 5.13.4.5.2". According to Article 5.13.4.5.2, "a permanent steel casing may be considered as structurally effective in resisting axial loads and bending moments (i.e. may be considered as part of the longitudinal reinforcement) if the casing thickness is greater than 1/8-inch".	Minimum diameter = 30*in.*, for manual inspection. Minimum thickness of casing =1/8*in.*. According to Article 5.13.4.5.2 of AASHTO BDS (2012), "Shells that are more than 0.12" thickness may be considered as part of the reinforcement. In corrosive environments, a minimum of 0.06" shall be deducted from the shell thickness in …	It should be calculated as per table 5.12.3-1 of AASHTO BDS (2012)- These are general provisions for clear concrete cover.

Continued Table A.1. Comparison of DOTs design requirements

DOT/ Codes	Connection method for Type II/oversized shaft [See note 1]	Embedment length required [See note 2 and 10]	Casing contribution in strength	Minimum thickness and diameter of casing [See note 6]	Minimum concrete cover for drilled shaft
		expected values of material properties". [See note 8] • AASHTO BDS (2012), Article 5.11.2.1 and 5.11.2.2 should be used for calculating embedment length. For seismic zones 2, 3 and 4 multiply this with 1.25 as per requirement of Article 5.10.11.4.3. [See note 2]	AASHTO provisions for CFT columns can be used for calculating strength of encased drilled shaft.	determining resistance."	
California	Non-contact splice into top of drilled shaft.	Seismic Design Criteria Version 1.6 (2010) Section 8.2.4, refers to AASHTO SGS, for calculating minimum required development length. [See note 8]	As per, Analysis of Laterally Loaded Long or Intermediate Drilled Shafts of Small or Large Diameter in Layered Soil (2008), effect of permanent steel casing can be used for enhancement of structural capacity of drilled shaft.	Minimum diameter is 24*in.*, when water is anticipated. As per, Bridge Design Specifications (2003) Section 4.6.6.1, where permanent steel casing is used and the shell is smooth pipe and more than 0.12 inch in thickness, it may be considered as load carrying in the absence of corrosion.	As per, Bridge Design Specifications (2003) Section 4.6.6.2.5, "The reinforcement shall be placed a clear distance of not less than 2 inches from the permanently cased or 3 inches from the uncased sides. When shafts are constructed in corrosive or marine environments, or when concrete is placed by the water or slurry displacement methods, the clear distance should not be less than 4 inches for uncased shafts and shafts with permanent casings not sufficiently corrosion resistant".

Continued Table A.1. Comparison of DOTs design requirements

DOT/ Codes	Connection method for Type II/oversized shaft [See note 1]	Embedment length required [See note 2 and 10]	Casing contribution in strength	Minimum thickness and diameter of casing [See note 6]	Minimum concrete cover for drilled shaft
Florida	Refers to FHWA (Brown et al. 2010).	Refers to FHWA (Brown et al. 2010).	As per, Florida DOT's Soils and Foundations Handbook (2000) Section 8.2.3, drilled shafts may be constructed using temporary or permanent casing, however, the drilled shaft design methods are applicable only for computing the resistance of the uncased portions of the shaft. Portions of the shaft constructed with temporary casing will most commonly have reduced side shear resistance versus constructing the same portion of the shaft using slurry.	According to, Structures Design Guidelines (2013) Section 3.6, minimum diameter of shaft = 48*in.* for non-redundant shafts.	According to, Structures Design Guidelines (2013) Section 3.6, minimum concrete cover = 6*in.* for all kinds of shafts.
Illinois	Non-contact splice into top of drilled shaft.	According to, Bridge Manual (2012) Section 3.15.5.4, "When splicing of longitudinal bars is necessary, they should be mechanically spliced. Mechanical splices for vertical bars shall be staggered according to LRFD Article 5.10.11.4.1f. An exception to using mechanical splices is when nominal extensions of the drilled shaft cages are required in construction due to variable field conditions. In most instances, the cage can be lengthened by lap	Not Specified.	Contractor is responsible for determining the casing thickness. Refer Article 516.06(d) of the Standard Specifications.	Not Specified.

Continued Table A.1. Comparison of DOTs design requirements

DOT/ Codes	Connection method for Type II/oversized shaft [See note 1]	Embedment length required [See note 2 and 10]	Casing contribution in strength	Minimum thickness and diameter of casing [See note 6]	Minimum concrete cover for drilled shaft
		splicing additional bars at the base of the cage as the moment demand in this area is greatly diminished". See Figure B.1.			
Kansas.	As per, Bridge Construction Manual (2008) Section 5.4.8 of Bridge Construction Manual, "the shaft reinforcement must extend into the column by the splice length shown in the plans. This is done either by extending the shaft steel (if the shaft is the same size as the column) or by inserting a splice or dowel bar that extends into the shaft and into the column".	See Figure B.8.	There is some resistance provided by the casing. KDOT does not allow for the casing contributing to the shaft resistance. (Risch, Loren, Chief, Bureau of Structures & Geotechnical Services, KDOT, Personal communication to Muhammad Hassan, July 03, 2013)	As per, Design Manual (2013) Section 3.4.6.2, minimum diameter =3'-0". For standard wall thickness of tubes/casing refer to Table A.2.	As per, Design Manual (2013) Section 3.4, for drilled shafts, use 3 in. cover for shafts < 3 ft., 4 in. cover, for shafts 3 ft. to 5 ft., and 6 in. of cover for shafts > 5 ft.
Louisiana	Refers to AASHTO LRFD Specifications.	Refers to AASHTO LRFD Specifications.	Refers to AASHTO LRFD Specifications.	As per, LADOTD Bridge Design Manual (2006) Section 6, "drilled shafts used in abutments shall have a minimum diameter of 2'-0", however, a diameter of 2'-6" is preferable".	As per, LADOTD Bridge Design Manual (2006) Section 6, "detailed clearances for the reinforcement to the outside of the drilled shaft will be 3" for shafts with a diameter of 2'-6" or less and 6*in.* for shafts greater than 2'-6" ".

Continued Table A.1. Comparison of DOTs design requirements

DOT/ Codes	Connection method for Type II/oversized shaft [See note 1]	Embedment length required [See note 2 and 10]	Casing contribution in strength	Minimum thickness and diameter of casing [See note 6]	Minimum concrete cover for drilled shaft
Massachusetts	Non-contact splice into top of drilled shaft.	According to, MassDOT LRFD Bridge Manual - Part I (2013) Section 3.2.3, "Continuous steel reinforcing shall be maintained whenever possible throughout the length of the shaft. Splices should be avoided in the longitudinal steel where practical. If splices in the adjacent longitudinal reinforcement are necessary, they shall be made with mechanical reinforcing bar splicers and shall be staggered a minimum of 2'-0". "Column longitudinal reinforcement shall be extended into drilled shafts in a staggered manner to avoid a weakened section with a sudden change in stiffness".	Not Specified.	Not Specified.	Minimum Cover =5*in.*. For typical details see Figures 0.2 and 0.3.

Continued Table A.1. Comparison of DOTs design requirements

DOT/ Codes	Connection method for Type II/oversized shaft [See note 1]	Embedment length required [See note 2 and 10]	Casing contribution in strength	Minimum thickness and diameter of casing [See note 6]	Minimum concrete cover for drilled shaft
Missouri.	Not Specified.	Refers to AASHTO LRFD Specifications- Reinforcing steel shall extend 10 ft. below the point of fixity of the drilled shaft.	As per, Engineering Policy Guidelines for Design of Drilled Shafts (2011) Section 751.37.1.3, "all drilled shafts shall have permanent casing (corrugated metal pipe or steel pipe) installed through overburden soils to prevent caving of these soils during construction unless conditions are such that the shafts can be more effectively and reliably constructed without casing or using temporary casing". As per, Engineering Policy Guidelines for Design of Drilled Shafts (2011) Section 751.37.6 , "if permanent casing is used, and the shell consists of smooth pipe greater than 0.12 in. thick, it may be considered load carrying. A1/8" shall be subtracted off of the shell thickness to account for corrosion. Casing could also be corrugated metal pipe"	As per, Engineering Policy Guidelines for Design of Drilled Shafts (2011) Section 751.37.1.1, "the length to diameter ratio of drilled shafts should generally be in the following range: $3 \leq L/D \leq 30$. Minimum Diameter of drilled shaft= 18"". As per, Engineering Policy Guidelines for Design of Drilled Shafts (2011) Section 751.37.1.3, "drilled shaft greater than 6 ft. in diameter shall have a minimum casing thickness of ½" specified unless a greater thickness is required by design for strength".	Refer to Table A.3.

Continued Table A.1. Comparison of DOTs design requirements

DOT/ Codes	Connection method for Type II/oversized shaft [See note 1]	Embedment length required [See note 2 and 10]	Casing contribution in strength	Minimum thickness and diameter of casing [See note 6]	Minimum concrete cover for drilled shaft
Nevada.	See Figure B.11.	Not Specified.	According to, NDOT structures manual (2008) Section 17.4.3, "a casing may be used to maintain the excavation, especially when placing a shaft within the water table. This casing, if left in place after construction, shall not be considered in the determination of the structural resistance of the shaft. However, it should be considered when evaluating the seismic response of the foundation because the casing will provide additional resistance".	According to, NDOT structures manual (2008) Section 17.4.4-4 , "the diameter of a drilled shaft supporting a single column shall be at least 1½ ft. greater than the greatest dimension of the column cross section".	According to, NDOT structures manual (2008) Section 17.4.4-2 "the design and detailing of drilled shafts must conform to the clearances for reinforced steel cages as specified in the NDOT Standard Specifications: + 4 in. for drilled shafts having a diameter of less than 5 ft., or + 6 in. for drilled shafts having a diameter of 5 ft. or more".
Oregon	Non-Contact Lap splice. For connection detail refer to Figures B.12 and B.13.	As per, Bridge Design and Drafting Manual 2004 (2013) Section 1.1.5.5, "the splice region is ($1.7L_{db} + a$) rounded up to the nearest 3 inches." Note that L_{db} is the basic development length per AASHTO BDS Article 5.11.2.1.Where a=0.5*(shaft spiral dia.-column spiral dia.).	As per, Bridge Design and Drafting Manual 2004 (2013) Section 1.1.5.5, "if permanent casing is desired it should be taken into account in the structural analysis of the bridge because it increases the stiffness and strength of the shaft and may significantly affect the overall response of a bridge subject to large lateral loads".	Not Specified.	As per, Bridge Design and Drafting Manual 2004 (2013) Section 1.1.5.5, "if Shaft Diameter is ≤ 3 ft. than concrete cover= 3 in., if 5 ft. > D > 3 ft. then concrete cover=4 in, if dia. is ≥5 ft. then cover = 6 in."

Continued Table A.1. Comparison of DOTs design requirements

DOT/ Codes	Connection method for Type II/oversized shaft [See note 1]	Embedment length required [See note 2 and 10]	Casing contribution in strength	Minimum thickness and diameter of casing [See note 6]	Minimum concrete cover for drilled shaft
South Carolina.	Non-Contact Lap splice	According to, SCDOT seismic design specifications for highway bridges (2011) Section 8.4.9, "longitudinal column reinforcement shall be extended into oversized shafts in a staggered manner with the minimum embedment lengths of $2D_{c,\,max}$ and $3D_{c,\,max}$, where $D_{c,\,max}$ is the largest cross sectional dimension of the column". Refer Figure B.15 for typical detail.	According to, SCDOT Bridge Design Memorandum – DM0111 (2011), SCDOT Bridge Design Manual Section 19.3.3 should include, "The casing shall not be considered in the determination of the structural resistance of the shaft. However, it should be considered when evaluating the seismic response of the foundation because the casing will provide additional resistance."	According to, SCDOT Bridge Design Memorandum – DM0111 (2011), SCDOT Geotechnical Design Manual Section 16.4 should include, "Drilled shaft sizes (diameters) can range from 30 inches (2-1/2 feet) to 144 inches (12 feet). Drilled shaft sizes typically used by SCDOT range from 42 inches (3-1/2 feet) to 84 inches (7 feet) in diameter".	SCDOT require a 4-inch minimum concrete cover for drilled shafts in both soil and rock conditions.
Washington	Non-Contact Lap splice. Refer Figures B.18 and B.19.	As per TRAC Report WA-RD 417.1(1997) titled "Noncontact Lap Splices in Bridge Column-Shaft Connections", "column longitudinal reinforcement in drilled shafts is typically straight. Embedment shall be a minimum length equal to $l_{ns} = l_s + s$. where: l_s = the larger of $1.7 \times l_{ac}$ or $1.7 \times l_d$ (for Class C lap splice) where: l_{ac} = development length from the Seismic Guide Spec. 8.8.4 for the column longitudinal reinforcement. l_d = tension development	Washington DOT Design Memorandum (2012), allows steel casing to be considered in the calculation of structural capacity of piles, shafts, and connections of pile-to-pile cap and column-to-shaft foundation.	See note 8.	According to, Bridge Design Manual (LRFD) (2012) Section 7.8.2, "Cover requirements vary depending on the drilled shaft diameter and shall be as specified below: • Diameter less than or equal to 3′-0″ = 3″ • Diameter greater than 3′-0″ and less than 5′-0" = 4″ • Diameter greater than or equal to 5′-0″ = 6″ "

Continued Table A.1. Comparison of DOTs design requirements

DOT/ Codes	Connection method for Type II/oversized shaft [See note 1]	Embedment length required [See note 2 and 10]	Casing contribution in strength	Minimum thickness and diameter of casing [See note 6]	Minimum concrete cover for drilled shaft
		length from AASHTO LRFD Section 5.11.2.1 for the column longitudinal reinforcement. *s* = distance between the shaft and column longitudinal reinforcement" According to, Bridge Design Manual (LRFD) (2012) Section 7.4.4, "the requirements of the AASHTO seismic 8.8.10 for development length of column bars extended into oversized pile shafts for SDC C and D shall not be used. All applicable modification factors for development length, except one, in AASHTO LRFD 5.11.2 may be used when calculating l_d. The modification factor in 5.11.2.1.3 that allows l_d to be decreased by the ratio of (A_s required)/ (A_s provided), shall not be used".			

Table Notes:

- Difference between Type I and Type II connections is defined in Caltrans Seismic Design Criteria (2010). See Section 1.3.2 for further details.

- As per AASHTO BDS (2012) Article 5.11.5.2.1, bars spliced by noncontact lap splices shall not be spaced farther apart transversely than one-fifth the required lap splice length or 6.0*in.*. For the column/shaft splice, all the reinforcing is spliced in the same location. Since there is less than twice the required reinforcing a Class C splice is required.

- For connection detail of Type II shafts, for which spacing can be greater than 6*in.*, reference to the Washington DOT document is given. Refer to Figure 1.2 of the report for typical connection detail.

- These provisions are for CFT not RCFT (i.e., Reinforced Concrete-filled Tube).

- These are based on Caltrans Seismic Design Criteria (SDC), 2006 edition. In revised 2010 edition, of Caltrans SDC required difference in diameter is increased from 18*in.* to 24*in.*.

- Minimum thickness of casing can be either calculated from the requirement for reinforcement or for required strength during driving. Minimum thickness of casing required to achieve requisite strength during driving is function of site condition and driving equipment. Larger thickness of casing is required for casings installed with help of vibratory or impact hammer (Brown et al. 2010).

- Thickness of casing will decrease with passage of time due to effects of corrosion. While calculating the strength of shaft including effect of casing, reduction in thickness of casing over the shaft design life should be considered. If soil pH is less than 4.5 and/or soil resistivity is less than 2000-*ohm-cm*, than conditions are considered as aggressive. Furthermore, if sulfate content is more than 200 parts-per-million (ppm) and/or chloride content is more than 100 *ppm*, then soil is also considered aggressive. These conditions will cause corrosion at higher rate. Hannigan et al. (2006) report a conservative estimate for a corrosion rate of 0.003 *inch/year* for steel piles buried in fill or disturbed natural soil (Brown et al. 2010).

- The development length l_d shall be determined by multiplying the basic tension development length l_{db} as specified in AASHTO BDS Article 5.11.2.1 by, "the compounded modification factors of 0.9 and 0.6 for epoxy-coated and non-epoxy-coated reinforcement, respectively. Expected values of 68*ksi* and 5*ksi* for f_{ye} and f'_{ce} respectively, shall be used in calculating l_{db}"

- According to Washington DOT Design Memorandum (2012), "the cross-section for CFT and RCFT shall be adjusted for corrosion rates as specified below but not less than 1/16 *inch* at the end of design life (75 years minimum) after corrosion.
    - Soil embedded zone (undisturbed soil): 0.001 *inch/year*
    - Soil embedded zone (fill or disturbed natural soils) 0.003 *inch/year*
    - Immersed Zone (fresh water): 0.002 *inch/year*
    - Immersed Zone (salt water): 0.004 *inch/year*
    - Scour Zone (salt water): 0.005 *inch/year*
    - The minimum thickness shall not be taken less than 3/8 *inch* at the time of installation."

- This table specifies minimum length of column/splice cage reinforcement that should be extended into drilled shaft. For further understanding, refer Figure 1.2 of the report and Figures B.5, B.12, B.13, B.15, and B.19.

Table A.2. Standard Tool Casings Standard Available (From Kansas DOT)

Outside Diameter	Wall Thickness Range
18*in.* thru 24*in.*	Min. 1/4*in.*; 9/32*in.*; 5/16*in.*; 3/8*in.* Max.
30*in.* thru 36*in.*	Min. 5/16*in.*; 3/8*in.*; 7/16*in.* Max.
42*in.* thru 60*in.*	Min. 3/8*in.*; 7/16*in.*; 1/2*in.* Max.
66*in.* thru 96*in.*	Min. 13/32*in.*; 7/16*in.*; 9/16*in.*; 3/4*in.* Max

Table A.3. Minimum Concrete Cover Requirements

Outside Diameter, *ft.*	Casing Remains, *in.*
2	3
3	3
4	4
5 or larger	6

A.2 Summary of Requirements for DOTs not mentioned in Table A.1

This section briefly describes the structural design and detailing requirements for drilled shafts specified by DOTs not mentioned in Table A.1. The DOTs included here (presented in a list by alphabetical order), for the most part, follow the requirements provided in the AASHTO BDS or the AASHTO SGS. Small deviations from those provisions, when found, are highlighted for each state. Section 1.3.1 of the report summarizes the design and detailing requirements for all DOTs.

- Alabama DOT, Bridge Bureau Structures Design and Detail Manual (2008), mentions AASHTO LRFD Standard Specifications for Highway Bridges, as a basis document. This manual also specifies a minimum concrete cover of 6*in.* for the shaft, and recommends that drilled shaft diameter be 6*in.* larger than column diameter.

- Alaska DOT follows AASHTO SGS. For all non-seismic aspects of design, it refers to the AASHTO BDS (Marx, Elmer E., Senior Bridge Design Engineer, State of Alaska Department of Transportation and Public Facilities, Personal communication to Muhammad Hassan, June 10, 2013).

- Arkansas Highway and Transportation Department states that they strictly follow the AASHTO BDS for the structural design of drilled shafts (Fuselier, Carl J, Division Head - Bridge, Arkansas Highway and Transportation Department, Personal communication to Muhammad Hassan, June 26, 2013).

- According to Arizona DOT, AASHTO BDS provisions shall be followed for structural designing of drilled shafts (ADOT Bridge Design Guidelines (2011)). According to the ADOT Bridge Design Guidelines (2011) Appendix A-Example 2.2, "Where the distance between spliced rebar exceeds 6*in.*, the development length must be increased to reflect the lack of a contact splice. This is done by assuming a 1:1 distribution between bars resulting in increasing the lap length by the distance of separation." "For the column/shaft splice, all the reinforcing is spliced in the same location. Since there is less than twice the required reinforcing a Class C splice is required." According to section 10.8.5 of ADOT Bridge Design Guidelines (2011), "Drilled shafts of six feet or more in diameter or which may be constructed using slurry or wet method, shall have 6*in.* minimum clear cover of the reinforcements to the outside edge of the shaft."

- Colorado DOT requires that "caisson design" shall be in compliance with Chapters 10 and 11 of the latest AASHTO BDS (Mohseni, Mansour, Professional Engineer I, Colorado Department of Transportation, Personal communication to Muhammad Hassan, June 11, 2013).

- Connecticut DOT generally follows the AASHTO provisions. However, they heavily rely on the results of load tests because codes are perceived to be fairly conservative, at least with respect to axial capacity (Fontaine, Leo L, Connecticut Department of Transportation, Personal communication to Muhammad Hassan, June 29, 2013).

- In Delaware, driven piles are found to be more effective for the type of soils found in that state, and DelDOT rarely uses drilled shafts (Hastings, Jason N., Bridge Design Engineer, Delaware Department of Transportation, Personal communication to Muhammad Hassan, June 27, 2013). DelDOT Bridge Design Manual (2005) Section 6.2.4 specifies that, if a casing is used, the minimum thickness of steel casing should be 0.25*in.*. It refers to FHWA Drilled Shaft Manual for the design of drilled shafts. It also refers to AASHTO BDS for specific criteria for seismic design.

- Georgia DOT follow AASHTO BDS and FHWA guidelines for structural design of caissons/drilled shaft (Customer Service Unit, Georgia DOT, Personal communication to Muhammad Hassan, July 8, 2013). The Bridges and Structures Manual (2013) specifies that, for allowing easy access for inspection purposes, diameter of drilled caissons should be more than 48*in.*.

- Hawaii DOT follows AASHTO BDS for the design of drilled shaft (Santo, Paul, Bridge Design Engineer, Hawaii DOT, Personal communication to Muhammad Hassan, September 26, 2013).

- Indiana DOT Design Manual (2013) Section 408-4.0, mentions that AASHTO BDS shall be followed for structural design of drilled shaft. A typical detail of drilled shaft is shown in Figure B.4.

- Idaho Transportation Department, Bridge Design LRFD Manual (2008), require that AASHTO BDS and the AASHTO LRFD SGS shall be followed for structural design of drilled shaft.

- Iowa DOT, LRFD bridge design manual (2012) Section 6.3, mentions that structural design of drilled shafts for bridge foundations is governed by the AASHTO LRFD Specifications, and advises designers to consult the FHWA "Drilled Shafts: Construction Procedures and LRFD Design Methods" by Brown et al. (2010) for more design information.

- Kentucky Transportation Cabinet, Structural Design (2005) Section SD-503, states that "Where drilled shafts pass through soil, use permanent casing". According to Geotechnical Guidance Manual (2005), "Design procedures are presented in the FHWA IF-99-029, Drilled Shafts: Construction Procedures and Design Methods". According to Section 2.3 of Special Note 11c-Drilled Shafts (Kentucky Transportation Cabinet (KYTC) 2012), minimum thickness of casing is specified as 3/8*in.*. It is advised to the neglect effect of the permanent casing while calculating structural capacity of encased drilled shaft (Hite, Mark, Kentucky Transportation Cabinet, Personal communication to Muhammad Hassan, July 8, 2013). Typical detail of drilled shaft is shown in Figure B.9.

- Maine Department of Transportation, Bridge Design Guide (2003) Section 5.8, follows the procedures given in FHWA (1988) for design of drilled shaft.

- Maryland DOT does not have provisions specifically related to structural design of drilled shafts. However, some county-specific documents (e.g., Anne Arundel County Maryland, Design Manual (2006) Section 4-II-G) states that all components of highway bridges shall be designed in accordance with the AASHTO Standard Specifications for Highway Bridges.

- Michigan DOT currently follows AASHTO BDS for the design of drilled shaft (Zokvic, Vladimir, P.E., MDOT Bridge Standards, Personal communication to Muhammad Hassan, July 01, 2013).

- Mississippi DOT requires drilled shaft foundations for Mississippi DOT projects to be designed in accordance with the FHWA (Brown et al. 2010) document (Ferguson, Sean, P.E., MDOT Geotechnical, Personal communication to Muhammad Hassan, July 01, 2013).

- Minnesota DOT, LRFD Bridge Design Manual (2013), mention that AASHTO BDS shall be followed. It also requires the use of permanent casings whenever shafts are constructed in water. Minimum concrete cover is 3*in.*.

- According to Montana DOT, Montana Structures Manual (2002) Section 20.4, AASHTO BDS shall be followed for the structural design of drilled shaft. For typical drilled shaft details, refer to Figure B.10.

- Nebraska DOR (Department of Roads), Geotechnical Policies and Procedures (2012) Section 7.1E, requires that both AASHTO BDS and FHWA guidelines should be followed. According to Bridge office policies and procedures (Nebraska Department of Roads Bridge Division 2013) Section 2.3.6, drilled shafts shall be constructed using permanent casing.

- New Hampshire DOT follows AASHTO and FHWA for the design of drilled shafts (Daigle, Kevin, E.I.T., NH Department of Transportation, Personal communication to Muhammad Hassan, June 27, 2013).

- New Jersey DOT, Design Manual for Bridges and Structures (2009), indicates that the AASHTO LRFD Guidelines and AASHTO BDS shall be followed for design of drilled shafts. According to Section 16.3.4, "The Federal Highway Administration Publication Number FHWA-IF-99-025, titled "Drilled Shafts: Construction Procedures and Design Methods" may be studied for assistance in designing drilled shafts."

- New York DOT, NYSDOT LRFD Bridge Design Specifications (2011), indicates that the AASHTO BDS shall be followed.

- North Dakota DOT, Design Manual (2013), Section IV LRFD Bridge Design Specifications, does not specify any provision which should be used in addition to AASHTO BDS for structural design of drilled shaft.

- North Carolina DOT structural design of drilled shafts shall be in accordance with the current edition of the AASHTO LRFD Specifications. NCDOT do not consider presence of the permanent casing when computing the shaft structural capacity (Hanks, Brian, North Carolina DOT, Personal communication to Muhammad Hassan, July 12, 2013).

- Ohio DOT indicates that the FHWA (Brown et al. 2010) shall be used as reference for designing drilled shafts. Furthermore, enhancement of structural capacity due to presence of permanent casing in drilled shaft can be considered for resisting axial loads and bending moments (Antonios, Teddy, Transportation Engineer 4, Office of Structural Engineering, Ohio DOT, Personal communication to Muhammad Hassan, July 01, 2013). According to Bridge Design Manual (2007) Section 202.2.3.3, the minimum diameter for drilled shafts that support pier columns is specified as 42*in.* Section 301.5.7 specifies that, "minimum concrete cover for drilled shaft ties or spirals of diameter greater than 4.0*ft.* shall be 6*in.*, and 3*in.* for diameter equal or less than 4.0*ft.*".

- Pennsylvania DOT, Design Manual Part 4 (2012) Section 10.8, indicates that AASHTO BDS shall be used as the reference for designing drilled shafts. Minimum diameter is specified as 36*in.* for drilled shafts which need inspection. Refer to Figure B.14 for typical drilled shaft detail.

- Rhode Island LRFD, Bridge Design Manual (2007) Section 10.7, recommends using AASHTO BDS for structural designing of drilled shaft. The minimum drilled shaft diameter shall be 3*ft.*.

- South Dakota DOT generally follows AASHTO BDS for structural design of drilled shaft (Johnson, Steve, Bridge Design Engineer, SDDOT, Personal communication to Muhammad Hassan, July 08, 2013).

- Tennessee DOT typically follows AASHTO BDS and FHWA (Brown et al. 2010) for structural design of drilled shaft (Seger, Wayne J., Division of Structures, Director, Tennessee Department of Transportation, Personal communication to Muhammad Hassan, September 25, 2013).

- According to Texas DOT, Bridge Design Manual – LRFD (2013), AASHTO BDS should be followed for drilled shaft structural design. Texas DOT requires 30*in.* for specific girder bridge. However, 24 *in.* drilled shafts are commonly used for a concrete slab span bridge.

- Utah DOT exclusively follows AASHTO BDS and FHWA (Brown et al. 2010) guidelines for structural design of drilled shafts (Bischoff, Jon, Utah DOT, Personal communication to Muhammad Hassan, July 01, 2013).

- Vermont Agency of Transportation, Structures Design Manual (2010) Section 10.2.5, follows the AASHTO BDS for structural design of drilled shaft.

- Virginia DOT follows AASHTO BDS and specifies that design of the drilled shaft be accomplished with the help of L-Pile. The state recommends to ignore the effect of casing for determination of the section's strength (Hall, John M., Senior Geotechnical Engineer, VDOT – Central Office, Structure and Bridge Division, Geotechnical Section, Personal communication to Muhammad Hassan, July 12, 2013).

- According to Wisconsin DOT, WisDOT Bridge Design Manual (2013) Section 11.3.2, AAHTO BDS shall be followed for design of drilled shafts. Furthermore it is also mentioned that, for design methodologies refer to FHWA Publication IF-99-025, "Drilled Shafts: Construction Procedures and Design Methods".

- West Virginia DOT follows the latest AASHTO BDS for structural design of drilled shaft (Endres, Gerard G, P.E., West Virginia DOT, Personal communication to Muhammad Hassan, July 01, 2013).

- Wyoming DOT follows AASHTO BDS for structural design of drilled shaft (Fulton, Keith, State Bridge Engineer, Wyoming DOT, Personal communication to Muhammad Hassan, July 08, 2013).

APPENDIX B

Review of Concrete-Filled Steel Tubes (CSFST) Drilled Shaft design requirements from US DOTs, FHWA, AASHTO and others

Note: This Appendix has been prepared in collaboration with Mr. Muhammad Hassan, of NESPAK, Pakistan (Former MSc student at UB).

B.1 Standard Details

A number of states have provided standard details for drilled shafts. They are included in Figure B.1 to B.19, for the DOTs of Illinois (Figure B.1), Massachusetts (Figures B.2 and B.3), Indiana (Figure B.4), Kansas (Figures B.5 to B.8), Kentucky (Figure B.9), Montana (Figure B.10), Nevada (Figure B.11), Oregon (Figures B.12 and B.13), Pennsylvania (Figure B.14), South Carolina (Figure B.15), Texas (Figures B.16 and B.17), and Washington (Figures B.18 and B.19, as well as Figure 1.2 presented in the report).

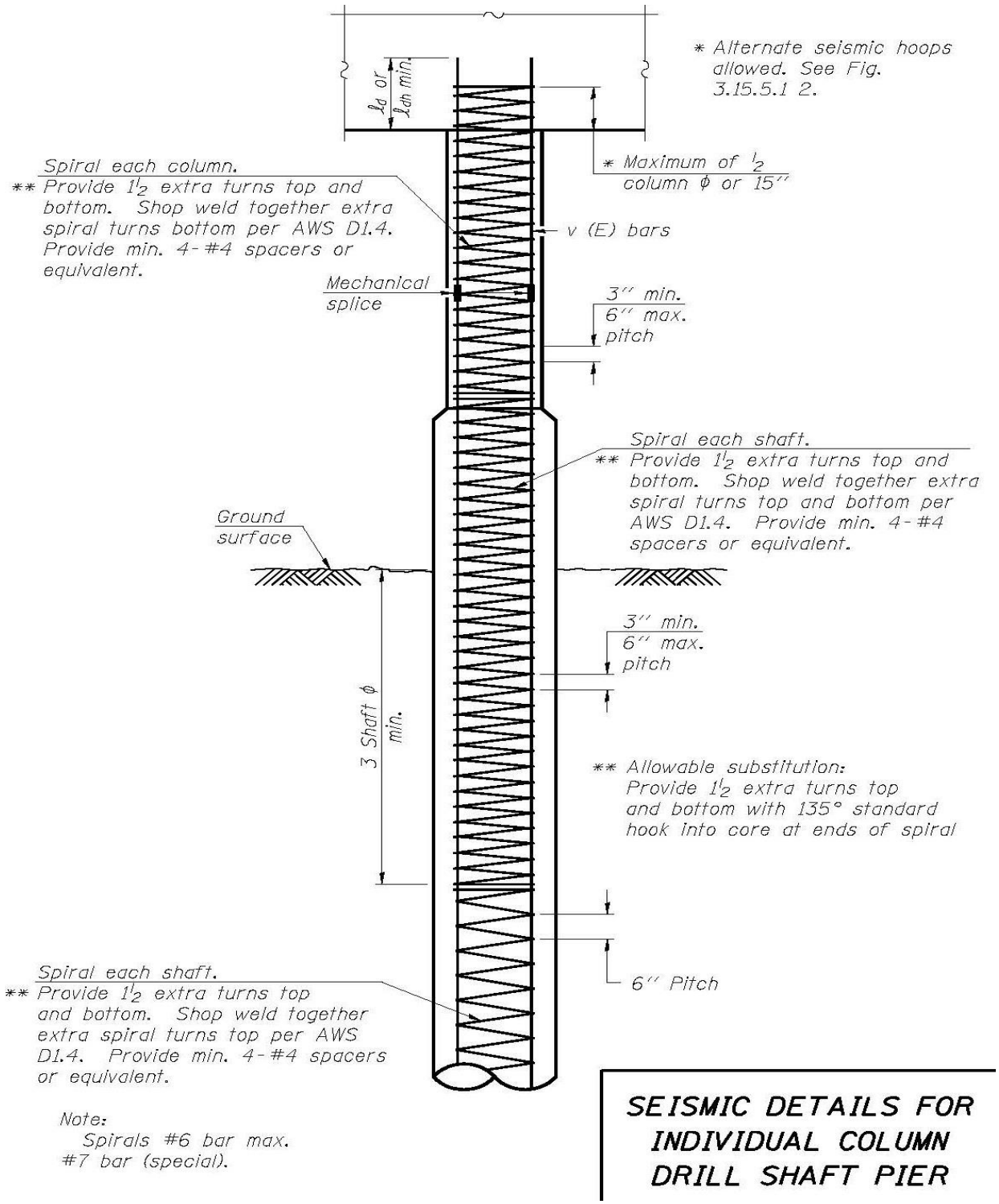

Figure B.1. Seismic detail for individual column shaft pier (From Illinois DOT Bridge Manual (2012)).

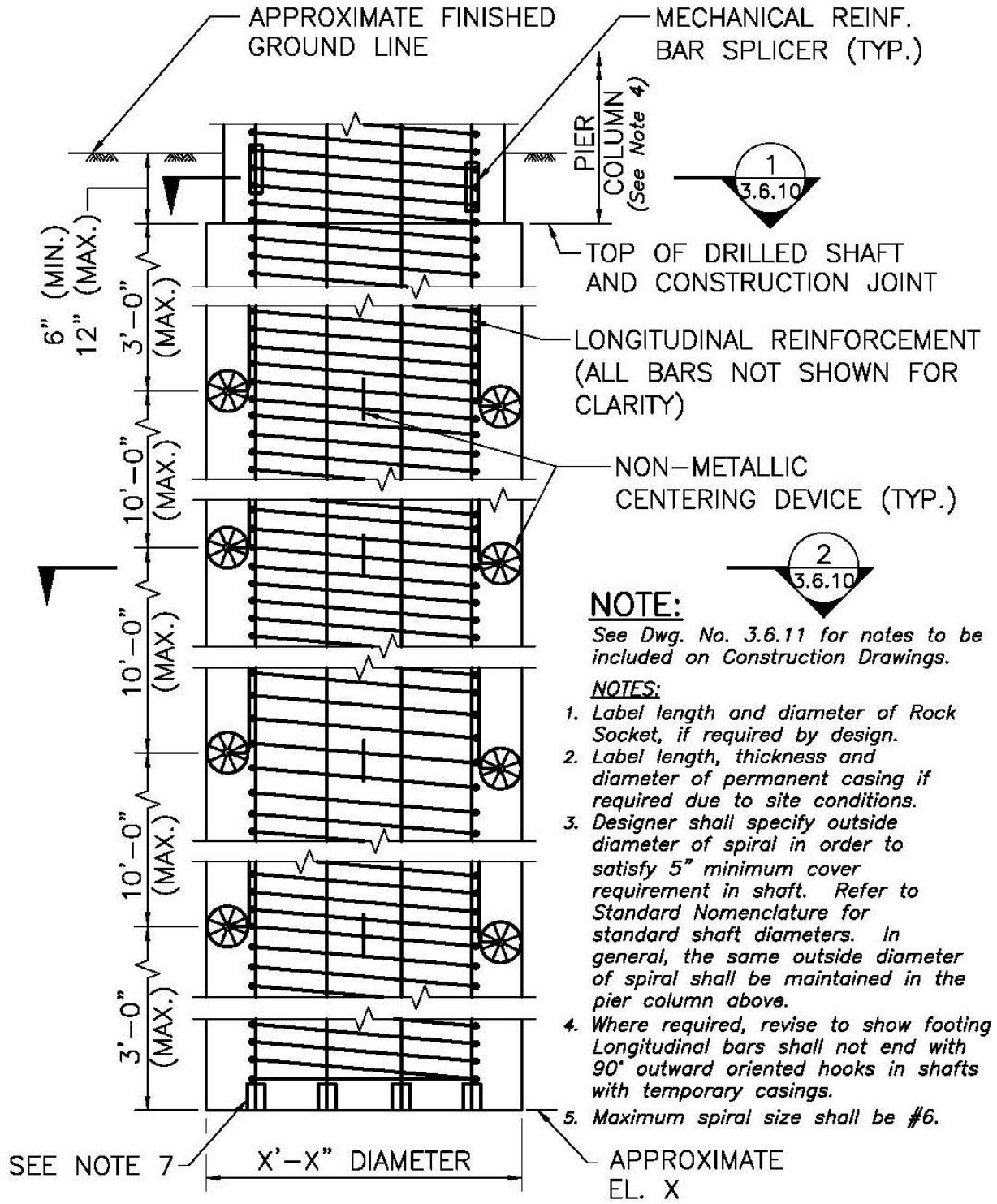

Figure B.2. Drilled shaft vertical section (From MassDOT Bridge Manual (2009)).

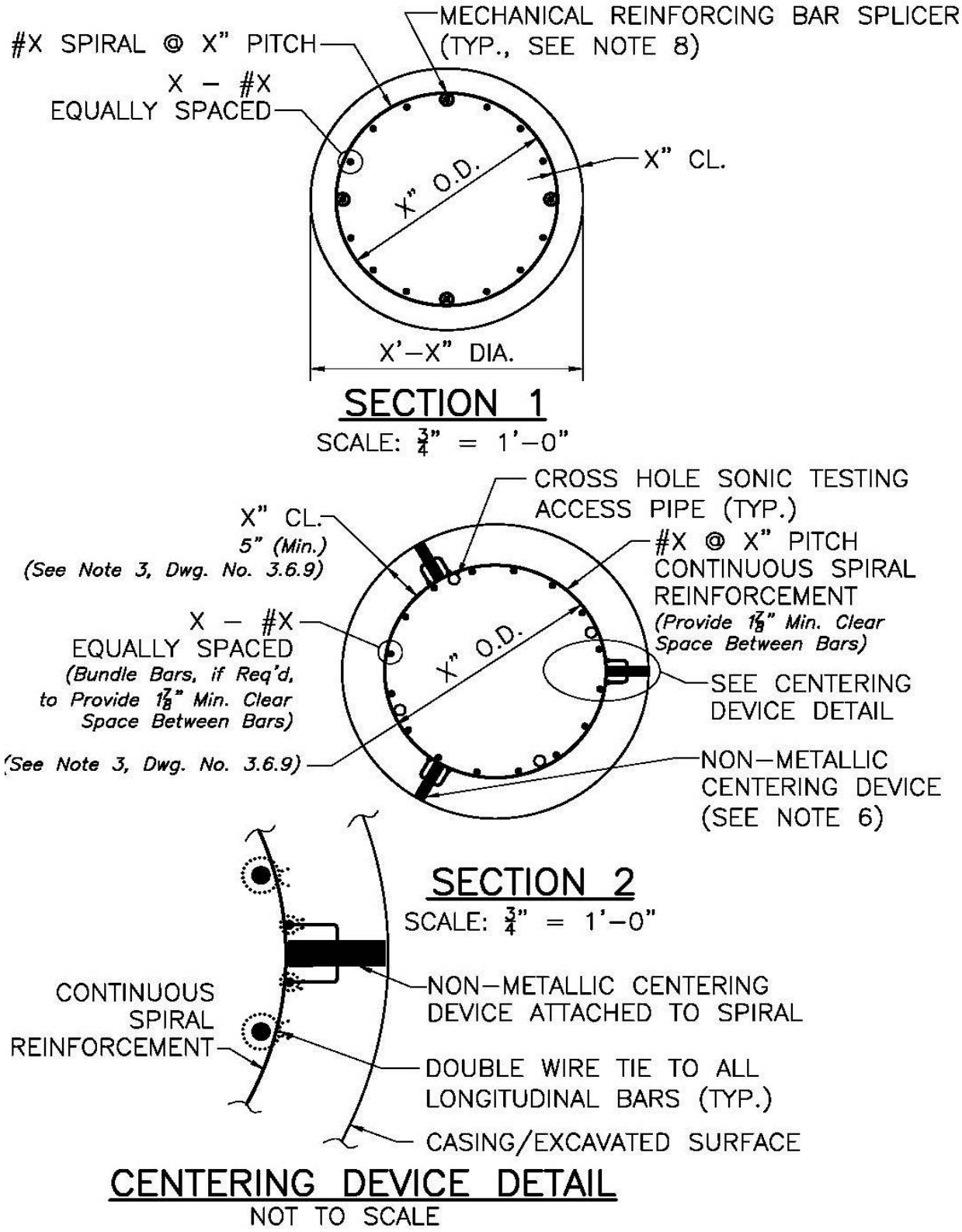

Figure B.3. Drilled shaft cross-section (From MassDOT Bridge Manual (2009)).

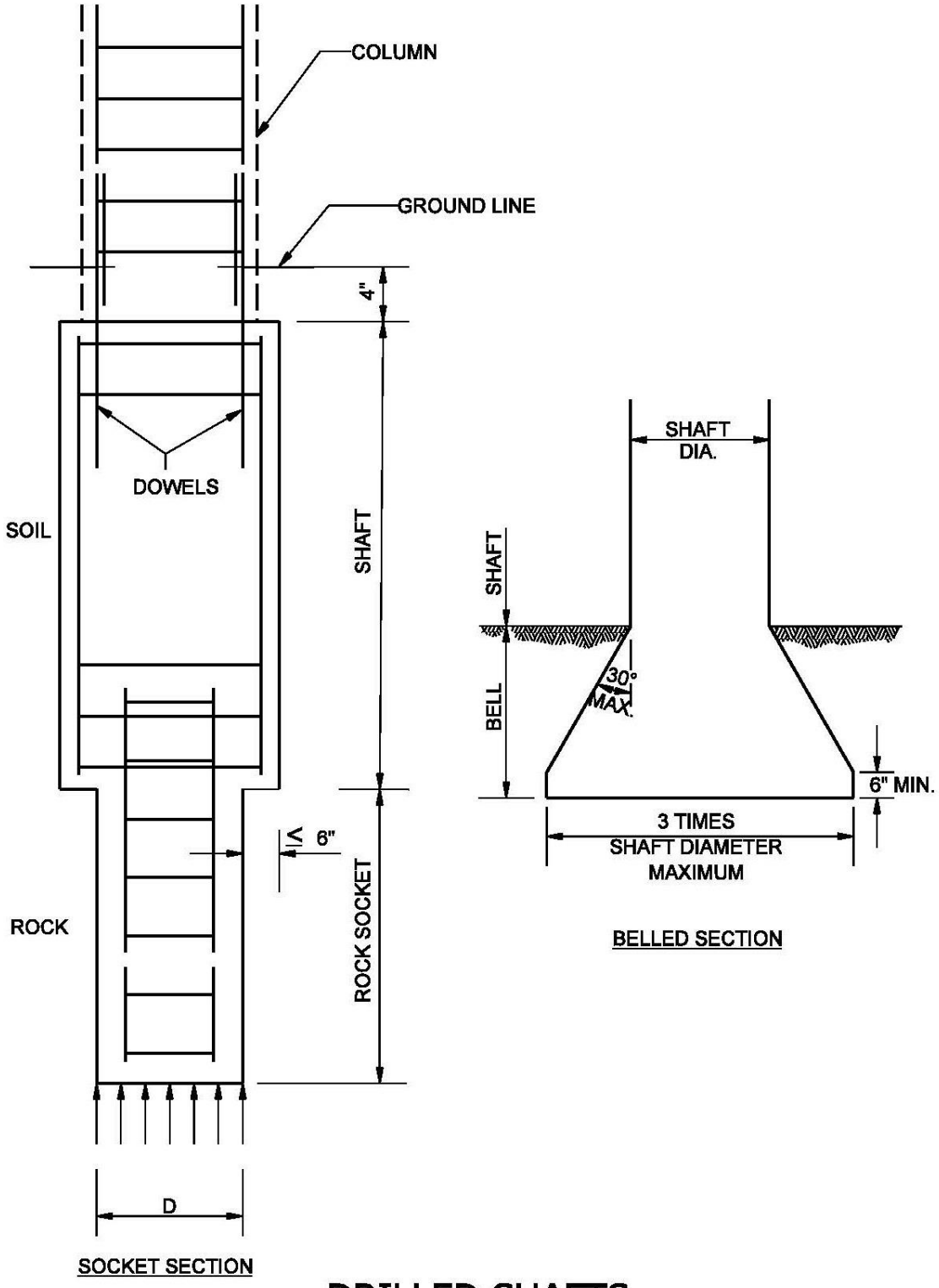

Figure B.4. Drilled shaft cross-section (From Indiana DOT Bridge Manual (2013)).

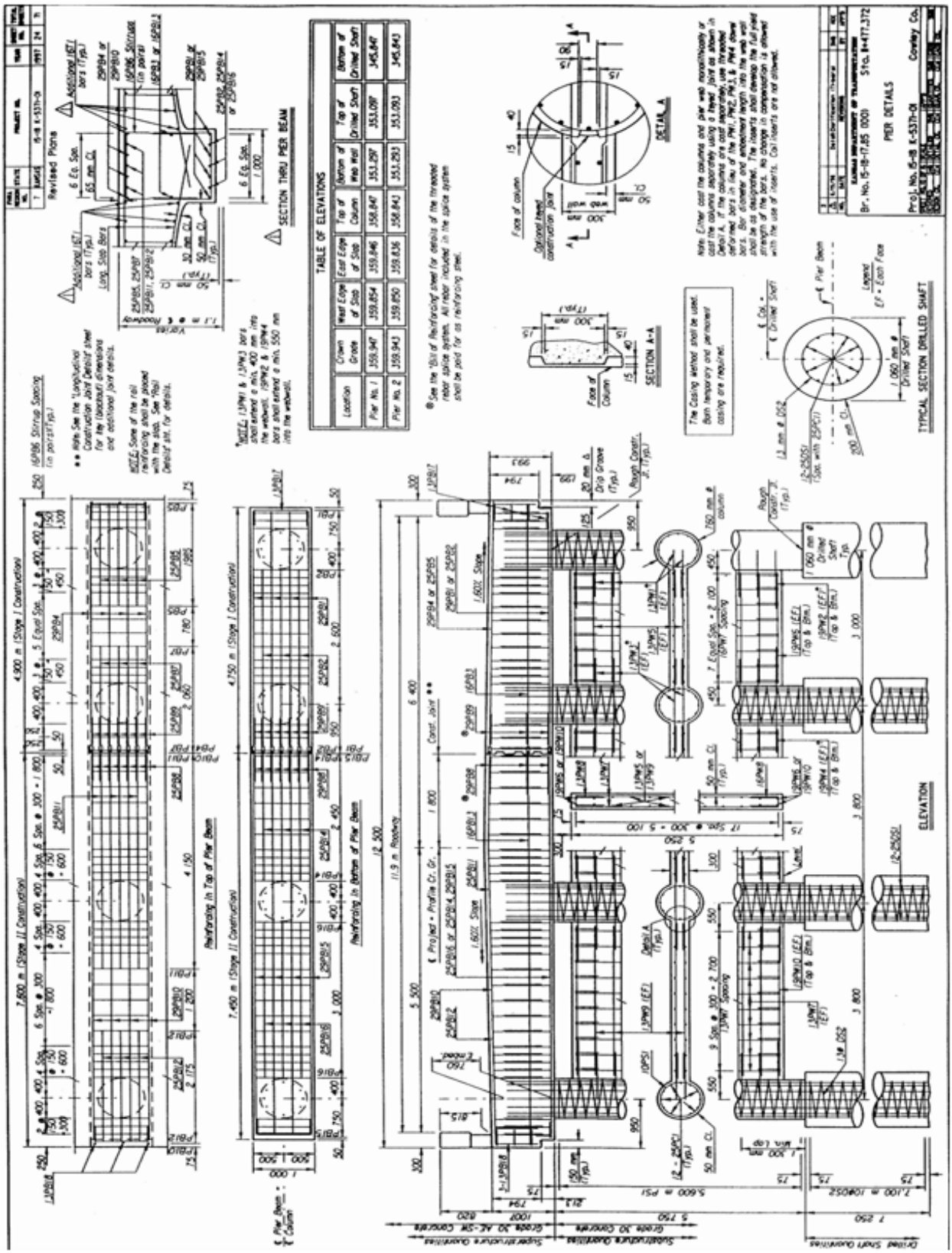

Figure B.5. Design detail of drilled shaft (From Kansas DOT Bridge Design Manual (2013)).

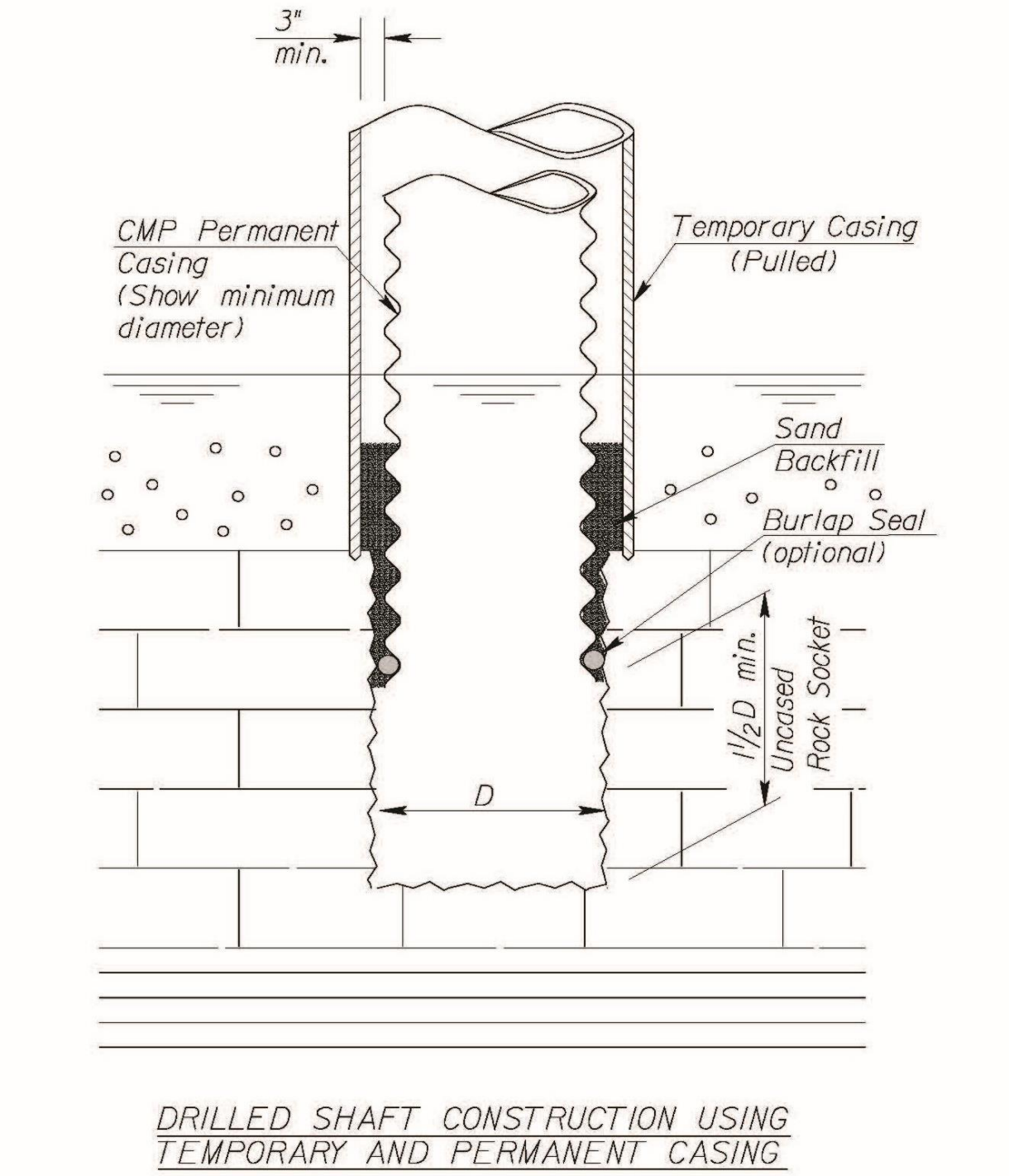

Figure B.6. Drilled shaft construction with temporary and permanent casing (From Kansas DOT Bridge Manual (2013)).

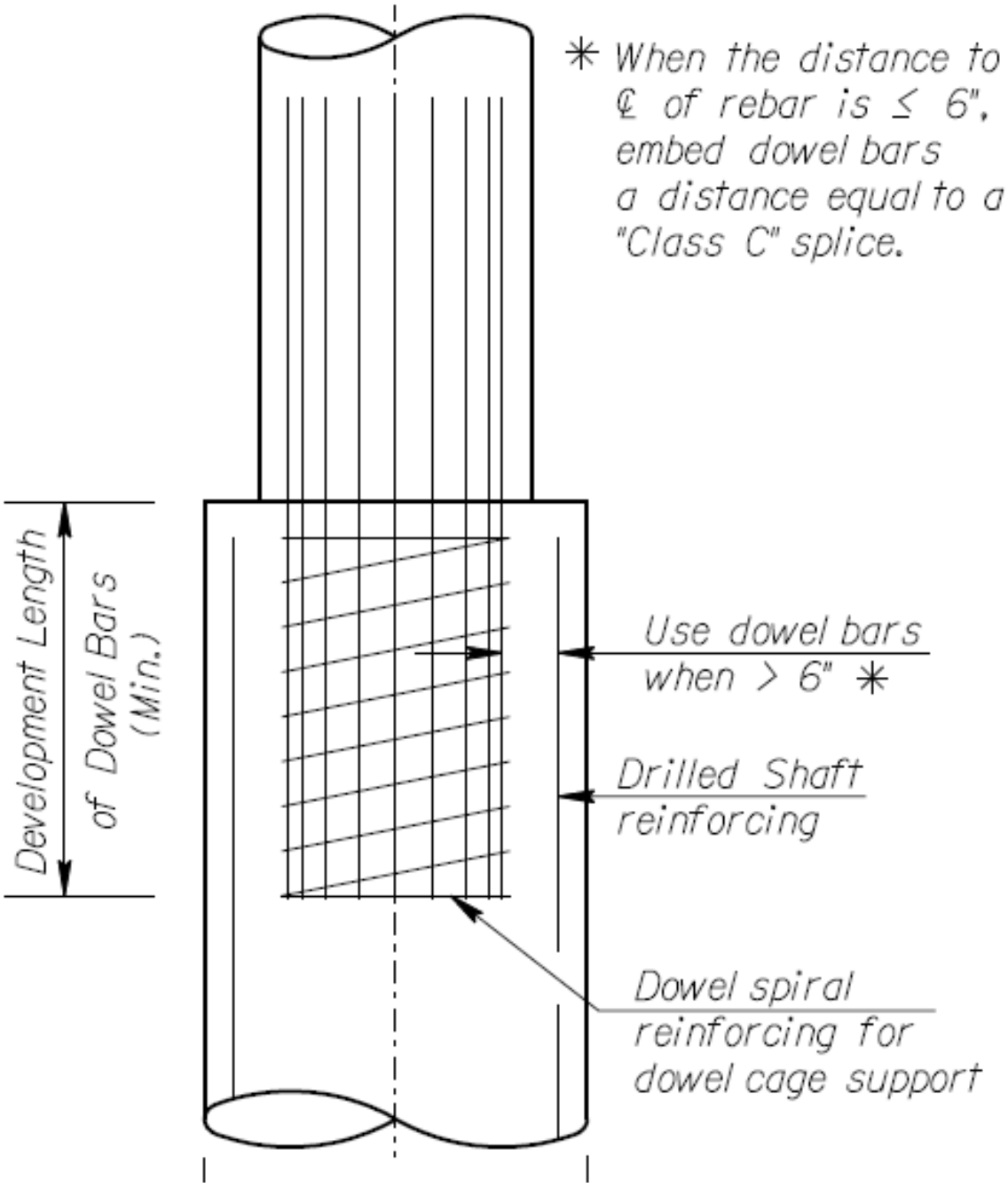

Figure B.7. Typical drilled shaft (From Kansas DOT Bridge Manual (2013)).

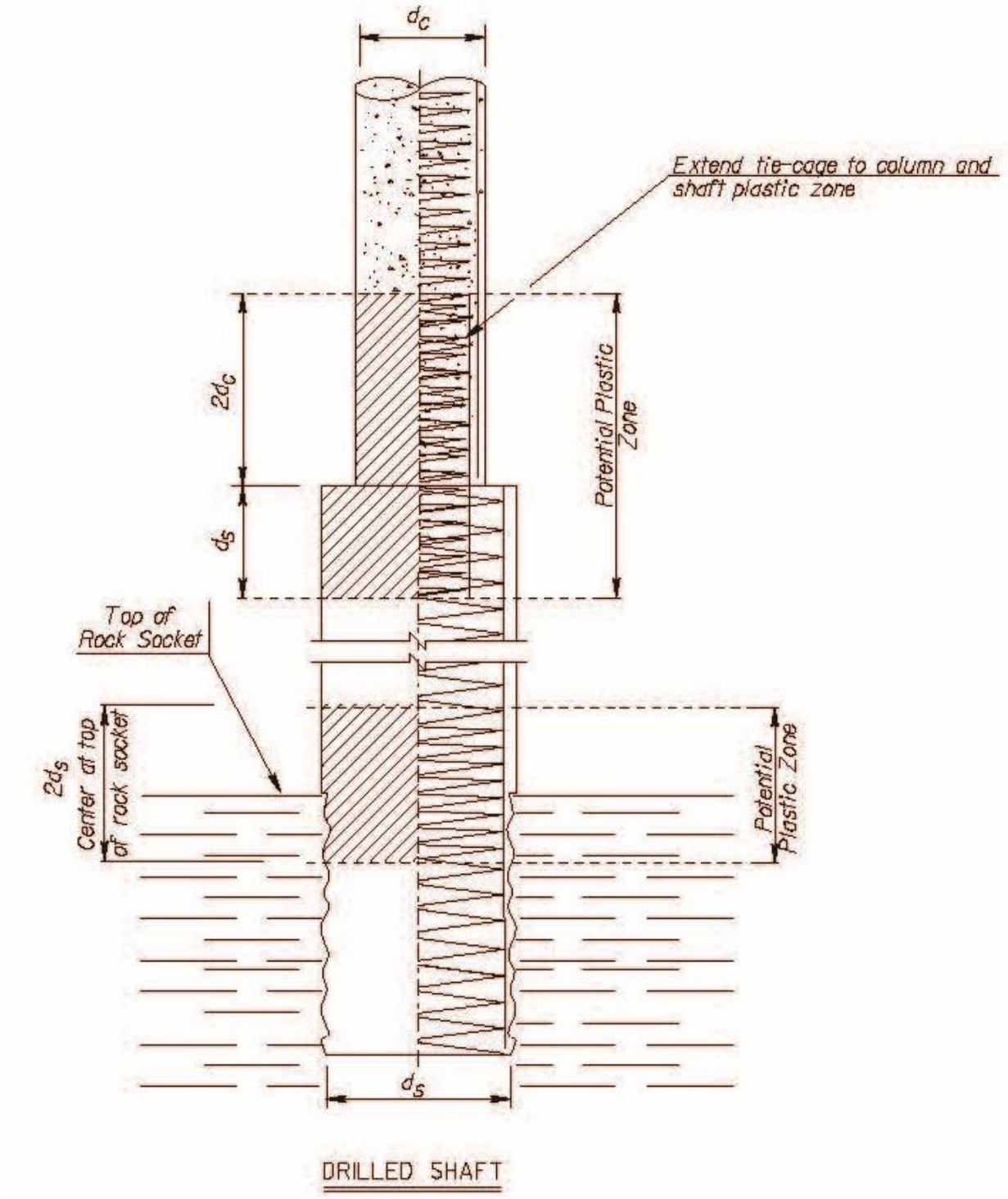

Figure B.8. Seismic detail for individual column shaft pier (From Kansas DOT Bridge Manual (2013)).

EXHIBIT 518

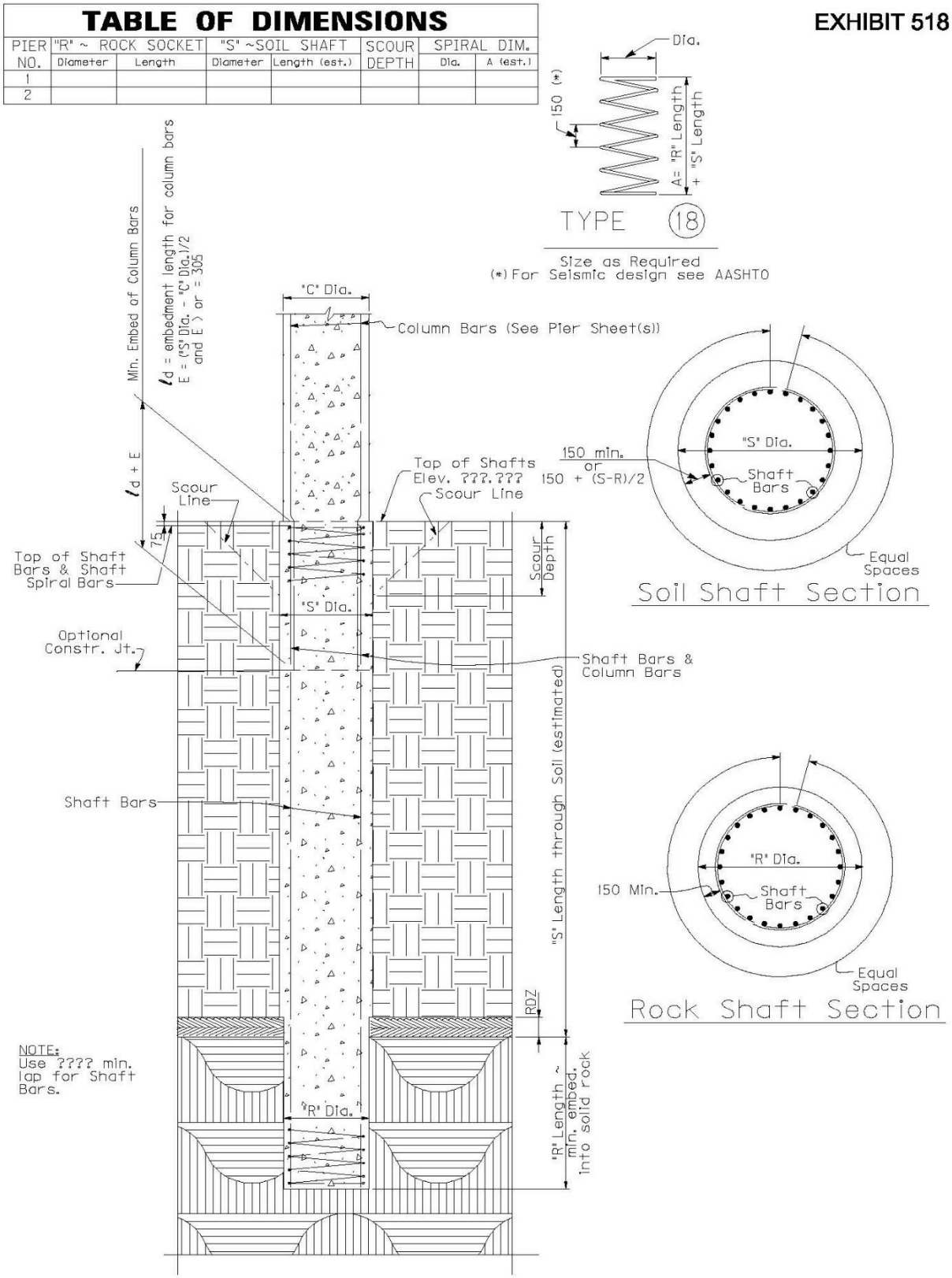

Figure B.9. Typical detail of drilled shafts (From Exhibit 518, Kentucky Transportation Cabinet Structure Design Manual (2005)).

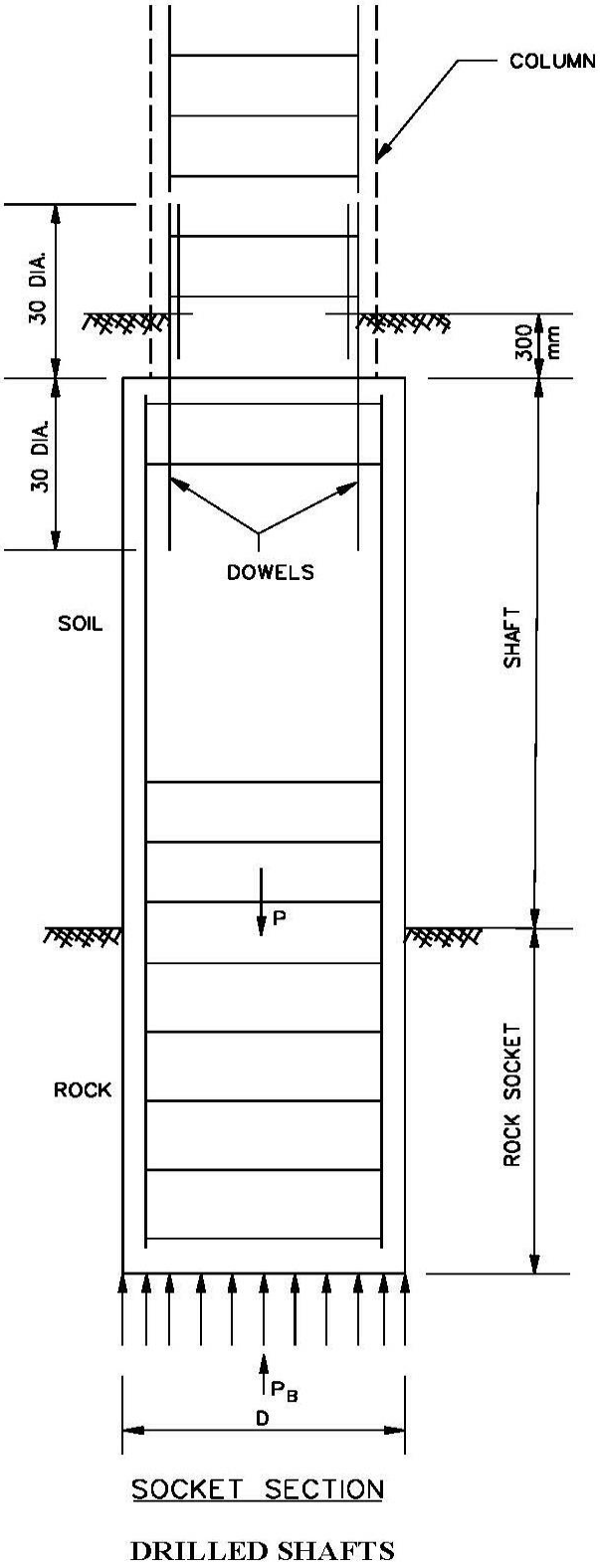

Figure B.10. Typical detail of drilled shaft (Montana Structures Manual (2002)).

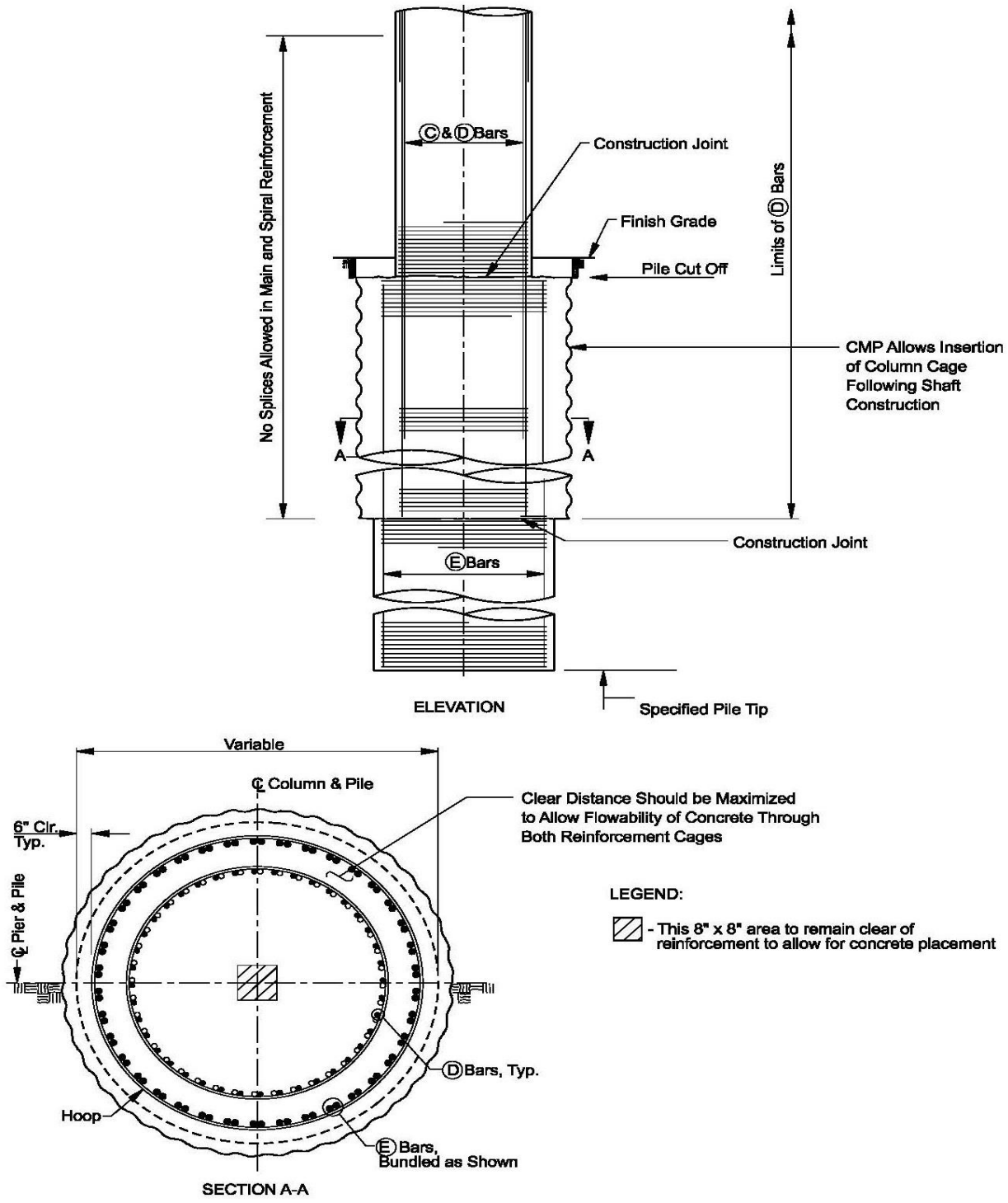

DRILLED SHAFT DETAIL

Figure B.11. Typical detail of drilled shaft (From Nevada DOT Structures Manual (2008))

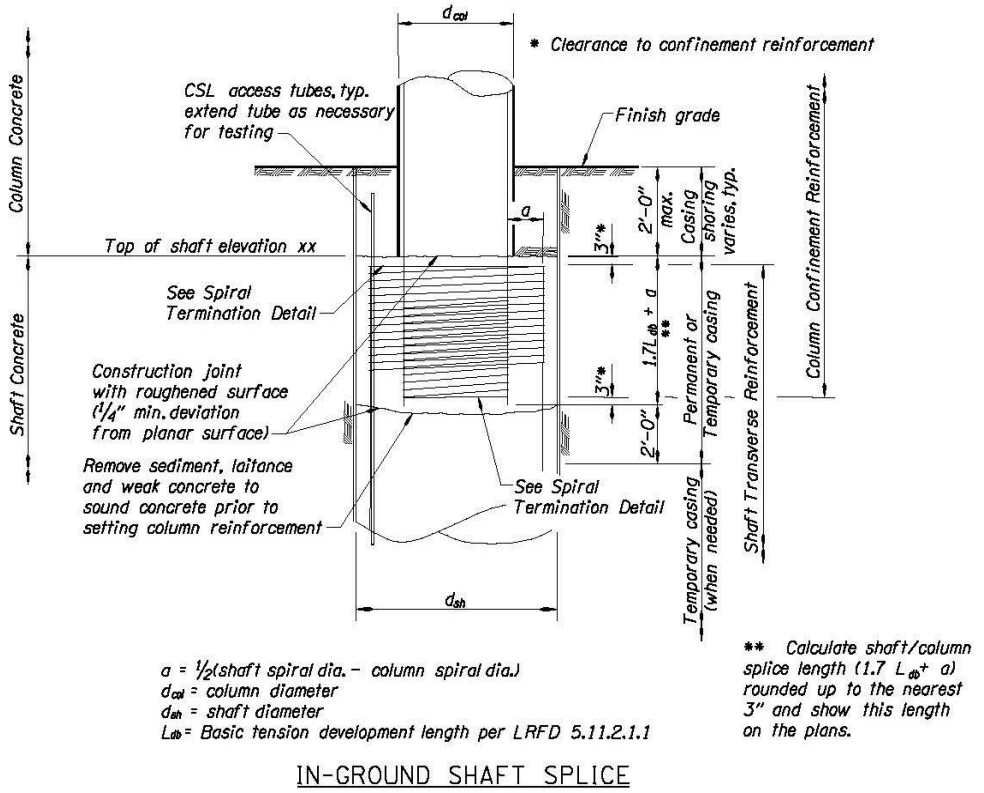

Figure B.12. Typical detail of drilled shaft in ground (From Oregon DOT Bridge Design and Drafting Manual (2013))

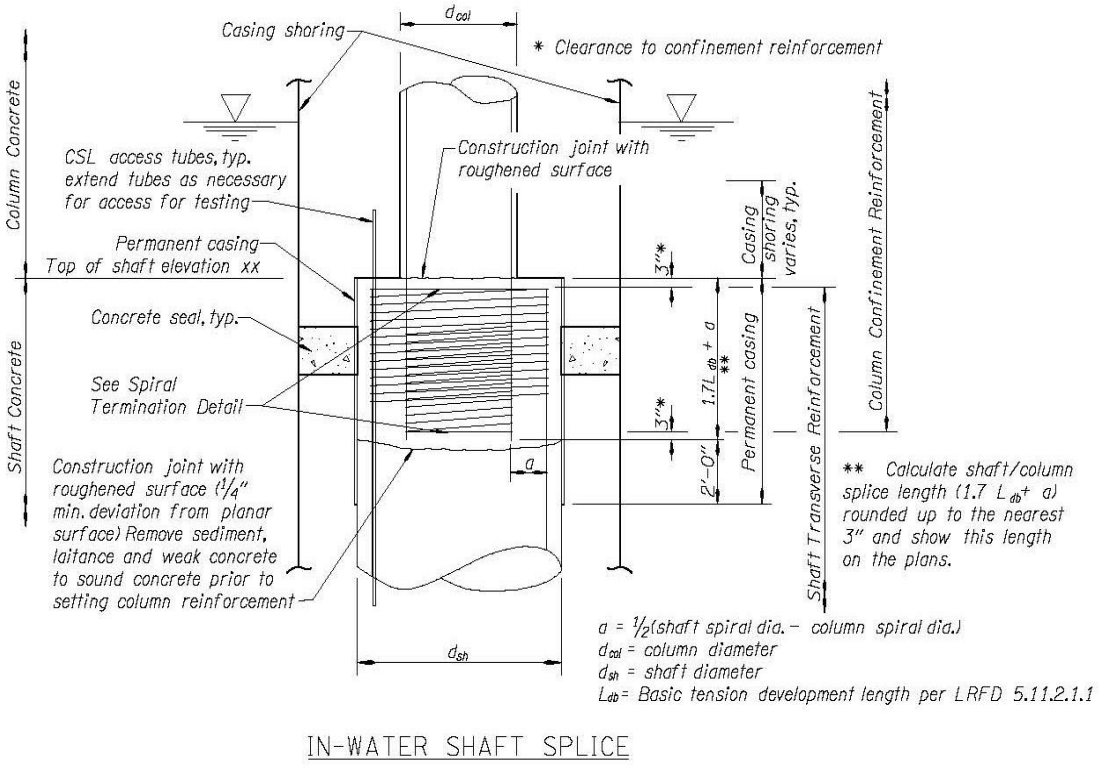

Figure B.13. Typical detail of drilled shaft in water (From Oregon DOT Bridge Design and Drafting Manual (2013))

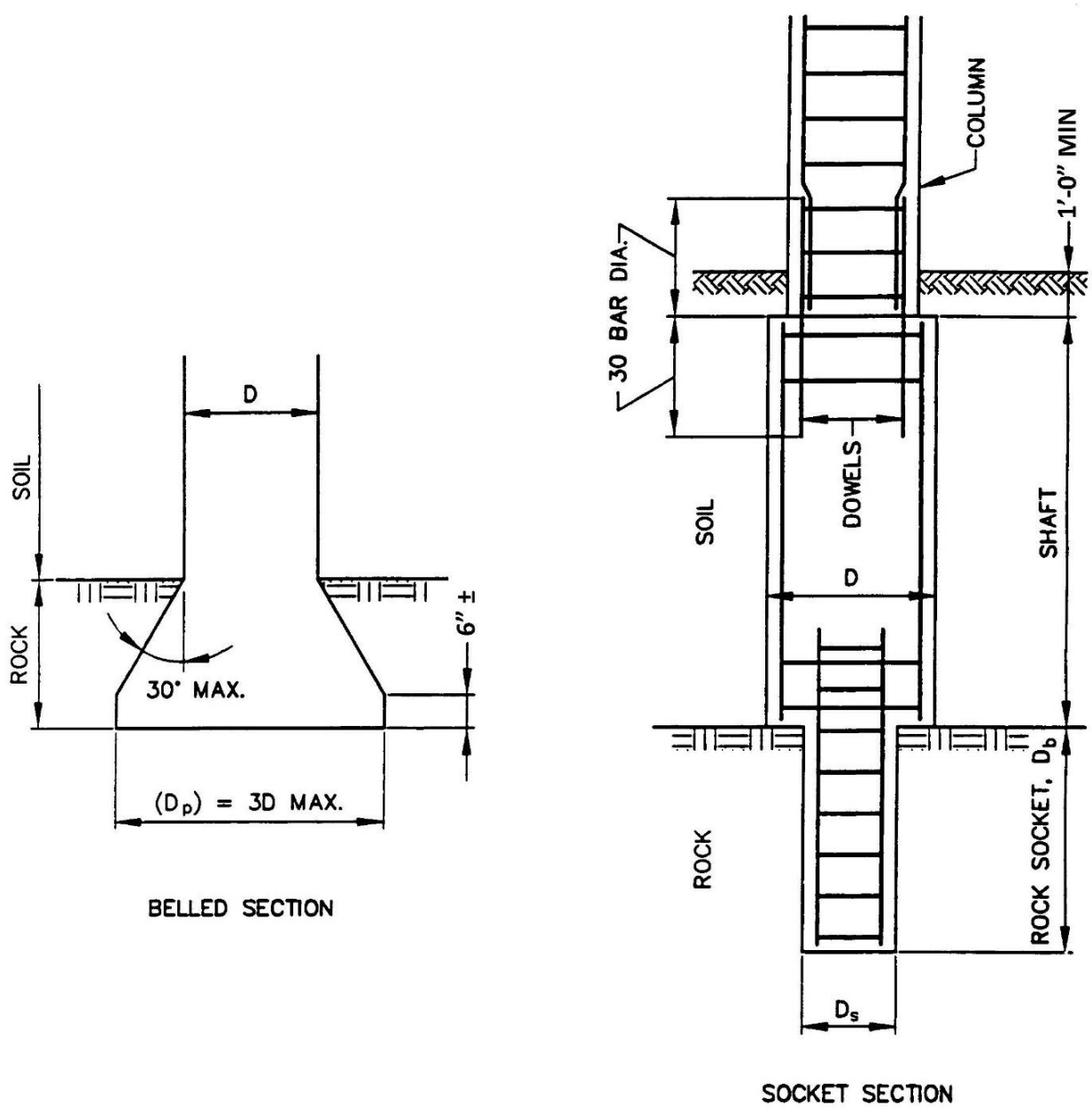

Figure B.14. Typical detail of drilled shaft (From Pennsylvania DOT, Design Manual Part 4, (2012))

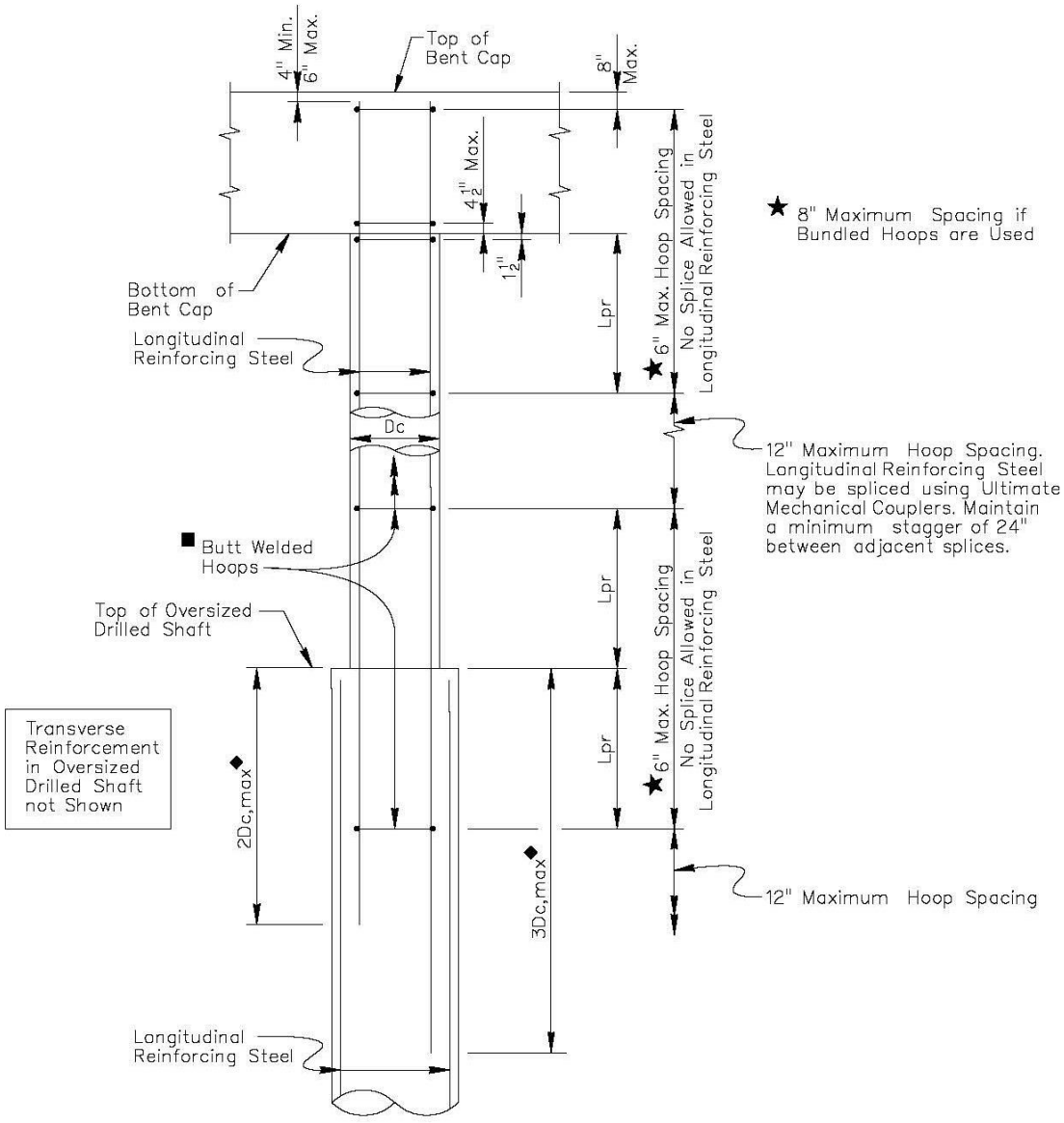

◆ Dc,max is the largest cross sectional dimension of the column.

■ Hoops shall have butt welded splices. The minimum size shall be #19 (#6) and the maximum size shall be #25 (#8). To prevent the hoop weld splices from being located on the same vertical plane, the locations of the splices shall be staggered around the perimeter of the column by a minimum distance of 1/3 of the hoop circumference.

Figure B.15. Typical seismic detail of drilled shaft (From SCDOT Seismic Design Specifications for Highway Bridges (2008))

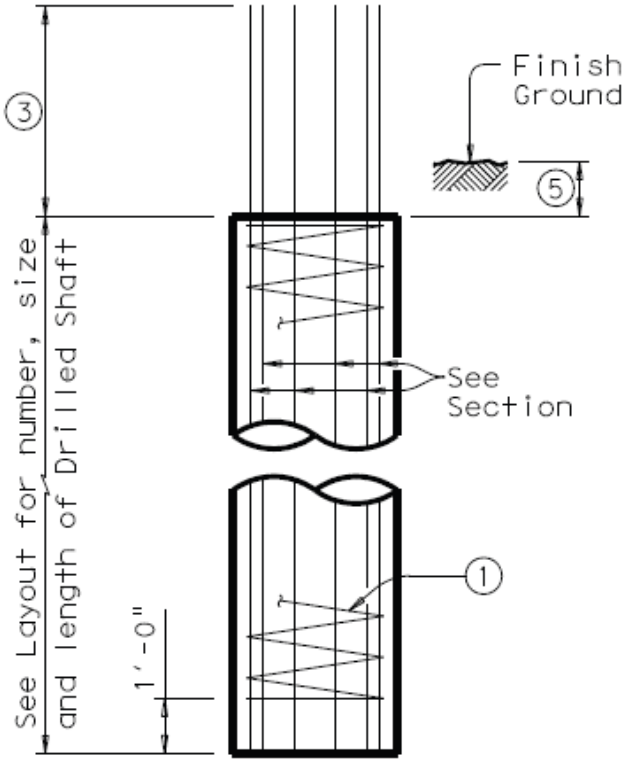

Figure B.16. Typical detail of drilled shaft diameter equal to column diameter (From Texas DOT Bridge Standards, (2012))

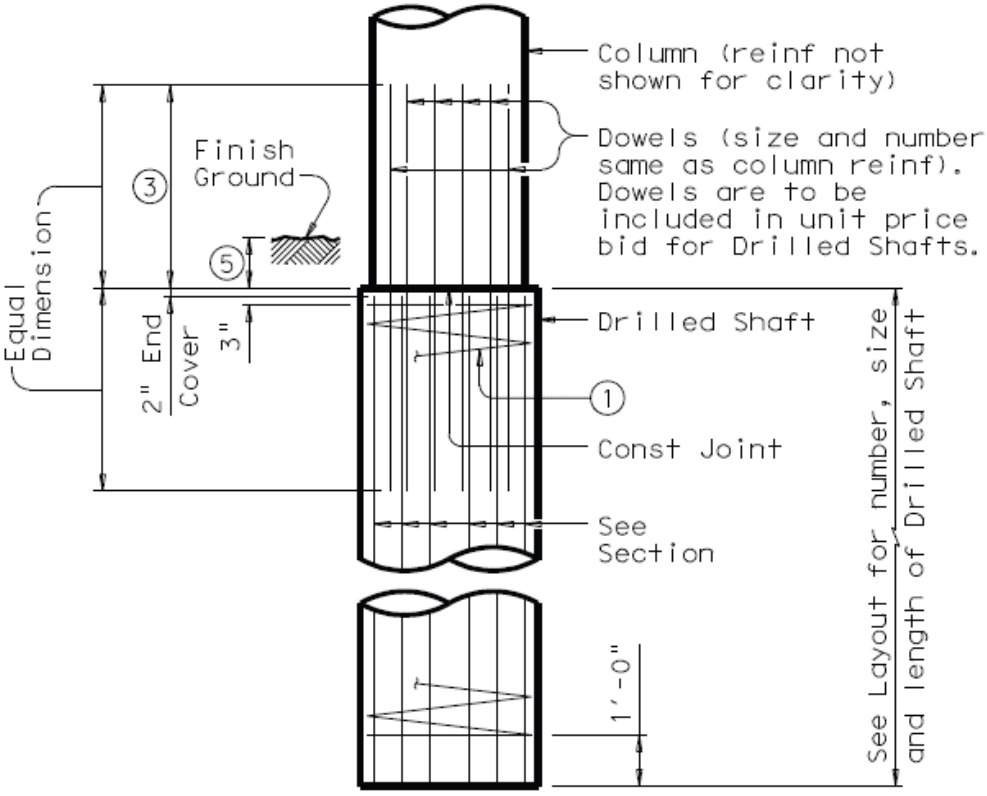

Figure B.17. Typical detail of drilled shaft diameter greater than column diameter (From Texas DOT Bridge Standards (2012))

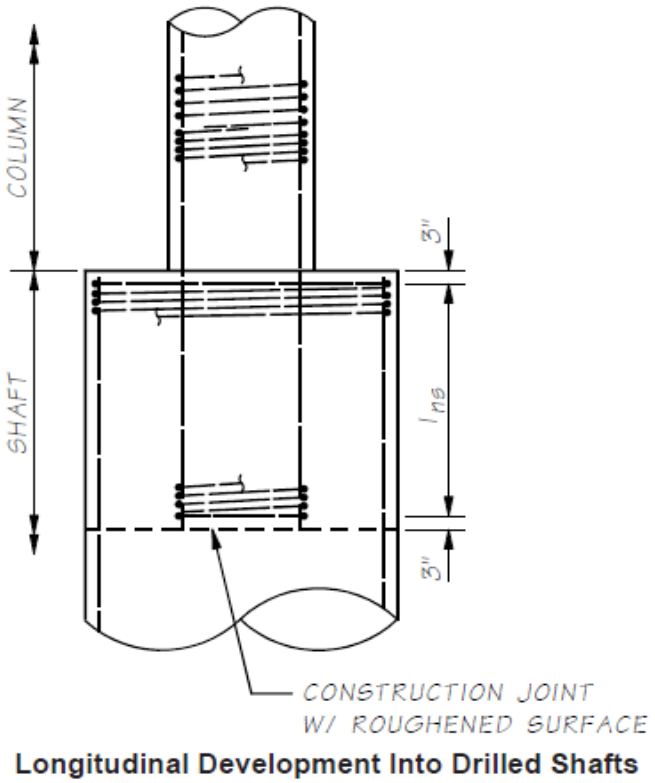

Figure B.18. Connection detail for drilled shaft (From Washington State DOT Bridge Design Manual (LRFD) (2012)).

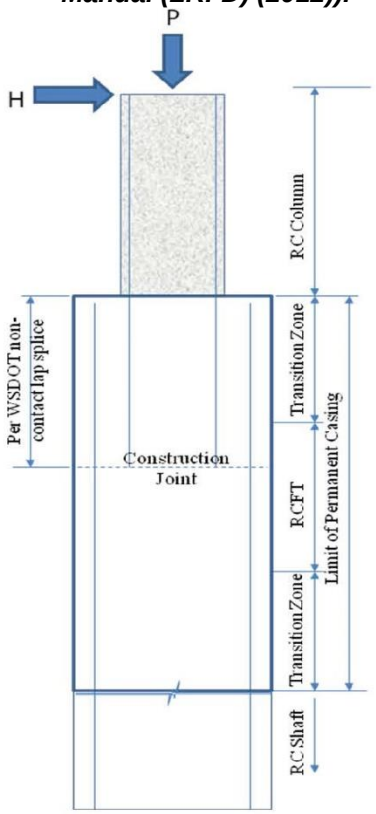

Figure B.19. Seismic Connection detail for drilled shaft (From Washington State DOT Design Memorandum (2012)).

B.2 International Codes Requirement

B.2.1 New Zealand Code

Some aspects related to structural strength of encased drilled shaft as per requirement of New Zealand code are presented elsewhere (see Section 1.4 of the report and Appendix C. Some additional aspects of designing are discussed in this section.

According to Section 14.3.6.9 of New Zealand's "Concrete Structures Standard-The Design of Concrete Structures" (Standards New Zealand 2006): "For piled foundation systems, the permanent shell or casing of a pile may be considered as providing a proportion of the strength of the pile. For steel casings, an appropriate allowance shall be made for loss of wall thickness by corrosion during the specified intended life of the structure". However, in commentary, further explanation is provided, according to Section C14.3.6.9: "For a cased pile, the effect or contribution of the steel shell may be included with respect to confinement for the potential plastic hinge region. However, no such contribution from the shell shall be allowed for in nominal flexural strength calculations because of lack of compatibility of strains between concrete and steel unless special provisions are made to transfer the associated bond forces to the steel. The presence of a steel pile casing can enhance the flexural capacity of the pile and allowance for this should be made either in the over-strength actions or by isolating the top of the casing so that it does not influence the flexural strength of the pile". In Section C14.3.6.9, guidance is provided on the allowance to be made for the corrosion of casing: "The rates of corrosion shown by experiments vary from practically nil to about 0.075 mm per year, a commonly used (average) figure being 0.05 *mm/year*".

As for development length of reinforcement, Section 8.7.2.5 of New Zealand's "Concrete Structures Standard-The Design of Concrete Structures" (Standards New Zealand 2006) states: "Bars spliced by non-contact lap splices in flexural members spaced transversely farther apart than $3d_b$ shall have splice length, L_{ds} , given by:

$$L_{ds} \geq L_d + 1.5\, S_L \qquad \text{(B.1)}$$

where L_{ds} is development length in tension which can be calculated by Section 8.6.3.2 or 8.6.3.2 and S_L is spacing between bars." These two clauses from the New Zealand code are provided below.

8.6.3.2 *Basic development length in tension*

Unless a more detailed determination of L_d is made in accordance with 8.6.3.3, the development length, L_{db} shall be calculated from:

$$L_{db} = \frac{(0.5\alpha_a f_y)}{\sqrt{f_c'}} d_b \qquad \text{(Eq. 8–2)}$$

where α_a = 1.3 for top reinforcement where more than 300 mm of fresh concrete is cast in the member below the bar, or 1.0 for all other cases.

The value of f_c' used in Equation 8–2 shall not exceed 70 MPa.

8.6.3.3 *Refined development length in tension*

The development length, L_d, in tension may be determined from:

$$L_d = \frac{\alpha_b}{\alpha_c \alpha_d} L_{db} \geq 300\,\text{mm} \quad \text{.....(Eq. 8–3)}$$

with α_b, α_c and α_d being defined as follows:

(a) Reinforcement provided in a flexural member (not subjected to seismic forces nor required for temperature or shrinkage in restrained members) in excess of that required:

$$\alpha_b = A_{sr}/A_{sp} \quad \text{.....(Eq. 8–4)}$$

(b) When cover to bars in excess of $1.5d_b$ or clear distance between adjacent bars in excess of $1.5\,d_b$ is provided:

$$\alpha_c = 1 + 0.5\left(\frac{c_m}{d_b} - 1.5\right) \quad \text{.....(Eq. 8–5)}$$

with the limitation of $1.0 \leq \alpha_c \leq 1.5$

where c_m = the lesser of the concrete cover or the clear distance between bars.

(c) When transverse reinforcement with at least 3 bars, spaced less than $8d_b$, transverse to the bar being developed, and outside it, are provided within L_d:

$$\alpha_d = 1 + \sqrt{\left(\frac{A_{tr}}{s}\right)\left(\frac{f_{yt}}{80nd_b}\right)} \quad \text{..... (Eq. 8–6)}$$

with the limitation of $1.0 \leq \alpha_d \leq 1.5$

Transverse reinforcement used for shear, flexure or temperature may be included in A_{tr}.

B.2.2 Canadian Code

The Canadian Highway Bridge Design Code (Canadian Standards Association 2006) provides only a single sentence on "Composite Tube Piles" (Clause 10.22.8), which states: "For composite tube piles, the applicable requirements of Clause 10.9.5 shall be met." This Clause 10.9.5 contains the provisions related to the strength of "composite columns consisting of hollow structural sections completely filled with concrete." These equations for the composite strength of encased drilled shaft are presented elsewhere (see Section 1.4 of the report and Appendix C).

Also relevant, Clause 10.22.8 of the Canadian Code states: "Bars spliced by non-contact lap splices in flexural members shall not be spaced transversely farther apart than; (a) 0.20 times the required lap splice length; and (b) more than 150*mm*". Additionally, according to Clause 4.7.4.4 of the Canadian Code for column connections, "The development length for all longitudinal steel shall be 1.25 times that specified in Clause 8.15.2", where Clause 8.15.9.3 describes requirements for Class A and Class B type splices. Clause 8.15.9.7 describes special requirement for splices in columns. Excerpts from the Canadian code are provided below.

8.15.2.2 Development length

The development length, ℓ_d, of reinforcing bars and deformed wire in tension shall be calculated as follows:

$$\ell_d = 0.45 \frac{k_1 k_2 k_3}{(d_{cs} + K_{tr})} \left[\frac{f_y}{f_{cr}} \right] A_b$$

where

$$K_{tr} = 0.45 \frac{A_{tr} f_y}{10.5 s n}$$

where

s = maximum centre-to-centre spacing of transverse reinforcement within a distance ℓ_d and the factor 10.5 is expressed in millimetres per newton

However, the term $(d_{cs} + K_{tr})$ shall not be taken greater than $2.5 d_b$.

8.15.2.3 Simplified development length

The development length, ℓ_d, of reinforcing bars and deformed wire in tension may be taken from Table 8.8 if the clear cover and clear spacing of the bars being developed are at least d_b and $1.4 d_b$, respectively.

Table 8.8
Minimum development length of reinforcing bars and deformed wire in tension
(See Clause 8.15.2.3.)

Cases	Minimum development length, ℓ_d
Components containing minimum stirrups or ties (Clause 8.9.1.3 or 8.14.4.3) within ℓ_d or slabs and walls with a clear spacing of not less than $2d_b$ between bars being developed	$0.18 k_1 k_2 k_3 \frac{f_y}{f_{cr}} d_b$
Other cases	$0.24 k_1 k_2 k_3 \frac{f_y}{f_{cr}} d_b$

8.15.2.4 Modification factors

The following modification factors shall be used in calculating the development length specified in Clauses 8.15.2.2 and 8.15.2.3:

(a) Bar location factor, k_1:
  (i) 1.3 for horizontal reinforcement placed so that more than 300 mm of fresh concrete is cast in the component below the development length or splice; and
  (ii) 1.0 for other cases.

(b) Coating factor, k_2:
  (i) 1.5 for epoxy-coated reinforcement with a clear cover less than $3d_b$ or a clear spacing between bars being developed less than $6d_b$;
  (ii) 1.2 for all other epoxy-coated reinforcement; and
  (iii) 1.0 for uncoated reinforcement.

(c) Bar size factor, k_3:
  (i) 0.8 for 20M and smaller bars and deformed wires; and
  (ii) 1.0 for 25M and larger bars.

The product $k_1 k_2$ need not be taken greater than 1.7.

8.15.9 Splicing of reinforcement

8.15.9.1 Lap splices

Lap splices shall not be used for bars larger than 35M.

Bars spliced by non-contact lap splices in flexural members shall not be spaced transversely farther apart than

(a) 0.20 times the required lap splice length; and
(b) more than 150 mm.

8.15.9.3 Splices of deformed bars and deformed wire in tension

Lap splices of deformed bars and deformed wire in tension shall be classified as Class A or Class B in accordance with Table 8.11. The minimum length of lap shall be 1.0l*d* for Class A splices and 1.3l*d* for Class B splices, but not less than 300 mm. In this regard, the development length, l*d* , shall be calculated in accordance with Clause 8.15.2.1, but without the modification factors for excess reinforcement specified in Clause 8.15.2.5.

Table 8.11
Classification of lap splices in tension
(See Clause 8.15.9.3.)

	Maximum percentage of A_s spliced within required splice length	
(A_s provided)/(A_s required)	50	100
≥ 2	Class A	Class B
< 2	Class B	Class B

8.15.9.7 Special requirements for columns

Where the bar stress due to factored loads is compressive, lap splices shall comply with Clause 8.15.9.4.

Where the bar stress due to factored loads is tensile and does not exceed 0.5*fy* , lap splices shall be Class B tension lap splices if more than one-half of the bars are spliced at any section and Class A tension lap splices if half or fewer of the bars are spliced at any section and alternate lap splices are staggered by l*d*.

Where the bar stress due to factored loads is greater than 0.5*fy* in tension, lap splices shall be Class B tension lap splices.

Where welded splices or mechanical connections are used, the amount of reinforcement spliced at any location shall not exceed 0.04 times the gross area of the section. Where the gross area of reinforcement exceeds 0.04 times the gross area of the section, connection or splice locations shall be spaced at least 750 mm apart.

B.2.3 Eurocode

Some aspects related to the structural strength of encased drilled shaft per the requirements of Eurocode are presented elsewhere (see Section 1.4 of the report and Appendix C). These are found in Eurocode 4, Part 2 (British Standards Institution 2005), Clause 6.7, which has provisions for the design of composite columns and composite compression members with concrete-filled rectangular and circular tubes.

According to Eurocode 2, Part 1-1 (National Standards Authority of Ireland (NSAI) 2005), if the clear distance between splice bars increases beyond 50*mm* or $4d_b$, then the lap length shall be increased by the clear distance between bars. Section 8.7.3 can be used to calculate lap splice length.

APPENDIX C

Requirements for Design and Detailing of Concrete-Filled Steel Tubes

Note: This Appendix has been prepared in collaboration with Mr. Muhammad Hassan, of NESPAK, Pakistan (Former MSc student at UB).

C.1 Requirement of maximum permitted D/t ratio

In this Appendix, the *D/t* ratios requirements for CFST members are outlined, summarized for different codes, with references to specific relevant clauses/articles for each code.

1. **American Institute of Steel Construction (AISC), "Specifications for Structural Steel Buildings (AISC 360-10)";**

According to AISC 360-10 Table *I* 1.1*B*, the maximum *D/t* ratio for a round HSS filled with concrete is 0.09 E/F_y for Compact/ Noncompact members and 0.31 E/F_y for Noncompact / Slender members. Note that for seismic applications, AISC 341-10 should be used instead.

2. **American Institute of Steel Construction (AISC), "Seismic Provisions for Structural Steel Buildings (AISC 341-10)" ;**

According to AISC Seismic Provision Table *D*1.1, the maximum D/t ratio for a round hollow structural section (HSS) filled with concrete shall be 0.076 E/F_y for highly ductile members and 0.15 E/F_y for moderately ductile members.

3. **American Concrete Institute (ACI), "Building Code Requirements for Structural Concrete (ACI 318-11)" ;**

According to ACI Section 10.13, minimum thickness of steel encasement for a composite member with a concrete core encased by structural steel is,

$$t > D\sqrt{\frac{F_y}{8E}} \qquad \text{(C.1)}$$

Note that this is a non-seismic requirement, but no additional specific provisions are provided for seismic detailing (in Chapter 21 of ACI).

4. **AASHTO LRFD Bridge Design Specifications (2012);**

According to AASHTO LRFD specifications, Article 6.12.2.3.2, requirement for *D/t* ratio for developing full plastic moment capacity is

$$\frac{D}{t} < 2.0\sqrt{\frac{E}{F_y}} \qquad \text{(C.2)}$$

For developing yield moment in composite section, requirement for *D/t* ratio is

$$2.0\sqrt{\frac{E}{F_y}} < \frac{D}{t} < 8.8\sqrt{\frac{E}{F_y}} \qquad \text{(C.3)}$$

Note that this is a general (non-seismic) requirement, but no additional specific provisions are provided for seismic detailing.

5. AASHTO Guide Specifications for LRFD Seismic Bridge Design (2012);

Although no limits are specified in the AASHTO SGS, the commentary indicates that the equations provide for strength are valid up to 0.14 (E/F_y).

6. Eurocode

According to Euro code 4, Part*1*-1, Table 6.3,

$$\frac{D}{t} \leq 90\,\frac{235}{F_y} \qquad \text{(C.4)}$$

Here, F_y is in MPa.

7. Canadian Code (CAN/CSA-S6-06);

According to Section 10.9.5.2 of Canadian Code, for hollow circular structural sections completely filled with concrete, outside diameter-to-thickness ratios of circular sections that do not exceed 28 000/$F_{y.}$, for F_y in MPa.

8. Japanese Code

According to Japanese code,

$$\frac{D}{t} \leq 1.5\,\frac{23500}{F_y} \qquad \text{(C.5)}$$

Here, F_y is in MPa.

9. Chinese Code

According to Chinese Code for normal columns;

$$\frac{D}{t} \leq 85\sqrt{\frac{235}{F_y}} \qquad \text{(C.6)}$$

Here, F_y is in MPa.

10. According to New Zealand Code for steel encased concrete core;

According to Section 10.3.11.6.1 of New Zealand Code for circular columns, the thickness of the steel encasement shall be equal to greater than,

$$t > D\sqrt{\frac{Fy}{8E}} \quad \text{(C.7)}$$

In all of above mentioned equations,

- D = Diameter of encased shaft/ composite column.
- t = Thickness of casing.
- E = Modulus of elasticity of steel.
- F_y = Steel yield stress.

C.2 Effective Flexural Stiffness

In this section different equations for calculating effective stiffness of CFST mentioned by different codes and standards are reviewed.

11. American Institute of Steel Construction (AISC) Specifications for Structural Steel Buildings (AISC 360-10);

According to AISC 360-10, the effective stiffness of a CSFT member can be calculated by:

$$EI_{eff} = E_s I_s + C_3 E_c I_c \quad \text{(C.8)}$$

where

$$C_3 = 0.6 + 2\left(\frac{A_s}{A_c + A_s}\right) \quad \text{(C.9)}$$

In the above equations and all subsequent ones, the subscript *s* refers to steel, *c* refers to concrete, and *g* refers to gross concrete section. *I* is the moment of inertia, *A* is area and *E* is modulus of elasticity.

12. AASHTO LRFD Bridge Design Specifications(2012);

According to the AASHTO BDS (2012), CFST stiffness value shall be greater of Equations 5.7.4.3-1 and 5.7.4.3-2, given in Article 5.7.4.3, and respectively equal to:

$$EI = \frac{\frac{E_c I_g}{5} + E_s I_s}{1 + \beta_d} \quad \text{(C.10)}$$

$$EI = \frac{\left(\frac{E_c I_g}{2.5}\right)}{1 + \beta_d} \quad \text{(C.11)}$$

where β_d = Ratio of maximum factored permanent load moment to maximum factored total load moment (to account for creep effects).

13. AASHTO Guide Specifications for LRFD Seismic Bridge Design (2011);

Although no equation in provided in the specification proper, the commentary to the AASHTO Guide Specification (2011) provides Equation C7.6-1 or C7.6-2 which are:

$$EI = E_S I_S + \frac{E_c I_c}{2.5} \qquad \text{(C.12)}$$

$$EI = E_S I_S \left(0.88 + \frac{0.352\, A_c}{n\, A_S}\right) \geq E_S I_S \qquad \text{(C.13)}$$

The first equation is a modified form of the equation given in Article 5.7.4.3 of AASHTO LRFD Specifications. The second equation is a modified form of the one given in Article 6.9.5.1 of AASHTO LRFD Specifications.

14. American Concrete Institute (ACI) 318-11;

According to ACI Section 10.13.5,

$$EI = \frac{\frac{E_c I_g}{5}}{1 + \beta_{dns}} + E_c I_{sx} \qquad \text{(C.14)}$$

Longitudinal bars located within the encased concrete core "shall be permitted to be used" in computing I_{sx}. The term β_{dns} shall be taken as the ratio of maximum factored axial sustained load to maximum factored axial load associated with the same load combination, but shall not be taken greater than 1.0.

15. Eurocode 4

According to Eurocode 4, BS EN 1994-1-1:2004, Article 6.7.3.3-2 for calculation of relative slenderness and the critical force, the effective flexural stiffness $(EI)_{eff}$ can be calculated from:

$$EI = E_a I_a + E_s I_s + K_e E_{cm} I_c \qquad \text{(C.15)}$$

where, K_e is a correction factor and E_{cm} is the modulus of elasticity for concrete. I_a, I_c, and I_s are the second moments of area of the structural steel section, the uncracked concrete section and the reinforcement for the bending plane being considered.

16. New Zealand Code (NZS 3101.2006.1)

According to New the Zealand code

$$EI = \frac{\frac{E_c I_g}{5}}{1 + \beta_d} + E_c I_t \qquad \text{(C.16)}$$

where β_d is the ratio of design axial dead load to total design axial load of a column or pier and I_t is moment of inertia of structural steel shape or pipe about centroidal axis of composite member section in mm^4.

C.3 Strength of encased drilled shafts

17. American Institute of Steel Construction (AISC) Specifications for Structural Steel Buildings (AISC 360-10);

AISC 360-10 states that the nominal strength of composite member can be determined either from plastic stress distribution method or from strain compatibility method. Tensile strength of concrete shall be neglected. Local buckling effects shall be considered.

In the plastic stress method, it is specified that steel can reach F_y in either tension or compression and that concrete in compression reach a maximum stress of $0.95f_c'$. In the strain compatibility method, a

maximum concrete strain 0.003 *in/in* is specified and linear distribution of strains across the section is assumed.

18. AASHTO LRFD Bridge Design Specifications (2012);

The AASHTO LRFD Bridge Design Specifications (2012), Articles 6.9.2.2, 6.9.5, and 6.12.3.2.2, provide guidelines for determining the capacity of CFST members. Roeder et al. (2010), reported that these provisions are conservative compared to AISC and ACI because pure flexure capacity is limited to the plastic moment of the steel section alone (and it is still the case in the 2012 Edition of AASHTO).

19. AASHTO Guide Specifications for LRFD Seismic Bridge Design (2011);

AASHTO Guide Specifications for LRFD Seismic Bridge Design (2011) Article 7.6, provides a design guideline that is similar to the AISC plastic stress distribution method. AASHTO provisions only deal with CFST without internal reinforcement. Two methods to calculate strength are described: Method 2 is a simplified and approximate method which gives slightly lesser values that those calculated by the Method 1. Therefore, values calculated by Method 2 shall be increased by 10 % for capacity design purposes. These equations adopted by the AASHTO SGS were originally derived by Bruneau and Marson (2004). Note that Method 2 below was adapted from a Eurocode approach.

a. Method 1: Exact Geometry

Moment resistance of concrete-filled pipe can be calculated by

$$M_{rc} = \varphi_f \left(C_r e + C_r^{'} e^{'} \right) \qquad \text{(C.17)}$$

where:

$$C_r = F_y \beta \frac{Dt}{2}$$

$$C_r{}' = f_c^{'} \left[\frac{\beta D^2}{8} - \frac{b_c}{2} \left(\frac{D}{2} - a \right) \right]$$

$$e = b_c \left[\frac{1}{(2\pi - \beta)} + \frac{1}{\beta} \right]$$

$$e' = b_c \left[\frac{1}{(2\pi - \beta)} + \frac{b_c^2}{1.5\beta D^2 - 6b_c(0.5D - a)} \right]$$

$$a = \frac{b_c}{2} tan\left(\frac{\beta}{4}\right)$$

$$b_c = D \sin\left(\frac{\beta}{2}\right)$$

β = central angle formed between neutral axis chord line and the center point of the pipe found by the recursive equation (rad.)

$$\beta = \frac{A_s F_y + 0.25\, D^2\, f_c' \left[sin\left(\frac{\beta}{2}\right) - sin^2\left(\frac{\beta}{2}\right) tan\left(\frac{\beta}{4}\right) \right]}{0.125 D^2 f_c' + DtF_y} \qquad \text{(C.18)}$$

where:

D = outside diameter of steel pipe, *in.*

t = pipe wall thickness, *in.*

F_y = nominal yield stress of steel pipe, *ksi.*

$f_c{}'$ = nominal uniaxial concrete compressive strength, *ksi.*

Figures C.1 and C.2 illustrate the geometric properties and free-body diagram used to calculate the moment resistance of concrete-filled pipe per the above equations. Note that in Figure C.1, the shaded area shows the concrete above the neutral axis in compression.

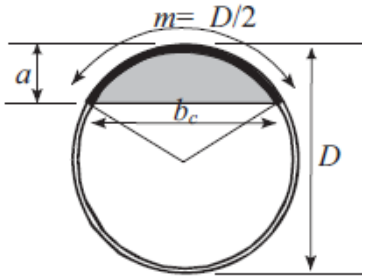

Figure C.1: Flexure of concrete-filled pipe (From AASHTO SGS (2011)).

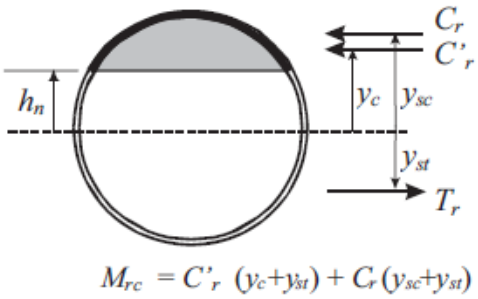

Figure C.2: Free-body diagram used to calculate moment resistance of concrete-filled pipe (From AASHTO SGS (2011)).

b. Method 2: Approximate Geometry

A conservative moment resistance of concrete-filled pipe can be calculated by:

$$M_{rc} = \varphi_f \left[\left(Z - 2th_n^2\right)F_y + \left(\frac{2}{3}(0.5D - t)^3 - (0.5D - t)h_n^2\right)f_c^{'}\right] \qquad \text{(C.19)}$$

where:

$$h_n = \frac{A_c f_c^{'}}{2Df_c^{'} + 4t\left(2F_y - f_c^{'}\right)}$$

φ_f = 1.0 resistance factor for structural steel in flexure
A_c = area of the concrete core, in^2
D = outside diameter of steel pipe, $in.$
t = pipe wall thickness, $in.$
Z = plastic section modulus of steel pipe, in^3
F_y = nominal yield stress of steel pipe, ksi.

Figure C.3 shows the geometric properties used in above equations

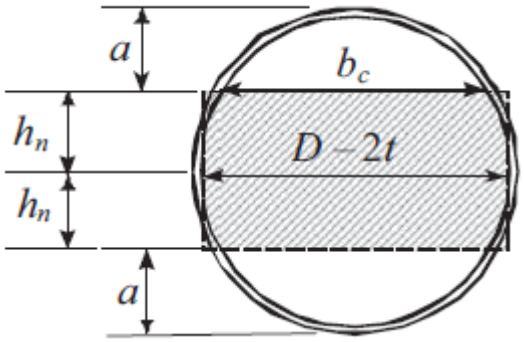

Figure C.3: Flexure of Concrete-Filled Pipe-Illustrates Approximation Made in Method 2 (From AASHTO SGS (2011)).

20. American Concrete Institute (ACI) 318-11

ACI uses a strain compatibility method with maximum permitted concrete strain of 0.003*in/in* and linear distribution of strains across the section. According to Section 10.2.7.1, "Concrete stress of $0.85f'_c$ shall be assumed uniformly distributed over an equivalent compression zone bounded by edges of the cross-section and a straight line located parallel to the neutral axis at a distance $a = \beta_1 c$ from the fiber of maximum compressive strain". According to Section 10.2.7.3, "for f'_c between 2500 and 4000*psi*, β_1 shall be taken as 0.85. For f'_c above 4000*psi*, β_1 shall be reduced linearly at a rate of 0.05 for each 1000*psi* of strength in excess of 4000*psi*, but β_1 shall not be taken less than 0.65".

21. Eurocode 4

Eurocode 4 also use a plastic stress diagram similar to the AISC approach, except that for concrete stresses are taken as $1.0f'_c$ instead of $0.95f'_c$.

22. Canadian Code (CAN/CSA-S6-06)

The Canadian code provisions are similar to AASHTO Guide Specification, based on the Bruneau and Marson (2004) equations.

23. Japanese Code

The Standard for Structural Calculation of Steel Reinforced Concrete Structures, 5th Ed. (in Japanese) by Architectural Institute of Japan (AIJ 2001), uses allowable stress design. The procedure given in the Japanese Code for calculating the ultimate bending strength of a beam-column is as follows:

M_u of a beam-column of length not greater than 12 times the width or diameter of the steel tube section is calculated by:

$$N_u = {}_cN_u + {}_sN_u \qquad \text{(C.20)}$$

$$M_u = {}_cM_u + {}_sM_u \qquad \text{(C.21)}$$

For a circular CFST beam-column:

$${}_cN_u = (\theta_n - \sin\theta_n \cos\theta_n)\frac{({}_cD^2 . {}_c\sigma_{cB})}{4} \qquad \text{(C.22)}$$

$${}_cM_u = \sin^3\theta_n \frac{({}_cD^2 . {}_c\sigma_{cB})}{12} \qquad \text{(C.23)}$$

$$ {}_sN_u = \{\beta_1\theta_n + \beta_2(\theta_n - \pi)\}\left(1 - \left(\frac{{}_st}{D}\right)\right) D.\ {}_st.\ {}_s\sigma_y \quad \text{(C.24)} $$

$$ {}_sM_u = \left(\beta_1 + \beta_2\right)\sin\theta_n \frac{\left(1 - \left(\frac{{}_st}{D}\right)\right)^2}{2}\ D^2.\ {}_st.\ {}_s\sigma_y \quad \text{(C.25)} $$

where;

$$ \theta_n = \cos^{-1}(1 - 2x_{n1}) $$

$$ x_{n1} = \frac{x_n}{{}_cD} $$

$$ {}_c\sigma_{cB} = {}_cr_u.F_c + \frac{1.56\ {}_st.\ {}_s\sigma_y}{D - 2\ {}_st} $$

x_n: Position parameter of neutral axis

${}_cD$: Width or diameter of a concrete section

${}_st$: Thickness of a steel tube section

${}_s\sigma_y$: Yield stress of steel tube

APPENDIX D

Review of finite element modeling methods of reinforced concrete members

Some of existing finite element modeling methods for reinforced concrete have been described in this Appendix. The following provides a description of accepted existing finite element models applicable to reinforced concrete and typically implemented in finite element analysis packages. The dominant method of representing reinforced concrete members and continuums when using finite elements consists of developing separate models for the concrete and the steel, and combining those models, either at the element scale by using additional constitutive matrices, or at the structural scale by using different elements for each material and some mechanism or elements to tie them together.

This section presents various recognized techniques for modeling reinforced concrete, including techniques to model plain concrete, reinforcing bars, and the bond between concrete and rebars. Constitutive models for concrete and reinforcement bars, and their implementations in finite element software packages, are presented in Sections D.1 and D.2, respectively. In Section D.3, implementation of shear mechanisms to transfer axial load from concrete to steel tube is discussed. Section D.4 discusses the strut-and-tie model as a simplified method for load transfer analysis.

Generally, there are three different finite element modeling techniques that are widely used to simulate reinforced concrete behavior. They are discrete, embedded and distributed models.

In the discrete modeling technique, concrete and reinforcement are defined separately with their corresponding elements and properties. In this method, an interface must be defined to represent the interaction between the concrete and reinforcing bars in terms of transferring forces and relative displacements. In the embedded modeling technique, reinforcing is considered as a member that is built into the concrete element. In this case, a perfect bond is considered to exist between the reinforcing bars and concrete. Therefore, they work together as one unit. The embedded modeling technique is simpler to use compared to discrete models, but it cannot capture the interaction between the reinforcing bars and the surrounding concrete, such as those due to bar slippage and other phenomenon.

In the distributed modeling technique, an equivalent homogeneous material model is used to represent reinforced concrete. That is equivalent to “smearing” the properties of reinforcement into the concrete elements. In such models, the contribution of concrete and steel is not calculated separately and perfect bond is again considered.

Each of these models has its own advantages. However, the discrete model is the only model that can consider the bond slip mechanism directly. Therefore, it is more useful in modeling the more complex aspects of the behavior of reinforced concrete structures, at the cost of complications in the modeling process. The following paragraphs give an overview of existing concrete constitutive models typically implemented in finite element analysis softwares.

D.1 Concrete modeling

The nonlinear behavior of concrete can be related to a combination of material plasticity and damage. A constitutive model for concrete should include both of these phenomena in order to capture the real behavior of the concrete.

The approaches for defining the stress-strain behavior of concrete under various stress states can be divided into three main groups: (1) Linear elasticity; (2) Non-linear elasticity; and (3) Linear-perfect-plasticity (Chen 2007). In order to simulate the damage of concrete, each of these groups has to address the concrete failure criteria (cracking and crushing). Some researchers have described the behavior of concrete using plasticity theories alone (e.g., (Bazant 1978; Chen 2007)) or continuum damage theory alone (e.g. (Loland 1980; Ortiz and Popov 1982)). However, models that are based only on plasticity theory, are not capable of describing the degradation of material stiffness due to micro cracking, while models based only on continuum damage theory cannot capture irreversible deformations, crack opening and closures, or inelastic volumetric expansion in compression (Cicekli et al. 2007).

Among the constitutive models which use both plasticity and damage theories, the one proposed by Lee and Fenves (1998) is commonly used and implemented in finite element analysis packages. This model accounts for concrete strength degradation down to any residual value or zero, in either tension or compression after reaching the maximum tensile and compressive strengths, respectively. Lee and Fenves (1998) have developed a plastic-damage model based on the "fracture-energy" damage definition similar to the model proposed by Lubliner et al. (1989) which is also known as the Barcelona model. They have defined two damage factors (for tensile and compressive damage) together with a yield function consisting of multiple hardening variables to consider different damage states. The yield function used by Lee and Fenves (1998) is a modified version of that developed by Lubliner et al. (1989). The proposed plastic-damage model, uses the effective stress concept (Kachanov 1986) for the evolution of yield surface, which makes calibration of the model with experimental results more convenient. Furthermore, to address the effect of opening and closing of cracks in concrete (stiffness degradation and recovery respectively), a "stiffness recovery scheme" has been defined in the model (Lee and Fenves 1998).

Lee and Fenves (1998) showed that, their constitutive model can accurately predict the behavior of concrete under monotonic and cyclic loading. Also, they have shown that, opening and closing of cracks are well captured by the model in terms of stiffness degradation and recovery.

Available concrete constitutive models in finite element analysis packages are typically smeared crack models, and damage plasticity models. In particular:

- ANSYS (2004) uses a nonlinear plastic material which is capable of modeling crushing of concrete in compression and cracking due to tension. Cracking is considered as "smeared" in three orthogonal directions at each integration point. In this model, the failure criterion can be defined by a formulation proposed by Willam and Warnke (1975).

- The concrete model available in ADINA (Bathe 1978) is based on the work done by Kotsovos and Spiliopous (1995) and Kotsovos and Pavlovic (1995). It considers nonlinear behavior in compression up to a maximum compressive strength followed by a drop to zero strength. The stress-strain law and failure surface is based on experimental tests. Smeared cracking concept also is used in this model.

- DIANA (De Witte and Jansen 2010) includes different plasticity models such as Mohr-Coulomb or Drucker-Prager, for compressive behavior of concrete. This can be combined with cracking models, such as smeared crack or total strain crack models based on fixed and rotating crack concepts for tensile behavior.

- Available concrete constitutive models in Abaqus (Simulia 2012) are a smeared crack concrete model, a brittle cracking model, and a concrete damage plasticity (CDP) model. The smeared crack concrete model is designed for the case when concrete is subjected to essentially monotonic straining at low confining pressures. This model consists of an isotropically hardening yield surface that is active in compression. Also, the model has an independent "crack detection surface" that can determine the crack induced failures. This constitutive model uses smeared cracking concepts based on oriented damage elasticity to define the reversible part of its response after a cracking failure (Simulia 2012). The brittle cracking model is proposed for the cases when concrete behavior is dominated by tensile cracking failure and compressive failure is not important. Therefore, it is

assumed that the compressive behavior is always linear elastic. The brittle cracking model captures the anisotropy induced by cracking and uses a brittle failure criterion to allow removal of elements from a mesh. This model uses the smeared cracking to represent the discontinuous macrocrack brittle behavior (Simulia 2012). The concrete damaged plasticity (CDP) model is intended for applications in which the concrete is subjected to cyclic or any other arbitrary loadings. This model assumes an isotropic damage for concrete and considers the degradation of elastic stiffness induced by plastic strains both in tension and compression. Stiffness recovery effects under cyclic loading also can be taken into account. The compressive behavior consists of an elastic part until initial yield, and a plastic region that consists of a strain hardening part followed by strength degradation after the ultimate strength point. Under tension, the stress-strain behavior follows a linear elastic relationship until the failure stress (which corresponds to the initiation of micro-cracking in concrete), after which the stress-strain behavior follows a softening part (which macroscopically represents the propagation of micro-cracks). Under cyclic behavior, the complex degradation mechanisms that involve the opening and closing of previously formed micro-cracks is approximated by simple user-defined parameters that shape the rate of stress and stiffness degradation. The CDP model, assumes that the reduction of elastic modulus is given in terms of a scalar degradation variable which can be a function of either cracking stress or cracking displacement for the tensile and crushing (inelastic) strain for compressive behavior (Simulia 2012).

- LS-Dyna (LSTC 2013) has a variety of concrete constitutive models such as: MAT_CONCRETE_DAMAGE (MAT 72), MAT_WINFRITH_CONCRETE (MAT 85), MAT_CSCM _CONCRETE (MAT 159) (LSTC 2013). Among these models, the Winfrith concrete model allows up to three orthogonal crack planes for each element. These cracks can be reviewed using LS-Prepost (LSTC 2013). This material is pressure dependent and able to simulate the effect of confinement pressure on strength and ductility. Work by others has shown that the ability to properly model the tension behavior of the concrete has a significant impact on the ability to numerically replicate the behavior of concrete-filled tubes and that the Winfrith model is superior in that respect (Imani 2014).

Concrete is commonly modeled using three-dimensional solid elements, such as the 4-node linear tetrahedron, 6-node linear triangular prism, 8-node linear brick, 10-node quadratic tetrahedron, 15-node quadratic triangle, or 20-node quadratic brick, typically found in the library of finite element programs. Each of three-dimensional solid elements has 3 degrees of freedom per node. Some useful features of these elements are constant and linear pressure, reduced integration and hourglassing control (Simulia 2012).

D.2 Reinforcement modeling

Reinforcement in concrete structures is typically provided by means of rebars which can be modeled as smeared, embedded or discrete members in concrete. Metal plasticity material models are typically used for rebars to describe their behavior. Rebars are superposed on a mesh of elements used to model the concrete. A brief discussion on reinforcement material models and elements is presented in this section.

There are several models for metal plasticity analysis. One can choose among rate-independent and rate-dependent plasticity models, or between Mises yield surface for isotropic materials and Hill's yield surface for anisotropic materials, and for rate-independent modeling, between isotropic and kinematic hardening. Commonly a rate-independent elasto-plasticity model with kinematic hardening which uses the Mises yield condition with an associated plastic flow rule, is used for modeling of steel reinforcement.

As mentioned before, rebar can be defined as smeared layers in concrete elements. It can also be included in continuum concrete elements using embedment technique or it can be modeled discretely. In the latter two methods, rebars can be modeled using three dimensional solid elements, or one-dimensional elements such as beams or truss members (when the bending stiffness of reinforcement is negligible).

In the embedded technique, the bond between reinforcement and concrete is complete which means that there is no slippage of reinforcement in the concrete. However, if slippage of the rebars is likely to affect the response of the reinforced concrete structure, a bond-slip relationship can be defined at the interface of reinforcement and concrete, allowing to consider the effect of reinforcement slippage. Generally, bond-slip behavior in reinforced concrete structures can be modeled in three different scales: rib scale, bar scale and member scale (Cox and Herrmann 1998).

At the rib scale, the interaction between reinforcement bars and concrete is taken into account by modeling the geometrical details of the rebars, including their ribs, and the surrounding concrete. Analyses at this scale typically allow to investigate the mechanics of bond only in the early response, as it is numerically challenging to model the bond for large slips at this scale given that, in such cases, the material around the ribs will be damaged and deformed excessively by the movement of ribs. Also note that these models are not used to analyze entire members or structures, because a structure or member modeled to the level of details to capture the size of every ribs on each rebar would require a large computational capacity to analyze (Cox and Herrmann 1998) .

In bar scale models, rebars are modeled as plain bars and the bond-slip behavior is accounted for by defining a stress-slippage law at the interface of reinforcement and concrete. Bar scale models idealize the interaction between concrete and reinforcement by defining a connecting element as the interface between steel and concrete. The forces acting between the reinforcement and concrete such as adhesion, friction and bearing forces at the ribs are idealized as tangential and normal stress at the interface element. Although the idealized interface cannot capture the local effects of ribs on the surrounding concrete, such as crushing, shearing, and transverse cracking, this modeling technique is appropriate for considering the effects of rebar slippage on the stiffness and strength of reinforced concrete structures.

Finally, at the member scale, the effect of bond-slip is considered in global response of elements (i.e., beam, column or connection response), without explicitly modeling local effects. Several researchers have proposed macro models (such as special beam-column elements) that inherently consider the effect of bond slip behavior without an explicit definition of rebar-concrete interface. This kind of models is suitable for analyzing large structural models that include several reinforced concrete elements. Typically, member-scale models are appropriate for representing the bond behavior for one particular structural element. This is because in collecting experimental data at member scale, it is often impossible to define the bond state during the test and also distinguish between bond response and other structural response of elements. Therefore, the developed model is a function of the element design parameters. Generally, member-scale models don’t have the capability of implementation within a continuum finite element model. Indeed, at this scale, bond data includes cumulative information about the bond behavior such as total bar slip or total bar stress transfer over a large anchorage zone. Thus, they cannot provide information about the distribution of slippage or stresses along the rebars which is required for a continuum finite element model.

D.3 Shear transfer mechanisms

In steel encased concrete columns, the axial load from concrete to steel tube, generally transfers by the means of friction in the interface of concrete and steel. However, shear mechanisms can also be used for load transferring, particularly in applications where questions arise as to whether friction alone is sufficient to achieve load transfer. For example, shear studs which have been installed within a cast-in-steel-shell (CISS) pile at the new East Span of the San Francisco-Oakland Bay Bridge by Caltrans (Gebman et al. 2006).

Although there are no provisions that require the use of shear mechanisms for the design of composite columns (or piles) in bridge and building codes, design standards from the American Petroleum Institute (API 1993) and the United Kingdom Department of Energy (HSE 1995) provide design equations and recommendations for using shear keys in grouted pile-to-structure connections, in offshore structures. Figure D.1 shows details of the connection and shear keys recommended by API (1993).

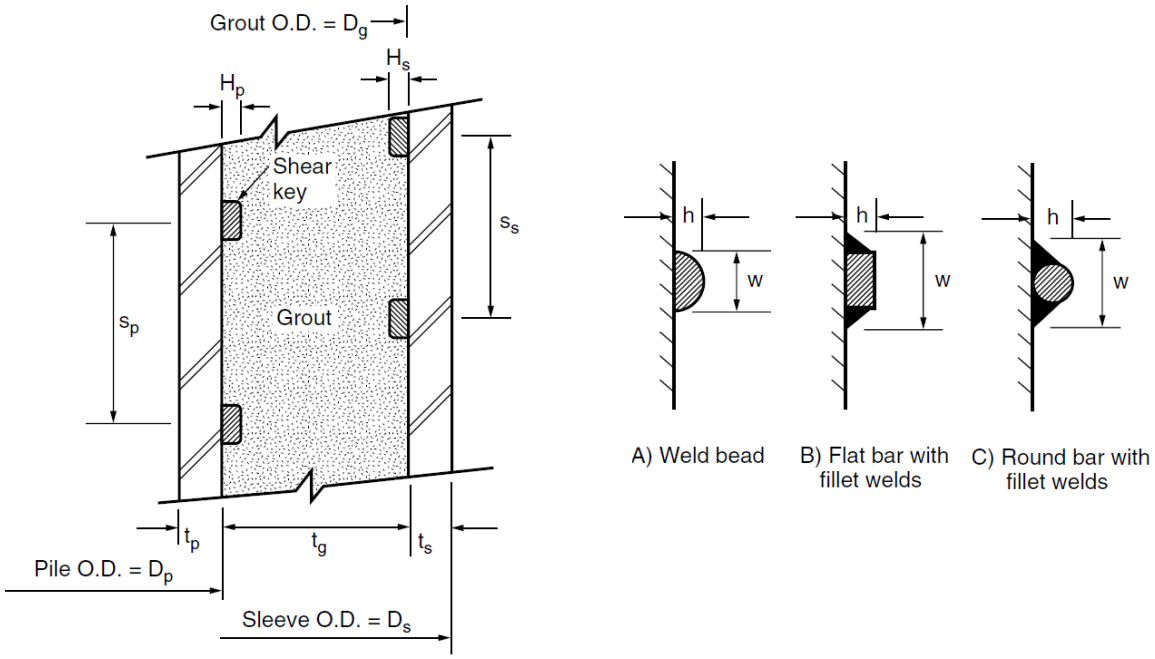

Figure D.1: Recommended shear key details (API 1993).

where w/h is specified to be between 1.5 and 3.0.

API (1993) increases the nominal axial load capacity of the pile when shear keys are used at the interface between steel and grout. The magnitude in this increase in the axial load capacity depends on the shear key outstand dimension (h in the Figure D.1), shear key spacing (s), and unconfined grout compressive strength. The spacing between shear keys (s) should not be more than 10 times the shear key outstand dimension (h).

Gebman et al. (2006) have studied the effect six different types of mechanisms for transferring the axial force from a concrete column to a cast-in-steel-shell (CISS) piles. Mechanisms used by Gebman et al. (2006) are shown in Figure D.2.Cyclic compression and tension tests have been done using 15.25 in and 24 in diameter CISS pile units.

They also have developed finite element models in Abaqus and compared the nonlinear numerical analysis results with their experimental results. In these finite element models, shear mechanisms were modeled explicitly. Figure D.3 shows a typical result for the tests by Gebman et al. (2006).

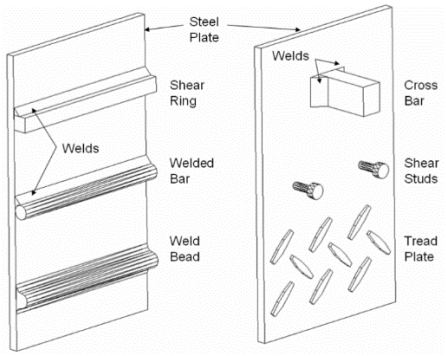

Figure D.2: Mechanisms studied by Gebman et al. (2006).

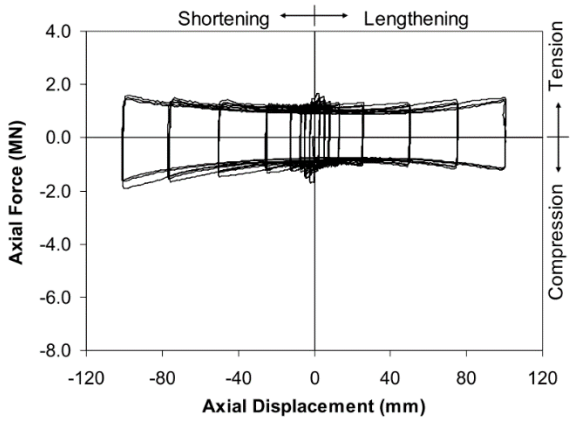

Figure D.3: Hysteretic response for a test unit including shear studs at a D/t ratio of 128 (Gebman et al. 2006).

D.4 Simplified analysis techniques

Although using finite element analysis is a valid approach when seeking to investigate the behavior of reinforced concrete structure response, this modeling technique is computationally expensive and time consuming. The use of simplified analysis methods can be advantageous for hand calculations. Strut-and-tie models have been proposed as a tool for simplified analysis of reinforced concrete connections such as column-to-beam or column-to-footing connections (Marsh et al. 2013; Schlaich and Schafer 1991). They have also been used to represent the force transfer mechanism in non-contact splices (McLean and Smith 1997).

To model the load transfer within non-contact lap splices under pure tension, McLean and Smith (1997) proposed a two dimensional strut-and-tie model for columns with rectangular ties (Figure D.4) and a three dimensional model for circular columns (Figure D.5). Load applied to one bar splice transfers through the surrounding concrete via compression struts to the other splice bar. McLean and Smith (1997) developed these models based on review of existing research at that time and have verified them through two dimensional panel and three dimensional column-shaft experimental tests for rebars less than No. 11.

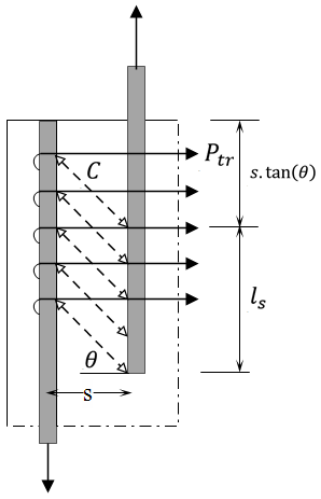

Figure D.4: Two dimensional strut-and-tie model for non-contact lap splices based on the model proposed by McLean and Smith (1997).

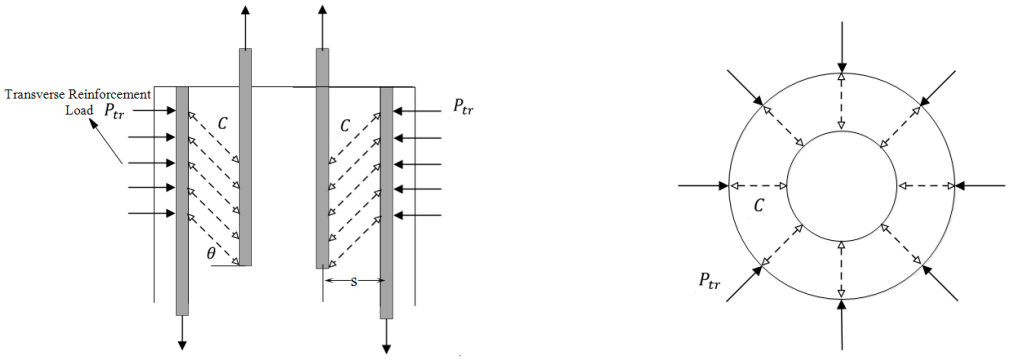

(a) Elevation view (b) Cross-section view

Figure D.5: Three dimensional strut-and-tie model for non-contact lap splices based on the model proposed by McLean and Smith (1997).

A limit for the maximum distance between transverse reinforcement for the model to be valid has been defined by McLean and Smith (1997), and the required non-contact lap splice length (l_{ns}) is calculated as:

$$l_{ns} = l_s + s.\tan(\theta) \qquad \text{(D.1)}$$

where, l_s, s and θ, are the standard required splice length, distance between splices, and angle of the compression struts, respectively. A value of 45° for θ, has been recommended by McLean and Smith (1997). The proposed strut-and-tie model has been incorporated by Washington State DOT into the Washington State Bridge Design Manual (2012) with some modifications.

In other studies, Gebman et al. (2006) used a strut-and-tie model to design the shear mechanisms investigated in their study (neglecting the bond between concrete and steel tube), and Schlaich and Shafer (1991) and Marsh et al. (2013) proposed strut-and-tie models for column to shaft socket connections considering both rough and smooth surfaces at the column and shaft interface.

APPENDIX E

Plastic stress distribution method

The plastic stress distribution method (PSDM) that was used throughout the report, also called fiber or layer analysis (Bruneau et al. 2011), is based on the plastic stress distribution on the composite section that is shown in Figure E.1. However, in order to simplify the calculations, internal rebars were replaced by an equivalent steel ring with a same area of total internal reinforcement. Figure E.2, shows the simplified RCFST section and the corresponding stress distribution. Note that no tensile strength was considered for concrete and the confining effect due to the steel tube on the compressive strength of the concrete parts was considered using equations proposed by Susantha et al. (2001), described below. Confining effect of transverse reinforcement was not considered in calculations. However, it must be recognized that for the shafts used in the parametric study, the confinement provided by the tube and reinforcement have only a small effect on the total flexural strength of composite section. For example, Table E.1 presents the calculated resultant forces for each part of a 24*in.* diameter composite RCFST section. The location of neutral axis can be found by considering the equilibrium of normal forces acting on the section (summing up all the resultant normal forces in this table), and, with knowledge of that location of the neutral axis, the plastic moment capacity of the section can be calculated. Note that, throughout the report, the moment contributed by each part of the cross-section was calculated with respect to the geometrical center of the composite RCFST section, per conventional structural analysis.

A comparison between the plastic moment that is calculated with the PSDM described above and the complete moment curvature obtained from fiber-section analysis done by OpenSees for the RCFST shaft of Analysis Group G-1, is presented in Figure E.3. As shown, the results obtained for flexural strength are in good agreement.

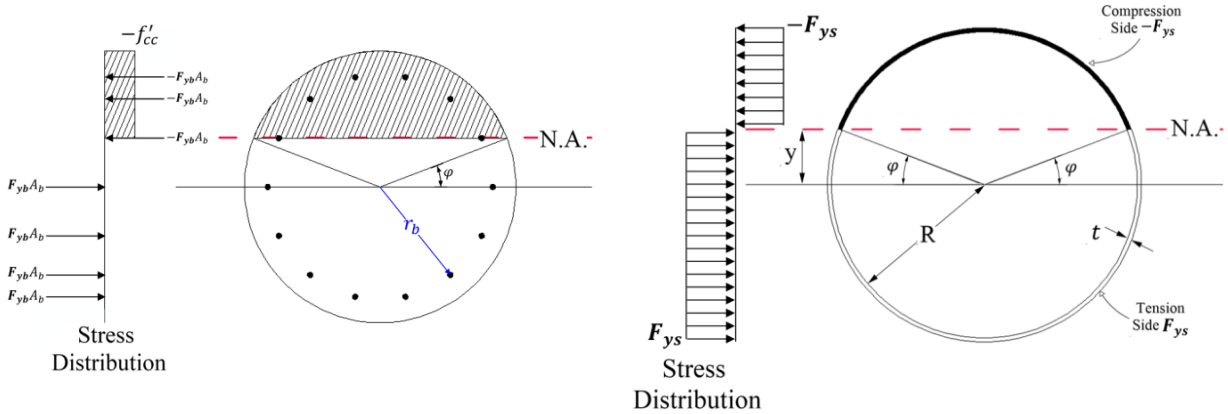

(a) Reinforced concrete part (b) Steel tube part

Figure E.1: Plastic stress distribution on RCFST section's: (a) Reinforced concrete part; (b) Steel tube part.

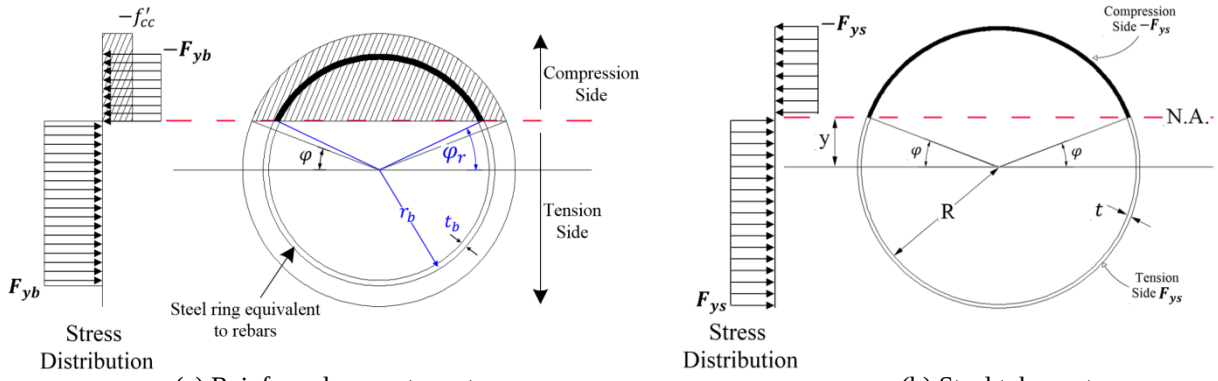

(a) Reinforced concrete part (b) Steel tube part

Figure E.2: Simplified plastic stress distribution on RCFST section's: (a) Reinforced concrete part; (b) Steel tube part.

Table E.1. Resultant normal forces of each part of composite RCFST section in PSDM.

Part	Resultant normal force	
	Compressive	**Tensile**
Steel tube	$-(\pi - 2\varphi)RtF_{ys}$	$(\pi + 2\varphi)RtF_{ys}$
Concrete	$-\left(\frac{\pi - 2\varphi}{2} - \cos(\varphi)\sin(\varphi)\right)R^2 f'_{cc}$	$zero$
Internal reinforcement	$-(\pi - 2\varphi_r)r_b t_b F_{yb}$	$(\pi + 2\varphi_r)r_b t_b F_{yb}$
External forces	$-P$	N/A

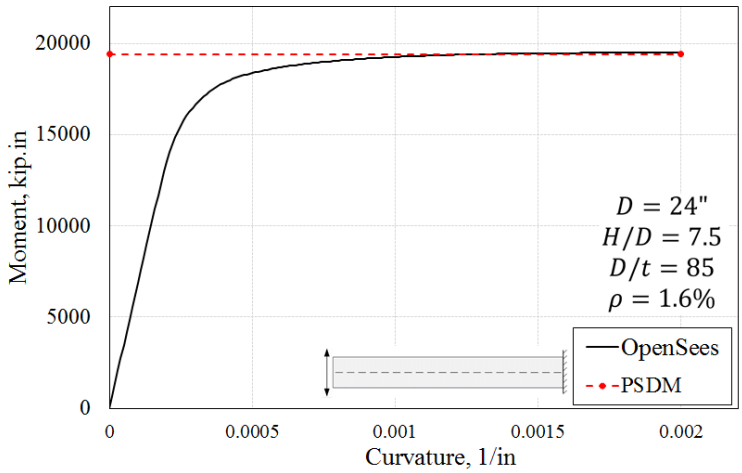

Figure E.3: Moment-curvature curve of RCFST shaft of the analysis Group G-1 calculated by OpenSees and the PSDM.

The analytical model proposed by Susantha et al. (2001) for uniaxial compressive strength of concrete confined by steel tube as part of a CFST column can be summarized as Equation (E.1) below:

$$f'_{cc} = f'_c + 4f_{rp} \quad \text{(E.1.a)}$$

$$f_{rp} = \beta \left(\frac{2t}{D-2t}\right) F_{ys} \quad \text{(E.1.b)}$$

$$\beta = \nu_c - \nu_s \quad \text{(E.1.c)}$$

$$\nu_c = 0.2312 + 0.3582\nu'_c - 0.1524\left(\frac{f'_c}{F_{ys}}\right) + 4.843\nu'_c\left(\frac{f'_c}{F_{ys}}\right) - 9.169\left(\frac{f'_c}{F_{ys}}\right)^2 \quad \text{(E.1.d)}$$

$$\nu'_c = \frac{0.881}{10^6}\left(\frac{D}{t}\right)^3 - \frac{2.58}{10^4}\left(\frac{D}{t}\right)^2 + \frac{1.953}{10^2}\left(\frac{D}{t}\right) + 0.4011 \quad \text{(E.1.e)}$$

where,
f'_{cc}: Confined compressive strength of the concrete
f'_c: Unconfined compressive strength of the concrete
f_{rp}: Lateral pressure at the peak load
t: Thickness of the steel tub
D: Diameter of the steel tube
F_{ys}: Steel tube yield stress
ν_c: Poisson ratio of steel tube filled with concrete
ν_s: Poisson ratio of steel tube (taken equal to 0.5)

The confined compressive strength calculated by Equation (E.1) for each analysis group is shown in Table E.2 below.

Table E.2. Calculated confined compressive strength for analysis groups

Analysis Group	*D*, *in.*	*t*, *in.*	F_{ys}, *ksi*	f'_c, *ksi*	f'_{cc}, *ksi*
G-1 and G-6	24	0.281	79	5.2	6.5
G-2, G-3, G-4, G-5, G-7, G-8, G-11, and G-12	100	1.18	79	5.2	6.6
G-9 and G-10	100	1.00	79	5.2	6.0

APPENDIX F

Properties of finite element models used in the analytical program

Table F.1 presents the details of the finite element models used in the analytical program.

Table F.1. Properties of the finite elements models used in the analytical program.

Analysis Group	RCFST shaft part						Reinforced concrete column part				
	D_i, *in.*	H_s, *in.*	t_s, *in.*	Internal reinforcement		Cover, *in.*	D_c, *in.*	H_c, *in.*	Reinforcement		Cover, *in.*
				Long.	Trans.				Long.	Trans.	
G-1, G-6	24	180, 120, 72	0.281	12#7	#3@12”	2	N/A	N/A	N/A	N/A	N/A
G-2, G-5, G-7, G-11	100	750,500,300	1.18	32#18	dbl.#5@12”	2	N/A	N/A	N/A	N/A	N/A
G-3, G-4, G-8	100	750	1.18	32#18	dbl.#5@12”	2	88	220	42#18	dbl.#5@15”	1.5
G-9	100	750	1.00	32#18	dbl.#5@12”	2	N/A	N/A	N/A	N/A	N/A
G-10	100	750	1.00	32#18	dbl.#5@12”	2	88	220	42#18	dbl.#5@15”	1.5

where:
D_i: Inside dimension of steel tube, *in.*
H_s: Shaft height, *in.*
t_s: Steel tube wall thickness, *in.*
D_c: Diameter of the attached column, *in.*
H_c: Height of the attached column, *in.*

For all the finite element models of the analytical program:
Unconfined uniaxial compressive strength of concrete (f_c'): 5.2*ksi*
Steel tube yield stress (F_{ys}): 79*ksi*
Reinforcing bar yield stress (F_{yb}): 68*ksi*

APPENDIX G

Design of flexural specimens

Design aspects and some details specific to each of the specimens are presented in the following sections.

G.1 Specimen S1

Specimen S1 was considered to be the reference specimen against which all results from many of the other specimens were compared. The objective of testing this specimen was to investigate development of required composite action in RCFST shafts, relying only on the friction naturally developing between the steel tube and the concrete core. The properties of the shaft section of Specimen S1 with outer diameter of $20in.$ and D/t ratio of 80 are presented in Tables G.1 and G.2.

Table G.1. Specimen S1 shaft's steel tube properties

Outside diameter (D_s), *in.* (nominal)	Wall thickness (t), *in.* (nominal)	D/t	Steel Grade	Nominal yield strength (f_y), ksi	Expected yield strength (f_{ye}), ksi	$\frac{H_s}{D_s}$
20	0.25	77	A252 Grade 2	35	55	7

Table G.2. Specimen S1 shaft's reinforced concrete core properties

f'_c, *ksi*	Reinforcing ratio (ρ_s), %	Long. reinforcing	Trans. reinforcing	Nominal yield strength (f_y), *ksi*	Expected yield strength (f_{ye}), *ksi*
4	1.25	12 #5 A706Gr60	#4 @4" A706Gr60	60	68

Figure G.1 shows a sample of the calculated value of α_c (defined by Equation (2.15) of the report) that is obtained for different diameters and reinforcing ratios of column section of the specimen. Large values of α_c indicate a greater safety margin to develop the expected plastic flexural strength of the shaft without yielding the reinforced concrete column framing into the shaft. In this figure, the solid lines correspond to the different diameters of reinforced concrete column, the dotted lines correspond to different reinforced concrete column reinforcement ratio, and the intersections of dotted and solid lines show possible design configurations. A column section with diameter of D_c=0.8D_s and reinforcing ratio of ρ_s= 5% was chosen for Specimen S1. As indicated in Figure G.1, the α_c ratio for this sample column section is 1.1. Note that the values shown in Figure G.1 are a sample of how the design was done. The final design values were obtained by performing several iterations to find the best possible configurations. Finalized design values are presented in Table 2.9 of the report.

Figure G.2 shows a sample moment diagram along Specimen S1 for the maximum applied lateral load. The properties of the reinforced concrete column part of the Specimen S1 are presented in Table G.3. Note

that, the confining effect of the transverse reinforcing was not considered in calculating the yield moment of the reinforced concrete column for all designed specimens.

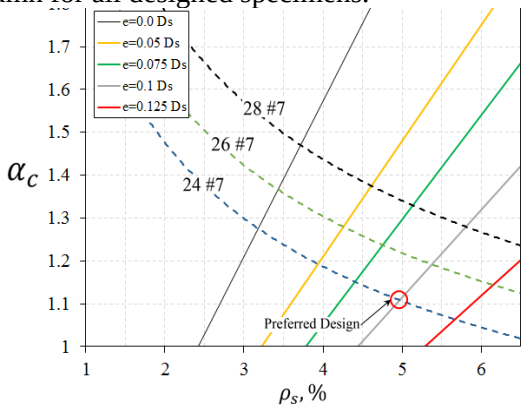

(a) $H_c/D_c = 2.5$

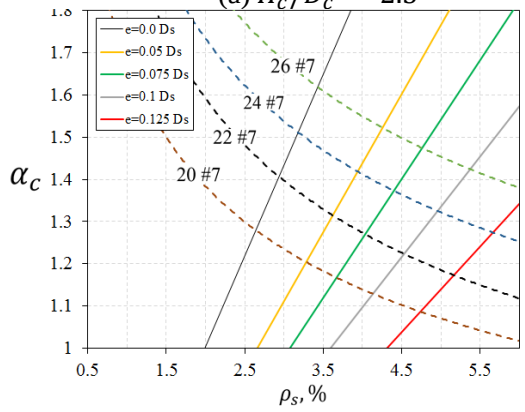

(b) $H_c/D_c = 2.0$

Figure G.1: Values of α_c for different diameter and reinforcement ratios of concrete part for: (a) H_c/D_c=2.5 and H_c/D_c=2.0.

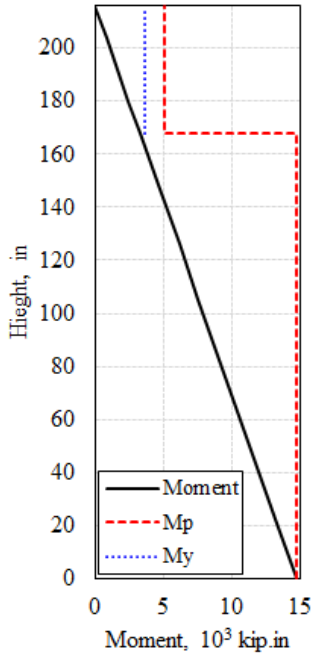

Figure G.2: Moment diagram for Specimen S1

Table G.3. Specimen S1 column part's properties

D_c, *in.*	H_c, *in.*	f'_c, *ksi*	Reinforcing ratio (ρ_s), %	Long. reinforcing	Trans. reinforcing	Nominal yield strength (f_y), *ksi*
16	40	4	6.0	20 #7 A706Gr60	#4 @4" A706Gr60	60

The shear capacity check for both the reinforced concrete column and the shaft was done according to Chapter 8 of the AASHTO Guide Specifications for LRFD Seismic Bridge Design (2011). For Specimen S1, since no axial force is applied, the shear strength of the concrete core was neglected and only the shear strength due to transverse reinforcement was considered. Also, for the shaft, only the shear strength of the steel tube was considered. The shear capacity checks for the reinforced concrete column and the RCFST shaft of Specimen S1 were done as following (based on knowledge at the time of specimen design).

Shear capacity of the reinforced concrete column:

According to Section 8.6.3 of the AASHTO Guide Specifications for LRFD Seismic Bridge Design (2011), the shear reinforcement capacity can be calculated as:

$$V_S = \frac{\pi}{2}\left(\frac{A_{sp} f_{yh} D'}{s}\right) \leq 0.25\sqrt{f_c'} A_e \qquad \text{(G.1)}$$

where:

A_{sp} = area of hoop reinforcing bar = 0.2 in^2

f_{yh} = yield stress of the confinement steel = 60 ksi.

D' = core diameter of column measured from center of hoop = 16.5 in
s = spacing of hoop reinforcement = 4 in
f_c' = compressive strength of concrete = 4 ksi
$A_e = 0.8A_g = (0.8)\left(\frac{\pi}{4}\right)(19^2) = 227\ in^2$
therefore:

$$V_S = 78\ kips \leq 0.25\sqrt{f_c'}A_e = 113\ kips$$

and:

$$\phi_s V_s = (0.9)(78) = 70\ kips\ >\quad V_u = \frac{M_{ps}}{Hs + H_c} = \frac{14800}{216} = 69\ kips$$

Shear capacity of the RCFST shaft:

The shear resistance of the circular steel tube was calculated as follows:

$$V_{S_{tube}} = 0.58F_y(0.5A_g) \qquad \text{(7.10.2-15) Washington DOT BDM (2014)} \qquad \text{(G.2)}$$

where:

F_y = nominal yield strength of the steel tube=35 ksi
A_g = area of the steel tube = 23.2 in^2

therefore: $V_{S_{tube}} = 235\ kips$ and:

$$\phi_s V_s = (0.9)(235) = 212\ kips\ >\quad V_u = \frac{M_{ps}}{Hs + H_c} = \frac{14800}{216} = 69\ kips$$

The value of V_u, was calculated above for the H_c/D_c ratio of 2.5. Note that if the case of H_c/D_c=2.0 had been used instead, the shear capacity of the column would have had to be increased by either decreasing the transverse reinforcing distance or using rebars with larger diameter (but the RCFST shaft part would still have had adequate shear strength).

G.2 Specimen S2R

The mechanism for transferring loads from a reinforced concrete column to a CFST shaft part was studied in Section 2.2.12. Based on those findings, per the model described in Section 2.2.12, the reinforced concrete column loads can be transferred to the steel tube part of the CFST shaft provided that a sufficient reinforced concrete column reinforcement's extension length is provided. A schematic view of the proposed Specimen S2R is shown in Figure G.3 below. As shown in that figure, although the column reinforcement extends some distance into the shaft to a length defined as the transition zone, there is no shaft reinforcement in that transition zone. This specimen therefore allows to investigate the adequacy of the load transfer mechanism described in Section 2.2.12.

For this specimen, the transition zone length is set to be equal to the sum of the diameter of the column and the development length of the rebars. Two options existed at the bottom of the shaft: it could be left un-reinforced, or instead reinforced to provide a total flexural strength identical to that of Specimen S1 (i.e., the reference RCFST shaft in this experimental program), to investigate whether the proposed transition zone for this specimen allows to develop the same plastic moment capacity of at the base of the RCFST shaft section. The second option was chosen for this specimen. Figure G.4 shows a sample moment diagram along Specimen S2R for the maximum applied lateral load. The length of the rebars at that location was taken as at least $D_s + l_d$. For the diagram shown in Figure G.4, the length of RCFST part at the bottom of the shaft is chosen to be $3D_s$.

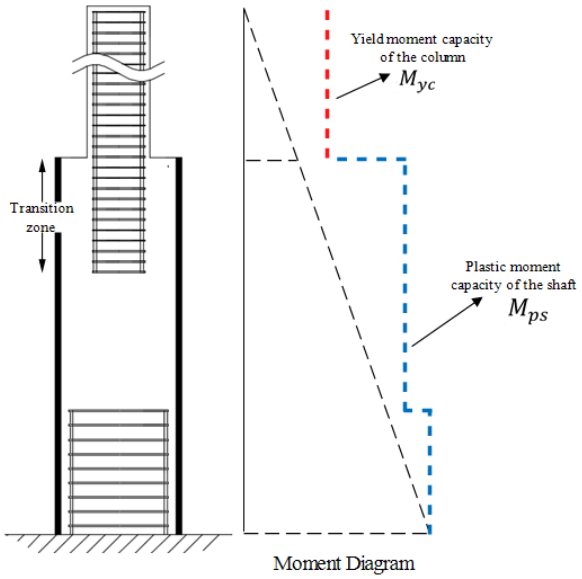

Figure G.3: Schematic view of the proposed Specimen S2R.

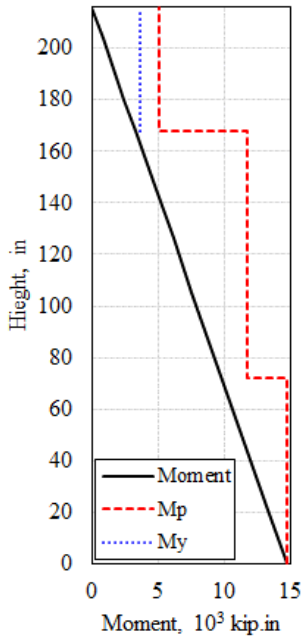

Figure G.4: Moment diagram for Specimen S2R

G.3 Specimen S3

Specimen S3 was chosen to be similar to Specimen S1 but with a friction-less coating on the interior surface of the steel tube. The objective of this test was to investigate a case where there is little friction (if any) at the interface of the reinforced concrete core and the steel tube in the RCFST shaft. As shown in Section 2.2.6, the lack of friction at the interface of the steel tube and concrete core, prevents the development of full composite action in the RCFST shaft, and therefore, the plastic capacity of the RCFST shaft decreases. In order to reduce the friction at the interface of the concrete and steel tube, different materials can be used to coat the interior surface of the steel tube. For example, Gebman et al. (2006) used a water-bentonite coating in order to reduce the friction at the concrete and steel interface. Roeder et al. (2009) used grease for this purpose.

The moment diagram and capacity of each part of Specimen S3 are symbolically provided in Figure G.5. The moment capacity of the RCFST shaft part was calculated (according to findings in Section 2.2) by summation of the steel tube and reinforced concrete core plastic moment capacities. The resulting α_c ratio is 1.79 for Specimen S3. However, it is recognized that in the actual specimen (compared to the model), it may be practically impossible to achieve zero friction at the interface, and the experimentally obtained capacity of the RCFST shaft can be more than the theoretical one. For this reason, the reinforced concrete column part of the specimen was designed to be similar to the one used in Specimen S1. The shear capacity check for the reinforced concrete column and the RCFST shaft parts of Specimen S3 is presented in the following.

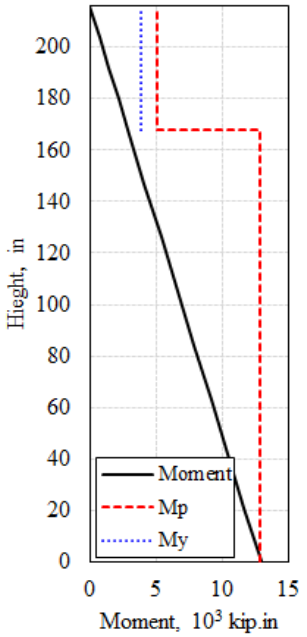

Figure G.5: Moment diagram for Specimen S3

Shear Capacity of RCFST shaft:

The maximum shear force in this specimen is lower than Specimen S1's maximum applied shear and therefore, no shear capacity check is necessary.

G.4 Specimen S4

Specimen S4 was chosen identical to Specimen S3. Except, grease coating was used instead of Bentonite slurry.

G.5 Specimen S5

The design procedure for Specimen S5 was similar to the Specimen S1 but with different dimensions for the RCFST shaft and the reinforced concrete column parts.

G.6 Specimen S6R

Specimen S6R was considered to be similar to the Specimen S4, except that shear transfer mechanisms were used on the interior surface of steel tube to achieve full composite action. Design of the shear transfer mechanisms can be done according to Gebman et al. (2006) and API 2A-LRFD (1993), as mentioned in Appendix D. For the proposed Specimen S6R, shear rings (i.e., flat bars with square cross-section) were considered at the top of the shaft to provide the shear transfer mechanism. Design was done according to Section H.4.3.2 of API 2A-LRFD (neglecting the D/t ratio limit specified by API 2A-LRFD). Note that the shear strength of the ring, per API 2A-LRFD, is smaller than the one reported by Gebman et al. (2006), suggesting a satisfactory and conservative design. Four shear rings with $0.25 in.^2$ square cross-section, spaced no more than $8 in.$ from each other, are found adequate to transfer the internal axial load that was calculated using Equation (2.2).

APPENDIX H

Construction and preparation of the test specimens

H.1 Flexural specimens

H.1.1 General

Flexural specimens were constructed according to the construction schedule presented in Section H.1.4 (for Specimen S1 as a representative case). Photos of the construction and instrumentation of the flexural specimens are presented in the following sections. In the following, construction steps that were similar for all flexural specimens are shown only for Specimen S1; those that were different for other specimens are shown in different sub-sections of Section H.1.5.

For Specimen S2R, per the objective of the test, the shaft part's internal reinforcing was terminated at a height of $10ft.$ from the strong floor ($7ft.$ from top of the foundation) and a gap of about $21in.$ was left without reinforcement between that point and the bottom of the reinforcing cage of the column part that was extended in the shaft. Figure H.1a shows the details of the internal reinforcing cages for Specimen S2R. A DYWIDAG bar was placed through a plastic sleeve that was placed axially along the specimen and through the strong floor and was anchored at both ends (i.e., at the top of the specimen and below the strong floor). The bar was pre-tensioned to a certain amount of force before testing the specimen in order to apply the desired axial compression load on Specimen S2R. A load cell was placed at the bottom end of the bar to monitor the axial load applied on the specimen. Figures H.1b and H.1c show the details of the axial DYWIDAG placement. Note that the DYWIDAG bar was free to move along the plastic sleeve and it was not embedded in the concrete.

Construction of Specimens S3 and S4 was similar to what is described in the construction schedule presented in Section H.1.4, except that bentonite slurry and grease were applied for Specimens S3 and S4, respectively, on the interior surface of the steel tube before pouring concrete. Photos of the bentonite and grease applications are presented in Section H.1.5.

For Specimen S6R, a grease coating was applied at the interior surface of the shaft tube. A thicker layer of coating was applied on that surface compared to Specimen S4. Four shear rings were welded at the top of the shaft's steel tube. Construction steps of Specimen S5 were similar to Specimen S1.

Figures H.2 and H.3 show the ready-to-test views of a typical 20*in.* diameter specimen and of the30 *in.* diameter Specimen S5, respectively.

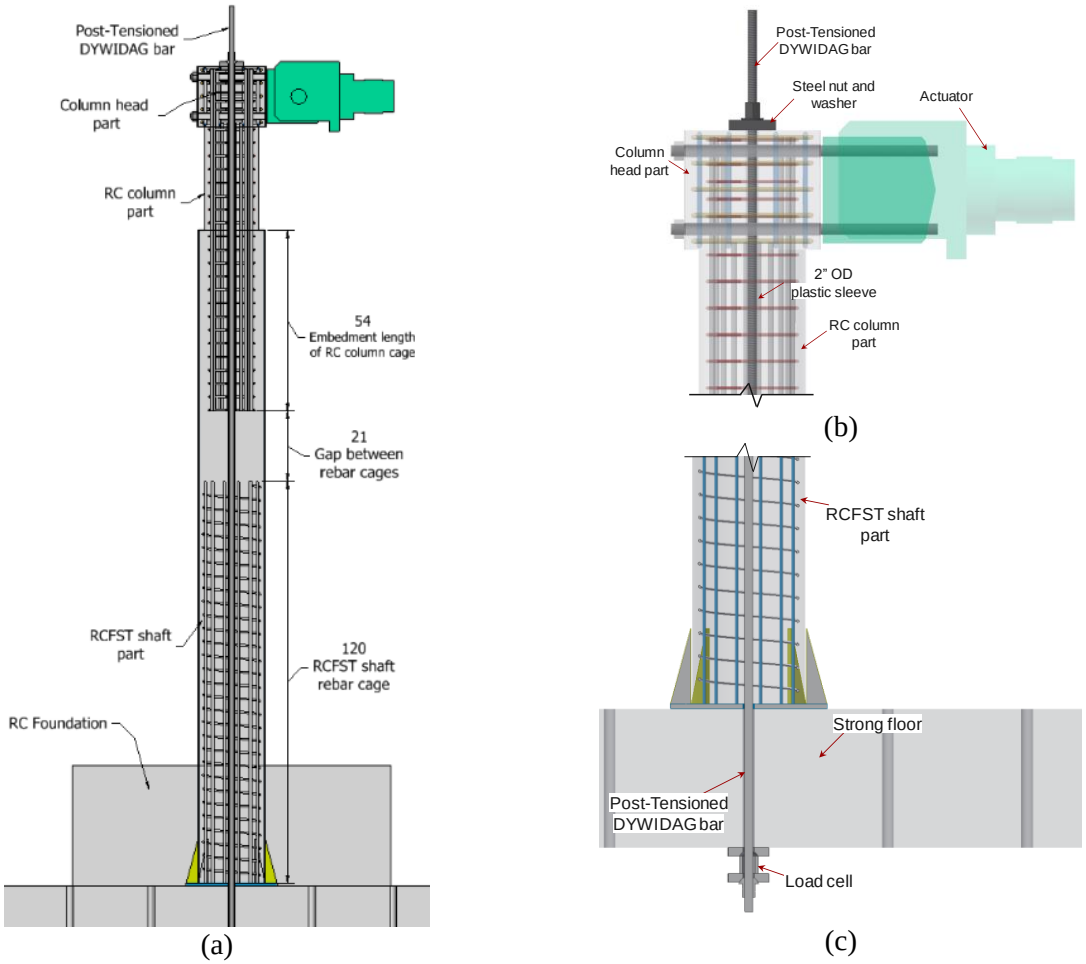

Figure H.1: Specimen S2R's: (a) Internal reinforcing details. (b) DYWIDAG placement details at the top. (c) DYWIDAG placement details at the bottom.

Figure H.2: Global view of the flexural specimen's test setup (20in. diameter specimen is shown).

Figure H.3: Global view of Specimen S5 ready for test.

H.1.2 Instrumentation

Different instruments were used to measure the local and global responses of the flexural specimens. These include strain gauges, string potentiometers, LVDTs, and the laser-based Krypton K600 high performance dynamic mobile coordinate measurement system (SEESL 2014). A number of strain gauges were placed along the steel tube on its outer surface to measure both longitudinal and transverse strains. Also, strain gauges were installed on the internal longitudinal rebars in order to monitor strains along the rebars. String pots were used along the height of the steel tube to measure the elongation and shortening of the compression and tension sides of the shaft along its height. The Krypton K600 device was used to measure displacements near the base of the specimen, possible displacements of the foundation, and slippage of the concrete core inside the steel tube. In an attempt to measure slippage at the interface of steel tube and the concrete core, four Krypton device's LEDs were placed on a square grid of $9 \times 9in.$ on the steel tube at $7ft.$ high for $20in.$ diameter specimens ($9 \times 16.5in.$ at $7.5ft.$ height for the $30in.$ specimen) and four LEDs were placed on the concrete core in holes cut in the steel tube on a similar grid at a $1.5in.$ longitudinal offset ($2.25in.$ for the $30in.$ specimen). Figure H.4 shows the position of these LEDs on the $20in.$ diameter specimens. This technique has been previously used by Lu and Kennedy (1994) and Brown (2013) to measure slippage between the steel tube and the concrete core in concrete-filled members.

Table H.1 lists the number of different instruments that were used for each specimen. Details of the instrumentation plan for the flexural specimens are presented in Appendix M.

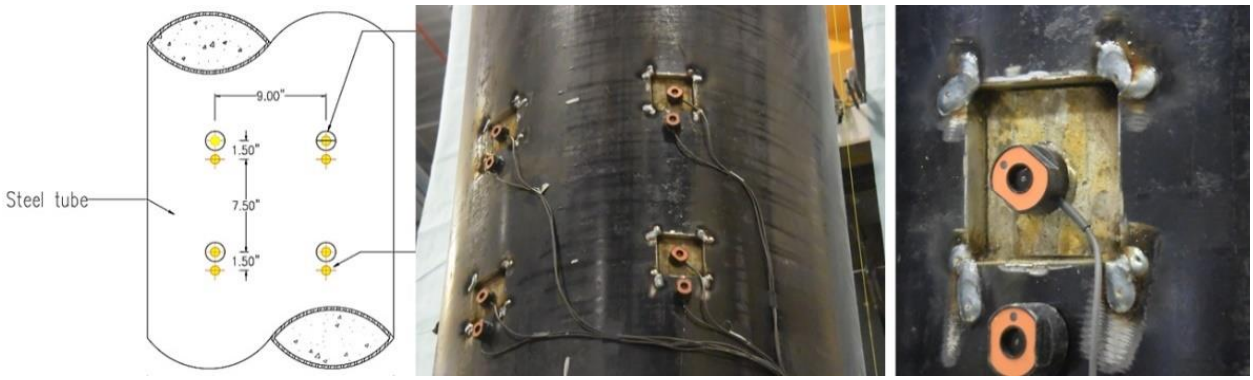

Figure H.4: Schematic view of slippage measuring LEDs.

Table H.1. Quantity of instruments that were used for each flexural specimen.

Specimen	Quantity			
	Strain Gauge	String Pot.	Krypton LED	Load Cell
S1	46	25	20	N/A
S2R	44	25	20	1
S3	42	25	20	N/A
S4	42	25	20	N/A
S5	46	25	23	N/A
S6R	42	25	21	N/A

H.1.3 Material properties of flexural specimens

Material properties of different parts of each flexural specimen were measured by performing uniaxial tension and compression tests on the steel coupons and concrete cylinders, respectively. At least three samples were tested for the steel tube, longitudinal reinforcement of the RCFST shaft part, and concrete part of each flexural specimen. Figure H.5 shows the uniaxial test setup for typical steel tube coupons and concrete cylinders. The measured uniaxial stress-strain relationships of the steel tube coupons are shown in Figure H.6. The average uniaxial stress-strain curve of the steel tube part of each specimen is shown in Figure H.7. Measured uniaxial stress-strain relationships of the concrete for the RCFST shaft part of the flexural specimens are shown in Figure H.8. Note that axial LVDTs were not used in testing Specimen S1 concrete cylinders and therefore uniaxial stress-strain relations corresponding to Specimen S1 cylinders are not shown in this figure. Figure H.9 shows the uniaxial test setup and measured stress-strain relations for the RCFST shafts' longitudinal rebars. The average measured material properties of the steel tube and shaft concrete for each flexural specimen are presented in Table 2.10. Average yield and ultimate stress for rebars were $75.2ksi$ and $96.6ksi$ respectively.

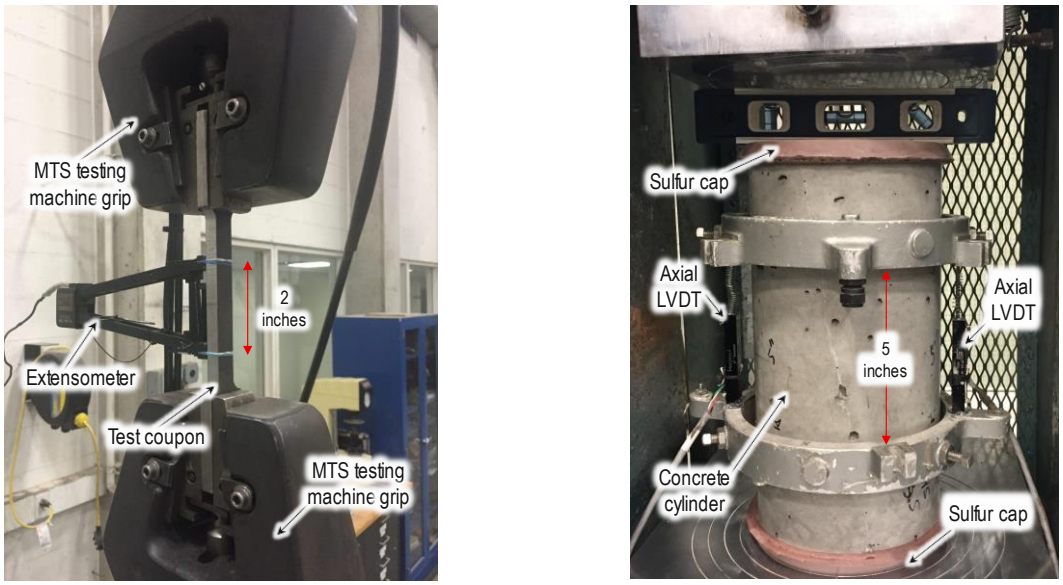

(a) (b)

Figure H.5: Uniaxial test setup for: (a) tension test of steel coupons; (b) compression test of concrete cylinders.

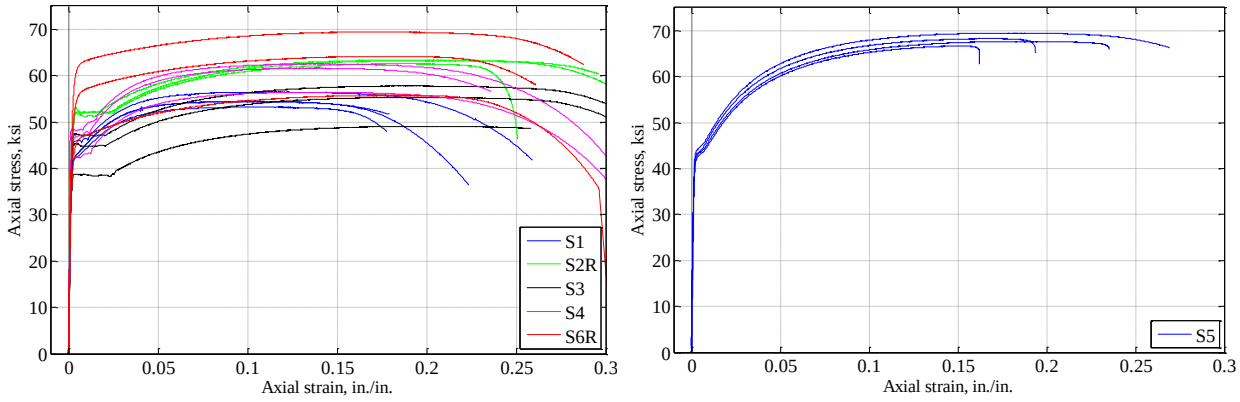

(a) (b)

Figure H.6: Measured uniaxial stress-strain relation of: (a) 20in. steel tubes; (b) 30in. steel tube.

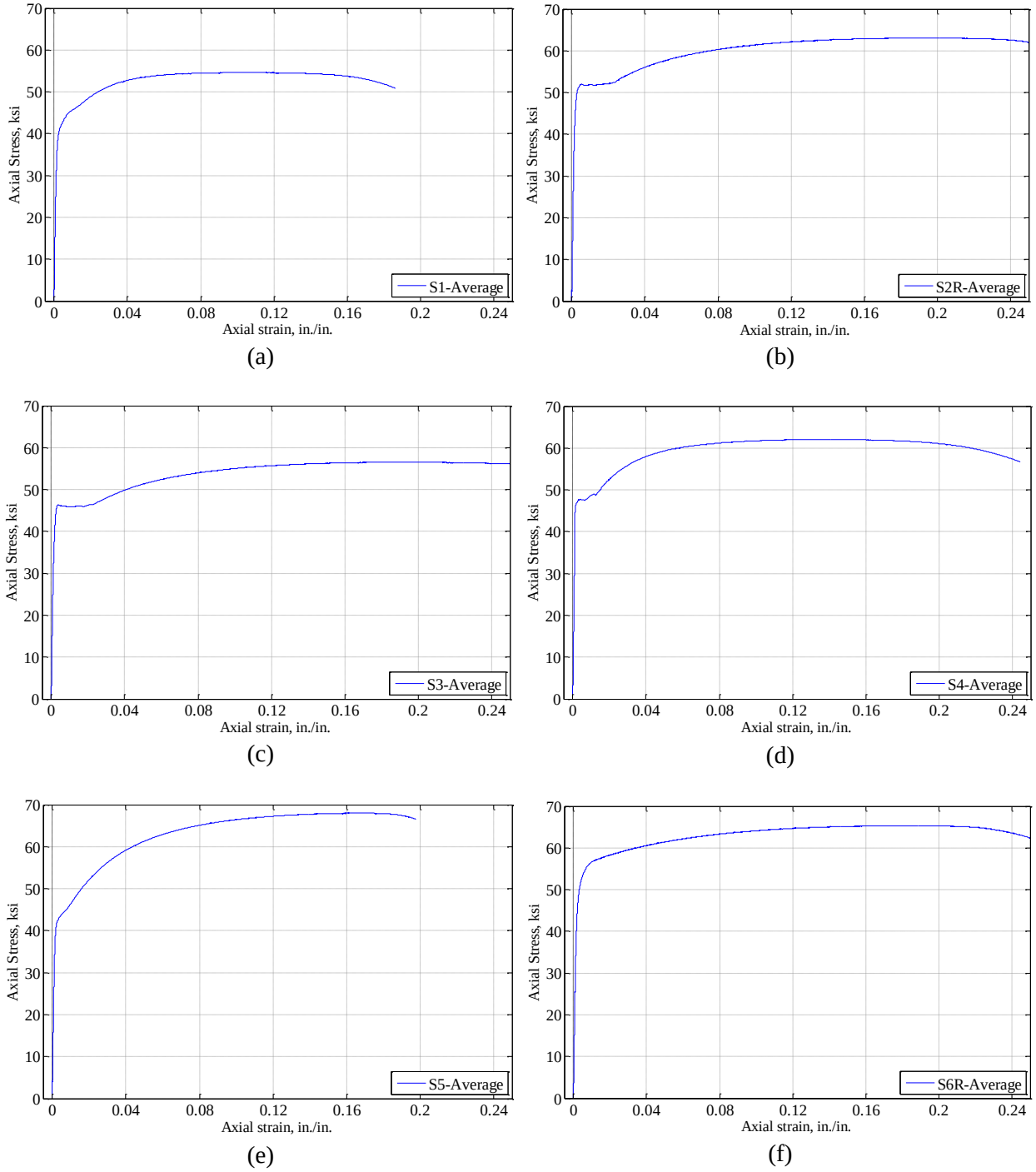

Figure H.7: Average uniaxial stress-strain relation of the steel tube part of Specimen: (a) S1; (b) S2R; (c) S3; (d) S4; (e) S5; (f) S6R.

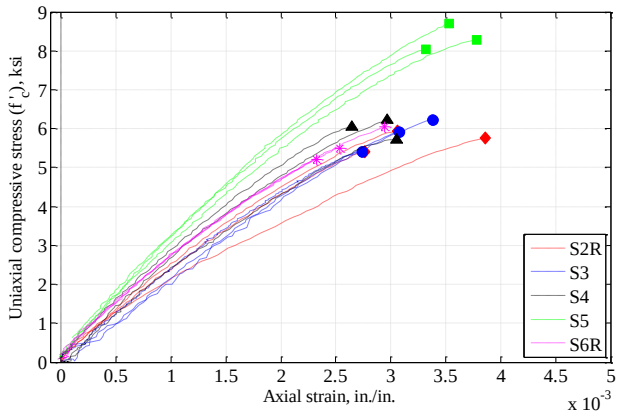

Figure H.8: Measured uniaxial stress-strain relation of concrete of RCFST shaft part of the flexural specimens.

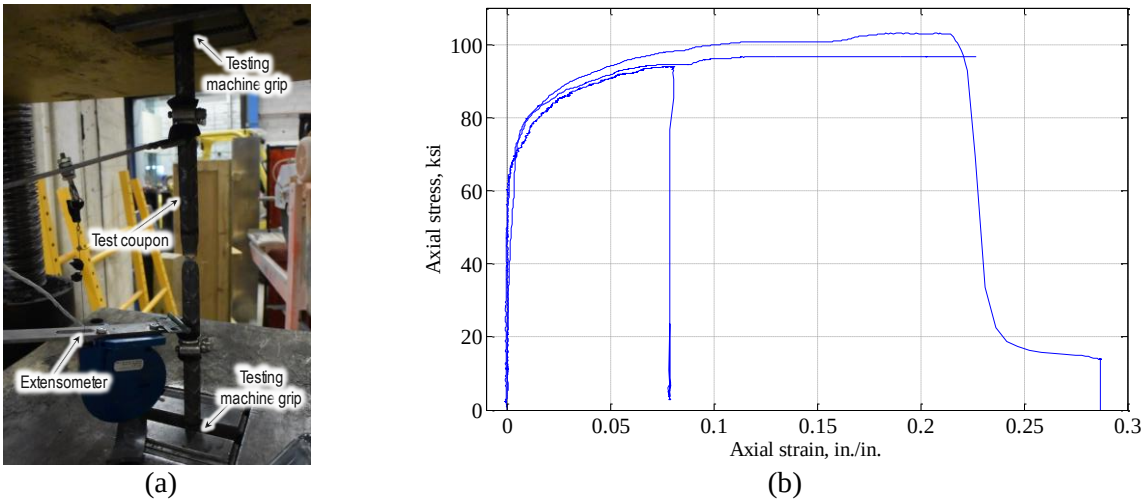

(a) (b)

Figure H.9:RCFST shaft longitudinal rebar: (a) uniaxial tension test setup; (b) uniaxial stress-strain relations.

Table H.2. Average material properties obtained from uniaxial tests for flexural specimens.

Specimen	Steel tube				Concrete
	F_y, ksi	ϵ_y, μin./in.	F_u, ksi	E_s, ksi	f'_c, ksi
S1	46.0	1500	55.1	30100	5.0
S2R	51.9	1700	63.1	30900	5.7
S3	46.1	1600	57.0	29400	5.8
S4	47.4	1400	62.1	33400	6.0
S6R	55.0	1900	66.8	29600	5.6
S5	41.5	1400	68.0	30300	8.3

H.1.4 Detailed test preparation schedule

Table H-3 shows the detailed schedule and construction sequence of Specimen S1.

Table H-3. Testing schedule

No.	ACTIVITY	10/1/2015 Thu 1	10/2/2015 Fri 2	10/3/2015 Sat 3	10/4/2015 Sun 4	10/5/2015 Mon 5	10/6/2015 Tue 6	10/7/2015 Wed 7	10/8/2015 Thu 8	10/9/2015 Fri 9	10/10/2015 Sat 10	10/11/2015 Sun 11	10/12/2015 Mon 12	10/13/2015 Tue 13	10/14/2015 Wed 14	10/15/2015 Thu 15	10/16/2015 Fri 16	10/17/2015 Sat 17	10/18/2015 Sun 18	10/19/2015 Mon 19	10/20/2015 Tue 20	10/21/2015 Wed 21	10/22/2015 Thu 22	10/23/2015 Fri 23
1	Put instrumentation on the RCFST shaft part rebars (See drawing D-I-03).																							
2	Weld the base plate at the bottom of the steel tube (See drawing D-RCFST-02).																							
3	Weld the stiffeners at the bottom of the steel tube (See drawing D-RCFST-02).																							
4	Weld Type BP-RT1 anchor bars to the base plate (See drawing D-RCFST-02).																							
5	Put the shaft rebar cage inside the steel tube and fix it at place (See drawing D-RCFST-01).																							
6	Put LSG#1 to LSG#4 strain gauges that are going to be embedded in the foundation (See drawing D-I-02).																							
7	Construct the formwork for reinforced concrete foundation.																							
8	Put the reinforced concrete foundation pre-fabricated rebar cage inside the formwork.																							
9	Install the plastic sleeves that will be used for DYWIDAG bars, inside the reinforced concrete foundation rebar cage.																							
10	Put the specimen lifting hooks inside the reinforced concrete foundation rebar cage (See drawing D-LH-01).																							
11	Lift the steel tube with its contents and place it in the middle of the reinforced concrete foundation rebar cage.																							
12	Put the extra rebars around the steel tube (in the foundation) and tie them (See drawing D-RT-01).																							

Continued Table H-3. Testing schedule

No.	ACTIVITY	10/1/2015 Thu 1	10/2/2015 Fri 2	10/3/2015 Sat 3	10/4/2015 Sun 4	10/5/2015 Mon 5	10/6/2015 Tue 6	10/7/2015 Wed 7	10/8/2015 Thu 8	10/9/2015 Fri 9	10/10/2015 Sat 10	10/11/2015 Sun 11	10/12/2015 Mon 12	10/13/2015 Tue 13	10/14/2015 Wed 14	10/15/2015 Thu 15	10/16/2015 Fri 16	10/17/2015 Sat 17	10/18/2015 Sun 18	10/19/2015 Mon 19	10/20/2015 Tue 20	10/21/2015 Wed 21	10/22/2015 Thu 22	10/23/2015 Fri 23
13	Construct the reinforced concrete column part rebar cage (See drawing D-RCC-02).																							
14	Put the column rebar cage inside the shaft rebar cage and fix it at place (See drawing D-TZ-01).																							
15	Put two bars at the top level of the RCFST shaft to be used by string pots (See drawing D-I-08).																							
16	Pour foundation concrete																							
17	Pour concrete in the steel tube until the top level of the steel tube (i.e., only the RCFST shaft part).																							
18	Cure time for concrete (RCFST shaft and reinforced concrete foundation parts).												Item No. 18 finishes on 11/8/2015.											
19	Construct the formwork at the top of the specimen for the reinforced concrete column part.																							
20	Install the column head rebar cage at the top of the reinforced concrete column rebar cage (See drawings D-CH-01 and D-CH-02).																							
21	Install the Type CH-Hook rebar at top of the reinforced concrete column part (See drawings D-CH-02 and D-CH-03).																							
22	Install the plastic sleeves for actuator attachment rods (See drawing D-CH-02).																							
23	Mix 4*ksi* concrete in the SEESL.																							

Continued Table H-3. Testing schedule

No.	ACTIVITY	10/22/2015 Thu 22	10/23/2015 Fri 23	10/24/2015 Sat 24	10/25/2015 Sun 25	10/26/2015 Mon 26	10/27/2015 Tue 27	10/28/2015 Wed 28	10/29/2015 Thu 29	10/30/2015 Fri 30	10/31/2015 Sat 31	11/1/2015 Sun 32	11/2/2015 Mon 33	11/3/2015 Tue 34	11/4/2015 Wed 35	11/5/2015 Thu 36	11/6/2015 Fri 37	11/7/2015 Sat 38	11/8/2015 Sun 39	11/9/2015 Mon 40	11/10/2015 Tue 41	11/11/2015 Wed 42	11/12/2015 Thu 43
18	Cure time for concrete (RCFST shaft and reinforced concrete foundation parts).	Item No. 18 started from 10/12/2015.																					
23	Mix 4*ksi* concrete in the SEESL.																						
24	Pour and vibrate the concrete for the top part of the specimen (i.e., reinforced concrete column and column head parts).																						
25	Cure time for concrete of the top part of the specimen (see item 24 above).																						
26	Instrumentation of the specimen (See Appendix 3).																						
27	Drill the LED holes on the steel tube wall (See drawing D-I-05).																						
28	Lift the specimen and take off the reinforced concrete foundation formwork.																						
29	Lift and move the specimen to the testing location (See Section H.1.5)																						
30	Prepare the DYWIDAG bars for tying the specimen to the strong floor.																						
31	Install the DYWIDG bars and tie the foundation to strong floor.																						
32	Test the Specimen.																						

Note: At least two days were needed to take off the instrumentation, remove the DYWIDAG bars, detach the specimen, and test the next specimen.

H.1.5 Photos of construction process of flexural specimens

This appendix presents figures and pictures of the construction process for test specimens. Figures are ordered according to construction sequence.

H.1.5.1 Specimen S1

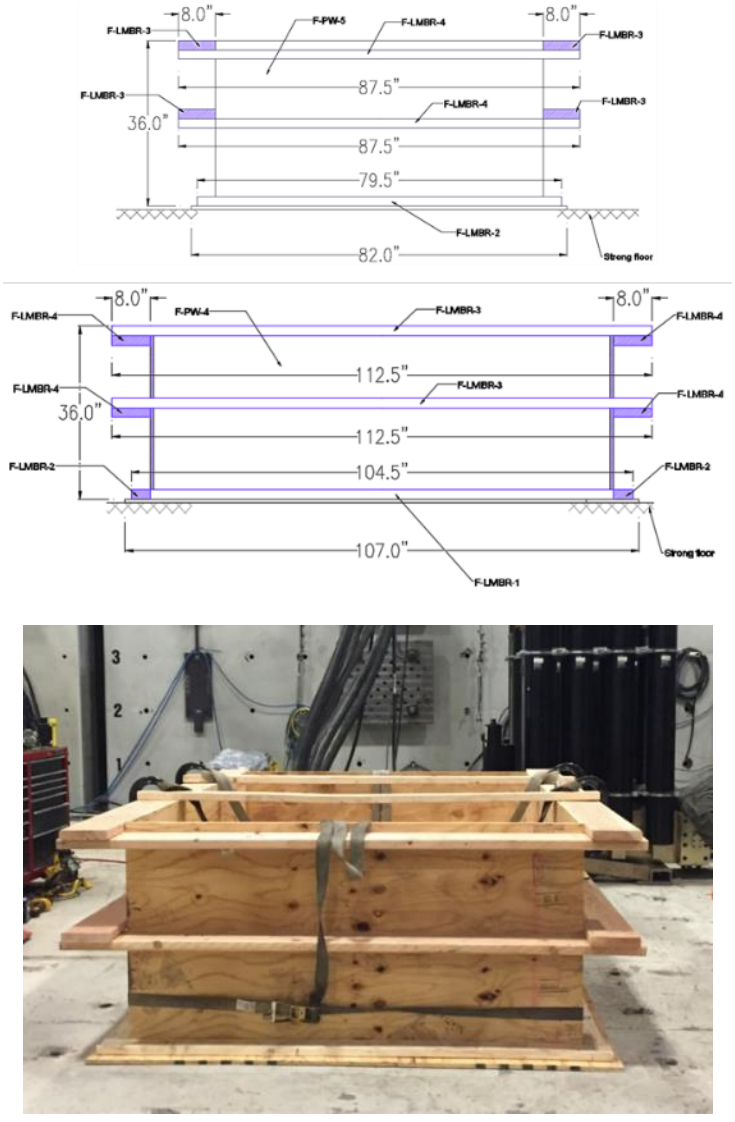

Figure H-10: Construction of foundation's formwork.

Figure H-11: Construction of foundation's rebar cage.

Figure H-12: Foundation rebar cage placement in the formwork.

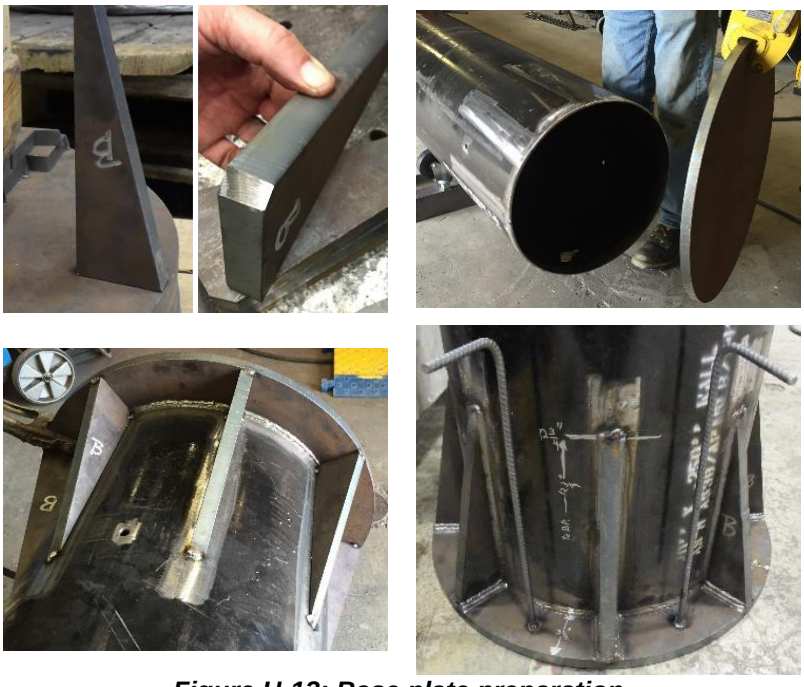

Figure H-13: Base plate preparation.

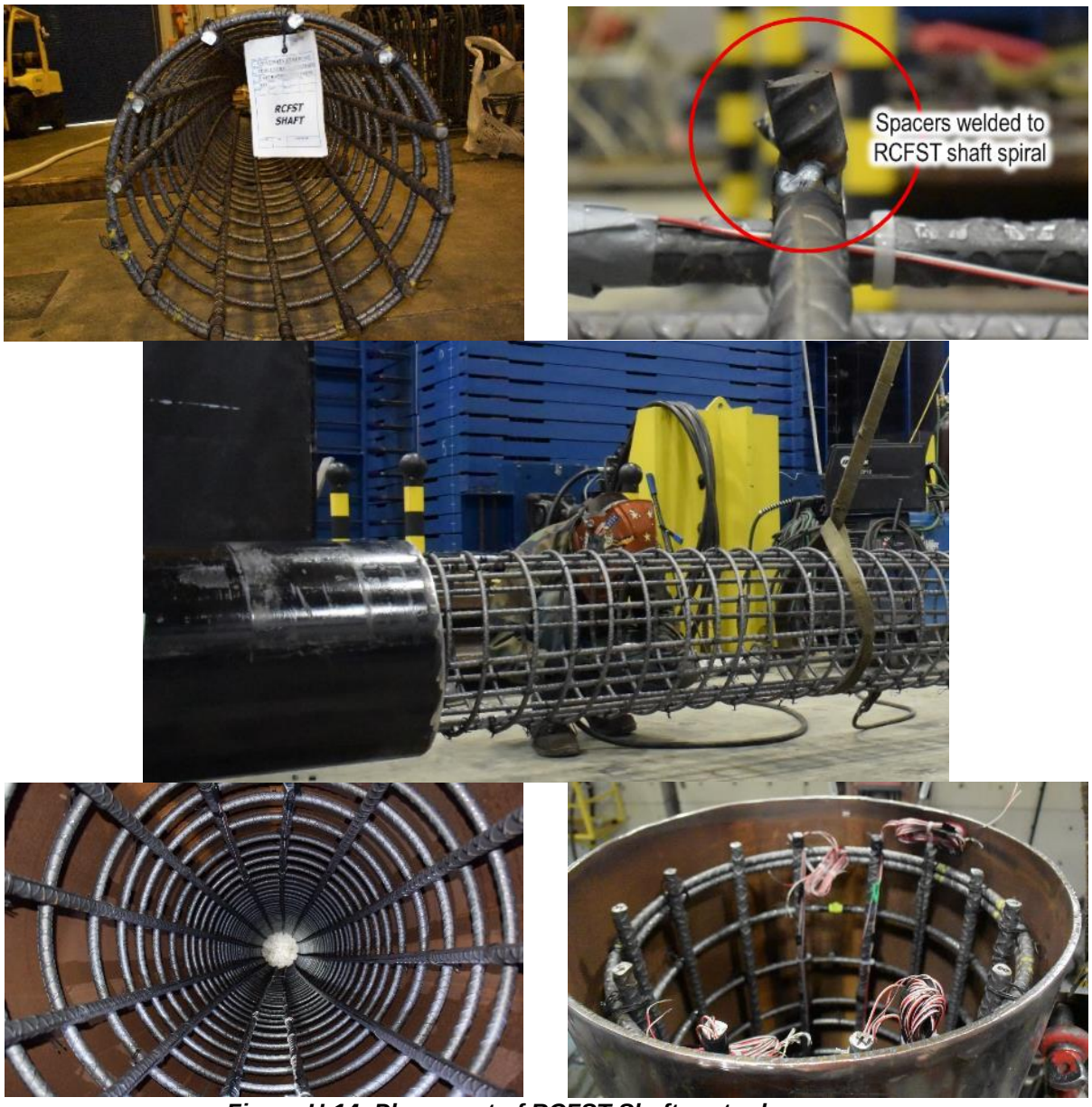

Figure H-14: Placement of RCFST Shaft part rebar cage.

Figure H-15: Placement of RCFST Shaft part in the foundation part.

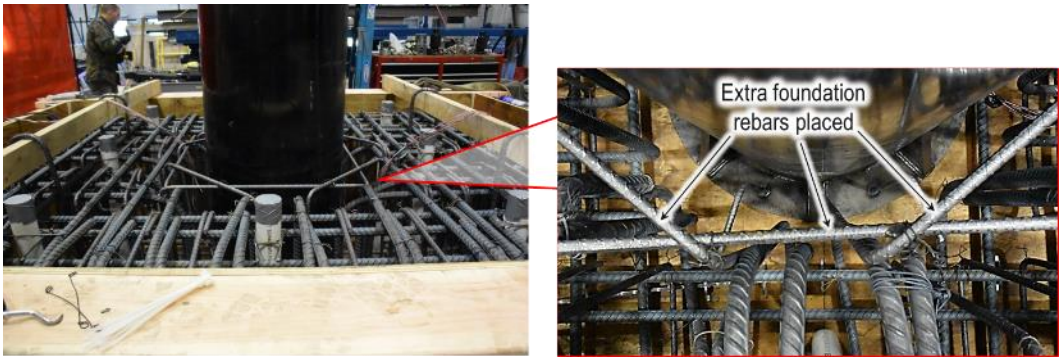

(a)

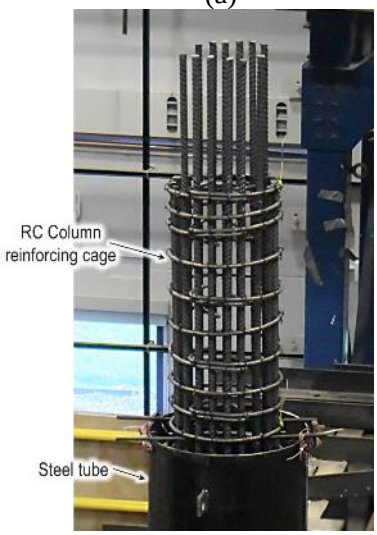

(b)

Figure H-16: (a) Placement of foundation's extra rebars. (b) Placement of the reinforced concrete column part's rebar cage at the top of RCFST shaft part.

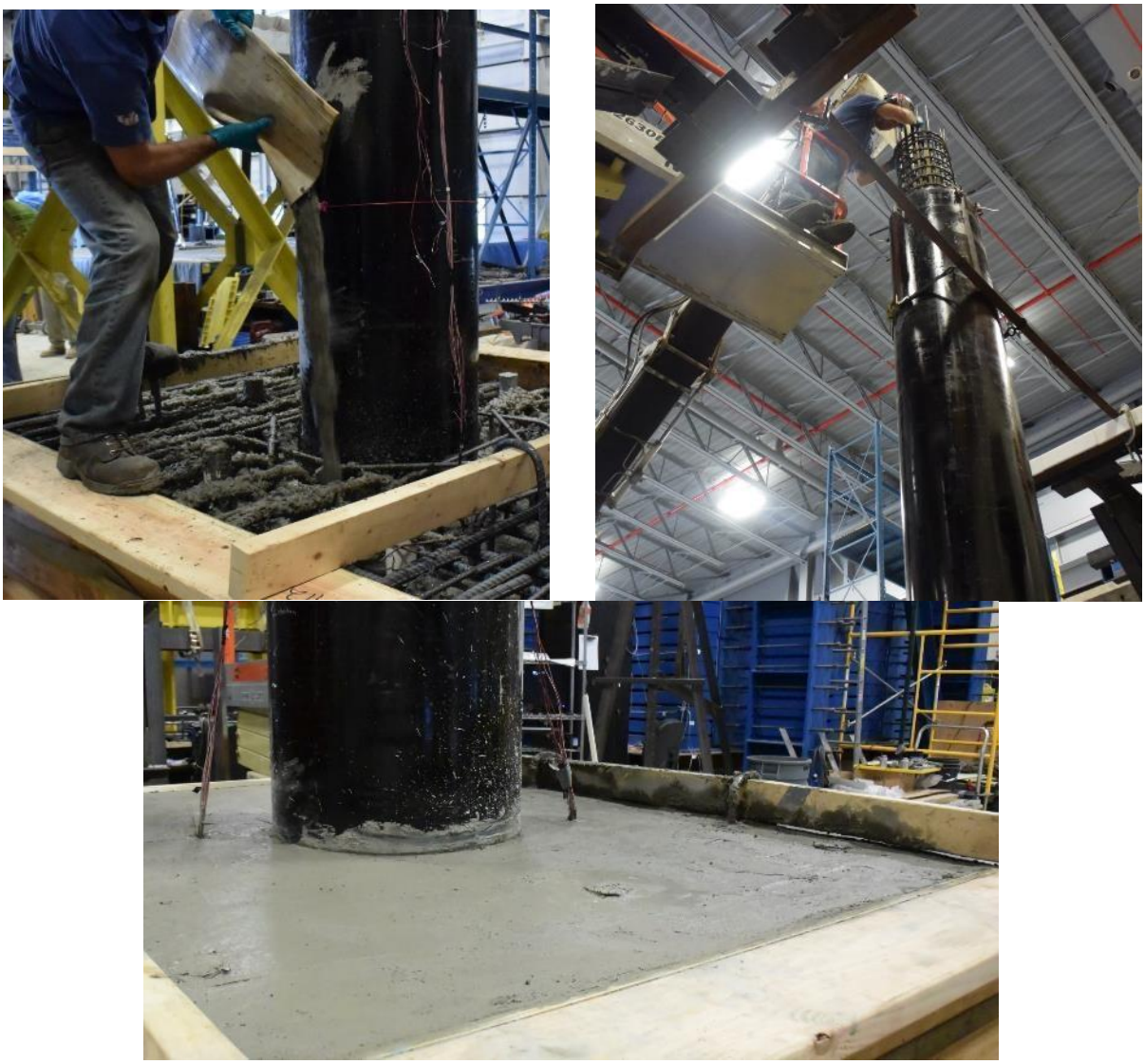

Figure H-17: Self-consolidating concrete poured in the foundation and RCFST shaft part.

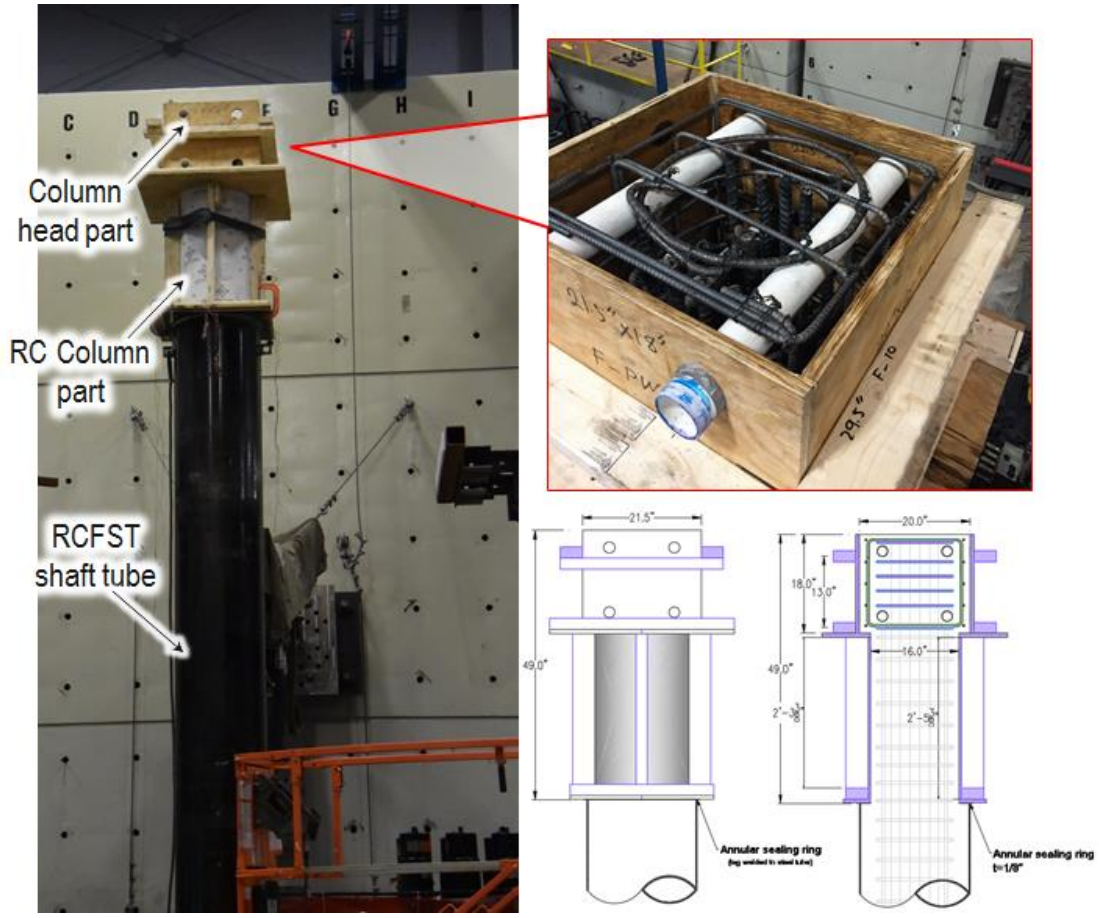

Figure H-18: Reinforced concrete column part's formwork placement.

Figure H-19: Reinforced concrete column part concrete pour and vibration.

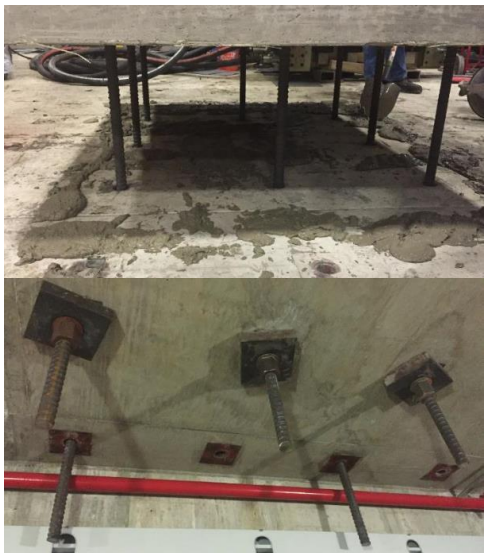

Figure H-20: Specimen fixing on the strong floor using post-tensioned DYWIDAG bars, showing bars when foundation was uplifted to place hydrostone, and bars tied to underside of strong floor.

H.1.5.2 Specimen S2R

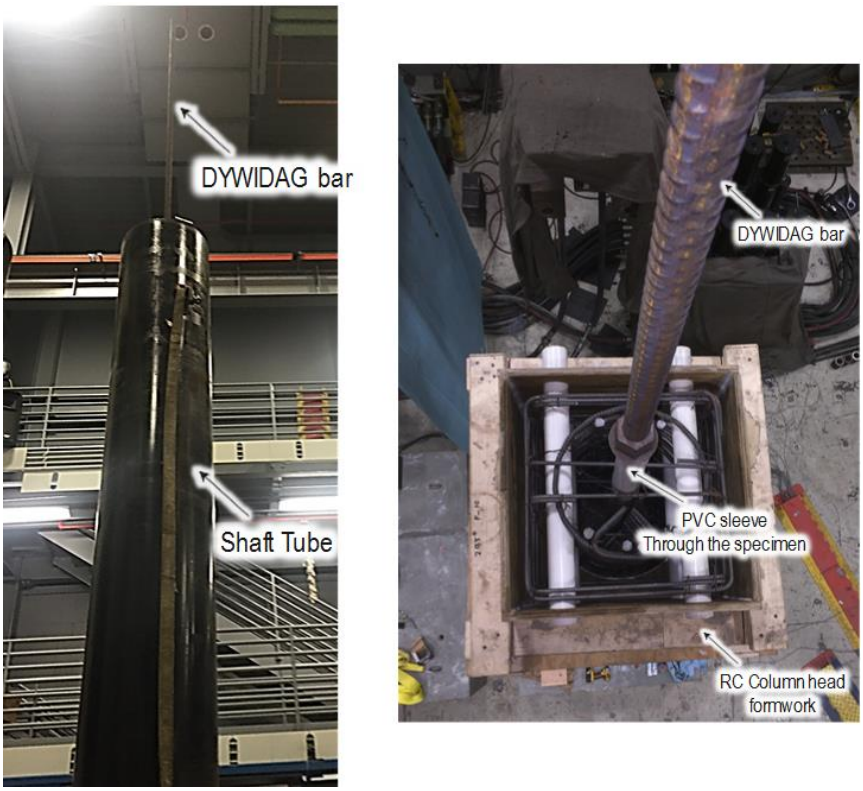

Figure H-21: DYWIDAG bar placement through the axial axis of Specimen S2R.

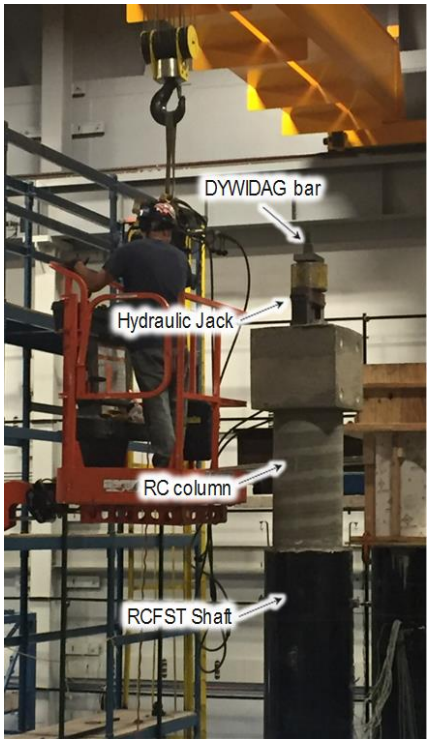

Figure H-22: Pre-tensioning the axial DYWIDAG using hydraulic jack in Specimen S2R.

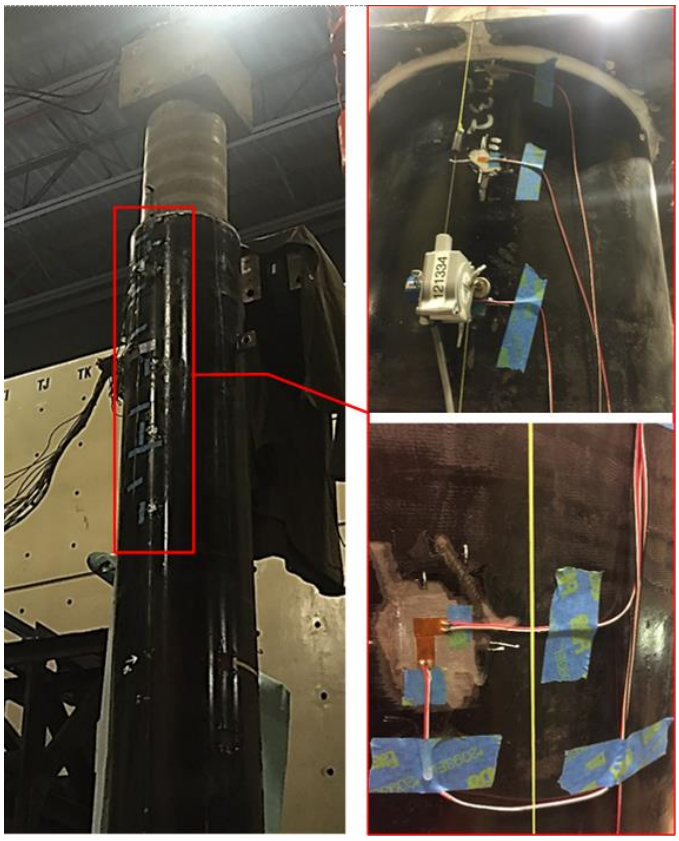

Figure H-23: Instrumentation at the top of the shaft in Specimen S2R.

H.1.5.3 Specimens S3 and S4

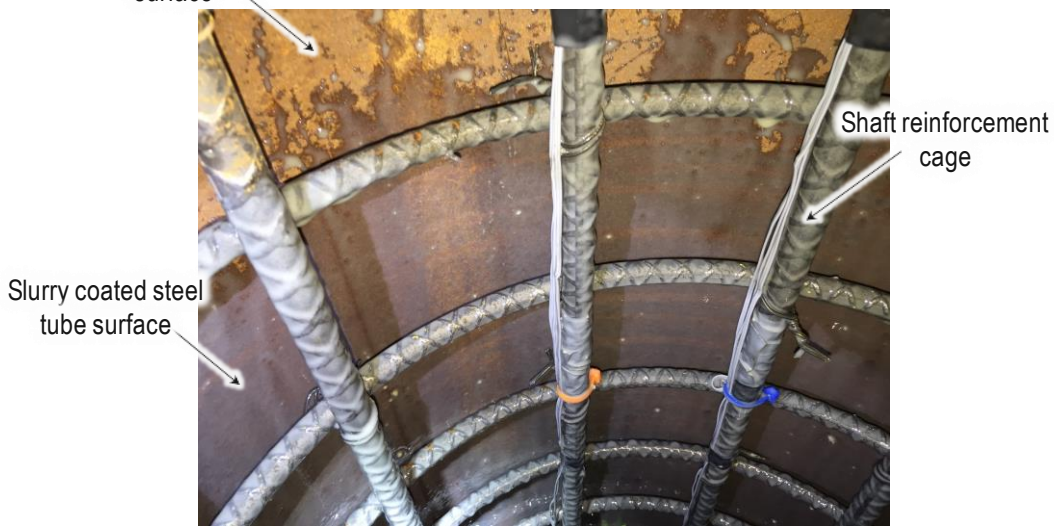

Figure H-24: Applying bentonite slurry to Specimen S3.

TECHNICAL DATA

PREMIUM GEL®

API BENTONITE

DESCRIPTION

PREMIUM GEL is a 200 mesh, 90 bbl yield sodium bentonite for freshwater drilling, slurry walls, and tunnel boring. PREMIUM GEL complies with API 13A Section 9, Specifications for Drilling Fluid Materials.

RECOMMENDED USE

May be used for all types of freshwater mud rotary drilling where higher solids are desired. PREMIUM GEL can also be used as a seal for earthen structures, slurry trenching, tunnel boring, and foundation drilling.

CHARACTERISTICS

- Cools and lubricates bit
- Mixes quickly and easily
- Reduces fluid loss into the formation
- Removes cuttings
- Stabilizes borehole

MIXING AND APPLICATION:

Mixing ratios are based on the use of freshwater; water purity will affect bentonite performance. For best results, acidic and hard make-up water should be pretreated with SODA ASH to a pH of 8.5-9.5. Add PREMIUM GEL slowly through jet/hopper mixer.

PACKAGING

50 lb (22.7 kg) bag, 48 per pallet, 100 lb (45.4 kg) bag, 35 per pallet, 1 ton or 2 ton supersacks, or bulk. All pallets are plastic-wrapped.

DRILLING FLUID AND SLURRY TRENCHING - PREMIUM GEL MIXING RATIO IN POUNDS (KG) PER 100 GALLONS (380 LITERS) OF WATER		
Condition	**Lbs (kg) of PREMIUM GEL**	**% Solids**
Normal Conditions	30 - 50 lbs (13.5 - 22.5 kg)	3.5 - 5.7%
Sand and Gravel	50 - 70 lbs (22.5 - 31.5 kg)	5.7 - 7.7%
Fluid Loss Control	70 - 80 lbs (31.5 - 36 kg)	7.7 - 8.8%
SLURRY PROPERTIES - 6.04% SOLIDS		
Property	**Typical Value**	**Specification/Procedure**
Viscosity FANN 600 rpm	40 cps	30 cps Min - API 13A Section 9
Viscosity FANN 6 rpm	11 cps	ACC TP-2005
Viscosity FANN 3 rpm	11 cps	ACC TP-2005
Yield - 42 gal bbl of 15 cps slurry/ton	90 to 120 bbl/tn	90 Min - API 13A Section 9
Marsh Funnel, seconds/quart	42 seconds	ACC TP-1014
Apparent Viscosity (AV)	15 to 25 cps	ACC TP-2005
Plastic Viscosity (PV)	9 to 10	ACC TP-2005
Yield Point, lb/100 ft^2	15 to 25 lb/100 ft^2	ACC TP-2005
Filtrate, 30 minutes @ 100 psi, ml	13 to 15 ml	15 ml Max - API 13A Section 9
Filter Cake, in	3/32 in	N/A
pH	9.03	ACC TP-1018
GENERAL PROPERTIES		
Property	**Typical Value**	**Specification/Procedure**
Moisture %	7.4%	ACC TP-2006
Free Swell	28	ASTM D-5890
Plate Water Absorption	622.80%	ASTM E946-92
Specific Gravity	2.5	Generally Recognized
Bulk Density Non-compacted	53 lbs/ft^3	ACC TP-1005
Bulk Density Compacted	72 lbs/ft^3	ACC TP-1005
Grit % (<75 micron)	3.2%	4.0% Max - API 13A Section 9
Particle Sizing	70% Min passing #200 mesh sieve	ACC TP-1015

Figure H-25: Technical data of bentonite provided by the supplier.

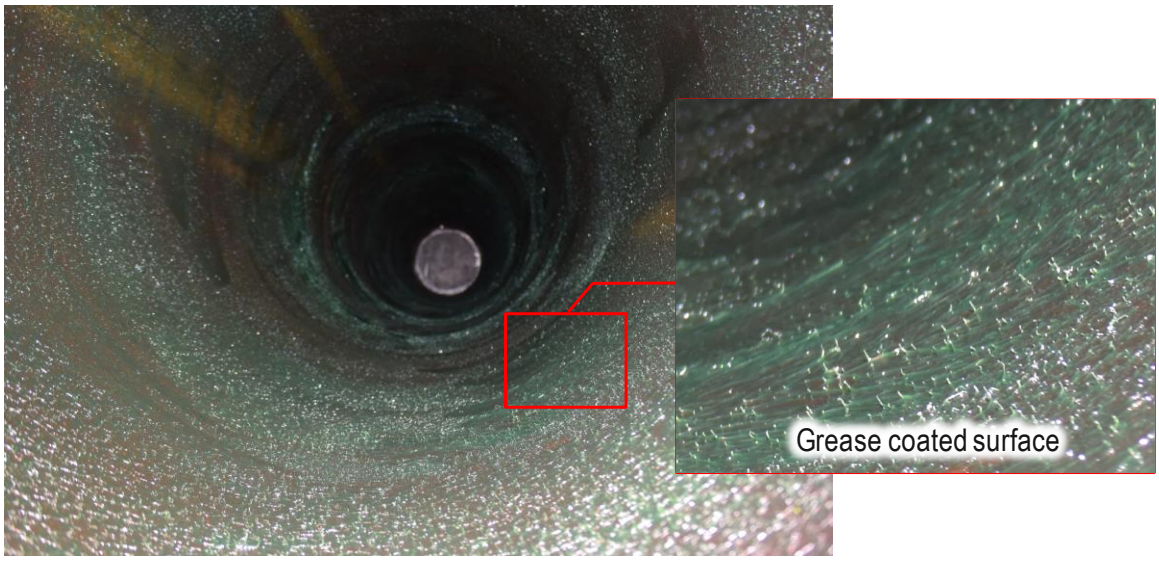

Figure H-26: Greased interior surface of the steel tube of Specimen S4.

H.1.5.4 Specimen S5

Figure H-27: Foundation rebar cage place in the foundation form work for Specimen S5.

Figure H-28: Rebar strain gages and shaft rebar cage placement in Specimen S5.

Figure H-29: Specimen S5's steel tube placement in its foundation rebar cage.

Figure H-30: Specimen S5's reinforced concrete column rebar cage placement at the top of the shaft before concrete pouring.

Figure H-31: Concrete pouring for foundation and shaft parts of Specimen S5.

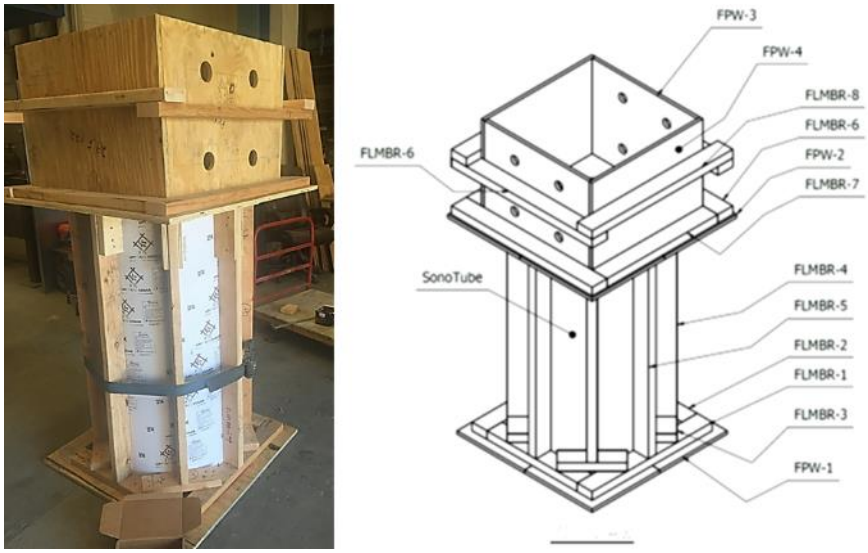

Figure H-32: Specimen S5's reinforced concrete column and column head parts form work.

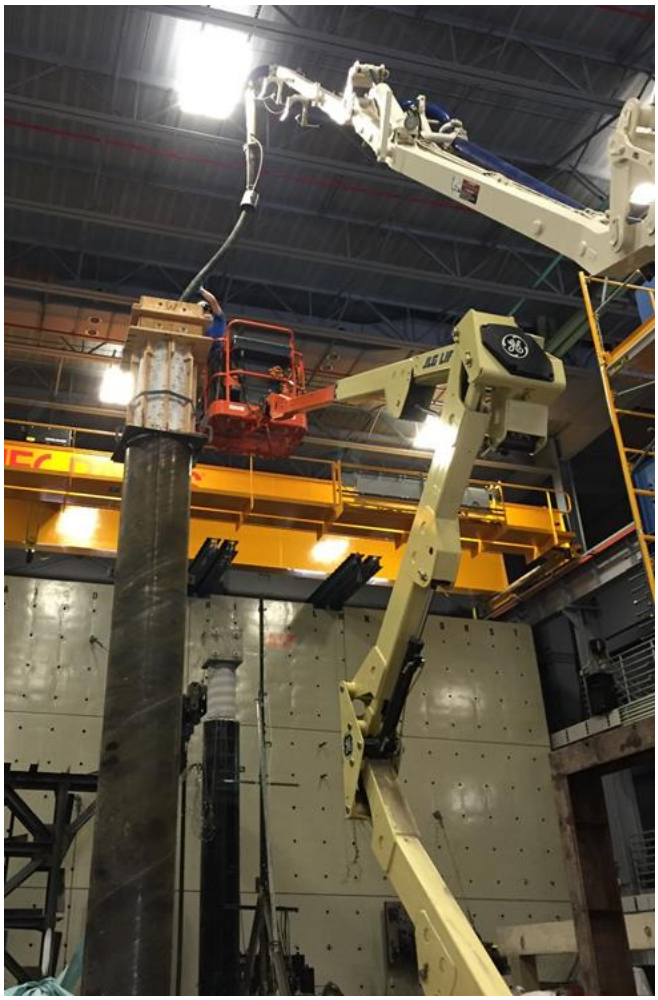

Figure H-33: Concrete pouring for reinforced concrete column and column head parts of Specimen S5.

Figure H-34: Moving Specimen S5 to test location.

H.1.5.5 Specimen S6R

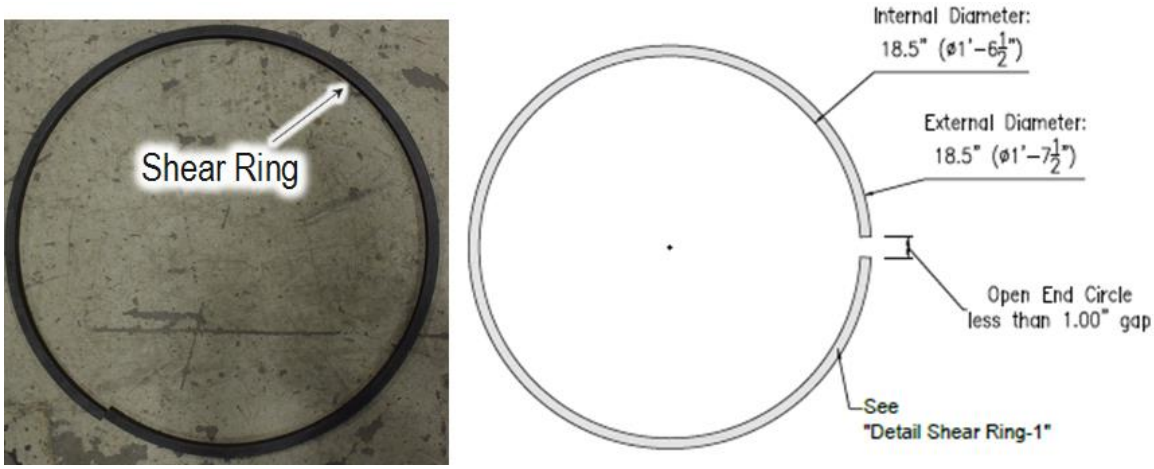

Figure H-35: Shear rings used as shear transferring mechanism in Specimen S6R.

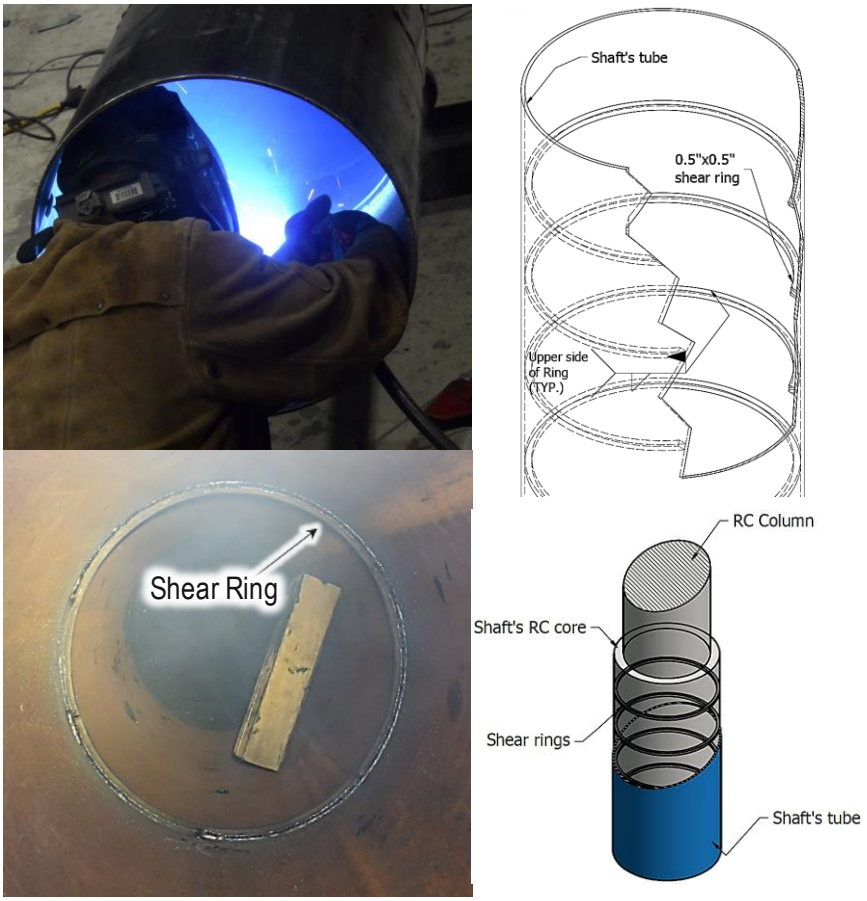

Figure H-36: Shear rings welding at the top of the shaft in Specimen S6R.

Figure H-37: Greased coating at the interior surface of the steel tube in Specimen S6R.

H.2 Shear specimens

H.2.1 General

Welding of the shear specimens and stiffener modules were done by a fabricator and shipped to the SEESL, where concrete casting and the rest of the test preparation were performed. In order to achieve the minimum variation in material properties among the 12OD shear specimens, all of them were constructed from a single HSS12.75x0.25 steel tube and a single batch of $4ksi$ normal weight ready-mix concrete delivered by a mixer truck. As the length of the ordered HSS steel tube was about $12in.$ shorter than the total length needed to build all the 12OD shear specimens, it was decided to make the hollow shear specimen 6 $in.$ shorter at each end (see Figure H.38). Note that, finite element analyses were conducted to verify and ensure that this modification would not change the behavior and results for that particular specimen (mainly because the stiffener modules were designed for concrete-filled 12OD shear specimens, which were much stronger than needed for the specimen consisting of a hollow steel tube alone).

Figures H.39 and H.40 show the constructed 12OD and 16OD shear specimens, respectively. Figure H.41 shows the constructed stiffener modules for 12OD shear specimens. The assembled 12OD shear specimen and its ready-to-test state on the pantograph is shown in Figure 2.112. The $4ksi$ normal weight concrete for the 12OD shear specimens was cast indoor, and the concrete was vibrated during the casting process. Note that 88 and 40 high strength A490 bolts were used in the assembly of each 12OD and 16OD shear specimen test setup, respectively. All the bolted connections were designed as slip-critical. All the bolts were lubricated before each test and torqued to at least 70% of their yield strength values. A hydraulic power torque was used for tightening the bolts.

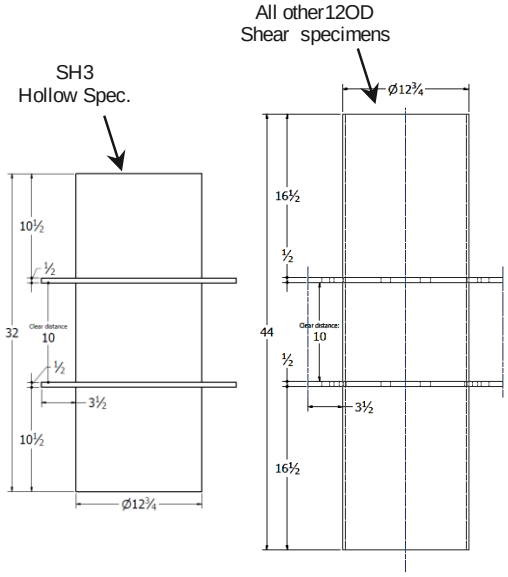

Figure H.38: Comparison of length of the steel tube of SH3 specimen and other 12OD shear specimens.

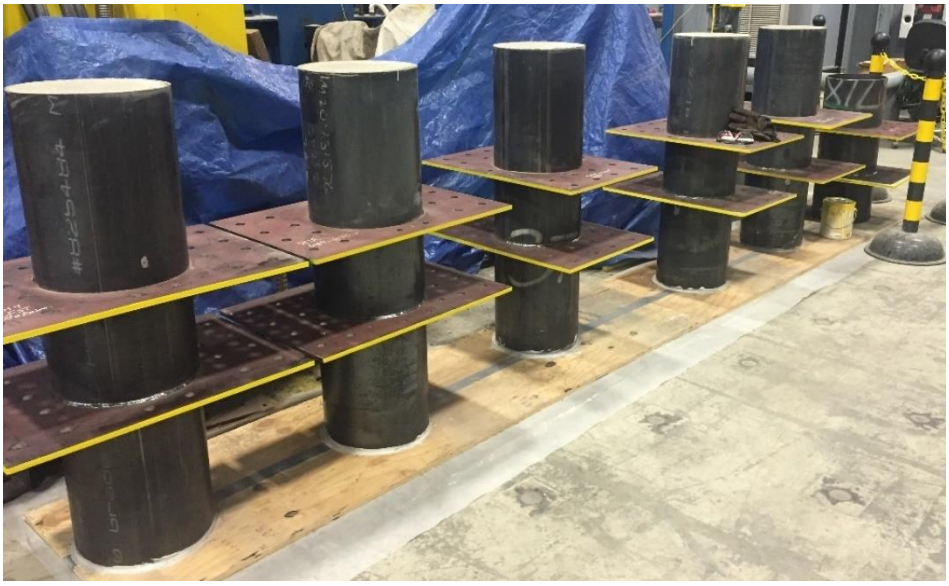

Figure H.39: Constructed 12OD shear specimens

Figure H.40: Constructed SH2 (16OD) shear specimens

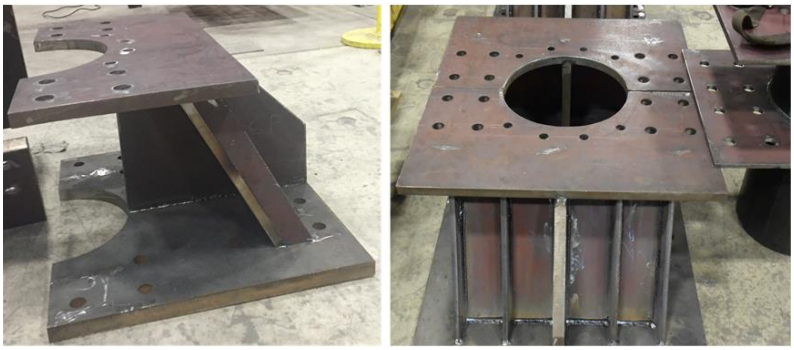

Figure H.41: Constructed stiffener modules for 12OD shear specimens

Figure H.42: The assembled 12OD shear specimen and its ready-to-test state on the pantograph.

H.2.2 Instrumentation

The measuring devices that were used in the shear tests, including strain gauges, string pots, and Krypton system, are listed in Table H.4. There was also an internal load-cell and displacement sensor in the actuator. Figure H.43 shows the location of the strain gauges and string pots on the test setup. The locations of the krypton LEDs are shown in Figure H.44. Detailed drawings of the instrumentation plan for shear tests are provided in Appendix M.

Table H.4. Number of instruments used for each shear specimen.

Specimen	Quantity		
	Strain Gauge	String Pot.	Krypton LED
SH2	10	6	13
SH3	10	6	27
SH4	10	6	27
SH5	10	6	27
SH6	10	6	19
SH7	10	6	19
SH1R	10	6	19

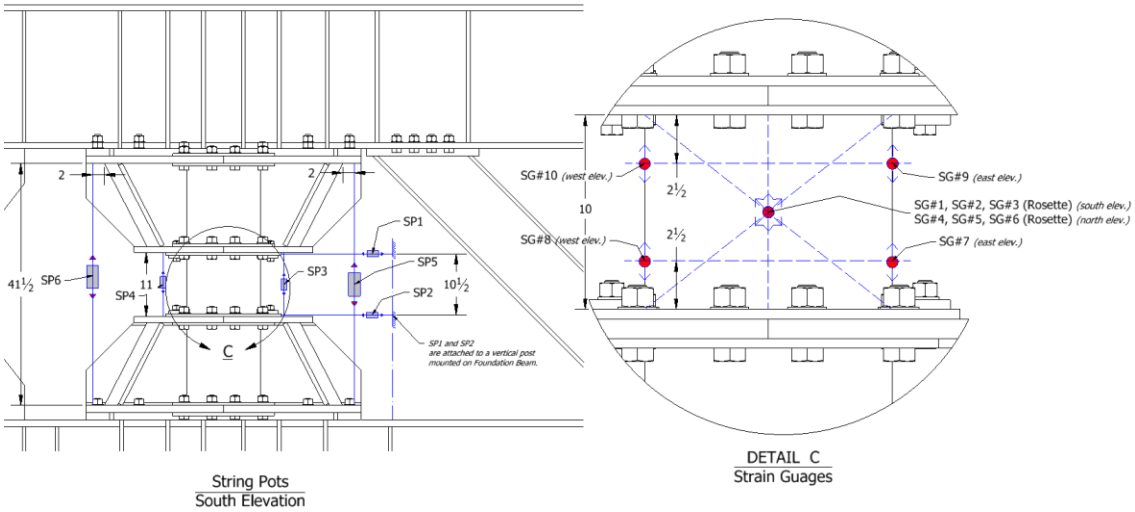

Figure H.43: Location of strain gauges and string-pots on the shear test setup.

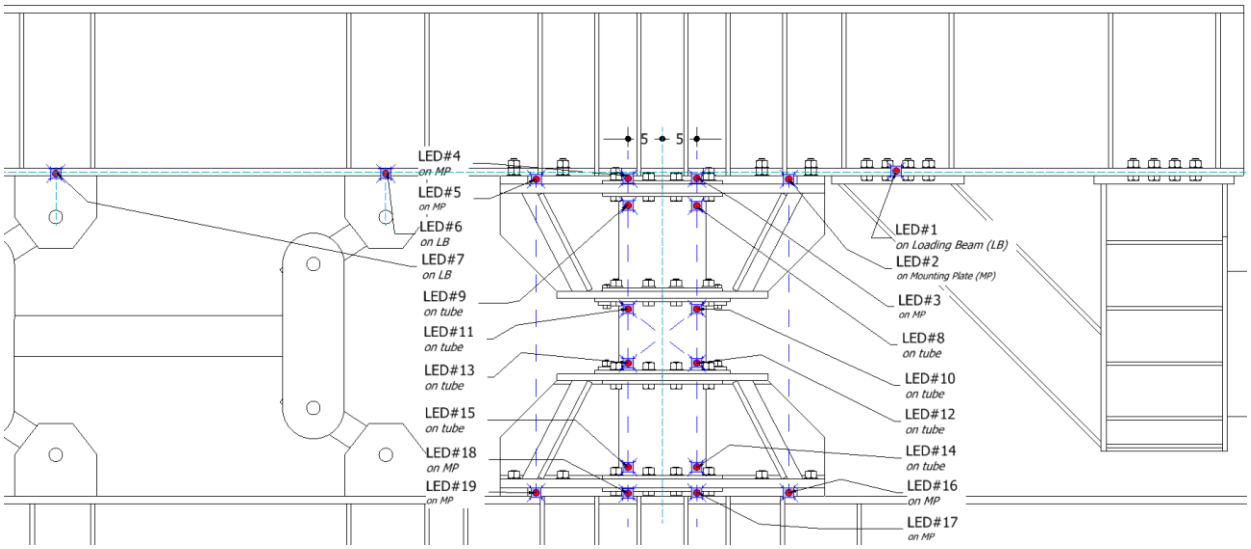

Figure H.44: Location of Krypton LEDs on the shear test setup.

H.2.3 Material properties of shear specimens

The properties of the steel tube, concrete, and rebars used in the shear specimens are presented in this section. The measured uniaxial stress-strain relationships of the steel tube coupons are shown in Figure H.45. The average uniaxial stress-strain curve of the steel tube part of each specimen is shown in Figure H.46. Measured uniaxial stress-strain relationships of the concrete for the 12OD shear specimens are shown in Figure H.47. Concrete cylinder tests were performed after testing the first and last 12OD concrete-filled shear specimens, and the average strength was used as the concrete strength (variation of concrete strength between the first and last specimen was not significant (see Figure H.47)). The average measured material properties of the steel tube and concrete for each shear specimen are presented in Table 2.11.

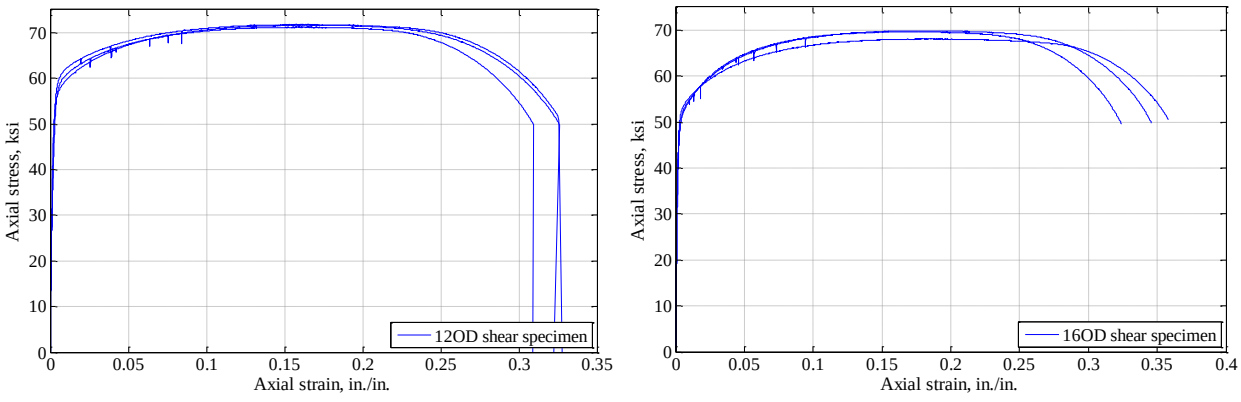

(a) (b)

Figure H.45: Measured uniaxial stress-strain relation of: (a) 12OD shear specimens steel tubes; (b) 16OD shear specimen steel tube.

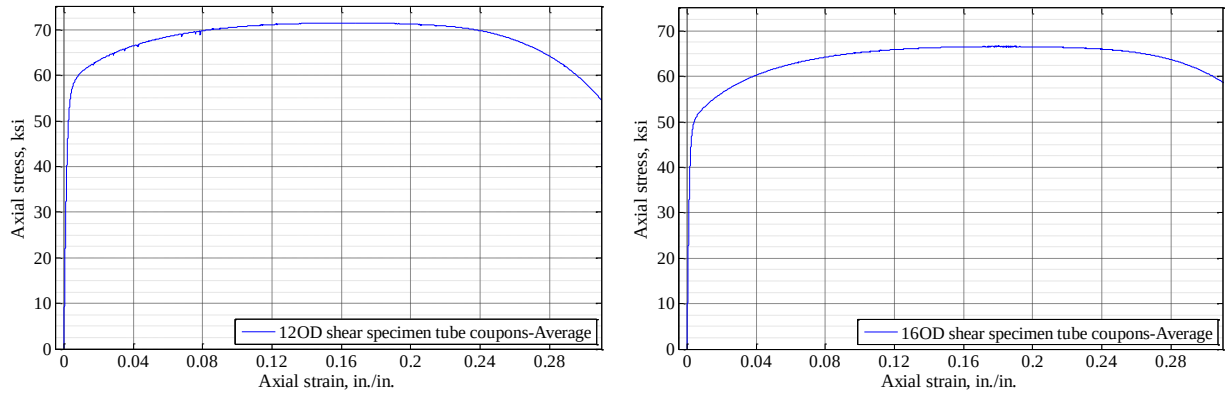

(a) (b)

Figure H.46: Average uniaxial stress-strain relation of: (a) 12OD shear specimens steel tubes; (b) 16OD shear specimen steel tube.

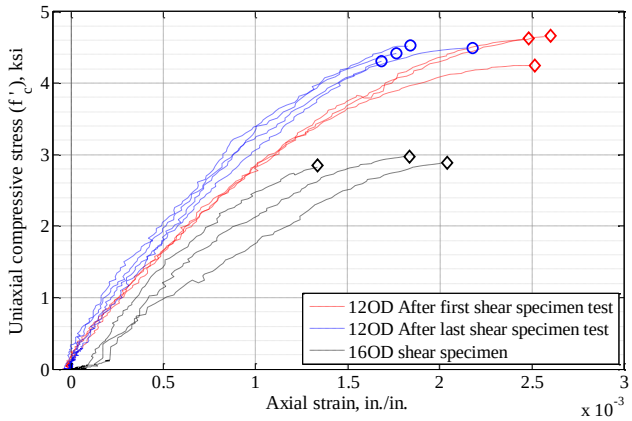

Figure H.47: Measured uniaxial stress-strain relation of concrete of the shear specimens.

Table H.5. Average material properties obtained from uniaxial tests for shear specimens.

Shear Specimen	Steel tube				Concrete
	F_y, ksi	ϵ_y, μin./in.	F_u, ksi	E_s, ksi	f'_c, ksi
12OD specimens	58.0	1900	71.5	30100	4.5
16OD specimen (SH2)	50.6	1700	68.3	29000	2.9

APPENDIX I

Test results

I.1 Flexural specimens test results

I.1.1 Cyclic loading protocol

Figure 2.99 shows the cyclic loading protocol proposed in IR2. In this figure, the first 4 cycles are elastic loading, increasing in amplitude up to first yield strength (F_y) of the specimen (i.e., force-controlled cycles). After reaching first yield in the specimen at the end of cycle 4, the protocol calls for continued testing (in displacement-controlled cycles), by subjecting the specimen to displacements amplitudes equal to multiples of the equivalent yield displacement (Δ'_y), with two cycles applied at each displacement amplitude (i.e., at $2\Delta'_y$, $3\Delta'_y$, $4\Delta'_y$, etc.), until the specimen fails. Based on this loading protocol, Specimen S1 was tested under the cyclic displacement protocol shown in Figure 3.1. Displacement amplitudes were chosen according to the calculated first yield (Δ_y=2.2 $in.$) and equivalent yield (Δ'_y=3.4 $in.$) points of a structural model of Specimen S1 that was analyzed in OpenSees. Figure I.3 shows these corresponding points on the pushover curve. In this model, the compressive strength of the concrete cylinders of Specimen S1 that were tested before the specimen test date were used. For the self-consolidating concrete used for the shaft, that cylinder was tested on the 27th day of curing. For the steel tubes and rebar cages, no tension tests were done before the test date and therefore, the material properties (mill certificates) that were provided by suppliers for the delivered materials were used to calculate the load protocol displacement values.

Displacement amplitudes of the initial four cycles were equal to $\pm$0.25, $\pm$0.5, $\pm$0.75, and $\pm$1.0 times the first yield point displacement (Δ_y). After the fourth cycle, displacements continued to be applied as a function of the equivalent yield point displacement (Δ'_y). Amplitude of the displacement cycles increased by an amount equal to Δ'_y with two cycles applied at each displacement amplitude until rupture occurred in the steel tube.

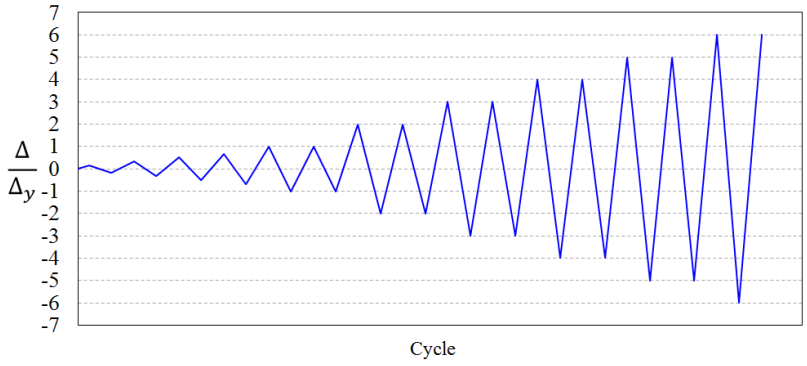

Figure I.1: Cyclic loading history

(a) Cycles 1 to 6

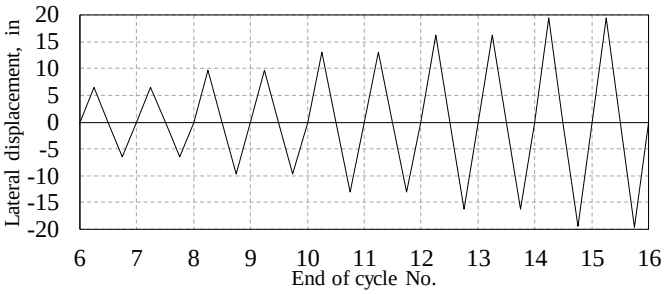

(b) Cycles 7 to 16

Figure I.2: Loading history for Specimen S1: (a) Cycles at displacements up to Δ'_y; (b) Cycles at displacements above that value. .

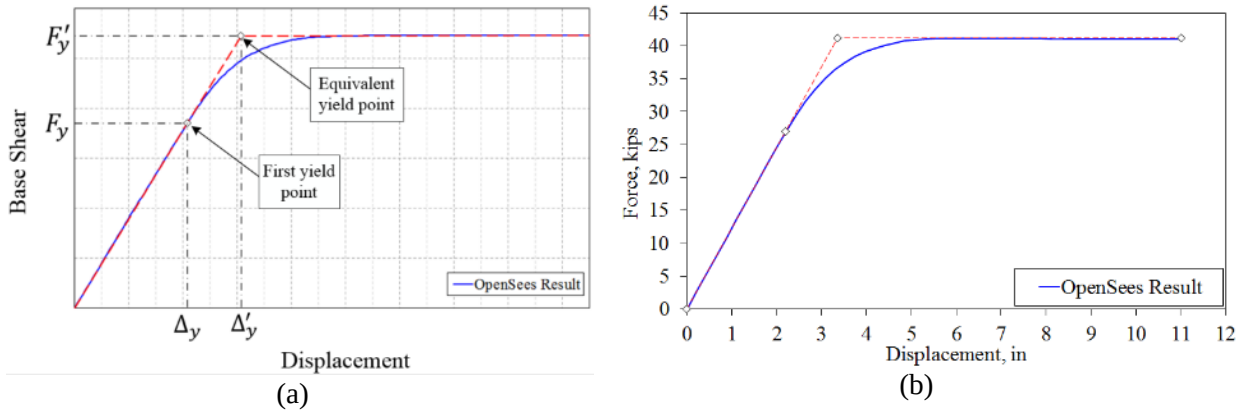

(a) (b)

Figure I.3: OpenSees pushover results for Specimen S1: (a) Definition of first and equivalent points; (b) First and equivalent points.

I.1.2 Force-Displacement relationships of flexural specimens

The experimentally-obtained Force-Displacement curve for the flexural specimens and their backbone curves are shown in Figures 3.2 and 3.3, respectively. The points when some of the key observations were made during the test (corresponding to the onset of visible local buckling, maximum strength, and rupture of steel tube) are marked on these curves. Tables I.1 to I.6 present each cycle's peak displacements at the center of the height of the column head and the force applied by the actuator at those corresponding displacements for each flexural specimen.

For Specimen S1, the maximum strength of the specimen was achieved at the peak positive and negative displacements of the 9th cycle (i.e., C9P = 9.74 *in.* and C9N = -9.90 *in.*), which were $45.50\ kips$ and $-45.39\ kips$, respectively. Local buckling of the specimen started to develop during the 7th cycle and it was observed at the peak positive displacement of the 7th cycle (C7P). Figure I.6 shows the region on the

steel tube where local buckling developed, namely about $2in.$ above the foundation surface on both sides of the steel tube. Comparing the strain at the onset of local buckling with the yield strain (ϵ_y) of the steel tube corresponding to Specimen S1 presented in Table H.2 of Appendix H, it is observed that local buckling of steel tube developed shortly after yielding of steel tube. This observation was also consistently made for all other flexural specimens.

After reaching maximum flexural strength and initiation of local buckling at the bottom of the steel tube, the flexural strength of the specimen decreased upon cyclic displacements at greater amplitude. As shown in Figure 3.2a, this decrease was not significant from the Cycle 9 until the peak positive displacement was reach at the 15th cycle (i.e., C15P=19.49 $in.$).

A first rupture of the steel tube occurred suddenly (and was heard) at negative displacement of -18.28 $in.$ under a lateral load of -39.9 $kips$ during the second half of the 15th cycle close to its peak negative displacement (i.e., C15N= -19.49 $in.$). Figure I.8 shows pictures of the lower part of the specimen at the point C15N when this first rupture occurred. A second rupture on the opposite side (i.e., east side) of the steel tube, occurred during the reversed displacement, at a positive displacement of 15.45 $in.$ during the first half of the 16th cycle under a lateral force of 27.7$kips$. Following the second rupture, the lateral force dropped to 20.9 *kips* at the peak positive displacement of the 16th cycle (i.e., C16P=19.55 $in.$). Figure I.9 shows pictures of the lower part of the specimen at the point C16P. At the peak negative displacement of the 16th cycle (i.e., C16N= -18.80 $in.$), the lateral load reached -17.4$kips$. Pictures of the lower part of the specimen at the point C16N are shown in Figure I.10. Figure I.11 shows the crushed concrete inside the lower part of shaft part and the developed crack interface on the west side of Specimen S1 at the displacement C16N.

As described in Section 2.3.5, Specimen S2R was constructed and tested with a different transition zone (i.e., the RCFST shaft had no internal reinforcing along the reinforced concrete column-to-RCFST shaft transition zone) and under axial load. Specimen S2R, resisted a maximum lateral load of 46.0 $kips$ at the positive peak displacement of the 9th cycle (C9P) and -46.54 *kips* at the negative peak displacement of the 11th cycle (C11N). The development of local buckling at the bottom of the steel tube was visually observed at the peak displacement of the 7th cycle (C7P= +6.73 $in.$). At this point, specimen resistance was 43.74 *kips*, which is 95% of the maximum lateral load resisted by the specimen. Figure I.12 shows the development of local buckling at the lower part of the steel tube for different peak displacements. Comparing the experimentally obtained strains at the buckling zone of the steel tube with its yield strain shows that the buckling developed after yielding (see Figure I.13). First rupture of the steel tube occurred on the east side of the steel tube during first half of the 16th cycle at a positive displacement of 17.5 $in.$ under a lateral load of 35 $kips$. Upon load reversal, the west side of the steel tube ruptured as the displacement reached -16.6 $in.$ under a lateral load of -31.2 $kips$. It was observed that the steel tube started to tear due to accumulative plastic strain at the points of highest curvature along the buckled zone. It appeared that when cracking initiated locally, it was not through the entire thickness of the tube, but this could not be verified by measurements. This might have created a progressive reduction in the effective thickness of the steel tube before through-thickness fracture eventually developed in the steel tube. Figure I.14 shows the tearing of the steel tube that was visually observed at the C14P and C14N points on the east and west sides of the steel tube, respectively. Figures I.15 and I.16 show the ruptured steel tube at the east and west sides of the steel tube, respectively. It was observed that even in the absence of internal reinforcing over the middle part of the RCFST shaft, forces were able to transfer from the reinforced concrete column part to the shaft part and the shaft was still able to develop its theoretical plastic moment. This suggests that the load transferring mechanism that is described in Section 2.2.12.1 (Page 63 of the main report) could be used as an alternative transition zone design.

Specimen S3 had bentonite slurry at the interior surface of the steel tube. The objective of testing this specimen, was to investigate the effect of having a bentonite-coating on the interface of the steel tube and core concrete of the RCFST shaft. Specimen S3, resisted a maximum lateral load of 38.3 $kips$. First buckling was observed at C7P and rupture happened at the bottom of the steel tube on the east side at first half of the 15th cycle at a positive displacement of 23.8 $in.$ The slippage of the concrete core with respect

to the steel tube at the shaft part due to reduced interface friction by the bentonite coating was measured during the test. However, the amount of slippage was relatively small (particularly when compared to that measured for Specimen S4 which had a grease coating, as will be shown later). Slippage comparisons for different specimens are presented in Section I.1.3.2 of the report. Note that at end of the Specimen S3 test and after rupture of the shaft tube, it was observed that the concrete at the bottom of the shaft had some moist areas, which had not been observed in other tested specimens (see Figure I.17). This was observed through the developed crack and in the concrete that fell out of the steel tube through the cracked area. The moist concrete was most probably caused by the presence of the bentonite slurry in the pipe. This was also observed in other small areas on the surface of the concrete core after cutting open a part of the steel tube at the bottom of the shaft. This could have affected, to some degree, the ability of friction forces to develop at the steel-tube to concrete interface in those areas, but not sufficiently to prevent attainment of the plastic moment of the composite section, as will be discussed in Section I.1.2.2. Figure I.18 shows the condition of the concrete-to-steel tube interface of Specimen S3 after the test where part of the steel tube has been removed.

Specimen S4 was built with a grease coating at the interior surface of the steel tube. The objective of testing this specimen was to investigate the non-composite behavior of the RCFST shafts, which according to finite element analyses done in the analytical program could happen when significant friction force cannot develop at the interface of the steel tube and the concrete core. Specimen S4 resisted a maximum force of +43.7 $kips$ at the peak positive displacement of the 9th cycle (i.e., C9P). Initiation of local buckling development was observed at the 7th cycle. Rupture at the bottom of the steel tube occurred at the east side of the tube during the first half of the 16th cycle, at a positive displacement of +16.4 in. Slippage of the concrete core with respect to the steel tube at the shaft part was visually observed from the 12th cycle. Significantly more slippage developed than what was observed in Specimen S3 (with bentonite coating). The measured slippage values are presented in Section I.1.3.3 of the report.

Specimen S5, was built with a 30 in. outside diameter spiral-welded steel tube with a D/t ratio of 96. The objective of testing this specimen was to investigate the effect of diameter and thickness of the steel tube as well as the effect of spiral weld on the composite behavior of the RCFST shafts. Specimen S5 resisted a maximum lateral load of 83.1 $kips$ at the peak positive displacement of 11th cycle. Local buckling was visually observed at the 7th cycle. The actuator's maximum stroke of 20 in. was reached at the 11th cycle. Therefore, testing continued with cycles of same displacement amplitude until failure of the specimen. Maximum flexural strength of the specimen reduced progressively after the 11th cycle and failure occurred by rupture of the steel tube at the bottom of the RCFST. First rupture happened just prior to reaching the maximum negative displacement during the 18th cycle (i.e., C18N) at a negative displacement of -20.2 in. on the west side of the steel tube. Rupture on the east side occurred during the following displacement half-cycle, toward the maximum positive displacement of 19th cycle, at a displacement of +16.6 in. Testing continued for an additional cycle, after which the crack had propagated to a length of 30 in. on the west side, and 22.5in.. on the east side of the tube.

The objective of testing Specimen S6R was to investigate the possibility of developing the full composite strength of the RCFST shaft by means of a shear transfer mechanism (i.e., the rings) in the absence of adequate friction at the concrete-to-steel tube interface. Specimen S6R was constructed with a thick coating of grease on the interior surface of the steel tube, and with shear rings welded at the top of the steel tube. This specimen resisted a maximum lateral load of 42.8 $kips$ at the peak positive displacement of the 9th cycle (i.e., C9P). Initiation of local buckling was observed at the 7th cycle, and rupture at the bottom of the steel tube occurred at the west side of the tube during second half of the 15th cycle at a negative displacement of -17.2 in. No visible slippage at the interface was observed during the test.

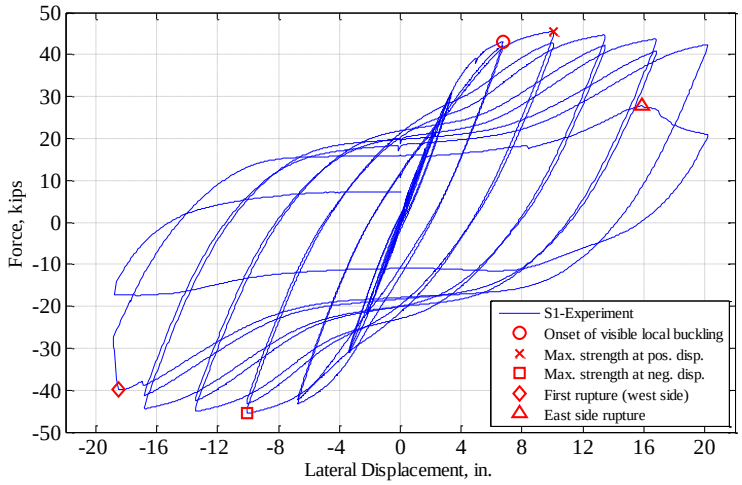

(a)

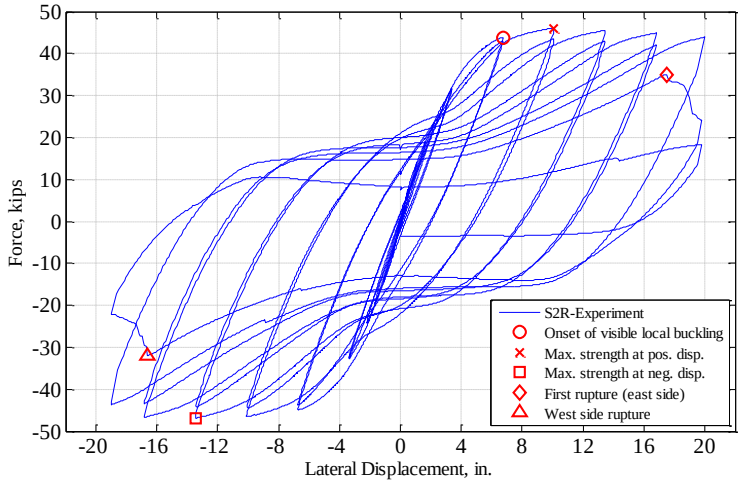

(b)

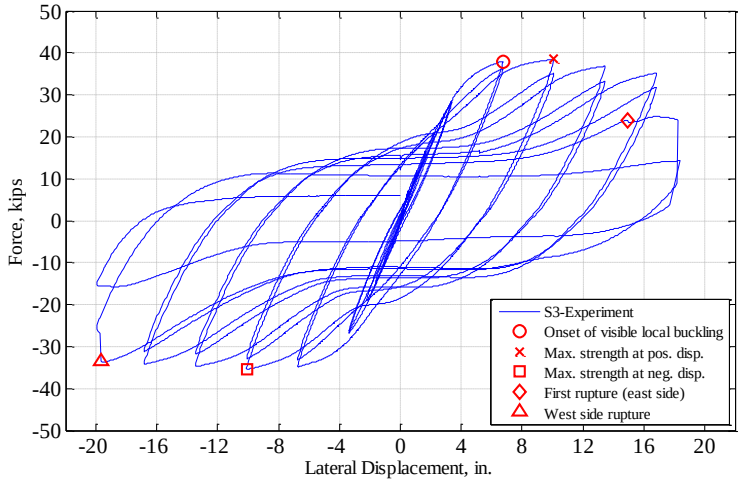

(c)

Figure I.4: Force-Displacement curve measured from test of Specimen: (a) S1; (b) S2R; (c) S3; (d) S4; (e) S5; (f) S6R.

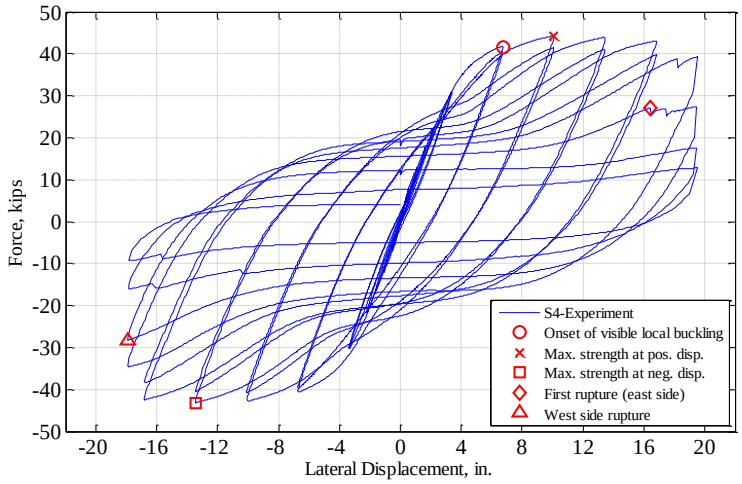

(d)

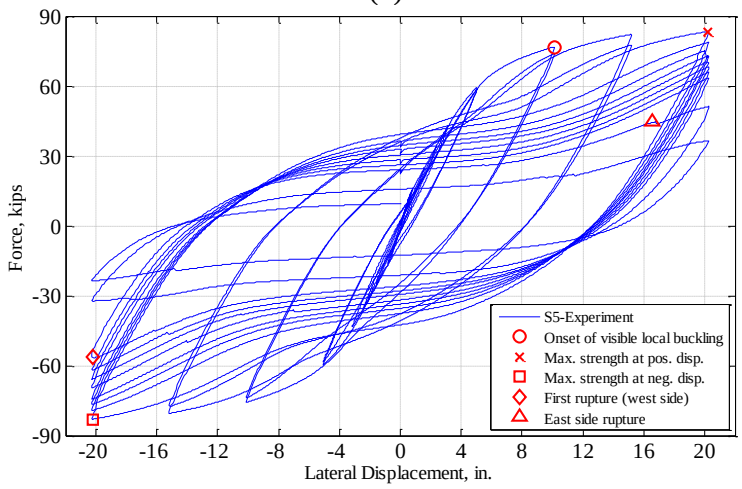

(e)

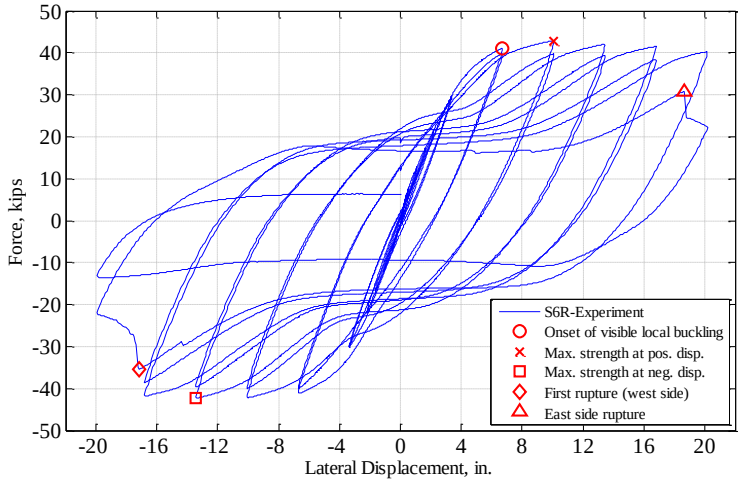

(f)

Continued Figure 3.2: Force-Displacement curve measured from test of Specimen: (a) S1; (b) S2R; (c) S3; (d) S4; (e) S5; (f) S6R.

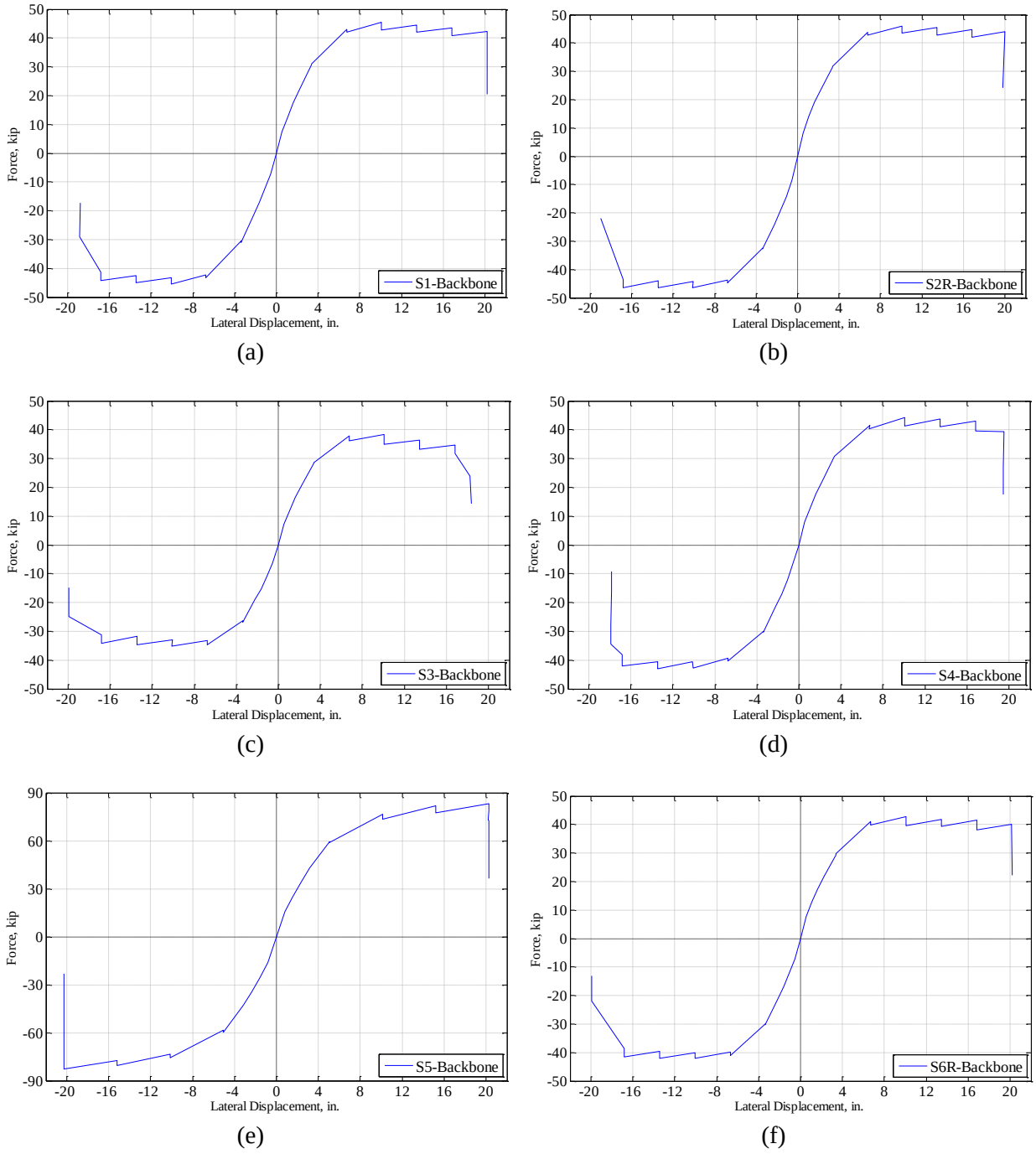

Figure I.5: Force-Displacement backbone curve for Specimen: (a) S1; (b) S2R; (c) S3; (d) S4; (e) S5; (f) S6R.

Table I.1: Peak displacements and corresponding forces for Specimen S1.

Cycle	Label	Displacement, *in.*	Force, *kips*	Cycle	Label	Displacement, *in.*	Force, *kips*
1	C1P	+0.52	7.45	9	C9P	+9.74	45.50
	C1N	-0.53	-7.14		C9N	-9.99	-45.39
2	C2P	+1.06	12.36	10	C10P	+9.74	42.79
	C2N	-1.06	-11.99		C10N	-10.00	-43.32
3	C3P	+1.55	17.27	11	C11P	+13.00	44.65
	C3N	-1.59	-16.92		C11N	-13.35	-45.04
4	C4P	+2.07	21.95	12	C12P	+13.01	42.10
	C4N	-2.14	-21.65		C12N	-13.39	-42.48
5	C5P	+3.18	30.76	13	C13P	+16.28	43.75
	C5N	-3.29	-31.03		C13N	-16.65	-44.39
6	C6P	+3.18	30.97	14	C14P	+16.27	40.86
	C6N	-3.30	-30.64		C14N	-16.67	-41.14
7	C7P	+6.53	42.92	15	C15P	+19.49	42.24
	C7N	-6.63	-43.10		C15N	-18.73	-39.90
8	C8P	+6.54	41.89	16	C16P	+19.55	27.72
	C8N	-6.63	-42.10		C16N	-18.75	-17.40

Table I.2: Peak displacements and corresponding forces for Specimen S2R.

Cycle	Label	Displacement, *in.*	Force, *kips*	Cycle	Label	Displacement, *in.*	Force, *kips*
1	C1P	+0.55	8.25	10	C10P	+10.10	43.41
	C1N	-0.55	-8.38		C10N	-10.10	-44.33
2	C2P	+1.10	14.13	11	C11P	+13.47	45.41
	C2N	-1.11	-14.40		C11N	-13.47	-46.54
3	C3P	+1.65	19.05	12	C12P	+13.46	42.70
	C3N	-1.66	-19.40		C12N	-13.46	-43.93
4	C4P	+2.21	23.51	13	C13P	+16.83	44.62
	C4N	-2.21	-24.19		C13N	-16.84	-46.35
5	C5P	+3.37	31.43	14	C14P	+16.84	41.94
	C5N	-3.37	-32.81		C14N	-16.83	-43.41
6	C6P	+3.37	31.74	15	C15P	+19.97	43.89
	C6N	-3.37	-32.43		C15N	-19.02	-43.41
7	C7P	+6.73	43.74	16	C16P	+19.84	24.06
	C7N	-6.73	-44.79		C16N	-19.00	-21.88
8	C8P	+6.73	42.88	17	C17P	+19.77	18.26
	C8N	-6.73	-43.74		C17N	N/A	N/A
9	C9P	+10.10	46.00				
	C9N	-10.11	-46.49				

Table I.3: Peak displacements and corresponding forces for Specimen S3.

Cycle	Label	Displacement, *in*.	Force, *kips*	Cycle	Label	Displacement, *in.*	Force, *kips*
1	C1P	+0.55	7.29	10	C10P	+10.10	35.01
	C1N	-0.55	-6.34		C10N	-10.10	-32.94
2	C2P	+1.10	11.84	11	C11P	+13.46	36.37
	C2N	-1.10	-10.82		C11N	-13.47	-34.56
3	C3P	+1.65	16.55	12	C12P	+13.47	33.25
	C3N	-1.66	-15.21		C12N	-13.47	-31.85
4	C4P	+2.21	20.72	13	C13P	+16.82	34.77
	C4N	-2.21	-19.06		C13N	-16.84	-34.11
5	C5P	+3.36	28.21	14	C14P	+16.84	31.63
	C5N	-3.37	-26.82		C14N	-16.84	-31.15
6	C6P	+3.36	28.54	15	C15P	+18.26	24.00
	C6N	-3.37	-26.42		C15N	-19.93	-24.78
7	C7P	+6.73	37.83	16	C16P	+18.40	14.25
	C7N	-6.73	-34.73		C16N	-19.91	-14.76
8	C8P	+6.73	36.16				
	C8N	-6.73	-33.11				
9	C9P	+10.10	38.26				
	C9N	-10.11	-35.26				

Table I.4: Peak displacements and corresponding forces for Specimen S4.

Cycle	Label	Displacement, *in*.	Force, *kips*	Cycle	Label	Displacement, *in.*	Force, *kips*
1	C1P	+0.57	7.88	10	C10P	+9.94	41.37
	C1N	-0.50	-7.02		C10N	-10.02	-40.61
2	C2P	+1.11	12.93	11	C11P	+13.26	43.68
	C2N	-1.04	-12.13		C11N	-13.29	-43.14
3	C3P	+1.66	17.66	12	C12P	+13.27	41.15
	C3N	-1.56	-16.91		C12N	-13.36	-40.47
4	C4P	+2.18	22.22	13	C13P	+16.56	43.09
	C4N	-2.12	-21.52		C13N	-16.70	-42.49
5	C5P	+3.34	30.73	14	C14P	+16.58	39.57
	C5N	-3.27	-30.37		C14N	-16.68	-37.34
6	C6P	+3.35	30.19	15	C15P	+19.06	39.30
	C6N	-3.27	-29.99		C15N	-17.81	-33.16
7	C7P	+6.68	41.82	16	C16P	+19.06	27.79
	C7N	-6.65	-40.68		C16N	-17.87	-27.94
8	C8P	+6.69	40.48	17	C17P	+19.06	17.66
	C8N	-6.65	-39.72		C17N	-17.91	-15.54
9	C9P	+9.93	43.20	18	C18P	+19.06	12.82
	C9N	-9.99	-41.85		C18N	-17.91	-8.90

Table I.5: Peak displacements and corresponding forces for Specimen S6R.

Cycle	Label	Displacement, *in.*	Force, *kips*	Cycle	Label	Displacement, *in.*	Force, *kips*
1	C1P	+0.55	7.78	10	C10P	+10.10	39.60
	C1N	-0.55	-7.20		C10N	-10.10	-40.00
2	C2P	+1.10	12.81	11	C11P	+13.46	41.88
	C2N	-1.10	-12.17		C11N	-13.47	-42.06
3	C3P	+1.65	17.27	12	C12P	+13.47	39.38
	C3N	-1.66	-16.96		C12N	-13.47	-39.63
4	C4P	+2.21	21.67	13	C13P	+16.82	41.43
	C4N	-2.21	-21.71		C13N	-16.84	-41.49
5	C5P	+3.36	29.31	14	C14P	+16.84	38.16
	C5N	-3.37	-30.27		C14N	-16.84	-38.54
6	C6P	+3.36	29.68	15	C15P	+18.26	40.07
	C6N	-3.37	-29.95		C15N	-19.93	-21.84
7	C7P	+6.73	41.06	16	C16P	+18.40	22.20
	C7N	-6.73	-41.02		C16N	-19.91	-13.03
8	C8P	+6.73	39.71				
	C8N	-6.73	-39.86				
9	C9P	+10.10	42.82				
	C9N	-10.11	-42.09				

Table I.6: Peak displacements and corresponding forces for Specimen S5.

Cycle	Label	Displacement, *in.*	Force, *kips*	Cycle	Label	Displacement, *in.*	Force, *kips*
1	C1P	+0.79	15.50	11	C11P	+20.27	83.14
	C1N	-0.79	-16.01		C11N	-20.28	-82.90
2	C2P	+1.57	24.72	12	C12P	+20.27	78.66
	C2N	-1.58	-25.25		C12N	-20.27	-78.64
3	C3P	+2.36	34.17	13	C13P	+20.21	73.21
	C3N	-2.37	-34.63		C13N	-20.27	-76.63
4	C4P	+3.15	43.10	14	C14P	+20.27	72.65
	C4N	-3.15	-43.11		C14N	-20.28	-74.24
5	C5P	+5.07	59.44	15	C15P	+20.26	70.06
	C5N	-5.07	-59.70		C15N	-20.27	-69.50
6	C6P	+5.07	58.98	16	C16P	+20.26	68.17
	C6N	-5.07	-58.59		C16N	-20.28	-65.78
7	C7P	+10.14	76.36	17	C17P	+20.27	65.81
	C7N	-10.15	-75.45		C17N	-20.27	-62.15
8	C8P	+10.14	73.54	18	C18P	+20.27	63.36
	C8N	-10.14	-73.63		C18N	-20.27	-54.68
9	C9P	+15.20	81.76	19	C19P	+20.27	51.20
	C9N	-15. 21	-80.41		C19N	-20.28	-32.15
10	C10P	+15.20	77.23	20	C20P	+20.28	36.46
	C10N	-15.21	-77.59		C20N	-20.27	-23.38

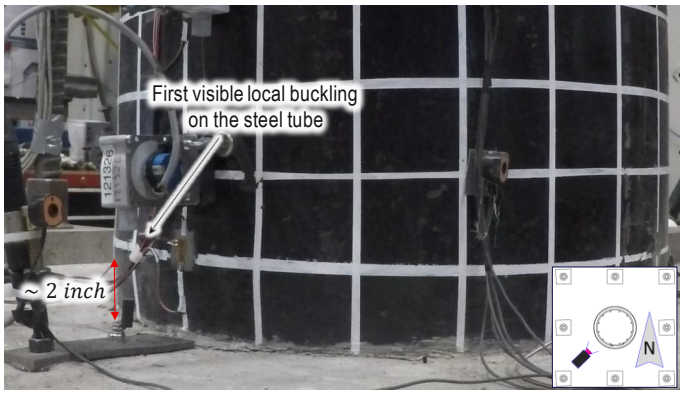

Figure I.6: Visible local buckling observed at C7P for Specimen S1.

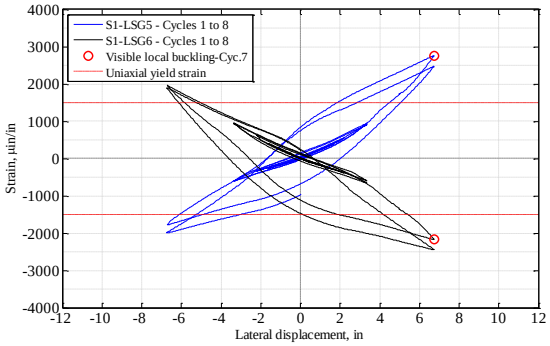

Figure I.7: Strain gage history vs. lateral displacement of LSG#5 (on the east side of the steel tube) and LSG#6 (on the west side of the steel tube) for Specimen S1.

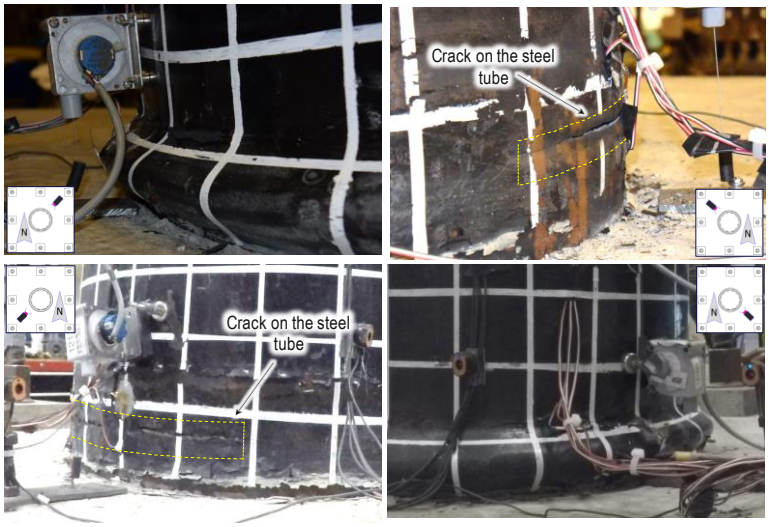

Figure I.8: Lower part of Specimen S1 at C15N

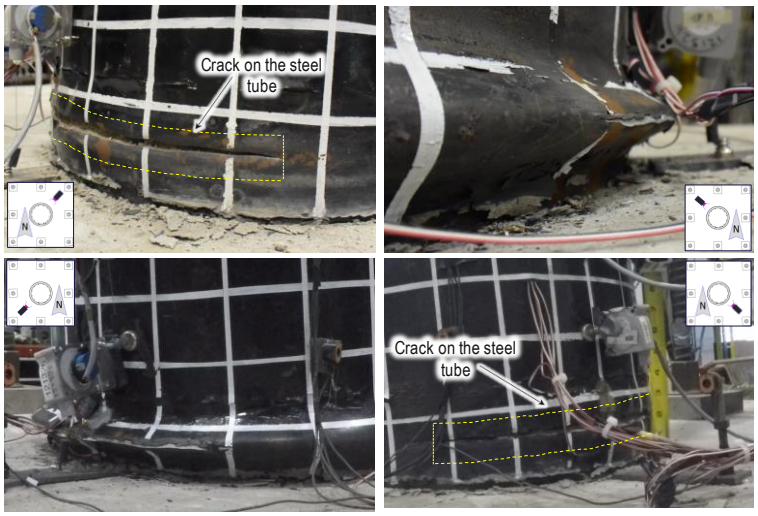

Figure I.9: Lower part of Specimen S1 at C16P

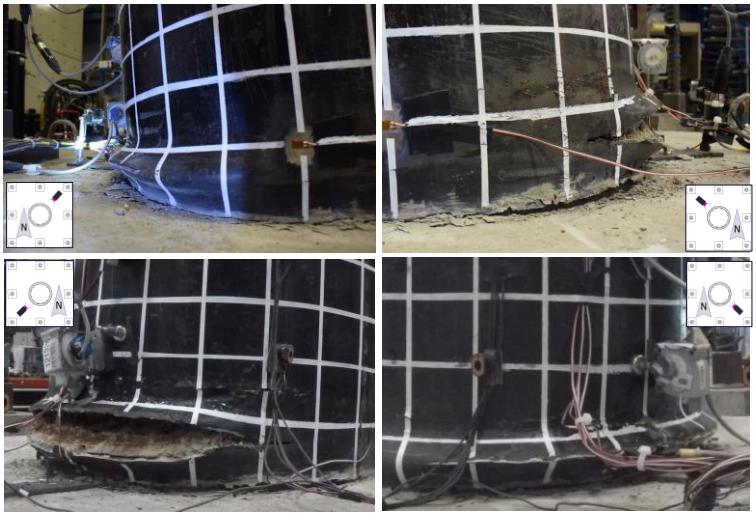

Figure I.10: Lower part of Specimen S1 at C16N

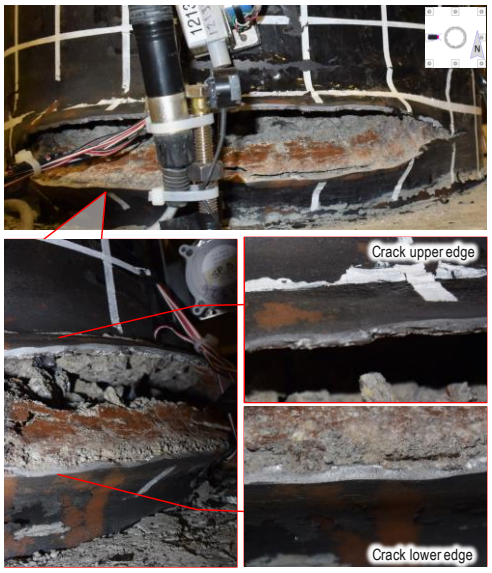

Figure I.11: Interior concrete part of the shaft and crack interface of Specimen S1 at C16N

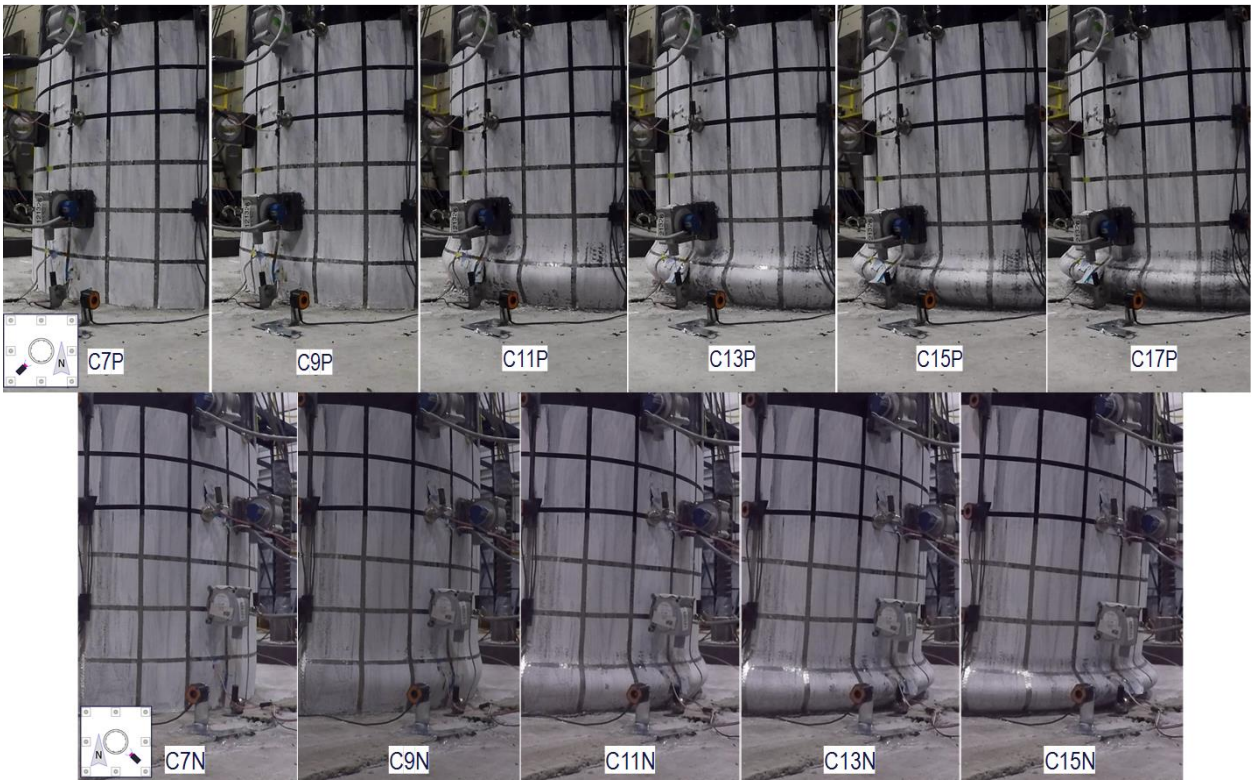

Figure I.12: Development of tube local buckling at lower part of Specimen S2R at different peak displacements.

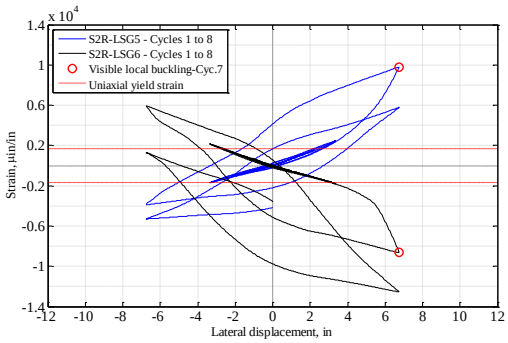

Figure I.13: Strain gage history vs. lateral displacement of LSG#5 (on the east side of the steel tube) and LSG#6 (on the west side of the steel tube) for Specimen S2R.

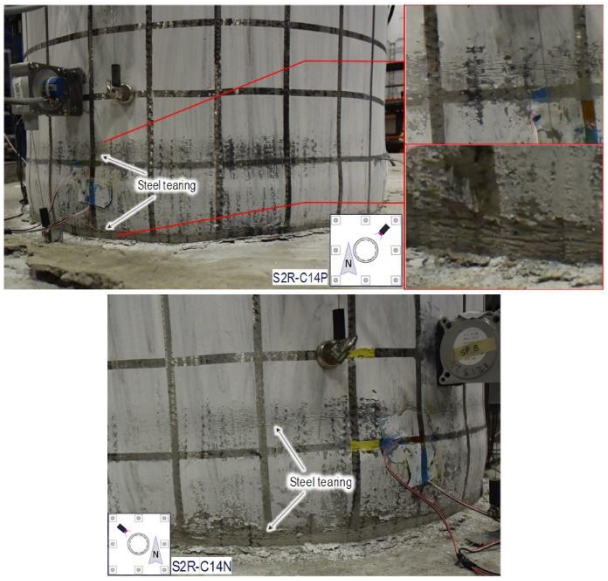

Figure I.14: Tearing of steel tube at the lower part of Specimen S2R before tube rupture.

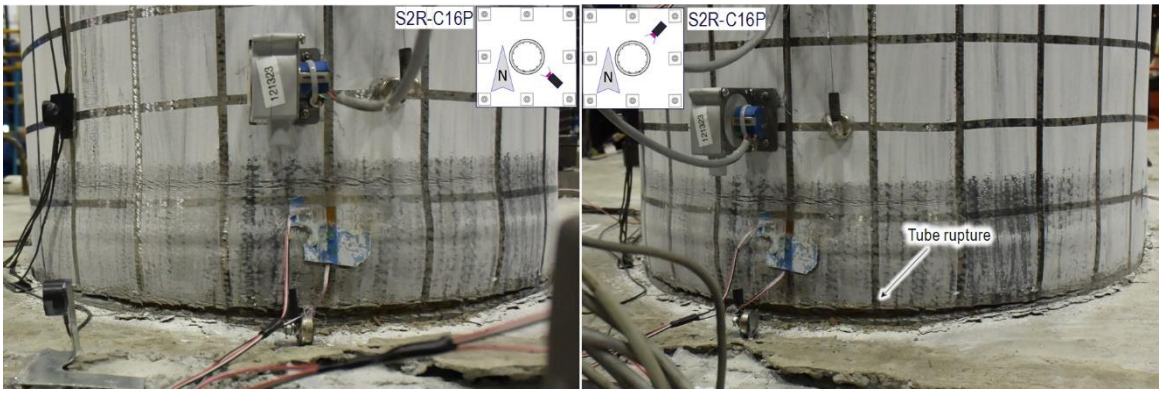

Figure I.15: First tube rupture at east side of Specimen S2R at C16P.

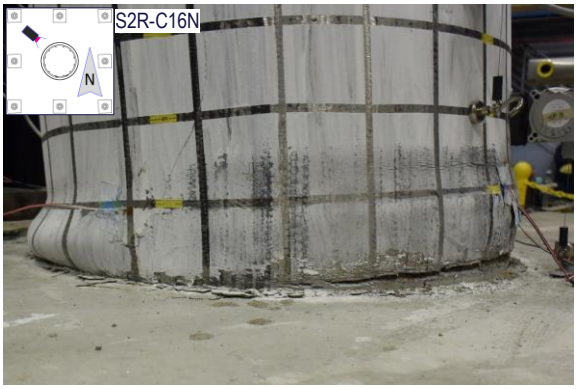

Figure I.16: West side tube rupture at lower part of Specimen S2R at C16N.

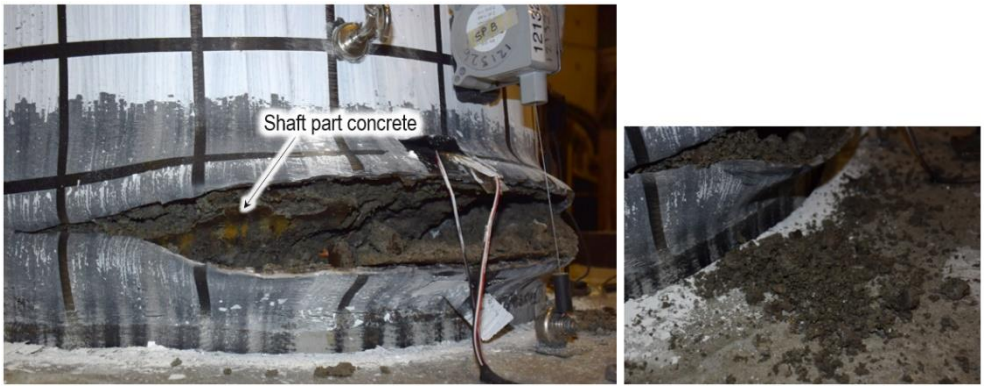

Figure I.17: Specimen S3 shaft part's concrete core condition after rupture of steel tube.

Figure I.18: Specimen S3 (with bentonite) shaft part's interface post-testing condition.

I.1.2.1

Axial load

As discussed in the main body of the report, the axial load on Specimen S2R was applied by means of a DYWIDAG bar that was placed along the specimen and pre-tensioned to about 10% of the axial capacity (squash load) of the reinforced concrete column part. The axial load applied on Specimen S2R and its variation during the cycles is shown in Figure I.19 below. As shown in the figure, axial load on the specimen increased as the lateral displacement at the top of the specimen increases. This happened dominantly because of elongation of the pre-tensioned DYWIDAG bar that occurred in each cycle because the DYWIDAG was placed at the center of the cross-section, where tension developed as the position of the neutral axis shifted away from the center of the cross-section. Figure I.20 shows a schematic view of the distribution of the stresses on the cross-section of the RCFST shaft and the DYWIDAG that was obtained by finite element analysis of Specimen S2R under flexural loading. The progressive increase in axial force throughout the test program was found to be a consequence of the increase in height of the specimen during the inelastic cycles. The increase in height of the specimen was observed in finite element analysis of Specimen S2R, which is discussed in Appendix J. The increase in height of the specimen was not measured during the test. As shown in Figure I.19, the values of the axial load varied between 92.6$kips$ and 143.0$kips$ (i.e., peaking at approximately 15% of the axial capacity of the reinforced concrete column).

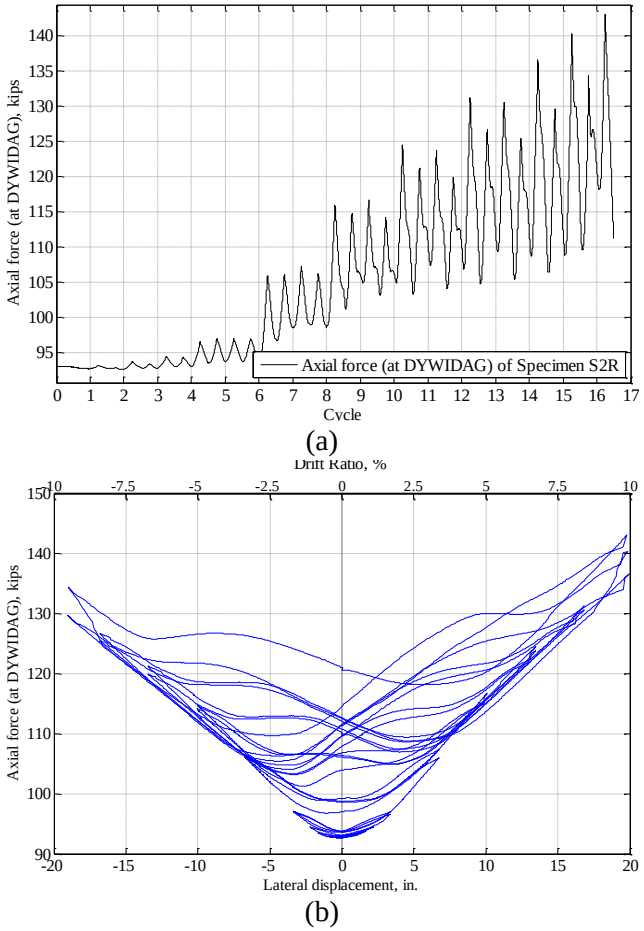

Figure I.19: Specimen S2R's applied axial load versus: (a) Cycles; (b) Lateral displacement.

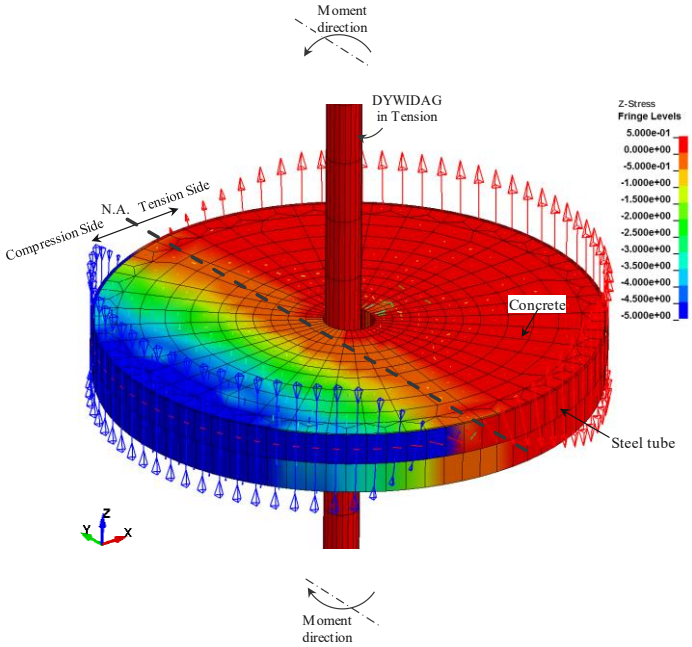

Figure I.20: Schematic view of the distribution of normal stresses at the cross-section and the tension force in the DYWIDAG obtained by finite element analysis.

I.1.2.2 Friction coefficients

To investigate the condition of the interface between the steel tube and the concrete core, and to measure the friction coefficient, the shaft of the flexural specimens was cut-off from the footing and laid out horizontally on the lab floor after the test; a piece of the steel tube at the bottom of the shaft was then cut-off to allow to observe the condition at the interface between the steel tube and the concrete core.

Figure I.21 shows the part that was cut from Specimen S4 for observation. As seen in this figure, there was still a significant coating of grease on the surface of the concrete, although some of it possibly had been "absorbed" by the concrete. Then, a simple setup was prepared in order to calculate the existing friction coefficient of the surface. Figure I.22 shows the friction test setup; it consisted of a weight suspended by a wire and pulley configured such as to make it possible to apply a known lateral force to the free plate. The friction coefficient is directly obtained by the ratio of pulling force and the weight applied on top of the plate (including the plate self-weight). Using this setup, the coefficient of friction was measured for different normal forces for the existing surface conditions. Also, this test was repeated for a number of different surface conditions, specifically including the cases with applied grease or bentonite slurry.

Figure I.22 and Table I.7 show the resulting measured friction coefficients for these cases. The measured friction coefficient for the steel tube on the dry surface of the shaft concrete, was about 0.60. Note that, for surfaces coated with bentonite, the friction coefficient was relatively high, being equal to 0.6 for Specimen S3, and generally above 0.4 for three other cases in which the concrete surface was coated (after it was exposed by removal of the steel tube) with different bentonite conditions, namely wet bentonite and dry (hydrated and non-hydrated) bentonite.

For Specimen S4, the existing friction coefficient value reached as high as 0.3 for low interface forces and it degraded as the interface force increased. In that case, the measured friction coefficient at the existing interface was lower than 0.2 for normal interface forces of more than 60*lbs.* This trend was also observed in many other cases tested, but less noticeably so. It was also observed that a larger load than the friction force was needed to initiate the sliding at first (which is typically referred to as the "breakaway" friction).

The lowest friction coefficient was obtained for Specimen S6R, for which a thick layer of grease was applied on the interior of the steel tube, and for which an average measured friction coefficient of about

0.11 was measured. The average measured friction coefficients for all other considered surface conditions are presented in Table I.7.

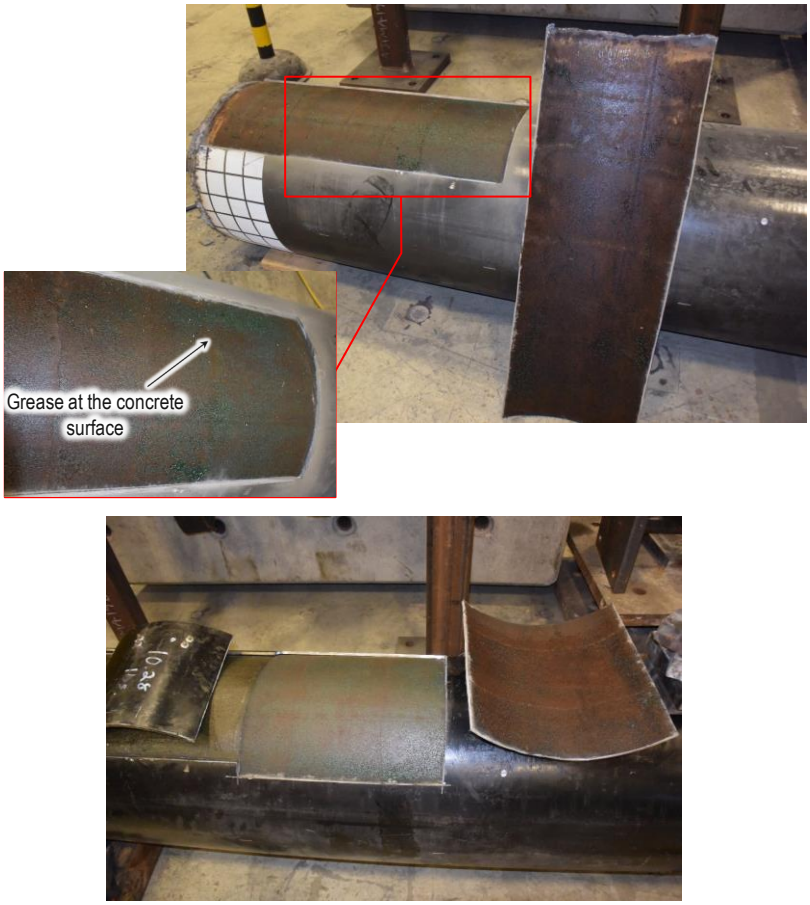

Figure I.21: Condition of the interface of the steel tube and concrete core of Specimen S4 after testing.

Figure I.22: Friction coefficient measuring test setup.

Table I.7: Friction test results for different surface conditions

Surface Condition	Range of normal forces considered for average, lb.	Average friction coefficient, μ
Specimen S3 (Bentonite Slurry)	<50	0.60
Specimen S4 (Existing Greased Surface)	>50	0.18
Specimen S6R (Thick layer of grease)	>50	0.11
Steel on concrete	<50	0.60
Fresh bentonite (wet)	all	0.49
Non-hydrated bentonite (dry)	all	0.47
Hydrated bentonite (<24hr hydration)(dry)	all	0.42
PE Sheet + fresh Grease	>50	0.27
2 x PE Sheet + fresh Grease	>50	0.31
Fresh grease	>50	0.11
Thick layer of grease	>50	0.07
2 x PE Sheet + dry surface	>50	0.34

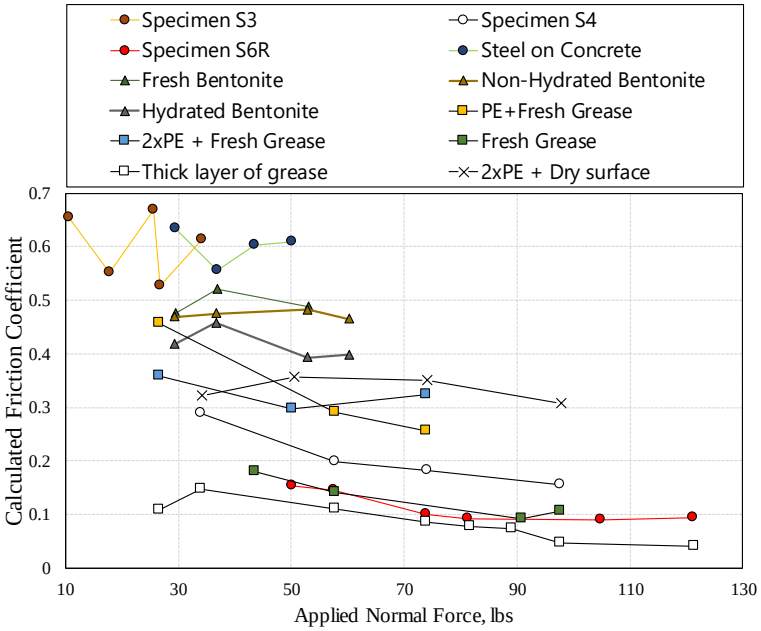

Figure I.23 Measured friction coefficient at the interface of the steel tube and concrete core for different surface conditions.

I.1.3 Comparison of flexural specimen test results

I.1.3.1 Calculation of the flexural specimens' analytical strengths

In order to compare the flexural specimen results with each other, the experimentally obtained strength for each flexural specimen was normalized to its analytical strength value, and normalized values were compared to each other. The analytical strengths were calculated using the PSDM considering each specimen's test condition (such as applied axial load and composite or non-composite behavior) and the variation of each specimen's measured material properties that are presented in Section H.1.3. The confining effects of the steel tube were considered in the PSDM calculations, using the proposed model by Susantha et al. (2001) per the procedure presented in Appendix E.

For analytical strength calculations of Specimen S2R, which was axially post-tensioned to an axial value of 92.6$kips$ before testing, but for which this axial load increased up to 143$kips$ during the test, this variation in axial load was considered in calculating the dispersion of the strength values. Also for this case, in addition to the PSDM calculations (which considers material strength but no second order effects), a simple discrete finite element model of the specimen was developed in OpenSees to consider the possible P-Δ effects and variations of axial load due to lateral deformations of the specimen (that is discussed in Section I.1.2.1). The OpenSees model is a fiber model that makes it possible to capture the variations that occurred during the test in the pre-tension load in the DYWIDAG bar used to apply axial load on the specimen. Figure I.24 shows a detailed schematic view of the developed discrete finite element model in OpenSees. No strain hardening of steel and no material damage for steel and concrete were considered in the model. Figure I.25 compares the push over results of the OpenSees model and PSDM calculated using average material properties. As mentioned above, no material damage was defined in the model. Therefore, as shown in Figure I.25, the push over curve didn't exhibit any strength degradation. In fact, the amount of applied lateral load still slightly increased at larger drifts because of the development of an extra axial load in the DYWIDAG bar because of its inclination. In order to compare the strength calculated by the OpenSees model with the PSDM values, the amount of applied horizontal load at a drift of 10.10$in.$ was taken as the maximum strength. This drift corresponds to the point where the maximum strength of Specimen S2R was reached during the test. As shown in Figure I.25, the PSDM values calculated considering the full range of axial loads reached during the test is slightly less than the maximum strength calculated by OpenSees model at that drift.

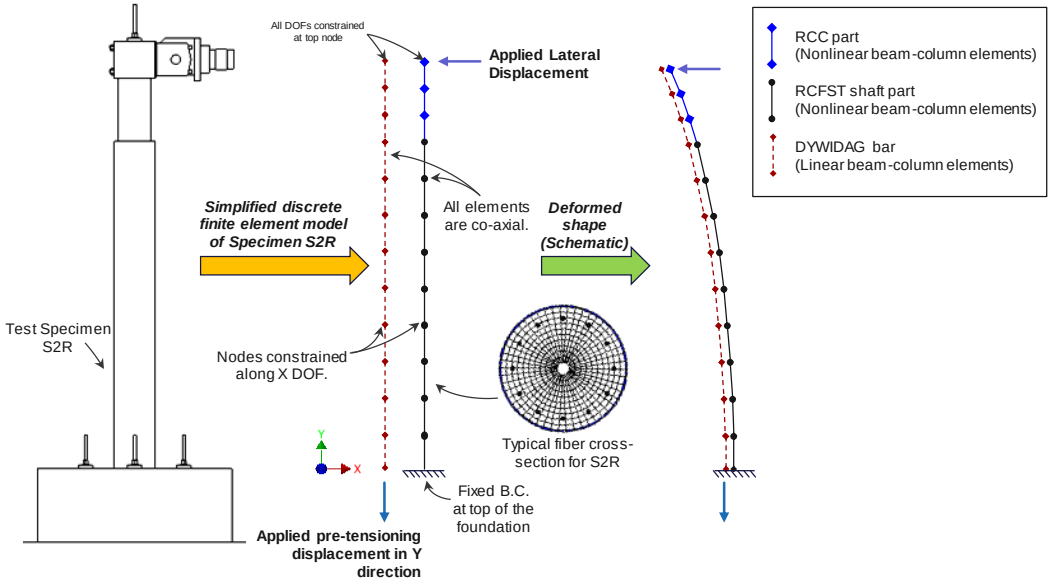

Figure I.24: Schematic of the developed discrete finite element model of Specimen S2R.

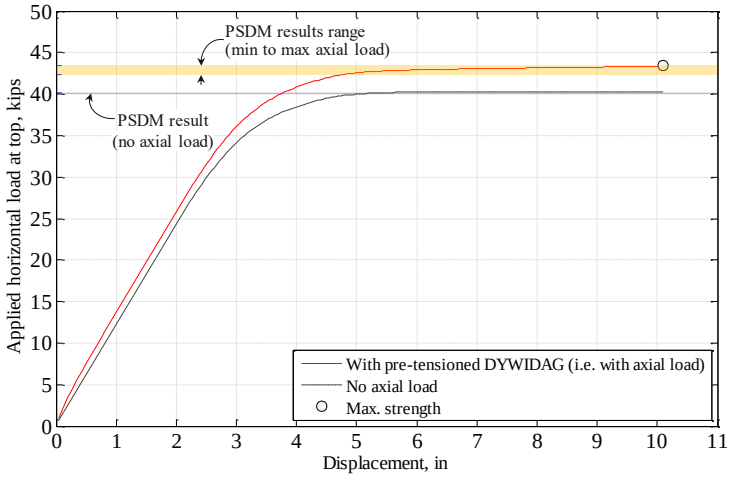

Figure I.25: Comparison of Specimen S2R PSDM and OpenSees model results.

I.1.3.2 Force-Displacement relationship comparisons

The experimental hysteresis curves obtained for the flexural specimens are compared in Figures I.26 to I.30. To facilitate comparison across the entire response, the full hysteretic curves have been broken down in subsets, in three series of cycles regrouped together as cycles 1 to 8, cycles 9 to 12, and cycles 13 to the end of the test. Normalized hysteresis curves are also presented in these figures. The applied lateral force (on the vertical axis of the figures) is normalized by the lateral force that creates a moment equal to the composite cross-section strength calculated by PSDM, using the each specimen's measured material properties. The average values of measured material properties were used in the PSDM strength calculations. Comparison of the normalized hysteresis curves of the specimens shows that, generally, the behavior of specimens is similar.

The Force-Displacement backbone of the tested specimens are compared in Figures I.31 to I.35 . The normalized Force-Displacement backbones are also presented in these figures. Again, results are generally similar for all specimens.

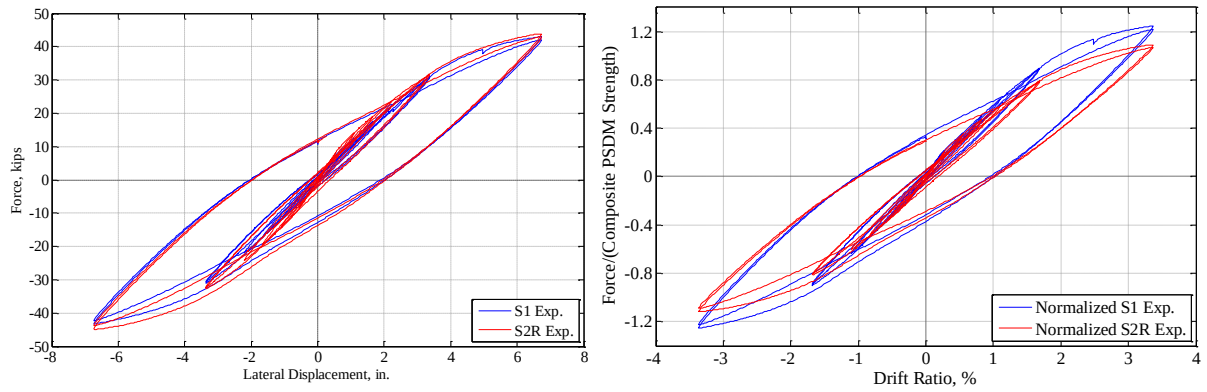

(a) cycles 1 to 8

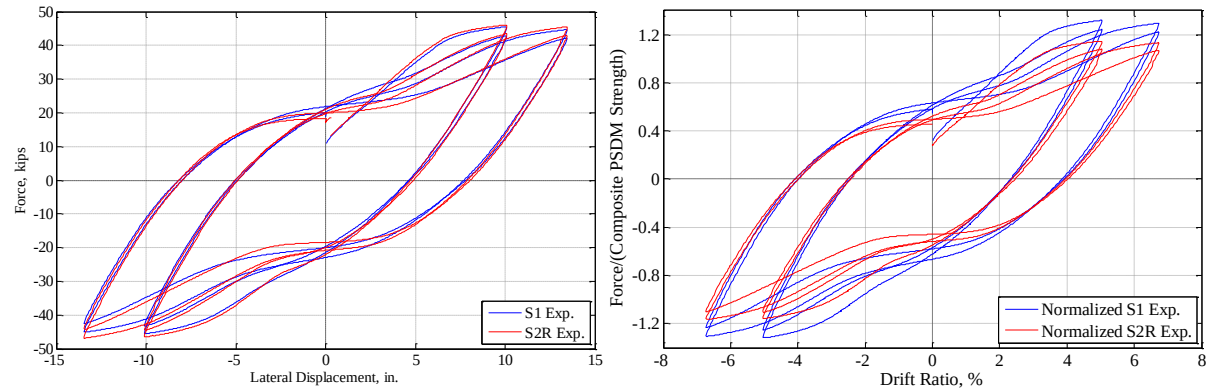

(b) cycles 9 to 12

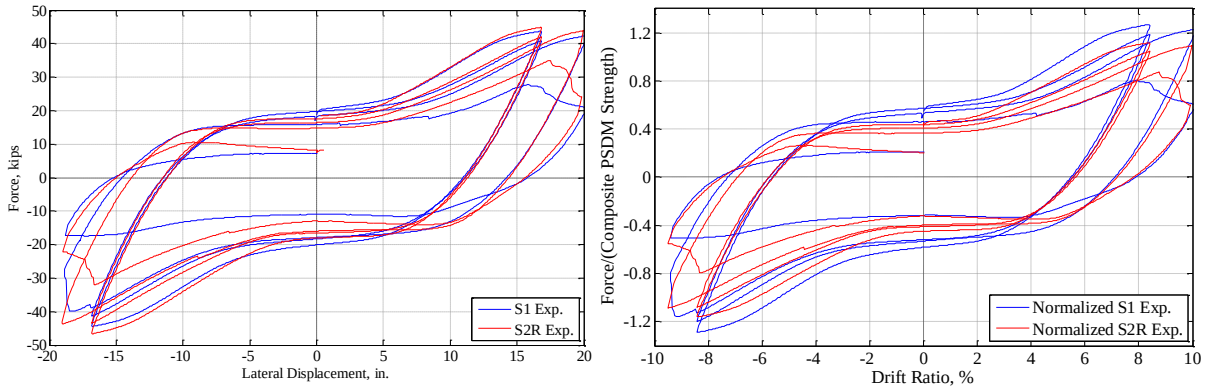

(c) cycles 13 to end.

Figure I.26: Comparison of hysteresis and normalized hysteresis curves for Specimens S1 and S2R: (a) cycles 1 to 8; (b) cycles 9 to 12; (c) cycles 13 to end.

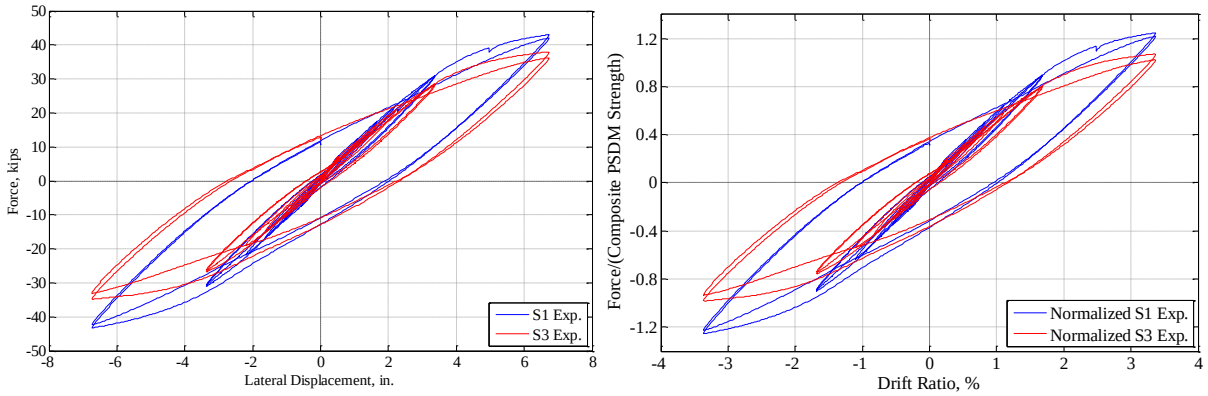

(a) cycles 1 to 8

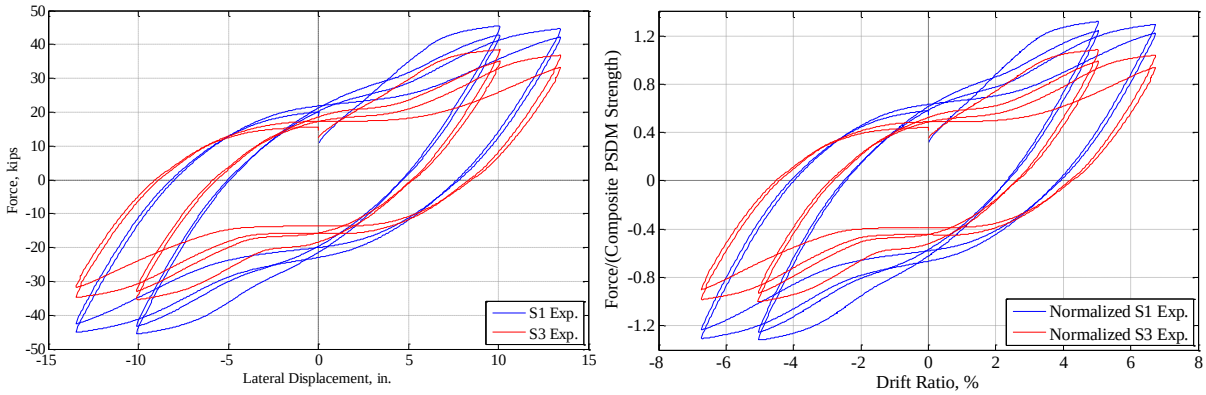

(b) cycles 9 to 12

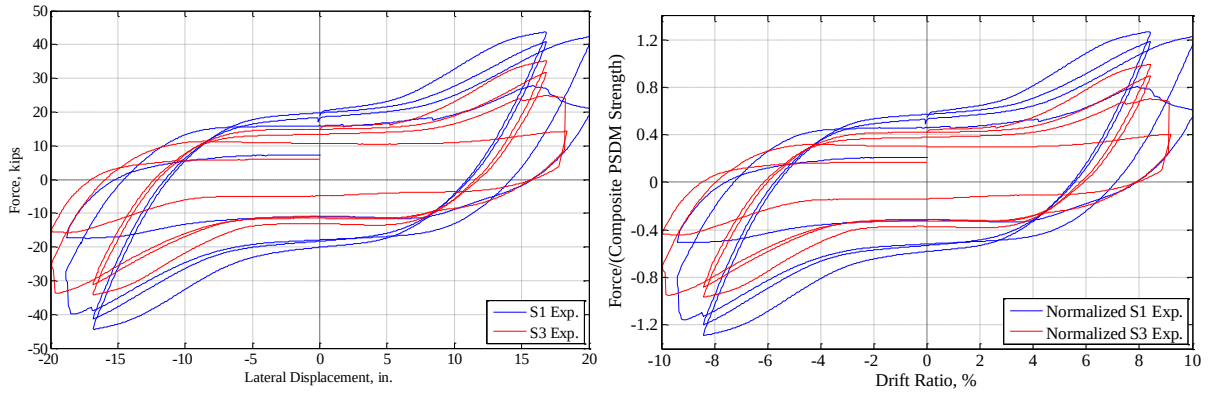

(c) cycles 13 to end.

Figure I.27: Comparison of hysteresis and normalized hysteresis curves for Specimens S1 and S3: (a) cycles 1 to 8; (b) cycles 9 to 12; (c) cycles 13 to end.

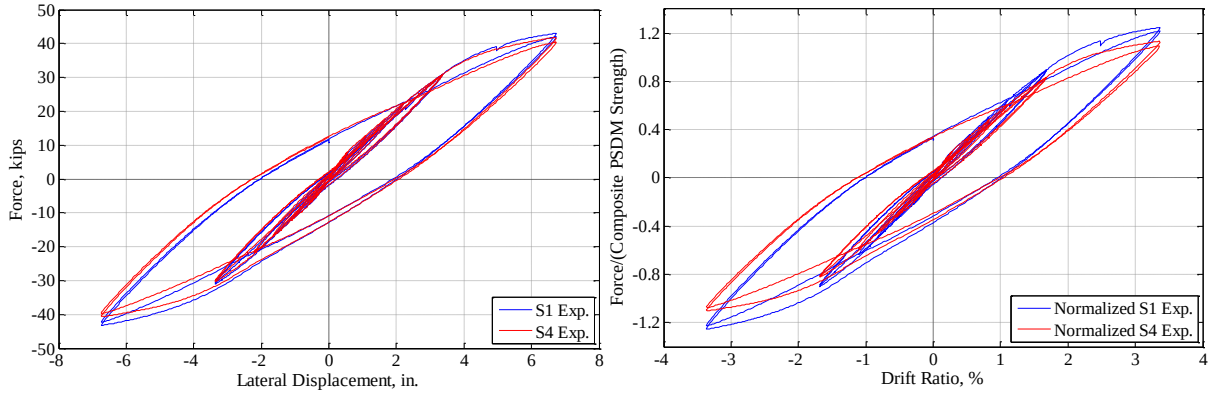

(a) cycles 1 to 8

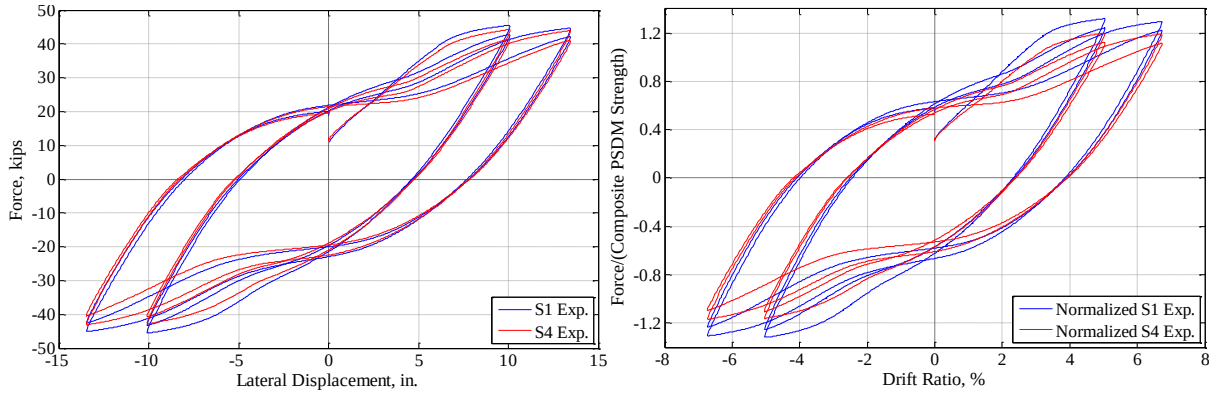

(b) cycles 9 to 12

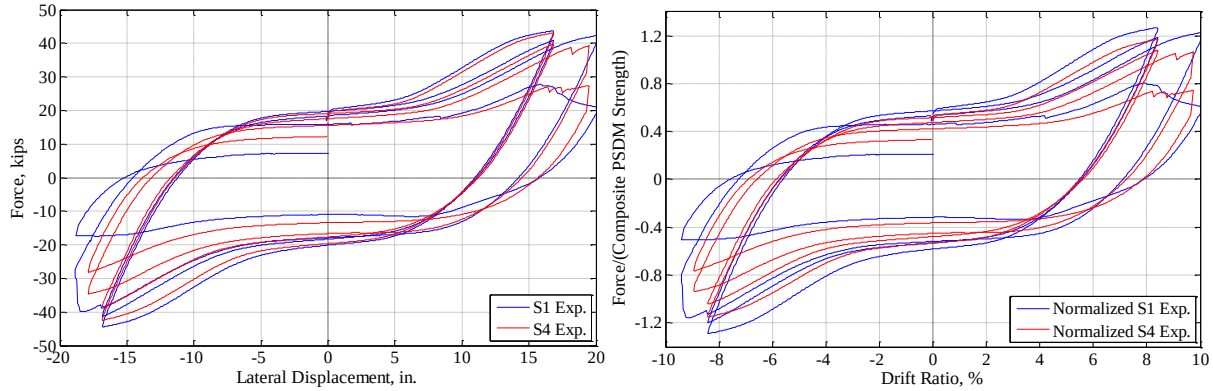

(c) cycles 13 to end.

Figure I.28: Comparison of hysteresis and normalized hysteresis curves for Specimens S1 and S4: (a) cycles 1 to 8; (b) cycles 9 to 12; (c) cycles 13 to end.

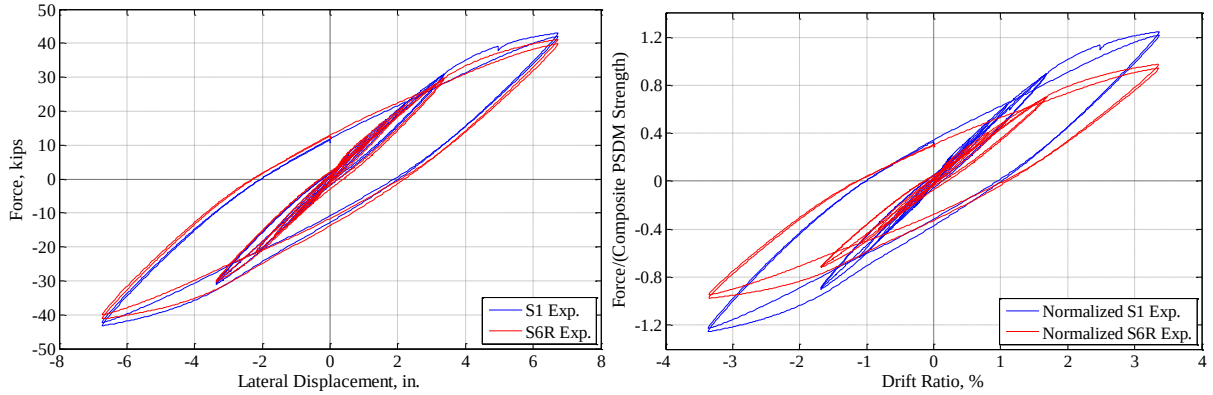

(a) cycles 1 to 8

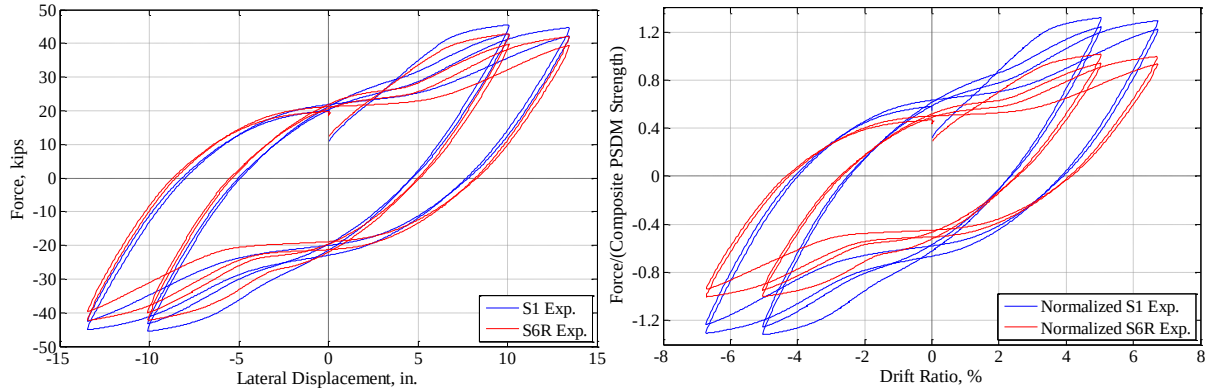

(b) cycles 9 to 12

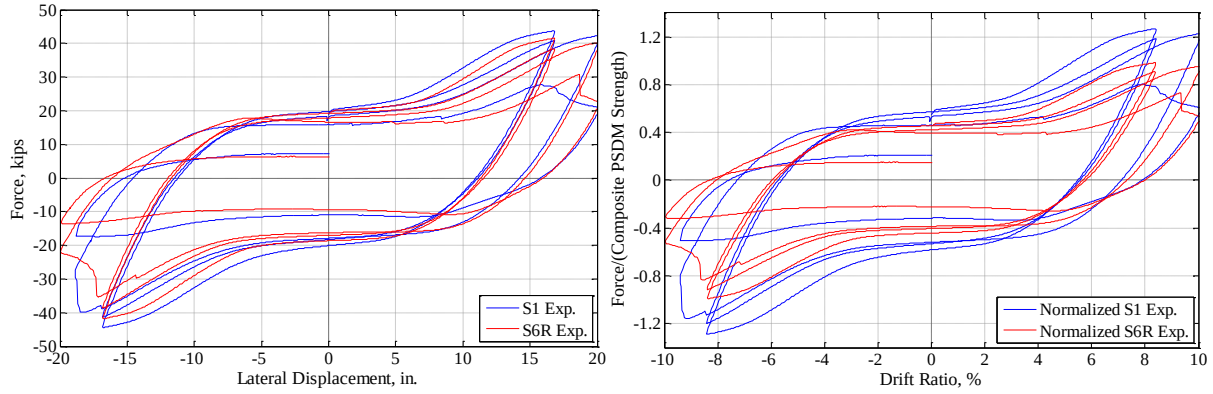

(c) cycles 13 to end.

Figure I.29: Comparison of hysteresis and normalized hysteresis curves for Specimens S1 and S6R: (a) cycles 1 to 8; (b) cycles 9 to 12; (c) cycles 13 to end.

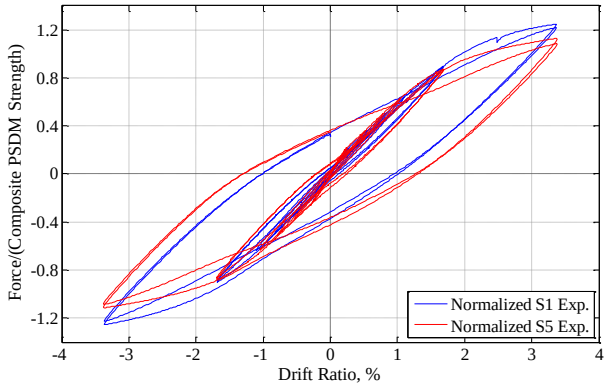

(a) cycles 1 to 8

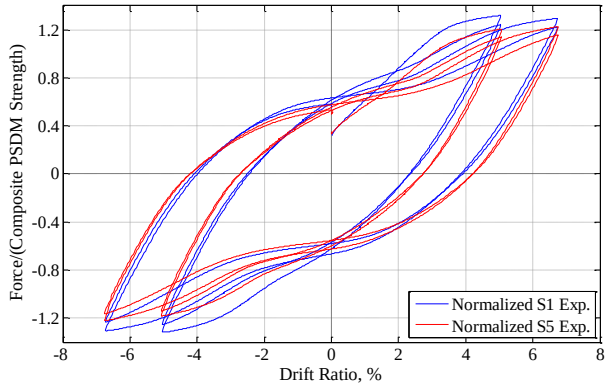

(b) cycles 9 to 12

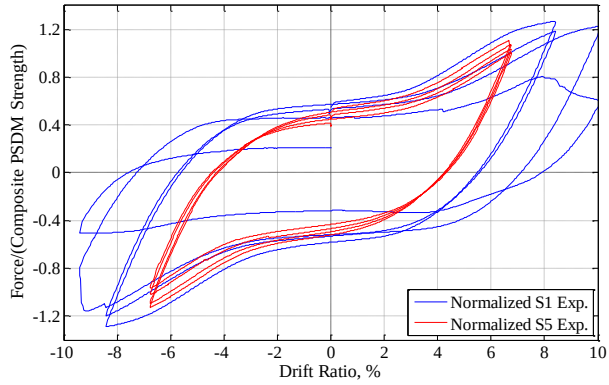

(c) cycles 13 to end.

Figure I.30: Comparison of normalized hysteresis curves for Specimens S1 and S5: (a) cycles 1 to 8; (b) cycles 9 to 12; (c) cycles 13 to end.

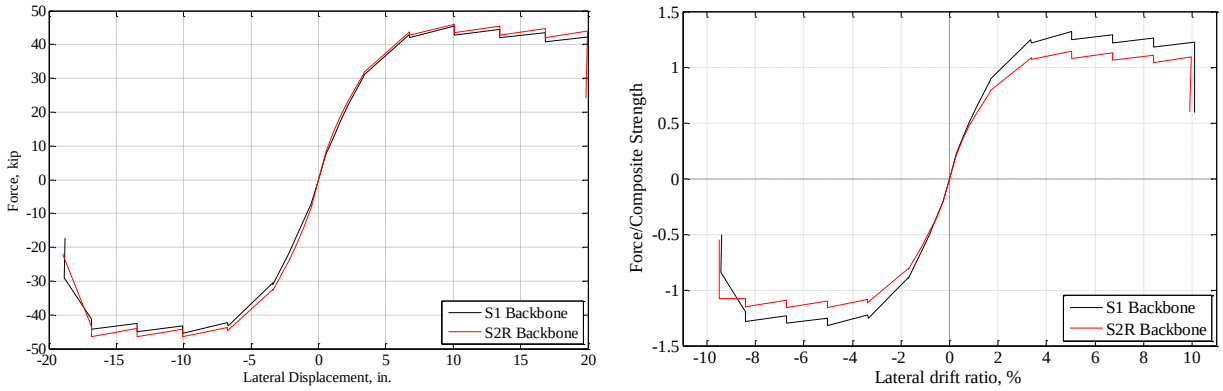

(a) (b)

Figure I.31: (a)Comparison of backbone curves for Specimens S1 and S2R. (b) Comparison of normalized backbone curves for Specimens S1 and S2R.

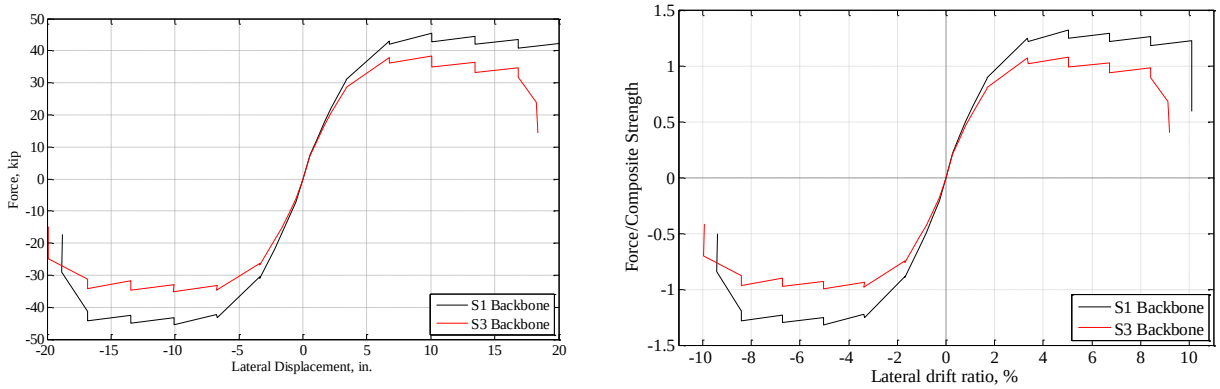

(a) (b)

Figure I.32: (a)Comparison of backbone curves for Specimens S1 and S3. (b) Comparison of normalized backbone curves for Specimens S1 and S3.

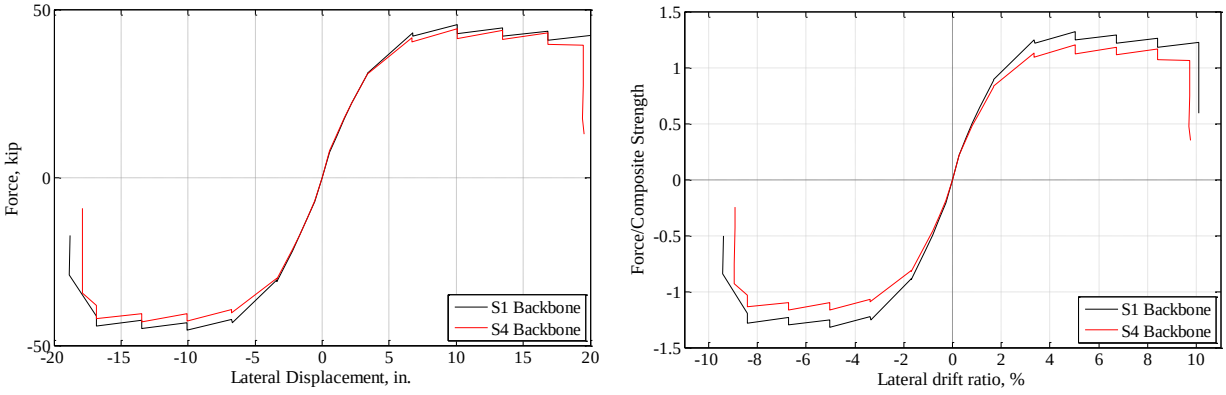

(a) (b)

Figure I.33: (a)Comparison of backbone curves for Specimens S1 and S4. (b) Comparison of normalized backbone curves for Specimens S1 and S4.

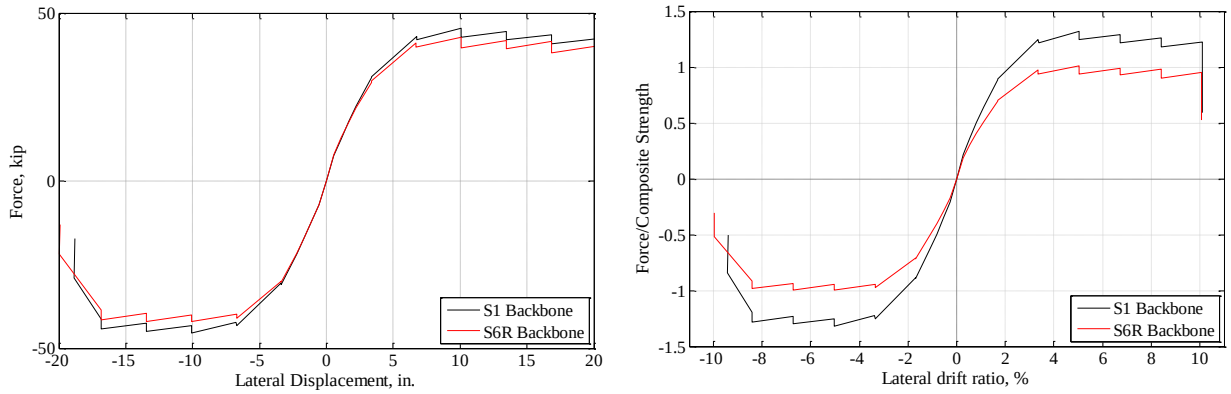

Figure I.34: (a)Comparison of backbone curves for Specimens S1 and S6R. (b) Comparison of normalized backbone curves for Specimens S1 and S6R.

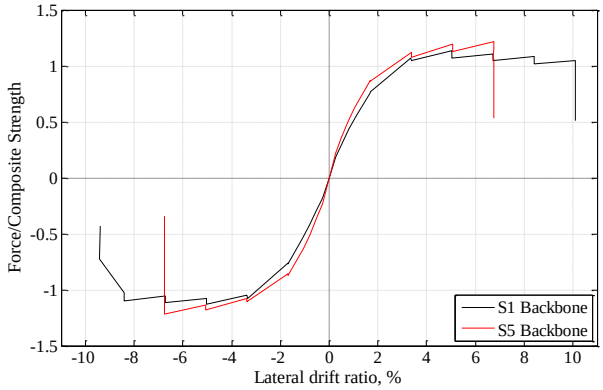

Figure I.35: Comparison of normalized backbone curves for Specimens S1 and S5.

I.1.3.3 Slippage Comparisons

The average slippage at the interface of the steel tube and the concrete core, as measured using 8 Krypton LEDs on each tested specimens, are compared in Figure I.36 for the flexural specimens. As shown in that figure, the slippage values are insignificant, typically less than $0.05in.$, except for Specimen S4 (i.e., the specimen with grease coating on the interior surface of the steel tube), which is significantly higher than for all other specimens. The maximum slippage for Specimen S4 was more than a third of inch ($0.36\ in.$). The maximum slippage values obtained at each cycle are shown in Figure I.37 for all flexural specimens. As shown in this figure, for Specimen S1, the slippage is within $0.0046in.$ and doesn't increase at greater lateral displacements. For Specimen S2R, as shown in Figure I.37b, the measured slippage values are within $0.0041in.$ As the lateral displacement of Specimen S2R becomes larger, the measured slippage values go slightly negative, which could be because of the applied axial load.

Measured slippage for Specimen S3 is shown in Figure I.37c. The measured slippage for this specimen increases as the lateral displacement increases. However, as shown in Figure I.36, the measured slippage is still significantly less compared to the slippage experienced by Specimen S4. The maximum measured slippage for Specimen S3 was $0.017in.$, which is 3.6 times more than the maximum measured slippage for Specimen S1, but still about 20 times less that for Specimen S4. The measured peak slippage values at different cycles for Specimen S4 are shown in Figure I.37d. This slippage increases at greater lateral displacements and, as mentioned earlier, reaches up to $0.36in.$, which is about 78 times more than the slippage measured for Specimen S1. For the larger diameter specimen (Specimen S5), the slippage values

are within 0.0081 *in.*, which is 1.77 times the maximum slippage for Specimen S1. The lack of correlation of slippage with lateral displacement is similar to what was observed for Specimen S1. Figure I.37f shows the slippage values for Specimen S6R, which had grease coating on the interior surface of its steel tube, and shear rings at the top of the RCFST shaft. As shown in the figure, the slippage values are increasing with lateral displacement and maximum slippage reaches 0.033 *in.* at the maximum lateral displacement, which is 10.6 times less than the specimen with grease coating and without shear rings (i.e., Specimen S4). Note that a camera was installed at the top of the shaft to record possible differential movement between the steel tube and concrete infill at that location. Slippage between the steel tube and the concrete core was visually observable at the top of the RCFST shaft only for Specimen S4; for all other specimens, no visible slippage was observed. Figures I.38 and I.39, respectively show the condition of the top of the RCFST shaft part for Specimen S4, for which the slippage was visually observed and another specimen for which there was no visual slippage (i.e., Specimen S3 in this case).

The average slippage for Specimens S1 and S3 is compared in Figure I.40 (with fine resolution for the vertical axis in this figure). As shown in the figure, although some slippage was measured for the specimen with bentonite slurry coating on the inside of the steel tube, it was not significant, but certainly increased compared to the results for Specimen S1 at greater lateral displacement, indicating some possible decrease in the friction resistance at the steel-concrete interface.

Figure I.41 shows the comparison of the average slippages for Specimens S1, S4 (greased), and S6R (greased with shear rings at top of the shaft), with a magnified vertical axis clipping Specimen S4 values for the cycles at large lateral displacement to better see the differences at lower displacement values. As shown in the figure, the slippage in Specimen S6R (contrary to Specimen S4) remained within about 0.03 *in*. This indicates that the shear rings at the top of the steel tube of the RCFST shaft were able to prevent slippage.

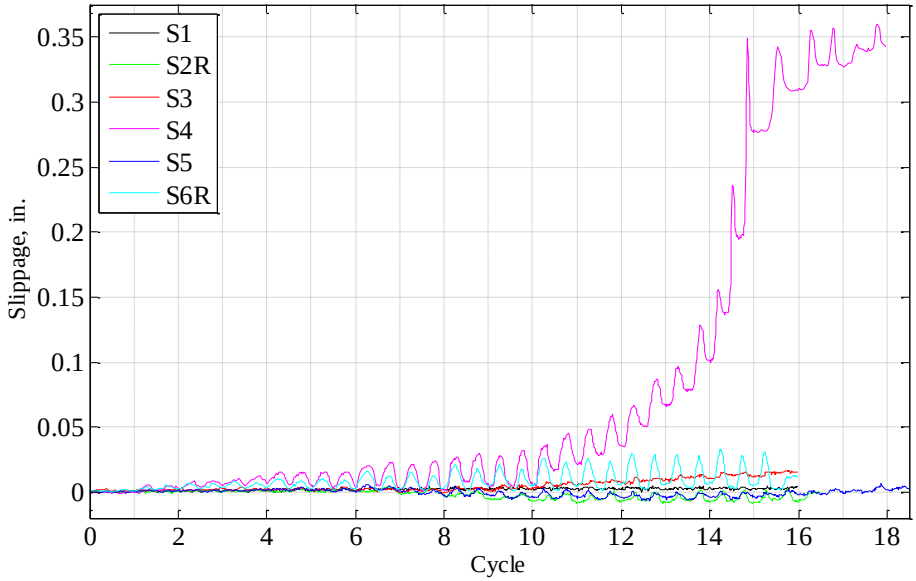

Figure I.36: Comparison of measured slippage at the interface of steel tube and concrete core of Specimens measured by Krypton LEDs.

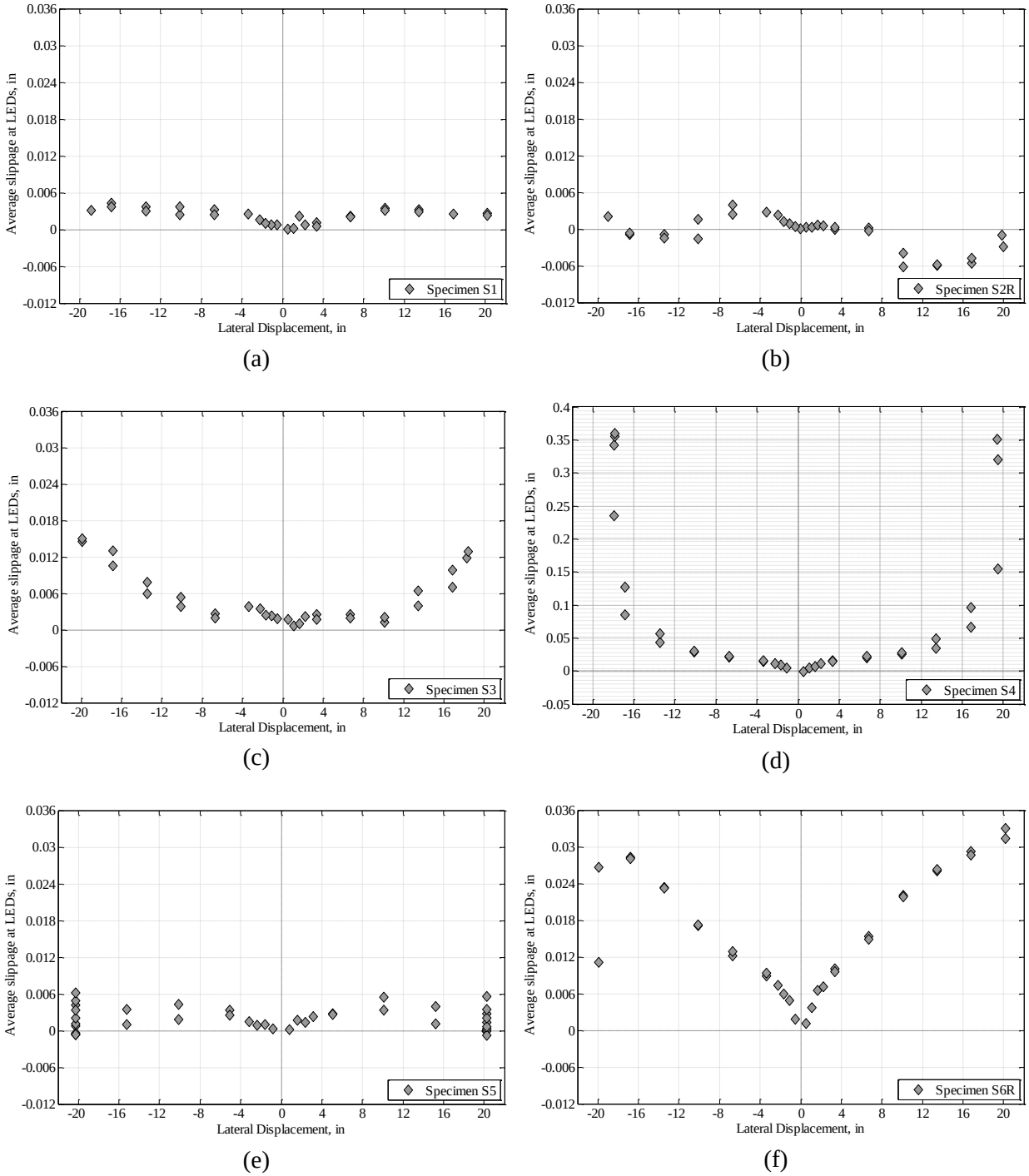

Figure I.37: Average slippage at LEDs for Specimen: (a) S1; (b) S2R; (c) S3; (d) S4 (different vertical scale); (e) S5; (f) S6R.

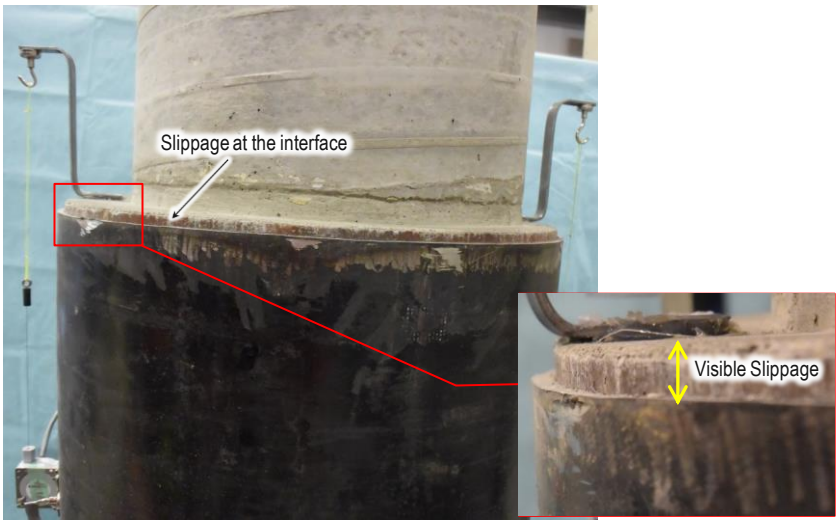

(a)

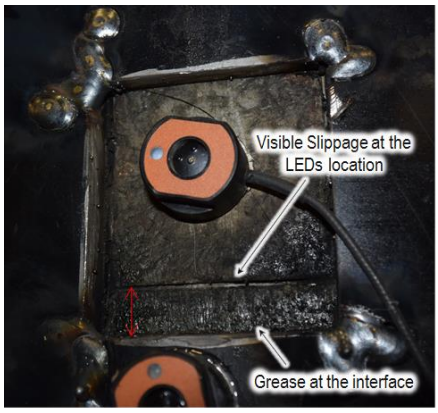

(b)

Figure I.38: Visible slippage at the end of the test of Specimen S4: (a) at top of the shaft part, (b) at the location of the installed Krypton LEDs.

Figure I.39: Top of the shaft part of Specimen S3.

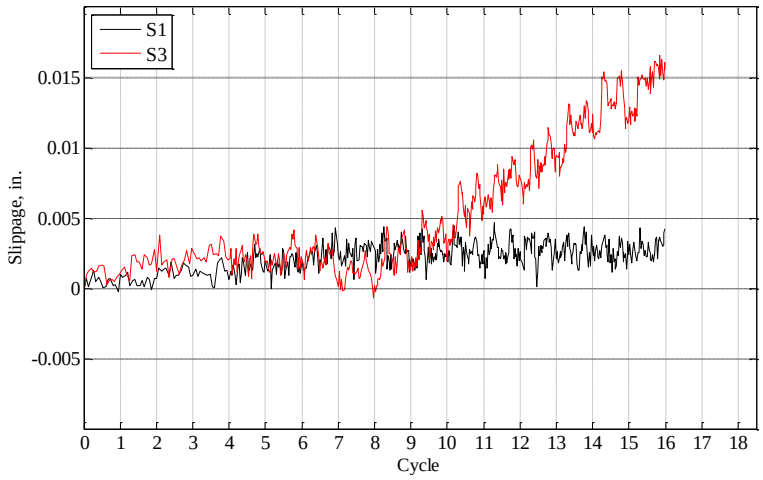

Figure I.40: Comparison of measured slippage at the interface of steel tube and concrete core of Specimens S1 and S3 measured by Krypton LEDs.

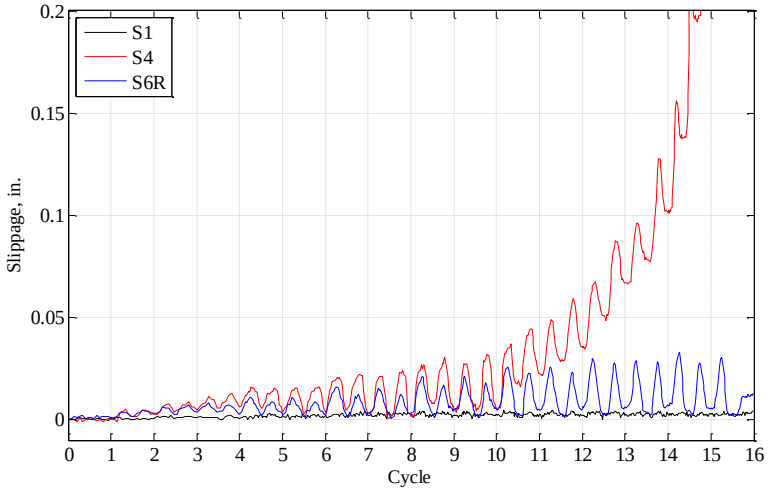

Figure I.41: Comparison of measured slippage at the interface of steel tube and concrete core of Specimens S1, S4, and S6R measured by Krypton LEDs.

I.1.3.4 Lateral deformation profile

The lateral deformation of flexural specimens was recorded by a series of string pots attached to the specimens, as presented in Appendix M. Figures I.42 and I.43 show the deformed shape of the flexural specimens at the peak positive and negative displacements of the elastic and inelastic cycles respectively. Figure I.44 compares the lateral deformation of each flexural specimen normalized per the maximum value at the top of the column (i.e., at actuator level) for the first and last cycles. As shown in this figure, the deformed shape of the flexural specimens in the first cycle is close to that of an end-loaded cantilever beam (that follows a 3rd order polynomial function) during the initial elastic cycles, and changes into an almost linear function during the more inelastic cycles (with rotation more concentrated at the bottom of the specimen).

The normalized lateral deformations of Specimen S2R, which was axially loaded are compared to the corresponding normalized deformations of Specimen S1 at first and final cycles in Figure I.45a. As shown in this figure, the lateral deformation profiles of both specimens are similar to each other. The same

comparison was also done for Speicmens S5 and S1 in Figure I.45b. The lateral deformation profiles of these specimens are also similar to each other.

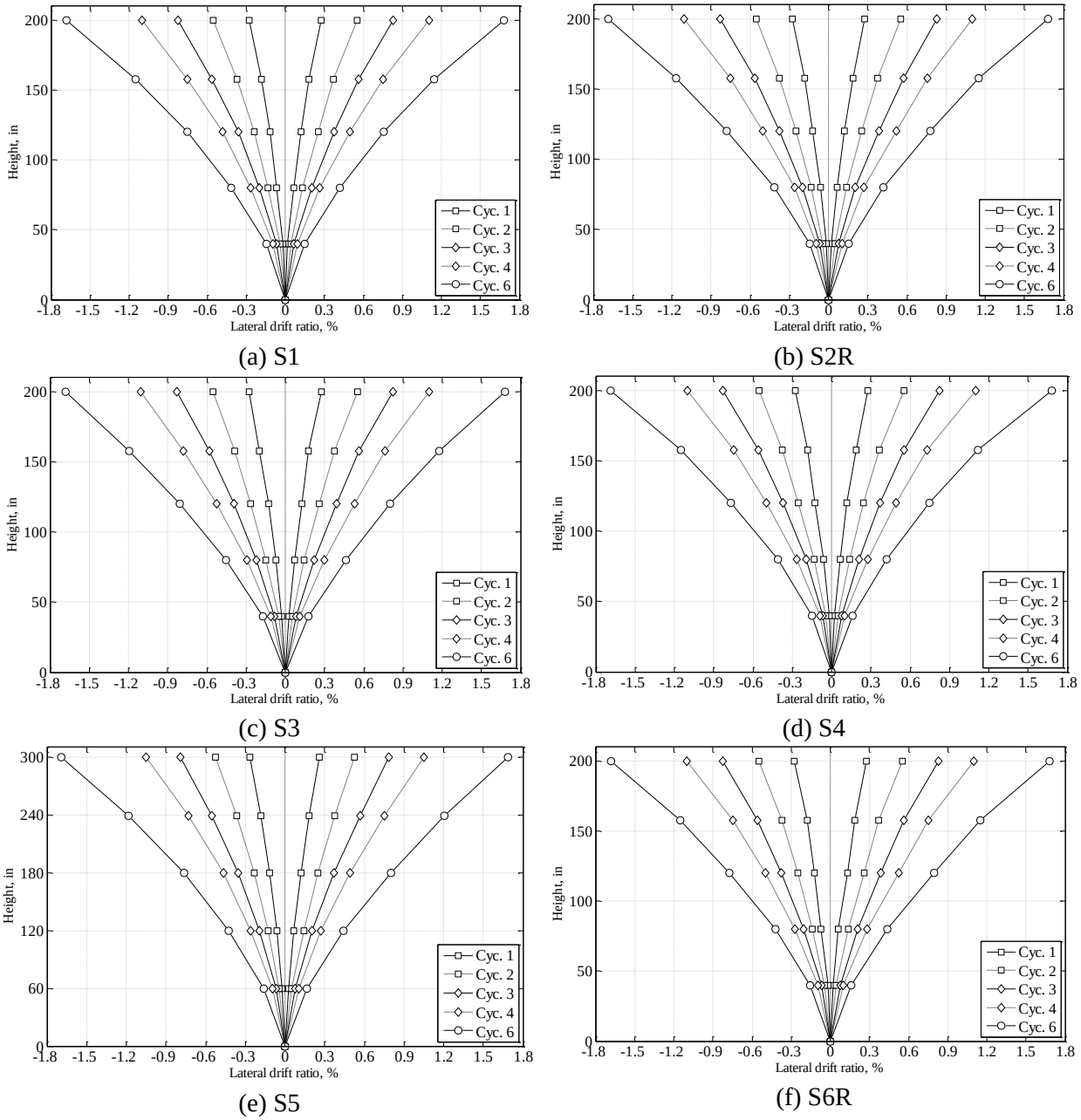

Figure I.42: Deformed shape at the peak positive and negative displacement of elastic cycles for Specimen: (a) S1; (b) S2R; (c) S3; (d) S4; (e) S5; (f) S6R.

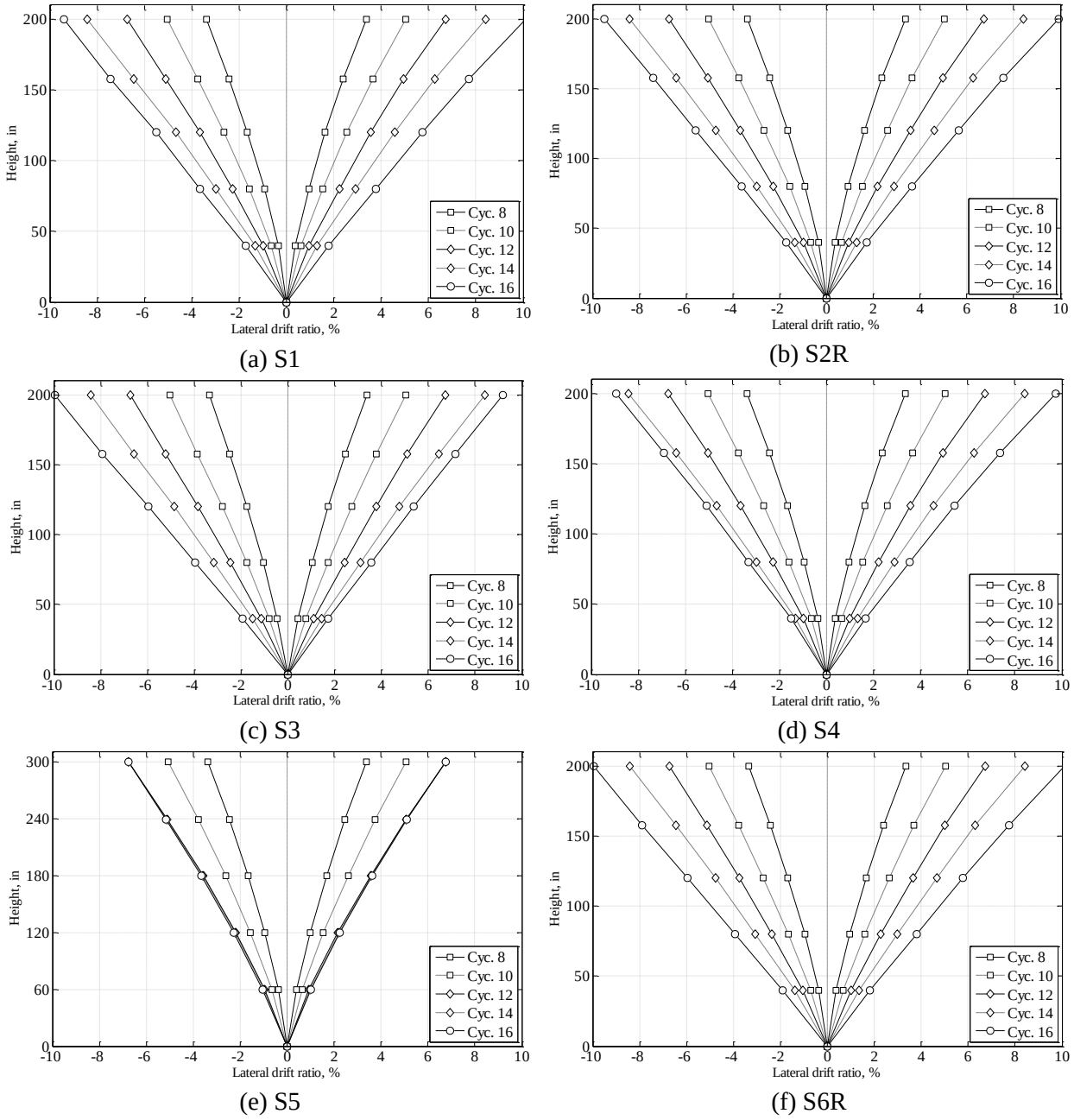

Figure I.43: Deformed shape at the peak positive and negative displacement of inelastic cycles for Specimen: (a) S1; (b) S2R; (c) S3; (d) S4; (e) S5; (f) S6R.

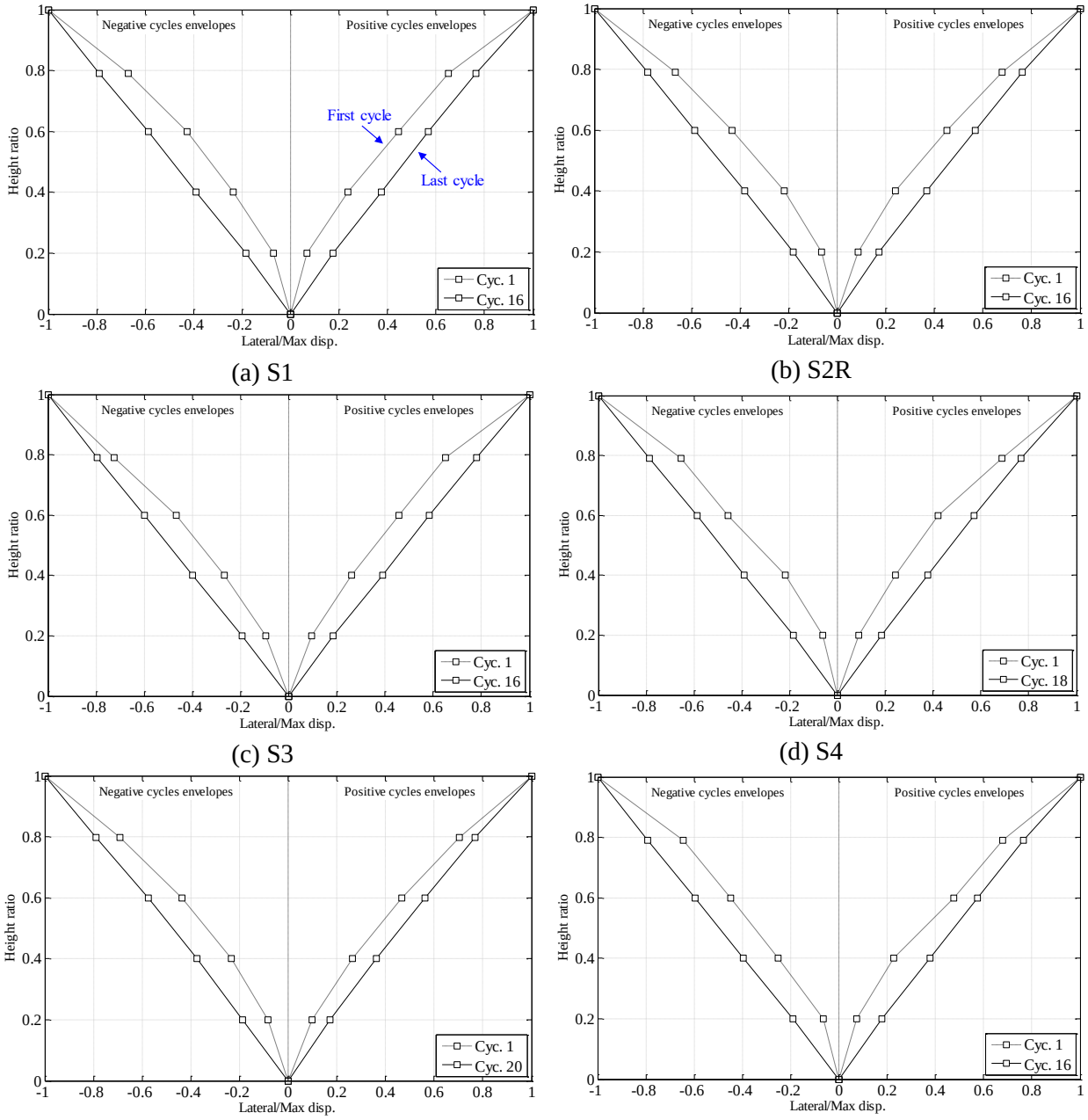

(a) S1

(b) S2R

(c) S3

(d) S4

(e) S5

(f) S6R

Figure I.44: Modal lateral deformation shape of the flexural specimens at the first and final cycles.

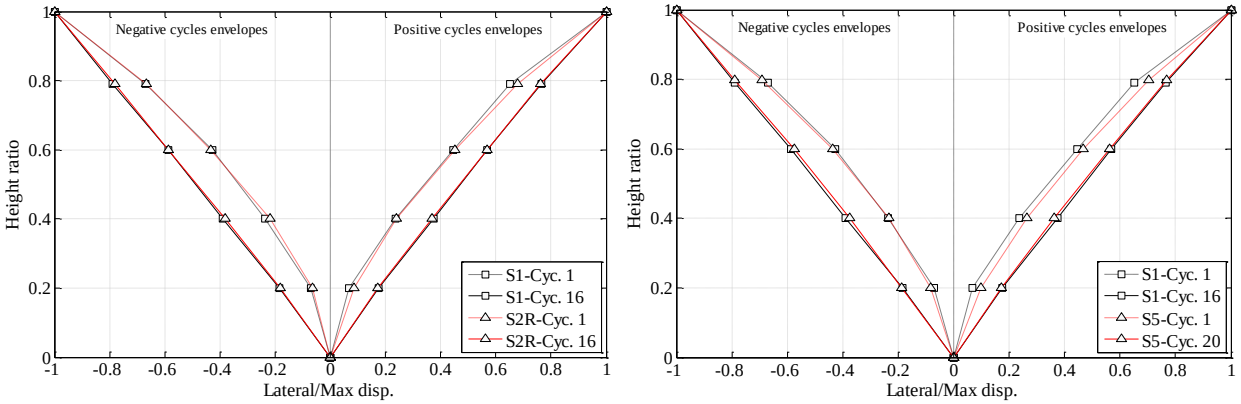

Figure I.45: Comparison of modal lateral deformation shapes of Specimens: (a) S1 and S2R, (b) S1 and S5.

I.1.3.5 Torsion check

As shown in Section 2.3.5 of the report, the specimen was built to be symmetric with respect to loading plane. Therefore, theoretically, no out of plane (i.e., sidesway) movement was expected during the test. However, due to unavoidable imperfections that existed in the construction process and test setup preparation, the constructed flexural specimens were not perfectly symmetric or aligned and some small sideway movements was measured during the test. Although, the small sideways movements do not have an impact on the strength of the specimen (the circular shafts have the same flexural strength in any loading direction), it could produce errors on data readings interpretation for the top string pots and actuator's load cell and displacement sensor. To check for sideways movements, the 3-D movement of the top of the flexural specimens was tracked by using 3 horizontal string pots at the actuator level of the specimen as shown in Figure I.46a. Using the recorded displacement from these string pots and by solving the following system of equations, the displacement and rotation of the top of the specimen were calculated.

$$\textbf{SOE}: \begin{cases} \vec{\boldsymbol{a}} - \vec{\boldsymbol{\alpha}} + \vec{\boldsymbol{F}} + \vec{\boldsymbol{\alpha}}' - \vec{\boldsymbol{a}}' = 0 \\ \vec{\boldsymbol{b}} - \vec{\boldsymbol{\beta}} + \vec{\boldsymbol{F}} + \vec{\boldsymbol{\beta}}' - \vec{\boldsymbol{b}}' = 0 \\ \vec{\boldsymbol{c}} - \vec{\boldsymbol{\gamma}} + \vec{\boldsymbol{F}} + \vec{\boldsymbol{\gamma}}' - \vec{\boldsymbol{c}}' = 0 \\ \vec{\boldsymbol{\alpha}}' = \mathrm{R}\vec{\boldsymbol{\alpha}} \\ \vec{\boldsymbol{\beta}}' = \mathrm{R}\vec{\boldsymbol{\beta}} \\ \vec{\boldsymbol{\gamma}}' = \mathrm{R}\vec{\boldsymbol{\gamma}} \end{cases} \qquad \text{(I.1)}$$

where **R** is a rotation tensor:

$$\mathrm{R} = \begin{bmatrix} cos(\theta) & -sin(\theta) \\ sin(\theta) & cos(\theta) \end{bmatrix} \qquad \text{(I.2)}$$

$\vec{a}$ = Position vector showing initial state of Sting pot SP9's attaching string.
$\vec{b}$ = Position vector showing initial state of Sting pot SP8's attaching string.
$\vec{c}$ = Position vector showing initial state of Sting pot SP7's attaching string.
$\vec{a}'$ = Position vector showing deformed state of Sting pot SP9's attaching string.

$\vec{b}'$ = Position vector showing deformed state of Sting pot SP8's attaching string.
$\vec{c}'$ = Position vector showing deformed state of Sting pot SP7's attaching string.
$\vec{F}$ = Displacement vector showing the movement of the top of the specimen.
θ = Rotation of the top of the specimen.
and $\vec{\alpha}$, $\vec{\alpha}'$, $\vec{\beta}$, $\vec{\beta}'$, $\vec{\gamma}$, and $\vec{\gamma}'$ are vectors as shown in Figure I.46.

Figure I.47a shows the footprint of the movement of the top of the flexural specimen during the test for the first three tested flexural specimens. The vertical axis shows the drift ratio of the specimen in the direction perpendicular to the actuator. Results showed that the transverse movement of the flexural specimens was insignificant, being less than 0.8% transverse drift ratio. Figure I.47b shows the rotation of the top of the flexural specimens during the test for the same three specimens. As shown in the figure, the rotation at the top was also insignificant, being less than 3 degrees.

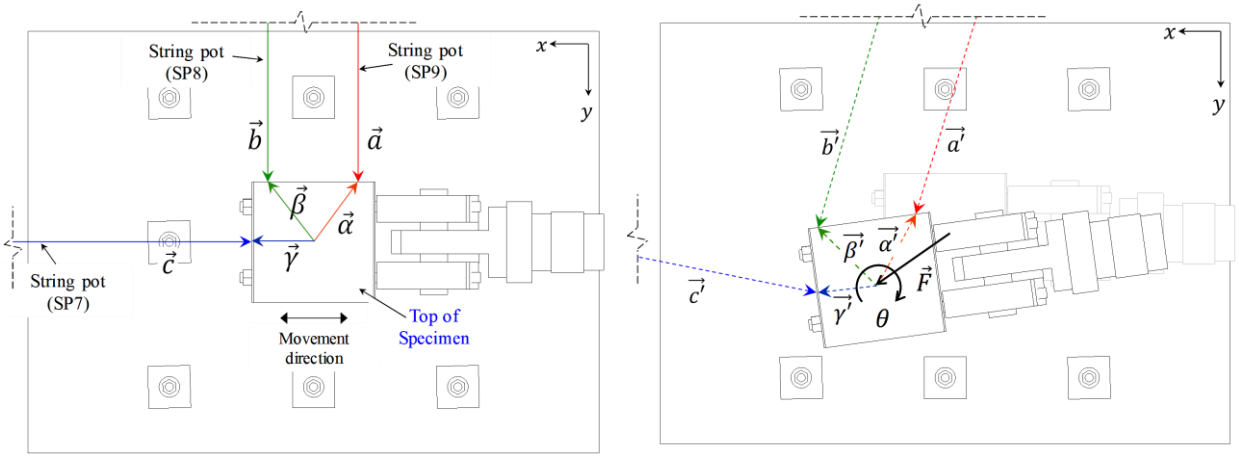

(a) Initial state (Top view)　　(b) Deformed state (Top view)

Figure I.46: String pot configurations for measuring the top movement of the flexural specimens.

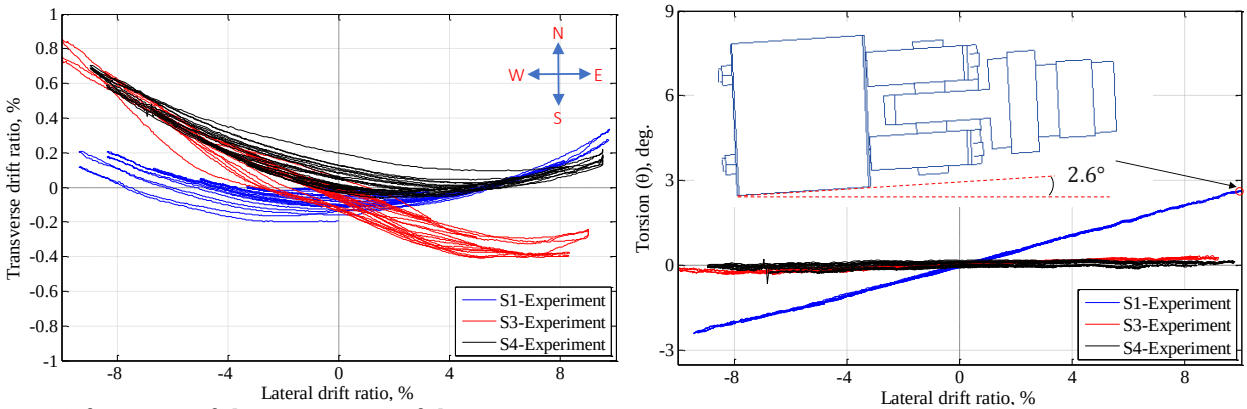

(a) footprint of the movement of the specimen　　(b) Rotation at the top of the specimen

Figure I.47: Movements at the top of the flexural specimens during the test.

I.2 RCFST shear test database

The test setups, test specimen properties, test results, and comparisons of the shear strengths obtained experimentally by the researchers presented in Table 3.11 and using the proposed equation are shown Tables I.9 to I.14. Note that for the Roeder et al. (2016) tests, the specimens that reportedly had a dominant flexural failure were excluded in the calculation of mean and standard variation. These specimens are hatched in Table I.10 and indicated in Figure I.48. For the Ye et al. (2016) tests, the specimens with shear span-to-depth ratio of less than 0.1 were also excluded in the evaluation of the proposed shear formula.

Table I.8. Summary of the existing test data on shear strength of RCFST members.

Research	Test Setup	Loading type	Diameter range, *in.*	$\frac{a}{D}$ range	$\frac{P}{P_0}$ range
Roeder et al. (2016)	Single curvature	Monotonic four point bending	20	0.25 - 1.0	0 and 0.085
Ye et al. (2016)	Double curvature	Monotonic three point bending	4.7	0.15 - 0.75	0 - 0.73
Nakahara and Tsumura (2014)	Double curvature	Cyclic Pantograph	6.5	0.5	0 - 0.4
Xiao et al. (2012)	Single curvature	Monotonic three point bending	6.5	0.14 - 1.0	0 - 0.62
Xu et al. (2009)	Single curvature	Monotonic three point bending	5.5	0.1 - 0.5	0
Qian et al. (2007)	Single curvature	Monotonic three point bending	7.7	0.1 - 0.3	0 - 0.77

Table I.9. Nakahara and Tsumura (2014) test specimens properties, results, and comparison with proposed formula.

Specimen	OD, *in.*	a, *in.*	$\frac{a}{OD}$	t, *in.*	$\frac{D}{t}$	f'_c, ksi	E_c, ksi	f_y, ksi	$\frac{P}{P_o}$	P, ksi	V_{exp}, kip	V_{CFST}, kip	$\frac{V_{exp}}{V_{CFST}}$	$\frac{V_{Strut}}{V_{CFST}}$	$\frac{V_{tube}}{V_{CFST}}$	$\frac{V_{conc}}{V_{CFST}}$
N1	6.5	3.3	0.5	0.193	33.9	9.3	5336	79	0	0	150	120	1.25	0.00	0.95	0.05
N2	6.3	3.1	0.5	0.089	70.5	9.6	5655	73	0.1	41	109	56	1.94	0.00	0.84	0.16
N3	6.5	3.3	0.5	0.193	33.9	9.3	5336	79	0.3	174	162	126	1.28	0.00	0.88	0.12
N4	6.3	3.1	0.5	0.089	70.5	9.6	5655	73	0.3	123	96	61	1.58	0.00	0.76	0.24
N5	6.5	3.3	0.5	0.197	33.0	7.0	4887	79	0.1	51	153	123	1.25	0.00	0.94	0.06
N6	6.5	3.3	0.5	0.197	33.0	7.0	4887	79	0.2	102	156	124	1.25	0.00	0.92	0.08
N7	6.5	3.3	0.5	0.197	33.0	7.0	4887	79	0.4	205	148	125	1.19	0.00	0.89	0.11
N8	6.3	3.1	0.5	0.089	70.5	9.6	5655	73	0.15	61	102	57	1.78	0.00	0.82	0.18
N9	6.3	3.1	0.5	0.089	70.5	9.6	5655	73	0.2	82	112	59	1.92	0.00	0.80	0.20

Table I.10. Roeder et al. (2016) test specimens properties, results, and comparison with proposed formula.

Specimen	OD, in.	a, in.	$\frac{a}{OD}$	t, in.	$\frac{D}{t}$	f'_c, ksi	E_c, ksi	f_y, ksi	$\frac{P}{P_o}$	P, ksi	V_{exp}, kips	V_{CFST}, kips	$\frac{V_{exp}}{V_{CFST}}$	$\frac{V_{Strut}}{V_{CFST}}$	$\frac{V_{tube}}{V_{CFST}}$	$\frac{V_{conc}}{V_{CFST}}$
R1	20	20	1	0.233	86	6	3965	50	0	0	322	313	1.03	0.00	0.85	0.15
R2	20	10	0.5	0.233	86	6.2	4031	50	0	0	550	313	1.75	0.00	0.85	0.15
R3	20	10	0.5	0.233	86	6.7	4190	50	0	0	552	318	1.74	0.00	0.85	0.15
R4	20	10	0.5	0.233	86	6.6	4159	50	0	0	543	318	1.71	0.00	0.85	0.15
R12	20	10	0.5	0.233	86	6.2	4031	54	0	0	651	337	1.93	0.00	0.86	0.14
R17	20	10	0.5	0.233	86	9.5	4976	55	0	0	547	356	1.54	0.00	0.84	0.16
R18	20	10	0.5	0.349	57	8.6	4758	57	0	0	832	515	1.62	0.00	0.89	0.11
R19	20	10	0.5	0.349	57	9.1	4891	57	0	0	952	517	1.84	0.00	0.89	0.11
R7	20	7.5	0.38	0.233	86	6.5	4111	50	0	0	705	531	1.33	0.53	0.47	0.53
R8	20	7.5	0.38	0.233	86	6.5	4121	54	0	0	802	554	1.45	0.51	0.49	0.51
R10	20	7.5	0.38	0.233	86	6.2	4014	54	0	0	665	542	1.23	0.50	0.50	0.50
R11	20	7.5	0.38	0.233	86	6.6	4162	57	0	0	600	576	1.04	0.50	0.50	0.50
R13	20	7.5	0.38	0.233	86	5.3	3737	54	0.085	202	710	516	1.38	0.45	0.55	0.45
R16	20	7.5	0.38	0.233	86	8.6	4750	57	0	0	765	649	1.18	0.58	0.42	0.58
R21	20	7.5	0.38	0.233	86	0.0	0	57	0	0	449	305	1.47	0.00	1.00	0.00
R14	20	5.0	0.25	0.233	86	8.6	4747	55	0	0	826	848	0.97	0.92	0.08	0.92
R15	20	5.0	0.25	0.233	86	8.8	4802	55	0	0	796	828	0.96	0.96	0.04	0.96
R20	20	5.0	0.25	0.233	86	2.8	2704	57	0	0	712	542	1.31	0.46	0.54	0.46

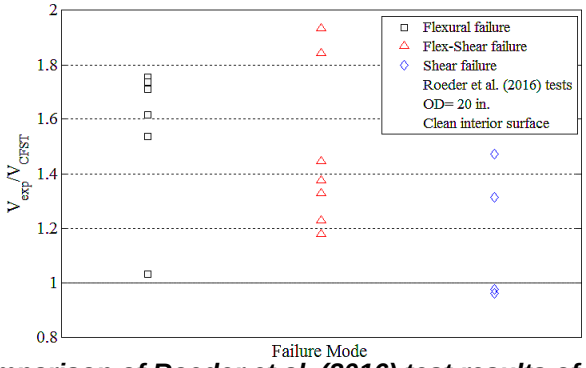

Figure I.48: Comparison of Roeder et al. (2016) test results of different failure modes and the proposed shear strength formula.

Table I.11. Qian et al. (2007) test specimens properties, results, and comparison with proposed formula.

Specimen	OD, *in.*	a, *in.*	$\frac{a}{OD}$	t, *in.*	$\frac{D}{t}$	f'_c, *ksi*	E_c, *ksi*	f_y, *ksi*	$\frac{P}{P_o}$	P, *ksi*	V_{exp}, *kips*	V_{CFST}, *kips*	$\frac{V_{exp}}{V_{CFST}}$	$\frac{V_{Strut}}{V_{CFST}}$	$\frac{V_{tube}}{V_{CFST}}$	$\frac{V_{conc}}{V_{CFST}}$
Q3	7.7	0.8	0.1	0.217	35	5.9	3922	48	0.43	209	281	120	2.33	0.27	0.73	0.27
Q4	7.6	0.8	0.1	0.295	26	5.9	3922	61	0.46	299	375	182	2.06	0.17	0.83	0.17
Q5	7.7	0.8	0.1	0.217	35	5.9	3922	48	0.72	348	378	109	3.48	0.29	0.71	0.29
Q6	7.6	0.8	0.1	0.295	26	5.9	3922	61	0.77	499	409	159	2.58	0.20	0.80	0.20
Q11	7.7	0.8	0.1	0.217	35	8.1	4596	48	0.41	237	272	133	2.04	0.33	0.67	0.33
Q12	7.6	0.8	0.1	0.295	26	8.1	4596	61	0.45	326	277	195	1.42	0.22	0.78	0.22
Q13	7.7	0.8	0.1	0.217	35	8.1	4596	48	0.69	395	336	122	2.76	0.36	0.64	0.36
Q14	7.6	0.8	0.1	0.295	26	8.1	4596	61	0.3	217	263	200	1.32	0.21	0.79	0.21
Q18	7.6	2.3	0.3	0.295	26	8.1	4596	61	0.45	326	387	224	1.73	0.31	0.69	0.31
Q19	7.7	2.3	0.3	0.217	35	8.1	4596	48	0.69	395	391	160	2.44	0.47	0.53	0.47
Q30	7.7	0.8	0.1	0.217	35	9.8	5065	48	0.4	260	376	143	2.63	0.37	0.63	0.37
Q31	7.6	0.8	0.1	0.295	26	9.8	5065	61	0.44	348	271	205	1.33	0.26	0.74	0.26
Q32	7.7	0.8	0.1	0.217	35	9.8	5065	48	0.67	433	226	132	1.71	0.40	0.60	0.40
Q33	7.6	0.8	0.1	0.295	26	9.8	5065	61	0.29	232	291	210	1.39	0.25	0.75	0.25
Q1	7.7	0.8	0.1	0.217	35	5.9	3922	48	0	0	286	123	2.32	0.26	0.74	0.26
Q2	7.6	0.8	0.1	0.295	26	5.9	3922	61	0	0	289	190	1.52	0.16	0.84	0.16
Q7	7.7	1.2	0.15	0.217	35	5.9	3922	48	0	0	439	138	3.17	0.35	0.65	0.35
Q8	7.6	1.2	0.15	0.295	26	5.9	3922	61	0	0	458	205	2.23	0.23	0.77	0.23
Q9	7.7	0.8	0.1	0.217	35	8.1	4596	48	0	0	501	134	3.73	0.33	0.67	0.33
Q10	7.6	0.8	0.1	0.295	26	8.1	4596	61	0	0	283	201	1.41	0.21	0.79	0.21
Q15	7.7	1.2	0.15	0.217	35	8.1	4596	48	0	0	230	155	1.49	0.43	0.57	0.43
Q16	7.6	1.2	0.15	0.295	26	8.1	4596	61	0	0	225	222	1.01	0.29	0.71	0.29
Q17	7.6	2.3	0.3	0.295	26	8.1	4596	61	0	0	395	226	1.75	0.31	0.69	0.31
Q28	7.7	0.8	0.1	0.217	35	9.8	5065	48	0	0	326	143	2.28	0.37	0.63	0.37
Q29	7.6	0.8	0.1	0.295	26	9.8	5065	61	0	0	398	210	1.89	0.25	0.75	0.25
Q34	7.7	1.2	0.15	0.217	35	9.8	5065	48	0	0	289	167	1.73	0.48	0.52	0.48
Q35	7.6	1.2	0.15	0.295	26	9.8	5065	61	0	0	220	235	0.94	0.33	0.67	0.33

Table I.12. Xiao et al. (2012) test specimens properties, results, and comparison with proposed formula.

Specimen	OD, *in.*	a, *in.*	$\frac{a}{OD}$	t, *in.*	$\frac{D}{t}$	f'_c, *ksi*	E_c, *ksi*	f_y, *ksi*	$\frac{P}{P_o}$	P, *ksi*	V_{exp}, *kips*	V_{CFST}, *kips*	$\frac{V_{exp}}{V_{CFST}}$	$\frac{V_{Strut}}{V_{CFST}}$	$\frac{V_{tube}}{V_{CFST}}$	$\frac{V_{conc}}{V_{CFST}}$
X1	6.3	2.5	0.40	0.217	29	3.8	3137	55	0.00	0	141	95	1.48	0.10	0.90	0.10
X2	6.3	2.5	0.40	0.217	29	4.7	3509	55	0.00	0	152	97	1.56	0.12	0.88	0.12
X3	6.3	2.5	0.40	0.217	29	4.3	3348	55	0.00	0	146	96	1.52	0.11	0.89	0.11
X4	6.5	2.6	0.40	0.173	38	3.8	3137	50	0.00	0	116	77	1.51	0.15	0.85	0.15
X5	6.5	2.6	0.40	0.173	38	4.7	3509	50	0.00	0	128	80	1.60	0.18	0.82	0.18
X6	6.5	2.6	0.40	0.173	38	4.3	3348	50	0.00	0	118	78	1.51	0.17	0.83	0.17
X7	6.5	2.6	0.40	0.118	55	3.8	3137	59	0.00	0	84	65	1.30	0.19	0.81	0.19
X8	6.5	2.6	0.40	0.118	55	4.7	3509	59	0.00	0	93	68	1.38	0.23	0.77	0.23
X9	6.5	2.6	0.40	0.118	55	4.3	3348	59	0.00	0	87	66	1.31	0.21	0.79	0.21
X10	6.3	2.5	0.40	0.217	29	3.8	3137	55	0.32	105	164	93	1.76	0.10	0.90	0.10
X11	6.3	2.5	0.40	0.217	29	4.7	3509	55	0.31	109	169	95	1.77	0.12	0.88	0.12
X12	6.3	2.5	0.40	0.217	29	4.3	3348	55	0.31	106	175	94	1.86	0.11	0.89	0.11
X13	6.5	2.6	0.40	0.173	38	3.8	3137	50	0.31	89	142	76	1.87	0.15	0.85	0.15
X14	6.5	2.6	0.40	0.173	38	4.7	3509	50	0.30	94	147	79	1.87	0.18	0.82	0.18
X15	6.5	2.6	0.40	0.173	38	4.3	3348	50	0.30	90	152	77	1.96	0.17	0.83	0.17
X16	6.5	2.6	0.40	0.118	55	3.8	3137	59	0.30	77	108	64	1.68	0.19	0.81	0.19
X17	6.5	2.6	0.40	0.118	55	4.7	3509	59	0.28	80	109	68	1.61	0.23	0.77	0.23
X18	6.5	2.6	0.40	0.118	55	4.3	3348	59	0.28	77	111	66	1.68	0.21	0.79	0.21
X19	6.3	2.5	0.40	0.217	29	3.8	3137	55	0.64	210	158	84	1.89	0.11	0.89	0.11
X20	6.3	2.5	0.40	0.217	29	4.7	3509	55	0.62	219	182	86	2.11	0.13	0.87	0.13
X21	6.5	2.6	0.40	0.173	38	3.8	3137	50	0.62	179	146	69	2.11	0.17	0.83	0.17
X22	6.5	2.6	0.40	0.173	38	4.7	3509	50	0.60	188	157	73	2.16	0.20	0.80	0.20
X23	6.5	2.6	0.40	0.118	55	3.8	3137	59	0.60	154	123	61	2.00	0.20	0.80	0.20
X24	6.5	2.6	0.40	0.118	55	4.7	3509	59	0.56	160	130	65	2.01	0.24	0.76	0.24
X25	6.3	0.9	0.14	0.217	29	3.8	3137	55	0.00	0	112	105	1.07	0.18	0.82	0.18
X26	6.3	0.9	0.14	0.217	29	4.7	3509	55	0.00	0	118	109	1.08	0.22	0.78	0.22
X27	6.3	0.9	0.14	0.217	29	4.3	3348	55	0.00	0	124	107	1.15	0.20	0.80	0.20
X28	6.3	0.9	0.14	0.217	29	4.3	3348	55	0.00	0	157	107	1.47	0.20	0.80	0.20
X29	6.5	0.9	0.14	0.173	38	4.3	3348	50	0.00	0	146	88	1.65	0.27	0.73	0.27
X30	6.5	0.9	0.14	0.118	55	4.3	3348	59	0.00	0	101	76	1.34	0.32	0.68	0.32
X31	6.5	0.9	0.14	0.173	38	3.8	3137	50	0.00	0	118	86	1.38	0.24	0.76	0.24
X32	6.5	0.9	0.14	0.173	38	4.7	3509	50	0.00	0	129	91	1.43	0.29	0.71	0.29
X33	6.5	0.9	0.14	0.173	38	4.3	3348	50	0.00	0	126	88	1.43	0.27	0.73	0.27
X34	6.5	0.9	0.14	0.118	55	3.8	3137	59	0.00	0	90	73	1.23	0.29	0.71	0.29
X35	6.5	0.9	0.14	0.118	55	4.7	3509	59	0.00	0	96	78	1.23	0.34	0.66	0.34
X36	6.5	0.9	0.14	0.118	55	4.3	3348	59	0.00	0	92	76	1.22	0.32	0.68	0.32
X37	6.3	0.9	0.14	0.217	29	3.8	3137	55	0.32	105	202	103	1.96	0.18	0.82	0.18
X38	6.3	0.9	0.14	0.217	29	4.7	3509	55	0.31	109	225	109	2.07	0.22	0.78	0.22
X39	6.3	0.9	0.14	0.217	29	4.3	3348	55	0.31	106	214	106	2.01	0.20	0.80	0.20

Continued Table I.12. Xiao et al. (2012) test specimens properties, results, and comparison with proposed formula.

Specimen	OD, *in.*	a, *in.*	$\frac{a}{OD}$	t, *in.*	$\frac{D}{t}$	f'_c, *ksi*	E_c, *ksi*	f_y, *ksi*	$\frac{P}{P_o}$	P, *ksi*	V_{exp}, *kips*	V_{CFST}, *kips*	$\frac{V_{exp}}{V_{CFST}}$	$\frac{V_{Strut}}{V_{CFST}}$	$\frac{V_{tube}}{V_{CFST}}$	$\frac{V_{conc}}{V_{CFST}}$
X40	6.5	0.9	0.14	0.173	38	3.8	3137	50	0.31	89	185	86	2.17	0.24	0.76	0.24
X41	6.5	0.9	0.14	0.173	38	4.7	3509	50	0.30	94	202	91	2.22	0.29	0.71	0.29
X42	6.5	0.9	0.14	0.173	38	4.3	3348	50	0.30	90	191	89	2.16	0.27	0.73	0.27
X43	6.5	0.9	0.14	0.118	55	3.8	3137	59	0.30	77	152	73	2.07	0.29	0.71	0.29
X44	6.5	0.9	0.14	0.118	55	4.7	3509	59	0.28	80	169	79	2.14	0.33	0.67	0.33
X45	6.5	0.9	0.14	0.118	55	4.3	3348	59	0.28	77	157	76	2.06	0.31	0.69	0.31
X46	6.3	0.9	0.14	0.217	29	3.8	3137	55	0.64	210	211	95	2.22	0.20	0.80	0.20
X47	6.3	0.9	0.14	0.217	29	4.7	3509	55	0.62	219	236	101	2.34	0.23	0.77	0.23
X48	6.3	0.9	0.14	0.217	29	4.3	3348	55	0.62	211	270	99	2.73	0.22	0.78	0.22
X49	6.5	0.9	0.14	0.173	38	3.8	3137	50	0.62	179	230	80	2.87	0.26	0.74	0.26
X50	6.5	0.9	0.14	0.173	38	4.7	3509	50	0.60	188	236	87	2.73	0.30	0.70	0.30
X51	6.5	0.9	0.14	0.173	38	4.3	3348	50	0.60	180	202	84	2.41	0.28	0.72	0.28
X52	6.5	0.9	0.14	0.118	55	3.8	3137	59	0.60	154	172	71	2.42	0.30	0.70	0.30
X53	6.5	0.9	0.14	0.118	55	4.7	3509	59	0.56	160	185	77	2.41	0.34	0.66	0.34
X54	6.5	0.9	0.14	0.118	55	4.3	3348	59	0.57	155	193	74	2.60	0.32	0.68	0.32
X55	6.3	3.2	0.50	0.256	25	2.9	2764	65	0.00	0	169	124	1.36	0.00	0.98	0.02
X56	6.3	6.3	1.00	0.256	25	2.9	2764	65	0.00	0	121	124	0.98	0.00	0.98	0.02
X57	6.5	3.3	0.50	0.161	40	2.9	2764	59	0.00	0	99	75	1.33	0.00	0.96	0.04
X58	6.5	6.5	1.00	0.161	40	2.9	2764	59	0.00	0	73	75	0.97	0.00	0.96	0.04

Table I.13. Xu et al. (2009) test specimens properties, results, and comparison with proposed formula.

Specimen	OD, *in.*	a, *in.*	$\frac{a}{OD}$	t, *in.*	$\frac{D}{t}$	f'_c, *ksi*	E_c, *ksi*	f_y, *ksi*	$\frac{P}{P_o}$	P, *ksi*	V_{exp}, *kips*	V_{CFST}, *kips*	$\frac{V_{exp}}{V_{CFST}}$	$\frac{V_{Strut}}{V_{CFST}}$	$\frac{V_{tube}}{V_{CFST}}$	$\frac{V_{conc}}{V_{CFST}}$
Xu16	5.5	0.6	0.1	0.145	38	4.9	3576	53	0	0	93	62	1.49	0.22	0.78	0.22
Xu17	5.5	1.1	0.2	0.145	38	4.9	3576	53	0	0	83	75	1.11	0.37	0.63	0.37
Xu18	5.5	1.7	0.3	0.145	38	4.9	3576	53	0	0	80	72	1.11	0.33	0.67	0.33
Xu19	5.5	2.8	0.5	0.145	38	4.9	3576	53	0	0	68	52	1.32	0.00	0.94	0.06

Table I.14. Ye et al. (2016) test specimens properties, results, and comparison with proposed formula.

Specimen	OD, *in.*	a, *in.*	$\frac{a}{OD}$	t, *in.*	$\frac{D}{t}$	f'_c, *ksi*	E_c, *ksi*	f_y, *ksi*	$\frac{P}{P_o}$	P, *ksi*	V_{exp}, *kips*	V_{CFST}, *kips*	$\frac{V_{exp}}{V_{CFST}}$	$\frac{V_{Strut}}{V_{CFST}}$	$\frac{V_{tube}}{V_{CFST}}$	$\frac{V_{conc}}{V_{CFST}}$
Ye1	4.7	0.7	0.15	0.079	60	4.6	3481	49	0	0	54	35	1.54	0.42	0.58	0.42
Ye2	4.7	0.7	0.15	0.079	60	4.6	3481	49	0	0	54	35	1.55	0.42	0.58	0.42
Ye3	4.7	0.7	0.15	0.079	60	4.6	3481	49	0.24	32	60	36	1.68	0.41	0.59	0.41
Ye4	4.7	0.7	0.15	0.079	60	4.6	3481	49	0.24	32	57	36	1.58	0.41	0.59	0.41
Ye5	4.7	0.7	0.15	0.079	60	4.6	3481	49	0.59	78	71	35	2.02	0.42	0.58	0.42
Ye6	4.7	0.7	0.15	0.079	60	4.6	3481	49	0.59	78	72	35	2.04	0.42	0.58	0.42
Ye7	4.7	0.7	0.15	0.079	60	4.6	3481	49	0.73	97	75	34	2.17	0.43	0.57	0.43
Ye8	4.7	0.7	0.15	0.079	60	4.6	3481	49	0.73	97	71	34	2.07	0.43	0.57	0.43
Ye9	4.7	0.4	0.08	0.079	60	4.6	3481	49	0.49	65	104	28	3.76	0.27	0.73	0.27
Ye10	4.7	0.4	0.08	0.079	60	4.6	3481	49	0.49	65	97	28	3.52	0.27	0.73	0.27
Ye11	4.7	0.7	0.15	0.079	60	4.6	3481	49	0.49	65	65	36	1.82	0.42	0.58	0.42
Ye12	4.7	0.7	0.15	0.079	60	4.6	3481	49	0.49	65	64	36	1.80	0.42	0.58	0.42
Ye13	4.7	2.4	0.5	0.079	60	4.6	3481	49	0.49	65	39	24	1.63	0.00	0.79	0.21
Ye14	4.7	2.4	0.5	0.079	60	4.6	3481	49	0.49	65	44	24	1.81	0.00	0.79	0.21
Ye15	4.7	3.5	0.75	0.079	60	4.6	3481	49	0.49	65	39	24	1.63	0.00	0.79	0.21
Ye16	4.7	3.5	0.75	0.079	60	4.6	3481	49	0.49	65	37	24	1.55	0.00	0.79	0.21
Ye17	4.7	0.7	0.15	0.079	60	8.3	4670	49	0.34	65	79	48	1.67	0.56	0.44	0.56
Ye18	4.7	0.7	0.15	0.079	60	8.3	4670	49	0.34	65	76	48	1.59	0.56	0.44	0.56
Ye19	4.7	0.7	0.15	0.118	40	4.6	3481	60	0.37	65	88	53	1.67	0.27	0.73	0.27
Ye20	4.7	0.7	0.15	0.118	40	4.6	3481	60	0.37	65	88	53	1.66	0.27	0.73	0.27

APPENDIX J

Finite element modeling of the test specimens

J.1 Finite element modeling and analysis of flexural tests

J.1.1 Finite element modeling of flexural tests

The finite element models of the tested specimens were constructed in LS-Dyna using the validated basic finite element models that were described in Section 2.2.4. Those finite element models were modified and re-analyzed here, in order to match the test specimens' dimensions and boundary conditions. Similar material models that were described in Section 2.2.4 were used for the concrete and steel parts as part of these re-analyses, except that the material properties used were those obtained from the coupon and cylinder tests for the specimens.

Figure J.1 shows the scheme developed for the finite element model for flexural specimens with no axial load. For sake of simplicity and reducing the analysis duration, a half of the flexural specimen was modeled and appropriate boundary conditions were defined on the symmetry plane. Also, only an inner part of the foundation block was modeled instead of all the foundation. The reduced dimensions of the foundation block were chosen in an iterative process by taking into account the effect of the foundation on the lateral stiffness of the specimen and based on performing a series of sensitivity push-over analyses starting from fully modelled foundation and simplifying it at each iteration.

The Winfrith concrete material model (MAT 85) with constant stress solid elements was used for the concrete parts. Table 2.2 presents the input parameters of the concrete material model. For the steel tube and baseplate's stiffeners, LS-Dyna's default shell element with 3 (or more) integration points through the element thickness was used. The baseplate part was modeled using constant stress solid elements. Bilinear elasto plastic material with 1% strain hardening was used for modeling of the steel parts. Kinematic hardening was considered for the steel material. Rebars were modeled using beam elements. For longitudinal rebars, a similar steel material model was used. Stirrups were modeled using elastic material. Table J.2 shows the input parameters for the nonlinear steel material. No failure criteria were defined for concrete and steel materials.

The contact relationships between different parts of the finite element model are shown in Figure J.2 (which has no purpose for interpretation of the results, but is provide here because it would be needed if the LS-Dyna model was to be independently re-created). Longitudinal and transverse reinforcement element nodes were merged with concrete elements, which provided a perfect bond between them. The contact at the interface of the tube and concrete core was defined using the *Automatic Single Surface Contact* algorithm. This contact type is a penalty-based contact, which allows the compression load to be transferred between slave nodes and master segments. The *Automatic Single Surface Contact* algorithm is a two-way treatment contact, which means that the master and slave nodes are checked for penetration through each other (note that analyses using one-way treatment contact algorithms were also conducted, but those contact elements only check the penetration of slave nodes through the master segments at the contact interface; results from those analyses were unsatisfactory and are not reported here). In the surface contact model used, a friction force develops at the interface when the adjacent parts press on each other and want to slide against each other. Sliding will occur when the shear force between the two surfaces reach the sliding force

resistance, which is equal to the compression force at the contact multiplied by a corresponding friction coefficient. The measured coefficient-of-friction values were used between the steel tube and the concrete core for analysis of each flexural test specimen.

Cyclic displacement was applied to the reinforced concrete column part at the actuator level. To reduce the runtime of the finite element analyses, the repeated cycles at each nonlinear displacement amplitude in the test loading protocol that was described in Section 2.3.3 were not considered in the cyclic displacement history applied to the finite element model. The self-weight of the specimens was applied using body force command.

In the finite element model of Specimen S2R the DYWIDAG bar used for pre-tensioning of the specimen was modeled using solid elements. Figure J.3 shows the scheme used for the finite element model of Specimen S2R. The concrete part's mesh was modified to accommodate the DYWIDAG hole at the center of the cross-section. A vertical (i.e., z-direction) displacement boundary condition was applied at the bottom of the DYWIDAG bar to create an axial load equivalent to the pre-tension load that was applied to Specimen S2R.

Results from finite element analyses of the flexural specimens are presented in the following section.

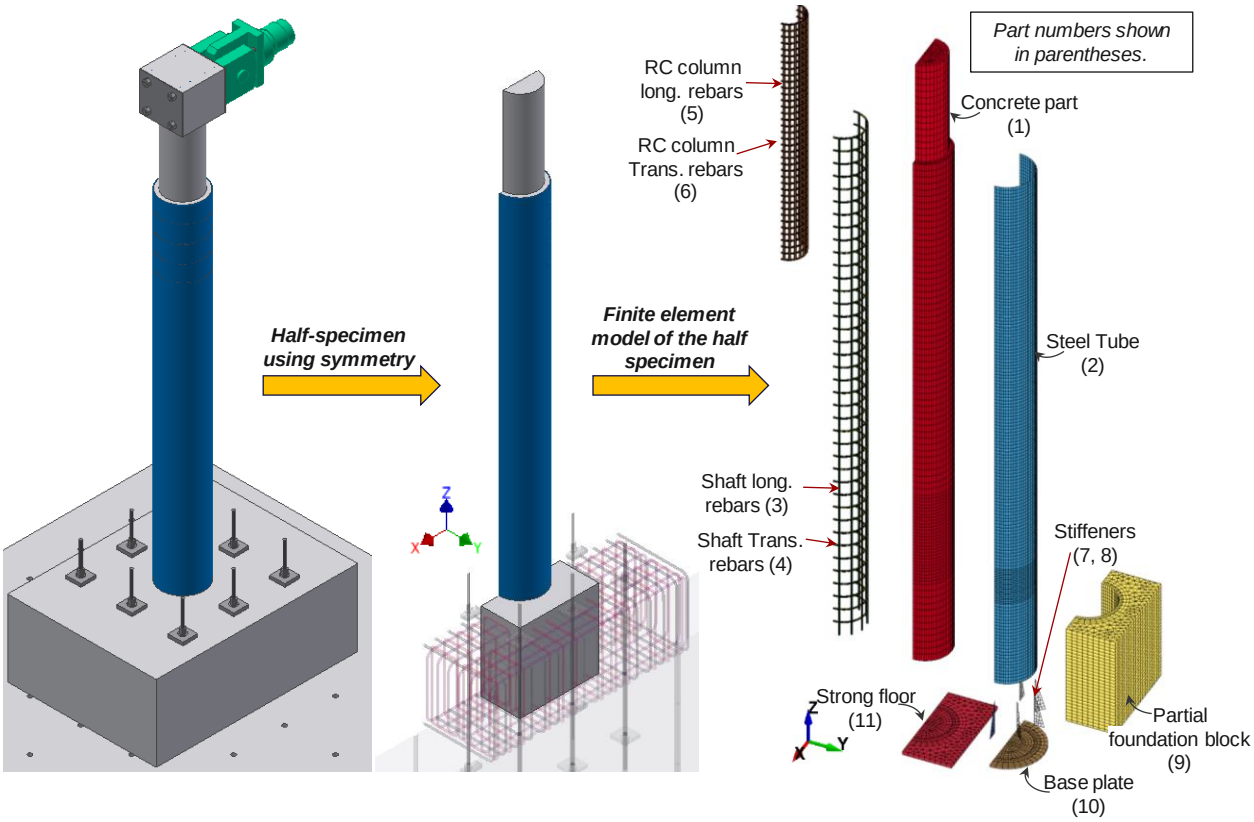

Figure J.1: Scheme of the developed finite element model for flexural specimens with no axial load.

Table J.1. Properties of the concrete material model

Material Model	Tangent Modulus, *ksi*	Poisson Ratio	Compressive Strength, UCS, *ksi*	Tensile Strength, UTS, *ksi*
Winfrith Concrete (MAT 84)	$\left(134\frac{lb}{ft^3}\right)^{\frac{3}{2}}.33.\sqrt{f_c'\ psi}$	0.2	Average f_c' values for each test	0.1xUCS

Table J.2. Properties of the concrete material model

Material Model	Tangent Modulus, E, *ksi*	Poisson Ratio, PR	Yield Stress, SIGY, *ksi*	Tangent Modulus, ETAN, *ksi*	Hardening parameter, BETA
Plastic Kinematic (MAT 003)	29000	0.3	Average F_y values for each test	0.1E	0

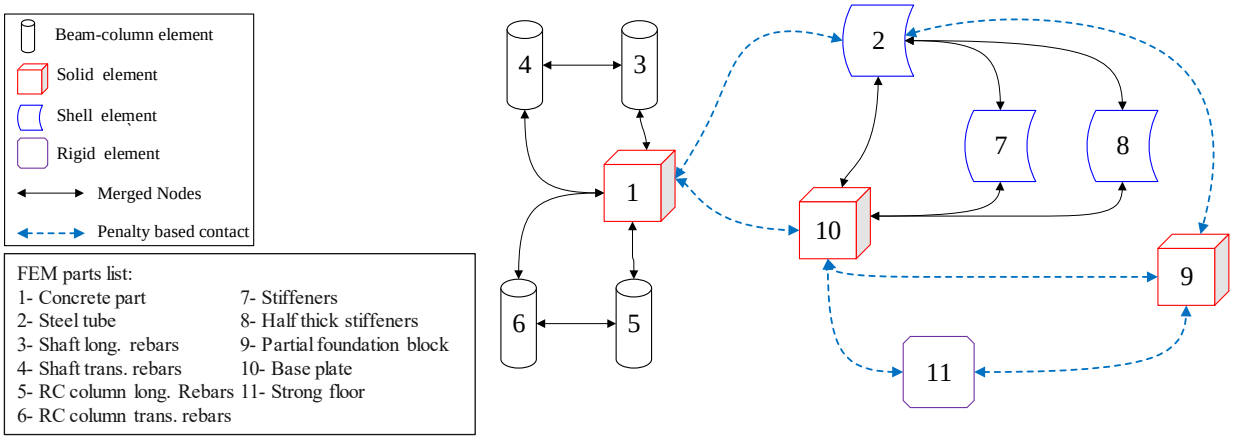

Figure J.2: The relationships between parts of the finite element model of flexural specimens

.

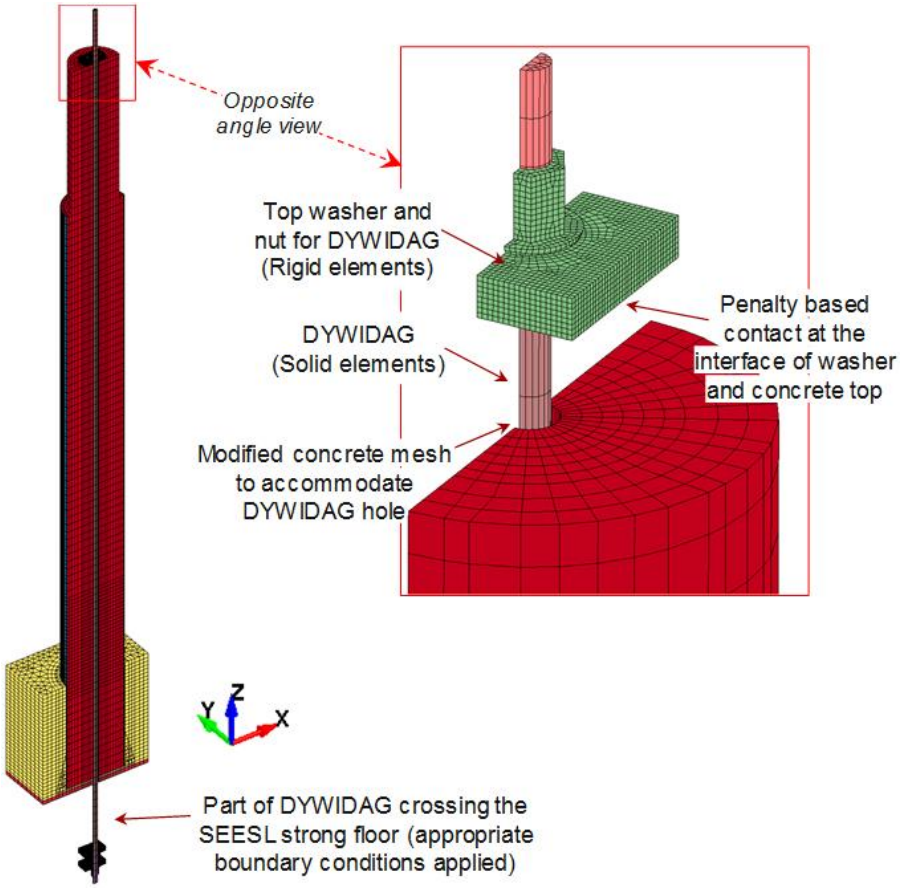

Figure J.3: Scheme of the finite element model of Specimen S2R.

J.1.2 Discussion of finite element analyses results of flexural tests

The results from the finite element analyses of the flexural test specimens are presented in this section. The hysteresis curves of the base moment-displacement relationships obtained from the finite element analyses are compared with the experimentally obtained results.

Figure J.4 compares the moment at the bottom of the RCFST shaft (i.e., top of the foundation) obtained from LS-Dyna finite element analysis with the experimental results of Specimen S1 test. As shown in this figure, the finite element analysis results are in good agreement with the experimental results. The initial stiffness of the specimen was well captured by the finite element model. The numerical results are generally slightly less than experimental results. At the drifts when maximum strength was achieved on negative and positives sides, the numerically-obtained base moments are 10% and 12% less than those obtained experimentally, respectively. Since, no failure criteria were defined for the materials and elements used in the finite element model, the model was not able to capture the strength degradation and failure of the specimen which was caused by initiation and propagation of cracking in the tube at the bottom of the shaft.

Figure J.5 shows the break-down of the base moment into the components carried by the steel tube and the reinforced concrete parts of the RCFST shaft. The percentage of the contribution of the steel tube and the reinforced concrete part of the RCFST shaft to the total strength of the specimen at peak drifts of each cycle is shown in Figure J.6. The point where the local buckling started to develop in the finite element model, the corresponding drift at the onset of visible local buckling observed during the test, and the point where the maximum experimental strength was obtained during test are also shown in this figure. As shown, the contribution of the steel tube is generally more than the contribution of the reinforced concrete part. The contribution of the steel tube is maximum right before the start of local buckling at the bottom of the shaft, at a drift equal to 3*in.* At this point the steel tube carries about 66% of the total base moment. The contribution of the steel tube starts to decrease after initiation of local buckling. The local buckling was visually observed to develop at a drift of 6*in.* during testing. At this point the steel tube contribution is about 59% of the total base moment. At a drift of about 10 $in.$, where the maximum strength was obtained during the test, the steel tube contribution is 55%. Figure J.7 shows the location of local buckling on the west side at the bottom of the shaft of the finite element model at a positive drift corresponding to the one when the maximum experimental strength was obtained (as a representative for location of local buckling), which is in good agreement with test observations.

Figure J.8 compares the moment at the bottom of the shaft obtained from LS-Dyna with the experimental results of Specimen S2R test. This specimen was axially loaded by a DYWIDAG bar to 93 $kips$ at the start of testing. In the finite element model, a similar axial load (90 $kips$) was applied to the specimen as described in Section 2.3.5. As shown in Figure J.8, the finite element results are closely matching the experimental results. Figures J.9 and J.10 show the moment carried by each part of the shaft and those parts' contribution to the total moment, respectively. As shown in Figure J.10, the contribution of the reinforced concrete part is more than the steel part at small drifts, which are mainly related to the elastic response range. This can be attributed to the presence of the axial load that produces compressive stresses on the cross-section of the reinforced concrete part of the shaft; therefore, a larger portion of the cross-section can contribute to the base moment. The maximum contribution of the steel tube, which happened right before initiation of local buckling, is about 59%; that is about 7% less compared to Specimen S1.

Figure J.11 compares the recorded axial load in the DYWIDAG bar from finite element analysis and testing. As was discussed in Appendix I, the axial load in the DYWIDAG bar increased with lateral drift. The increasing trend in the axial load was also captured by the finite element analysis of Specimen S2R. This increase in the axial load is attributed to the location of the neutral axis of the cross-section under bending with respect to the location of the DYWIDAG bar, which was located at the center of the cross-section (as described in Appendix H). It was also observed from the finite element analysis results that the specimen becomes longer as it goes through nonlinear cycles. The trace of the top of the specimen in the loading plane is plotted in Figure J.12 below for Specimens S1 and S2R. As shown in this figure, the top of the specimen moves upward during the test. The increase in height of Specimen S1, obtained from the finite element analysis, is about 0.6 in. For Specimen S2R, this elongation in height is somewhat restricted

by the axial load applied by the DYWIDAG bar, but still occurs (to a lesser extent); it is this lengthening that progressively increases the axial load during the test. The numerically-obtained value of increase in the height is about 0.3 $in.$ for Specimen S2R, that results in an approximate increase of 51 $kips$ in the axial load, which can be calculated analytically as:

$$\Delta F_{DYW} = \left(\frac{EA}{L}\right)_{DYW} \times \delta z = \frac{(29000)(1.58)}{270} \times 0.3 = 51\ kips \qquad \text{(J.1)}$$

where:

ΔF_{DYW}= increase in the axial load, $kips$.

$(\mathrm{EA}/L)_{DYW}$= axial stiffness of the DYWIDAG bar, $kip/in.$

δz= increase in the height of the specimen, $in.$

As shown in Figure J.11, at the start of analysis, the DYWIDAG force was 90 $kips$ and it had increased by 45 $kips$ at the end of analysis, which is close to the value calculated from Equation (J.1). However, for the experimental case, the remaining force in the DYWIDAG was recorded as 112$kips$, which was 19$kips$ more than the pre-tension force of the DYWIDAG. The numerically-obtained residual axial load from finite element analysis of Specimen S2R is therefore greater than the experimental one. The source of this difference could be related to crushing of the concrete at the bottom of the shaft during the test that could result in a settlement of the specimen at the larger amplitude cycles and a corresponding reduction of the axial force in the DYWIDAG bar (although the extent of crushing was not instrumented).

For Specimens S3 and S4, which had bentonite slurry and grease on the interior surface of their steel tube, respectively, the finite element analyses were performed considering three different friction coefficient values for each specimen. These models were analyzed for the cases: (i) with no friction (i.e., fully non-composite case, $\mu = 0$); (ii) with $\mu = 0.5$, and; (iii) with a friction coefficient equal to the average friction coefficient shown in Table I.7, which was obtained from the friction tests performed on specimen's steel tube-to-concrete interface after flexural testing of those specimens (as described in Appendix I). For this third case, the friction coefficients used for the finite element analyses were 0.6 and 0.15 for Specimens S3 and S4, respectively.

Figure J.13 shows the finite element results for Specimen S3 with different friction coefficient values. As shown, in all cases, the elastic stiffness was captured well. However, the case with zero friction showed less strength compared to the experimental results. The cases with $\mu = 0.5$ and 0.6 over-estimated the experimental strengths. Backbone curves for the three analyzed cases are compared to the experimental backbone curve in Figure J.14. The moments carried by the steel tube and the reinforced concrete components of the RCFST shaft and their contribution to the total base moment are shown in Figure J.15 for each friction case. As shown in this figure, the contribution of the steel tube for the non-composite case was more compared to the other two cases with friction. For all the cases, the maximum contribution of the steel tube happened right before the development of local buckling, and it amounted to 69% and 65% of the total strength obtained for the case with no friction (i.e., μ =0) and with friction (i.e., μ =0.5 and 0.6), respectively.

Figure J.16 shows the finite element results for Specimen S4 with different friction coefficient values. As shown, similarly to the results obtained for Specimen S3, the analytically-obtained elastic stiffness matched well with experimental results. The cases with zero friction and μ= 0.15 showed less strength compared to the experimental results, but the case with μ= 0.5 showed more strength than in other cases. Backbone curves for the three analyzed cases are compared to the experimental backbone curve in Figure J.17. The moments carried by the steel tube and the reinforced concrete components of the RCFST shaft and their contribution to the total base moment are shown in Figure J.15 for each friction case. The maximum contribution of the steel tube was about 68% for μ= 0 and μ=0.15, versus 65% for the case with μ=0.5.

Comparison of the finite element analysis and test results for Specimen S5 is shown in Figure J.19. For Specimen S5, the analytically-obtained results are shown to be in good agreement with the test results. The finite element analysis was extended beyond the maximum lateral displacement that was applied during the test (as discussed in Section 3.2.1, the applied lateral displacement during the test was limited to maximum $\pm 20\ in.$ stroke of the actuator) to maintain consistency with the other finite element analyses. The moments carried by the steel tube and the reinforced concrete components of the RCFST shaft and their contribution to the total base moment are shown in Figures J.20 and J.21. The maximum contribution of the steel tube to the total strength of the shaft was 60%. The location of local buckling at the bottom of Specimen S5's shaft is shown in Figure J.22.

In finite element modeling of Specimen S6R, the shear rings welded at the top of the shaft, were not modeled explicitly using elements. Instead, tie contacts between the steel tube and the concrete were used at the location of the shear rings. Tie contacts provide a perfect bond at the interface of the contact (i.e., between the steel tube and the concrete). Note that no observable deformations and cracks were observed in the concrete or the steel tube in the vicinity of the shear rings during the test. Also, no slippage was observed at the top of the shaft. Therefore, assuming a perfect bond between the steel tube and the concrete at the location of the shear rings, is a reasonable assumption. Figure J.23 shows the details of Specimen S6R at the location of shear rings.

Figure J.24 shows the finite element results for Specimen S6R. In general, the analytically-obtained response matches well with the experimental results in terms of stiffness and strength, and the unloading branches are in good agreement with the experimentally-obtained curves. For Specimen S6R, the strength values are more than those obtained experimentally. Figure J.25 compares the backbone curves obtained from the finite element analysis and the test. As shown, the strength value obtained by finite element analysis is 16% more compared to the maximum experimentally-obtained base moment value. This notable difference, which was not observed for the other flexural specimens comparisons, could be related to the existence of a difference between the material properties measured by the coupon and cylinder tests and the ones in the actual Specimen S6R; as discussed in Table 3.1 of Section 3.2.2, the strength calculated by PSDM using average measured material properties was also higher compared to that obtained for other specimens. The moments carried by the steel tube and the reinforced concrete components of the RCFST shaft and their contribution to the total base moment are shown in Figures J.26 and J.27.

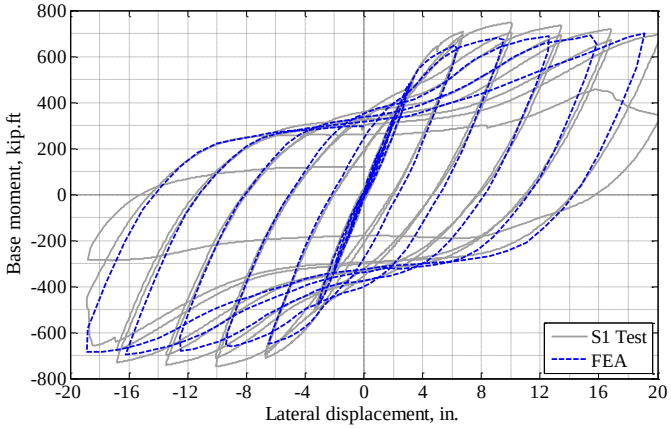

Figure J.4: Finite element analysis and experimental results comparison for Specimen S1.

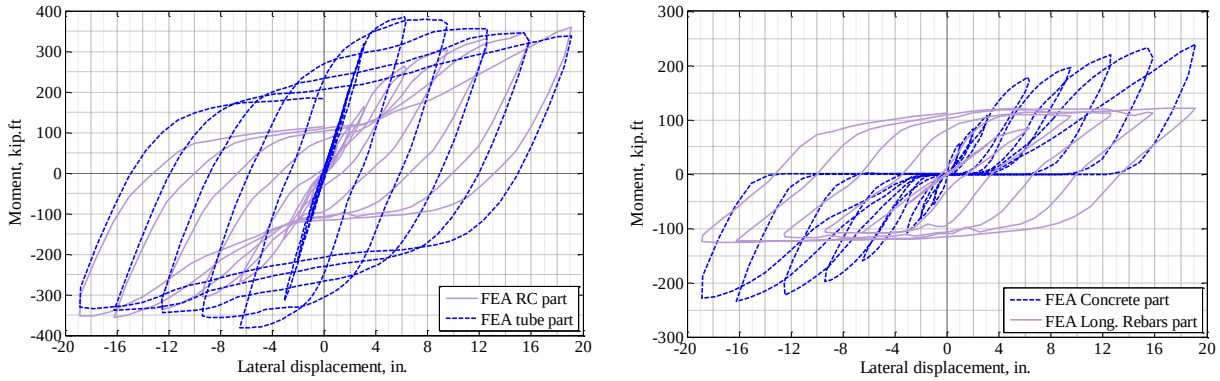

(a) Steel tube and reinforced concrete parts of RCFST shaft (b) Concrete and rebars of reinforced concrete part

Figure J.5: The moment carried by each part of the RCFST shaft of Specimen S1.

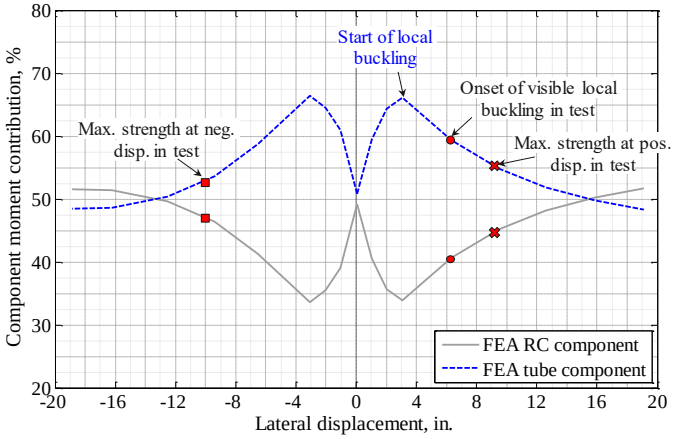

Figure J.6: Contribution of the steel tube and reinforced concrete part to the total moment of RCFST shaft of Specimen S1.

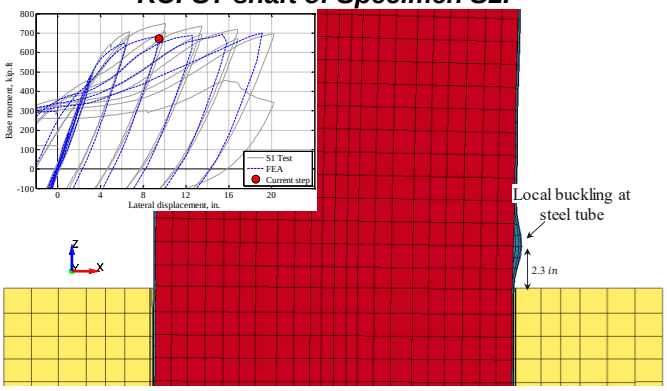

Figure J.7: The location of local buckling on the west side at the bottom of the shaft of the finite element model of Specimen S1.

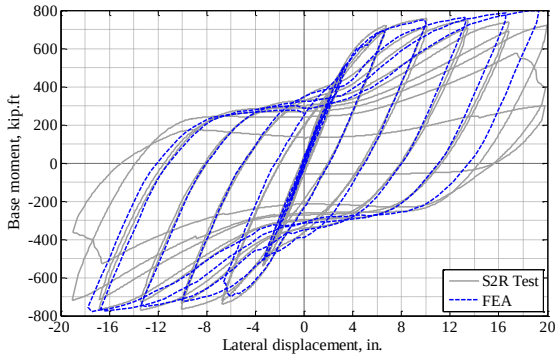

Figure J.8: Finite element analysis and experimental results comparison for Specimen S2R.

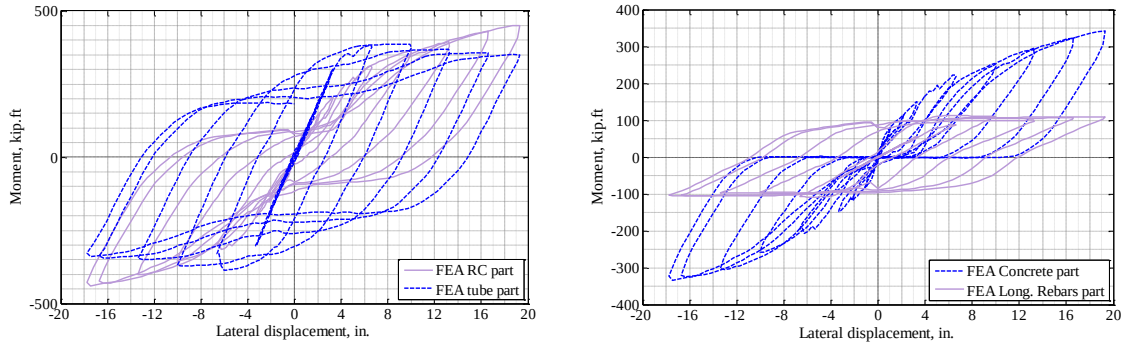

(a) Steel tube and reinforced concrete parts of RCFST shaft (b) Concrete and rebars of reinforced concrete part

Figure J.9: The moment carried by each part of the RCFST shaft of Specimen S2R.

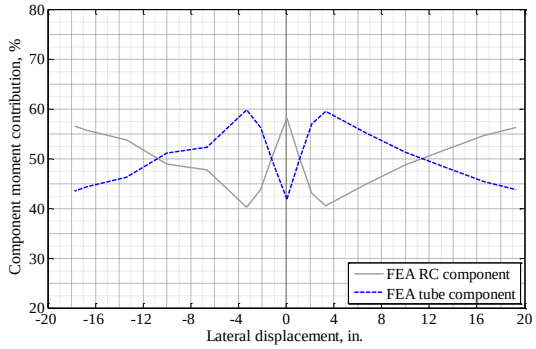

Figure J.10: Contribution of the steel tube and reinforced concrete part to the total moment of RCFST shaft of Specimen S2R.

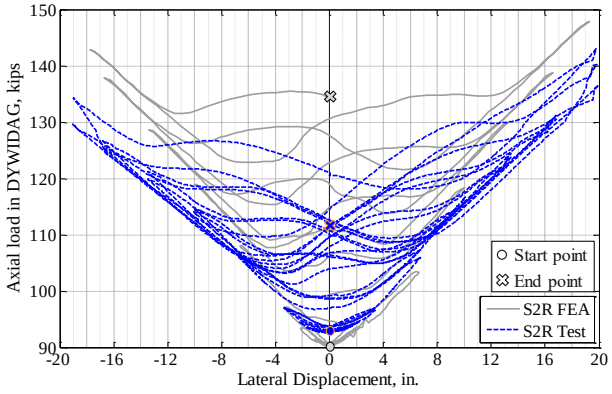

Figure J.11: Comparison of axial load in the DYWIDAG bar from finite element analysis and test of Specimen S2R.

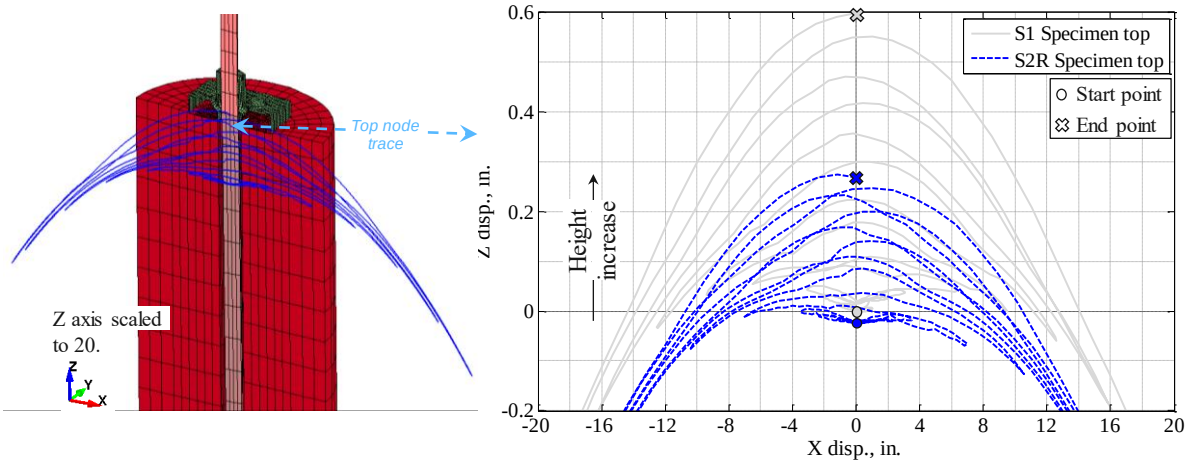

Figure J.12: The trace of the top of the specimen on the loading plane.

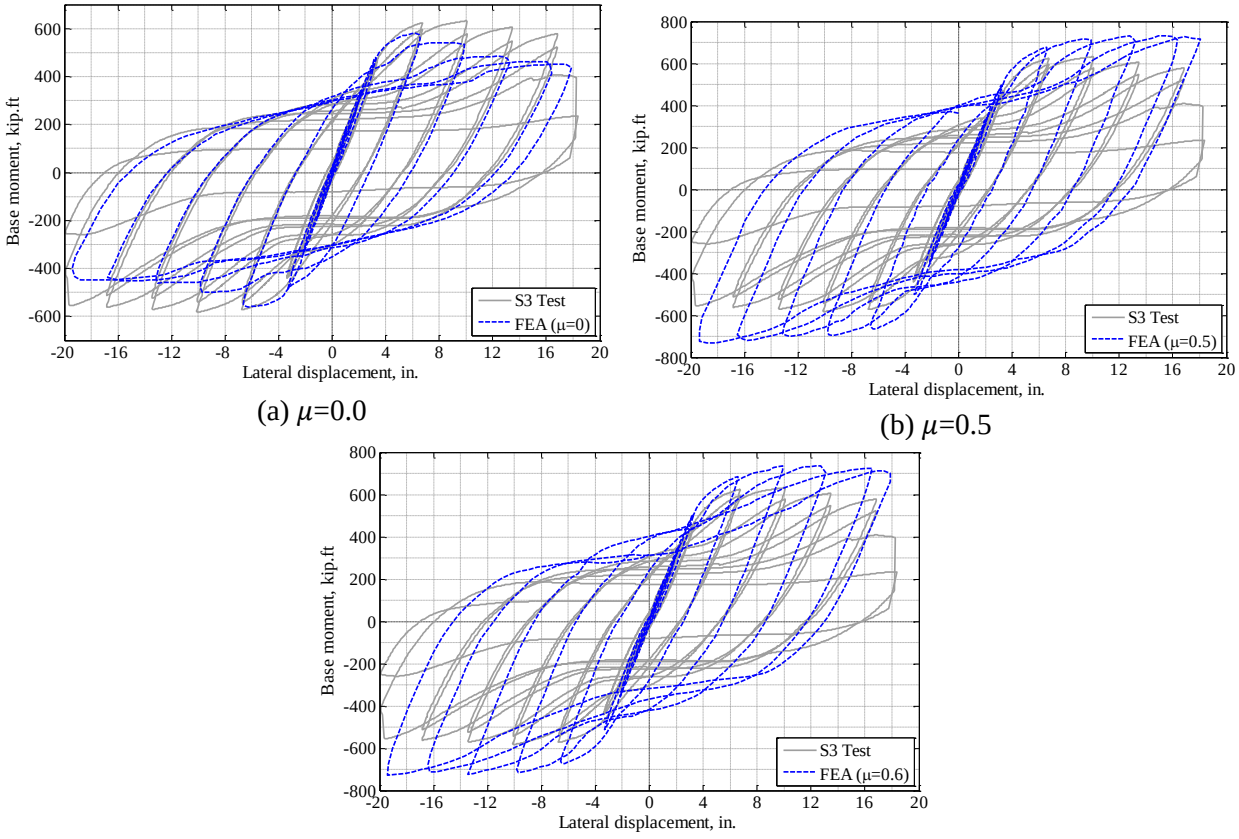

(a) μ=0.0

(b) μ=0.5

(c) μ=0.6

Figure J.13: Finite element analysis and experimental results comparison for Specimen S3.

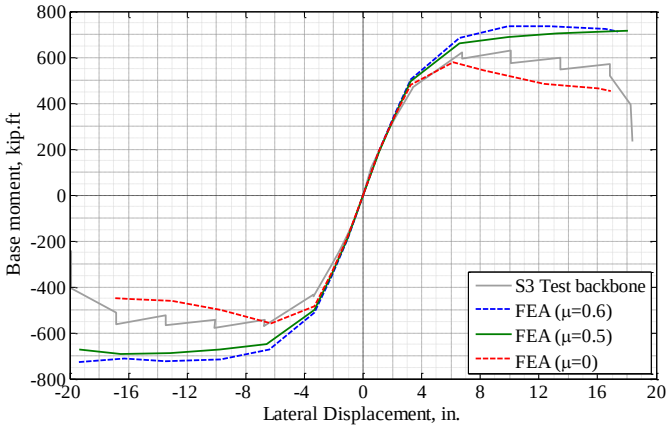

Figure J.14: Finite element and experimental results backbone comparison for Specimen S3.

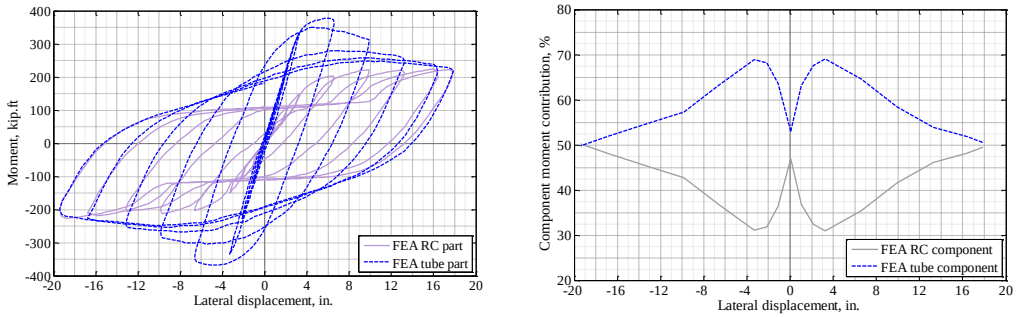

(a) μ=0.0

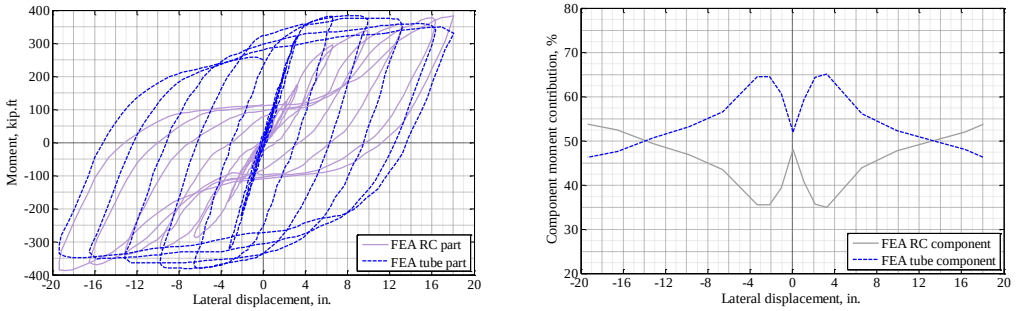

(b) μ=0.5

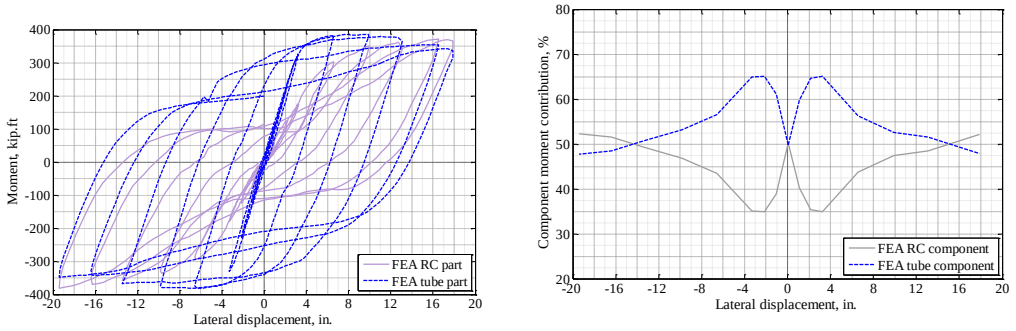

(c) μ=0.6

Figure J.15: Moments carried by each part of RCFST shaft of Specimen S3 for different friction cases.

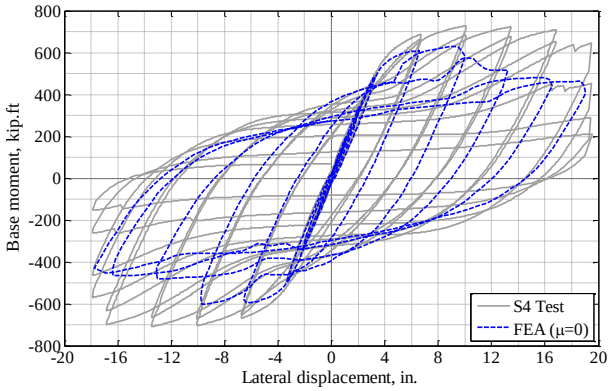

(a) μ=0.0

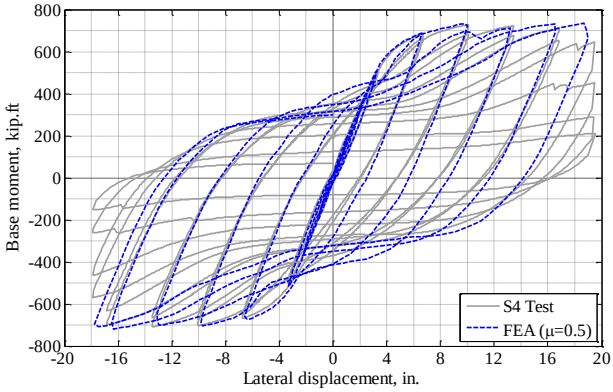

(b) μ=0.5

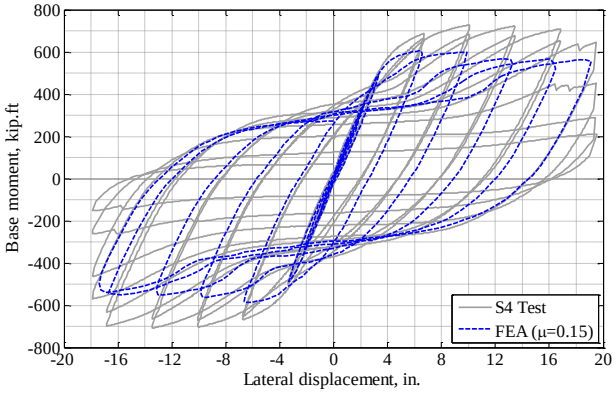

(c) μ=0.15

Figure J.16: Finite element analysis and experimental results comparison for Specimen S4.

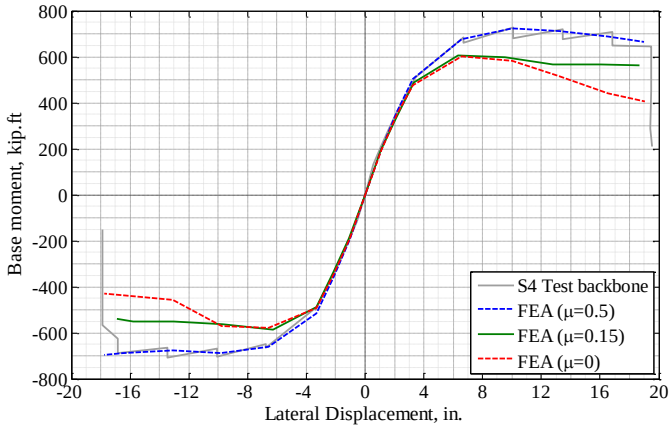

Figure J.17: Finite element and experimental results backbone comparison for Specimen S4.

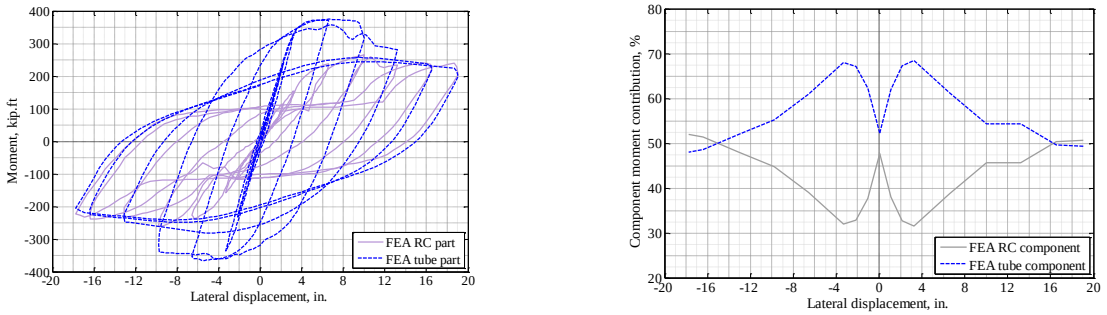

(a) μ=0.0

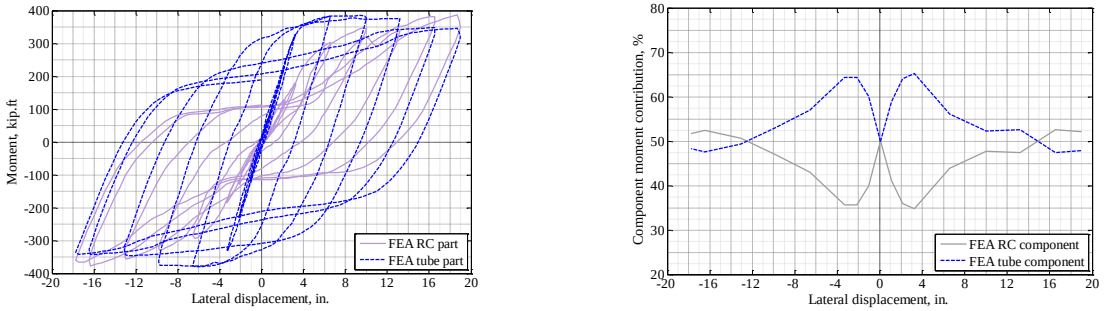

(b) μ=0.5

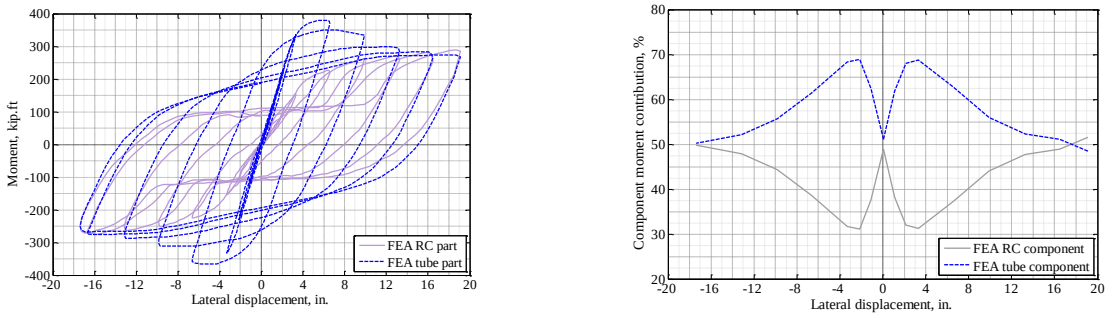

(c) μ=0.15

Figure J.18: Moments carried by each part of RCFST shaft of Specimen S4 for different friction cases.

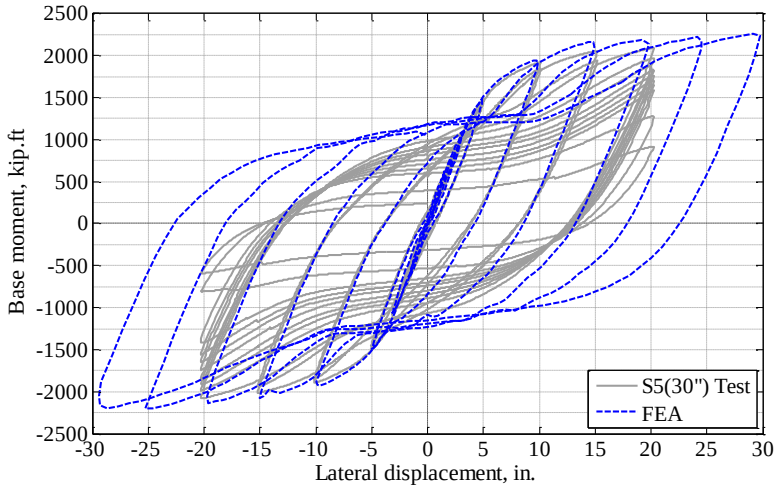

Figure J.19: Finite element analysis and experimental results comparison for Specimen S5.

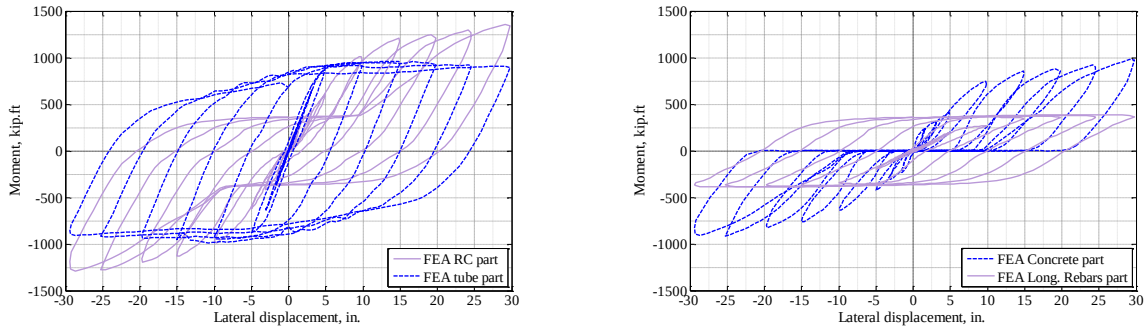

(a) Steel tube and reinforced concrete parts of RCFST shaft (b) Concrete and rebars of reinforced concrete part

Figure J.20: The moment carried by each part of the RCFST shaft of Specimen S5.

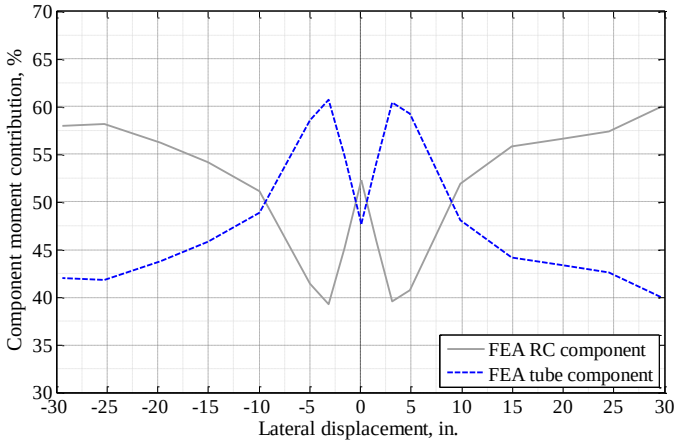

Figure J.21: Contribution of the steel tube and reinforced concrete part to the total moment of RCFST shaft of Specimen S5.

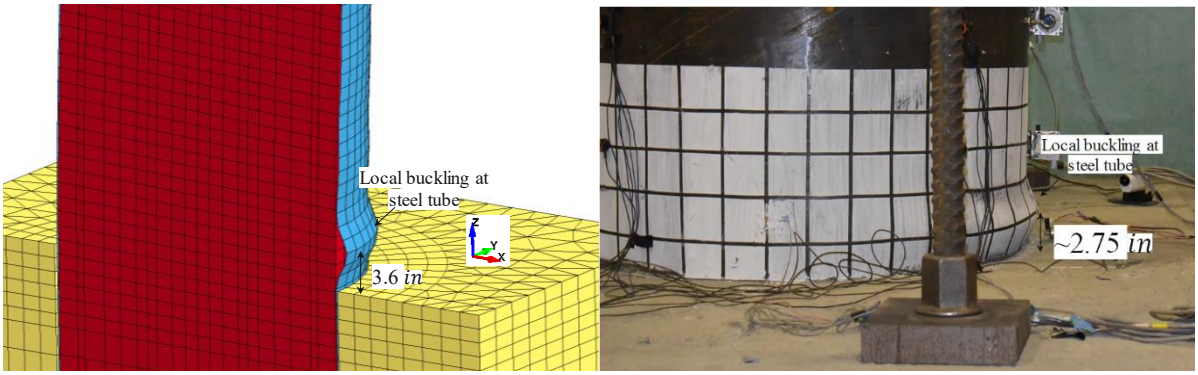

Figure J.22: The location of local buckling on the west side at the bottom of the shaft of the finite element model of Specimen S5.

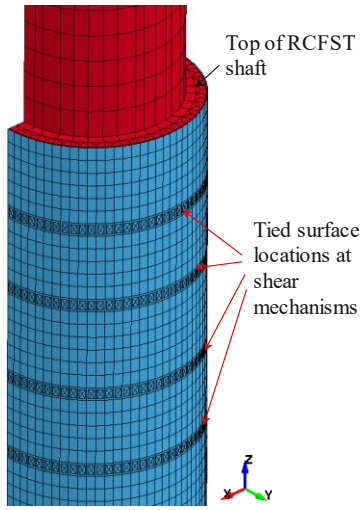

Figure J.23: The locations of tied contacts used for modeling shear mechanisms in Specimen S6R finite element model.

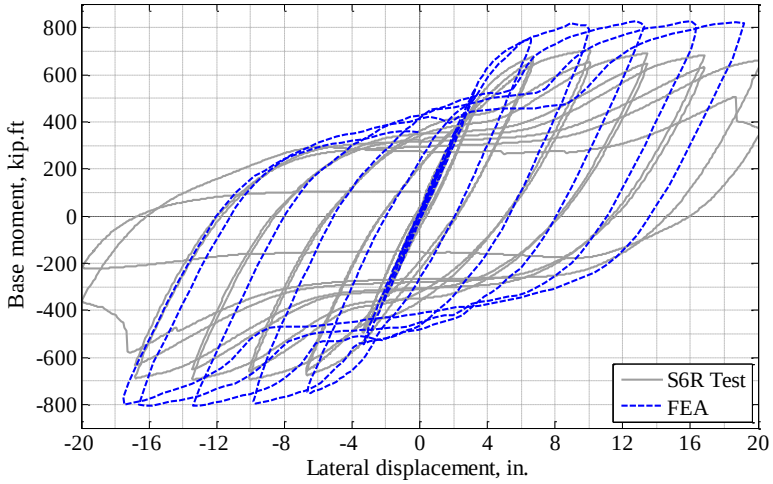

Figure J.24: Finite element analysis and experimental results comparison for Specimen S6R.

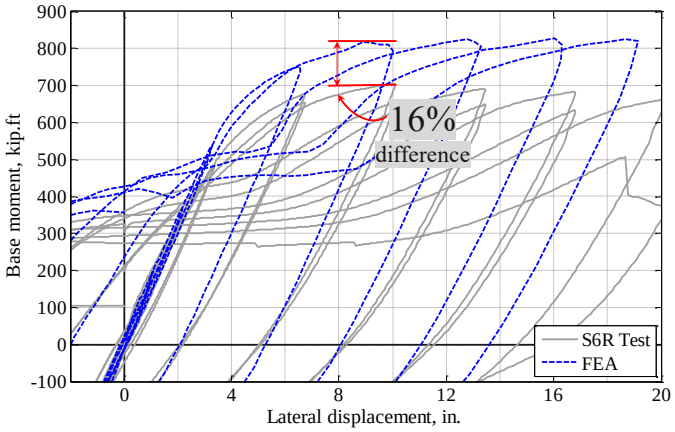

Figure J.25: Comparison of maximum strength results between finite element and experimental results for Specimen S6R.

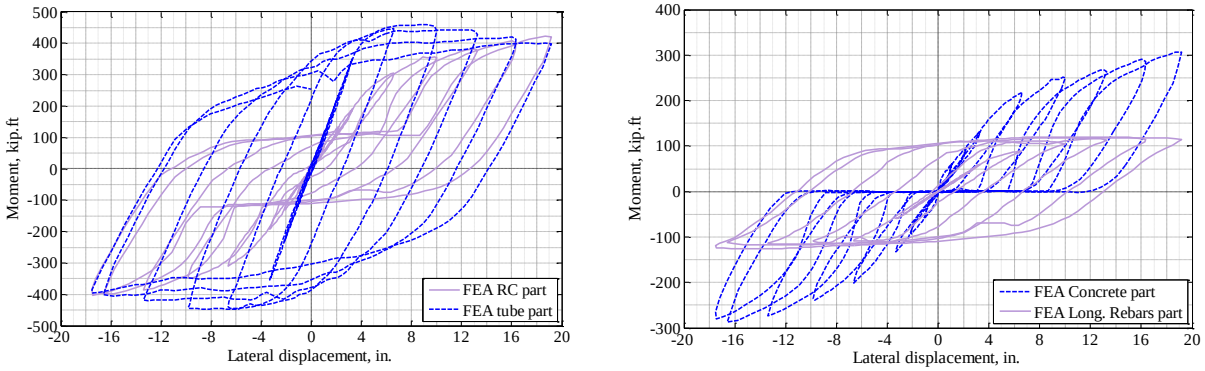

(a) Steel tube and reinforced concrete parts of RCFST shaft (b) Concrete and rebars of reinforced concrete part

Figure J.26: The moment carried by each part of the RCFST shaft of Specimen S6R.

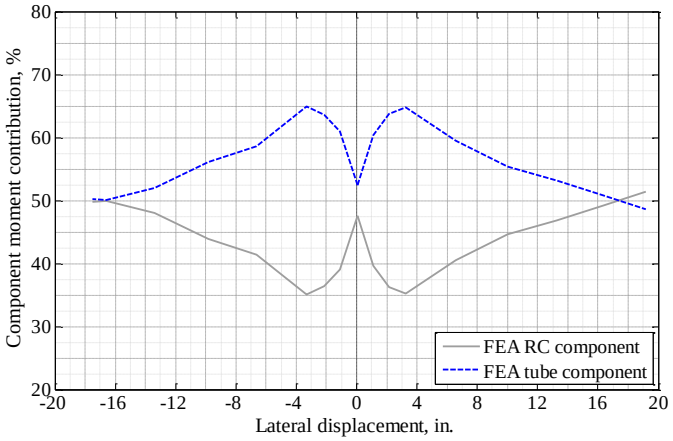

Figure J.27: Contribution of the steel tube and reinforced concrete part to the total moment of RCFST shaft of Specimen S6R.

J.2 Finite element analyses of RCFST shafts embedded in the soil

The details of the finite element models of the cases shown in Figure 3.7 of the report and their analyses results are presented in this Appendix. As it was mentioned in Section 3.2.4 of the report, to investigate the effect of soil embedment on the previous conclusions on the composite behavior of RCFST shafts, a finite element model of the $20in.$ flexural test specimen, but embedded in an elastic soil continuum, was analyzed in LS-Dyna. Different configurations of the RCFST shaft embedded in the soil were analyzed, considering the reinforced concrete column attached at top and different combinations of the attached shear transfer mechanism along the shaft, as schematically shown in Figure 3.7 of the report. The characteristics of the six configurations considered here are summarized as follows:

- Case (1): Similar to Specimen S1, but with RCFST shaft part embedded in soil.
- Case (2): Similar to Case (1), but with shear rings modeled at the top of the RCFST shaft.
- Case (3): Similar to Case (1), but with shear rings modeled at top of the RCFST shaft and below the location of maximum moment along the shaft (i.e., at a depth of $3.5D_s$).
- Case (4): A continuous RCFST shaft similar to Specimen S1, but with a height of $3D_s$ extending out of the soil.
- Case (5): Similar to Case (4) with shear rings modeled at the top.

- Case (6): Similar to Case (4) with two rings modeled the top and below the location of maximum moment under the soil (i.e., at a depth of $2D_s$).

In all the cases it was assumed that the base of the shaft was sitting on bedrock. The soil medium was modeled using elastic solid elements and analyses were conducted considering different values of the soil elastic moduli such as to achieve a depth of the maximum moment ranging from between 1 to 3 times the diameter of the shaft (D_s). For all the models, different friction coefficients (namely μ=0.1 and 0.5) were considered at the interface between the steel tube and the concrete core along the RCFST shaft. Note that the reinforced concrete column above the ground for Cases (1) to (3) was modeled as elastic in order to force development of the plastic hinge in the RCFST shaft part. The length of the transition zone inside the shaft (for development of the column rebars) was taken as similar to that used in Specimen S1, which was about $2.5D_s$. Figure J.28 shows the finite element mesh of the shaft and the surrounding soil continuum in LS-Dyna.

The contribution of steel and concrete to the total moment, the transferred internal axial load, and the neutral axis location along the length of the shafts embedded into soil were compared to the finite element results obtained for Specimen S1 under monotonic pushover load. These diagrams for the flexural test Specimen S1 are shown in Figure J.29. The moment distribution along the RCFST shaft part of Specimen S1 is shown in Figure J.29a at the point when the moment at the bottom of the shaft reached the composite moment value calculated by the PSDM (M_{PSDM}).

Recall that position of neutral axis is helpful to relatively illustrate how much compositeness develops in a RCFST. As explained in the analytical program of Chapter 2, for a fully composite RCFST cross-section, the neutral axes of the steel tube and the concrete core would be coaxial. Conversely, in a non-composite cross-section under flexure (and without external axial load), the neutral axes of the steel tube and concrete core are not coaxial. In that latter case, the steel tube's neutral axis is on the centerline of the cross-section, while the reinforced concrete part's neutral axis (after the concrete has cracked in tension) is not on the cross-section centerline and is located toward the compression side of the cross-section. Neutral axis positions between these limits express partial-compositeness.

It was also explained as part of the analytical work presented in Chapter 2 that, in a RCFST cross-section under bending moment, an internal axial load develops and transfers at the interface between the steel tube and the concrete core, which acts as uniform tensile and compressive loads on the steel tube and the reinforced concrete core of the RCFST cross-section, respectively. This internally transferring axial load moves the neutral axes of the steel tube and the reinforced concrete parts toward each other, resulting in development of composite action. The internal axial load between the steel tube and the reinforced concrete core can be transferred by the means of the friction bond that exists at the steel tube-to-concrete core interface along the shaft if an adequate friction coefficient is present. The interface friction force is a function of the friction coefficient at the interface ($\mu_{interface}$) and the normal force that is acting on that interface. As it was shown as part of the analytical work presented Chapter 2, if the friction force at the interface is insufficient to transfer the necessary internal axial load to develop the composite action, the transfer of internal axial load can be achieved instead using shear transferring mechanisms such as shear rings or studs.

Figure J.29b shows the diagram of the transferred internal axial load at the interface of the steel tube and the concrete core. Specimen S1 relied on the natural friction bond between the steel tube and the concrete core as the means of transferring the internal axial load. The natural friction coefficient between steel tube and the concrete core was taken equal to $\mu_{interface}$=0.5 in the analyses. As shown in this figure, the transferred internal axial load increases sharply within $0.5D_s$ at the top of the shaft, from zero to about 40 $kips$ and then increases gradually toward bottom of the shaft. Figure J.29c shows the distribution of the neutral axes on the concrete core and steel tube along the RCFST shaft at the corresponding plastic moment state. As shown, the neutral axis locations get close to each other at a distance of about $2.5D_s$ below the top of the shaft. The transferred internal axial load reached about $50kips$ at $2.5D_s$ from top of the shaft and increased to about $90kips$ at the bottom. It is also shown in Figure J.29a that in the top $0.5D_s$ of the shaft, the steel tube doesn't contribute significantly to the total moment resistance of the RCFST shaft.

In addition, to compare the maximum moment resistance obtained from each of the six analysis cases described above with the calculated M_{PSDM}, the transferred internal axial load and the neutral axis locations were also compared to ensure the composite action of the RCFST shaft in the soil. Recall that, for RCFST cross-sections, the difference between composite and non-composite moment capacity is not typically not significant (12% for the considered shaft). Therefore, to qualitatively gage the extent of compositeness developed, comparison of the transferred internal axial load and the location of neutral axes also performed for all cases considered.

Figure J.30 shows the moment and the transferred internal axial load distributions for Case (1). The moment distribution is shown at the point when the moment in the RCFST shaft immediately below the transition zone (-2.5D_s) reached the calculated M_{PSDM} for the RCFST cross-section. Note that the M_{PSDM} capacity within the transition zone is more than the shaft's M_{PSDM} as it includes the extra rebar cage of the top reinforced concrete column that is extended into the shaft. For this reason, in Cases (1), (2), and (3), the ability of reaching the composite $M_{PSDM}$for the RCFST cross-section *below* the transition zone has been investigated.

As shown in Figure J.30b, the transferred internal axial load at -2.5D_s is about 85$kips$, which is only 5$kips$ less than the transferred internal axial load at the bottom of Specimen S1 (see Figure J.29b). Case (1) results show that the M_{PSDM} capacity was reached at the bottom of the transition zone (-2.5D_s) when a friction coefficient of 0.5 was used at the interface (recall that this was the friction coefficient generally deemed sufficient to develop a maximum moment greater M_{PSDM} in RCFSTs).

A significantly lower friction coefficient at the interface cannot develop sufficient bond to transfer the internal axial load that is required to achieve composite action. Figure J.31 shows results for Case (1) with $\mu_{interface}$=0.1, which shows that the transferred internal axial load is significantly lower than that for the case with $\mu_{interface}$=0.5. As shown in this figure, the moment capacity of the RCFST shaft below the transition zone is between the calculated non-composite and composite M_{PSDM} capacity.

Results of the analyses presented in the analytical program, and the experimental results, showed that in the absence of adequate interface friction bond, using shear transfer mechanisms (namely, shear rings) at the top of cantilevering RCFST shaft resulted in composite behavior of the RCFST cross-section. Analyses of the RCFST shafts embedded in the soil in this section showed that, by providing the shear transfer mechanisms at the top of the shaft (Case (2)), the internally transferring axial force can be transferred between the steel tube and the concrete immediately below the shear transfer mechanisms. However, in this case, contrary to the cantilever case, composite behavior might not be achieved if the bottom end of the RCFST shaft (i.e., the end that sits on the solid rock) is free to move and the slippage between the steel tube and the concrete core can occur from that end. To better illustrate the effect of the shear transfer mechanism when only provided at top end of the shaft, the Case (2) finite element model was analyzed by considering friction coefficients of 0.5 and 0.1. Recall that this model is similar to Case (1) shaft, but with added shear rings at the top as shear transfer mechanism.

Figure J.32 shows the moment and transferred internal axial load diagrams for the analyzed Case (2) model with $\mu_{interface}$=0.5. As previously shown in Figure J.30, for the case with $\mu_{interface}$=0.5 the composite behavior was achieved only by means of the existing friction bond. From the transferred internal axial force shown in Figure J.32, it can be seen that the use of shear rings at the top together with a friction coefficient of 0.5 makes it possible to transfer the internal axial load over a shorter length at the top of the shaft, which can result in composite behavior immediately below the location of the shear rings. However as shown in Figure J.33, the use of shear rings at the top of the shaft when the friction coefficient was 0.1 didn't help to achieve composite behavior along the RCFST shaft. As shown in this figure, although the RCFST shaft was able to reach the calculated (M_{PSDM}) due to eventual strain hardening, the transferred internal axial load diagram shows that the transferred axial load is actually less than for Case (1).

In the case of low interface friction bond, the composite behavior can be achieved by providing extra shear transferring mechanism below the location of the maximum moment along the shaft. In fact, composite behavior can be achieved along a desired length of the shaft by providing shear transfer mechanisms at both ends of that length. Figure J.34 shows the moment and transferred internal axial load

diagrams for Case (3) which has two sets of shear rings attached at the top of the shaft and at -3.5D_s from the top. As shown, the shear rings transferred a sufficient internal axial load between the steel tube and the concrete core to achieve the composite behavior over the region that is between the shear rings.

The transferred internal axial load for Case (1), (2), and (3) were re-plotted in Figure J.35 for comparison. As shown for the cases with shear rings (Cases (1) and (2)), the internal axial load transferred immediately at the location of the shear rings, while for the case without rings (Case (1)), the internal axial load was transferred gradually over a longer length.

The neutral axes locations of the steel tube and the reinforced concrete core along the shaft obtained from the different analyzed cases are shown in Figure J.36. The neutral axes are seen to be closer to each other in Figure J.36a, c, and d, which correspond to the cases that achieved the composite M_{PSDM} compared to Figure J.36b that corresponds to Case (2), with $\mu_{int} = 0.1$ and that didn't behave as a composite RCFST cross-section.

Figure J.37 shows the moment and transferred internal axial load for Case (4) analyzed using different soil stiffness moduli. In Case (4) the RCFST shaft itself was extended out of the soil for a height of 3D_s and no reinforced concrete column exists at top of the RCFST shaft. In this case the interface friction force along the extended length of the RCFST shaft also contributes to transferring the internal axial load. As shown in Figure J.37, the transferred internal axial load at top of the soil was about 85$kips$, which resulted in composite behavior of the RCFST shaft even when the maximum moment occurred close to the soil level at about -0.5D_s. Note that the rate at which the transferred internal axial load is transferred from the steel to the concrete increases in the soil (compared to above ground), indicating that the bearing resistance of the soil in contact with outside surface of the steel tube also increases the pressure between the steel and concrete.

For Cases (5) and (6) exhibited similar behavior to what was observed for Cases (2) and (3), respectively, which further validates the findings related to required positioning of shear rings. The moment and transferred internal axial load diagrams for Cases (5) and (6) are shown in Figures J.38 and J.39, respectively.

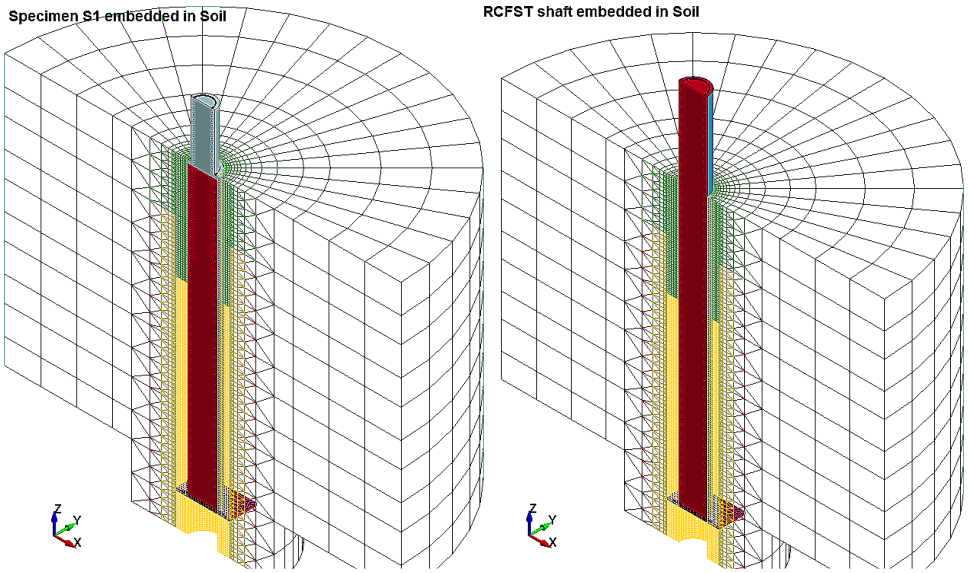

Figure J.28: Finite element mesh of the shaft and the surrounding soil continuum in LS-Dyna.

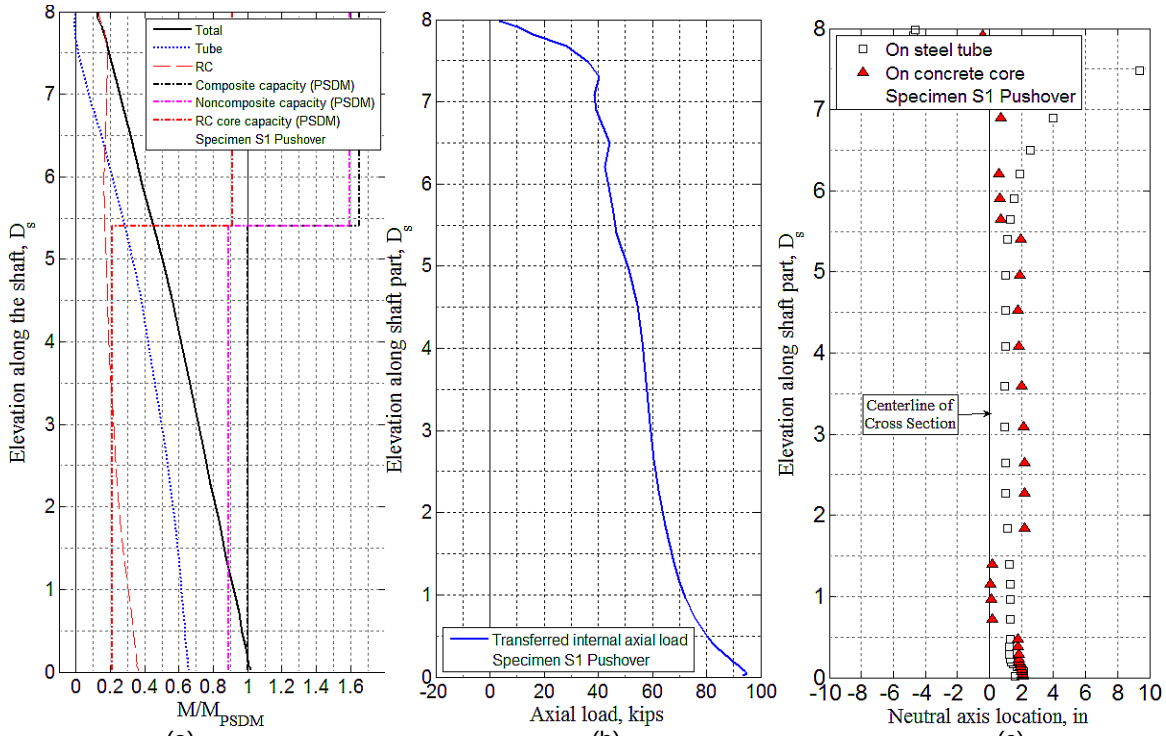

Figure J.29: Moment and transferred internal axial load and neutral axis location diagrams for test Specimen S1 (Cantilever, no soil).

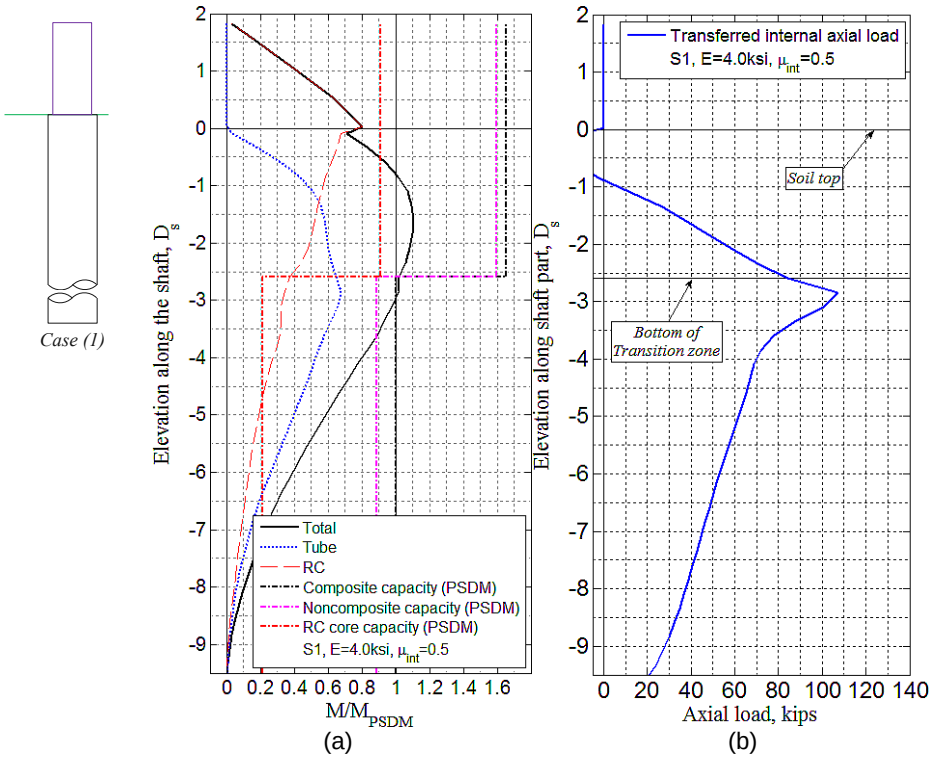

Figure J.30: Moment and transferred internal axial load diagrams for Case (1) with μ_{int}=0.5.

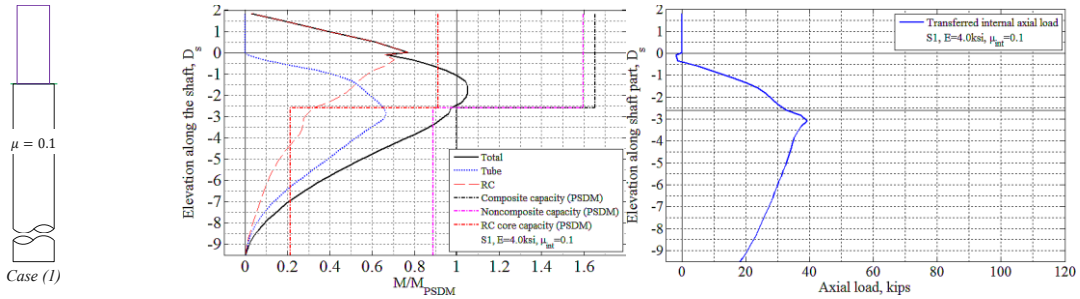

Figure J.31: Moment and transferred internal axial load diagrams for Case (1) with μ_{int}=0.1.

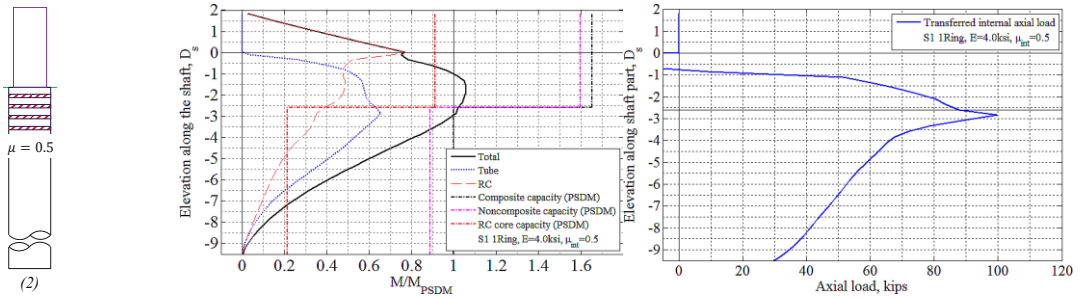

Figure J.32: Moment and transferred internal axial load diagrams for Case (2) with μ_{int}=0.5.

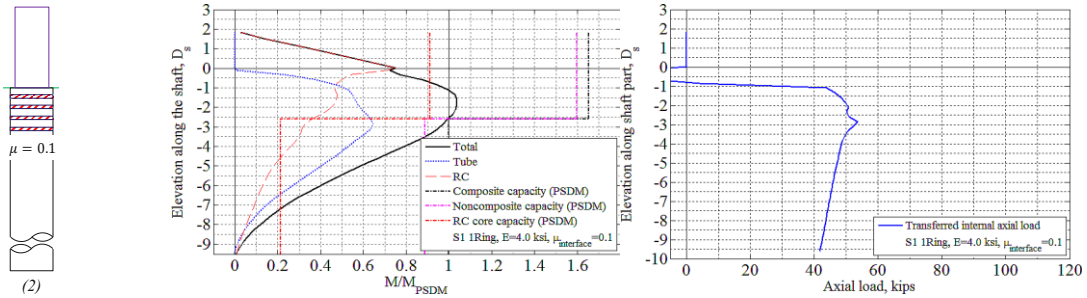

Figure J.33: Moment and transferred internal axial load diagrams for Case (2) with μ_{int}=0.1.

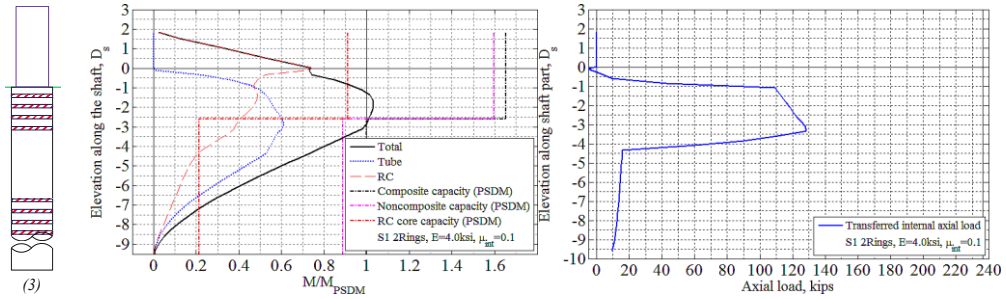

Figure J.34: Moment and transferred internal axial load diagrams for Case (3).

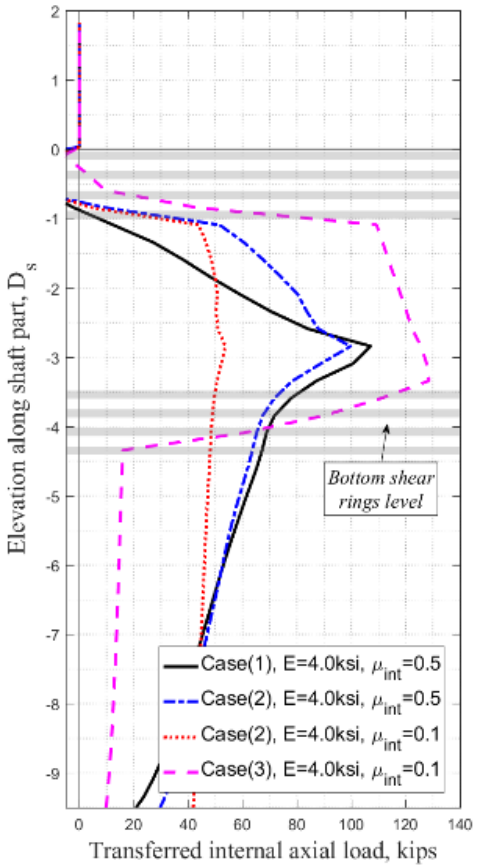

Figure J.35: Comparison of the transferred internal axial load in Cases (1), (2), and (3).

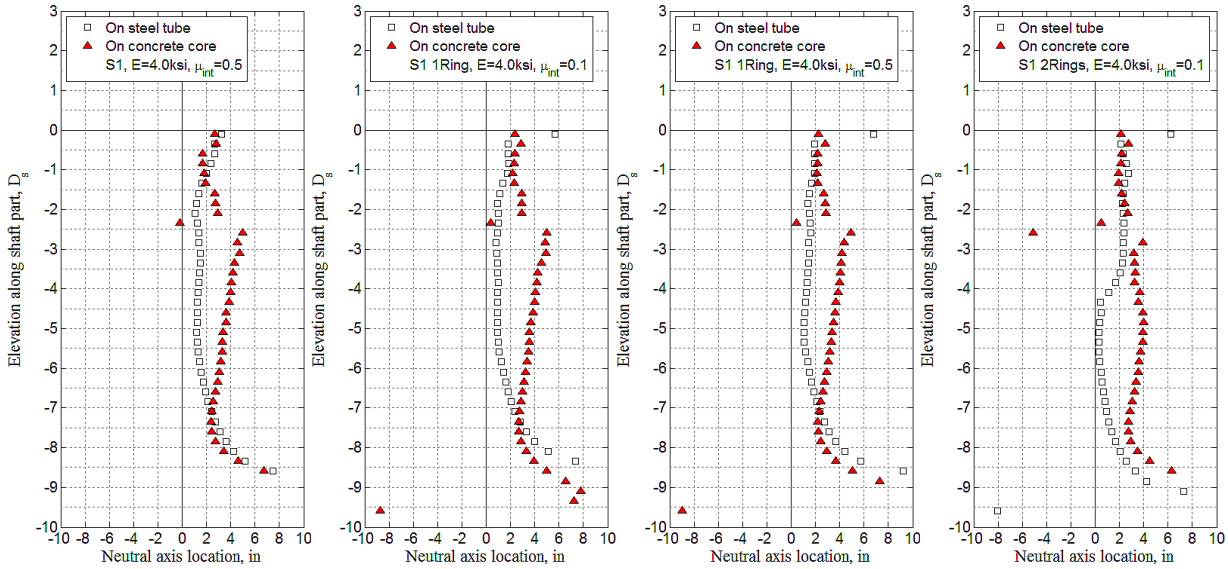

(a) Case (1), $\mu_{int} = 0.5$ (b) Case (2), $\mu_{int} = 0.1$ (c) Case (2),$\mu_{int} = 0.5$ (d) Case (3)

Figure J.36: Neutral axes locations along the RCFST shaft in Cases (1), (2), and (3).

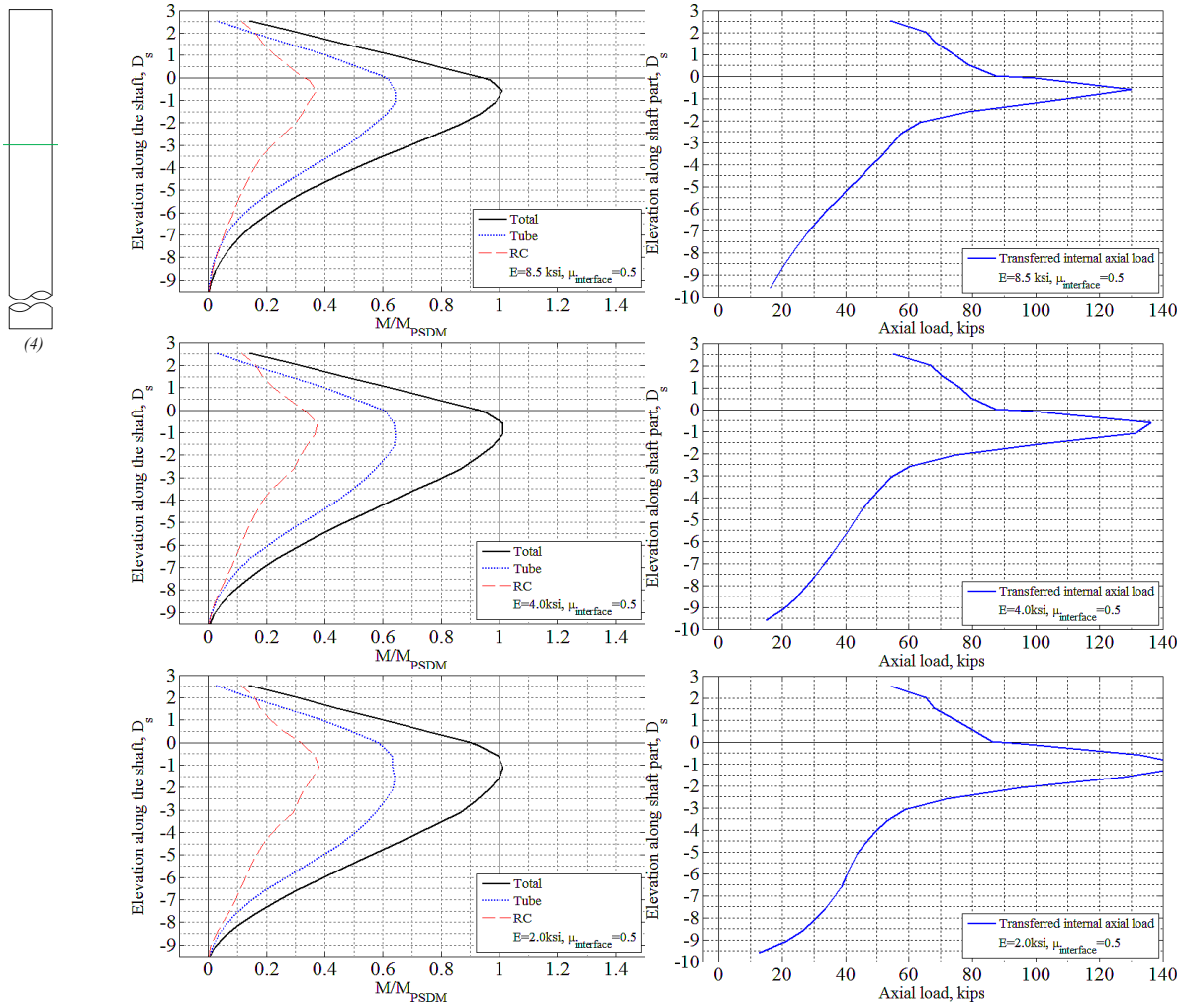

Figure J.37: Moment and transferred internal axial load diagrams for Case (4) embedded in different soils.

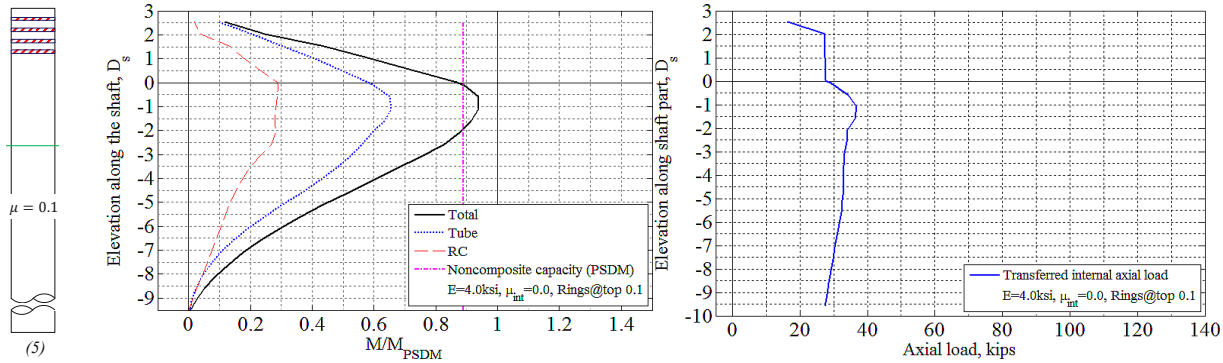

Figure J.38: Moment and transferred internal axial load diagrams for Case (5).

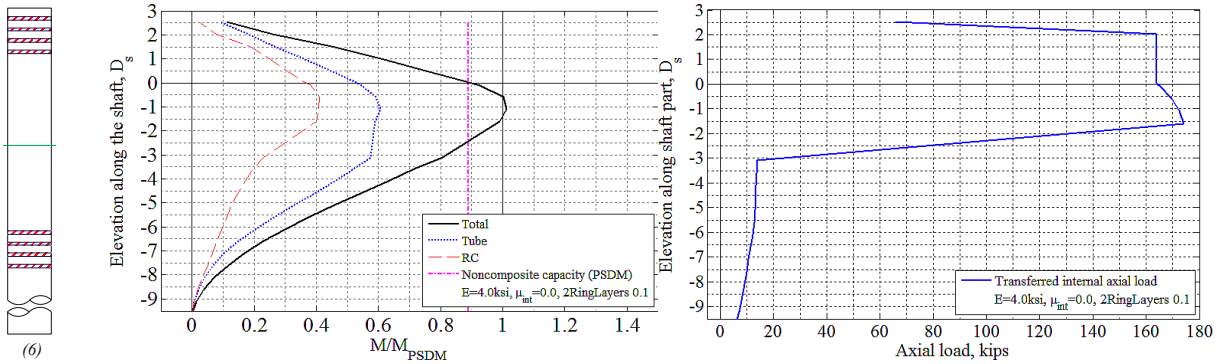

Figure J.39: Moment and transferred internal axial load diagrams for Case (6).

J.3 Finite element modeling and analysis of shear tests

J.3.1 Finite element modeling of shear tests

The LS-Dyna model of the shear specimen and test setup is schematically shown in Figure J.40. In order to include the effects of the flexibility of the pantograph device on the stiffness of the shear specimen and the amplitude of the applied lateral displacements, the shear specimen and the upper part of the pantograph were modeled, including the stiffener modules, loading beam, and the pantograph diagonals. A half-finite element model was built taking advantage of the symmetry existing in the test setup. Figures J.41 to J.43 show the details of different parts of the shear test setup finite element model.

A Winfrith concrete material model with constant stress solid elements was used for the concrete part. A bilinear elasto-plastic material with 1% strain hardening was used for modeling of the steel parts. Pre-tensioning forces of the bolts were applied by shortening the length of the bolts at the beginning of the analyses using temperature loading (and defining a thermal expansion coefficient along the axis of the bolt). The pre-tension force of the bolts were tuned to 70% of their yield strength. This finite element model was used prior to the shear tests for assessing the adequacy of the test setup and to design the cyclic loading protocol.

Specified material properties were used for pre-test finite element analyses. For post-test analyses, The average material properties presented in Table 2.11 were used for the steel tube and concrete. All other steel plates, were modeled assuming $50ksi$ for their yield strength. And bolts were modeled assuming $130ksi$ for their yield strength. For the steel tube, in addition to using the bilinear model, additional analyses were conducted with a "*piecewise linear plasticity*" model (MAT-024) by using the average effective stress-strain curve obtained from the coupon tests as input parameters, and results from those analyses were compared with each other. The applied cyclic loading was simplified, similarly to what was discussed before for flexural specimens in Section J.1.1.For comparison purposes, a push-over analysis was conducted using the actual effective stress-strain curve obtained from the average properties of the coupon tests. The results are compared with results from the previous finite element analysis and the experimentally obtained backbone curve for Specimen SH4.

Note that, as mentioned in Section 3.3.6, the test results for the RCFST shafts were generally similar to those for the CFST shear specimen (i.e., Specimen SH4). For this reason, finite element analyses were conducted only for the CFST shear specimen.

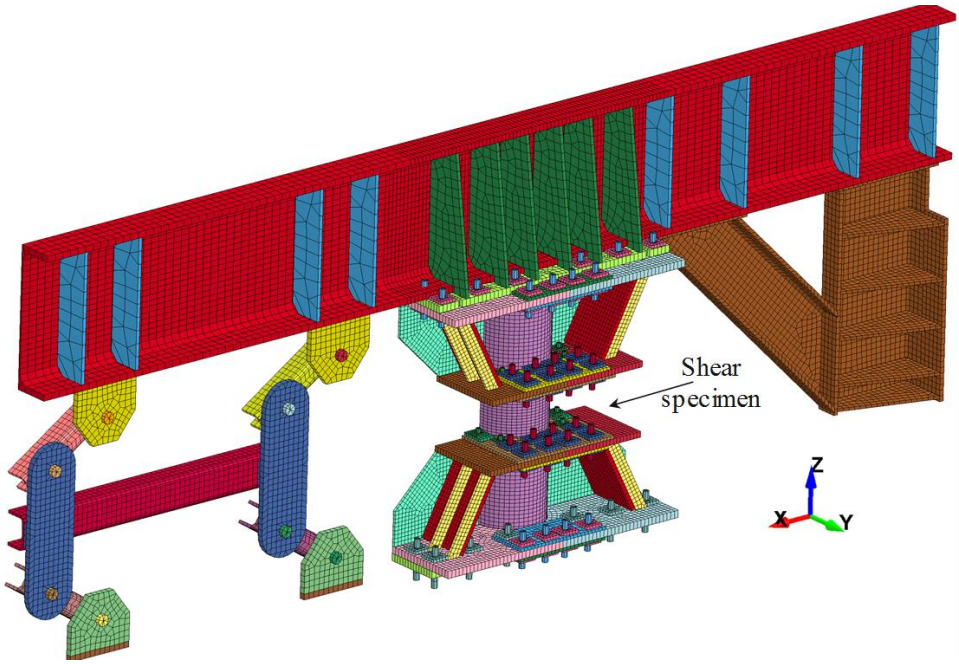

Figure J.40: Scheme of the developed LS-Dyna finite element model for shear tests.

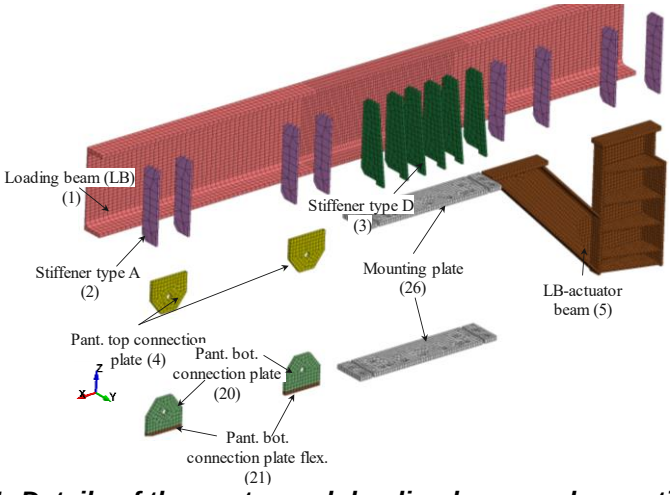

Figure J.41: Details of the pantograph loading beam and mounting plates.

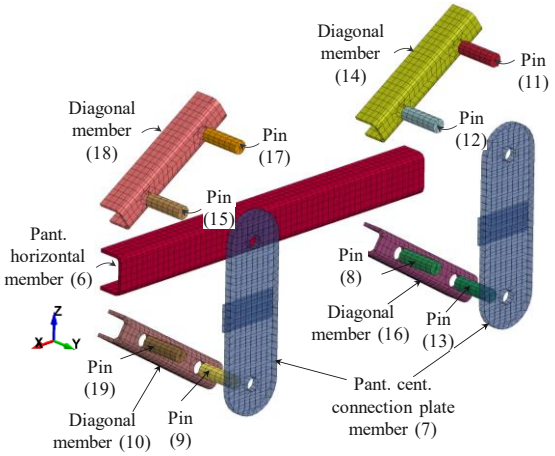

Figure J.42: Details of the pantograph's diagonals.

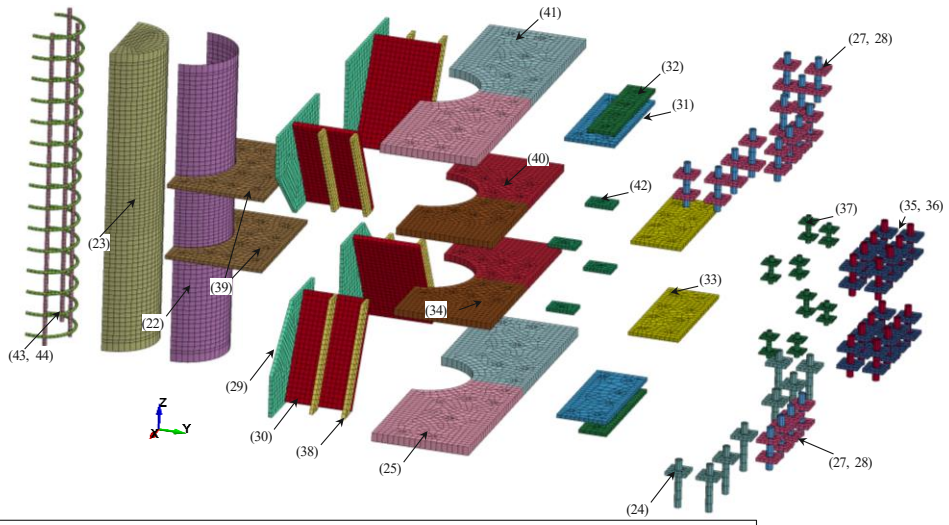

FEM 12OD shear specimen sub-system parts list:

22- Steel tube	30- S12D2-FP	37- SP3 bolts	43, 44- Internal reinforcement
23- Concrete	31- S12D2-SP1	38- S12D2-S1	
24- Bot. bolts	32- S12D2-SP4	39- S12D2-P2DP	
25- S12D2-BP (west)	33- S12D2-SP2	40- S12D2-DP (east)	
27, 28- Top bolts and washers	34- S12D2-DP (west)	41- S12D2-BP (east)	
29- S12D2-GP	35, 36- GP bolts and washers	42- S12D2-SP3	

Figure J.43: Details of the 12OD shear specimen and the stiffness modules.

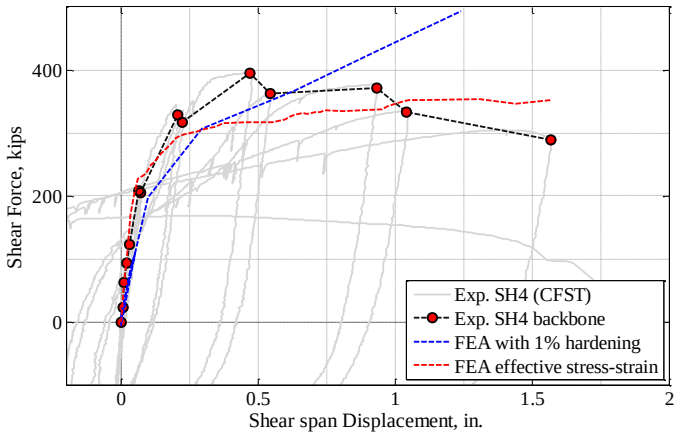

Figure J.44: Comparison of backbone curves for finite element analyses using different steel materials and test results for Specimen SH4.

APPENDIX K

Design examples

K.1 Example 1: Force-based design of RCFST

This example presents a RCFST used to support a single column bent. The plastic hinge is assumed to develop in the column, and therefore the RCFST is a capacity protected element. The cross-section of the shaft and its material properties are given in Table K.1. The factored design axial, shear, and moment values along the member are shown in Table K.2 and their corresponding diagrams are shown in Figure K.1. The design loads are coming from the plastic hinge in the column (assumed, not calculated). This example provides all calculations to ensure transfer of these loads into the RCFST and a check of the strength of the RCFST. Use of shear rings at top of the shaft as shear transfer mechanisms between the concrete and steel tube and their design process is also shown. This example also provides calculations for the shear strength of the designed RCFST shaft at its top and also below the soil level at an assumed location of a liquefiable layers. The outline of the calculations for the design Example 1 is as following:

1. Check of the limitations and requirements per revised AASHTO BDS (2014) Article 6.9.6.2.
2. Calculation of the nominal axial capacity per AASHTO BDS (2014) Article 6.9.6.3.
3. Calculation of the nominal flexural resistance per AASHTO BDS (2014) Article C6.12.2.3.3.
4. Generating of the material based P-M interaction curve.
5. Calculation of the nominal and factored stability-based P-M interaction curve per AASHTO BDS (2014) Article 6.9.6.3.4.
6. Check of the factored capacity of the RCFST shaft with the design demands.
7. Calculation of the factored stability-based P-M interaction curve per AASHTO SGS (2014) Article 7.6.2 and comparison with the results of item 5.
8. Design of shear transfer mechanisms at top of the shaft per proposed AASHTO BDS (2014) Article 6.9.6.3.5.
9. Calculation of the shear capacity of the RCFST shaft at its top (non-composite assumption) and below the soil level (composite assumption) per proposed equations for shear capacity of RCFST shafts.

All this process was included in Mathcad v15.0 software worksheets for design engineers. The Mathcad worksheets are printed in the following.

Table K.1. Shaft properties for Example 1.

Nominal diameter of steel tube	d_{tube}	$60in.$	
Nominal thickness of steel tube	t_{tube}	$0.625in.$	
Nominal yield strength of steel tube	F_{ytube}	$45ksi$	ASTM A252 – Gr. 3
Nominal compressive strength of concrete	f_c'	$4ksi$	
Nominal yield strength of rebar	f_{yst}	$60ksi$	
Cross-section rebar ratio	ρ_{st}	1.26%	(28) #10 bars
Rebar cage cover	cover	$2in.$	
Nominal diameter of transverse rebar	d_{tr}	$5/8in.$	

Table K.2. Factored loads along the member of Example 1.

Elevation, *ft*	Axial load, *kips*	Shear force, *kips*	Moment, *kip.ft*
10	5000.0	-500.0	0.0
8	5005.9	-500.0	1000.0
6	5011.8	-500.0	2000.0
4	5017.7	-500.0	3000.0
2	5023.6	-500.0	4000.0
0	5029.3	-499.5	5000.0
-5	4948.9	-120.0	8496.6
-10	4793.2	321.9	9336.4
-15	4582.4	606.0	7082.8
-20	4332.6	368.9	2841.0
-25	4067.5	103.4	258.9
-30	3811.4	-19.6	-465.1
-35	3575.1	-33.6	-327.8
-40	3363.6	-14.7	-92.4
-45	3181.4	-1.4	10.2
-50	3031.4	1.8	20.1
-55	2915.5	1.0	7.5
-60	2834.0	0.2	0.2
-65	2774.6	-0.1	-1.0
-70	2739.1	-0.1	-0.4

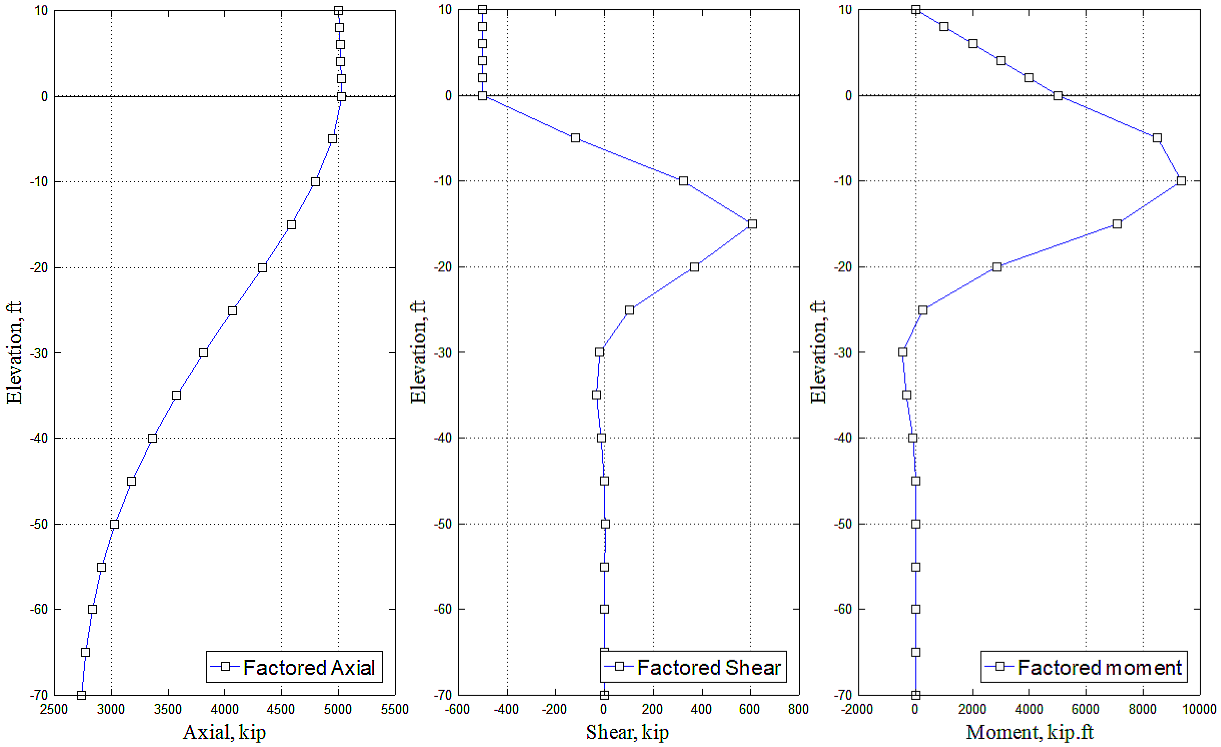

Figure K.1: Factored Axial, shear, and moment diagrams along the shaft of Example 1.

Mathcad ® Enabled Content.

Composite RCFST Shaft Design, *Hadi Kenarangi, University at Buffalo, 2017*

Composite RCFST shaft capacity check using the proposed modifications to AASHTO Bridge Design Specification.

Disclaimer

Disclaimer

While the research team of the Project NCHRP 12-93 have made every effort to ensure that the equations, calculations, diagrams, and solutions accurately represent the content of the references and the proposed revisions, the research team do not give any warranties on accuracy of the solutions produced by different set of input parameters. The user shall use engineering judgment and check the accuracy of the produced solutions and results.

Disclaimer

User Notices

User Notices

AASHTO LRFD Bridge Design Specification is noted as "**AASHTO BDS**"
AASHTO Guide Specifications for LRFD Seismic Bridge Design is noted as "**AASHTO SGS**"
Input variables that need to be defined by the user are highlighted in YELLOW.
Key results and design checks are highlighted in GREEN.
Intermediate results and checks are highlighted in BLUE.

User Notices

Description

Givens : Factored moment, axial load, and shear diagrams in the RCFST shaft. RCFST cross-section including the tube thickness and material properties, concrete material properties, and reinforcing layout and areas.

References:

- AASHTO. (2011; 2012; 2013; 2014). *AASHTO Guide Specifications for LRFD Seismic Bridge Design (2nd Edition) with 2012, 2014 and 2015 Interim Revisions.* American Association of State Highway and Transportation Officials (AASHTO).
- AASHTO. (2014; 2015). *AASHTO LRFD Bridge Design Specifications, U.S. Customary Units with 2015 and 2016 Interim Revisions (7th Edition).* American Association of State Highway and Transportation Officials (AASHTO).

Input

Notation

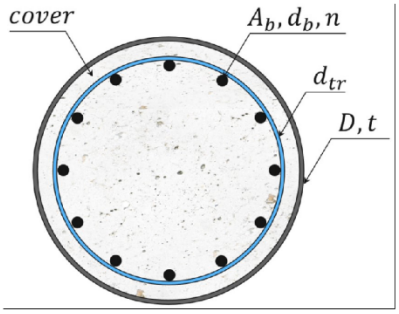

Unsupported length: L := 50ft (Assumed equal to the distance from top of the column to the depth of the fixity)

K := 2

Unfactored axial dead load: P := 5000kip (Maximum applied unfactored axial load was considered)

Cross section properties

Steel tube

Outside diameter of the steel tube: D := 60in

Thickness of the steel tube: t := 0.625in

Nominal yield strength of the steel tube: $f_{yst} := 45ksi$

Modulus of elasticity of steel: $E_s := 29000 \cdot ksi$

Concrete

Uniaxial compressive strength of the unconfined concrete: $f'_c := 4 \cdot ksi$

Uniaxial compressive strength of the confined concrete: $f'_{cc} := 4.75 \cdot ksi$

Unit weight of concrete: $w_c := 150 \frac{lb}{ft^3}$

Modulus of elasticity of concrete: $E_c := \left(w_c \cdot \frac{ft^3}{lb} \right)^{1.5} \cdot \sqrt{\frac{f'_{cc}}{ksi}} ksi = 4004 \cdot ksi$ (ACI318)

Shaft rebar

Cover: $cover := 2in$

Nominal diameter of the rebar: $d_b := 1.27in$

Nominal area of the rebar: $A_b := 1.27in^2$

Number of rebars: $n := 28$

Nominal diameter of the transverse rebar: $d_{tr} := \frac{5}{8}in$

Nominal yield strength of the rebar: $f_{yb} := 60ksi$

Computed section properties

Inside diameter of steel tube: $D_c := D - 2t = 58.75 \cdot in$

Rebar layer radius: $r_b := \frac{D_c}{2} - cover - d_{tr} - \frac{d_b}{2} = 26.115 \cdot in$

Equivalent rebar ring thickness: $t_b := \frac{n \cdot A_b}{2 \cdot \pi \, r_b} = 0.217 \cdot in$

Moment of inertia of the equivalent rebar ring: $I_r := \frac{\pi}{4}\left[\left(r_b + \frac{t_b}{2}\right)^4 - \left(r_b - \frac{t_b}{2}\right)^4\right] = 1.213 \times 10^4 \cdot in^4$

Total area of rebars: $A_r := n \cdot A_b = 35.56 \cdot in^2$

Area of concrete fill: $A_c := \pi \frac{D_c^2}{4}$

Moment of inertia of the concrete: $I_c := \pi \frac{D_c^4}{64}$

Plastic modulus of the concrete: $Z_c := \frac{D_c^3}{6}$

Area of the steel tube: $A_s := \pi \cdot \frac{D^2}{4} - A_c$

Moment of inertia of the steel tube: $I_s := \pi \frac{D^4}{64} - I_c$

Plastic modulus of the steel tube: $Z_s := \frac{D^3}{6} - Z_c$

Check limitations according to the revised AASHTO BDS Article 6.9.6.2-Limitations:

The following requirements shall be satisfied:

- Circular steel tubes shall be used.

  "OK"

- Spiral welded tubes formed from coil steel, straight-seam welded tubes formed from flat plates, or seamless pipes shall be used.

  "OK"

- Steel tubes with straight seam welds shall be permitted for CFSTs for all applications where the outside diameter is 24.0 in. or less. Steel tubes with straight seam welds shall be permitted for tubes larger than 24.0 in. in diameter if the concrete fill is designed with the addition of a low-shrinkage admixture to achieve a maximum of 0.04 percent shrinkage at 28 days, as tested in accordance with ASTM C157 Modified Standard Test Method for Length Change of Hardened Hydraulic-Cement Mortar or a positive means of shear transfer as described in 6.9.6.3.5 is provided.

  "OK"

- The wall thickness of the steel tube shall satisfy (6.9.6.2-1):

$$\text{if}\left(\frac{D}{t} \le 0.15\cdot\frac{E_s}{f_{yst}}, \text{"OK"}, \text{"Wall thickness requirement is not satisfied"}\right) = \text{"OK"}$$

- The specified minimum 28-day compressive strength of the concrete shall be the greater of 3.0 ksi and $0.075F_{yst}$.

$$\text{if}\left(f'_c \ge \max\left(3\text{ksi}, 0.075\cdot f_{yst}\right), \text{"OK"}, \text{"f'c is low"}\right) = \text{"OK"}$$

Calculating the nominal axial capacity per AASHTO BDS Article 6.9.6.3:

Compressive resistance of the column without consideration of buckling:

$$P_o := 0.95f'_c A_c + f_{yst}\cdot A_s + f_{yb}\cdot A_r = 17681\cdot\text{kip} \qquad (6.9.6.3.2\text{-}4)$$

Effective flexural stiffness:

$$C' := \min\left(0.15 + \frac{P}{P_o} + \frac{A_s + A_r}{A_s + A_r + A_c}, 0.9\right) = 0.486 \qquad (6.9.6.3.2\text{-}7)$$

$$EI_{eff} := E_s\cdot I_s + E_s\cdot I_r + C'\cdot E_c\cdot I_c = 2.98\times 10^9\cdot\text{kip}\cdot\text{in}^2 \qquad (6.9.6.3.2\text{-}6)$$

Note for comaprison reason, the effective flexural stiffness calculated using AASHTO SGS C7.6-1 is:

$$EI_{eff\_AASHTO\_SGS\_C7.6\_1} := E_s\cdot I_s + \frac{E_c\cdot I_c}{2.5} = 2.427\times 10^9\cdot\text{kip}\cdot\text{in}^2$$

The difference between AASHTO BDS Article 6.9.6.3 and AASHTO SGS C7.6-1 is:

$$\frac{EI_{eff\_AASHTO\_SGS\_C7.6\_1} - EI_{eff}}{EI_{eff}} = -18.555\cdot\%$$

Elastic critical buckling resistance of flexural buckling:

$$P_e := \frac{\pi^2 EI_{eff}}{(K \cdot L)^2} = 2.042 \times 10^4 \cdot kip \qquad (6.9.6.3.2\text{-}5)$$

Nominal compressive resistance:

$$P_n := if\left[P_e > 0.44P_o, 0.658^{\left(\frac{P_o}{P_e}\right)} \cdot P_o, 0.877P_e\right] = 12306 \cdot kip \qquad (6.9.6.3.2\text{-}2 \text{ \& } 3)$$

Calculating the nominal flexural resistance per AASHTO BDS Article C6.12.2.3.3 (PSDM):

$$r_m := \frac{D - t}{2} \qquad r_i := \frac{D - 2t}{2}$$

$$\theta_s(y) := asin\left(\frac{y}{r_m}\right) \qquad \theta_b(y) := if\left(-1 < \frac{y}{r_b} < 1, asin\left(\frac{y}{r_b}\right), if\left(\frac{y}{r_b} > 1, \frac{\pi}{2}, \frac{-\pi}{2}\right)\right)$$

$$c(y) := r_i \cdot \cos(\theta_s(y)) \qquad c_b(y) := r_b \cdot \cos(\theta_b(y))$$

$$\begin{aligned} P_{comp}(y) = {} & f_{yst} \cdot t \cdot r_m \cdot \left[\left(\pi - 2 \cdot \theta_s(y)\right) - \left(\pi + 2 \cdot \theta_s(y)\right)\right] \ldots \\ & + t_b \cdot r_b \cdot \left[f_{yb} \cdot \left(\pi - 2 \cdot \theta_b(y)\right) - \left(f_{yb} - 0.95f'_c\right) \cdot \left(\pi + 2 \cdot \theta_b(y)\right)\right] \ldots \\ & + \frac{0.95f'_c}{2}\left[\left(\pi - 2 \cdot \theta_s(y)\right) \cdot r_i^2 - 2 \cdot y \cdot c(y)\right] \end{aligned} \qquad (C6.12.2.3.3\text{-}1)$$

$$M_{comp}(y) := 0.95 \cdot f'_c \cdot c(y) \cdot \left[\left(r_i^2 - y^2\right) - \frac{c(y)^2}{3}\right] + 4 \cdot f_{yst} \cdot t \cdot c(y) \cdot \frac{r_m^2}{r_i} + 4 \cdot f_{yb} \cdot t_b \cdot c_b(y) \cdot r_b \qquad (C6.12.2.3.3\text{-}2)$$

Find the position of the neutral axis for the case of P_{comp}=0kip:

$y_{try} := 0in$

Given

$P_{comp}(y_{try}) = 0kip$

$y_B := Find(y_{try}) = 13.6 \cdot in$

$P_B := P_{comp}(y_B) = 0 \cdot kip$

$M_B := M_{comp}(y_B) = 13596 \cdot kip \cdot ft$

Find the position of the neutral axis for the case of M_{comp}=0kip.ft:

$y_{try} := -1in$

Given

$M_{comp}(y_{try}) = 0.001M_B$

$P_{comp}(y_{try}) > 0kip$

$y_A := Find(y_{try}) = -29.687 \cdot in$

$P_A := P_{comp}(y_A) = 17675.5 \cdot kip$

$M_A := M_{comp}(y_A) = 13.596 \cdot kip \cdot ft$

Generate 20 points of P-M curve by varying position of neutral axis:

$i := 1 .. 20$

$y_{cs_i} := y_B + \frac{(y_A - y_B)(i - 1)}{19}$ $M_{cs_i} := M_{comp}(y_{cs_i})$ $P_{cs_i} := P_{comp}(y_{cs_i})$

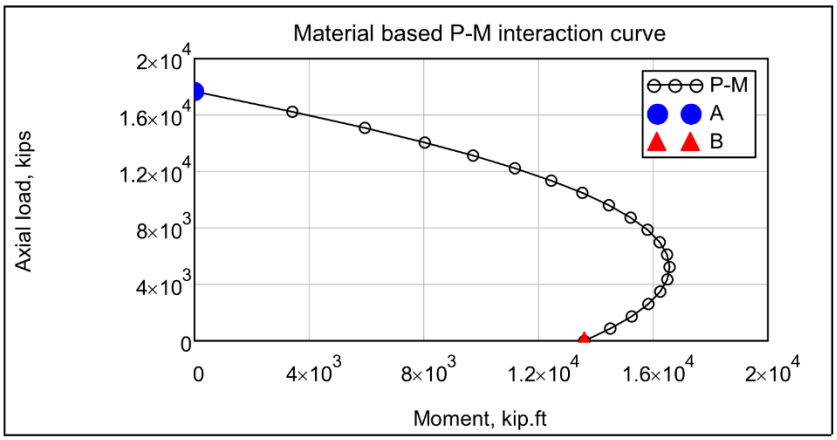

Nominal stability-based interaction curve according to AASHTO BDS Article 6.9.6.3.4:

The stability-based P-M interaction curve of CFSTs shall be constructed by joining points A′, A″, D, and B, as illustrated in Figure 6.9.6.3.4-1, where:

- Point A corresponds to P_o, determined as specified in Article 6.9.6.3.2.

$P_A = 17675 \cdot kip$ $M_A = 14 \cdot kip \cdot ft$

- Point A′ corresponds to the axial compression resistance without moment, P_n, determined as specified in Article 6.9.6.3.2.

$P_{A'} := P_n = 12306 \cdot kip$ $M_{A'} := 0kip \cdot ft$

- Point A″ is the intersection of the material-based interaction curve determined as specified in Article 6.12.2.3.3 and a horizontal line through Point A′.

$y_{try} := -1in$

Given

$P_{comp}(y_{try}) = P_{A'}$

$y_{A''} := \text{Find}(y_{try}) = -18.46 \cdot in$

$P_{A''} := P_{comp}(y_{A''}) = 1.231 \times 10^4 \cdot kip$

$M_{A''} := M_{comp}(y_{A''}) = 1.108 \times 10^4 \cdot kip \cdot ft$

- Point B corresponds to the composite plastic moment resistance without an axial load, M_o, determined as specified in Article C6.12.2.3.3.

$P_B = 0 \cdot kip$ $M_B = 13596 \cdot kip \cdot ft$

- Point C corresponds to the axial force, P_C, on the material-based interaction curve determined as specified in Article 6.12.2.3.3 that corresponds to the composite plastic moment resistance without axial load, M_o (Point B).

$y_{try} := -1in$

Given

$M_{comp}(y_{try}) = M_B$

$P_{comp}(y_{try}) > 0kip$

$y_C := \text{Find}(y_{try}) = -13.596 \cdot in$

$P_C := P_{comp}(y_C) = 1.044 \times 10^4 \cdot kip$

$M_C := M_{comp}(y_C) = 1.36 \times 10^4 \cdot kip \cdot ft$

- Point D is located on the material-based interaction curve determined as specified in Article 6.12.2.3.3 and is taken as the axial load, P_D, determined as:

$P_D := 0.5P_C \cdot \frac{P_n}{P_o}$ (6.9.6.3.4-1)

$y_{try} := 0in$

Given

$P_{comp}(y_{try}) = P_D$

$y_D := \text{Find}(y_{try}) = 4.122 \cdot in$

$P_D := P_{comp}(y_D) = 3632 \cdot kip$

$M_D := M_{comp}(y_D) = 16295 \cdot kip \cdot ft$

$P_{sb} := \begin{pmatrix} P_B & P_D & P_{A''} & P_{A'} \end{pmatrix}^T$ $M_{sb} := \begin{pmatrix} M_B & M_D & M_{A''} & M_{A'} \end{pmatrix}^T$

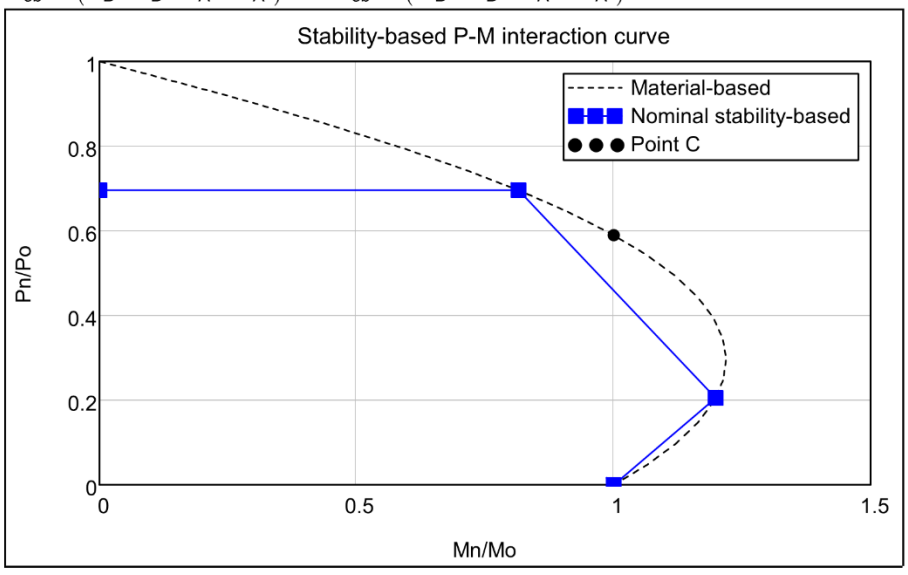

AASHTO BDS Article 6.9.6.3.1—The axial compressive load, P_u, and concurrent moment, M_u, calculated for the factored loadings by elastic analytical procedures shall satisfy the factored stability-based P-M interaction relationship. The factored interaction resistance curve shall be developed by applying the resistance factor, φ_c, for combined axial compression and flexure in composite CFSTs specified in Article 6.5.4.2 to the nominal stability-based P-M interaction curve as specified in Article 6.9.6.3.4.

From Article 6.5.4.2 of the AASHTO LRFD Bridge Design Specifications

- For axial compression, composite: $\phi_c := 0.9$

Factored axial and moment acting on the member:

Z := (ft)	P_u := (kip)	M_u := (kip·ft)
0	5029.34	5000
–5	4948.9	8496.58
–10	4793.2	9336.35
–15	4582.36	7082.79
–20	4332.64	2840.97
–25	4067.52	258.94
–30	3811.42	465.07
–35	3575.07	327.76
–40	3363.63	92.39
–45	3181.35	10.24
–50	3031.36	20.14
–55	2915.46	7.47
–60	2833.95	0.19
–65	2774.62	0.97
–70	2739.07	0.35

$P_{sb} := (P_B \quad P_D \quad P_{A''} \quad P_{A'})^T \qquad M_{sb} := \phi_c (M_B \quad M_D \quad M_{A''} \quad M_{A'})^T$

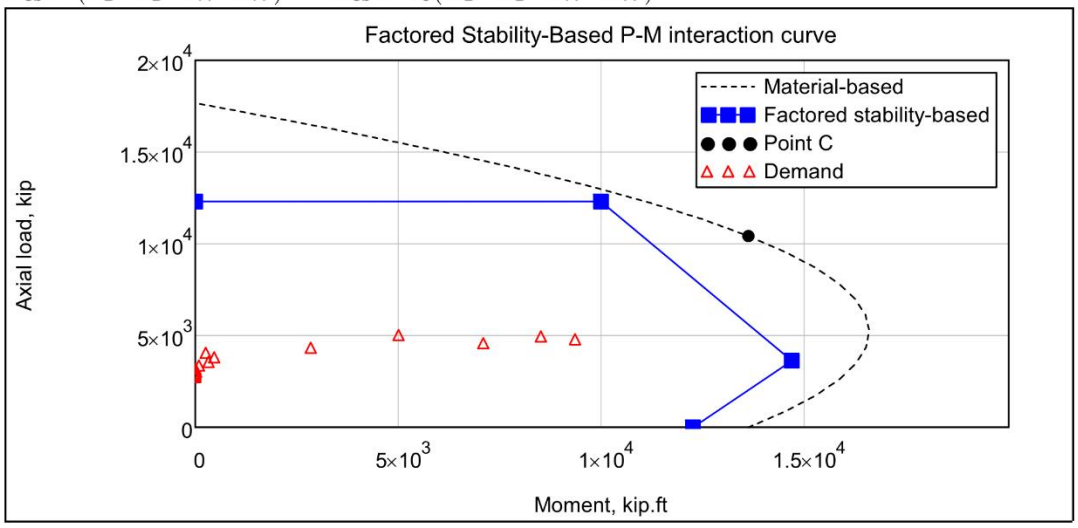

Proposed Article 6.9.6.3.5- Shear Transfer Between Concrete and Steel Tube

A positive method of shear transfer between the steel tube and concrete fill shall be provided within a distance of D/2 from the top of the steel tube where required to ensure composite action. Shear studs or welded rings may be used to transfer shear. The methods of Article 6.12.2.3.3 shall be used to calculate the amount of shear transfer required from bending demands. Consideration shall be given to shear transfer requirements arising from axial load applied to only the concrete fill or steel tube.

$r_m = 29.7 \cdot in$ $\theta_s(y_B) = 0.476$ (Defined previously)

$V_s := 4 \cdot \theta_s(y_B) \cdot r_m \cdot t \cdot f_{yst} = 1589 \cdot kip$

Design of shear rings to resist Vs:

Height of flat bars (shear rings): $h := \frac{3}{4} in$ (Square cross-section)

Distance between flat bars: $S_s := 8in$

Uniaxial compressive strength of unconfined concrete: $f'_c = 4 \cdot ksi$

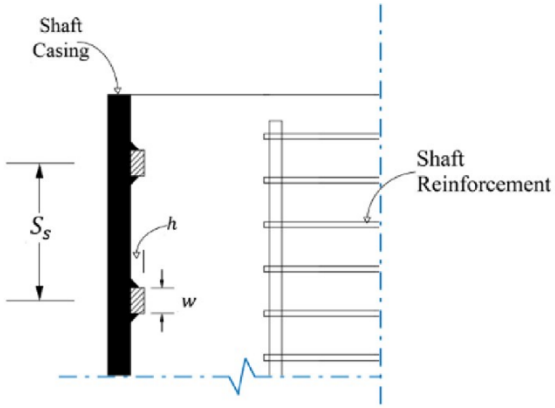

According to **C6.9.6.3.6-2** adopted from (H.4-1) of API2A-LRFD (1993):

Nominal resistance to shear transfer per inch of ring: $V_R := 0.9 \cdot f'_c \cdot h = 2.7 \cdot \frac{kip}{in}$

Inside circumference of the tube: $C := 2\pi \cdot D_c = 369 \cdot in$

Nominal resistance to shear transfer per ring: $V_{n\_ring} := C \cdot V_R = 997 \cdot kip$

From Article 6.5.4.2 of the AASHTO LRFD Bridge Design Specifications

- For shear connectors: $\phi_{sc} := 0.85$

Factored resistance to shear transfer per ring: $V_{ring} := \phi_{sc} \cdot V_{n\_ring} = 847 \cdot kip$

Number of required shear rings: $N_{ring} := ceil\left(\frac{V_s}{V_{ring}}\right) = 2$

use 3/4" shear rings 2@8"

Proposed non-composite shear capacity of RCFST at top of the shaft:

In non-composite RCFST members, the shear resistance of the developing strut (V_{Strut}) shall be taken as zero.

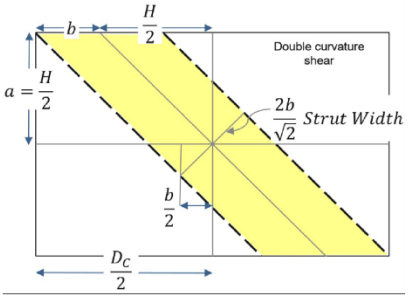

Figure: Elevation view of RCFST member under shear

Acting external axial load on the cross-section: $P_{axial} := 5029kip$

Axial load bearing on steel tube: $P_{st} := 0kip$

Axial load bearing on concrete core: $P_c := P_{axial}$ *(It was assumed that axial load is being carried by the concrete core only)*

Shear resistance of the developing strut: $V_{Strut} := 0kip$

Vertical component of the developing strut: $P_{Strut} := V_{Strut} = 0 \cdot kip$

Shear strength of the concrete: $\beta := 2.0$

$$V_c := 0.0316 \cdot \beta \cdot \sqrt{\frac{f'_c}{ksi}} \cdot A_c \cdot ksi \cdot \left(1 + \frac{P_{Strut} + P_c}{2 \cdot A_c \cdot ksi}\right) = 660 \cdot kip$$

Shear resistance of the concrete part of the RCFST: $V_{conc} := \max(V_{Strut}, V_c) = 660 \cdot kip$

Shear resistance of the steel tube part of the RCFST:

$$V_{st} := \frac{2 \cdot D \cdot t}{\sqrt{3}} \cdot \sqrt{f_{yst}^{\,2} - \left(\frac{P_{Strut} - P_{st}}{A_s}\right)^2} = 1949 \cdot kip$$

Nominal shear resistance of the non-composite RCFST: $V_n := V_{st} + V_{conc} = 2609 \cdot kip$

From Article 6.5.4.2 of the AASHTO BDS:

- For shear: $\phi_v := 1.0$

Factored nominal shear resistance of the non-composite RCFST: $V_{rc} := \phi_v \cdot V_n = 2609 \cdot kip$

Proposed composite shear capacity of RCFST below the soil level at the location of assumed liquefiable layers :

Acting external axial load on the cross section*: $P_{axial} := 4580kip$

Shear span*: $a := 0.4 \cdot D = 24 \cdot in$ $H := 2 \cdot a = 48 \cdot in$

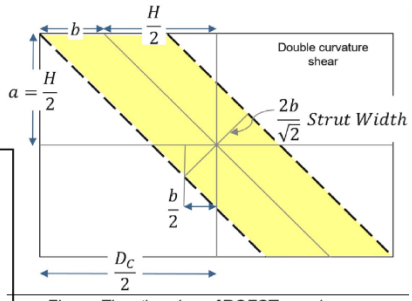

Figure: Elevation view of RCFST member under shear

* Acting axial load is taken at the assumed location of the liquefiable layers. Here taken as 21 ft. below soil level. The shear span develops according to the movement of two adjacent layers of soil sliding against each other. The length of the shear span is likely to be dependant on the relative lateral shear stiffness of the RCFST and the surrounding soil. For the sake of this example, the shear span was taken equal to that of the shear specimens tested by Kenarangi and Bruneau (2017) at the University at Buffalo.

Internal radius of steel tube: $R_c := \frac{D_c}{2} = 29.4 \cdot in$

Horizontal distance from centerline of the shear strut to its edge: $b := \min\left(\frac{D_c - H}{2}, \frac{H}{2}\right) = 5.4 \cdot in$

Cross sectional area of the the shear strut: $A_{Strut} := \sqrt{2} \cdot b \cdot \sqrt{4 \cdot R_c^2 - b^2} = 445 \cdot in^2$

Axial load bearing on steel tube: $P_{st} := \min\left(P_{axial} \cdot \frac{E_s \cdot A_s}{E_s \cdot A_s + E_c \cdot A_c}, A_s \cdot f_{yst}\right) = 1088 \cdot kip$

Axial load bearing on concrete core: $P_c := \min\left(P_{axial} - P_{st}, A_c \cdot f'_c\right) = 3492 \cdot kip$

Shear resistance of the developing strut: $V_{Strut} := \min\left(\frac{f'_c \cdot A_{Strut}}{\sqrt{2}}, A_s \cdot f_{yst} + P_{st}\right) = 1258 \cdot kip$

Vertical component of the developing strut: $P_{Strut} := V_{Strut}$

Shear strength of the concrete: $\beta := 2.0$ $V_c := 0.0316 \cdot \beta \cdot \sqrt{\frac{f'_c}{ksi}} \cdot A_c \cdot ksi \cdot \left(1 + \frac{P_{Strut} + P_c}{2 \cdot A_c \cdot ksi}\right) = 643 \cdot kip$

Shear resistance of the concrete part of the RCFST: $V_{conc} := \max\left(V_{Strut}, V_c\right) = 1258 \cdot kip$

Shear resistance of the steel tube part of the RCFST: $V_{st} := \frac{2 \cdot D \cdot t}{\sqrt{3}} \cdot \sqrt{f_{yst}^2 - \left(\frac{P_{Strut} - P_{st}}{A_s}\right)^2} = 1948 \cdot kip$

Nominal shear resistance of the composite RCFST: $V_n := V_{st} + V_{conc} = 3205 \cdot kip$

From Article 6.5.4.2 of the AASHTO BDS

- For shear: $\phi_v := 1.0$

Factored nominal shear resistance of the composite RCFST: $V_{rc} := \phi_v \cdot V_n = 3205 \cdot kip$

Mathcad ® Enabled Content.

Composite RCFST Shaft Design, *Hadi Kenarangi, University at Buffalo, 2017*

Axial-flexural interaction check using the proposed modifications to AASHTO SGS 7.6.1

Disclaimer

Disclaimer

While the research team of the Project NCHRP 12-93 have made every effort to ensure that the equations, calculations, diagrams, and solutions accurately represent the content of the references and the proposed revisions, the research team do not give any warranties on accuracy of the solutions produced by a new set of the input parameters. The user shall use engineering judgment and check the accuracy of the produced solutions and results.

Disclaimer

User Notices

User Notices

AASHTO LRFD Bridge Design Specification is noted as "**AASHTO BDS**"
AASHTO Guide Specifications for LRFD Seismic Bridge Design is noted as "**AASHTO SGS**"
Input variables that need to be defined by the user are highlighted in YELLOW.
Key results and design checks are highlighted in GREEN.
Intermediate results and checks are highlighted in BLUE.

User Notices

Description

Givens : Factored moment, axial load, and shear diagrams in the RCFST shaft. RCFST cross-section including the tube thickness and material properties, concrete material properties, and reinforcing layout and areas.

References:

- AASHTO. (2011; 2012; 2013; 2014). *AASHTO Guide Specifications for LRFD Seismic Bridge Design (2nd Edition) with 2012, 2014 and 2015 Interim Revisions.* American Association of State Highway and Transportation Officials (AASHTO).
- AASHTO. (2014; 2015). *AASHTO LRFD Bridge Design Specifications, U.S. Customary Units with 2015 and 2016 Interim Revisions (7th Edition).* American Association of State Highway and Transportation Officials (AASHTO).

Input

Notation

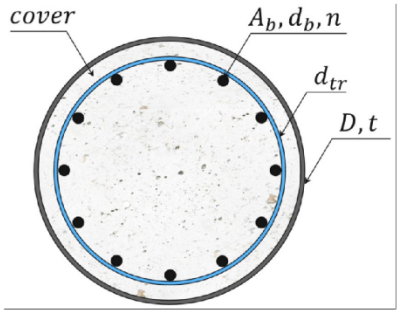

Unsupported length: $L := 50ft$

$K := 2$

Unfactored axial dead load: $P := 5029kip$

Cross section properties

Steel tube

Outside diameter of the steel tube: $D := 60in$

Thickness of the steel tube: $t := 0.625in$

Nominal yield strength of the steel tube: $f_{yst} := 45ksi$

Modulus of elasticity of steel: $E_s := 29000 \cdot ksi$

Concrete

Uniaxial compressive strength of the unconfined concrete: $f'_c := 4 \cdot ksi$

Uniaxial compressive strength of the confined concrete: $f'_{cc} := 4.75 \cdot ksi$

Unit weight of concrete: $w_c := 150 \frac{lb}{ft^3}$

Modulus of elasticity of concrete: $E_c := \left(w_c \cdot \frac{ft^3}{lb} \right)^{1.5} \cdot \sqrt{\frac{f'_{cc}}{ksi}} ksi = 4004 \cdot ksi$ (ACI318)

Shaft rebar

Cover: $cover := 2in$

Nominal diameter of the rebar: $d_b := 1.27in$

Nominal area of the rebar: $A_b := 1.27in^2$

Number of rebars: $n := 28$

Nominal diameter of the transverse rebar: $d_{tr} := \frac{5}{8}in$

Nominal yield strength of the rebar: $f_{yb} := 60ksi$

Computed section properties

Inside diameter of steel tube: $D_c := D - 2t = 58.75 \cdot in$

Rebar layer radius: $r_b := \frac{D_c}{2} - cover - d_{tr} - \frac{d_b}{2} = 26.115 \cdot in$

Equivalent rebar ring thickness: $t_b := \frac{n \cdot A_b}{2 \cdot \pi \, r_b} = 0.217 \cdot in$

Moment of inertia of the equivalent rebar ring: $I_r := \frac{\pi}{4}\left[\left(r_b + \frac{t_b}{2}\right)^4 - \left(r_b - \frac{t_b}{2}\right)^4\right] = 1.213 \times 10^4 \cdot in^4$

Total area of rebars: $A_r := n \cdot A_b = 35.6 \cdot in^2$

Area of concrete fill: $A_c := \pi \frac{D_c^2}{4} = 2710.9 \cdot in^2$

Moment of inertia of the concrete: $I_c := \pi \frac{D_c^4}{64} = 5.848 \times 10^5 \cdot in^4$

Plastic modulus of the concrete: $Z_c := \frac{D_c^3}{6} = 3.38 \times 10^4 \cdot in^3$

Area of the steel tube: $A_s := \pi \cdot \frac{D^2}{4} - A_c = 116.6 \cdot in^2$

Moment of inertia of the steel tube: $I_s := \pi \frac{D^4}{64} - I_c = 5.138 \times 10^4 \cdot in^4$

Plastic modulus of the steel tube: $Z_s := \frac{D^3}{6} - Z_c = 2.203 \times 10^3 \cdot in^3$

Calculating the nominal axial capacity per AASHTO BDS Article 6.9.6.3:

Compressive resistance of the column without consideration of buckling:

$$P_o := 0.95f'_c A_c + f_{yst} \cdot A_s + f_{yb} \cdot A_r = 17681 \cdot kip \quad (6.9.6.3.2\text{-}4)$$

Effective flexural stiffness:

$$C' := \min\left(0.15 + \frac{P}{P_o} + \frac{A_s + A_r}{A_s + A_r + A_c}, 0.9\right) = 0.488 \quad (6.9.6.3.2\text{-}7)$$

$$EI_{eff} := E_s \cdot I_s + E_s \cdot I_r + C' \cdot E_c \cdot I_c = 2.98 \times 10^9 \cdot kip \cdot in^2 \quad (6.9.6.3.2\text{-}6)$$

Elastic critical buckling resistance of flexural buckling:

$$P_e := \frac{\pi^2 EI_{eff}}{(K \cdot L)^2} = 2.04 \times 10^4 \cdot kip \quad (6.9.6.3.2\text{-}5)$$

Nominal compressive resistance:

$$P_n := \text{if}\left[P_e > 0.44P_o, 0.658^{\left(\frac{P_o}{P_e}\right)} \cdot P_o, 0.877P_e\right] = 12312 \cdot kip \quad (6.9.6.3.2\text{-}2 \text{ \& } 3)$$

From Article 6.5.4.2 of the AASHTO LRFD Bridge Design Specifications (AASHTO BDS):

- For axial compression, composite: $\phi_c := 0.9$
- For flexure: $\phi_f := 1.0$

6.9.6.3.2—Axial Compressive Resistance The factored resistance, P_r, of a composite CFST column subject to axial compression shall be determined as:

$$P_r := \phi_c \cdot P_n = 11081 \cdot kip \quad (6.9.6.3.2\text{-}1)$$

Revised Article 7.6.1—Combined Axial Compression and Flexure Concrete-filled

$$P_{rc} := A_c \cdot f'_c = 10843 \cdot kip \quad (7.6.1\text{-}4)$$

$$P_o = 17681 \cdot kip \quad (6.9.6.3.2\text{-}4) \text{ AASHTO BDS}$$

$$B := 1 - \frac{P_{rc}}{P_o} = 0.387 \quad (7.6.1\text{-}3)$$

Factored nominal capacity of the member (M_{rc}) determined in accordance with **Revised AASHTO SGS Article 7.6.2**:

$$t_b := \frac{n \cdot A_b}{2 \cdot \pi \, r_b} = 0.217 \cdot in \qquad (7.6.2\text{-}3)$$

$$Z_b := \frac{\left(2 \cdot r_b + t_b\right)^3 - \left(2 \cdot r_b - t_b\right)^3}{6} = 591.2 \cdot in^3 \qquad (7.6.2\text{-}4)$$

$$h_n := \frac{A_c \cdot f'_c}{2 \cdot D \cdot f'_c + 4\left(2 \cdot t \cdot f_{yst} + 2 \cdot t_b \cdot f_{yb} - t \cdot f'_c\right)} = 13.6 \cdot in \qquad (7.6.2\text{-}2)$$

$$M_{rc} := \phi_f \cdot \left[\begin{array}{l} \left(Z_s - 2 \cdot t \cdot h_n^{\,2}\right) \cdot f_{yst} + \left[\frac{2}{3}\left(\frac{D}{2} - t\right)^3 - \left(\frac{D}{2} - t\right) \cdot h_n^{\,2}\right] \cdot f'_c \ \ldots \\ + \left(Z_b - 2 \cdot t_b \cdot h_n^{\,2}\right) \cdot f_{yb} \end{array} \right] \qquad (7.6.2\text{-}1)$$

$M_{rc} = 13786 \cdot kip \cdot ft$

$M_{rc\_7.6.2\_SGS} := M_{rc}$

Factored nominal capacity of the member (M_{rc}) determined in accordance with **Article 6.12.2.3.3 AASHTO BDS:**

$$r_m := \frac{D - t}{2} = 29.7 \cdot in \qquad r_i := \frac{D - 2t}{2} = 29.4 \cdot in$$

$$\theta_s(y) := \operatorname{asin}\left(\frac{y}{r_m}\right) \qquad \theta_b(y) := \operatorname{if}\left(-1 < \frac{y}{r_b} < 1, \operatorname{asin}\left(\frac{y}{r_b}\right), \operatorname{if}\left(\frac{y}{r_b} > 1, \frac{\pi}{2}, \frac{-\pi}{2}\right)\right)$$

$$c(y) := r_i \cdot \cos\left(\theta_s(y)\right) \qquad c_b(y) := r_b \cdot \cos\left(\theta_b(y)\right)$$

$$\begin{aligned} P_{comp}(y) = {} & f_{yst} \cdot t \cdot r_m \cdot \left[\left(\pi - 2 \cdot \theta_s(y)\right) - \left(\pi + 2 \cdot \theta_s(y)\right)\right] \ \ldots \\ & + t_b \cdot r_b \cdot \left[f_{yb} \cdot \left(\pi - 2 \cdot \theta_b(y)\right) - \left(f_{yb} - 0.95 f'_c\right) \cdot \left(\pi + 2 \cdot \theta_b(y)\right)\right] \ \ldots \\ & + \frac{0.95 f'_c}{2}\left[\left(\pi - 2 \cdot \theta_s(y)\right) \cdot r_i^{\,2} - 2 \cdot y \cdot c(y)\right] \end{aligned} \qquad (C6.12.2.3.3\text{-}1)$$

$$M_{comp}(y) := 0.95 \cdot f'_c \cdot \left[c(y) \cdot \left[\left(r_i^{\,2} - y^2\right) - \frac{c(y)^2}{3}\right]\right] + 4 \cdot f_{yst} \cdot t \cdot c(y) \cdot \frac{r_m^{\,2}}{r_i} + 4 \cdot f_{yb} \cdot t_b \cdot c_b(y) \cdot r_b \qquad (C6.12.2.3.3\text{-}2)$$

Find the position of the neutral axis for the case of P_{comp}=0kip:

$y_{try} := 0in$

Given

$P_{comp}\left(y_{try}\right) = 0kip$

$y_B := \text{Find}\left(y_{try}\right) = 13.596 \cdot in$

$P_B := P_{comp}\left(y_B\right) = 0 \cdot kip$

$M_B := M_{comp}(y_B) = 13596 \cdot kip \cdot ft$

$M_{rc\_BDS} := \phi_f \cdot M_B = 13596 \cdot kip \cdot ft$

Compare M_{rc} from **Revised Article 7.6.2** and **Article 6.12.2.3.3 AASHTO BDS** :

Revised Article 7.6.2: $M_{rc\_7.6.2\_SGS} = 13786 \cdot kip \cdot ft$

Article 6.12.2.3.3 AASHTO BDS: $M_{rc\_BDS} = 13596 \cdot kip \cdot ft$

Continue with: $M_{rc} := M_{rc\_7.6.2\_SGS}$

$P_{SGS} := \begin{bmatrix} P_r & (1 - B) \cdot P_r & 0 \end{bmatrix}^T$ $M_{SGS} := \begin{pmatrix} 0 & M_{rc} & M_{rc} \end{pmatrix}^T$

Factored axial and moment acting on the member:

$$P_u := \begin{pmatrix} 5029.34 \\ 4948.9 \\ 4793.2 \\ 4582.36 \\ 4332.64 \\ 4067.52 \\ 3811.42 \\ 3575.07 \\ 3363.63 \\ 3181.35 \\ 3031.36 \\ 2915.46 \\ 2833.95 \\ 2774.62 \\ 2739.07 \end{pmatrix} kip \qquad M_u := \begin{pmatrix} 5000 \\ 8496.58 \\ 9336.35 \\ 7082.79 \\ 2840.97 \\ 258.94 \\ 465.07 \\ 327.76 \\ 92.39 \\ 10.24 \\ 20.14 \\ 7.47 \\ 0.19 \\ -0.97 \\ -0.35 \end{pmatrix} kip \cdot ft$$

$$\left(\frac{P_u}{P_r}+\frac{B\cdot M_u}{M_{rc}}\right)=\begin{pmatrix}0.594\\0.685\\0.694\\0.612\\0.471\\0.374\\0.357\\0.332\\0.306\\0.287\\0.274\\0.263\\0.256\\0.25\\0.247\end{pmatrix}$$

$$\text{if}\left[\left(\frac{P_u}{P_r}+\frac{B\cdot M_u}{M_{rc}}\right)_i<1\text{, "OK" , "NotOK"}\right]=\begin{pmatrix}\text{"OK"}\\\text{"OK"}\\\text{"OK"}\\\text{"OK"}\\\text{"OK"}\\\text{"OK"}\\\text{"OK"}\\\text{"OK"}\\\text{"OK"}\\\text{"OK"}\\\text{"OK"}\\\text{"OK"}\\\text{"OK"}\\\text{"OK"}\\\text{"OK"}\end{pmatrix}$$

$i := 1 .. 15$

(7.6.1-1)

$$\text{if}\left[\left(\frac{M_u}{M_{rc}}\right)_i<1\text{, "OK" , "NotOK"}\right]=\begin{pmatrix}\text{"OK"}\\\text{"OK"}\\\text{"OK"}\\\text{"OK"}\\\text{"OK"}\\\text{"OK"}\\\text{"OK"}\\\text{"OK"}\\\text{"OK"}\\\text{"OK"}\\\text{"OK"}\\\text{"OK"}\\\text{"OK"}\\\text{"OK"}\\\text{"OK"}\end{pmatrix}$$

(7.6.1-2)

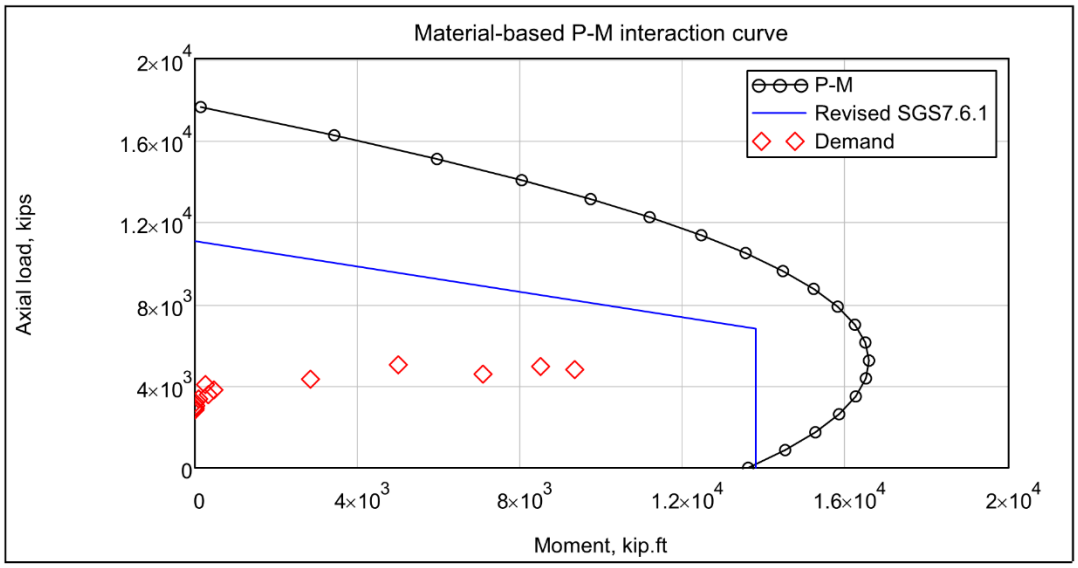
Material-based P-M interaction curve
P-M
Revised SGS7.6.1
Demand
Axial load, kips
Moment, kip.ft
2×10^4
1.6×10^4
1.2×10^4
8×10^3
4×10^3
0
0
4×10^3
8×10^3
1.2×10^4
1.6×10^4
2×10^4

K.2 Example 2: Displacement-based design of RCFST

This example presents a RCFST used to support a single reinforced concrete column bent of the same diameter, as shown in Figure K.2. In this example, the plastic hinge is allowed to develop in the RCFST below ground. The cross-section of the shaft and its material properties are given in Table K.3. The seismic displacement demand is given as $15in.$ at top of the column. This example provides calculations of the displacement capacity of the RCFST shaft to compare against demand. The outline of the calculations for the design Example 2 is as following:

1. Determination of the materials stress-strain behaviors to be used in generation of moment-curvature (M-ϕ) curves.

2. Calculation of the effective stiffness of the cross-section per AASHTO BDS (2014) Article 6.9.6.3.2.

3. Calculation of the first yield curvature and proposed limit states for the ultimate and damage curvatures per the proposed equations provided in Section 3.2.5 of the report.

4. Generating the M-ϕ curve by fiber-section analyses.

5. Calculation of idealized bi-linear M-ϕ curve per AASHTO BDS (2014) Article 8.5.

6. Calculation of plastic hinge length per AASHTO SGS (2014) Article 4.11.6-4.

7. Calculation of the equivalent yield displacement and displacement capacity of the RCFST shaft using the equivalent cantilever model.

All this process was included in Mathcad worksheets for design engineers. The Mathcad worksheets are printed in the following.

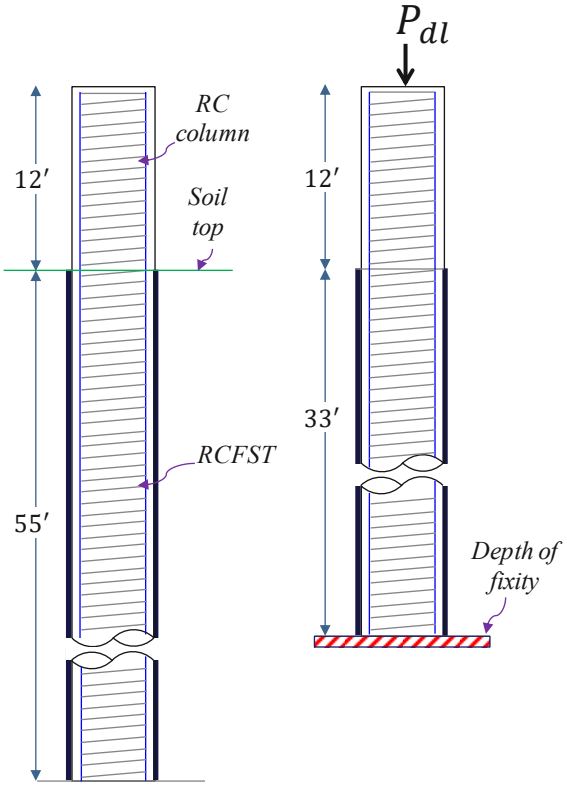

Figure K.2: RCFST geometry and equivalent cantilever model for Example 2.

Table K.3. Shaft properties for Example 2.

Nominal diameter of steel tube	d_{tube}	$48in.$	
Nominal thickness of steel tube	t_{tube}	$0.625in.$	
Nominal yield strength of steel tube	F_{ytube}	$45ksi$	ASTM A252 – Gr. 3
Nominal compressive strength of concrete	f_c'	$4ksi$	
Nominal yield strength of rebar	f_{yst}	$60ksi$	
Cross-section rebar ratio	ρ_{st}	2.5%	(20) #14 bars
Rebar cage cover	cover	$2in.$	
Nominal diameter of transverse rebar	d_{tr}	$5/8in.$	

Mathcad ® Enabled Content.

Composite RCFST Shaft Design, *Hadi Kenarangi, University at Buffalo, 2017*

Calculations of the displacement capacity of RCFST with allowed hinging below ground.

Disclaimer

Disclaimer

While the research team of the Project NCHRP 12-93 have made every effort to ensure that the equations, calculations, diagrams, and solutions accurately represent the content of the references and the proposed revisions, the research team do not give any warranties on accuracy of the solutions produced by different set of the input parameters. The user shall use engineering judgment and check the accuracy of the produced solutions and results.

Disclaimer

User Notices

User Notices

AASHTO LRFD Bridge Design Specification is noted as "**AASHTO BDS**"
AASHTO Guide Specifications for LRFD Seismic Bridge Design is noted as "**AASHTO SGS**"
Input variables that need to be defined by the user are highlighted in YELLOW.
Key results and design checks are highlighted in GREEN.
Intermediate results and checks are highlighted in BLUE.

User Notices

Description

- The seismic demand calculations, which are based on the calculated effective flexural stiffness are not presented in this worksheet.
- The M-ϕ curve was developed in OpenSees using the materials behavior calculated in this worksheet.
- Nonlinear pushover analysis of the equivalent cantilever column was substituted by hand calculations.

References:

- AASHTO. (2011; 2012; 2013; 2014). *AASHTO Guide Specifications for LRFD Seismic Bridge Design (2nd Edition) with 2012, 2014 and 2015 Interim Revisions.* American Association of State Highway and Transportation Officials (AASHTO).
- AASHTO. (2014; 2015). *AASHTO LRFD Bridge Design Specifications, U.S. Customary Units with 2015 and 2016 Interim Revisions (7th Edition).* American Association of State Highway and Transportation Officials (AASHTO).
- Brown NK, Kowalsky MJ, Nau JM. *Impact of D/t on seismic behavior of reinforced concrete filled steel tubes.* Journal of Constructional Steel Research. 2015;107:111-23.
- Denavit, Mark D., and Jerome F. Hajjar. *Characterization of behavior of steel-concrete composite members and frames with applications for design*. Newmark Structural Engineering Laboratory. University of Illinois at Urbana-Champaign., 2014.
- Susantha, K. a. S., Ge, H., & Usami, T. (2001). *Uniaxial stress–strain relationship of concrete confined by various shaped steel tubes.* Engineering Structures, 23(10), 1331–1347.

Input

Notation

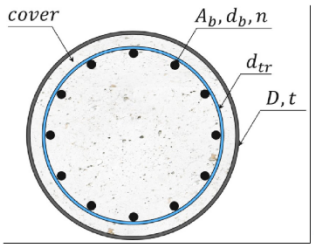

RCFST cross-section

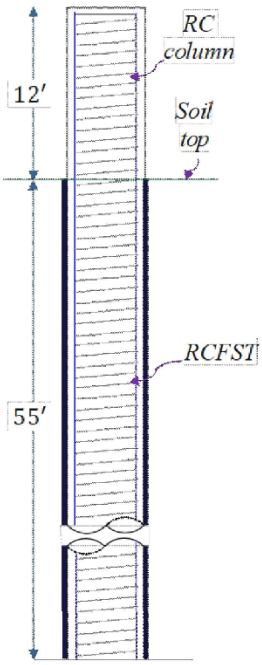

Figure (1): Model geometry

Unsupported length: $L := 45ft$ (Assumed equal to the distance from top of the column to the depth of the fixity)

$K := 2$

Unfactored axial dead load: $P := 1340kip$ (Positive is compression, Assumed equal to 10% of P_o)

Cross section properties

Steel tube

Outside diameter of the steel tube: $D := 48in$

Thickness of the steel tube: $t := \frac{5}{8}in = 0.625 \cdot in$

Nominal yield strength of the steel tube: $f_{yst} := 45ksi$

Modulus of elasticity of steel: $E_s := 29000 \cdot ksi$

Concrete

Uniaxial compressive strength of the unconfined concrete: $f'_c := 4 \cdot ksi$

Uniaxial compressive strength of the confined concrete: $f'_{cc} := 5.5 \cdot ksi$

Unit weight of concrete: $w_c := 150 \frac{lb}{ft^3}$

Modulus of elasticity of concrete: $E_c := \left(w_c \cdot \frac{ft^3}{lb} \right)^{1.5} \cdot \sqrt{\frac{f'_{cc}}{ksi}} ksi = 4308 \cdot ksi$ (ACI318)

Shaft rebar

Cover: $cover := 2in$

Nominal diameter of the rebar: $d_b := 1.693in$ (20#14)

Nominal area of the rebar: $A_b := 2.25in^2$

Number of rebars: $n := 20$

Nominal diameter of the transverse rebar: $d_{tr} := \frac{5}{8}in$

Nominal yield strength of the rebar: $f_{yb} := 60ksi$

Computed section properties

Inside diameter of steel tube: $D_c := D - 2t = 46.75 \cdot in$

Rebar layer radius: $r_b := \frac{D_c}{2} - cover - d_{tr} - \frac{d_b}{2} = 19.9 \cdot in$

Equivalent rebar ring thickness: $t_b := \frac{n \cdot A_b}{2 \cdot \pi \, r_b} = 0.36 \cdot in$

Moment of inertia of the equivalent rebar ring: $I_r := \frac{\pi}{4}\left[\left(r_b + \frac{t_b}{2}\right)^4 - \left(r_b - \frac{t_b}{2}\right)^4\right] = 8.914 \times 10^3 \cdot in^4$

Total area of rebars: $A_r := n \cdot A_b = 45 \cdot in^2$

Area of concrete fill: $A_c := \pi \frac{D_c^2}{4} = 1716.5 \cdot in^2$

Moment of inertia of the concrete: $I_c := \pi \frac{D_c^4}{64} = 2.345 \times 10^5 \cdot in^4$

Plastic modulus of the concrete: $Z_c := \frac{D_c^3}{6} = 1.703 \times 10^4 \cdot in^3$

Area of the steel tube: $A_s := \pi \cdot \frac{D^2}{4} - A_c = 93 \cdot in^2$

Moment of inertia of the steel tube: $I_s := \pi \frac{D^4}{64} - I_c = 2.61 \times 10^4 \cdot in^4$

Plastic modulus of the steel tube: $Z_s := \frac{D^3}{6} - Z_c = 1.403 \times 10^3 \cdot in^3$

Confined concrete behavior:

The analytical model proposed by Susantha et al. (2001) for the uniaxial compressive strength of the concrete confined by circular steel tube (Note: This model has been proposed for RCFST cross-section with no axial load. For the case with axial load, larger value for α is recommended. α is defined in Figure (2)):

Poisson ratio of the steel tube:

$$\nu_{st} := 0.3$$

Unconfined concrete peak strain:

$$\varepsilon_{co} := 0.002$$

Ultimate strain of confined concrete in circular RCFST per Susantha et al. (2001):

$$\varepsilon_{cu} := 0.025$$

Reduced unconfined compressive strength of concrete per Susantha et al. (2001):

$$f'_{rc} := 0.85 \cdot f'_c = 3.4 \cdot ksi$$

Poisson ratio of the steel tube filled with concrete (ν_e):

$$\nu'_e := \frac{0.881}{10^6}\left(\frac{D}{t}\right)^3 - \frac{2.58}{10^4}\left(\frac{D}{t}\right)^2 + \frac{1.953}{10^2}\left(\frac{D}{t}\right) + 0.4011 = 0.778$$

$$\nu_e := 0.2312 + 0.3582 \cdot \nu'_e - 0.1524\left(\frac{f'_{rc}}{f_{yst}}\right) + 4.843 \cdot \nu'_e\left(\frac{f'_{rc}}{f_{yst}}\right) - 9.169 \cdot \left(\frac{f'_{rc}}{f_{yst}}\right)^2$$

$$\beta := \nu_e - \nu_{st}$$

Lateral pressure at the peak load:

$$f_{rp} := \beta \cdot \left(\frac{2 \cdot t}{D - 2 \cdot t}\right) \cdot f_{yst} = 0.519 \cdot ksi$$

Confined uniaxial compressive strength of the concrete:

$$f'_{cc} := f'_{rc} + 4 \cdot f_{rp} = 5.5 \cdot ksi$$

Confined concrete peak strain:

$$\varepsilon_{cc} := \varepsilon_{co} \cdot \left[1 + 5 \cdot \left(\frac{f'_{cc}}{f'_{rc}} - 1\right)\right] = 0.0081$$

$$r := \frac{E_c}{\left(E_c - \frac{f'_{cc}}{\varepsilon_{cc}}\right)}$$

$$R_t := \frac{\sqrt{3 \cdot \left(1 - \nu_{st}^2\right)}}{2} \cdot \frac{f_{yst}}{E_s} \cdot \frac{D}{t} = 0.098$$

$$Z := \begin{cases} 0\text{MPa} & \text{if } R_t \cdot \frac{f'_{rc}}{f_{yst}} \le 0.006 \\ \left[10^5 \cdot \left(R_t \cdot \frac{f'_{rc}}{f_{yst}}\right) - 600\right]\text{MPa} & \text{if } R_t \cdot \frac{f'_{rc}}{f_{yst}} \ge 0.006 \wedge f_{yst} \le 283\text{MPa} \\ \left[10^6 \cdot \left(R_t \cdot \frac{f'_{rc}}{f_{yst}}\right) - 6000\right]\text{MPa} & \text{if } R_t \cdot \frac{f'_{rc}}{f_{yst}} \ge 0.006 \wedge f_{yst} \ge 336\text{MPa} \\ \left(\frac{f_{yst}}{283\text{MPa}}\right)^{13.4} \cdot \left[10^5 \cdot \left(R_t \cdot \frac{f'_{rc}}{f_{yst}}\right) - 600\right]\text{MPa} & \text{if } R_t \cdot \frac{f'_{rc}}{f_{yst}} \ge 0.006 \wedge 283\text{MPa} \le f_{yst} \le 336\text{MPa} \\ \text{"Error"} & \text{otherwise} \end{cases}$$

$$Z = 493 \cdot \text{MPa} \qquad R_t \cdot \frac{f'_{rc}}{f_{yst}} = 0.0074$$

$$\alpha := 1 - \frac{Z}{f'_{cc}}\left(\varepsilon_{cu} - \varepsilon_{cc}\right) = 0.779$$

$$f_{rc}(\varepsilon) := \begin{cases} f'_{cc} \cdot \dfrac{\frac{\varepsilon}{\varepsilon_{cc}} \cdot r}{r - 1 + \left(\frac{\varepsilon}{\varepsilon_{cc}}\right)^r} & \text{if } 0 \le \varepsilon \le \varepsilon_{cc} \\ f'_{cc} - Z \cdot \left(\varepsilon - \varepsilon_{cc}\right) & \text{if } \varepsilon_{cc} \le \varepsilon \le \varepsilon_{cu} \\ \alpha \cdot f'_{cc} & \text{if } \varepsilon \ge \varepsilon_{cu} \end{cases}$$

$$\varepsilon_i := 0, 0.001 .. 1.2 \cdot \varepsilon_{cu}$$

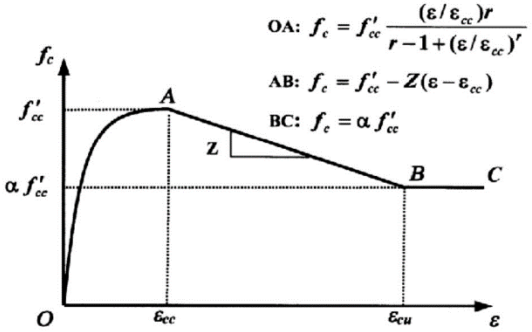

Figure (2): General form of the confined concrete stress-strain curve (compression side).

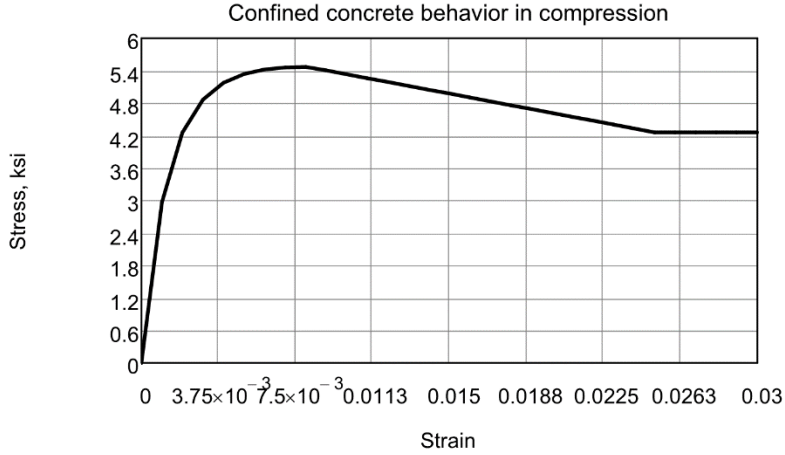

Figure (3): Confined concrete stress-strain curve (compression side).

Behavior of concrete in tension:

Ultimate tensile strength of concrete: $f'_t := 0.1 \cdot f'_c$

Tensile strain at crack: $\varepsilon_{cr} := \frac{f'_t}{E_c} = 9.284 \times 10^{-5}$

Tension softening stiffness: $E_t := E_c$

$$f_t(\varepsilon) := \begin{cases} (E_c \cdot \varepsilon) & \text{if } 0 \le \varepsilon \le \varepsilon_{cr} \\ \left[f'_t - E_t \cdot (\varepsilon - \varepsilon_{cr})\right] & \text{if } \varepsilon_{cr} \le \varepsilon \le \varepsilon_{cr} + \frac{f'_t}{E_t} \\ 0 & \text{if } \varepsilon_{cr} + \left(\varepsilon_{cr} + \frac{f'_t}{E_t}\right) \le \varepsilon \end{cases}$$

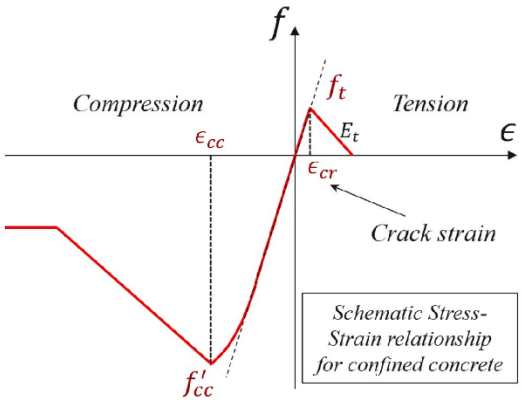

Figure (4): General form of the confined concrete stress-strain curve.

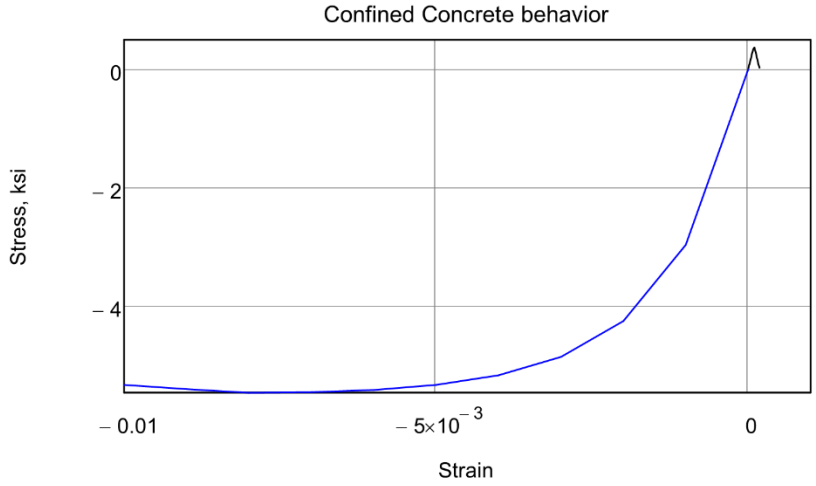

Figure (5): Confined concrete stress-strain curve including the tension side.

Steel tube material behavior:

Modulus of elasticity of steel: $E_s = 2.9 \times 10^4 \cdot ksi$

Nominal yield strength of steel tube: $f_{yst} = 45 \cdot ksi$

Strain hardening modulus (Denavit and Hajjar, 2012): $E_{sh} := \frac{E_s}{100}$

Strain at ultimate stress (Denavit and Hajjar, 2012): $\varepsilon_u := 120 \cdot \frac{f_{yst}}{E_s} = 0.186$

Fracture strain of the steel tube (Brown et al. 2015): $\varepsilon_{frac} := 0.025$

$$f_{st}(\varepsilon) := \begin{cases} \varepsilon \cdot E_s & \text{if } \varepsilon \le \frac{f_{yst}}{E_s} \\ f_{yst} + E_{sh} \cdot \left(\varepsilon - \frac{f_{yst}}{E_s} \right) & \text{if } \varepsilon \ge \frac{f_{yst}}{E_s} \end{cases}$$

$\varepsilon := 0, 10^{-4} .. \varepsilon_{frac}$

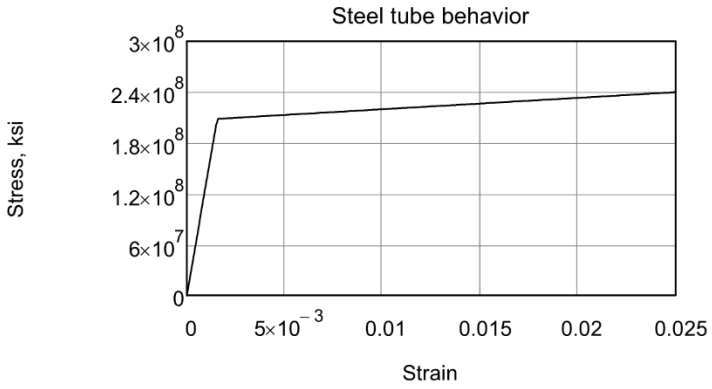

Figure (6): Steel tube stress-strain behavior.

Steel material behavior for the rebars should follow the actual stress-strain data as shown in Section 8.4.2 of AASHTO SGS. (Note: For simplicity here, a bilinear steel material behavior was assumed in this calculations.)

Effective stiffness of the RCFST cross-section per AASHTO BDS Article 6.9.6.3.2:

Compressive resistance of the column without consideration of buckling:

$$P_o := 0.95f'_c A_c + f_{yst} \cdot A_s + f_{yb} \cdot A_r = 13409 \cdot kip \qquad (6.9.6.3.2\text{-}4)$$

Effective flexural stiffness:

$$C' := \min\left(0.15 + \frac{P}{P_o} + \frac{A_s + A_r}{A_s + A_r + A_c}, 0.9\right) = 0.324 \qquad (6.9.6.3.2\text{-}7)$$

$$EI_{eff} := E_s \cdot I_s + E_s \cdot I_r + C' \cdot E_c \cdot I_c = 1.34 \times 10^9 \cdot kip \cdot in^2 \qquad (6.9.6.3.2\text{-}6)$$

Ultimate curvature calculation using the proposed equations:

Yield strain of the steel tube:

$$\varepsilon_y := \frac{f_{yst}}{E_s}$$

Fracture strain of the steel tube (Brown et al. 2015):

$$\varepsilon_{frac} = 0.025$$

Ultimate strain of confined concrete in circular RCFST per Susantha et al. (2001):

$$\varepsilon_{cu} = 0.025$$

(Collapsible region contains calculation of the plastic neutral axis using PSDM)

Distance from center to the plastic neutral axis by PSDM:

$$y_N = 5.4 \cdot in$$

Proposed ultimate curvature for composite RCFST cross-section (Kenarangi and Bruneau, 2017):
(Proposed in current NCHRP 12-93 project)

$$\phi_u := \min\left(\frac{\varepsilon_{frac}}{\frac{D}{2} - \frac{t}{2} + y_N}, \frac{\varepsilon_{cu}}{\frac{D}{2} - t - y_N}\right) = 8.6 \times 10^{-4} \cdot \frac{1}{in}$$

where:

$$\frac{\varepsilon_{frac}}{\frac{D}{2} - \frac{t}{2} + y_N} = 8.6 \times 10^{-4} \cdot \frac{1}{in} \quad \text{and} \quad \frac{\varepsilon_{cu}}{\frac{D}{2} - t - y_N} = 1.39 \times 10^{-3} \cdot \frac{1}{in}$$

Proposed damage controlling limit curvature (Kenarangi and Bruneau, 2017):

(Proposed in current NCHRP 12-93 project)

$$\phi_d := \min\left[\frac{1}{2}\left(\frac{\varepsilon_y}{\frac{D}{2} - \frac{t}{2}} + \frac{\varepsilon_{frac}}{\frac{D}{2} - \frac{t}{2} + y_N}\right), \frac{\varepsilon_{cu}}{\frac{D}{2} - t - y_N}\right] = 4.63 \times 10^{-4} \cdot \frac{1}{in}$$

Moment-curvature curve from fiber-section analysis:

(Collapsible region contains input of M-ϕ curve from external fiber-section analysis. The M-ϕ data should be inserted in the external file "M_Phi.csv" or directly inserted in "Data" matrix below.)

Insert moment-curvature curve of Composite RCFST that has been analyzed by fiber-section analyses software:

Data := M_Phi.csv

$$\begin{pmatrix} M \\ \phi \end{pmatrix} := \begin{pmatrix} Data^{\langle 2 \rangle}\ kip \cdot in \\ Data^{\langle 1 \rangle}\ \frac{1}{in} \end{pmatrix} \qquad \begin{pmatrix} \frac{M}{kip \cdot in} \\ \phi \cdot in \end{pmatrix}^T = (\{161,1\}\ \ \{161,1\})$$

$Data^T$ (Contains the moment and phi values)

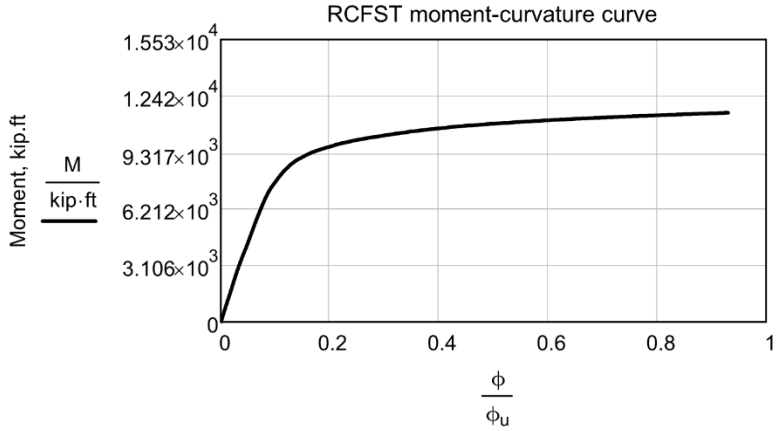

Figure (7): Moment-curvature curve inserted from fiber-section analysis software.

First yield curvature is defined as the curvature corresponding to the first yield on the tension side of the steel tube. This can be calculated using the fber-section anlaysis results.

$$\phi_y := 6.0 \times 10^{-5}\ \frac{1}{in}$$

Equivalent flexural stiffness (EI_{eq}) should be calculated by dividing the moment at first yield point by the corresponding curvature. The first yield point is defined as the point corresponding to the first yielding of the steel tube on the tension side.

Equivalent flexural stiffness of the composite RCFST: $EI_{eq} := 1.1835 \cdot 10^9 kip \cdot in^2$

Calculation of M_p per **AASHTO BDS Article 8.5** :

Note: ϕ has to be incremented evenly.

length(M) = 161 imax := length(M) i := 1 .. imax $d\phi := \phi_3 - \phi_2 = 5 \times 10^{-6} \cdot in^{-1}$

Area under *M-ϕ curve:* $$AUC := d\phi \cdot \left[\frac{1}{2} \cdot (M_1 + M_{imax}) + \sum_{i=2}^{imax-1} M_i \right] = 95.848 \cdot kip$$

$$PR := \text{polyroots}\left[\begin{pmatrix} \frac{AUC}{kip} & -\max(\phi)\cdot in & \frac{1}{\frac{2EI_{eq}}{kip\cdot in^2}} \end{pmatrix}^T\right] kip\cdot in$$

$$PR = \begin{pmatrix} 1.071\times 10^4 \\ 1.471\times 10^5 \end{pmatrix}\cdot kip\cdot ft \qquad M_p := \text{if}\left(PR_1 < \max(M), PR_1, PR_2\right) = 10712\cdot kip\cdot ft$$

Idealized plastic moment capacity: $M_p = 10712\cdot kip\cdot ft$

Curvature at equivalent yield: $\phi_{yi} := \frac{M_p}{EI_{eq}} = 1.086\times 10^{-4}\cdot\frac{1}{in}$

$$M_{idealized} := \begin{pmatrix} 0 & M_p & M_p \end{pmatrix}^T \qquad \phi_{idealized} := \begin{pmatrix} 0 & \phi_{yi} & \phi_u \end{pmatrix}^T$$

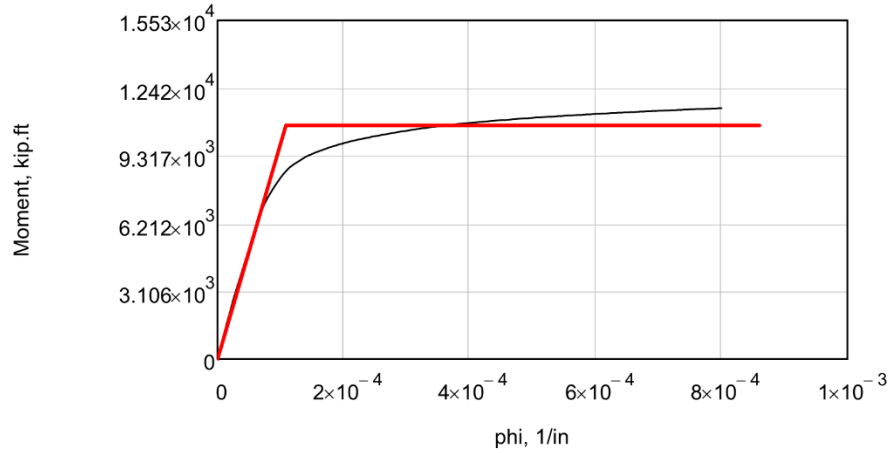

Figure (8): Idealized RCFST moment-curvature curve

Plastic hinge length according to AASHTO SGS Article 4.11.6-4:

The below-ground plastic hinge length, L_p, may be determined as:

Length of the cantilever pile: $H := 45ft$

Diameter of steel tube: $D = 48\cdot in$

Plastic hinge length: $L_p := \min(0.1\cdot H + 1.25\cdot D, 2\cdot D)$ (4.11.6-4)

$L_p = 2\cdot D$

Calculating the displacement capacity of the RCFST shaft using the equivalent cantilever model:

Analysis of this section could be determined by a nonlinear pushover analysis using SAP2000 or other finite element analysis software instead.

Height of the cantilever model: $L_{eq} := 45ft$

Calculated plastic hinge length: $L_p = 8\,ft$

Calculated ultimate curvature for composite RCFST cross-section: $\phi_u = 8.601 \times 10^{-4} \cdot \frac{1}{in}$

Calculated equivalent yield curvature for composite RCFST cross-section: $\phi_{yi} = 1.086 \times 10^{-4} \cdot \frac{1}{in}$

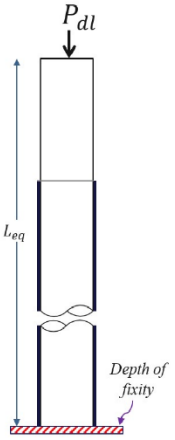

Equivalent yield displacement: $\Delta_{yi} := \frac{\phi_{yi} \cdot L_{eq}^2}{3} = 10.6 \cdot in$

Plastic curvature capacity: $\phi_{pc} := \phi_u - \phi_{yi} = 7.515 \times 10^{-4} \cdot \frac{1}{in}$

Plastic rotation capacity: $\theta_{pc} := \phi_{pc} \cdot L_p = 0.072 \cdot rad$

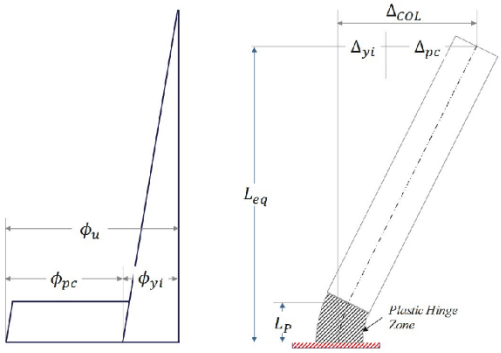

Figure (9): Plastic curvature distribution for a cantilever member.

Plastic displacement capacity: $\Delta_{pc} := \theta_{pc} \cdot \left(L - \frac{L_p}{2} \right) = 35.5 \cdot in$

Ultimate displacement capacity of the cantilever column: $\Delta_{col} := \Delta_{yi} + \Delta_{pc} = 46.1 \cdot in$

Structure demand/capacity check:

Displacement demand: $\Delta_D := 15in$ (at top of the column)

$$DOC := \begin{cases} \text{"Displacement capacity is OK"} & \text{if } \Delta_{col} \geq \Delta_D \\ \text{"Displacement demand is more than capacity"} & \text{otherwise} \end{cases}$$

DOC = "Displacement capacity is OK"

Seismic displacement demand/capacity ratio: $\frac{\Delta_D}{\Delta_{col}} = 0.326$

Plastic displacement demand: $\Delta_{pd} := \Delta_D - \Delta_{yi} = 4.443 \cdot in$

Displacement ductility demand: $\mu_D := 1 + \frac{\Delta_{pd}}{\Delta_{yi}} = 1.421$

Structure displacement ductility check for single column bent:

Displacement ductility demand: $\mu_D = 1.421$

$$DOC := \begin{cases} \text{"Displacement ductlity demand is OK"} & \text{if } \mu_D < 4.0 \\ \text{"Displacement ductlity demand is more than limit"} & \text{otherwise} \end{cases}$$

DOC = "Displacement ductlity demand is OK"

Calculated curvatures and idealized plastic moment:

First yield curvature: $\phi_y = 6 \times 10^{-5} \cdot \frac{1}{in}$

Curvature at equivalent yield: $\phi_{yi} = 1.086 \times 10^{-4} \cdot \frac{1}{in}$

Damage controlling curvature: $\phi_d = 4.628 \times 10^{-4} \cdot \frac{1}{in}$

Ultimate curvature: $\phi_u = 8.601 \times 10^{-4} \cdot \frac{1}{in}$

Idealized plastic moment capacity: $M_p = 1.071 \times 10^{4} \cdot kip \cdot ft$

APPENDIX L

Quantifying the economic impact

L.1 General

Investigation of the economic impacts of the proposed revisions was done by performing revised designs of actual bridge structures using the proposed revisions and comparing them with the designs made by current versions. The economic impacts of the proposed revisions are presented in this appendix.

L.2 Economic Impacts

A study of the economic impacts of the proposed revisions to AASHTO LRFD Bridge Specifications (2012) and AASHTO Guide Specifications for LRFD Seismic Bridge Design (2014) are presented in this section. Two aspects of the current research will result in significant economic savings:

- The investigation of the amount of composite action for CFST's, even with contaminated tubes, showed substantial composite behavior even if no additional steps are taken to transfer shear between the concrete and the steel tube.
- Additionally, a procedure for designing shear transfer mechanisms, in the form of shear rings welded to the inside of the steel tube, to ensure composite action in larger diameter CFSTs has been proposed.

Without the shear transfer provisions, some designers of large diameter shafts/tubes have been hesitant to consider composite action, and therefore typically designed assuming the steel tube was either not composite, or not present at all. Large diameter tubes are typically straight seam construction, and thus require modifications to the concrete fill in order to assume composite action under the current provisions, and this has dissuaded designers from taking advantage of composite behavior.

The economic impact of this change was investigated by performing both a reinforced concrete column design and a CFST design for a given set of loads for a large diameter shaft/tube. The design loads utilized were taken from an actual bridge structure that incorporated drilled shafts with non-structural steel tube. The governing load case for this particular bridge was a vessel collision scenario, which created large bending moments in the drilled shafts as shown in Figure L.1. Calculations were performed using AASHTO LRFD, Seventh Edition including 2015 Interim Revisions. Reinforced concrete columns were designed using Section 5.7 and CFSTs were designed using Section 6.9.6. The following assumptions and simplifications were made:

- Concrete compressive strength = 4*ksi*
- Steel tube yield strength = 50*ksi*
- Reinforcing steel yield strength = 60*ksi*
- Assume reinforced concrete columns require a 5/8*in.* non-structural steel tube for constructability
- Assume CFST does not require an internal cage of reinforcing steel
- Neglect corrosion allowance considerations for CFST steel tube
- Assume CFST's tube thickness is available in 1/8*in.* increments
- Assume shaft diameter is not governed by geotechnical requirements

- Perform designs based on axial load and moment requirements only (neglect shear and torsion)
- Perform designs based on strength requirements only (neglect serviceability)
- Assume design loads are constant (neglect change in design loads due to change in structure stiffness)

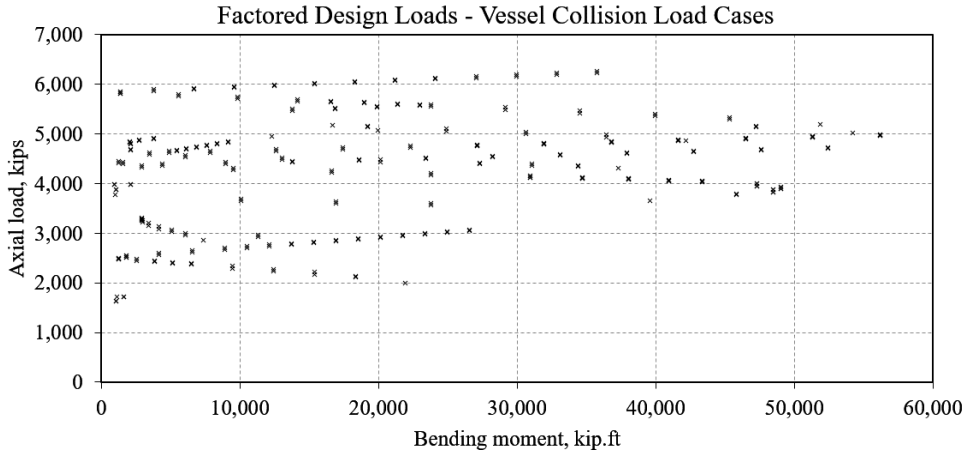

Figure L.1: Factored design loads

Reinforced concrete column designs were performed for column diameters of 9, 10, 11, and 12 *ft.* The 12 *ft.* diameter design resulted in 0.9% longitudinal steel, which is slightly more than the minimum required for reinforced concrete columns. The 9*ft.* diameter design resulted in 3.1% longitudinal steel, which approached the practical maximum assuming a single rebar cage would be utilized. Interaction diagrams for the smallest and largest diameter designs are provided in Figures L.2 and L.3.

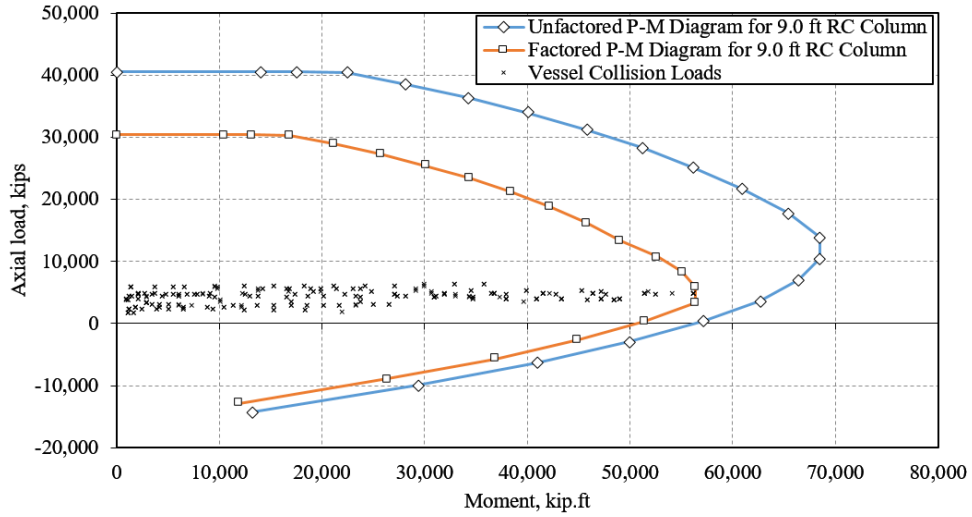

Figure L.2: P-M interaction diagram for 9.0 ft. reinforced concrete column.

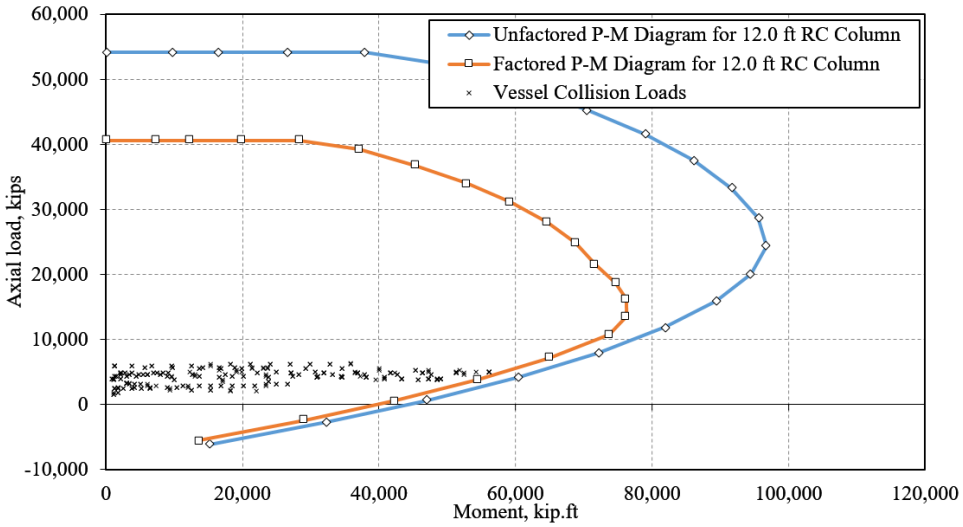

Figure L.3: P-M interaction diagram for 12.0ft. reinforced concrete column.

CFST designs were performed for column diameters of 6.5, 7.0, 7.5, 8.0, 8.5, and 9.0*ft.* The 6.5*ft.* diameter design resulted in a 2.25*in.* thick steel tube, which, based on manufacturer information, appears to be at or near the upper limit for availability. The 8.0, 8.5, and 9.0*ft.* designs all resulted in a required tube thickness of 1.25*in.* The tube thickness for the 8.0*ft.* diameter design was governed by strength requirements while the tube thickness for the 8.5 and 9.0*ft.* diameter designs were governed by *D/t* requirements. Interaction diagrams for the smallest and largest diameter designs are provided in Figures L.4 and L.5.

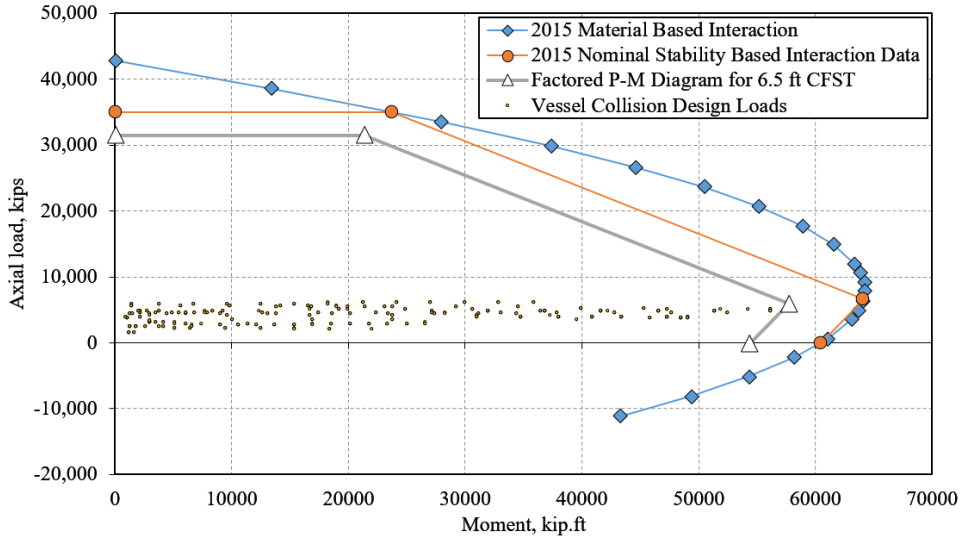

Figure L.4: Factored P-M interaction diagram for the designed 6.5 ft. CFST.

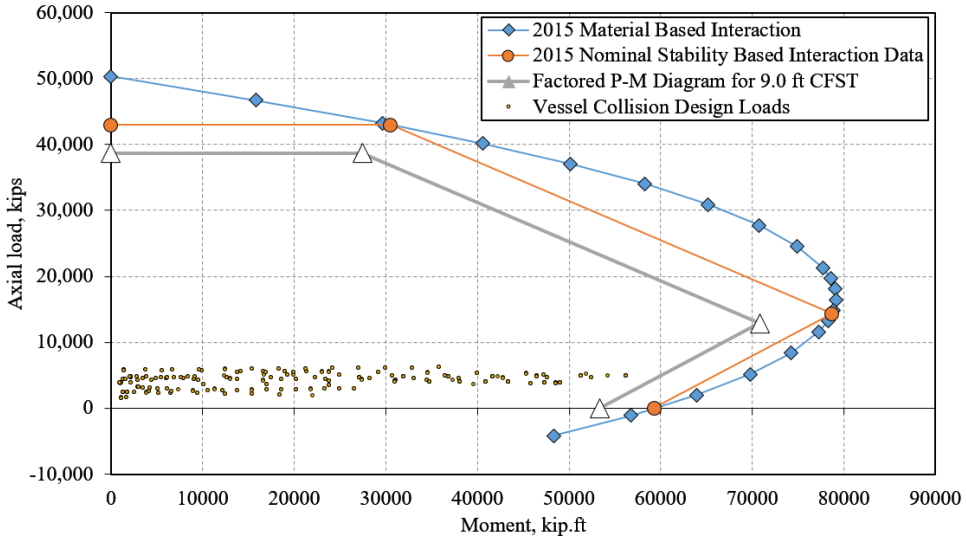

Figure L.5: Factored P-M interaction diagram for the designed 9.0 ft. CFST.

Installed material unit cost for each of the designs was evaluated to determine the optimal design. For the purpose of this evaluation the following unit costs for installed materials were used:

- Concrete – 200 *$/c.y.*
- Reinforcing steel – 1.00 *$/lb.*
- Steel tube – 1.33 *$/lb.*

The designs and their costs are summarized in Tables L.1 and L.2.

Table L.1. Reinforced concrete column design (4*ksi* concrete, 60*ksi* reinforcement, non-structural tube)

Outside Diameter of Concrete (*ft.*)	% Longitudinal Rebar	Non-structural Tube Thickness (*in.*)	Concrete Volume CY per *ft.* of shaft	Longitudinal Rebar Weight *lb.* per *ft.* of shaft	Spiral Weight *lb.* per *ft.* of shaft	Non-Structural Tube Weight *lb.* per *ft.* of shaft	Concrete Cost $ per *ft.* of shaft	Rebar Cost $ per *ft.* of shaft	Non-Structural Steel Tube Cost $ per linear *ft.* of shaft	Total Cost $ per *ft.* of shaft
9.0	3.1%	0.625	2.36	994	84	726	$471	$1,077	$965	$2,514
10.0	1.9%	0.625	2.91	749	93	806	$582	$842	$1,072	$2,496
11.0	1.3%	0.625	3.52	599	103	886	$704	$702	$1,179	$2,585
12.0	0.9%	0.625	4.19	504	113	966	$838	$617	$1,285	$2,740

Table L.2. CFST column design (4*ksi* Concrete, 50*ksi* tube)

Outside Diameter of Structural Tube (*ft.*)	Tube Thickness Required for Strength (*in.*)	Tube Thickness Required for D/T Ratio (*in.*)	Tube Thickness Required (*in.*)	% Steel	Concrete Volume CY per *ft.* of shaft	Tube Weight *lb.* per *ft.* of shaft	Concrete Cost $ per linear *ft.* of shaft	Steel Tube Cost $ per linear *ft.* of shaft	Total Cost $ per linear *ft.* of shaft
6.5	2.250	0.90	2.250	11.2%	1.09	1,822	$218	$2,423	$2,642
7.0	1.875	0.97	1.875	8.7%	1.30	1,646	$260	$2,189	$2,450
7.5	1.500	1.03	1.500	6.6%	1.53	1,419	$306	$1,887	$2,193
8.0	1.250	1.10	1.250	5.1%	1.77	1,266	$353	$1,684	$2,037
8.5	1.125	1.17	1.250	4.8%	2.00	1,346	$400	$1,791	$2,191
9.0	1.000	1.24	1.250	4.6%	2.25	1,426	$450	$1,897	$2,347

As can be seen above, the reinforced concrete column cost is minimized at 2,469 $/*ft.* for a 10 *ft.* diameter shaft while the CFST cost is minimized at 2,037 $/*ft.* for an 8.0*ft.* diameter shaft. It should also be noted that the cost for a 7.0*ft.* diameter CFST remains less than that of the optimized reinforced concrete column. This evaluation shows CFST to have about a 20% advantage when considering installed material cost. This is a significant savings, especially when many CFST's are used on a project.

Note that the above discussion assumes that unit costs for installed materials are constant for all shaft diameters. Depending on the diameters involved, this assumption may not result in accurate results. However, for the diameters under discussion herein, there is a real cost penalty for shafts larger than 10 *ft.* in diameter, as the equipment required for their installation is not widely available, and the cost of transporting the larger diameter tubes begins to escalate quickly.

The CFST designs did not utilize an internal reinforcing cage. The ability to eliminate the fabrication and installation of a reinforcing cage should reduce the construction and risk, and is a definite advantage of CFST construction.

APPENDIX M

CAD drawings

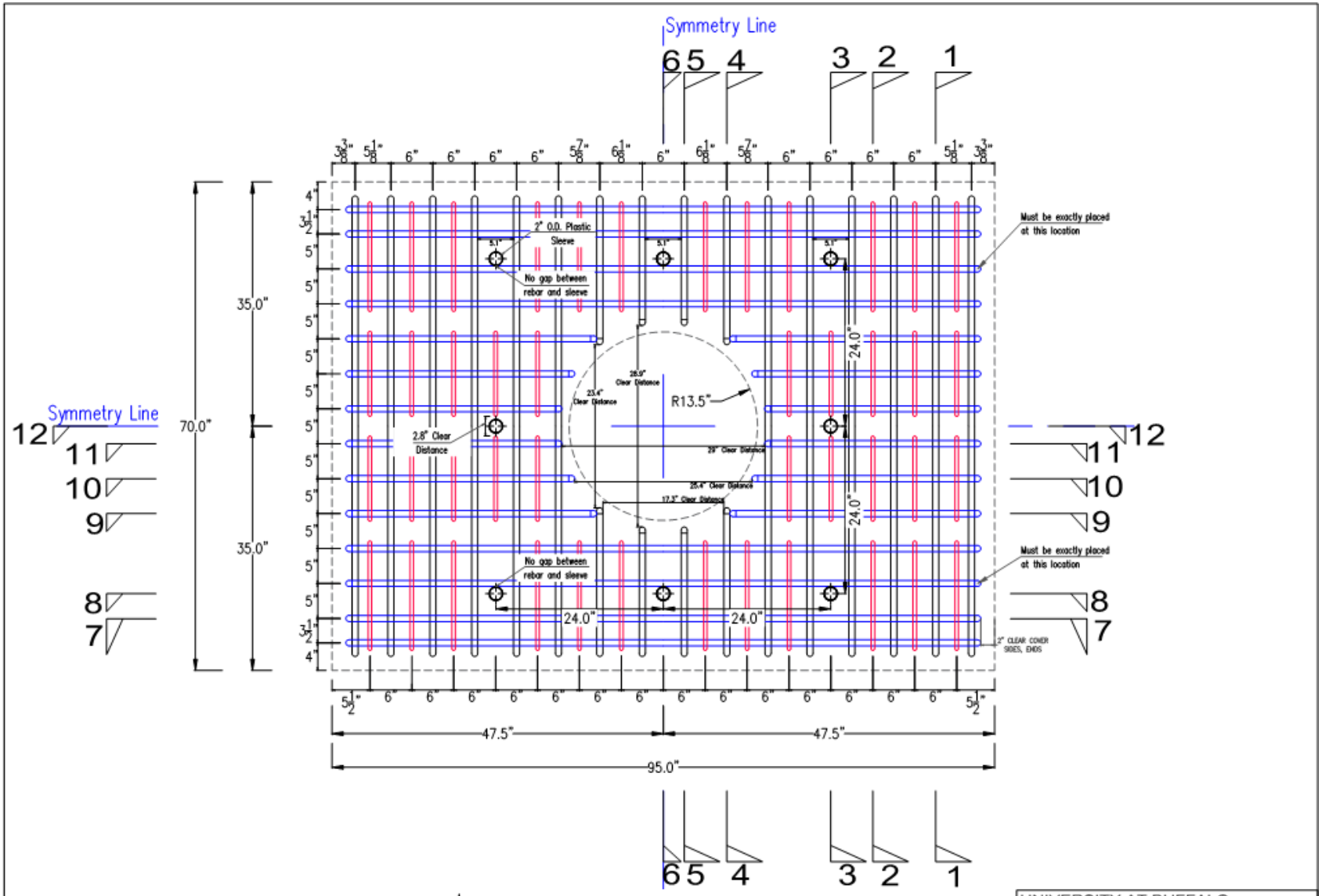

GENERAL NOTES:

1. ALL REBAR GRADE 60 ASTM A706
2. FOUNDATION CONCRETE fc'=4000psi
3. REBAR BENDS, etc. PER ACI 318-08
4. CONDUIT TO BE 2.0" DIAMETER PVC

PLAN – Dimensions

UNIVERSITY AT BUFFALO
206 KETTER HALL
Buffalo, NY 14226

RC foundation details

Page:	September 08, 2015	D-F-01
AI-2	By: Hadi Kanarangi	Rev: 00

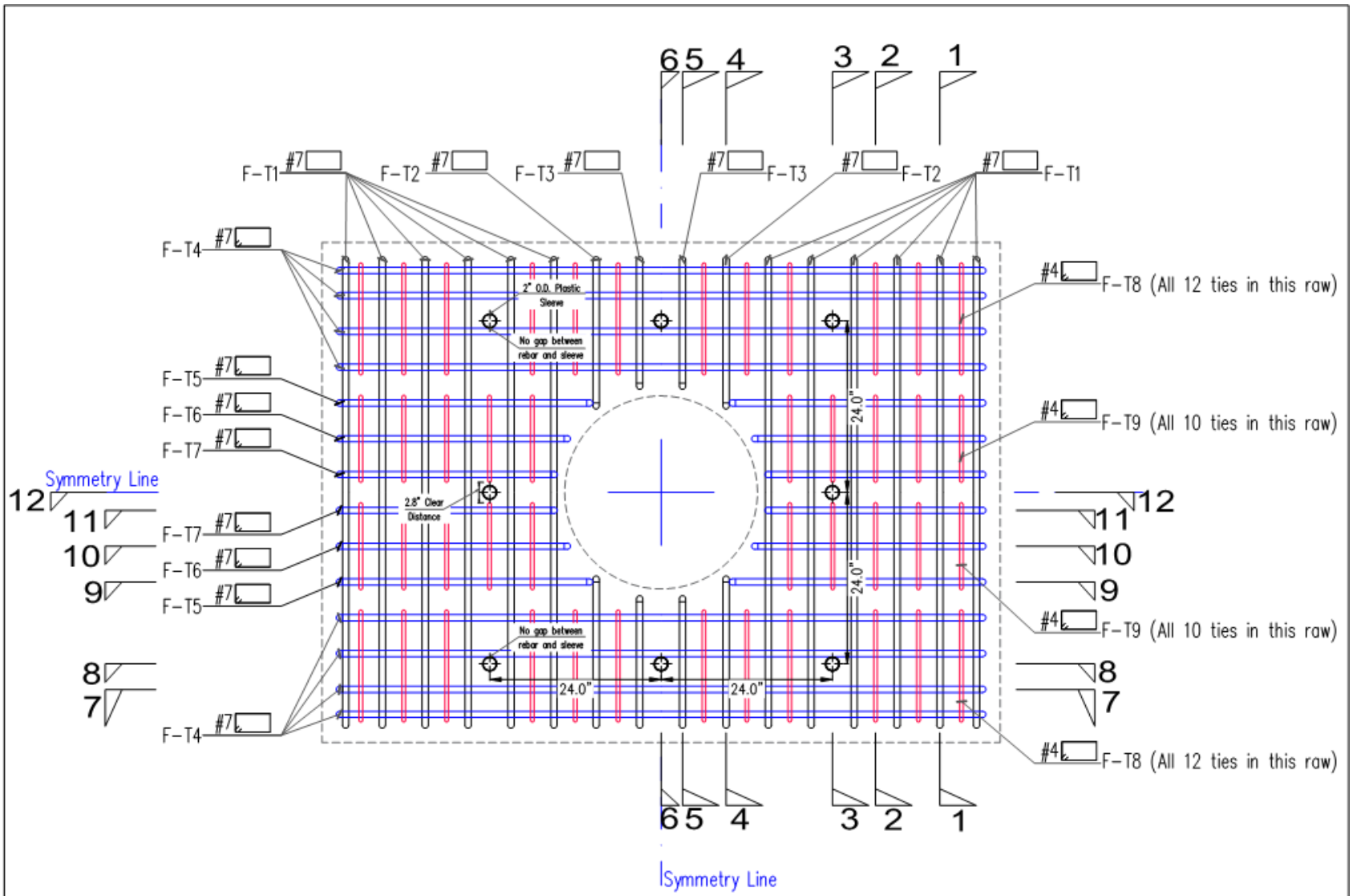

GENERAL NOTES:

1. ALL REBAR GRADE 60 ASTM A706
2. FOUNDATION CONCRETE fc'=4000psi
3. REBAR BENDS, etc. PER ACI 318-08
4. CONDUIT TO BE 2.0" DIAMETER PVC

PLAN – Reinforcement Types

UNIVERSITY AT BUFFALO 206 KETTER HALL Buffalo, NY 14226		
RC foundation details		
Page:	September 08, 2015	D-F-02
AI-3	By: Hadi Kanarangi	Rev: 00

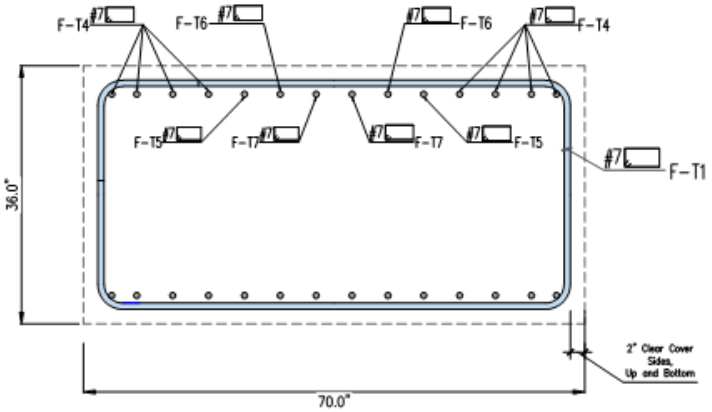

SECTION 1–1

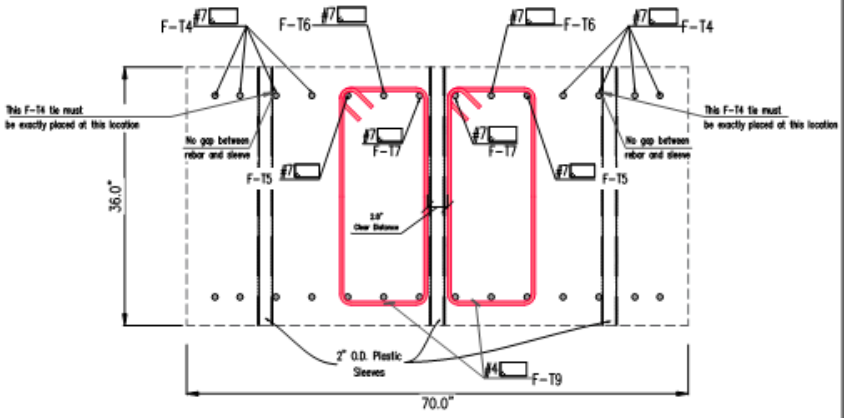

SECTION 3–3

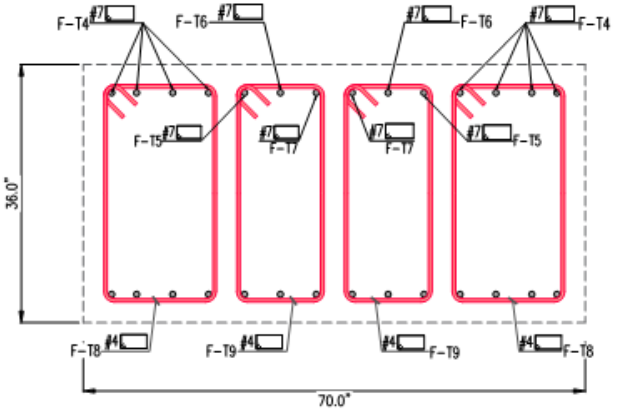

SECTION 2–2

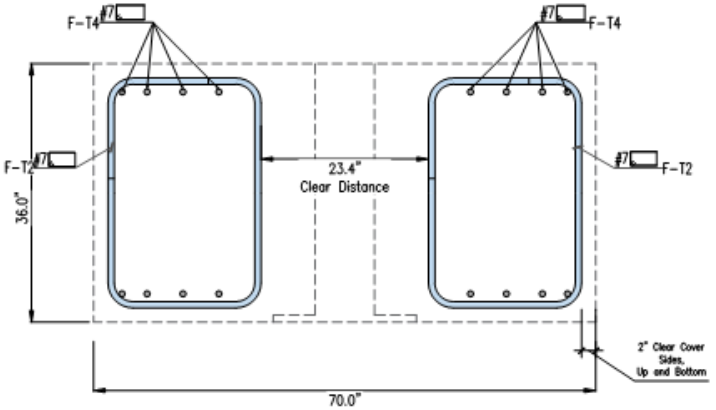

SECTION 4–4

GENERAL NOTES:

1. ALL REBAR GRADE 60 ASTM A706
2. FOUNDATION CONCRETE fc'=4000psi
3. REBAR BENDS, etc. PER ACI 318-08
4. CONDUIT TO BE 2.0" DIAMETER PVC

UNIVERSITY AT BUFFALO 206 KETTER HALL Buffalo, NY 14226		
RC foundation details		
Page:	September 08, 2015	D-F-03
AI-4	By: Hadi Kanarangi	Rev: 00

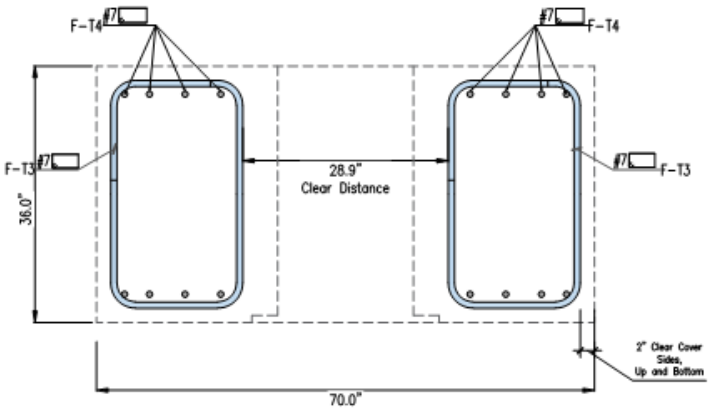

SECTION 5–5

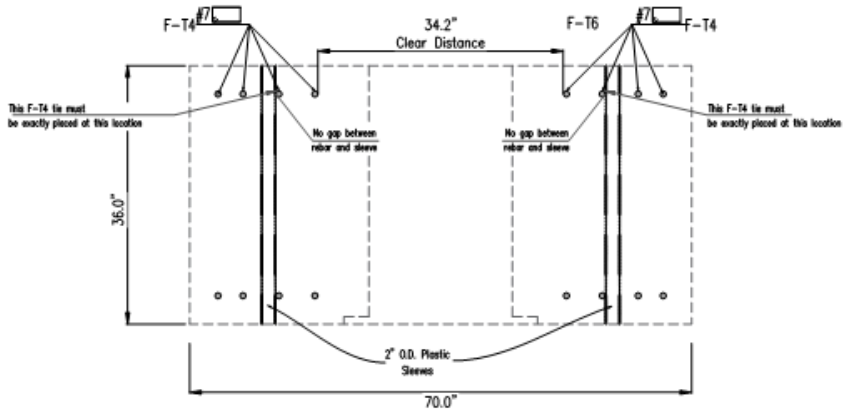

SECTION 6–6

GENERAL NOTES:

1. ALL REBAR GRADE 60 ASTM A706
2. FOUNDATION CONCRETE fc'=4000psi
3. REBAR BENDS, etc. PER ACI 318–08
4. CONDUIT TO BE 2.0" DIAMETER PVC

UNIVERSITY AT BUFFALO 206 KETTER HALL Buffalo, NY 14226		
RC foundation details		
Page:	September 08, 2015	D-F-04
AI–5	By: Hadi Kanarangi	Rev: 00

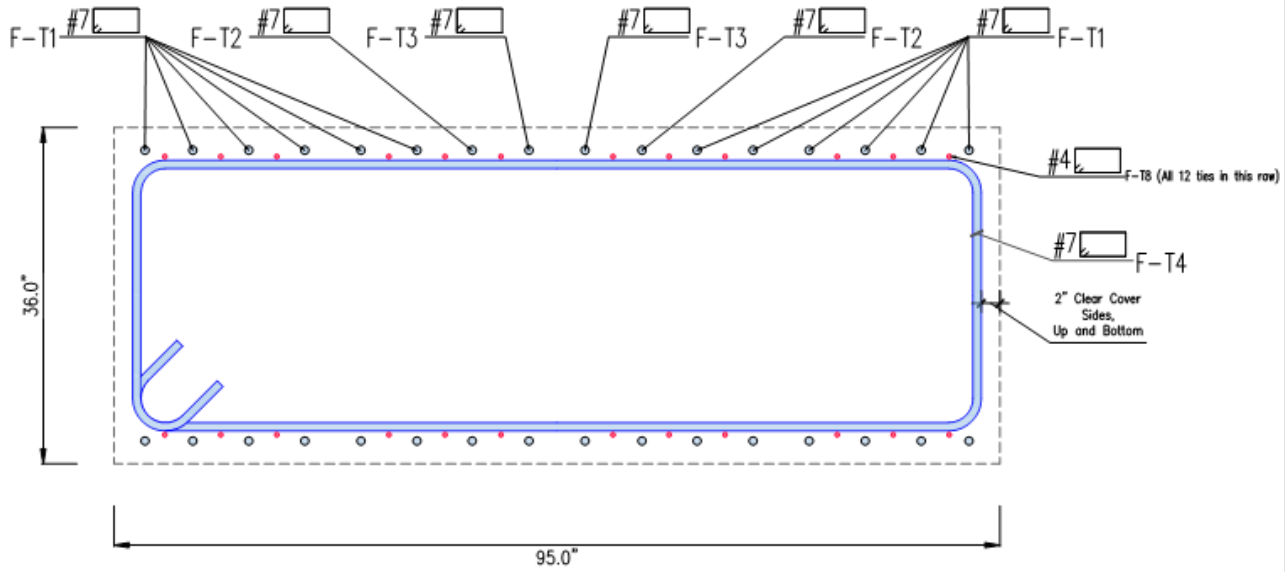

SECTION 7-7

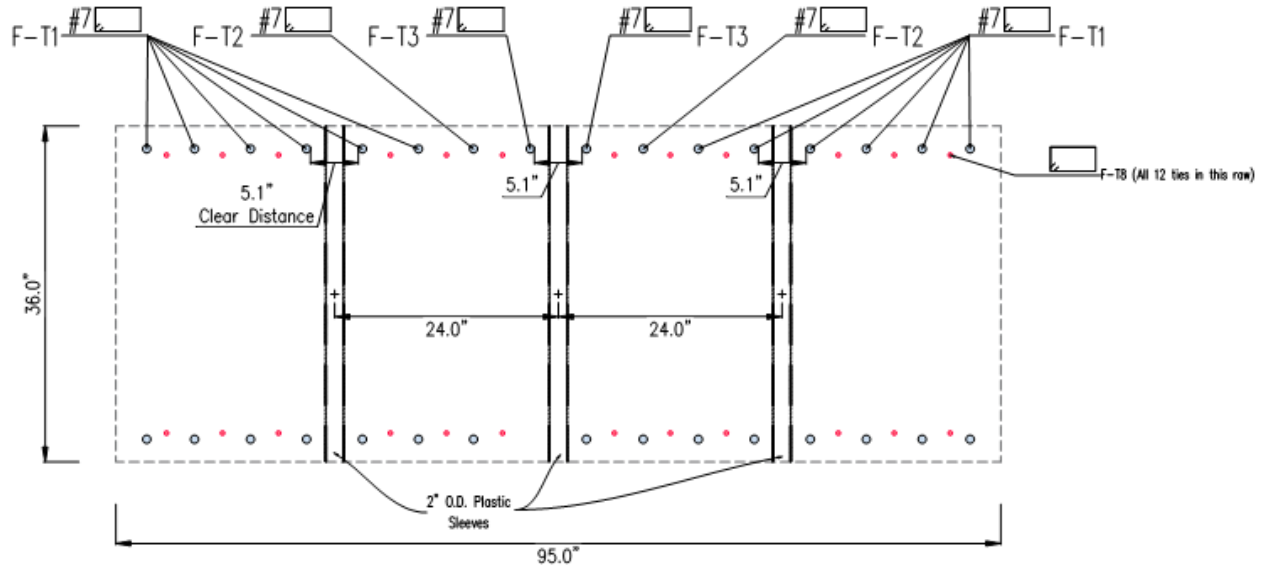

SECTION 8-8

UNIVERSITY AT BUFFALO 206 KETTER HALL Buffalo, NY 14226		
RC foundation details		
Page:	September 08, 2015	D-F-05
AI-6	By: Hadi Kenarangi	Rev: 00

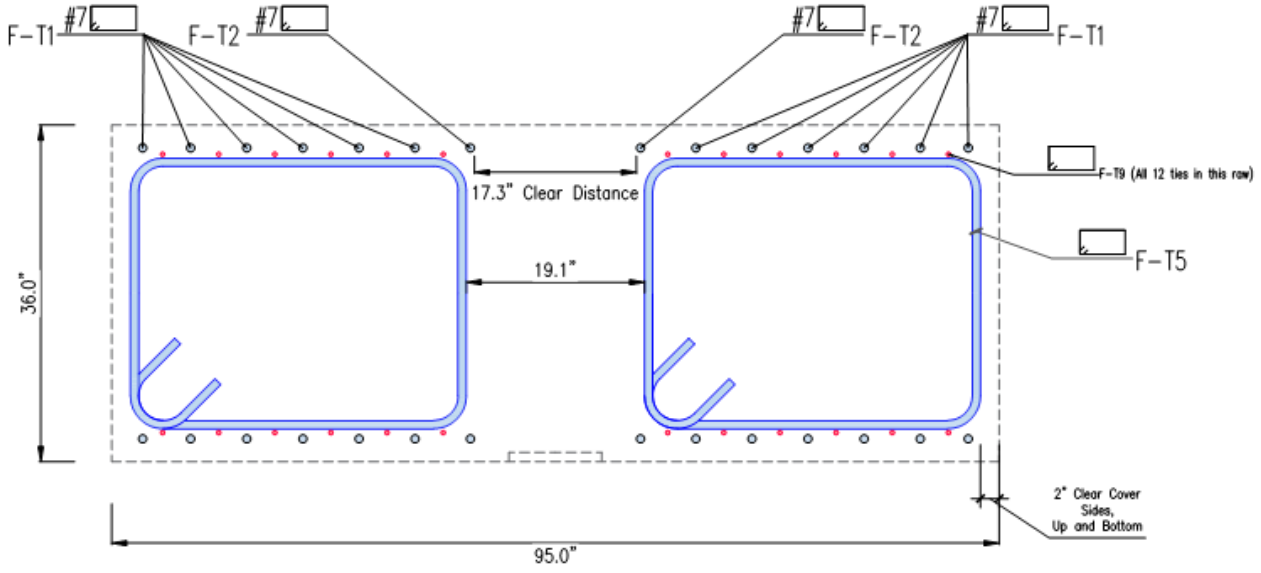

SECTION 9–9

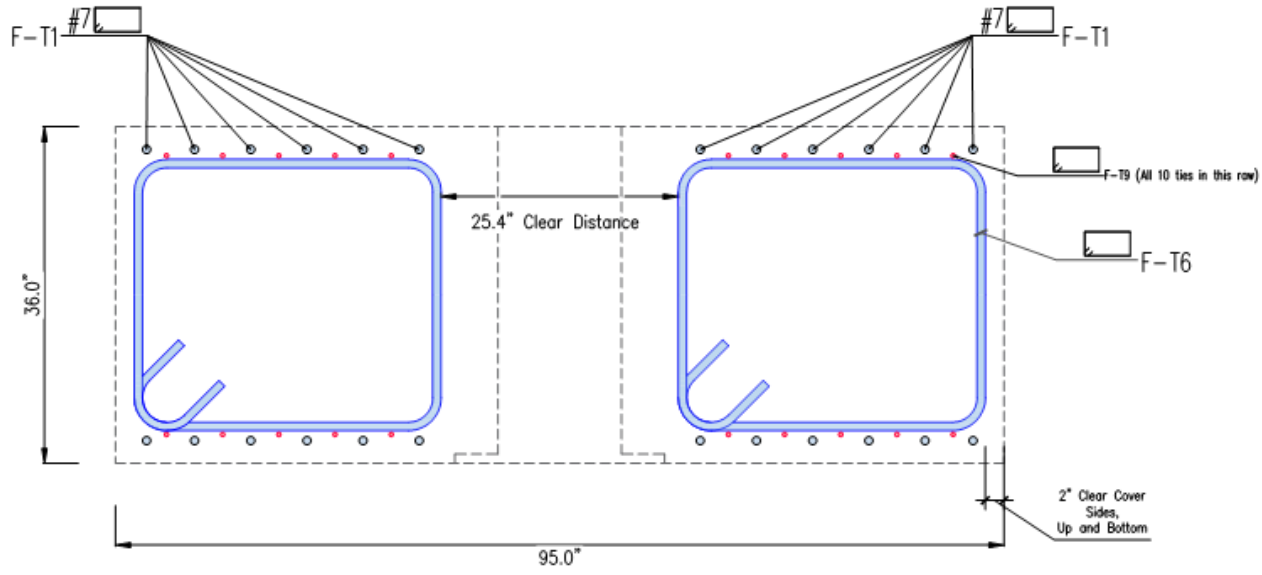

SECTION 10–10

UNIVERSITY AT BUFFALO 206 KETTER HALL Buffalo, NY 14226		
RC foundation details		
Page:	September 08, 2015	D-F-06
AI–7	By: Hadi Kenarangi	Rev: 00

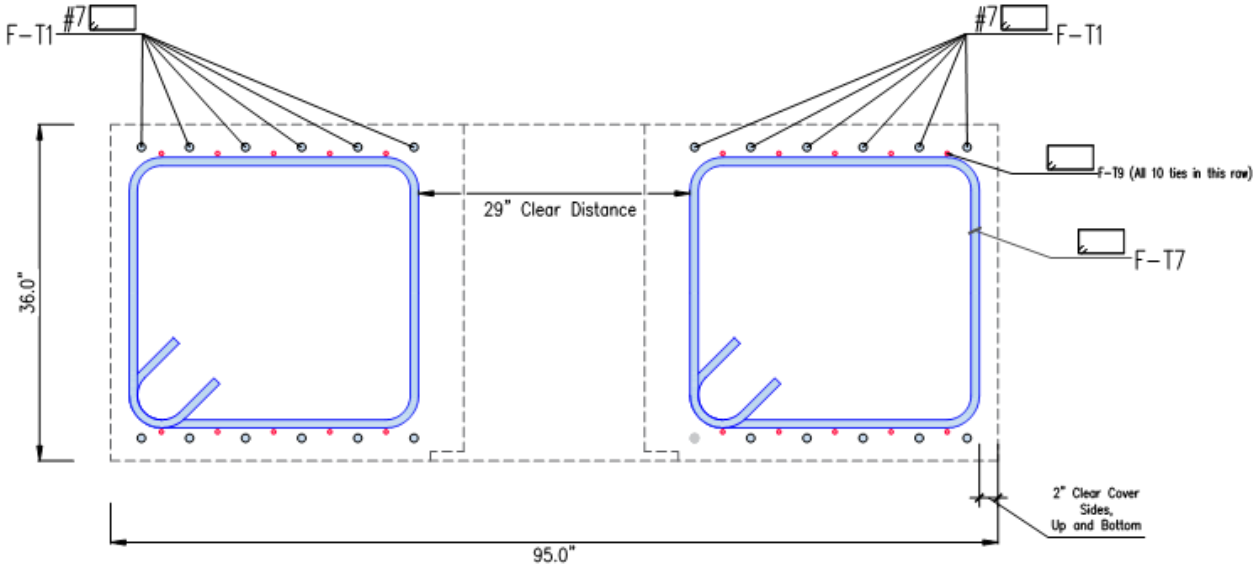

SECTION 11–11

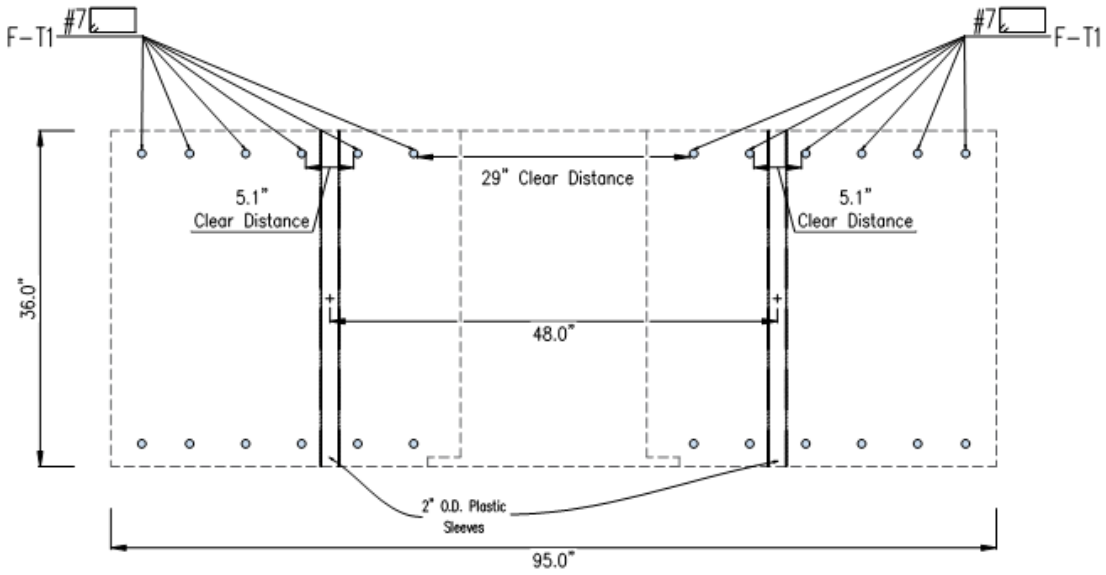

SECTION 12–12

UNIVERSITY AT BUFFALO 206 KETTER HALL Buffalo, NY 14226		
RC foundation details		
Page:	September 08, 2015	D-F-07
AI–8	By: Hadi Kenarangi	Rev: 00

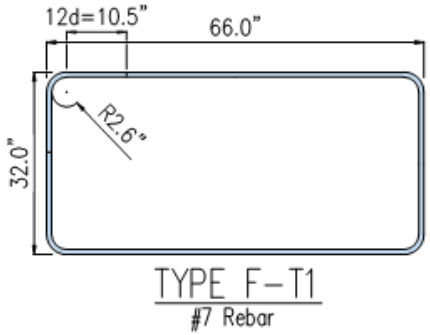

TYPE F–T1
#7 Rebar

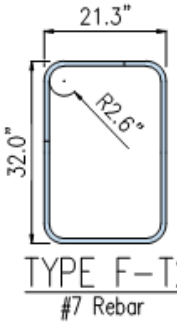

TYPE F–T2
#7 Rebar

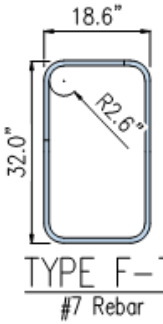

TYPE F–T3
#7 Rebar

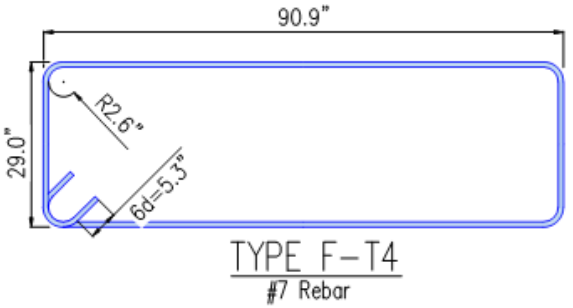

TYPE F–T4
#7 Rebar

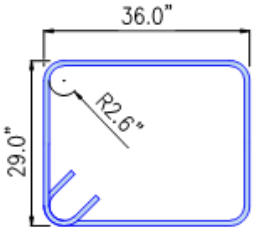

TYPE F–T5
#7 Rebar

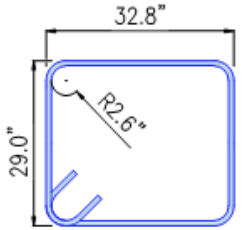

TYPE F–T6
#7 Rebar

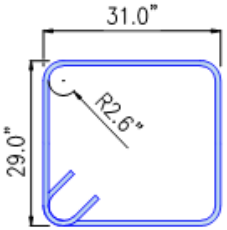

TYPE F–T7
#7 Rebar

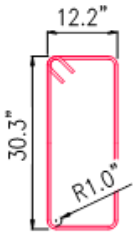

TYPE F–T8
#4 Rebar

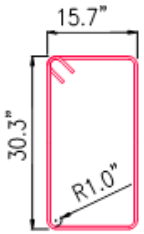

TYPE F–T9
#4 Rebar

Table 1. Foundation Rebars

Part	Type	Total Length, in/unit	Qty.	#	Area, in²	Weight, lb.	Shape
Foundation	F-T1	202.5	12	7	0.6	413.93	T2
	F-T2	113.5	4	7	0.6	77.34	T2
	F-T3	107.5	4	7	0.6	73.23	T2
	F-T4	251.8	8	7	0.6	343.19	T1
	F-T5	145.8	2	7	0.6	49.69	T1
	F-T6	135.8	2	7	0.6	46.28	T1
	F-T7	132.2	2	7	0.6	45.05	T1
	F-T8	100.3	24	4	0.2	136.97	T1
	F-T9	90.8	20	4	0.2	101.13	T1
					Total Weight	1283.81	

GENERAL NOTES:
1. ALL REBAR GRADE 60 ASTM A706
2. FOUNDATION CONCRETE fc'=4000psi
3. REBAR BENDS, etc. PER ACI 318–08
4. CONDUIT TO BE 2.0" DIAMETER PVC

UNIVERSITY AT BUFFALO
206 KETTER HALL
Buffalo, NY 14226

RC foundation details

Page:	September 08, 2015	D-F-08
AI–9	By: Hadi Kenarangi	Rev: 00

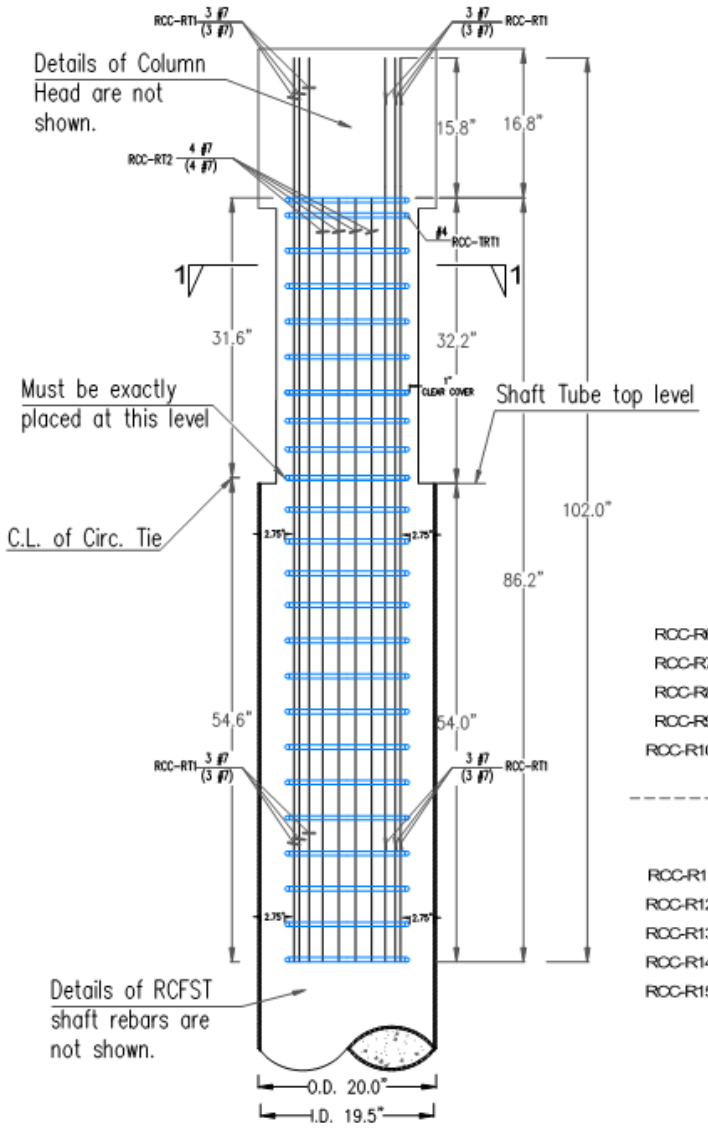

RC Column Part

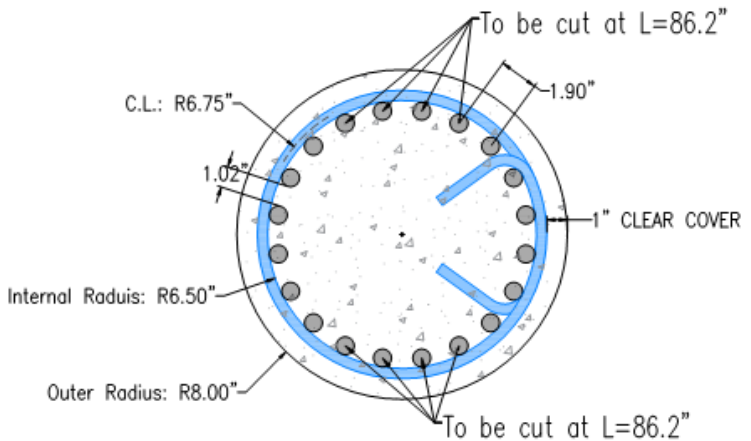

SECTION 1-1

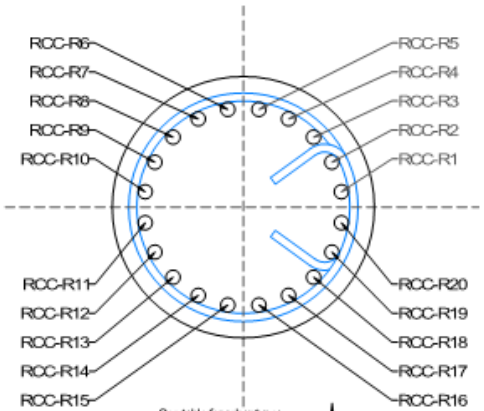

RC Column Rebar IDs

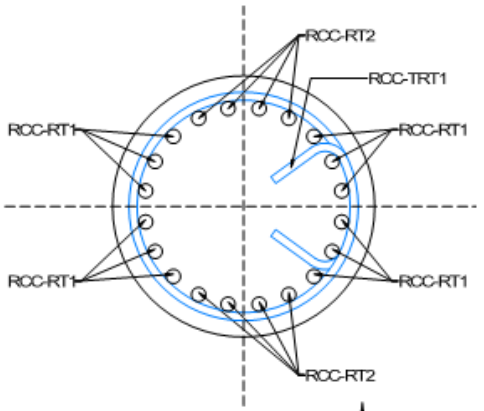

RC Column Rebar Types

UNIVERSITY AT BUFFALO 206 KETTER HALL Buffalo, NY 14226		
RC column part details		
Page:	September 08, 2015	D-RCC-01
AI-10	By: Hadi Kenarangi	Rev: 00

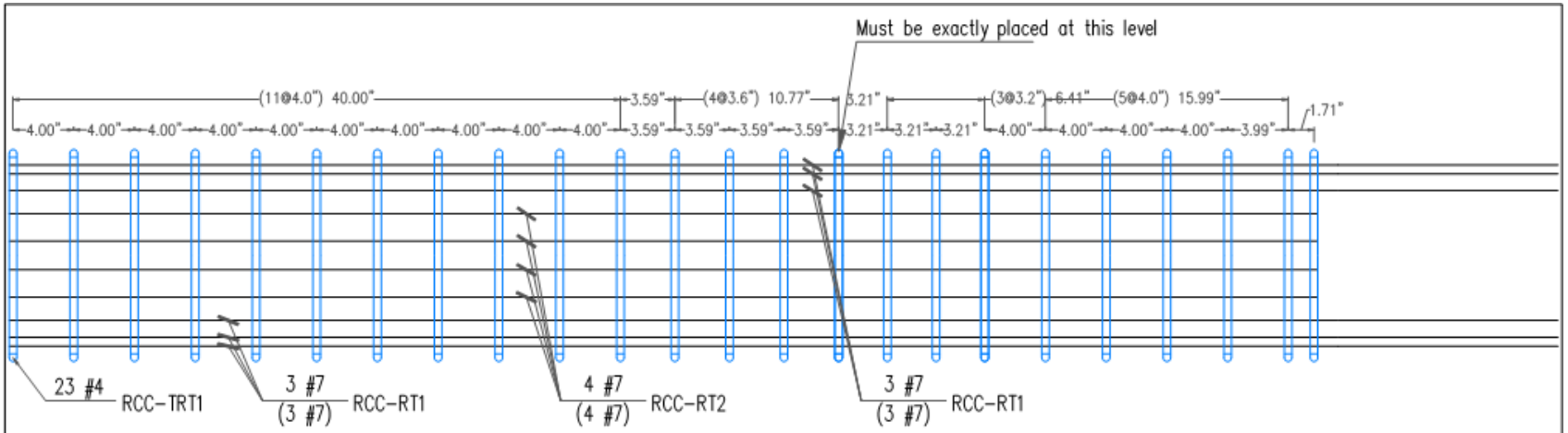

RC Column Rebar Cage Details

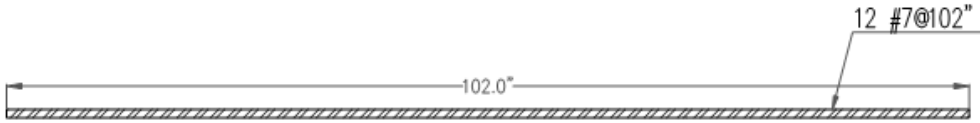

Type RCC-RT1
#7 Rebar

Type RCC-RT2
#7 Rebar

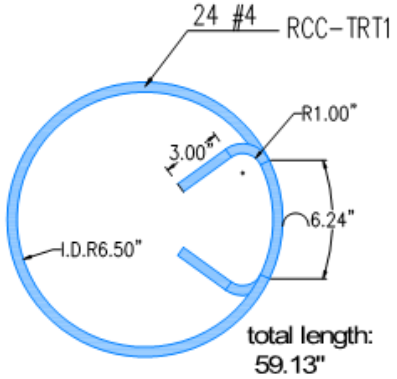

Type RCC-TRT1
#4 circ. tie

RC Column Rebar Types

UNIVERSITY AT BUFFALO 206 KETTER HALL Buffalo, NY 14226		
RC column part details		
Page:	September 08, 2015	D-RCC-02
AI-11	By: Hadi Kenarangi	Rev: 00

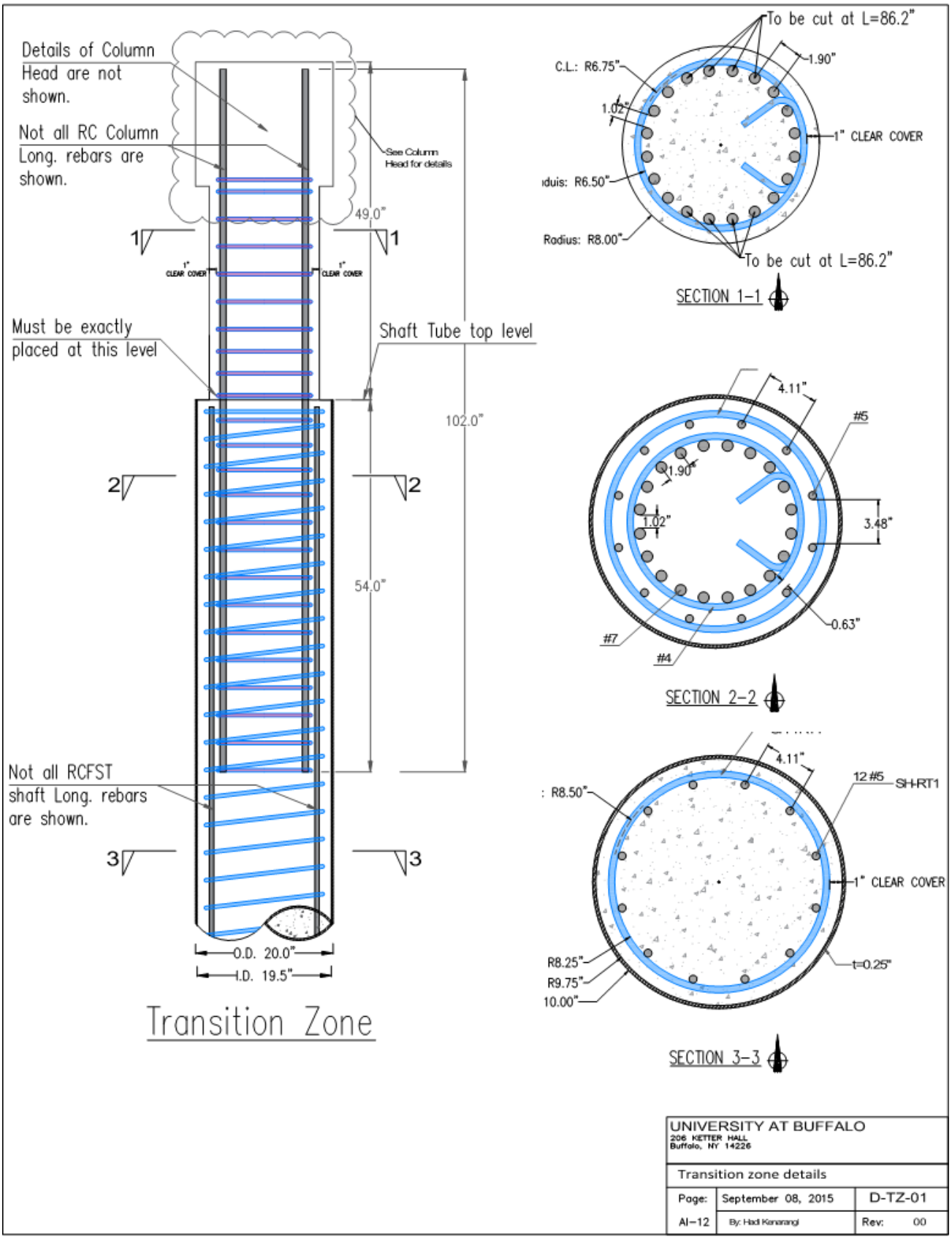
Details of Column Head are not shown.
Not all RC Column Long. rebars are shown.
See Column Head for details
49.0"
1
1
1" CLEAR COVER
1" CLEAR COVER
Must be exactly placed at this level
Shaft Tube top level
102.0"
2
2
54.0"
Not all RCFST shaft Long. rebars are shown.
3
3
O.D. 20.0"
I.D. 19.5"
Transition Zone
To be cut at L=86.2"
C.L.: R6.75"
1.90"
1.02"
1" CLEAR COVER
Radius: R8.00"
To be cut at L=86.2"
SECTION 1-1
4.11"
#5
1.90"
1.02"
3.48"
0.63"
#7
#4
SECTION 2-2
4.11"
12 #5
SH-RT1
R8.50"
1" CLEAR COVER
t=0.25"
R8.25"
R9.75"
10.00"
SECTION 3-3
UNIVERSITY AT BUFFALO
206 KETTER HALL
Buffalo, NY 14226
Transition zone details
Page:
September 08, 2015
D-TZ-01
AI-12
By: Hadi Kenarangi
Rev: 00

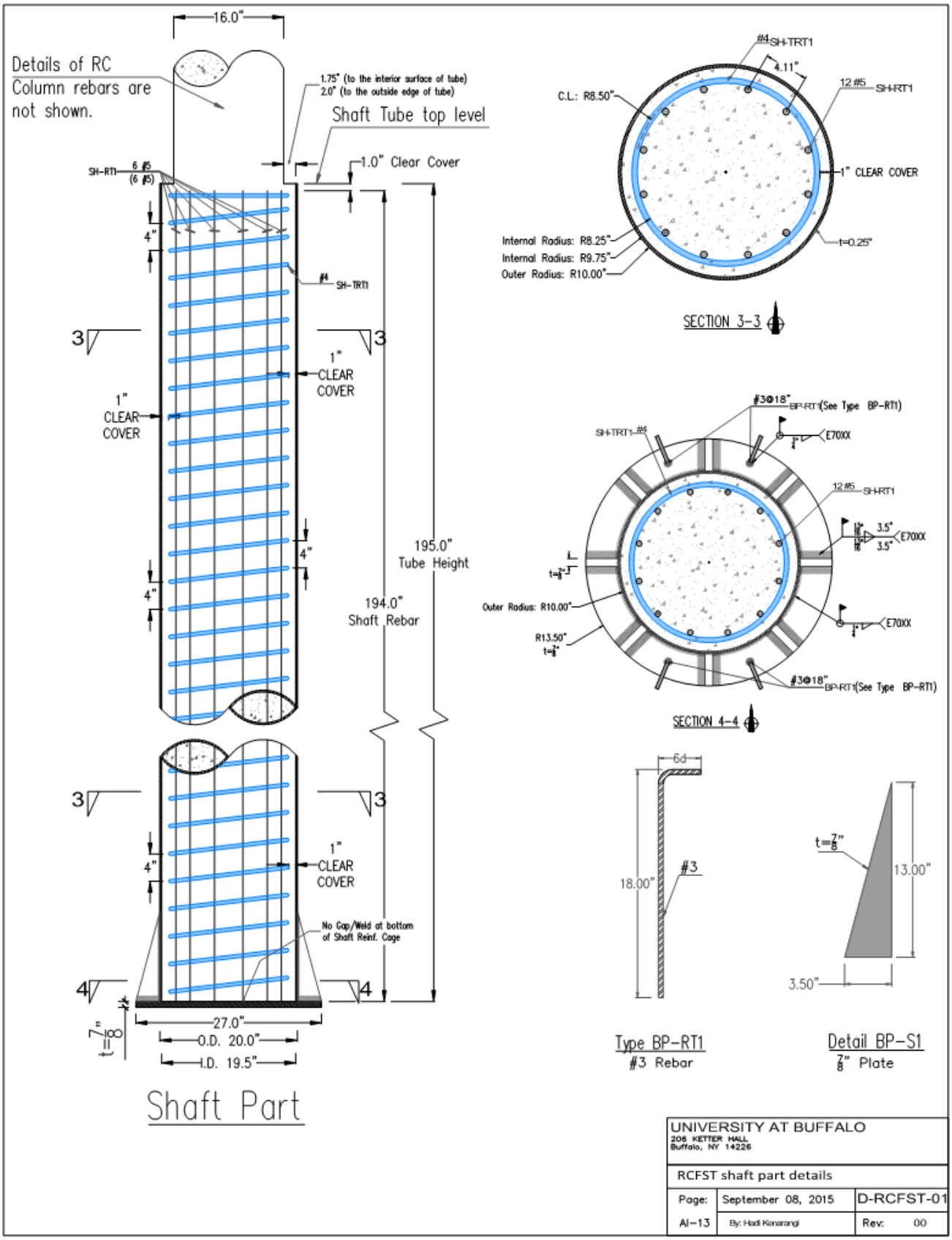
16.0"
Details of RC
Column rebars are
not shown.
1.75" (to the interior surface of tube)
2.0" (to the outside edge of tube)
Shaft Tube top level
1.0" Clear Cover
SH-RT1 6 #5 (6 #5)
4"
#4 SH-TRT1
3
3
1" CLEAR COVER
1" CLEAR COVER
4"
4"
195.0" Tube Height
194.0" Shaft Rebar
3
3
1" CLEAR COVER
4"
No Gap/Weld at bottom of Shaft Reinf. Cage
4
4
27.0"
O.D. 20.0"
I.D. 19.5"
7/8"
Shaft Part
#4 SH-TRT1
4.11"
12 #5 SH-RT1
C.L.: R8.50"
1" CLEAR COVER
Internal Radius: R8.25"
Internal Radius: R9.75"
Outer Radius: R10.00"
t=0.25"
SECTION 3-3
#3@18" BP-RT1 (See Type BP-RT1)
SH-TRT1 #4
E70XX
12 #5 SH-RT1
3.5"
3.5"
E70XX
t=7/8"
Outer Radius: R10.00"
R13.50"
t=7/8"
E70XX
#3@18" BP-RT1 (See Type BP-RT1)
SECTION 4-4
6d
18.00"
#3
Type BP-RT1
#3 Rebar
t=7/8"
13.00"
3.50"
Detail BP-S1
7/8" Plate
UNIVERSITY AT BUFFALO
208 KETTER HALL
Buffalo, NY 14226
RCFST shaft part details
Page:
September 08, 2015
D-RCFST-01
AI-13
By: Hadi Kenarangi
Rev: 00

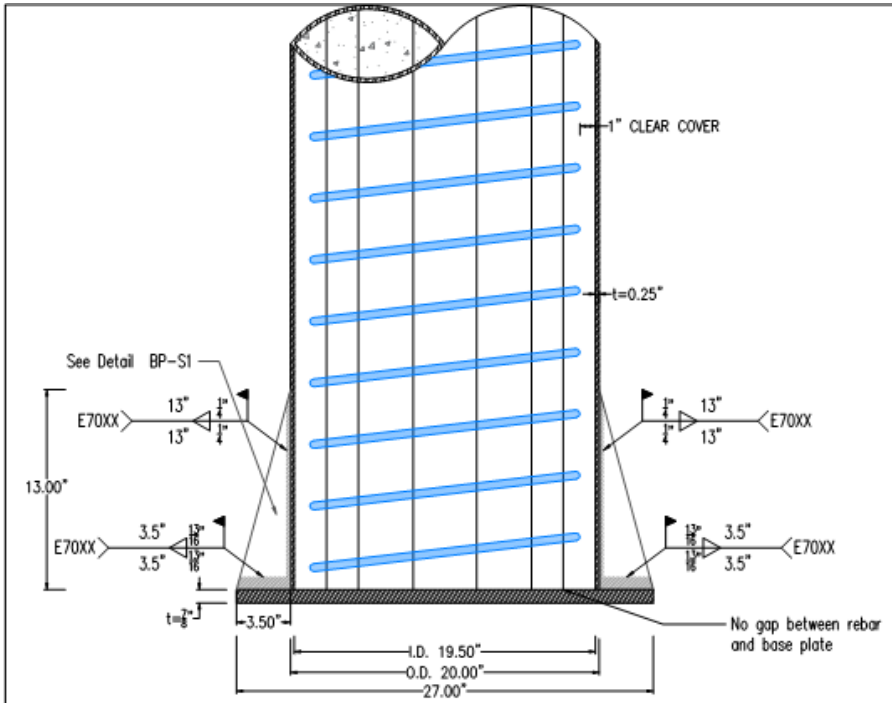

Shaft Bottom Part

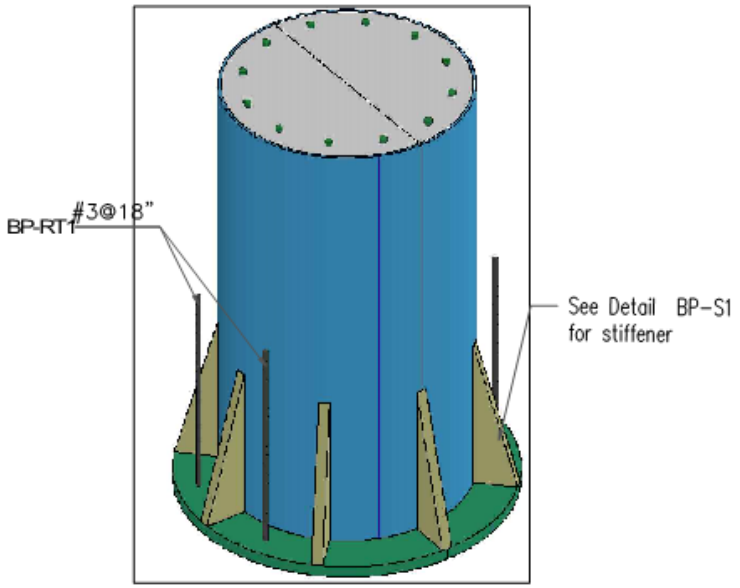

3D view of Shaft Bottom Part

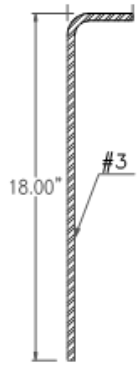

Type BP-RT1

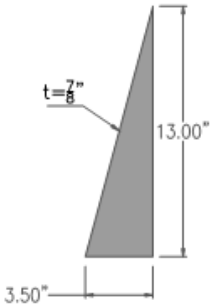

Detail BP-S1

UNIVERSITY AT BUFFALO 206 KETTER HALL Buffalo, NY 14226		
RCFST shaft part details		
Page:	September 08, 2015	D-RCFST-02
AI-14	By: Hadi Kenarangi	Rev: 00

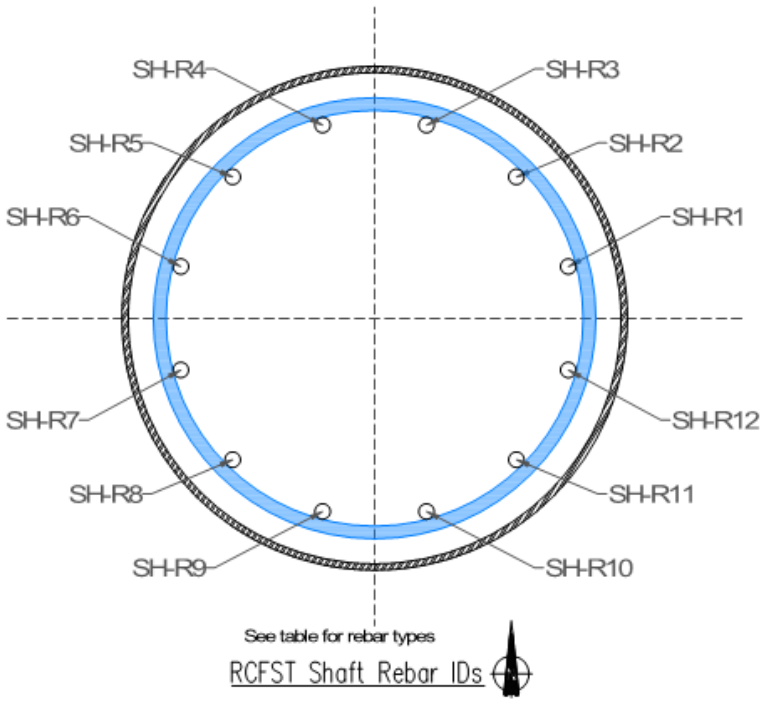

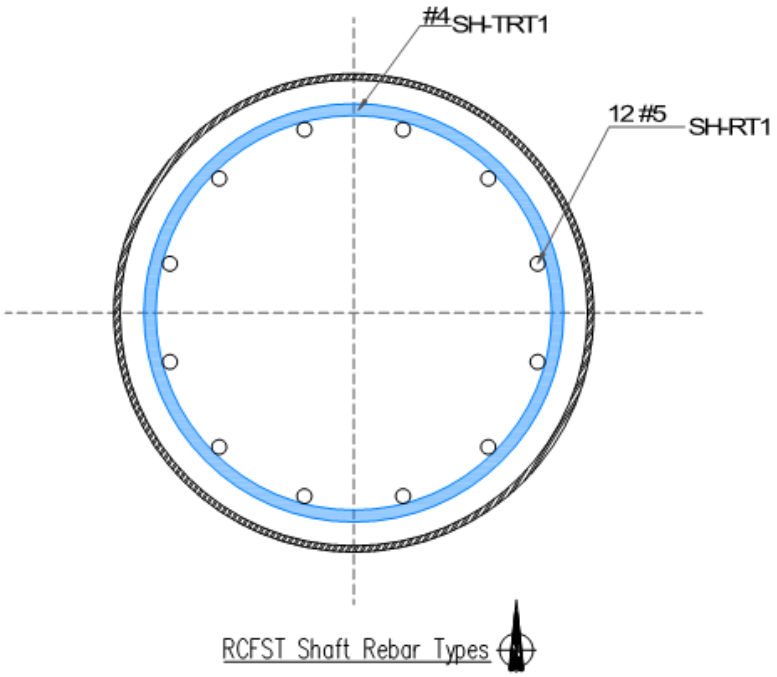

UNIVERSITY AT BUFFALO 206 KETTER HALL Buffalo, NY 14226		
RCFST shaft part details		
Page: AI-15	September 08, 2015 By: Hadi Kenarangi	D-RCFST-03 Rev: 00

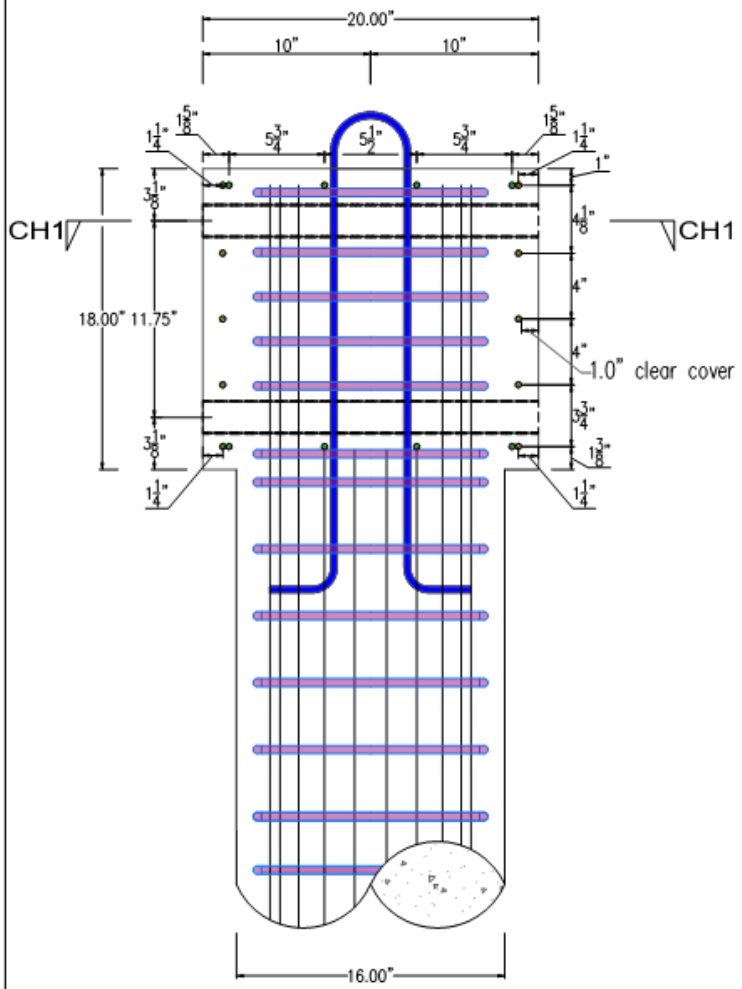

Column Head (North Elevation)
Rebar Cage Details – 1

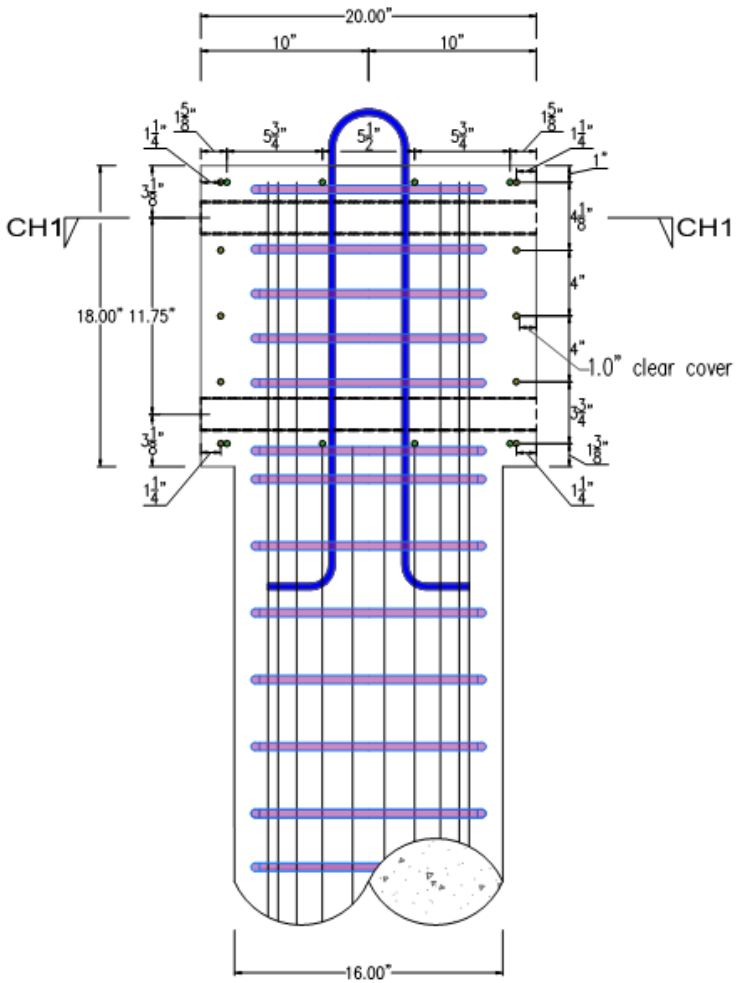

Column Head (North Elevation)
Rebar Cage Details – 2

UNIVERSITY AT BUFFALO 206 KETTER HALL Buffalo, NY 14226		
Column head details		
Page:	September 08, 2015	D-CH-01
AI–16	By: Hadi Kenarangi	Rev: 00

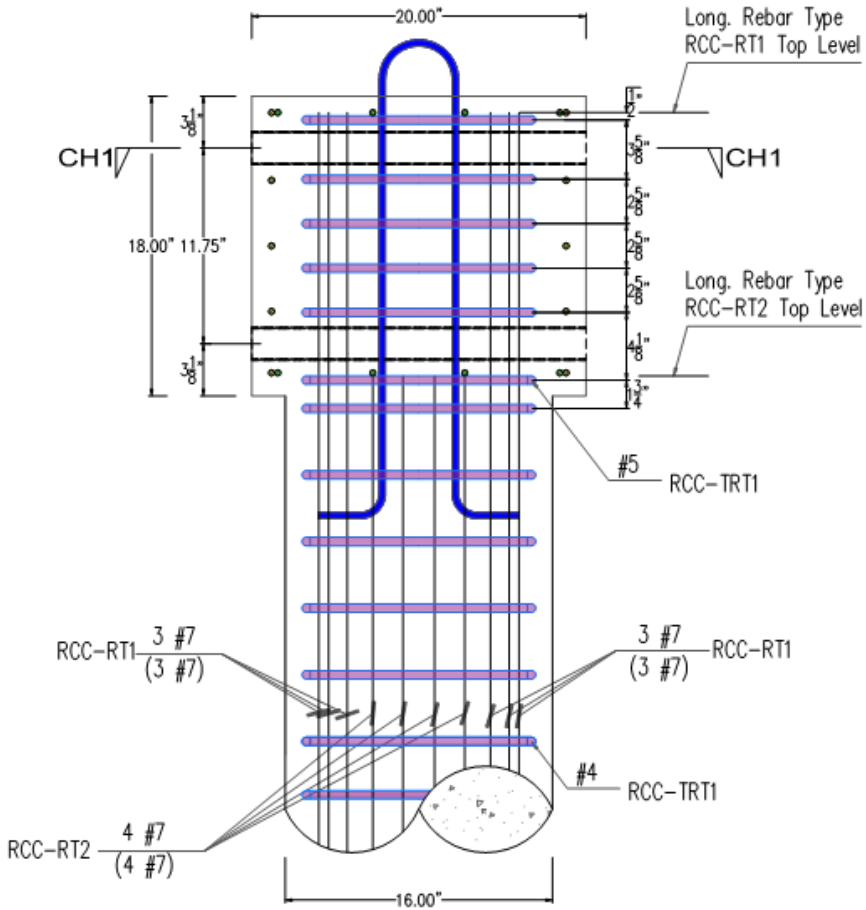

Column Head (North Elevation)
Extended Long. and Trans. Rebar Details

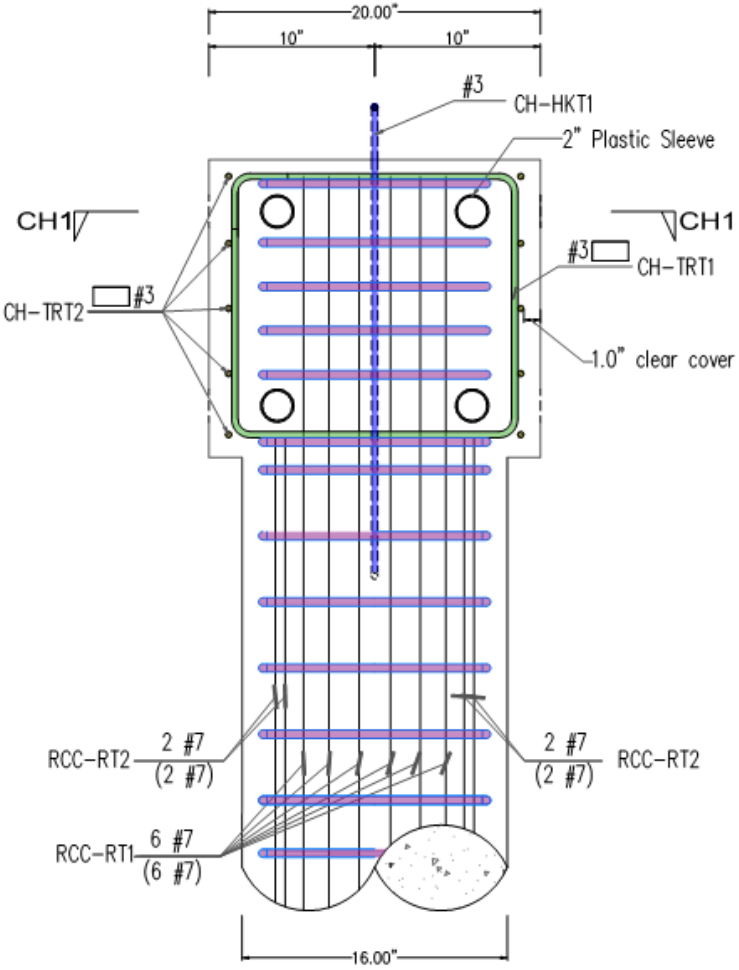

Column Head (East Elevation)
Rebar Cage Details

UNIVERSITY AT BUFFALO 206 KETTER HALL Buffalo, NY 14226		
Column head details		
Page:	September 08, 2015	D-CH-02
AI-17	By: Hadi Kenarangi	Rev: 00

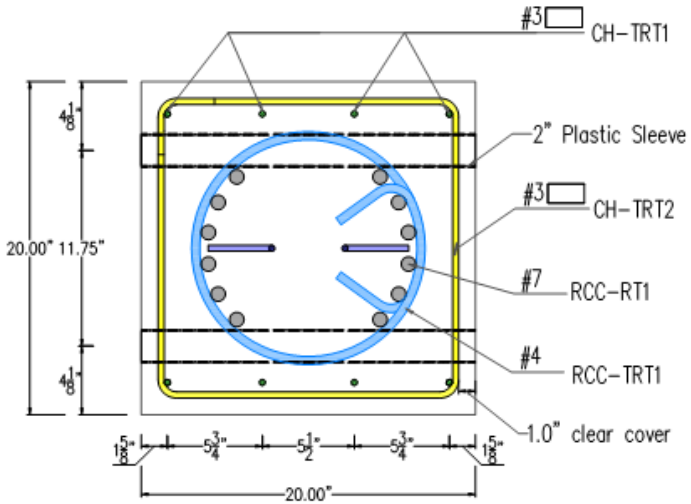

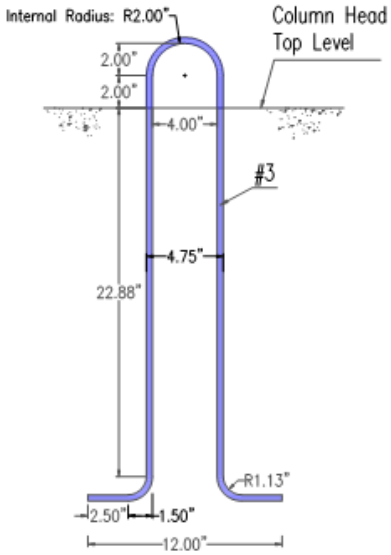

Type CH-HOOK
#3 Rebar

Section CH1-CH1

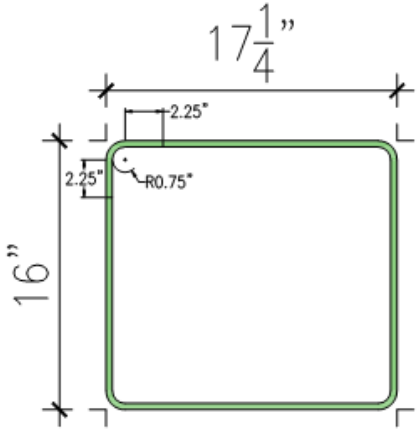

TYPE CH-TRT1
#3 Rebar

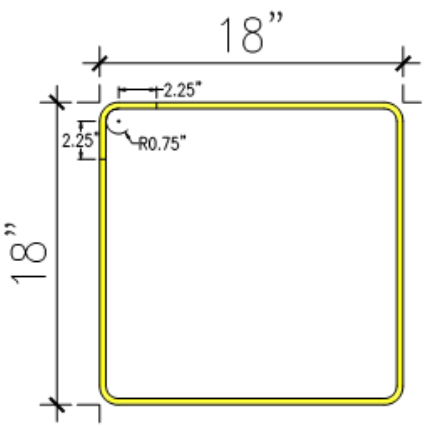

TYPE CH-TRT2
#3 Rebar

UNIVERSITY AT BUFFALO 206 KETTER HALL Buffalo, NY 14226		
Column head details		
Page:	September 08, 2015	D-CH-03
AI-18	By: Hadi Kenarangi	Rev: 00

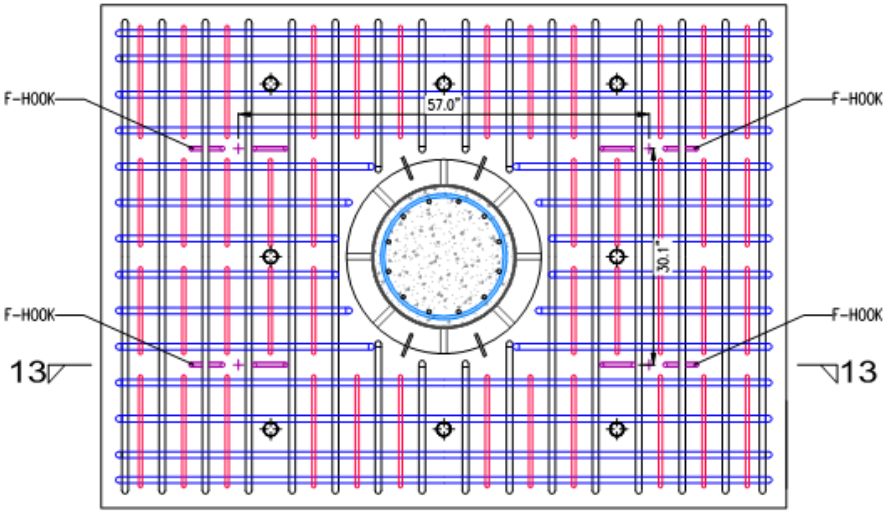

PLAN – Lifting Hooks Placement

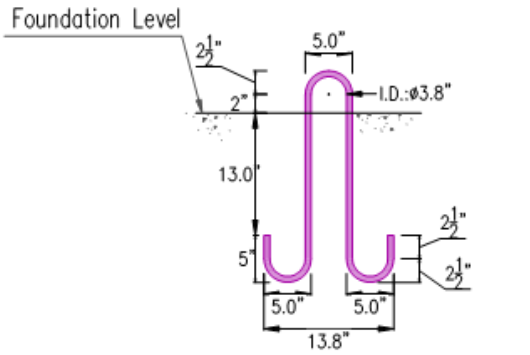

TYPE F-HOOK
#5 Rebar

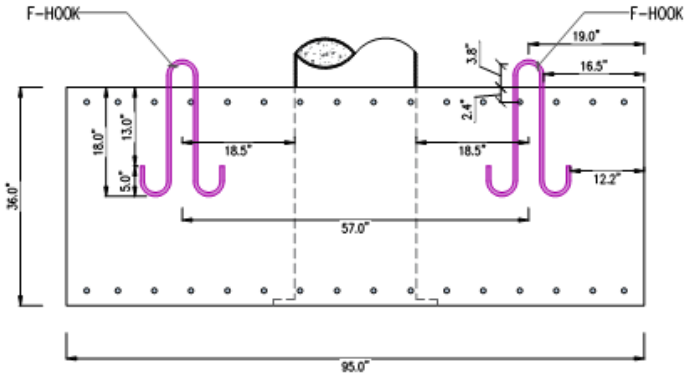

SECTION 13–13

UNIVERSITY AT BUFFALO 206 KETTER HALL Buffalo, NY 14226		
Lifting hook placement details		
Page:	September 08, 2015	D-LH-01
AI–19	By: Hadi Kenarangi	Rev: 00

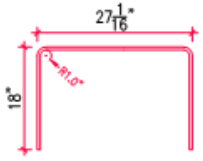

TYPE F-E1
#4 Rebar

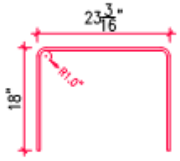

TYPE F-E2
#4 Rebar

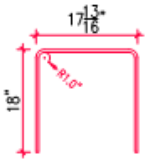

TYPE F-E3
#4 Rebar

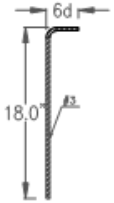

Type BP-RT1
#3 Rebar
Scale: B

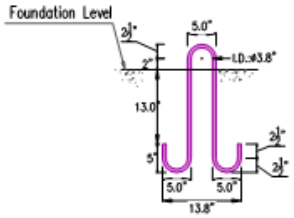

TYPE F-HOOK
#5 Rebar

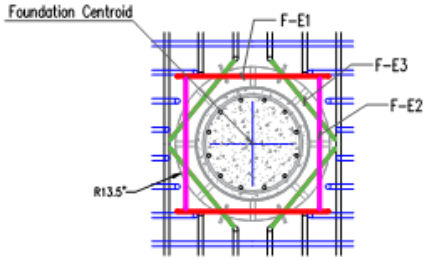

PLAN – Extra Reinforcements
Note: Shear Reinforcement is not shown

Table 2. Foundation Extra Rebars

Part	Type	Total length, in/unit	Qty.	#	Area, in²	Weight, lb.	Shape
footing	F-E1	67.8	2	4	0.2	0.4	S1
	F-E2	97.2	2	4	0.2	0.4	S1
	F-E3	51.8	4	4	0.2	11.5	S1
	F-HOOK	61.4	4	5	0.31	21.3	H1
					Total Weight	45.5	

Table 5. Other Rebars

Part	Type	Total Length, in/unit	Qty.	#	Area, in²	Weight, lb.	Shape
BP	BP-RT1	20.7	4	3	0.11	31.13	I3
					Total Weight	31.25	

GENERAL NOTES:
1. ALL REBAR GRADE 60 ASTM A706
2. FOUNDATION CONCRETE fc'=4000psi
3. REBAR BENDS, etc. PER ACI 318-08
4. CONDUIT TO BE 2.0" DIAMETER PVC

UNIVERSITY AT BUFFALO
206 KETTER HALL
Buffalo, NY 14226

Rebar types

Page:	September 08, 2015	D-RT-01
AI-20	By: Hadi Kenarangi	Rev: 00

M-20

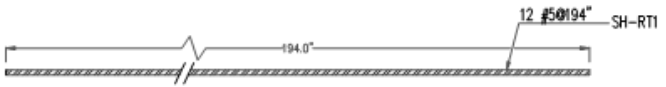

Type SH-RT1
#5 Rebar

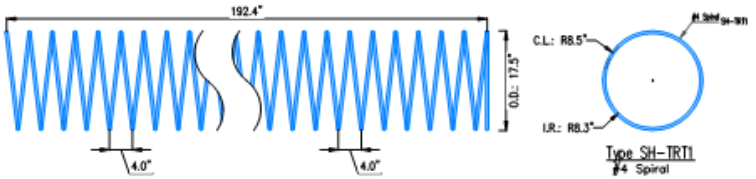

Type SH-TRT1
#4 Spiral

Shaft Rebar Types

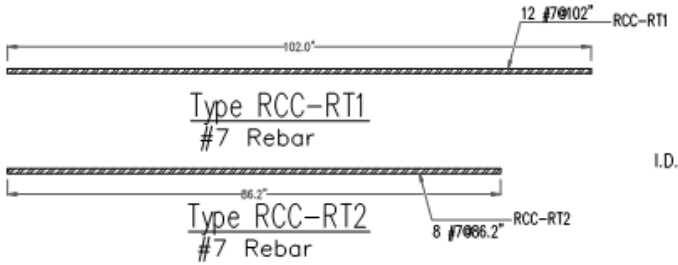

Type RCC-RT1
#7 Rebar

Type RCC-RT2
#7 Rebar

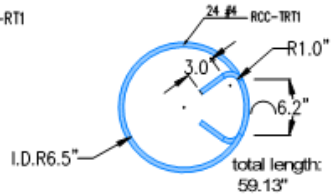

Type RCC-TRT1
#4 circ. tie
Scale: B

RC Column Rebar Types

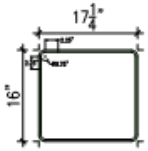

TYPE CH-TRT1
#3 Rebar

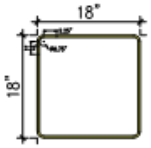

TYPE CH-TRT2
#3 Rebar

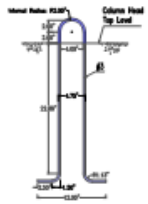

Type CH-HOOK
#3 Rebar

Table 3. RCFST Shaft Part Rebars

Part	Type	Total Length, in/unit	Qty.	#	Area, in²	Weight, lb.	Shape
Shaft	SH-RT1	194	12	5	0.31	202.3	Straight
	SH-TRT1	2570	1	4	0.2	140	Spiral
					Total Weight	342.3	

Table 4. RC Column and Column Head Part Rebars

Part	Type	Total Length, in/unit	Qty.	#	Area, in²	Weight, lb.	Shape
RC Column	RCC-RT1	102	12	7	0.6	208.5	Straight
	RCC-RT2	86.2	8	7	0.6	117.5	Straight
	RCC-TRT1	59.13	20	4	0.2	95.5	Circ. tie
Column Head	CH-TRT1	69.7	4	3	0.11	8.7	T2
	CH-TRT2	75.3	5	3	0.11	11.8	T2
	CH-HOOK	65	1	3	0.11	2.1	H2
					Total Weight	444.2	

GENERAL NOTES:
1. ALL REBAR GRADE 60 ASTM A706
2. FOUNDATION CONCRETE fc'=4000psi
3. REBAR BENDS, etc. PER ACI 318-08
4. CONDUIT TO BE 2.0" DIAMETER PVC

UNIVERSITY AT BUFFALO
206 KETTER HALL
Buffalo, NY 14226

Rebar types		
Page:	September 08, 2015	D-RT-02
AI-21	By: Hadi Kenarangi	Rev: 00

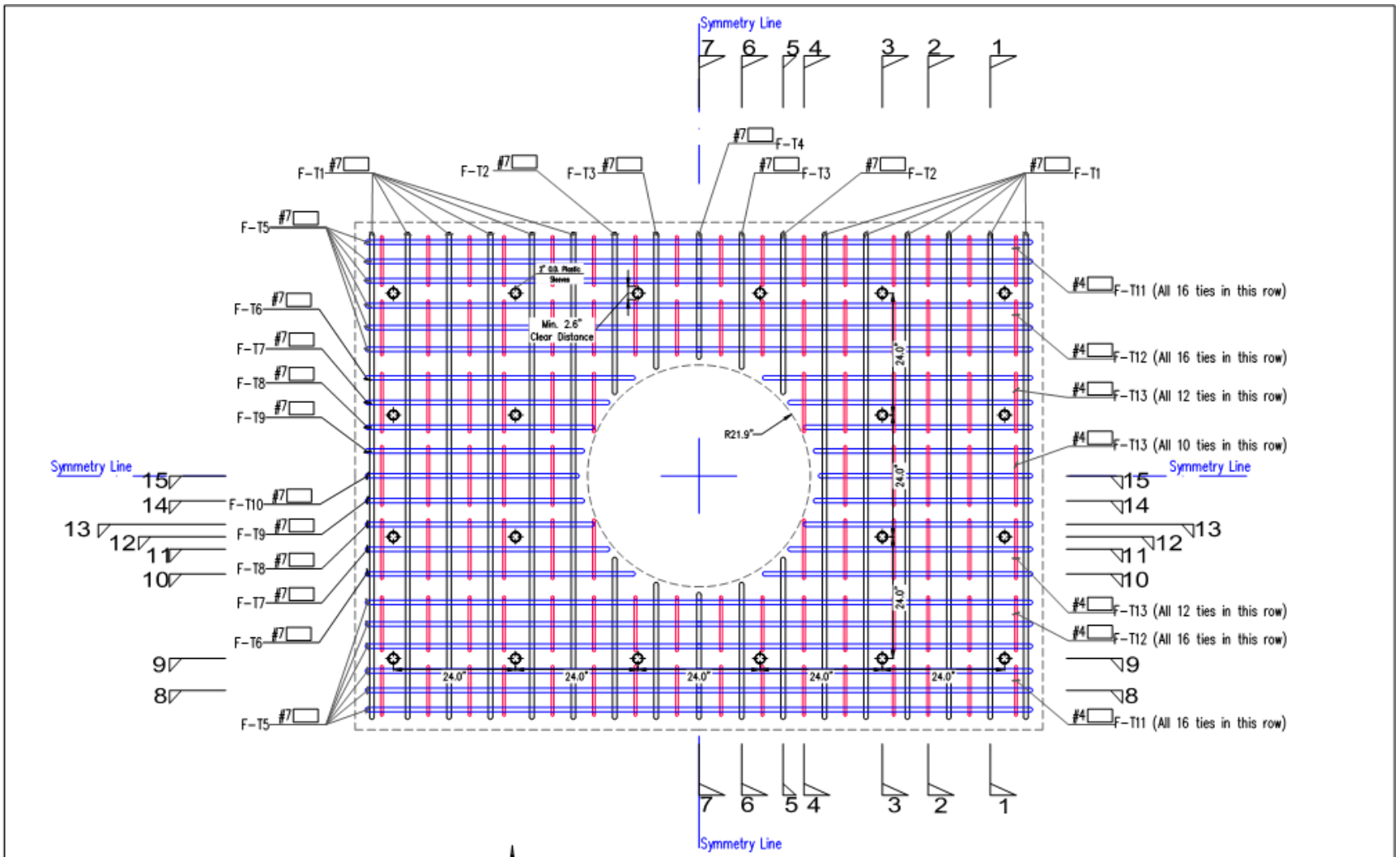

PLAN – Reinforcement Types

GENERAL NOTES:

1. ALL FOUNDATION REBAR GRADE 60 ASTM A706/A615
2. FOUNDATION CONCRETE fc'=4000psi
3. REBAR BENDS, etc. PER ACI 318-08
4. CONDUIT TO BE 2.0" DIAMETER PVC

UNIVERSITY AT BUFFALO 206 KETTER HALL Buffalo, NY 14226		
RC foundation details		
Page:	October 12, 2015	D-FS5-01
AI-2	By: Hadi Kenarangi	Rev: 00

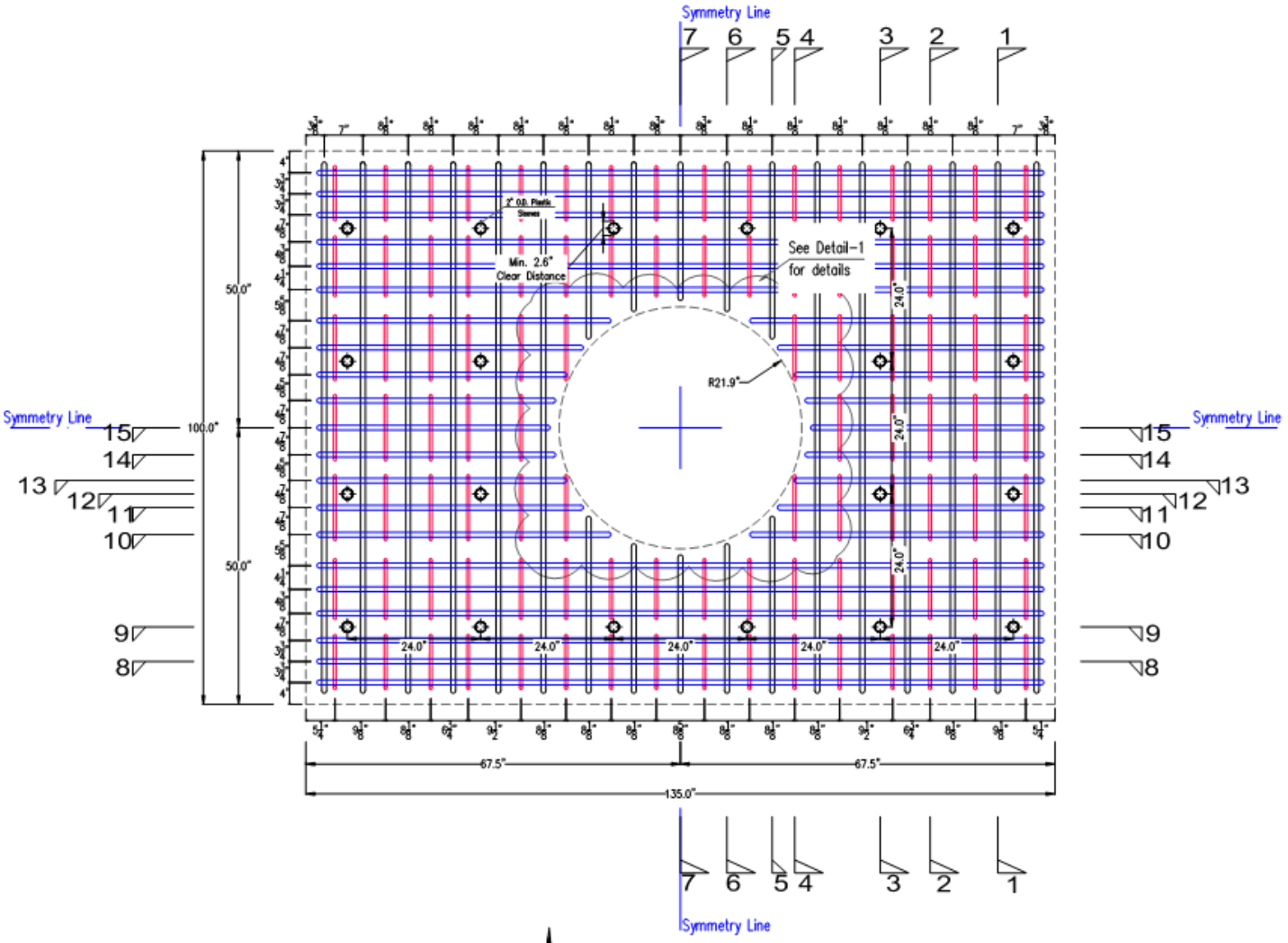

PLAN – Dimensions

GENERAL NOTES:

1. ALL FOUNDATION REBAR GRADE 60 ASTM A706/A615
2. FOUNDATION CONCRETE fc'=4000psi
3. REBAR BENDS, etc. PER ACI 318-08
4. CONDUIT TO BE 2.0" DIAMETER PVC

UNIVERSITY AT BUFFALO 206 KETTER HALL Buffalo, NY 14226		
RC foundation details		
Page:	October 12, 2015	D-FS5-02
AI-3	By: Hadi Kenarangi	Rev: 00

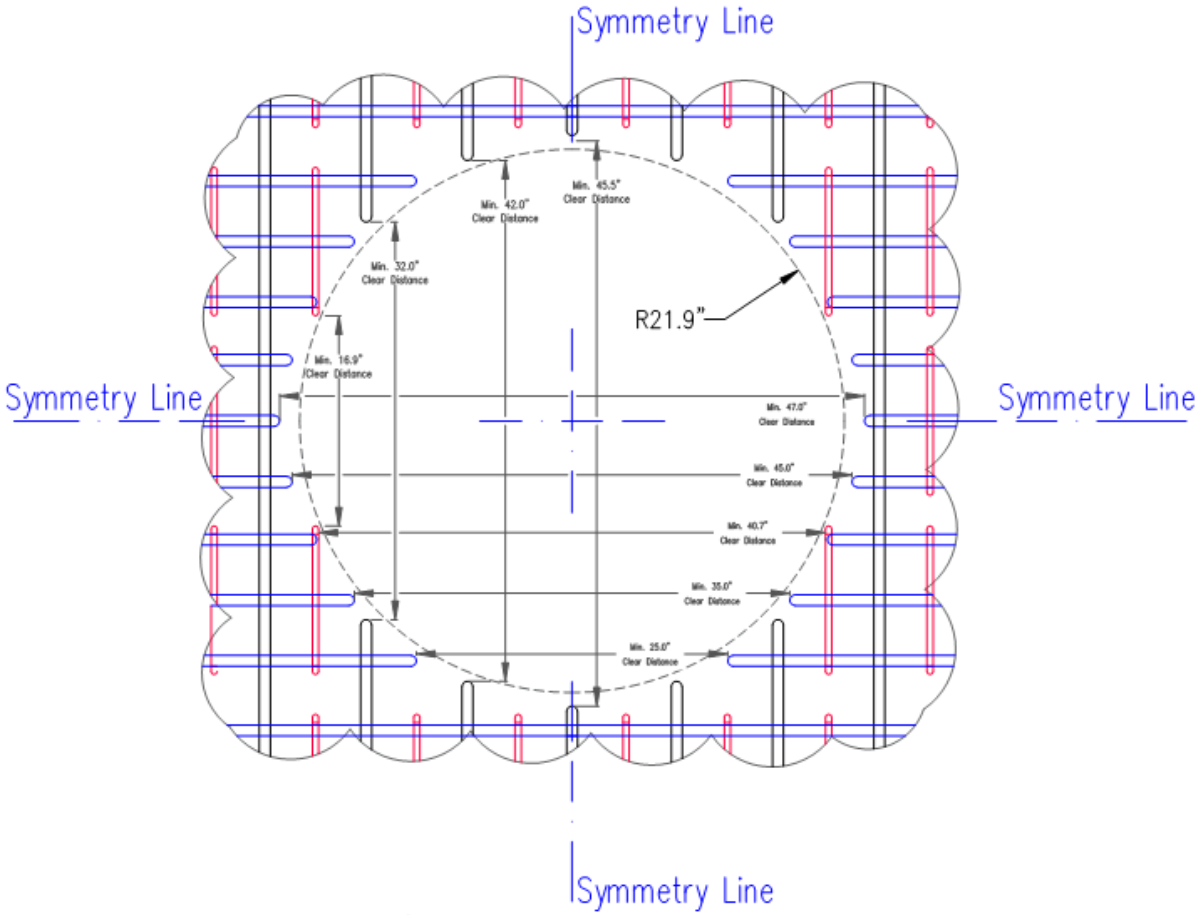

Detail–1

GENERAL NOTES:

1. ALL FOUNDATION REBAR GRADE 60 ASTM A706/A615
2. FOUNDATION CONCRETE fc'=4000psi
3. REBAR BENDS, etc. PER ACI 318–08
4. CONDUIT TO BE 2.0" DIAMETER PVC

UNIVERSITY AT BUFFALO 206 KETTER HALL Buffalo, NY 14226		
RC foundation details		
Page:	October 12, 2015	D-FS5-03
AI–4	By: Hadi Kenarangi	Rev: 00

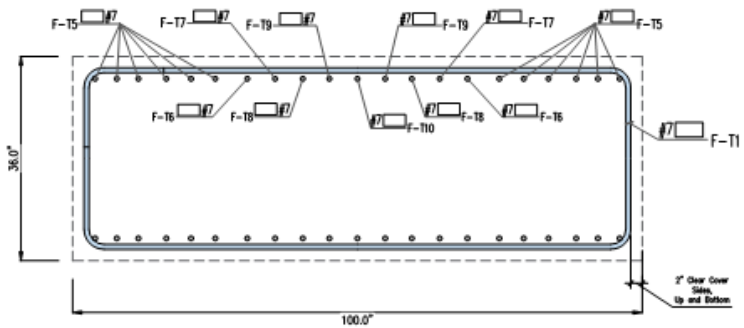

SECTION 1-1

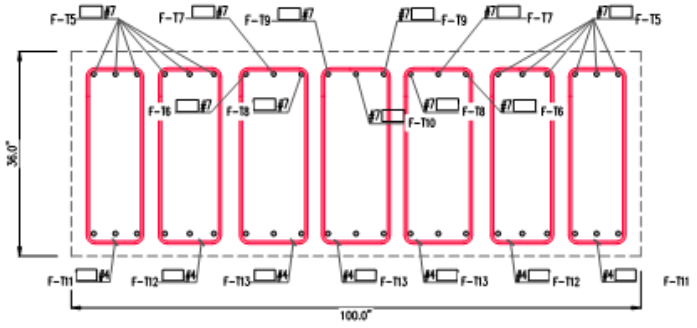

SECTION 2-2

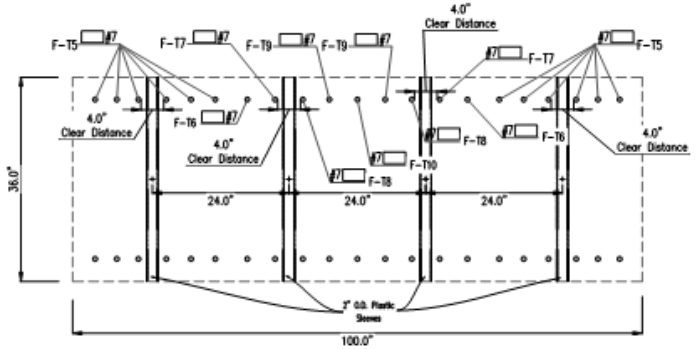

SECTION 3-3

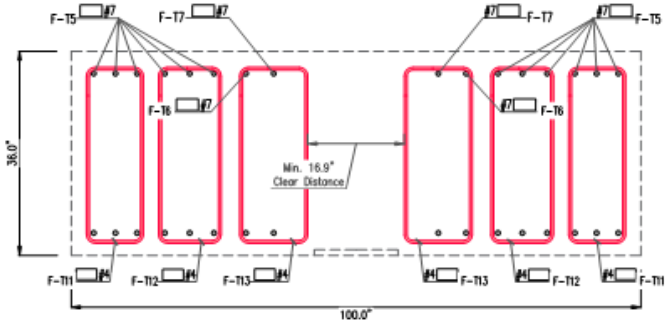

SECTION 4-4

GENERAL NOTES:

1. ALL FOUNDATION REBAR GRADE 60 ASTM A706/A615
2. FOUNDATION CONCRETE fc'=4000psi
3. REBAR BENDS, etc. PER ACI 318-08
4. CONDUIT TO BE 2.0" DIAMETER PVC

UNIVERSITY AT BUFFALO 206 KETTER HALL Buffalo, NY 14226		
RC foundation details		
Page:	October 12, 2015	D-FS5-04
AI-5	By: Hadi Kenarangi	Rev: 00

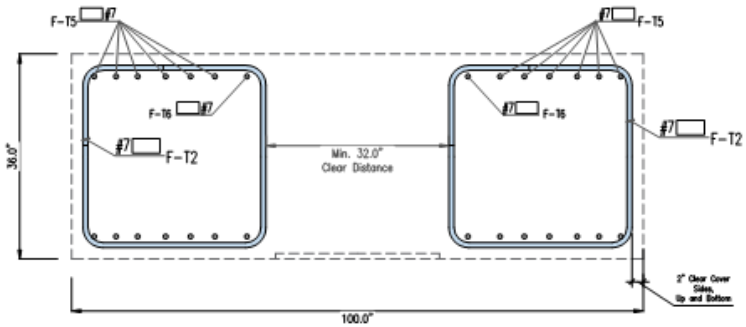

SECTION 5-5

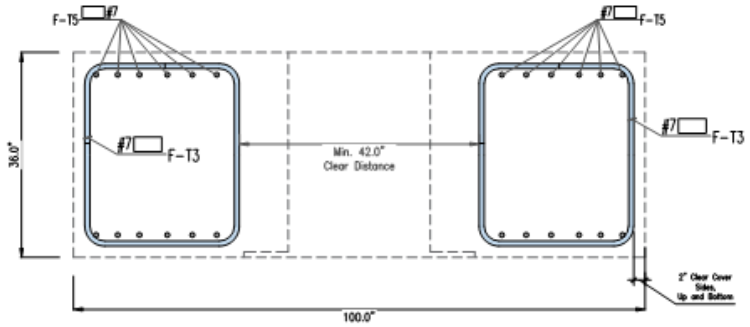

SECTION 6-6

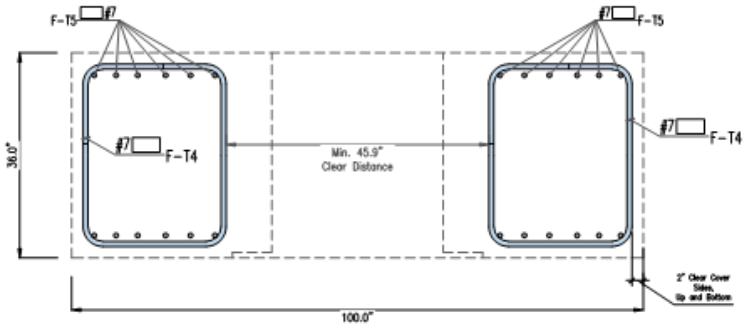

SECTION 7-7

GENERAL NOTES:

1. ALL FOUNDATION REBAR GRADE 60 ASTM A706/A615
2. FOUNDATION CONCRETE fc'=4000psi
3. REBAR BENDS, etc. PER ACI 318-08
4. CONDUIT TO BE 2.0" DIAMETER PVC

UNIVERSITY AT BUFFALO 206 KETTER HALL Buffalo, NY 14226		
RC foundation details		
Page:	October 12, 2015	D-FS5-05
AI-6	By: Hadi Kenarangi	Rev: 00

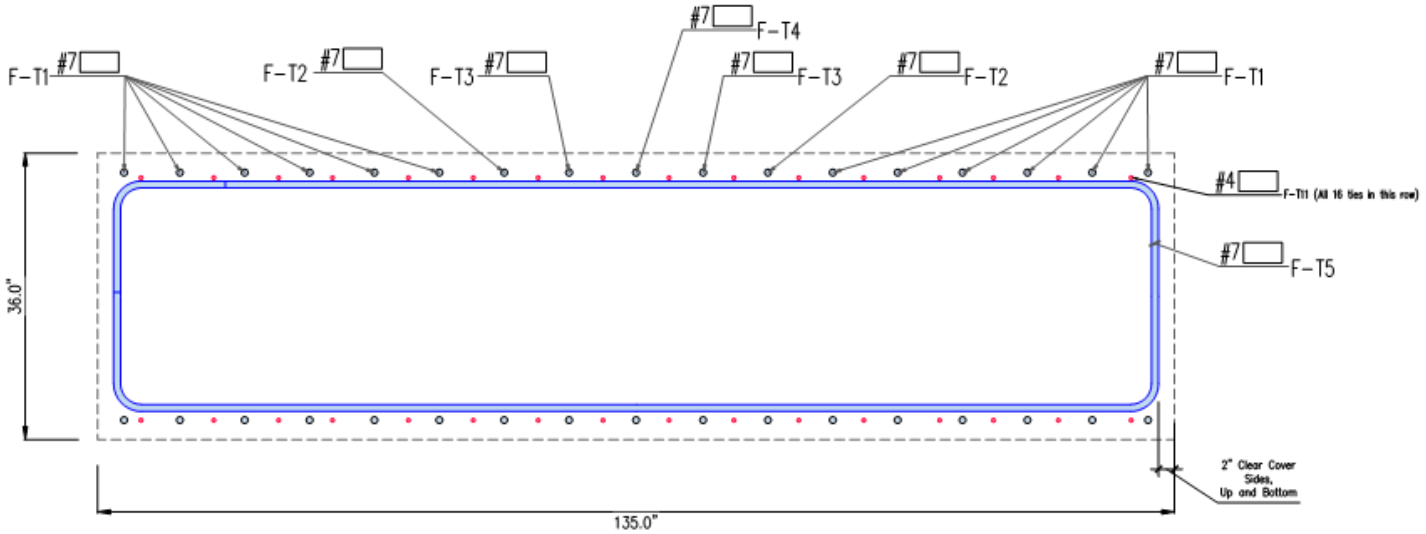

SECTION 8-8

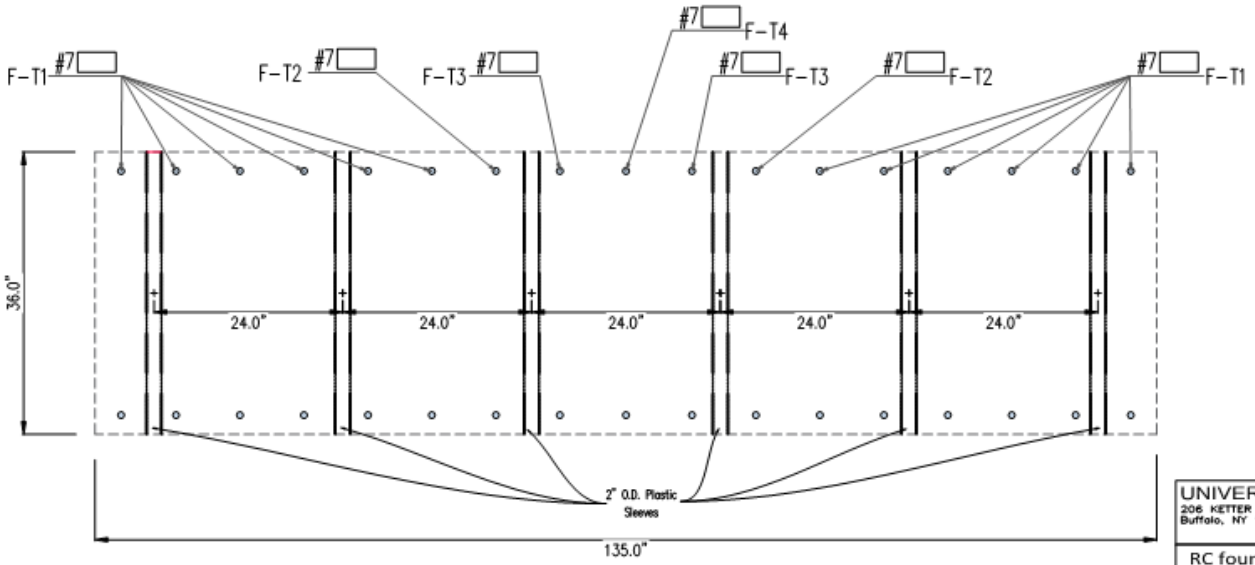

SECTION 9-9

UNIVERSITY AT BUFFALO
206 KETTER HALL
Buffalo, NY 14226

RC foundation details

Page:	October 12, 2015	D-FS5-06
AI-7	By: Hadi Kenarangi	Rev: 00

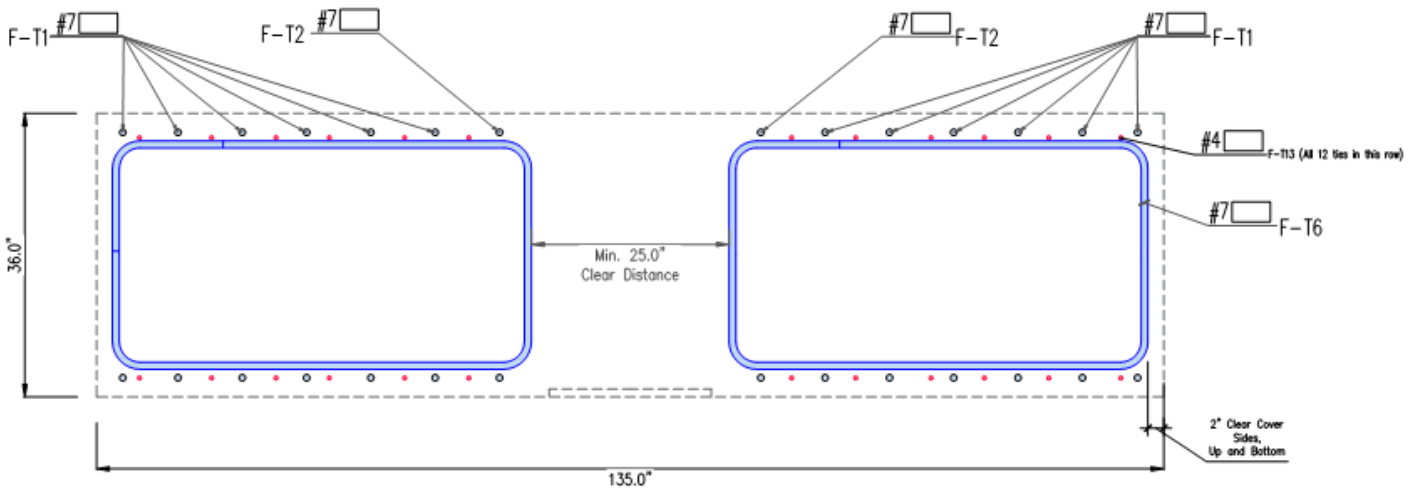

SECTION 10-10

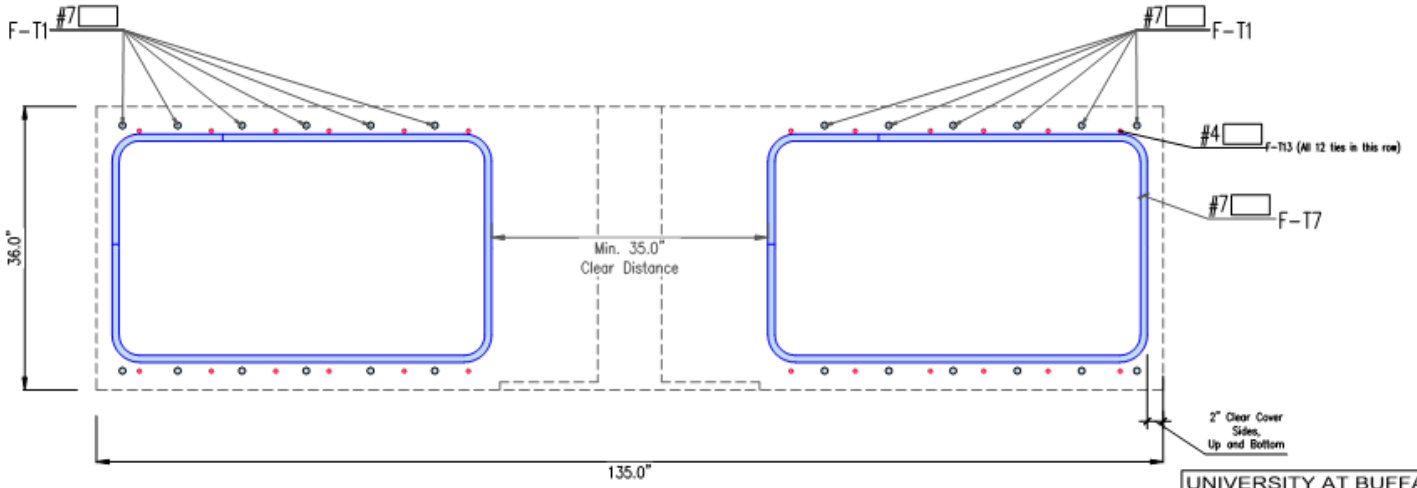

SECTION 11-11

UNIVERSITY AT BUFFALO
206 KETTER HALL
Buffalo, NY 14226

RC foundation details

Page:	October 12, 2015	D-FS5-07
AI-8	By: Hadi Kenarangi	Rev: 00

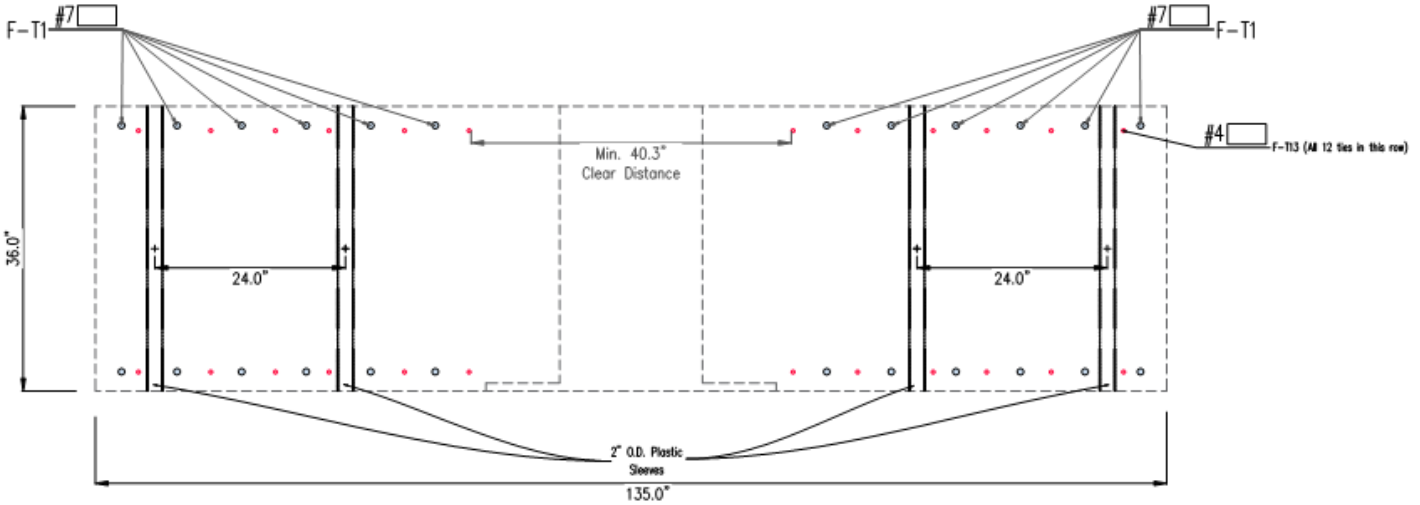

SECTION 12-12

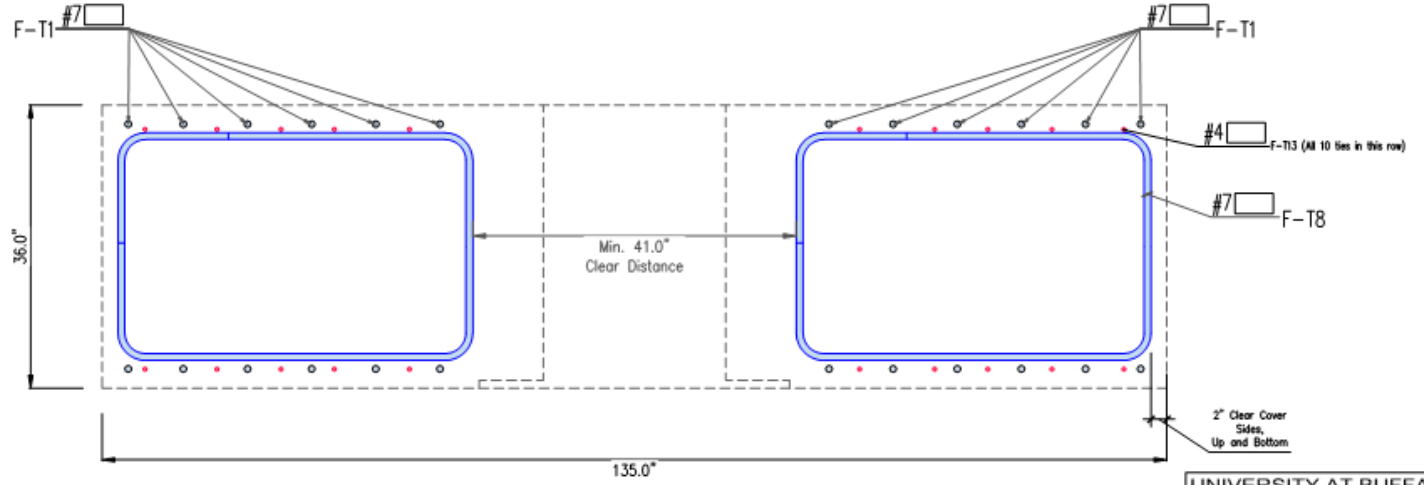

SECTION 13-13

UNIVERSITY AT BUFFALO
206 KETTER HALL
Buffalo, NY 14226

RC foundation details

Page:	October 12, 2015	D-FS5-08
AI-9	By: Hadi Kenarangi	Rev: 00

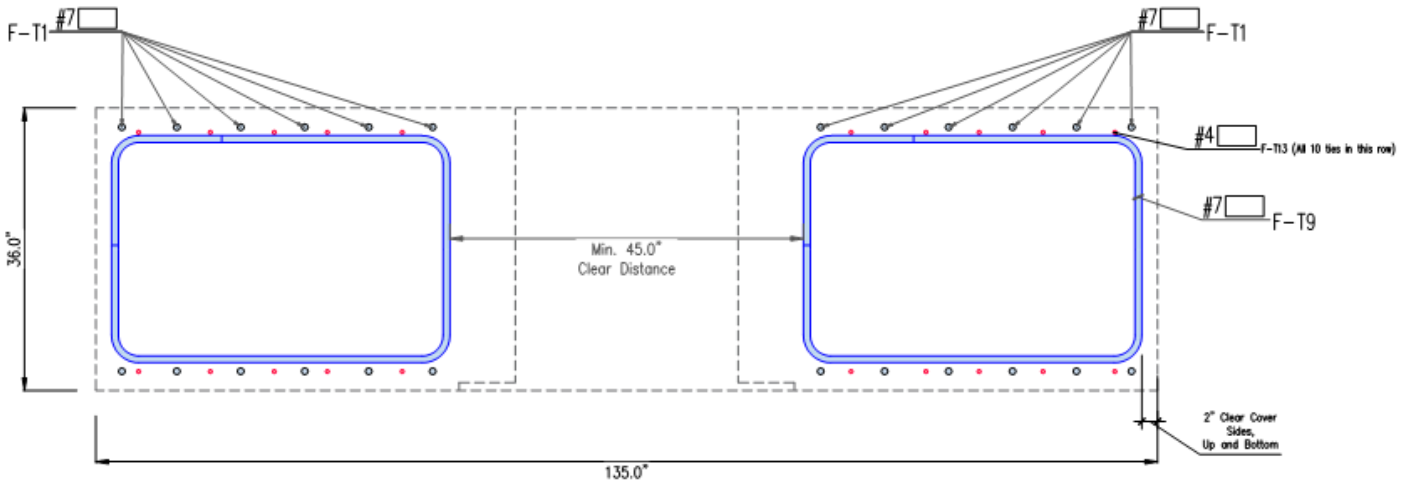

SECTION 14–14

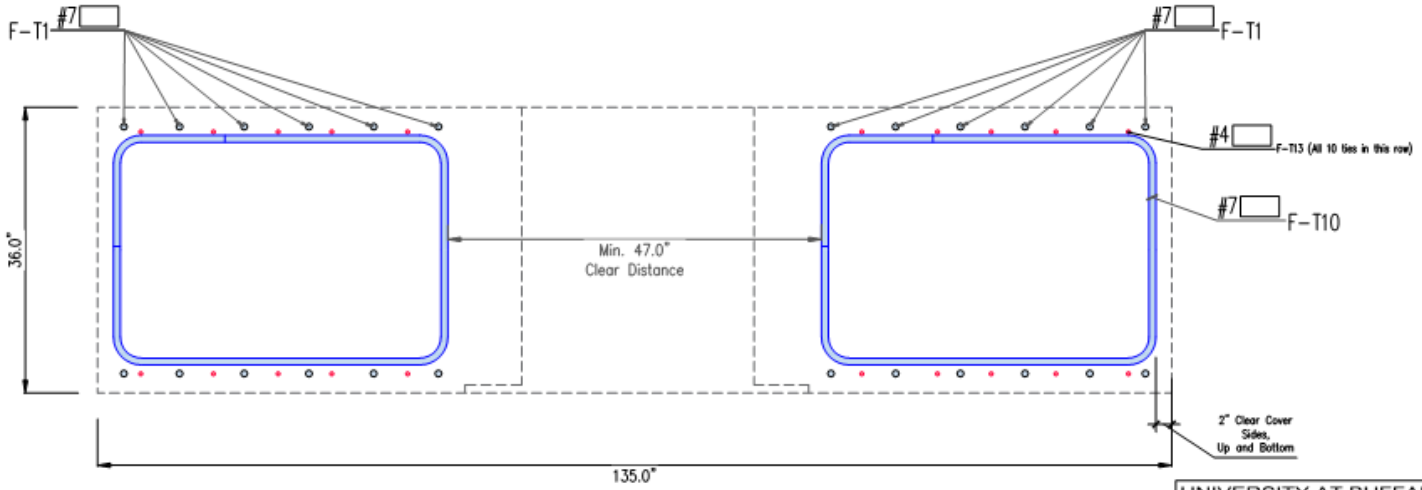

SECTION 15–15

UNIVERSITY AT BUFFALO
206 KETTER HALL
Buffalo, NY 14226

RC foundation details

Page:	October 12, 2015	D-FS5-09
AI–10	By: Hadi Kenarangi	Rev: 00

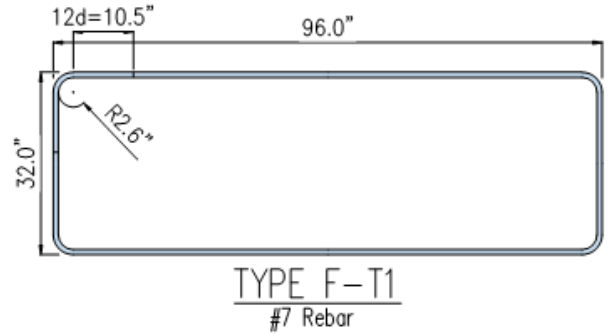

TYPE F-T1
#7 Rebar

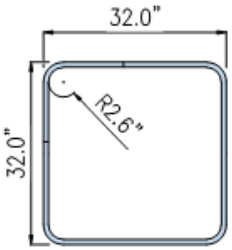

TYPE F-T2
#7 Rebar

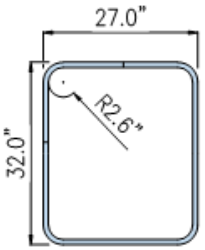

TYPE F-T3
#7 Rebar

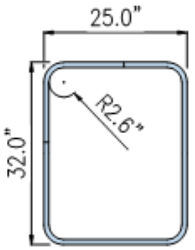

TYPE F-T4
#7 Rebar

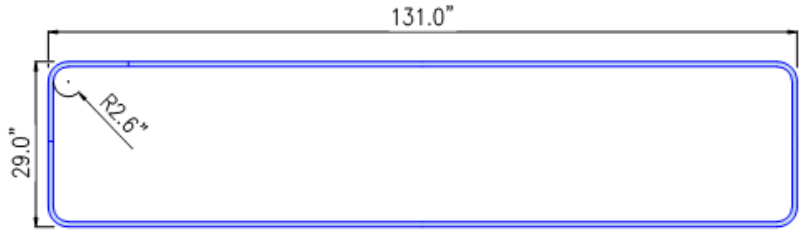

TYPE F-T5
#7 Rebar

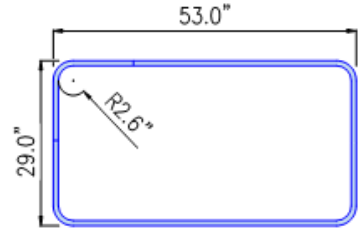

TYPE F-T6
#7 Rebar

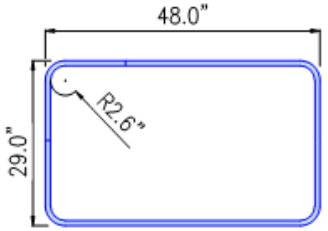

TYPE F-T7
#7 Rebar

Type 1 Foundation Rebars

Area	Item	Qty.	Size	Length	Mark	Shape	Lbs	A	B	C	D	E	G
Foundation		13	7	[illegible]	T-T1	T2	[illegible]	0-11	8-0	3-6	6-1	3-6	0-11
	2	[illegible]	7	13-2	T-T2	T2	130	0-11	2-6	2-6	2-6	2-6	0-11
	3	[illegible]	7	11-4	T-T3	T2	[illegible]	0-11	[illegible]	[illegible]	[illegible]	[illegible]	0-11
	4	[illegible]	7	11-0	T-T4	T2	98	0-11	[illegible]	[illegible]	[illegible]	[illegible]	0-11
	5	12	7	28-2	T-T5	T2	551	0-11	10-11	2-6	10-11	2-6	0-11
	6	[illegible]	7	13-2	T-T6	T2	124	0-11	4-6	2-6	4-6	2-6	0-11
	7	[illegible]	[illegible]	14-4	T-T7	T2	[illegible]	0-11	4-0	[illegible]	4-0	[illegible]	0-11
	8	[illegible]	7	13-10	T-T8	T2	[illegible]	0-11	[illegible]	[illegible]	[illegible]	[illegible]	0-11
	9	[illegible]	7	14-4	T-T9	T2	[illegible]	0-11	[illegible]	[illegible]	[illegible]	[illegible]	0-11
	10	[illegible]	7	12-4	T-T10	T2	[illegible]	0-11	[illegible]	[illegible]	[illegible]	[illegible]	0-11
		[illegible]					[illegible]						
	11	53	4	7-3 4/5	T-T11	T2	156	0-4	0-10	1-2	0-10	1-2	0-4
	12	53	4	7-3 4/5	T-T12	T2	156	0-4	0-11	1-2	0-10	1-2	0-4
	13	54	4	7-7 4/5	T-T13	T2	174	0-4	1-0	1-7	1-0	1-7	0-4
		266					40%						

Total Weight: 3,458 Lbs

GENERAL NOTES:

1. ALL FOUNDATION REBAR GRADE 60 ASTM A706/A615
2. FOUNDATION CONCRETE fc'=4000psi
3. REBAR BENDS, etc. PER ACI 318-08
4. CONDUIT TO BE 2.0" DIAMETER PVC

UNIVERSITY AT BUFFALO
206 KETTER HALL
Buffalo, NY 14226

RC foundation details

Page:	October 12, 2015	D-FS5-10
AI-11	By: Hadi Kenarangi	Rev: 02

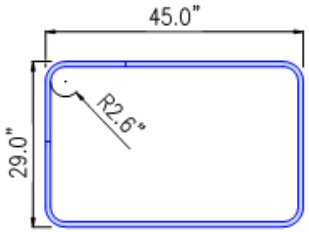

TYPE F-T8
#7 Rebar

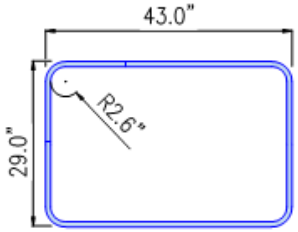

TYPE F-T9
#7 Rebar

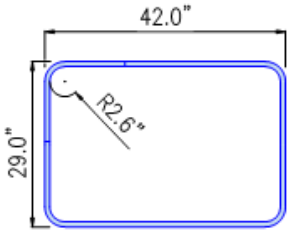

TYPE F-T10
#7 Rebar

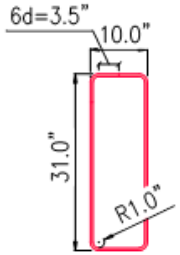

TYPE F-T11
#4 Rebar

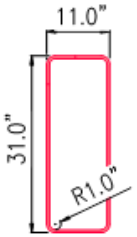

TYPE F-T12
#4 Rebar

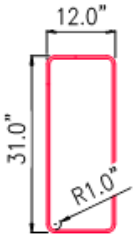

TYPE F-T13
#4 Rebar

Table 1. Concrete Rebars

Mark	Pcs	Qty	Size	Length	Shape	Weight	A	B	C	D	E	F
Foundation	1	12	7	29'-10"	F-T1	T2	358	2'-1	2'-0	2'-3	8'-3	2'-3	2'-11
	2	4	7	14'-4	F-T2	T2	114	2'-11	6'-6	6'-3	2'-9	2'-9	2'-11
	3	4	7	11'-6	F-T3	T2	92	2'-11	3'-3	3'-3	2'-9	2'-9	2'-11
	4	2	7	11'-0	F-T4	T2	44	2'-11	3'-0	2'-9	2'-1	2'-1	2'-11
	5	12	7	28'-2	F-T5	T2	676	2'-11	13'-11	2'-3	10'-11	2'-3	2'-11
	6	1	7	15'-3	F-T6	T2	153	2'-1	6'-3	3'-3	8'-3	2'-3	2'-11
	7	4	7	14'-6	F-T7	T2	117	2'-11	4'-0	3'-3	4'-3	2'-3	2'-11
	8	4	7	14'-10"	F-T8	T2	119	2'-11	3'-9	3'-3	3'-9	2'-3	2'-11
	9	4	7	15'-5	F-T9	T2	124	2'-11	3'-7	3'-3	3'-7	2'-3	2'-11
	10	2	7	15'-1	F-T10	T2	61	2'-11	3'-6	3'-3	3'-5	2'-3	2'-11
		52					2006						
	11	52	4	7'-8 1/8	F-T11	T2	156	2'-7	0'-10	2'-7	0'-10	2'-7	0'-4
	12	52	4	7'-8 1/8	F-T12	T2	156	2'-7	0'-1	2'-7	0'-11	2'-7	0'-4
	13	24	4	7'-4 1/8	F-T13	T2	74	2'-4	1'-0	2'-1	1'-1	2'-1	0'-4
		128					386						

Total Weight: 2,478 lb.

GENERAL NOTES:

1. ALL FOUNDATION REBAR GRADE 60 ASTM A706/A615
2. FOUNDATION CONCRETE fc'=4000psi
3. REBAR BENDS, etc. PER ACI 318-08
4. CONDUIT TO BE 2.0" DIAMETER PVC

UNIVERSITY AT BUFFALO
206 KETTER HALL
Buffalo, NY 14226

RC foundation details

Page:	October 12, 2015	D-FS5-11
AI-12	By: Hadi Kenarangi	Rev: 02

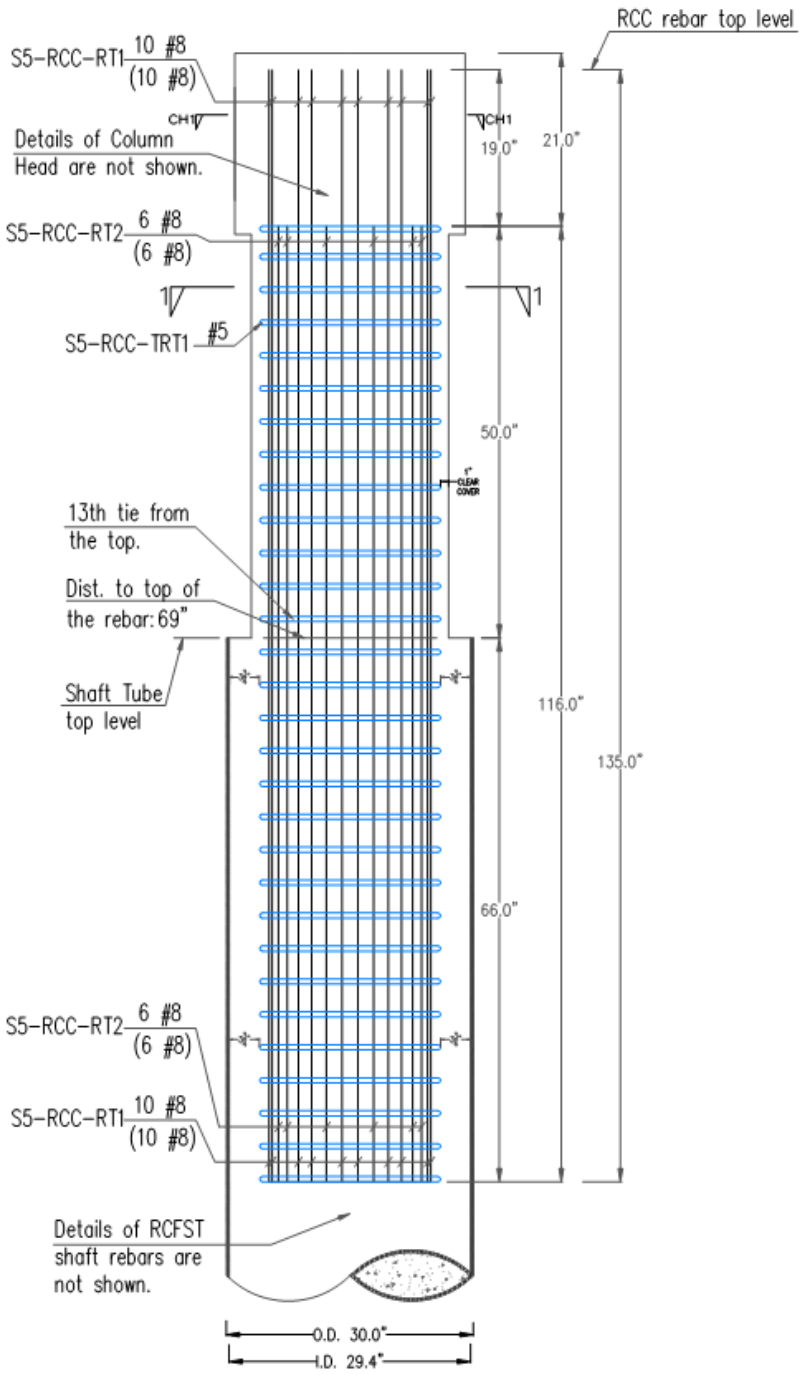

RC Column Part

GENERAL NOTES:

1. ALL REBAR GRADE 60 ASTM A706
2. CONCRETE fc'=4000psi
3. REBAR BENDS, etc. PER ACI 318-08
4. CONDUIT TO BE 2.0" DIAMETER PVC

UNIVERSITY AT BUFFALO 206 KETTER HALL Buffalo, NY 14226		
D30in RC Column Part Details 1		
Page:	May 29, 2016	D-RCC-1
AI-1	By: Hadi Kenarangi	Rev: 00

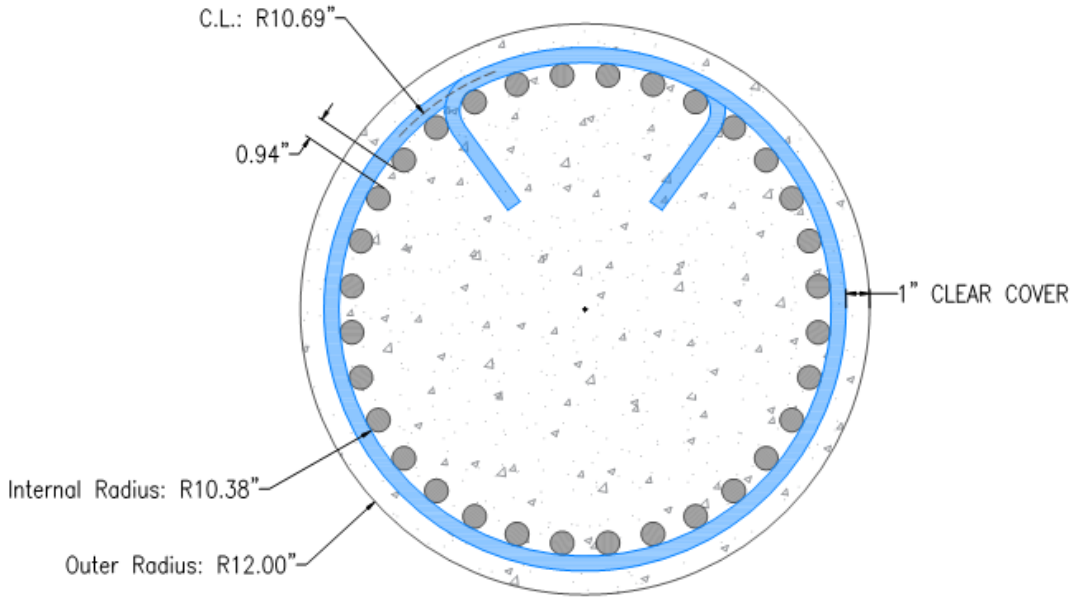

SECTION 1-1

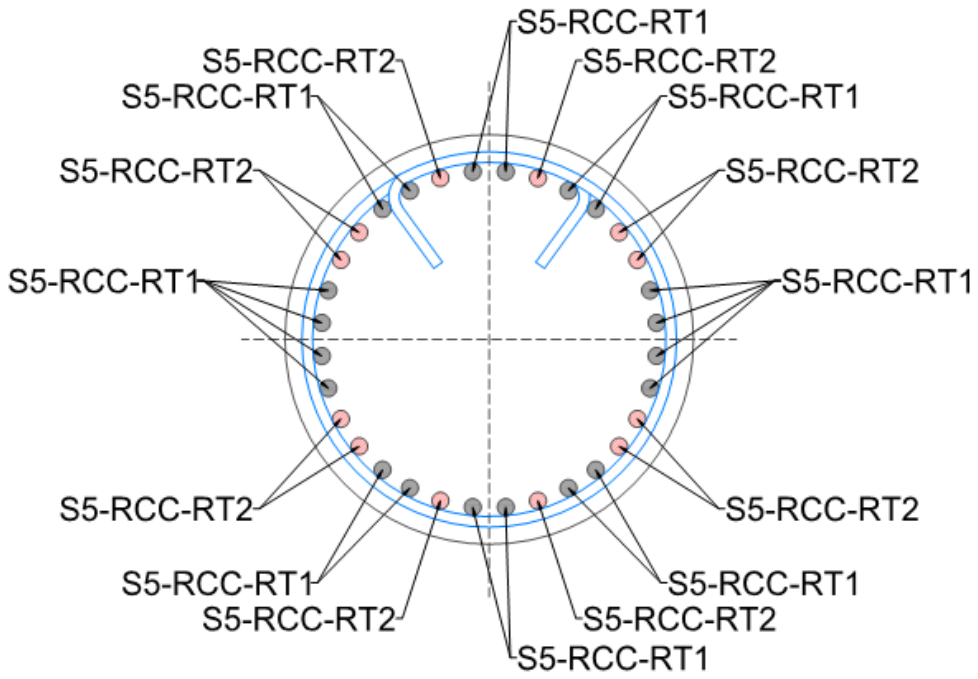

RC Column Rebar Types

GENERAL NOTES:
1. ALL REBAR GRADE 60 ASTM A706
2. CONCRETE fc'=4000psi
3. REBAR BENDS, etc. PER ACI 318-08
4. CONDUIT TO BE 2.0" DIAMETER PVC

UNIVERSITY AT BUFFALO 206 KETTER HALL Buffalo, NY 14226		
D30in RC Column Part Details 2		
Page:	May 29, 2016	D-RCC-2
AI-3	By: Hadi Kenarangi	Rev: 00

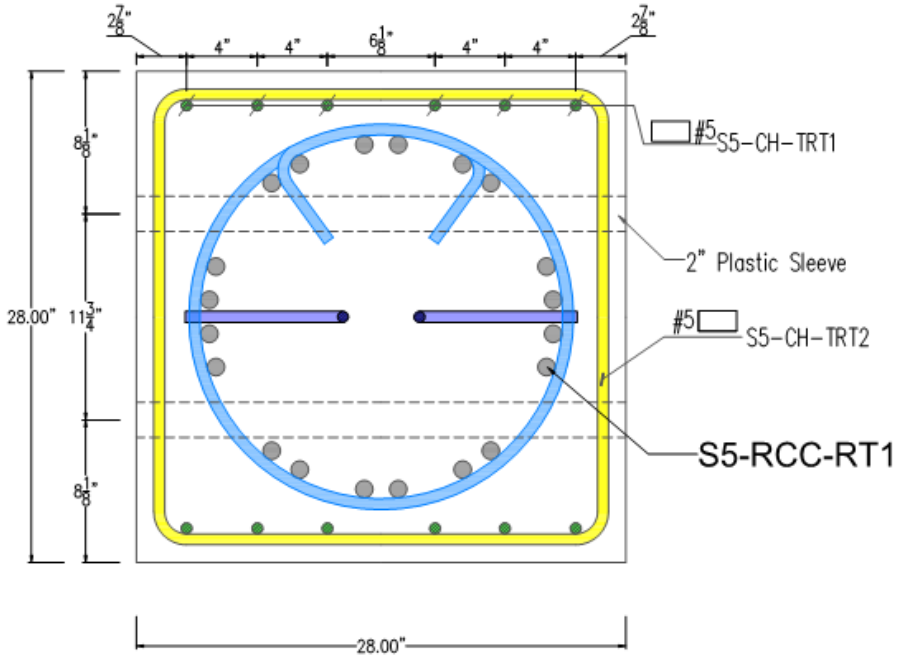

Section CH1-CH1

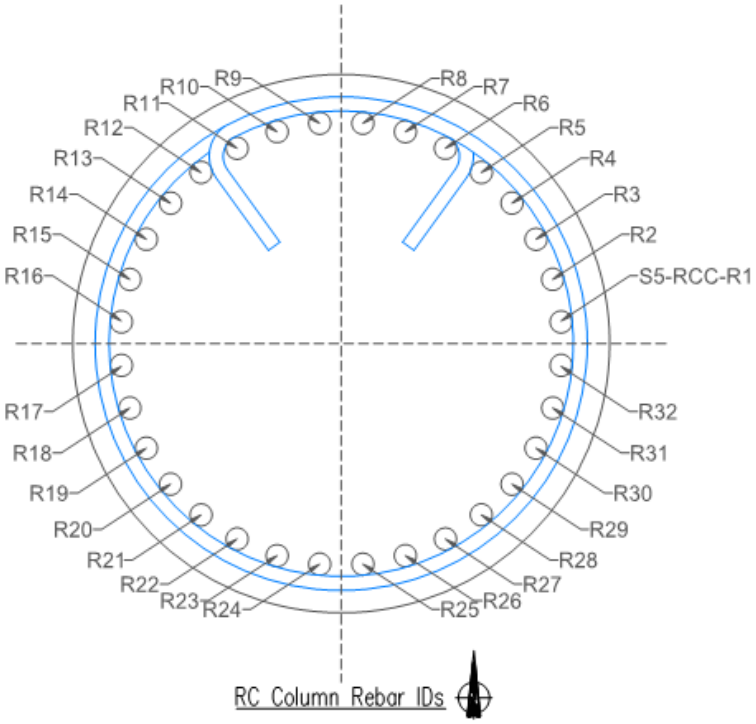

RC Column Rebar IDs

GENERAL NOTES:

1. ALL REBAR GRADE 60 ASTM A706
2. CONCRETE fc'=4000psi
3. REBAR BENDS, etc. PER ACI 318-08
4. CONDUIT TO BE 2.0" DIAMETER PVC

UNIVERSITY AT BUFFALO 206 KETTER HALL Buffalo, NY 14226		
D30in RC Column Part Details 3		
Page:	May 29, 2016	D-RCC-3
AI-2	By: Hadi Kenarangi	Rev: 00

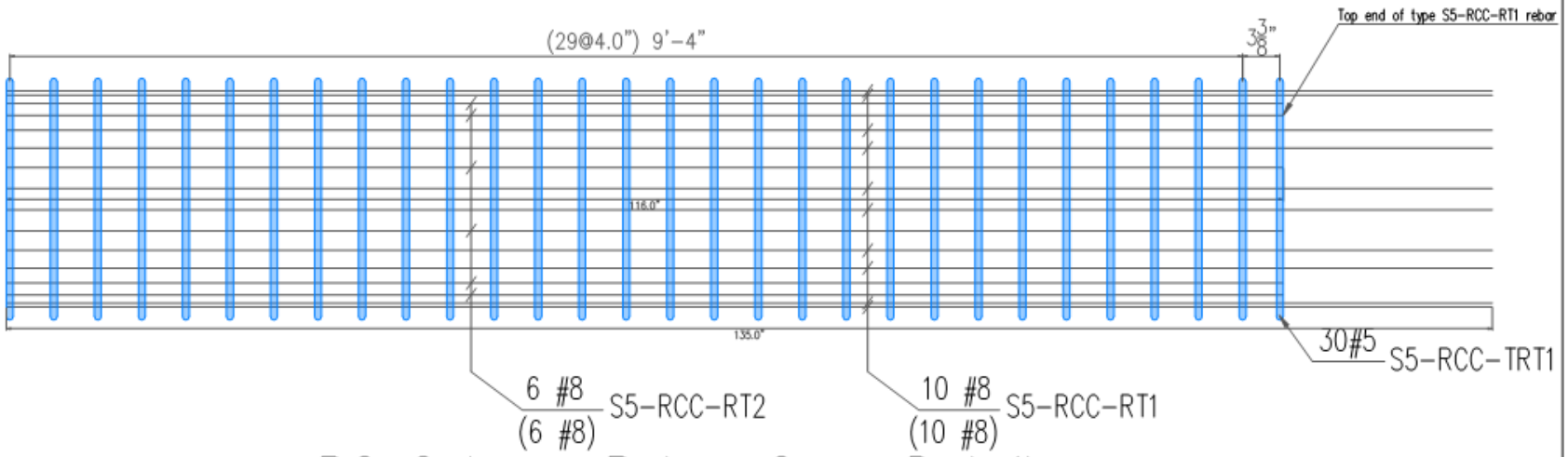

RC Column Rebar Cage Details

Type S5-RCC-RT1
#8 Rebar

Type S5-RCC-RT2
#8 Rebar

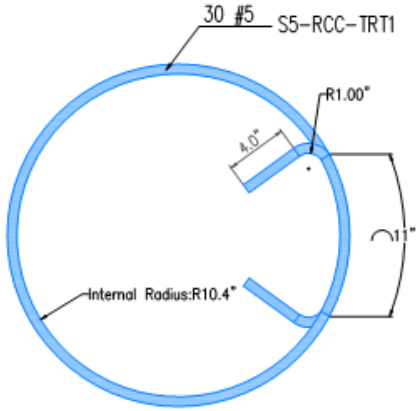

Type S5-RCC-TRT1
#5 circ. tie

RC Column Rebar Types

Table 4. D30in RC Column Part Rebars

Part	Type	Total Length, in/unit	Qty.	#	Area/unit mass in²/lb. per ft.	Weight, lb.	Shape
RCC	S5-RCC-RT1	135	20	8	0.79/2.67	801	Straight
	S5-RCC-RT2	116	12	8	0.79/2.67	310	Straight
	S5-RCC-TRT1	99	30	5	0.31/1.04	257	Circ. tie
					Total Weight	2168	

GENERAL NOTES:
1. ALL REBAR GRADE 60 ASTM A706
2. CONCRETE fc'=4000psi
3. REBAR BENDS, etc. PER ACI 318-08
4. CONDUIT TO BE 2.0" DIAMETER PVC

UNIVERSITY AT BUFFALO
206 KETTER HALL
Buffalo, NY 14226

D30in RC Column Part Details 4

Page:	May 29, 2016	D-RCC-4
AI-5	By: Hadi Kenarangi	Rev: 00

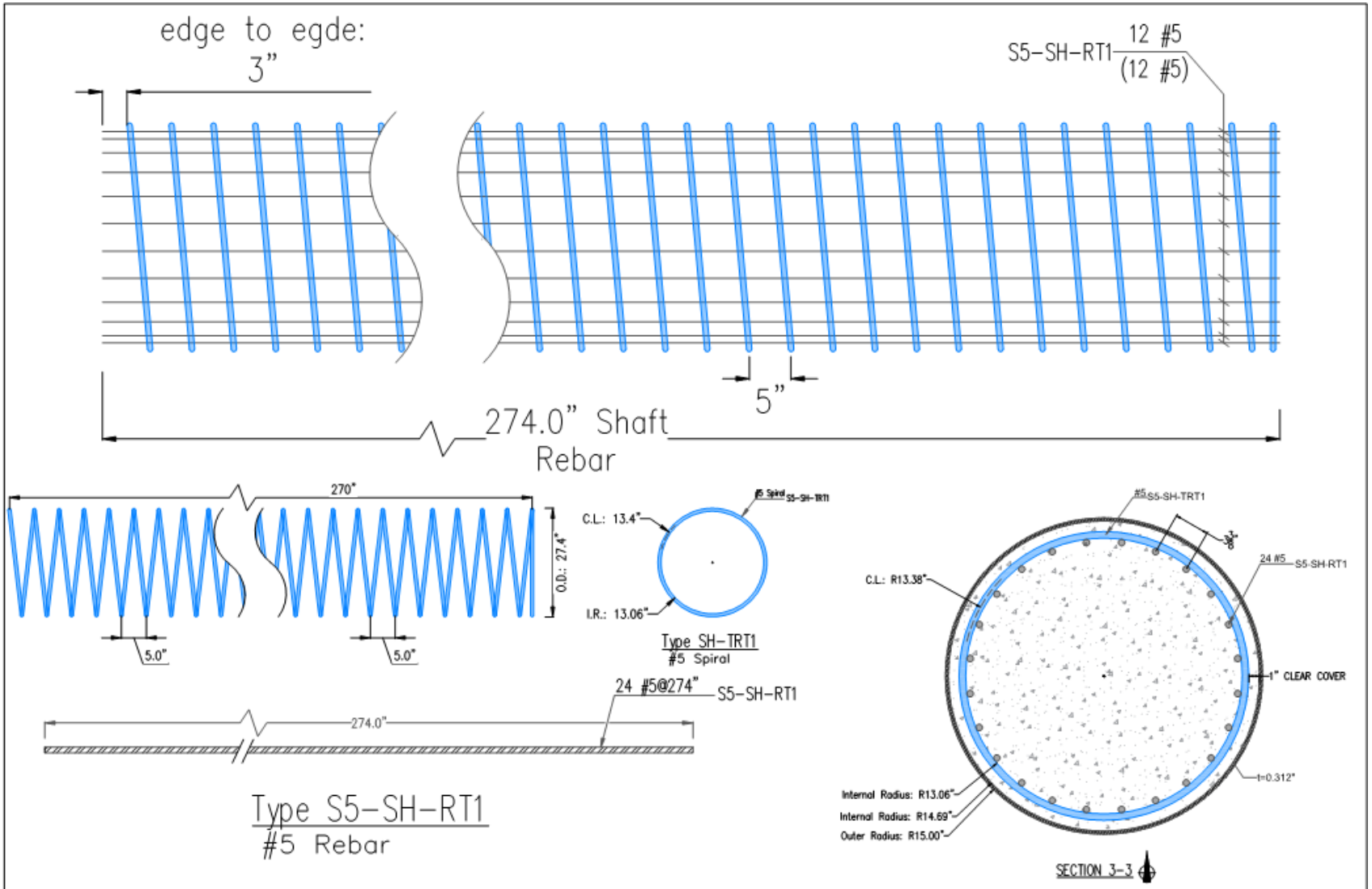

Table 3. D30in RCFST Shaft Part Rebars

Part	Type	Total Length, in/unit	Qty.	#	Area/unit mass in²/lb. per ft.	Weight, lb.	Shape
[illegible]	S5-SH-RT1	274	24	5	0.31/1.04	570	Straight
[illegible]	S5-SH-TRT1	4078	1	5	0.31/1.04	402	Spiral
					Total Weight	972	

GENERAL NOTES:

1. ALL REBAR GRADE 60 ASTM A706
2. CONCRETE fc'=4000psi
3. REBAR BENDS, etc. PER ACI 318-08
4. CONDUIT TO BE 2.0" DIAMETER PVC

UNIVERSITY AT BUFFALO
206 KETTER HALL
Buffalo, NY 14226

D30in RCFST Shaft Part Details 1

Page:	May 29, 2016	D-SH-1
AI-4	By: Hadi Kenarangi	Rev: 00

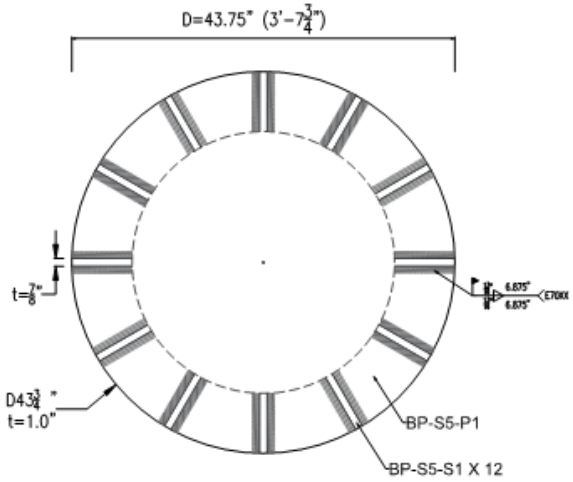

D30-Base Plate Details

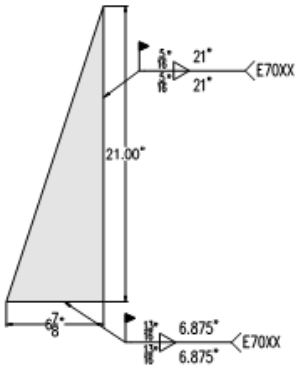

Detail BP-S5-S1

⅞" Plate

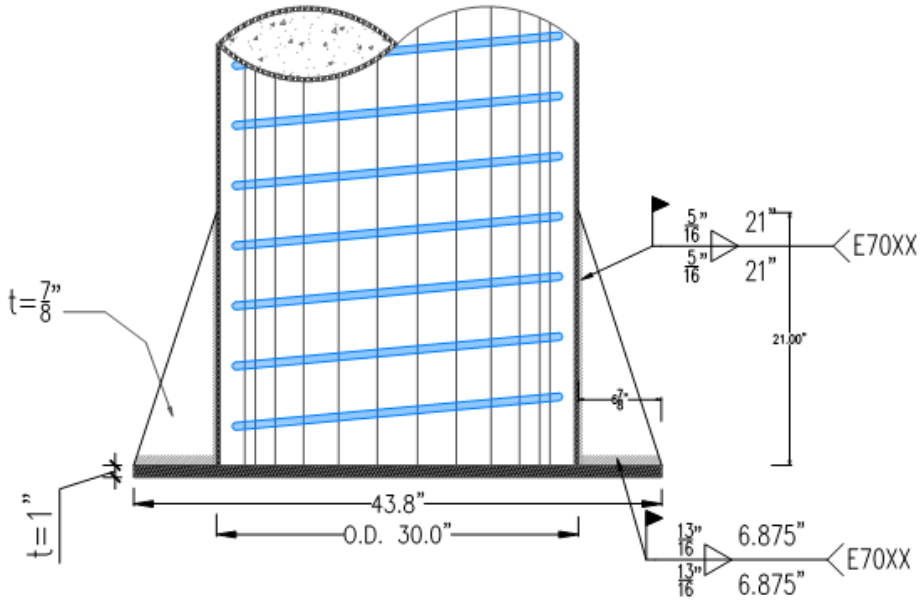

Shaft Bottom Part

UNIVERSITY AT BUFFALO 206 KETTER HALL Buffalo, NY 14226		
Base Plate Details		
Page: 00	May 29, 2016 By: Hadi Kenarangi	D30-ShaftBot Rev: 00

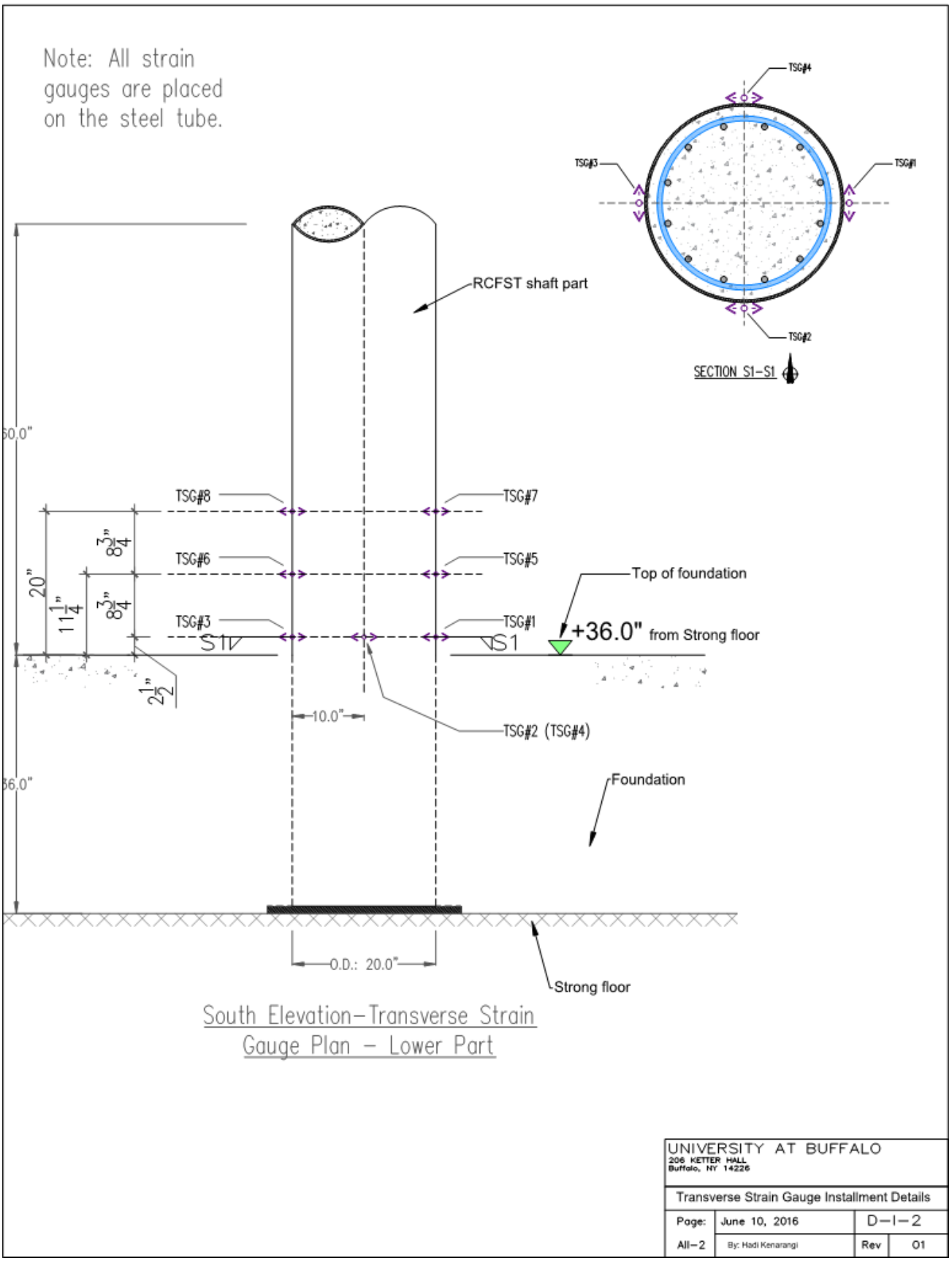
Note: All strain gauges are placed on the steel tube.
TSG#4
TSG#3
TSG#1
TSG#2
SECTION S1-S1
RCFST shaft part
TSG#8
TSG#7
TSG#6
TSG#5
TSG#3
TSG#1
S1
S1
Top of foundation
+36.0" from Strong floor
20"
8 3/4"
11 1/4"
8 3/4"
2 1/2"
10.0"
TSG#2 (TSG#4)
Foundation
O.D.: 20.0"
Strong floor
South Elevation-Transverse Strain Gauge Plan - Lower Part
UNIVERSITY AT BUFFALO
206 KETTER HALL
Buffalo, NY 14226
Transverse Strain Gauge Installment Details
Page:
June 10, 2016
D-I-2
All-2
By: Hadi Kenarangi
Rev
01

M-39

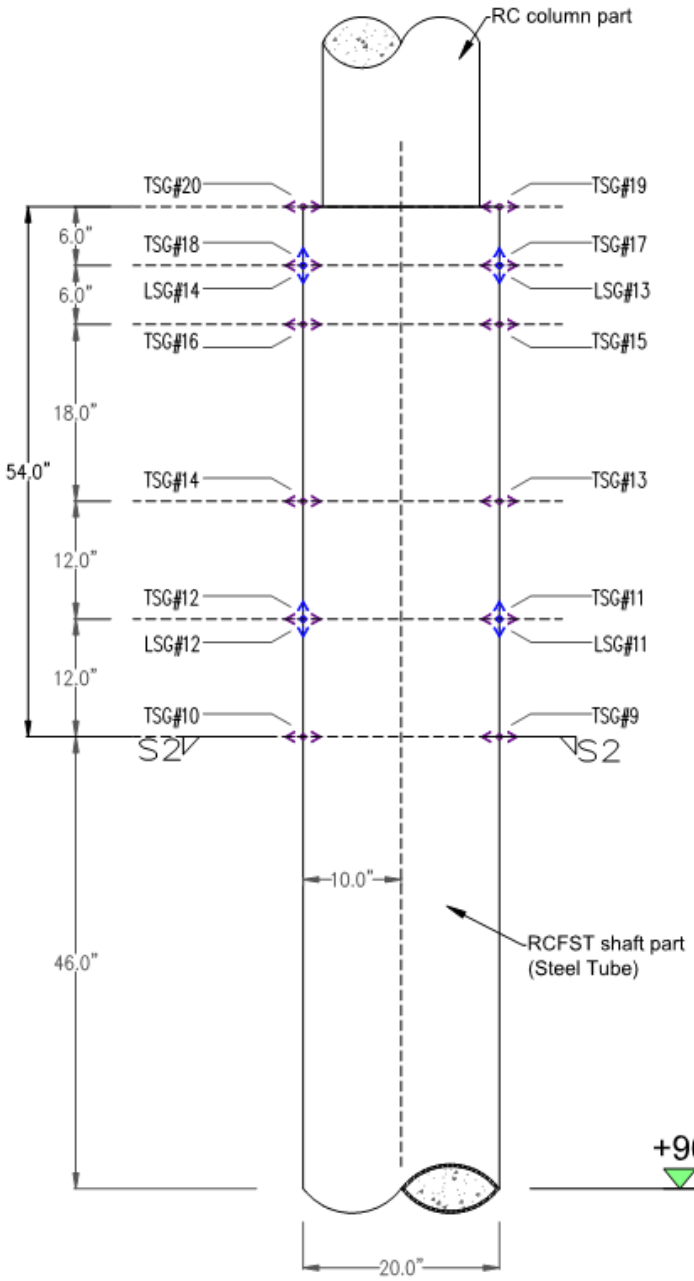

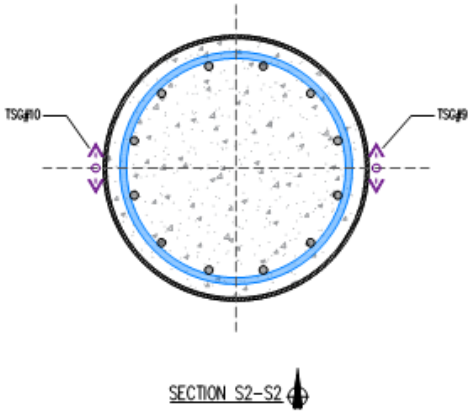

South Elevation-Transverse Strain Gauge Plan - Upper Part

Note:
1- All strain gauges are placed on the steel tube.
2- Upper part strain gauges will be used for Specimen S2R.

UNIVERSITY AT BUFFALO 206 KETTER HALL Buffalo, NY 14226			
Transverse Strain Gauge Installment Details			
Page:	June 10, 2016	D-I-3	
All-3	By: Hadi Kenarangi	Rev	01

M-40

Note: All strain gauges are placed on the steel tube.

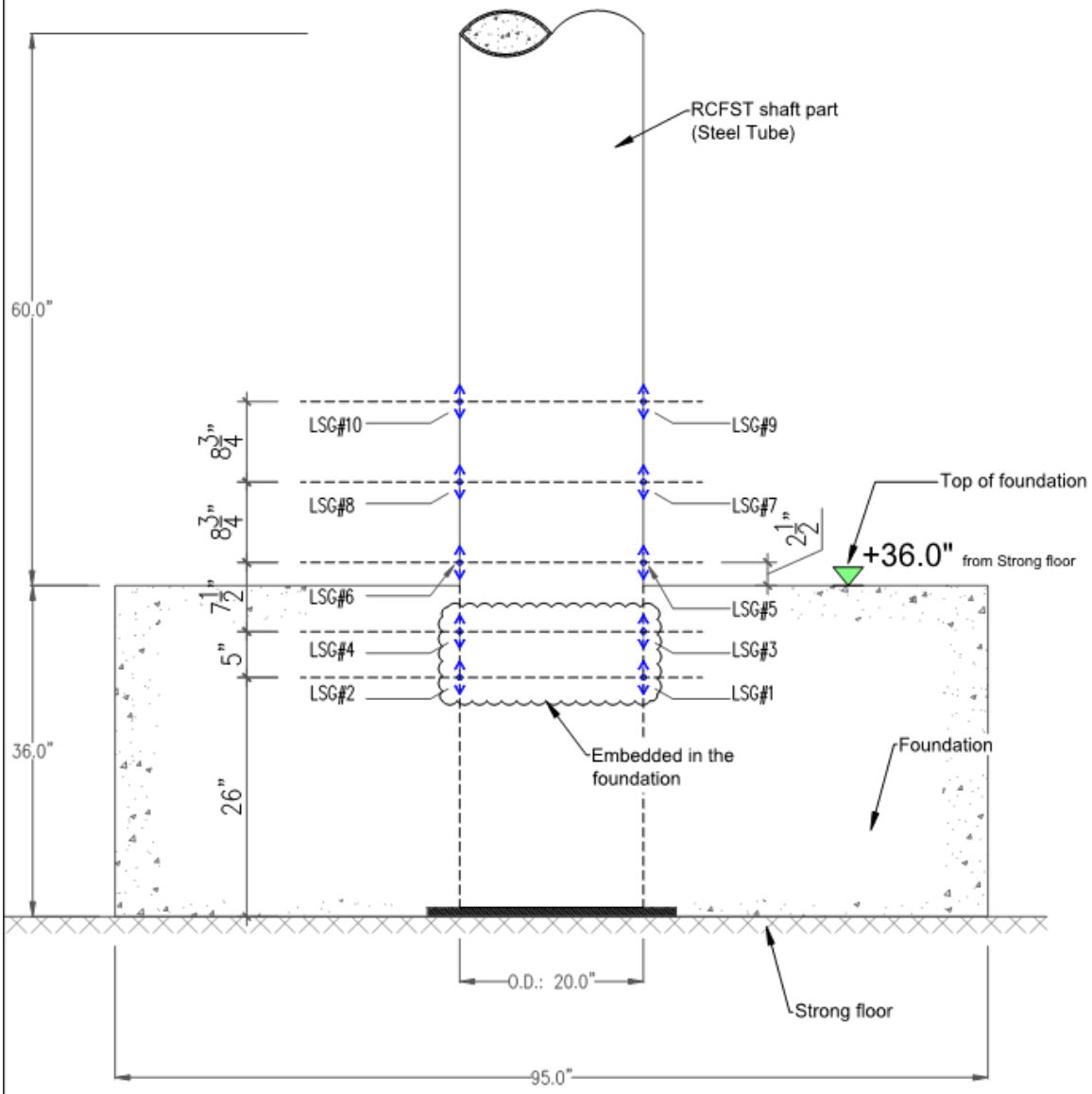

South Elevation–Longitudinal
Strain Gauge Plan – Lower Part

UNIVERSITY AT BUFFALO 206 KETTER HALL Buffalo, NY 14226			
Longitudinal Strain Gauge Installment Details			
Page:	June 10, 2016	D–I–4	
All–4	By: Hadi Kenarangi	Rev	00

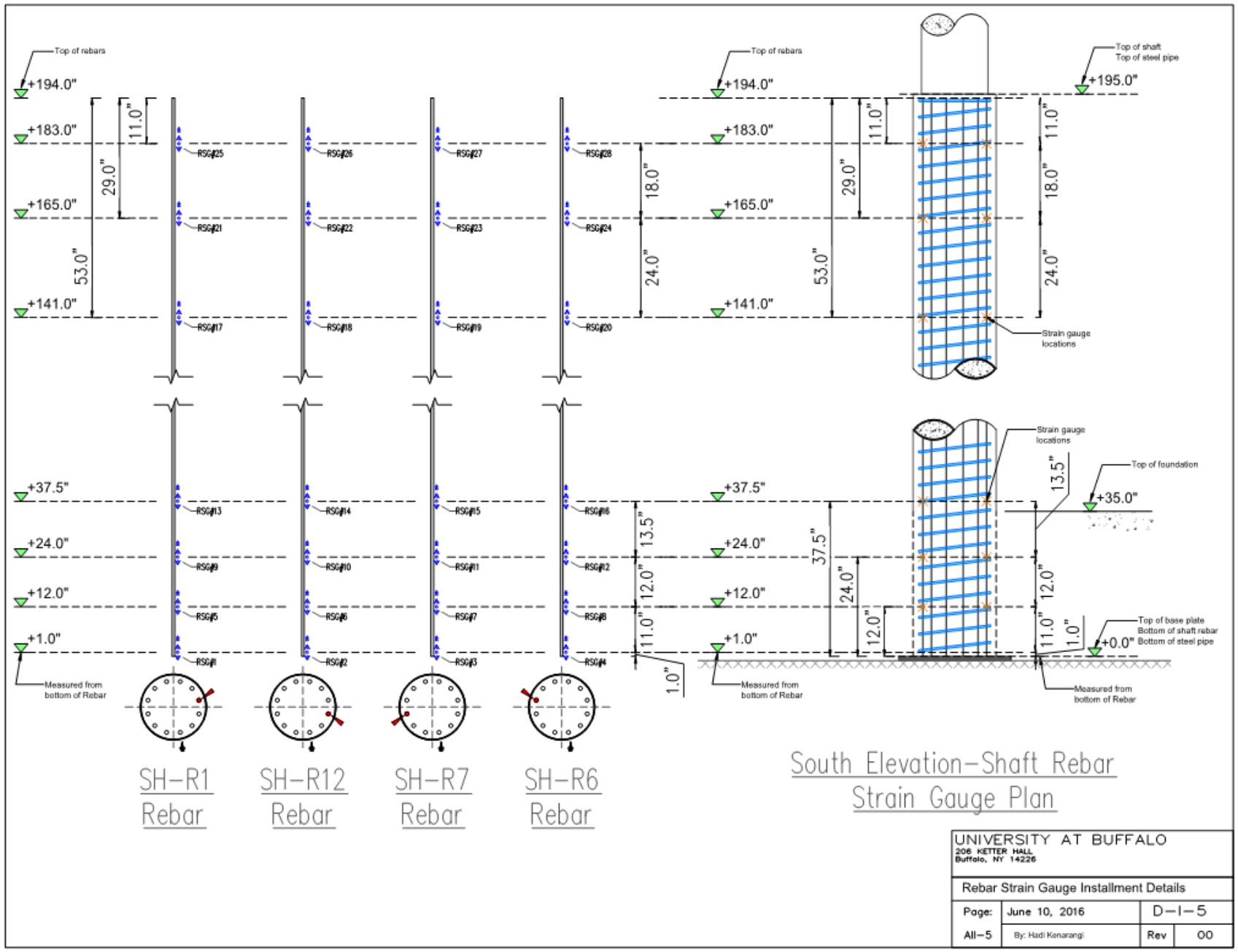
Top of rebars
+194.0"
+183.0"
+165.0"
+141.0"
11.0"
29.0"
53.0"
18.0"
24.0"
RSG#25
RSG#26
RSG#27
RSG#28
RSG#21
RSG#22
RSG#23
RSG#24
RSG#17
RSG#18
RSG#19
RSG#20
+37.5"
+24.0"
+12.0"
+1.0"
13.5"
12.0"
11.0"
1.0"
RSG#13
RSG#14
RSG#15
RSG#16
RSG#9
RSG#10
RSG#11
RSG#12
RSG#5
RSG#6
RSG#7
RSG#8
RSG#1
RSG#2
RSG#3
RSG#4
Measured from bottom of Rebar
Top of shaft
Top of steel pipe
+195.0"
Strain gauge locations
37.5"
24.0"
12.0"
Top of foundation
+35.0"
Top of base plate
Bottom of shaft rebar
Bottom of steel pipe
+0.0"
SH-R1 Rebar
SH-R12 Rebar
SH-R7 Rebar
SH-R6 Rebar
South Elevation-Shaft Rebar Strain Gauge Plan
UNIVERSITY AT BUFFALO
206 KETTER HALL
Buffalo, NY 14226
Rebar Strain Gauge Installment Details
Page:
June 10, 2016
D-I-5
All-5
By: Hadi Kenarangi
Rev
00

Table 2. Shaft rebar strain gauge placement details

No.	Label	Location*, in	Rebar No.	Orientation	Elevation
1	RSG#1	+1	SH-R1	Long.	East
2	RSG#2	+1	SH-R12	Long.	East
3	RSG#3	+1	SH-R7	Long.	West
4	RSG#4	+1	SH-R6	Long.	West
5	RSG#5	+12	SH-R1	Long.	East
6	RSG#6	+12	SH-R12	Long.	East
7	RSG#7	+12	SH-R7	Long.	West
8	RSG#8	+12	SH-R6	Long.	West
9	RSG#9	+24	SH-R1	Long.	East
10	RSG#10	+24	SH-R12	Long.	East
11	RSG#11	+24	SH-R7	Long.	West
12	RSG#12	+24	SH-R6	Long.	West
13	RSG#13	+37.5	SH-R1	Long.	East
14	RSG#14	+37.5	SH-R12	Long.	East
15	RSG#15	+37.5	SH-R7	Long.	West
16	RSG#16	+37.5	SH-R6	Long.	West
17	RSG#17	+141	SH-R1	Long.	East
18	RSG#18	+141	SH-R12	Long.	East
19	RSG#19	+141	SH-R7	Long.	West
20	RSG#20	+141	SH-R6	Long.	West
21	RSG#21	+165	SH-R1	Long.	East
22	RSG#22	+165	SH-R12	Long.	East
23	RSG#23	+165	SH-R7	Long.	West
24	RSG#24	+165	SH-R6	Long.	West
25	RSG#25	+183	SH-R1	Long.	East
26	RSG#26	+183	SH-R12	Long.	East
27	RSG#27	+183	SH-R7	Long.	West
28	RSG#28	+183	SH-R6	Long.	West

* From bottom end of rebar

Table 3. Steel tube strain gauge placement details

No.	Label	Location*, in	Orientation	Elevation
1	LSG#1	+26	Long.	East
2	LSG#2	+26	Long.	West
3	LSG#3	+31	Long.	East
4	LSG#4	+31	Long.	West
5	LSG#5	+38.5	Long.	East
6	LSG#6	+38.5	Long.	West
7	LSG#7	+47.25	Long.	East
8	LSG#8	+47.25	Long.	West
9	LSG#9	+56	Long.	East
10	LSG#10	+56	Long.	West
11	LSG#11**	+154	Long.	East
12	LSG#12**	+154	Long.	West
13	LSG#13**	+190	Long.	East
14	LSG#14**	+190	Long.	West
15	TSG#1	+38.5	Transverse	East
16	TSG#2	+38.5	Transverse	South
17	TSG#3	+38.5	Transverse	West
18	TSG#4	+38.5	Transverse	North
19	TSG#5	+47.25	Transverse	East
20	TSG#6	+47.25	Transverse	West
21	TSG#7	+56	Transverse	East
22	TSG#8	+56	Transverse	West
23	TSG#9**	+142	Transverse	East
24	TSG#10**	+142	Transverse	South
25	TSG#11**	+154	Transverse	West
26	TSG#12**	+154	Transverse	North
27	TSG#13**	+166	Transverse	East
28	TSG#14**	+166	Transverse	South
29	TSG#15**	+184	Transverse	West
30	TSG#16**	+184	Transverse	North
31	TSG#17**	+190	Transverse	East
32	TSG#18**	+190	Transverse	South
33	TSG#19**	+196	Transverse	West
34	TSG#20**	+196	Transverse	North

* From strong floor.
** Used for Specimen S2R only.

UNIVERSITY AT BUFFALO
206 KETTER HALL
Buffalo, NY 14226

Strain Gauge Tables			
Page:	June 10, 2016	D—I—6	
All—6	By: Hadi Kenarangi	Rev	01

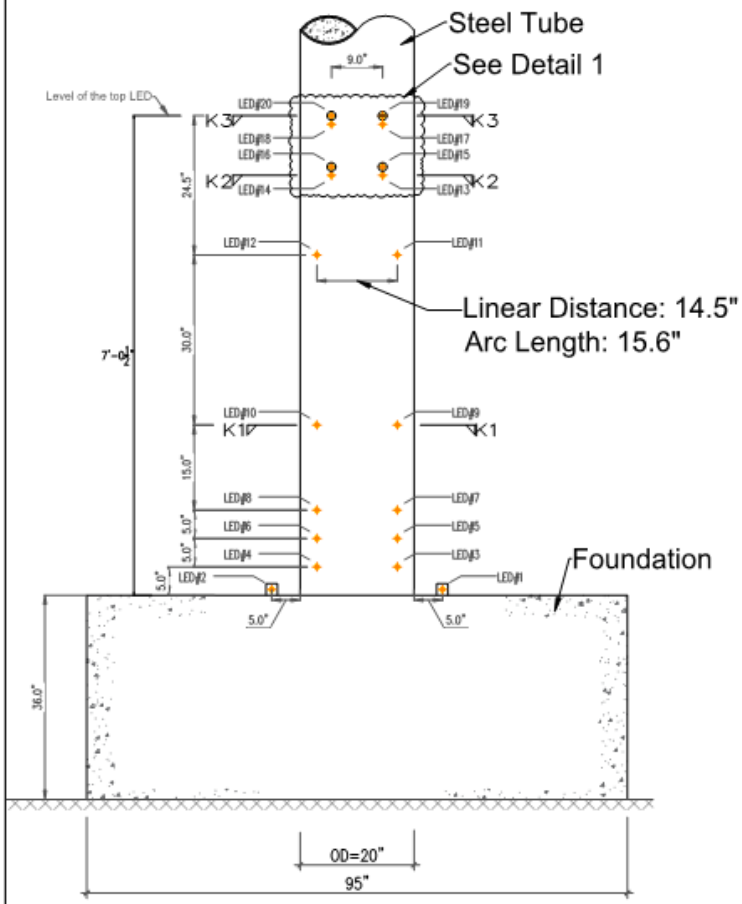

South Elevation–LED Plan

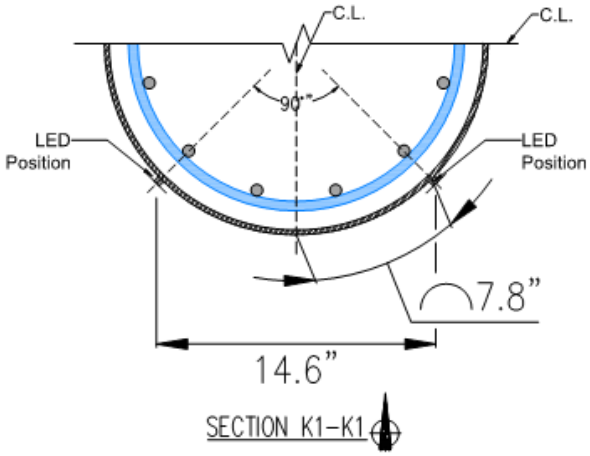

SECTION K1–K1

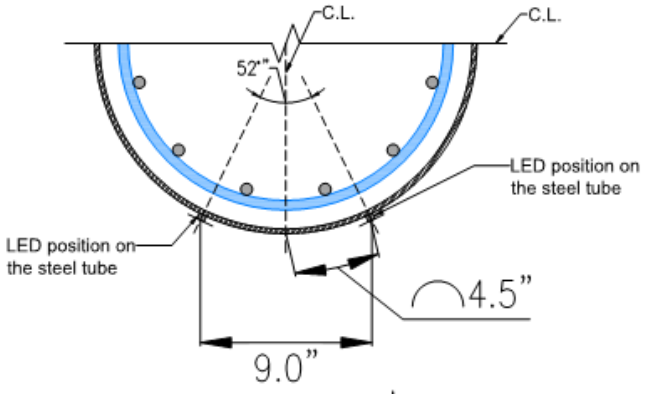

SECTION K2–K2

UNIVERSITY AT BUFFALO 206 KETTER HALL Buffalo, NY 14226			
Krypton LED Installment Details			
Page:	June 10, 2016	D–I–7	
All–7	By: Hadi Kenarangi	Rev	00

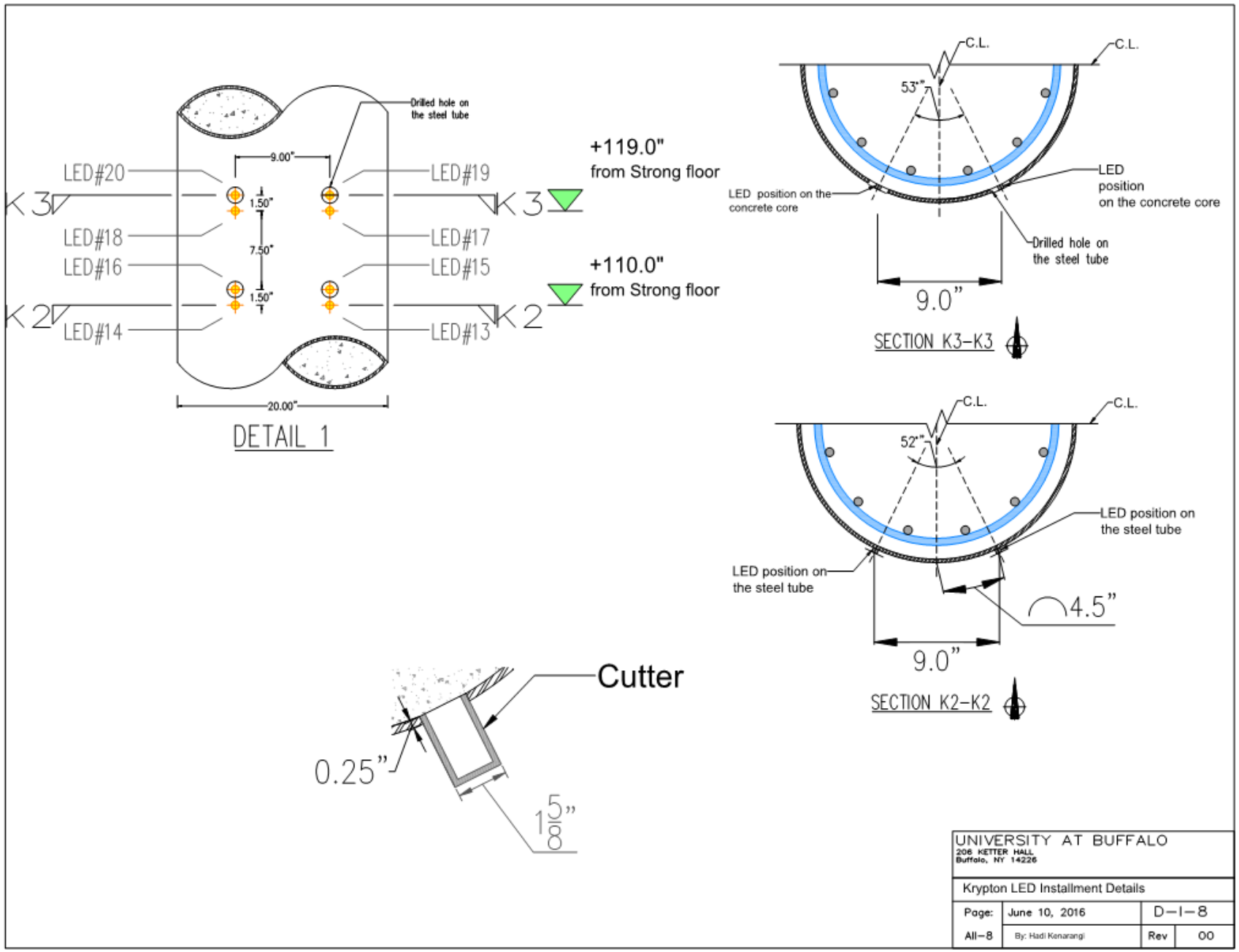

UNIVERSITY AT BUFFALO 206 KETTER HALL Buffalo, NY 14226			
Krypton LED Installment Details			
Page:	June 10, 2016	D-I-8	
All-8	By: Hadi Kenarangi	Rev	00

Table 4. Krypton LEDs placement details

No.	Label	Location*, in	Attached to	Elevation
1	LED#1	+36	Foundation	South
2	LED#2	+36	Foundation	South
3	LED#3	+41	Steel Pipe	South
4	LED#4	+41	Steel Pipe	South
5	LED#5	+46	Steel Pipe	South
6	LED#6	+46	Steel Pipe	South
7	LED#7	+51	Steel Pipe	South
8	LED#8	+51	Steel Pipe	South
9	LED#9	+66	Steel Pipe	South
10	LED#10	+66	Steel Pipe	South
11	LED#11	+96	Steel Pipe	South
12	LED#12	+96	Steel Pipe	South
13	LED#13	+110	Steel Pipe	South
14	LED#14	+110	Steel Pipe	South
15	LED#15	+111.5	Concrete Core	South
16	LED#16	+111.5	Concrete Core	South
17	LED#17	+119	Steel Pipe	South
18	LED#18	+119	Steel Pipe	South
19	LED#19	+120.5	Concrete Core	South
20	LED#20	+120.5	Concrete Core	South

* From strong floor

UNIVERSITY AT BUFFALO
206 KETTER HALL
Buffalo, NY 14226

Krypton LED Installment Table

Page:	June 10, 2016	D–I–9	
All–9	By: Hadi Kenarangi	Rev	00

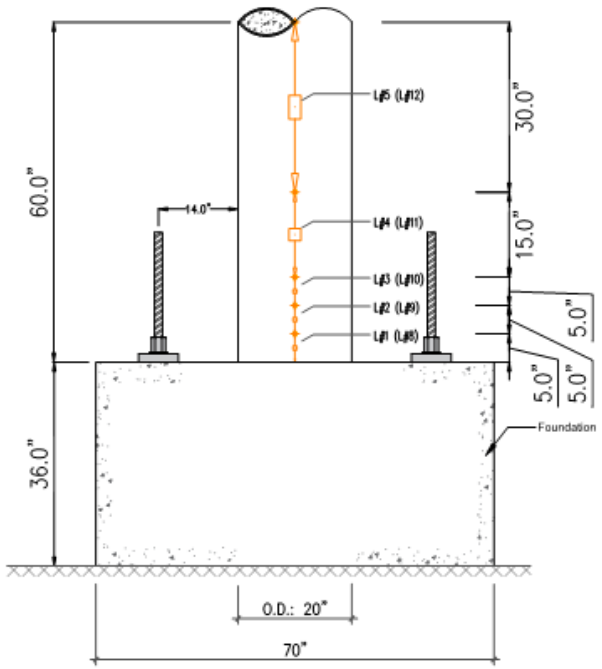

East Elevation–LVDT and String Pot Plan

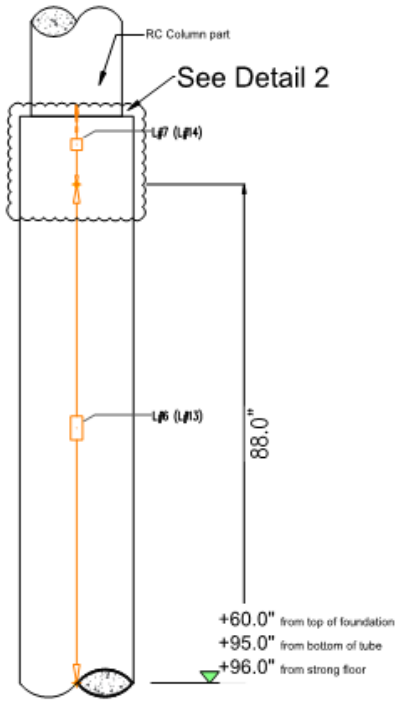

East Elevation–LVDT and String Pot Plan

Table 1. LVDT placement details

No.	Label	Length, in	Location*, in	Orientation	Elevation
1	L#1	5	+36	Vertical	East
2	L#2	5	+41	Vertical	East
3	L#3	5	+46	Vertical	East
4	L#4	15	+51	Vertical	East
5	L#5	30	+66	Vertical	East
6	L#6	88	+96	Vertical	East
7	L#7	14	+184	Vertical	East
8	L#8	5	+36	Vertical	West
9	L#9	5	+41	Vertical	West
10	L#10	5	+46	Vertical	West
11	L#11	15	+51	Vertical	West
12	L#12	30	+66	Vertical	West
13	L#13	88	+96	Vertical	West
14	L#14	14	+184	Vertical	West

* From strong floor to the bottom end attachment point.

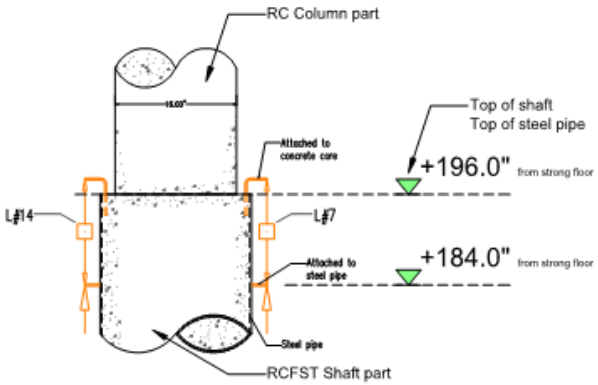

DETAIL 2
South Elevation

UNIVERSITY AT BUFFALO 206 KETTER HALL Buffalo, NY 14226			
LVDT Installment Plan			
Page:	June 10, 2016	D–I–10	
All–10	By: Hadi Kenarangi	Rev	00

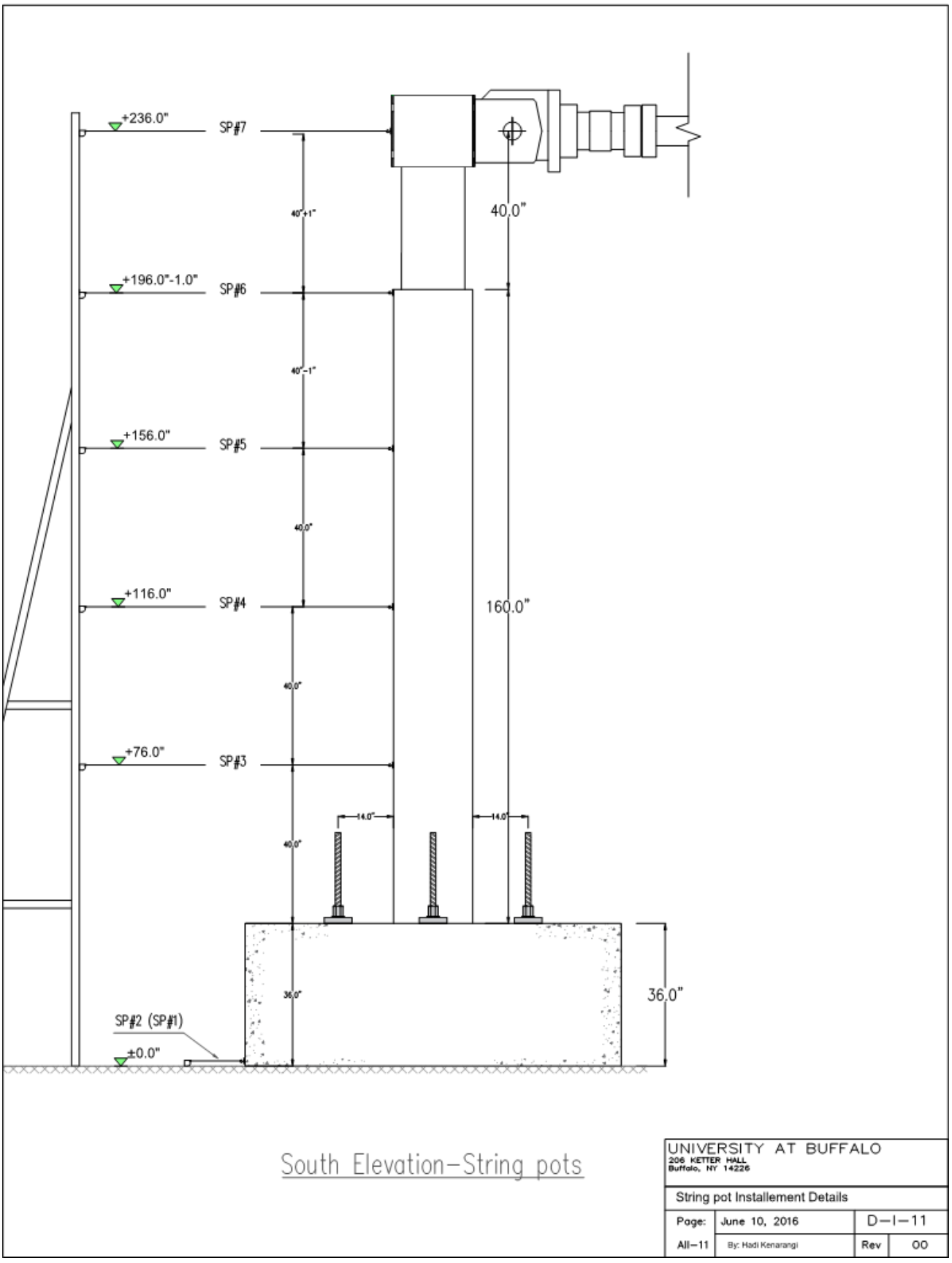

South Elevation–String pots

UNIVERSITY AT BUFFALO 206 KETTER HALL Buffalo, NY 14226			
String pot Installement Details			
Page:	June 10, 2016	D–I–11	
All–11	By: Hadi Kenarangi	Rev	00

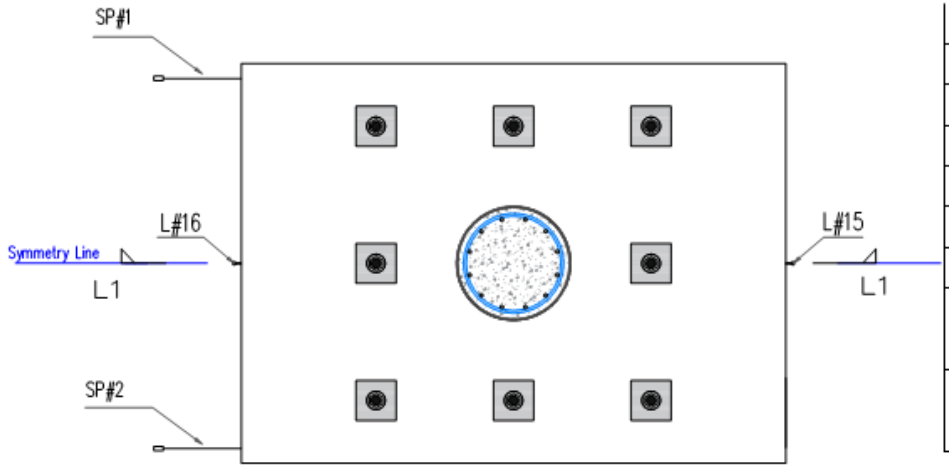

PLAN –Foundation LVDTs

Table 5. String pot placement details

No.	Label	Location*, in	Orientation	Elevation
1	SP#1	+5	Horizontal	West
2	SP#2	+5	Horizontal	West
3	SP#3	+76	Horizontal	West
4	SP#4	+116	Horizontal	West
5	SP#5	+156	Horizontal	West
6	SP#6	+196-1.0	Horizontal	West
7	SP#7	+236	Horizontal	West
8	SP#8	+236	Horizontal	North
9	SP#9	+236	Horizontal	North

* From strong floor.

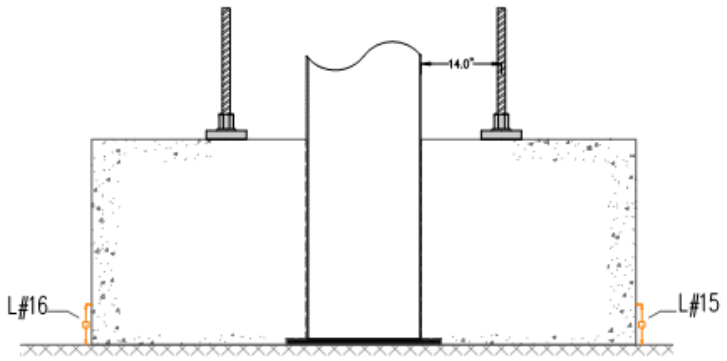

Section L1–L1

Continued Table 1. LVDT placement details

No.	Label	Length, in	Location*, in	Orientation	Elevation
15	L#15	5	+0.0	Vertical	East
16	L#16	5	+0.0	Vertical	West

* From strong floor to the bottom end attachment point.

UNIVERSITY AT BUFFALO
206 KETTER HALL
Buffalo, NY 14226

String pot Installement Details

Page:	June 10, 2016	D–I–12	
All–12	By: Hadi Kenarangi	Rev	00

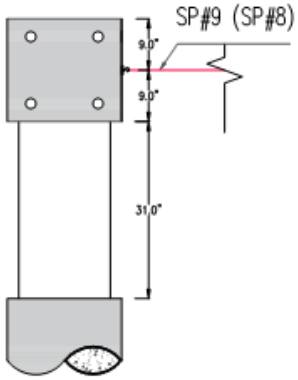

East Elevation
(Top String pots attachment)

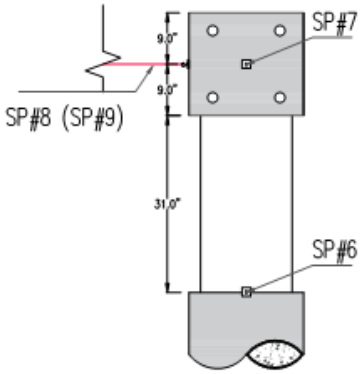

West Elevation
(Top String pots attachment)

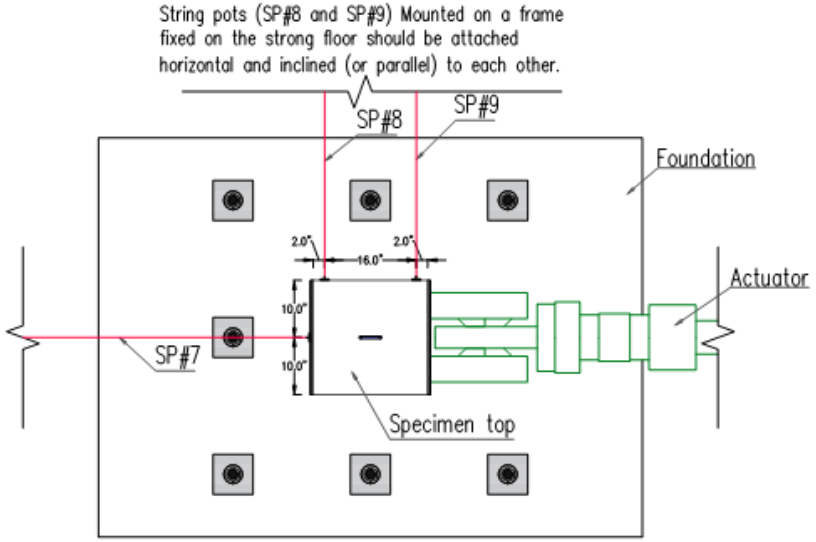

Top Elevation
LVDT attachment

UNIVERSITY AT BUFFALO 206 KETTER HALL Buffalo, NY 14226			
String pot Installement Details			
Page:	June 10, 2016		D-I-13
All-13	By: Hadi Kenarangi	Rev	00

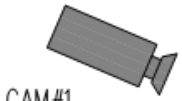

CAM#1

Mounted on the strong floor to monitor global view of the Specimen.

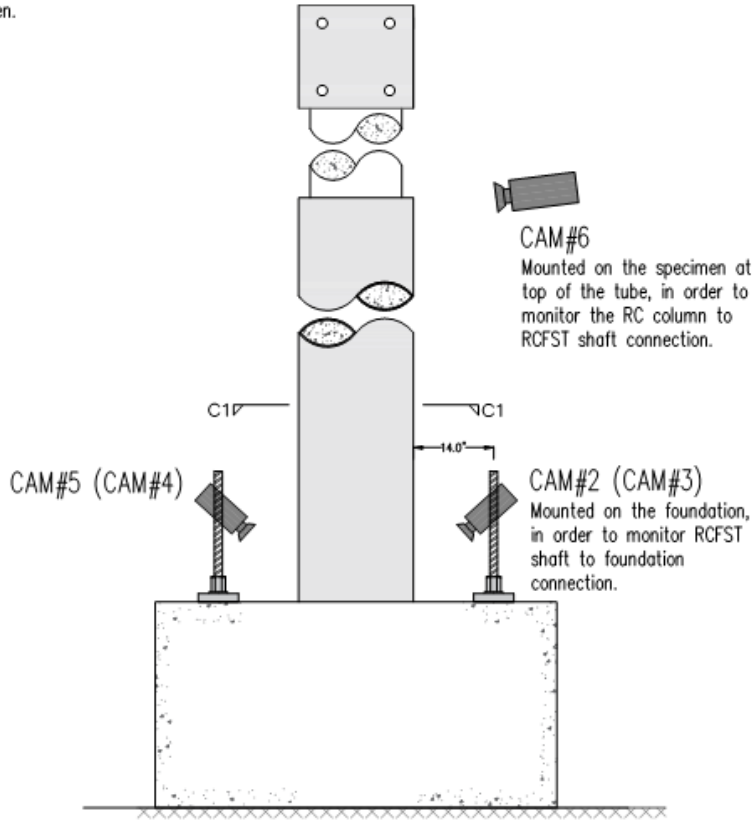

East Elevation–Video camera Plan

Table 5. Video camera placement details

No.	Label	Mounted on	Direction	Elevation
1	CAM#1	Strong floor	Global	South
2	CAM#2	Foundation top	Bottom of the tube	North
3	CAM#3	Foundation top	Bottom of the tube	North
4	CAM#4	Foundation top	Bottom of the tube	South
5	CAM#5	Foundation top	Bottom of the tube	South
6	CAM#6	Specimen	Column to Shaft	North
7	CAM#7	Mobile	Varies	Varies

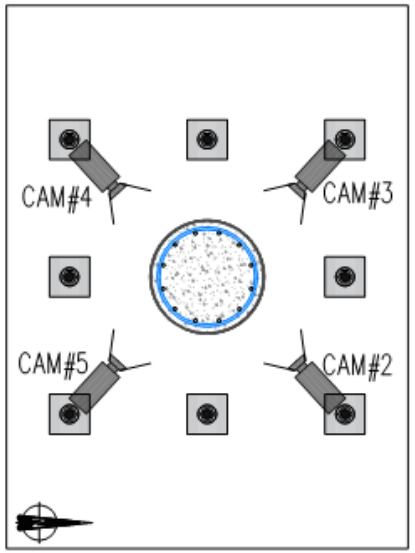

Section C1–C1

UNIVERSITY AT BUFFALO
206 KETTER HALL
Buffalo, NY 14226

Video Camera Installement Details

Page:	June 10, 2016	D–I–14	
All–14	By: Hadi Kenarangi	Rev	01

Note: All strain gauges are placed on the steel tube.

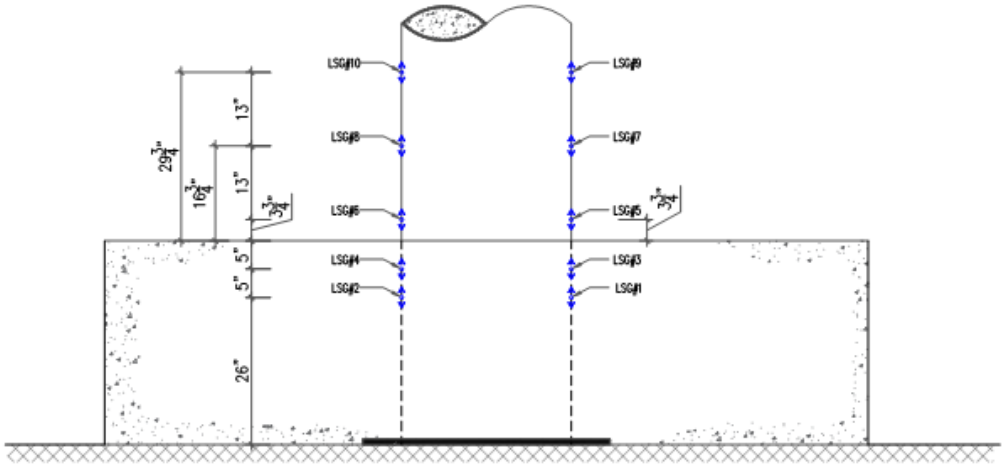

South Elevation–Longitudinal Strain Gauge Plan – Lower Part

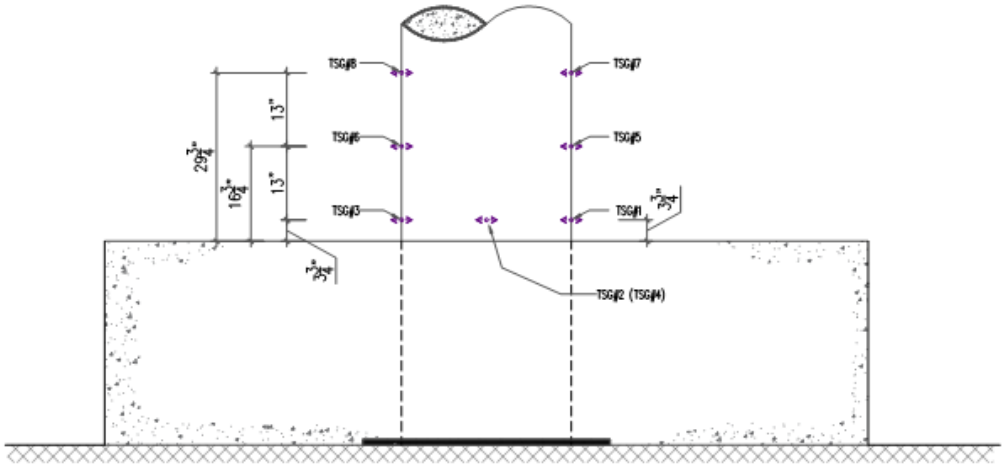

South Elevation–Transverse Strain Gauge Plan – Lower Part

UNIVERSITY AT BUFFALO 206 KETTER HALL Buffalo, NY 14226			
Transverse Strain Gauge Installment Details			
Page:	October 18, 2016	D–I–2	
All–2	By: Hadi Kenarangi	Rev	01

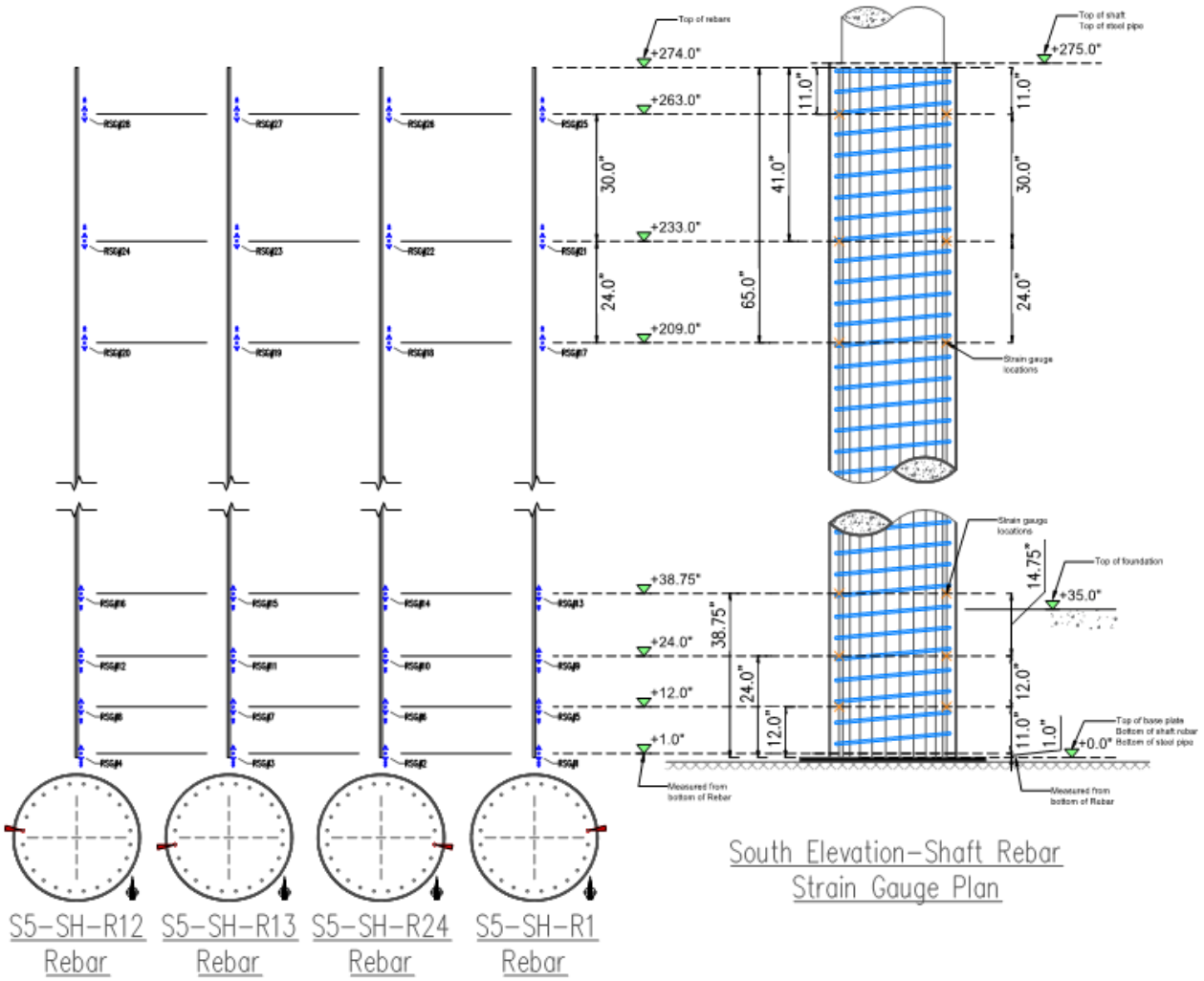

South Elevation–Shaft Rebar Strain Gauge Plan

UNIVERSITY AT BUFFALO 206 KETTER HALL Buffalo, NY 14226			
Rebar Strain Gauge Installment Details			
Page:	October 18, 2016	D–I–5	
All–5	By: Hadi Kenarangi	Rev	00

Table 2. Shaft rebar strain gauge placement details

No.	Label	Location*, in	Rebar No.	Orientation	Elevation
1	RSG#1	+1	S5-SH-R1	Long.	East
2	RSG#2	+1	S5-SH-R24	Long.	East
3	RSG#3	+1	S5-SH-R13	Long.	West
4	RSG#4	+1	S5-SH-R12	Long.	West
5	RSG#5	+12	S5-SH-R1	Long.	East
6	RSG#6	+12	S5-SH-R24	Long.	East
7	RSG#7	+12	S5-SH-R13	Long.	West
8	RSG#8	+12	S5-SH-R12	Long.	West
9	RSG#9	+24	S5-SH-R1	Long.	East
10	RSG#10	+24	S5-SH-R24	Long.	East
11	RSG#11	+24	S5-SH-R13	Long.	West
12	RSG#12	+24	S5-SH-R12	Long.	West
13	RSG#13	+38.75	S5-SH-R1	Long.	East
14	RSG#14	+38.75	S5-SH-R24	Long.	East
15	RSG#15	+38.75	S5-SH-R13	Long.	West
16	RSG#16	+38.75	S5-SH-R12	Long.	West
17	RSG#17	+209	S5-SH-R1	Long.	East
18	RSG#18	+209	S5-SH-R24	Long.	East
19	RSG#19	+209	S5-SH-R13	Long.	West
20	RSG#20	+209	S5-SH-R12	Long.	West
21	RSG#21	+233	S5-SH-R1	Long.	East
22	RSG#22	+233	S5-SH-R24	Long.	East
23	RSG#23	+233	S5-SH-R13	Long.	West
24	RSG#24	+233	S5-SH-R12	Long.	West
25	RSG#25	+263	S5-SH-R1	Long.	East
26	RSG#26	+263	S5-SH-R24	Long.	East
27	RSG#27	+263	S5-SH-R13	Long.	West
28	RSG#28	+263	S5-SH-R12	Long.	West

* From bottom end of rebar

Table 3. Steel tube strain gauge placement details

No.	Label	Location*, in	Orientation	Elevation
1	LSG#1	+26	Long.	East
2	LSG#2	+26	Long.	West
3	LSG#3	+31	Long.	East
4	LSG#4	+31	Long.	West
5	LSG#5	+39.75	Long.	East
6	LSG#6	+39.75	Long.	West
7	LSG#7	+52.75	Long.	East
8	LSG#8	+52.75	Long.	West
9	LSG#9	+65.75	Long.	East
10	LSG#10	+65.75	Long.	West
11	TSG#1	+39.75	Transverse	East
12	TSG#2	+39.75	Transverse	South
13	TSG#3	+39.75	Transverse	West
14	TSG#4	+39.75	Transverse	North
15	TSG#5	+52.75	Transverse	East
16	TSG#6	+52.75	Transverse	West
17	TSG#7	+65.75	Transverse	East
18	TSG#8	+65.75	Transverse	West

* From strong floor.

UNIVERSITY AT BUFFALO
206 KETTER HALL
Buffalo, NY 14226

Strain Gauge Tables			
Page:	October 18, 2016	D—I—6	
All—6	By: Hadi Kenarangi	Rev	01

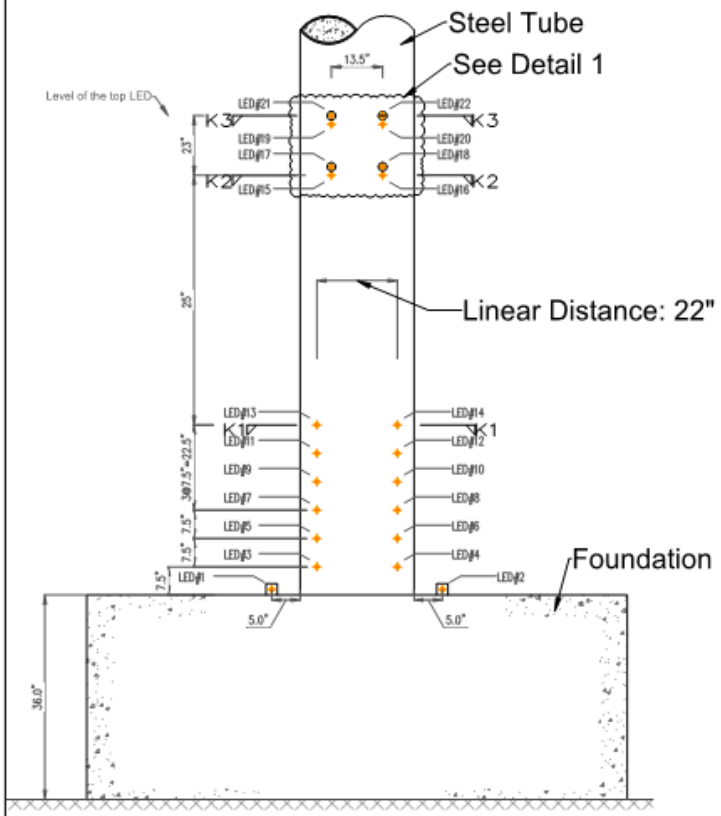

South Elevation–LED Plan
Not to scale

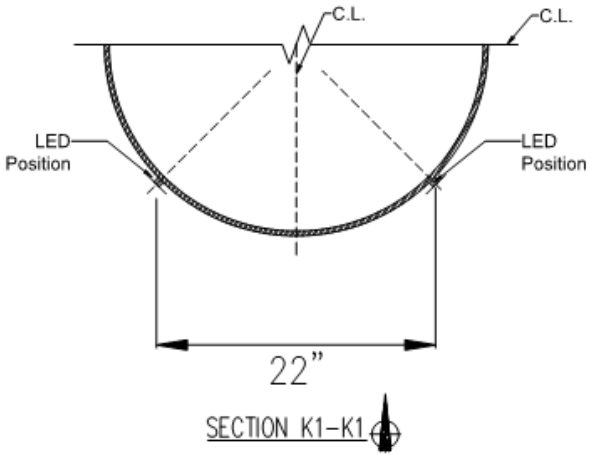

SECTION K1–K1

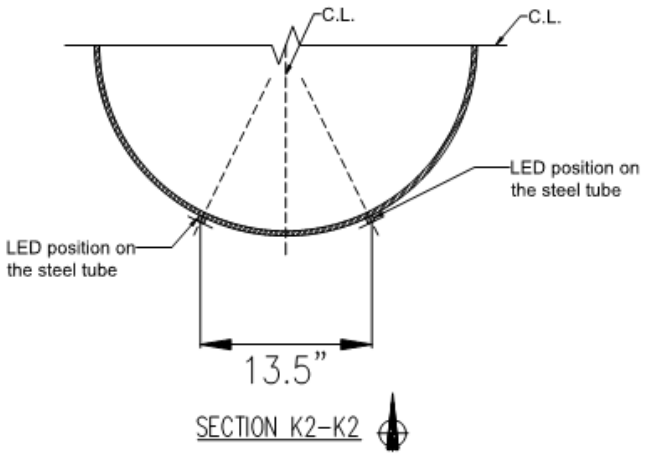

SECTION K2–K2

UNIVERSITY AT BUFFALO 206 KETTER HALL Buffalo, NY 14226			
Krypton LED Installment Details			
Page:	October 18, 2016	D–I–7	
All–7	By: Hadi Kenarangi	Rev	00

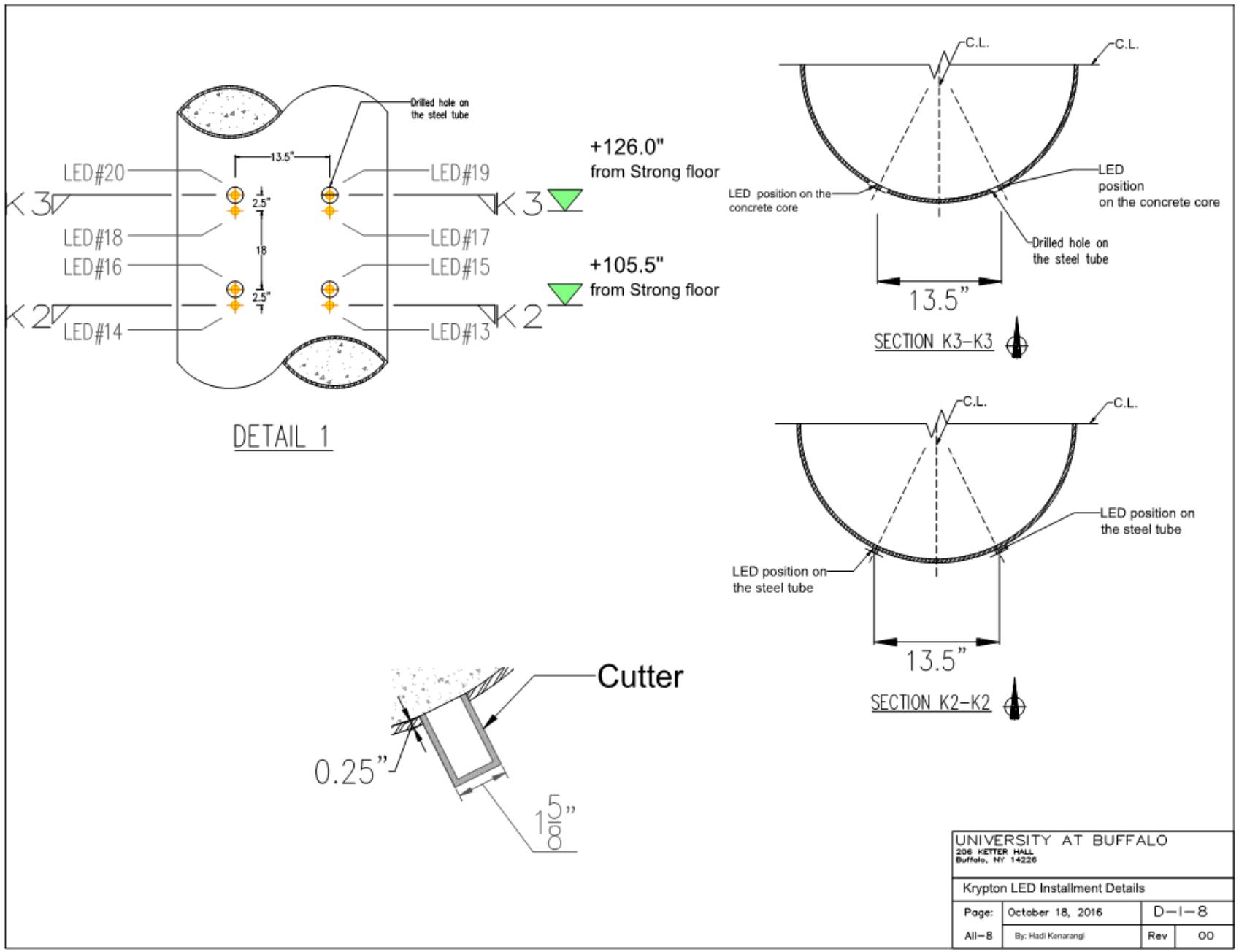
Drilled hole on the steel tube
13.5"
LED#20
LED#19
LED#18
LED#17
LED#16
LED#15
LED#14
LED#13
2.5"
18
2.5"
K 3
K 3
K 2
K 2
+126.0"
from Strong floor
+105.5"
from Strong floor
DETAIL 1
C.L.
C.L.
LED position on the concrete core
LED position on the concrete core
Drilled hole on the steel tube
13.5"
SECTION K3-K3
C.L.
C.L.
LED position on the steel tube
LED position on the steel tube
13.5"
SECTION K2-K2
Cutter
0.25"
1 5/8"
UNIVERSITY AT BUFFALO
206 KETTER HALL
Buffalo, NY 14226
Krypton LED Installment Details
Page:
October 18, 2016
D-I-8
All-8
By: Hadi Kenarangi
Rev
00

Table 4. Krypton LEDs placement details

No.	Label	Location*, in	Attached to	Elevation
1	LED#1	+36	Foundation	South
2	LED#2	+36	Foundation	South
3	LED#3	+41	Steel Pipe	South
4	LED#4	+41	Steel Pipe	South
5	LED#5	+46	Steel Pipe	South
6	LED#6	+46	Steel Pipe	South
7	LED#7	+51	Steel Pipe	South
8	LED#8	+51	Steel Pipe	South
9	LED#9	+66	Steel Pipe	South
10	LED#10	+66	Steel Pipe	South
11	LED#11	+96	Steel Pipe	South
12	LED#12	+96	Steel Pipe	South
13	LED#13	+110	Steel Pipe	South
14	LED#14	+110	Steel Pipe	South
15	LED#15	+111.5	Concrete Core	South
16	LED#16	+111.5	Concrete Core	South
17	LED#17	+119	Steel Pipe	South
18	LED#18	+119	Steel Pipe	South
19	LED#19	+120.5	Concrete Core	South
20	LED#20	+120.5	Concrete Core	South

* From strong floor

UNIVERSITY AT BUFFALO
206 KETTER HALL
Buffalo, NY 14226

Krypton LED Installment Table

Page:	October 18, 2016	D—I—9	
All—9	By: Hadi Kenarangi	Rev	00

Table 1. Longitudinal string pot placement details

No.	Label	Length, in	Location*, in	Orientation	Elevation
1	L#1	7.5	+36	Vertical	East
2	L#2	7.5	+43.5	Vertical	East
3	L#3	7.5	+51.0	Vertical	East
4	L#4	22.5	+58.5	Vertical	East
5	L#5	45.0	+81.0	Vertical	East
6	L#6	132.0	+126.0	Vertical	East
7	L#7	18.0	+258.0	Vertical	East
8	L#8	7.5	+36	Vertical	West
9	L#9	7.5	+43.5	Vertical	West
10	L#10	7.5	+51.0	Vertical	West
11	L#11	22.5	+58.5	Vertical	West
12	L#12	45.0	+81.0	Vertical	West
13	L#13	132.0	+126.0	Vertical	West
14	L#14	18.0	+258.0	Vertical	West

* From strong floor to the bottom end attachment point.

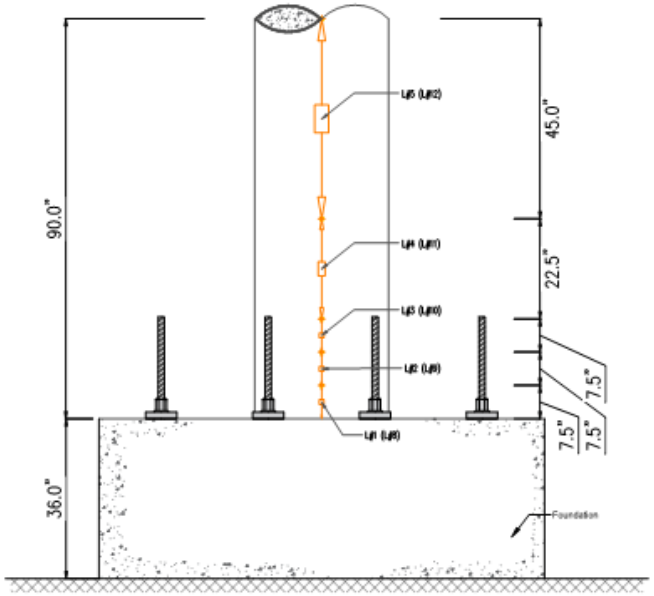

East Elevation–LVDT and String Pot Plan (lower half)

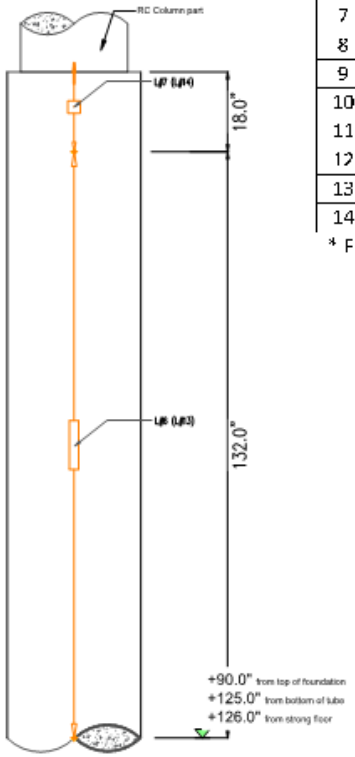

East Elevation–LVDT and String Pot Plan (upper half)

UNIVERSITY AT BUFFALO 206 KETTER HALL Buffalo, NY 14226			
LVDT Installment Plan			
Page:	October 18, 2016	D–I–10	
All–10	By: Hadi Kenarangi	Rev	00

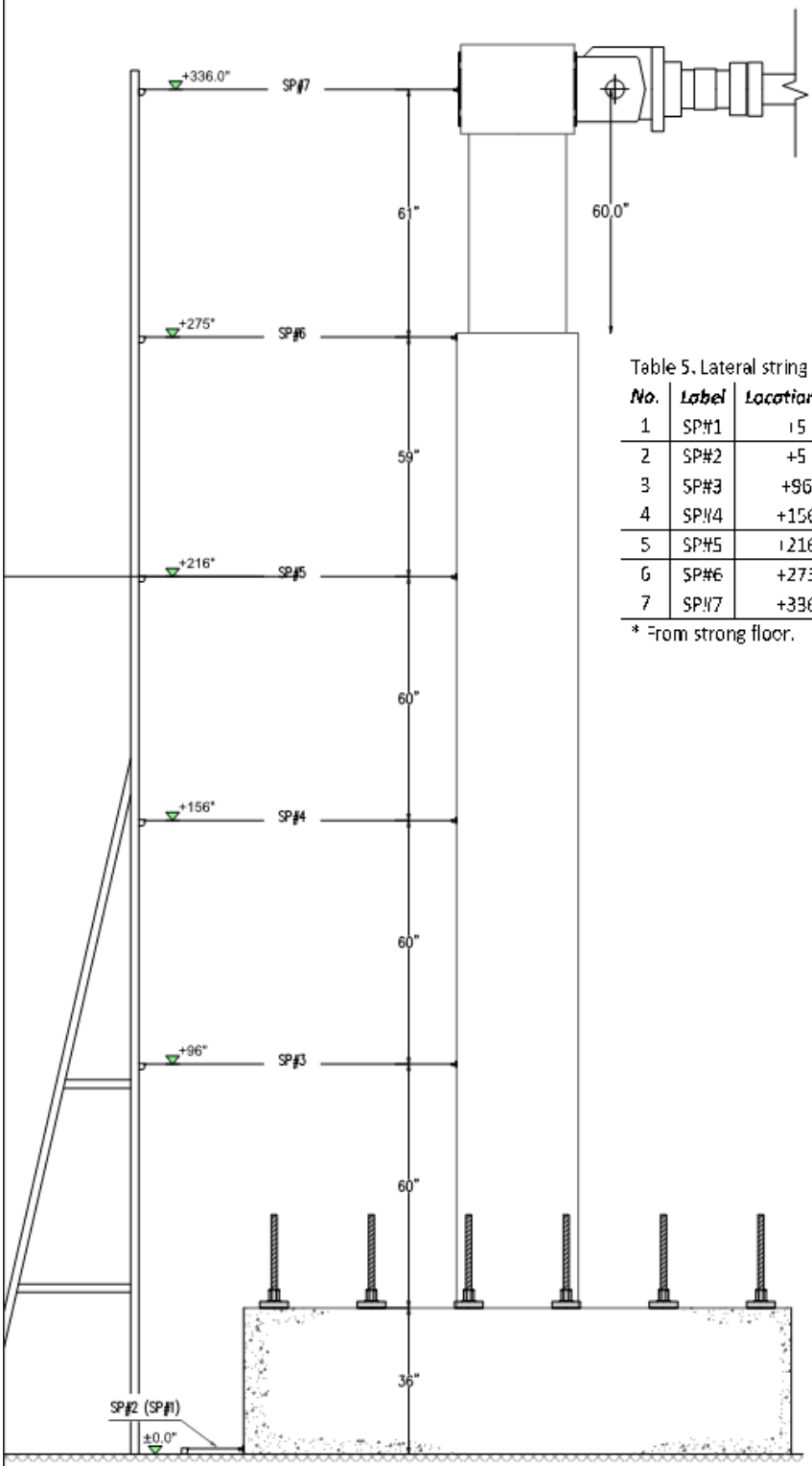

South Elevation–String pots

Table 5. Lateral string pot placement details

No.	Label	Location*, in	Orientation	Elevation
1	SP#1	+5	Horizontal	West
2	SP#2	+5	Horizontal	West
3	SP#3	+96	Horizontal	West
4	SP#4	+156	Horizontal	West
5	SP#5	+216	Horizontal	West
6	SP#6	+275	Horizontal	West
7	SP#7	+336	Horizontal	West

* From strong floor.

UNIVERSITY AT BUFFALO
206 KETTER HALL
Buffalo, NY 14226

String pot Installement Details

Page:	October 18, 2016	D–I–11	
All–11	By: Hadi Kenarangi	Rev	00

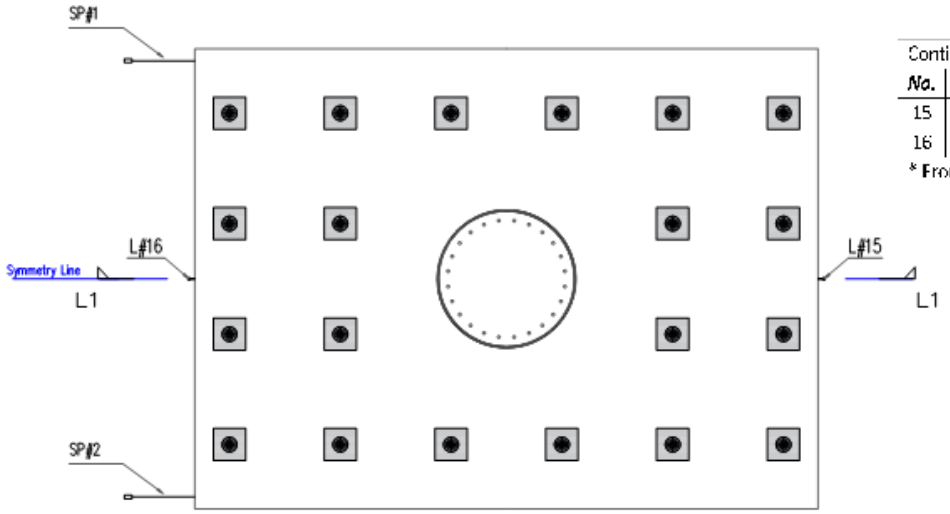

PLAN –Foundation LVDTs

Continued Table 1. LVDT placement details

No.	Label	Length, in	Location*, in	Orientation	Elevation
15	L#15	5	+0.0	Vertical	East
16	L#16	5	+0.0	Vertical	West

* From strong floor to the bottom end attachment point.

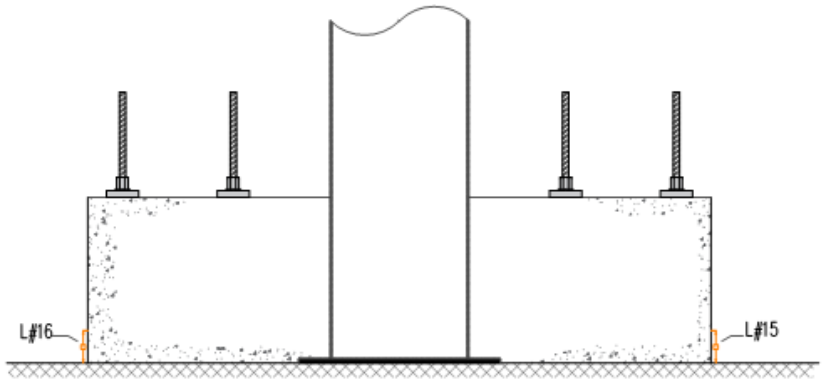

Section L1–L1

UNIVERSITY AT BUFFALO
206 KETTER HALL
Buffalo, NY 14226

String pot Installement Details

Page:	October 18, 2016	D–I–12	
All–12	By: Hadi Kenarangi	Rev	00

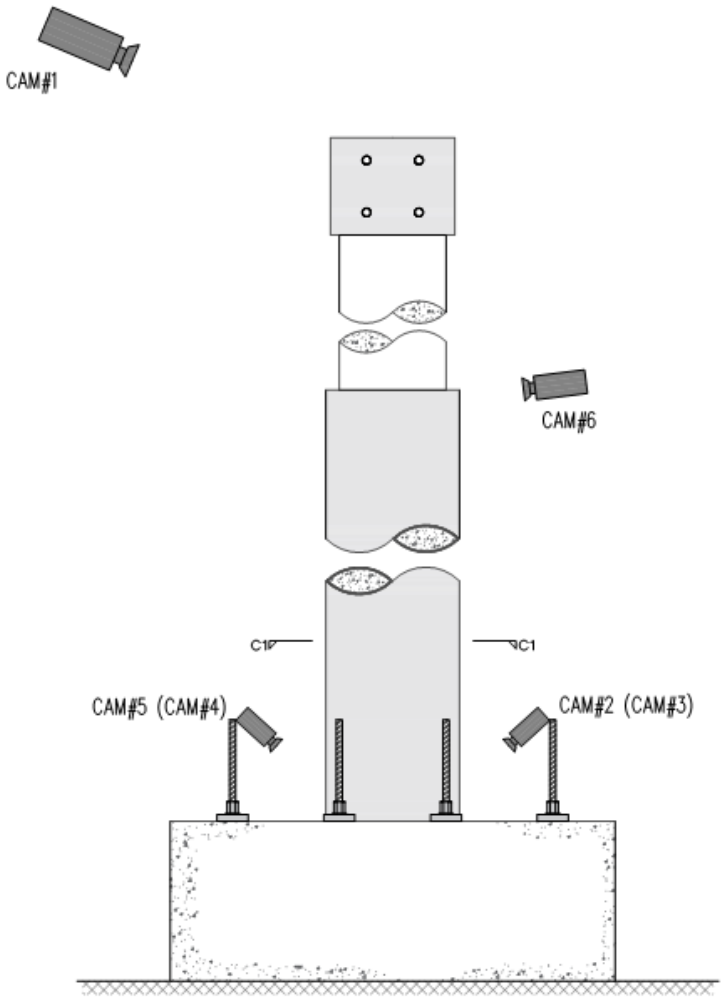

East Elevation–Video camera Plan

Table 6. Video camera placement details

No.	Label	Mounted on	Direction	Elevation
1	CAM#1	Strong floor	Global	South
2	CAM#2	Foundation top	Bottom of the tube	North
3	CAM#3	Foundation top	Bottom of the tube	North
4	CAM#4	Foundation top	Bottom of the tube	South
5	CAM#5	Foundation top	Bottom of the tube	South
6	CAM#6	Specimen	Column to Shaft	North
7	CAM#7	Mobile	Varies	Varies

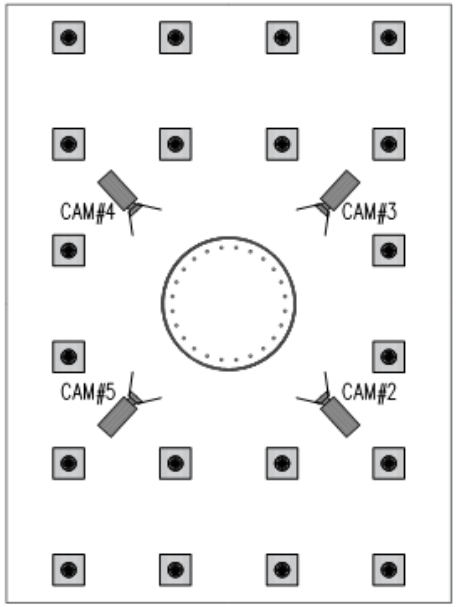

Section C1–C1

UNIVERSITY AT BUFFALO
206 KETTER HALL
Buffalo, NY 14226

Video Camera Installement Details

Page:	October 18, 2016	D–I–14	
All–14	By: Hadi Kenarangi	Rev	01

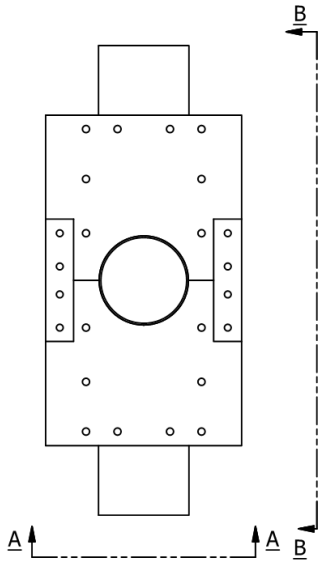

Base

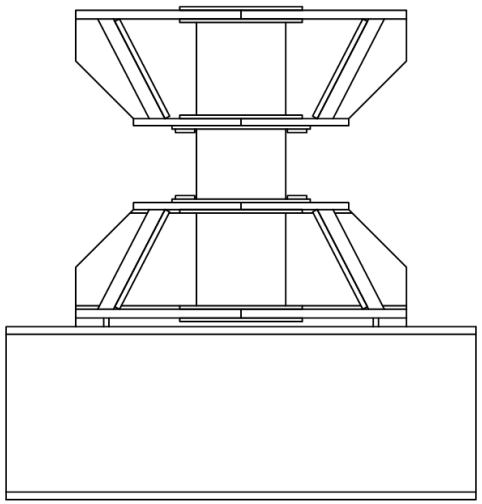

VIEW B-B
SCALE 0.09

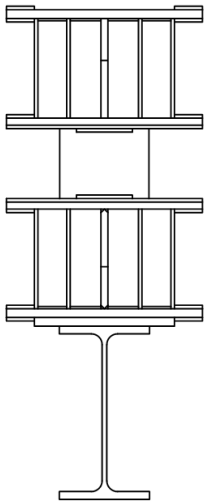

VIEW A-A
SCALE 0.09

Final Assembly in
SEESL lab.

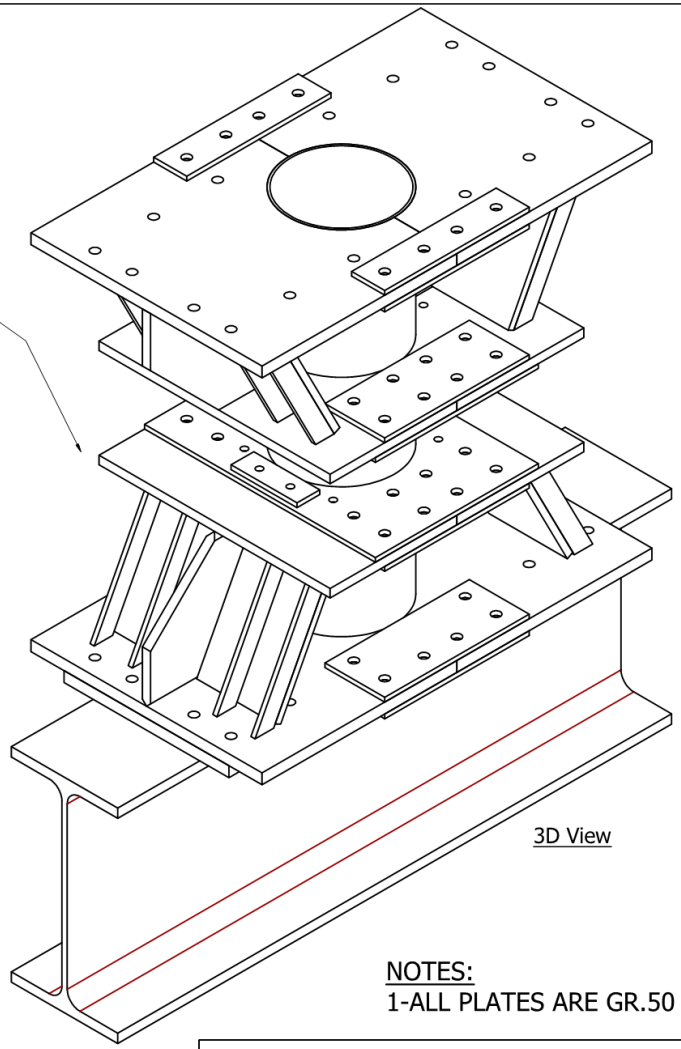

3D View

NOTES:
1-ALL PLATES ARE GR.50 STEEL

UNIVERSITY AT BUFFALO

206 KETTER HALL
BUFFALO, NY, 14226

Title: 12OD Shear Specimen Alternative Design No. 2

Page: 1of11	6/27/2016	STATUS: For Mnfctrng
	BY: Hadi Kenarangi	REV: 1

M-62

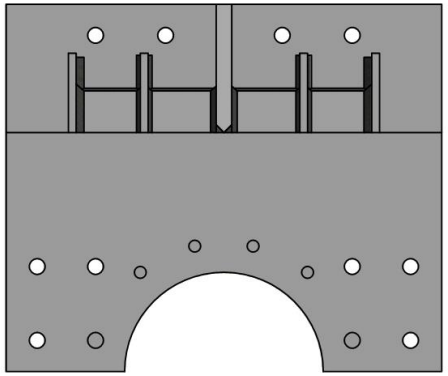

BASE

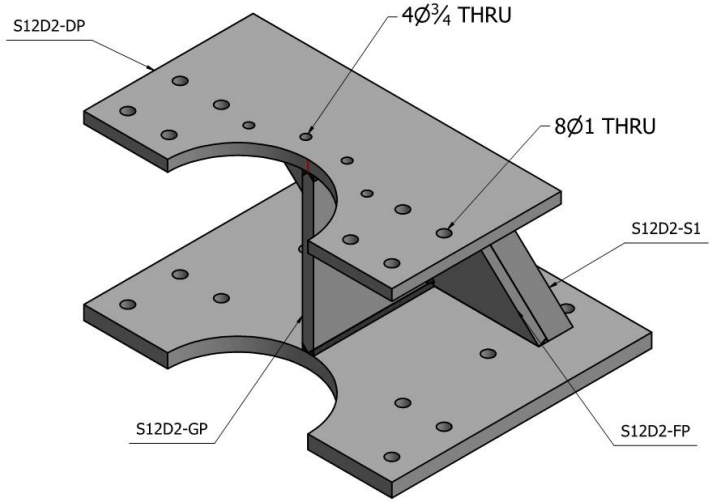

3D View
FRONT

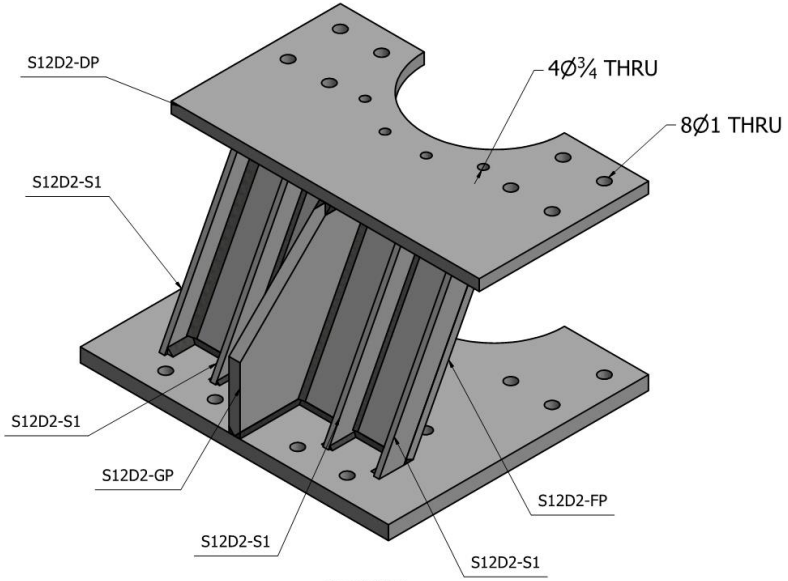

3D VIEW
BACK

NOTES:
1-ALL PLATES ARE GR.50 STEEL
2- 4 SERIES OF THIS ASSEMBLY IS NEEDED.

UNIVERSITY AT BUFFALO 206 KETTER HALL BUFFALO, NY, 14226		
Title: 12OD Shear Specimen Alternative Design No. 2		
Page: 2of11	6/27/2016	STATUS: For Mnfctrng
	BY: Hadi Kenarangi	REV: 1

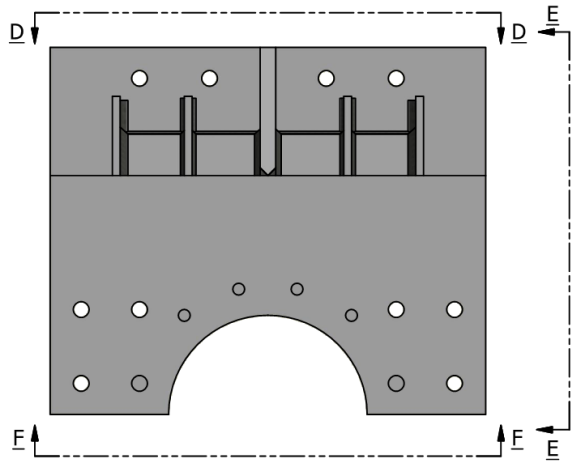

BASE

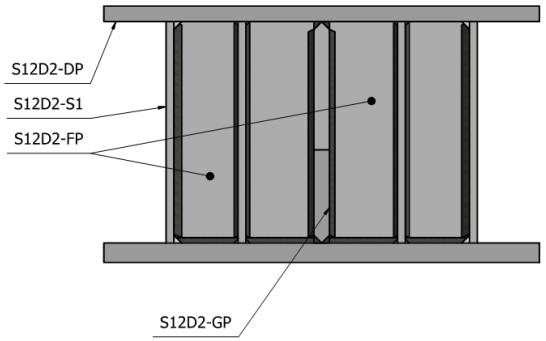

VIEW D-D
SCALE 0.2

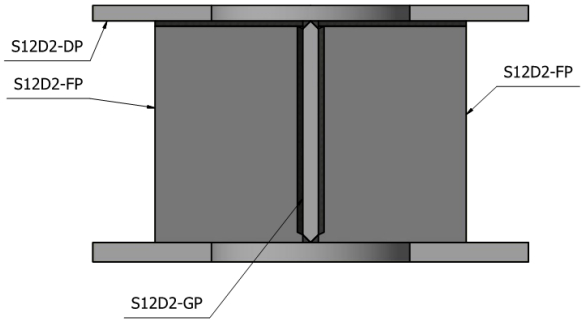

VIEW F-F
SCALE 0.2

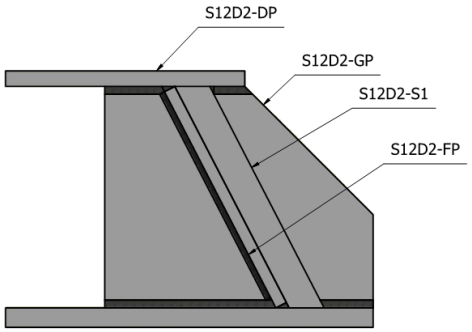

VIEW E-E
SCALE 0.2

NOTES:
1-ALL PLATES ARE GR.50 STEEL
2- 4 SERIES OF THIS ASSEMBLY IS NEEDED.

UNIVERSITY AT BUFFALO

206 KETTER HALL
BUFFALO, NY, 14226

Title: 12OD Shear Specimen Alternative Design No. 2

Page: 3of11	6/27/2016	STATUS: For Mnfctrng
	BY: Hadi Kenarangi	REV: 1

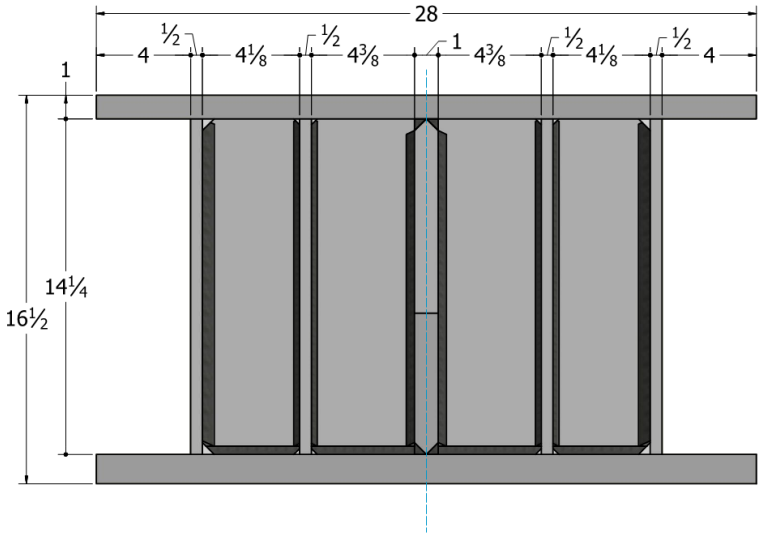

VIEW D-D

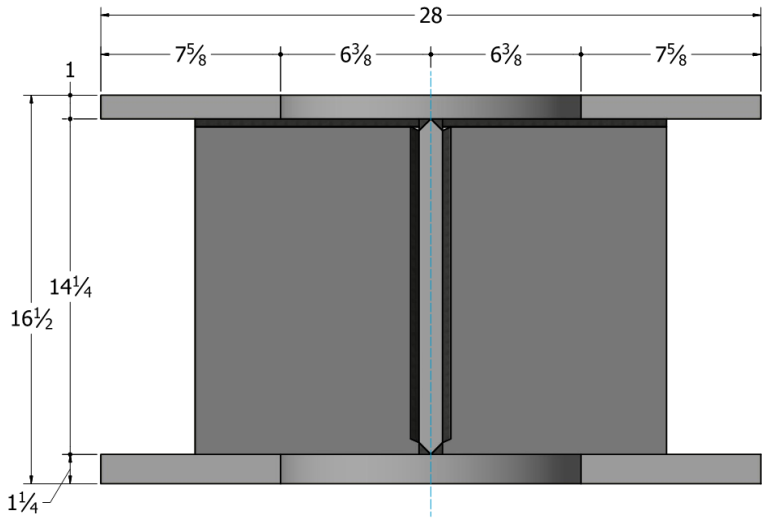

VIEW F-F

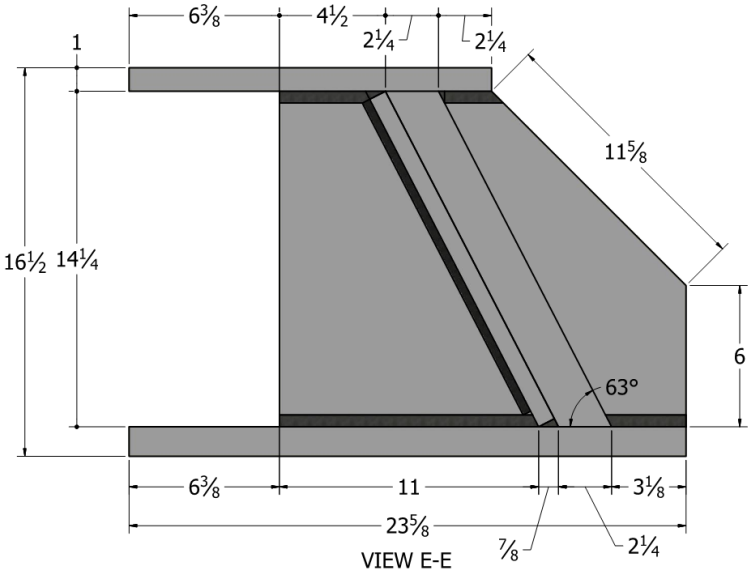

VIEW E-E

NOTES:
1-ALL PLATES ARE GR.50 STEEL
2- 4 SERIES OF THIS ASSEMBLY IS NEEDED.

UNIVERSITY AT BUFFALO

206 KETTER HALL
BUFFALO, NY, 14226

Title: 12OD Shear Specimen Alternative Design No. 2

Page: 4of11	6/27/2016	STATUS: For Mnfctrng
	BY: Hadi Kenarangi	REV: 1

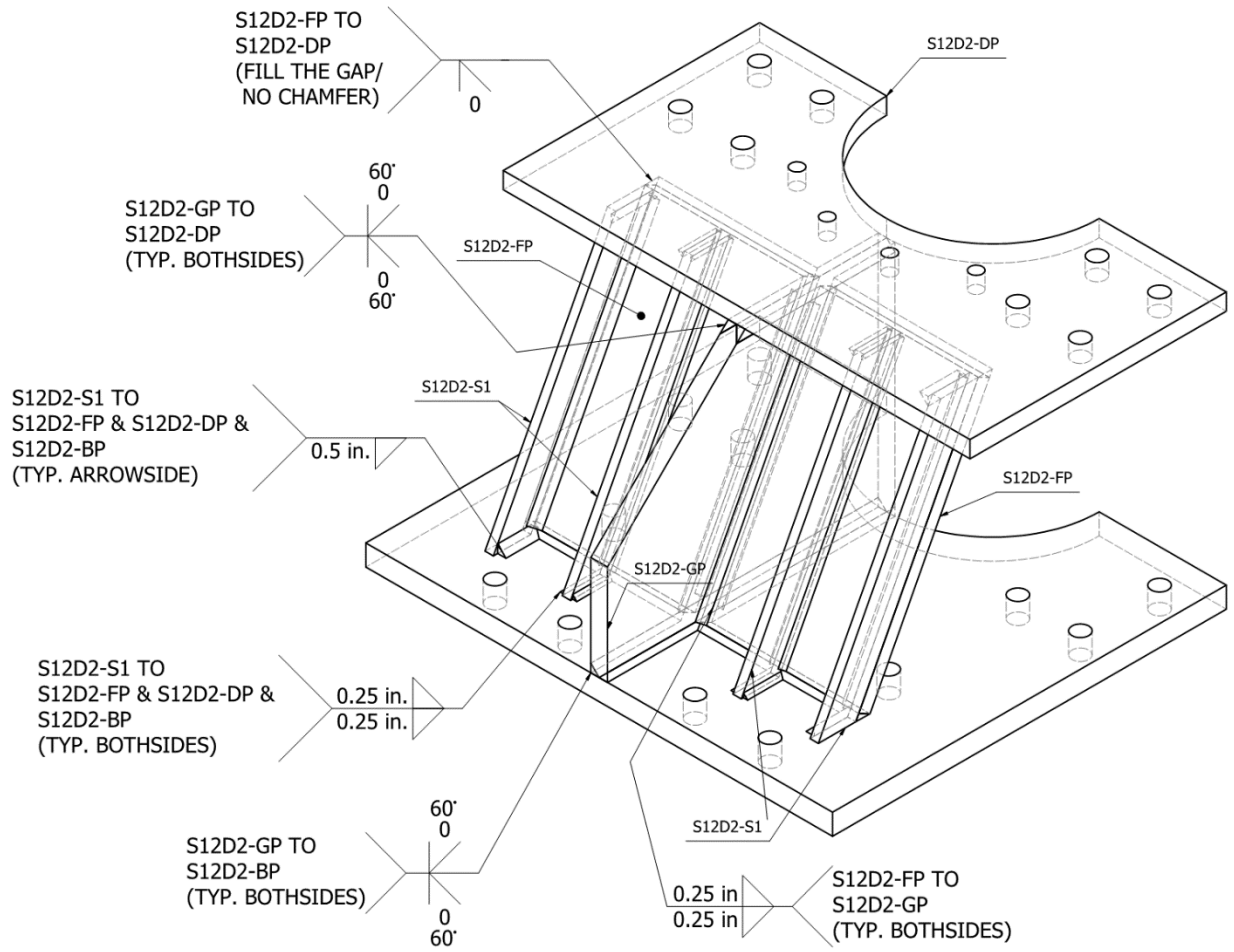

3D VIEW
WELDMENT

NOTES:
1-ALL PLATES ARE GR.50 STEEL
2- 4 SERIES OF THIS ASSEMBLY IS NEEDED.

UNIVERSITY AT BUFFALO

206 KETTER HALL
BUFFALO, NY, 14226

Title: 12OD Shear Specimen Alternative Design No. 2

Page: 5of11	6/27/2016	STATUS: For Mnfctrng
	BY: Hadi Kenarangi	REV: 2

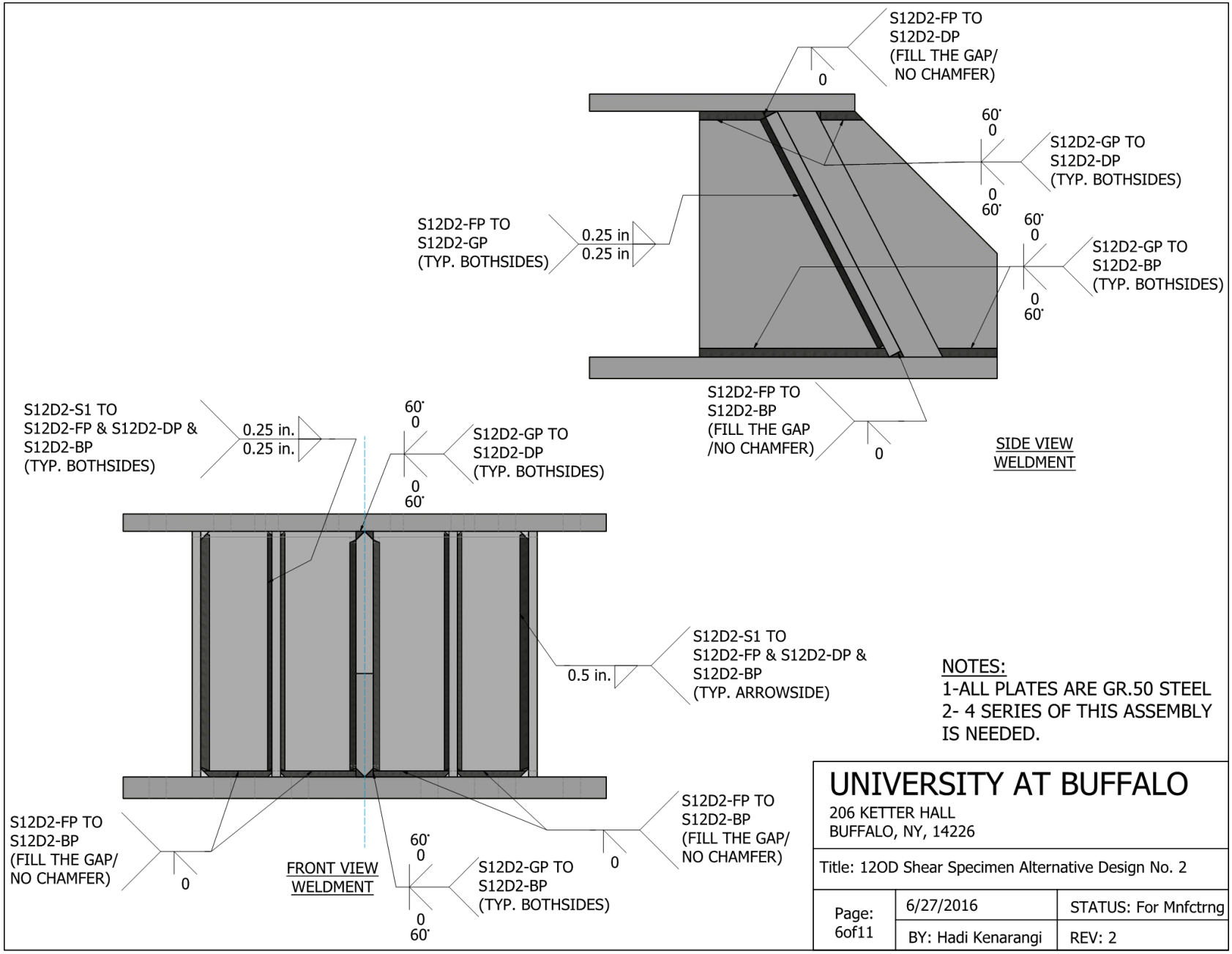

NOTES:
1-ALL PLATES ARE GR.50 STEEL
2- 4 SERIES OF THIS ASSEMBLY IS NEEDED.

UNIVERSITY AT BUFFALO

206 KETTER HALL
BUFFALO, NY, 14226

Title: 12OD Shear Specimen Alternative Design No. 2

Page: 6of11	6/27/2016	STATUS: For Mnfctrng
	BY: Hadi Kenarangi	REV: 2

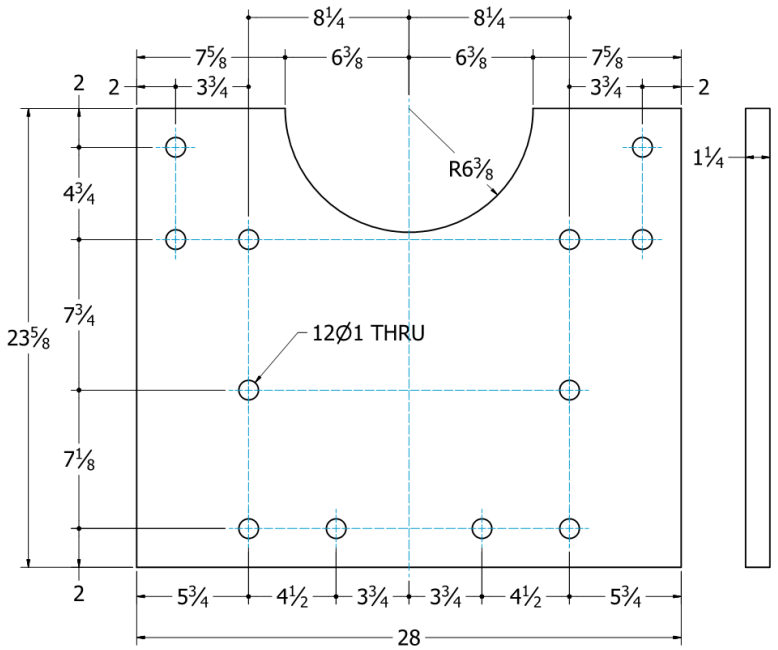

S12D2-BP
1¼ in thick plate

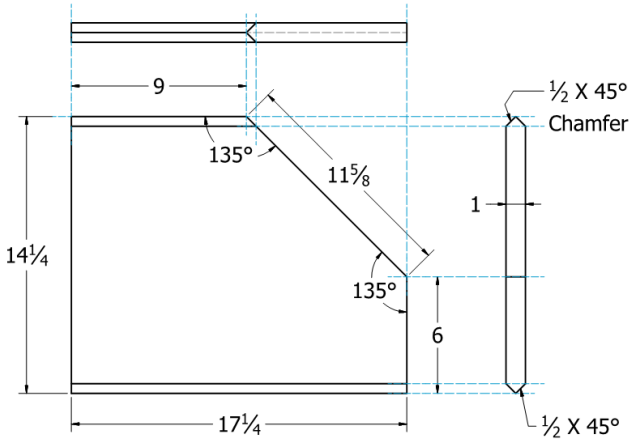

S12D2-GP
1 in thick plate

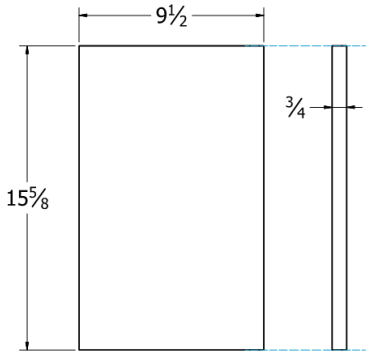

S12D2-FP
¾ in thick plate

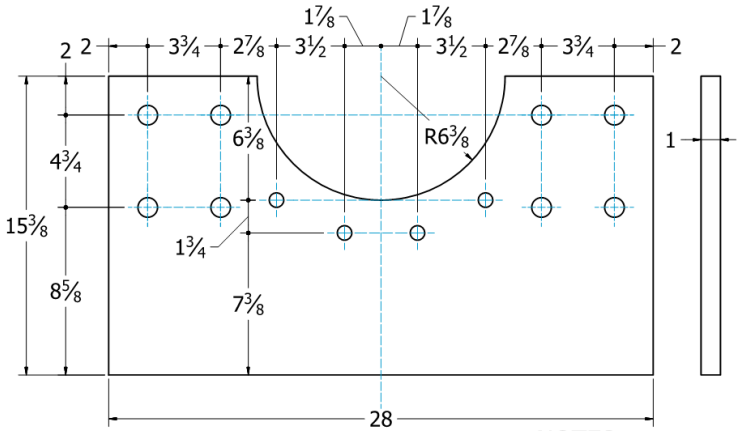

S12D2-DP
1in thick plate

NOTES:
1-ALL PLATES ARE GR.50 STEEL
2- 4 SERIES OF THIS ASSEMBLY IS NEEDED.

UNIVERSITY AT BUFFALO

206 KETTER HALL
BUFFALO, NY, 14226

Title: 12OD Shear Specimen Alternative Design No. 2

Page: 7of11	6/27/2016	STATUS: For Mnfctrng
	BY: Hadi Kenarangi	REV: 2

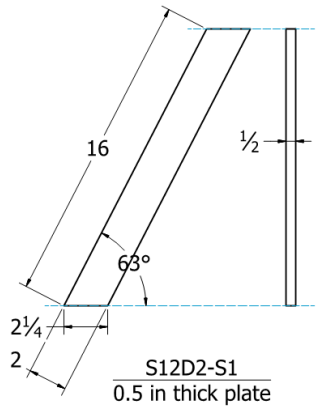

S12D2-S1
0.5 in thick plate

Parts List for four series of described assembly					
ITEM	QTY	PART NUMBER	DESCRIPTION	MATERIAL	VOLUME, in^3
1	4	S12D2-GP		Steel Gr.50	211.8
4	4	S12D2-BP		Steel Gr.50	735.3
9	16	S12D2-S1		Steel Gr.50	16.0
13	4	S12D2-DP		Steel Gr.50	366.7
15	8	S12D2-FP		Steel Gr.50	111.5

Note: 4 Series of this assembly is needed and shown in the table above.

NOTES:
1-ALL PLATES ARE GR.50 STEEL
2- 4 SERIES OF THIS ASSEMBLY IS NEEDED.

UNIVERSITY AT BUFFALO
206 KETTER HALL
BUFFALO, NY, 14226

Title: 12OD Shear Specimen Alternative Design No. 2

Page: 8of11	6/27/2016	STATUS: For Mnfctrng
	BY: Hadi Kenarangi	REV: 2

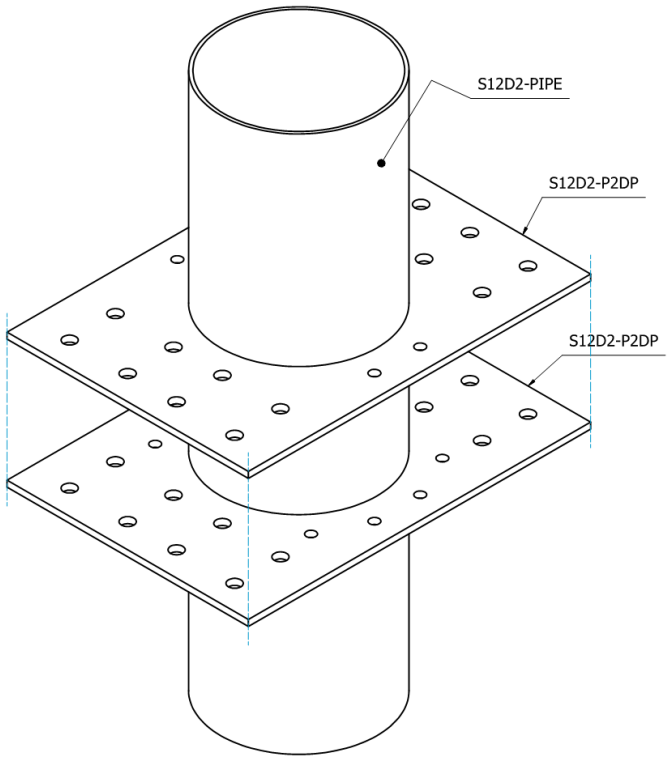

3D VIEW
FRONT

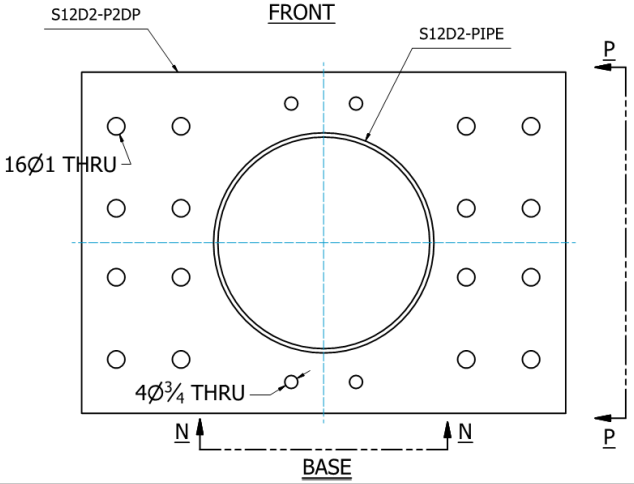

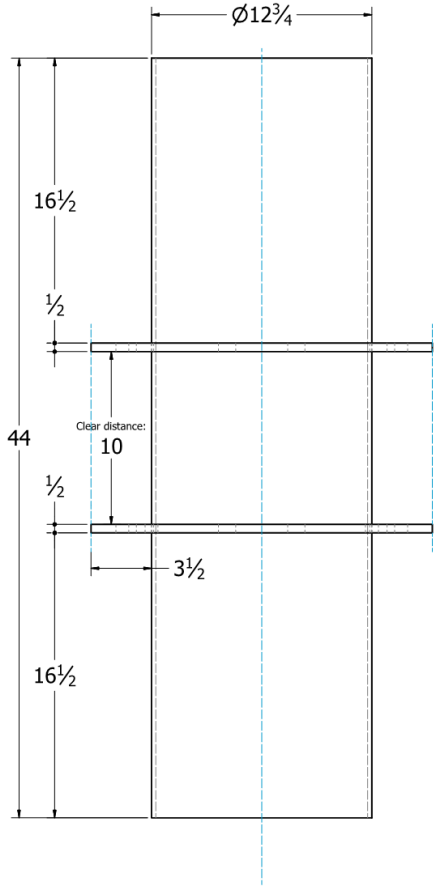

VIEW P-P

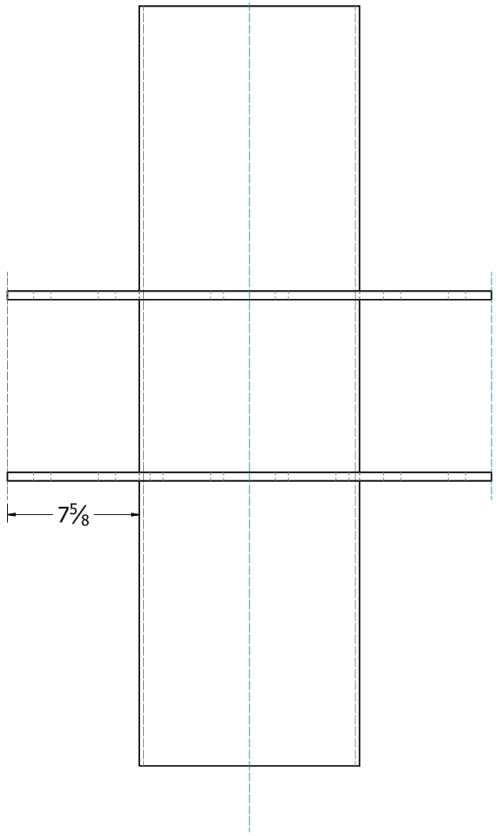

VIEW N-N

NOTES:
1-ALL PLATES ARE GR.50 STEEL
2- HSS PIPE TO HAVE LESS THAN 55ksi YIELD STRENGTH.
3- 6 SERIES OF THIS ASSEMBLY IS NEEDED.

UNIVERSITY AT BUFFALO

206 KETTER HALL
BUFFALO, NY, 14226

Title: 12OD Shear Specimen Alternative Design No. 2

Page: 9of11	6/27/2016	STATUS: For Mnfctrng
	BY: Hadi Kenarangi	REV: 1

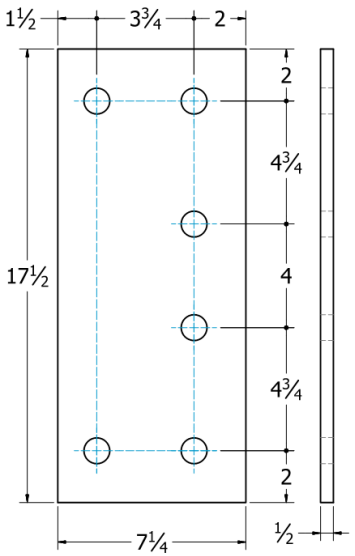

S12D2-SP1
½ in thick plate

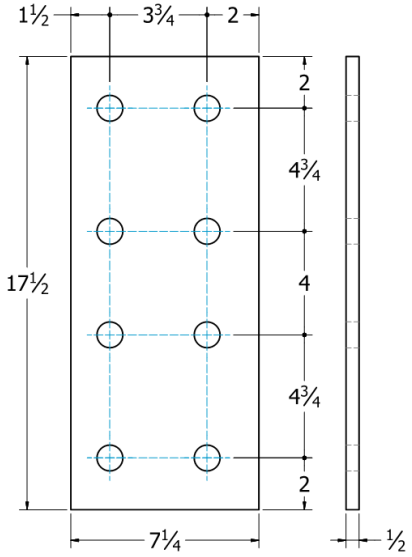

S12D2-SP2
½ in thick plate

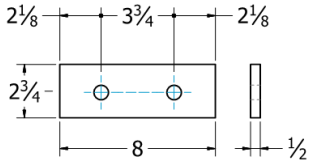

S12D2-SP3
½ in thick plate

Parts List - LOOSE (NO ASSEMBLY)					
ITEM	QTY	PART NUMBER	DESCRIPTION	MATERIAL	VOLUME
5	4	S12D2-SP2		Generic	61.1
6	4	S12D2-SP1		Generic	33.4
7	4	S12D2-SP3		Generic	63.4

NOTES:
1-ALL PLATES ARE GR.50 STEEL

UNIVERSITY AT BUFFALO
206 KETTER HALL
BUFFALO, NY, 14226

Title: 12OD Shear Specimen Alternative Design No. 2

Page: 11of11	6/27/2016	STATUS: For Mnfctrng
	BY: Hadi Kenarangi	REV: 1

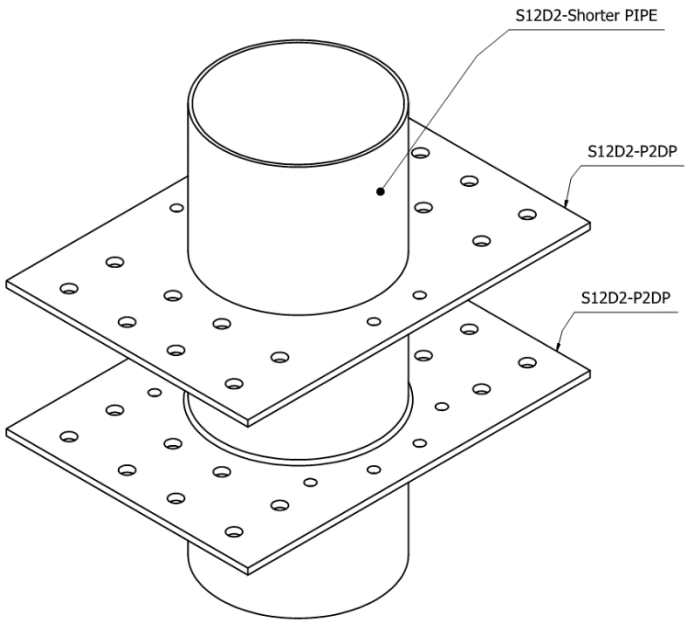

3D View
FRONT

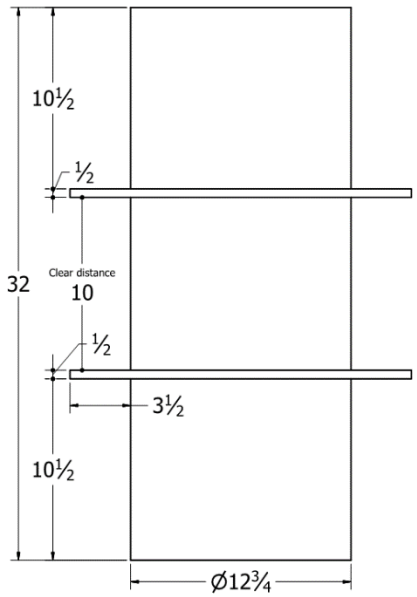

Front View

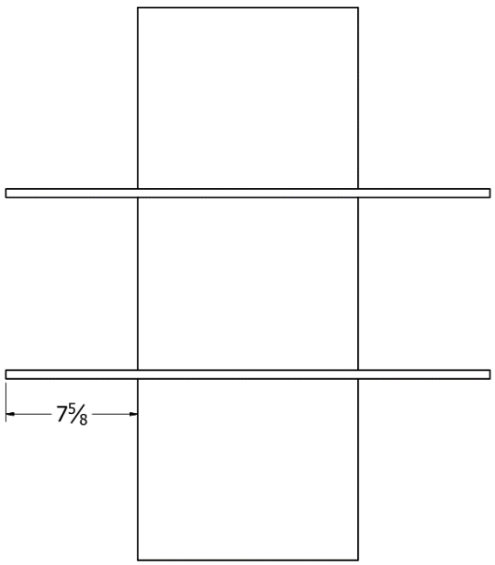

Side View

NOTES:
1-This configuration is to be applied to the shorter pipe only.

UNIVERSITY AT BUFFALO 206 KETTER HALL BUFFALO, NY, 14226		
Title: 12OD Shear Specimen Alternative Design No. 2		
Page: 12of12	6/27/2016	STATUS: For Mnfctrng
	BY: Hadi Kenarangi	REV:

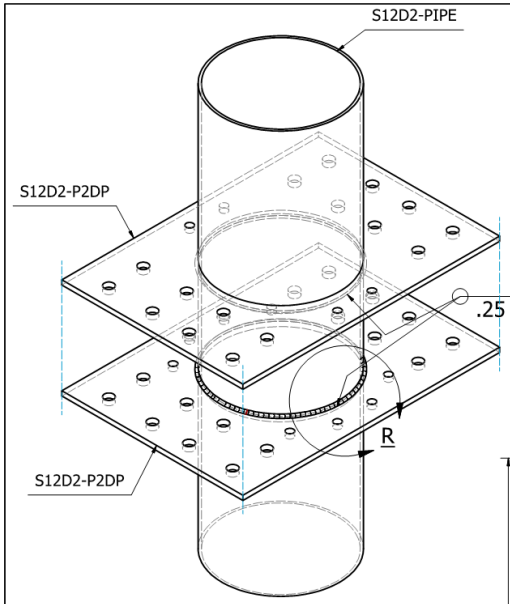

3D VIEW

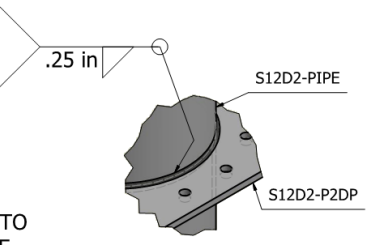

DETAIL R

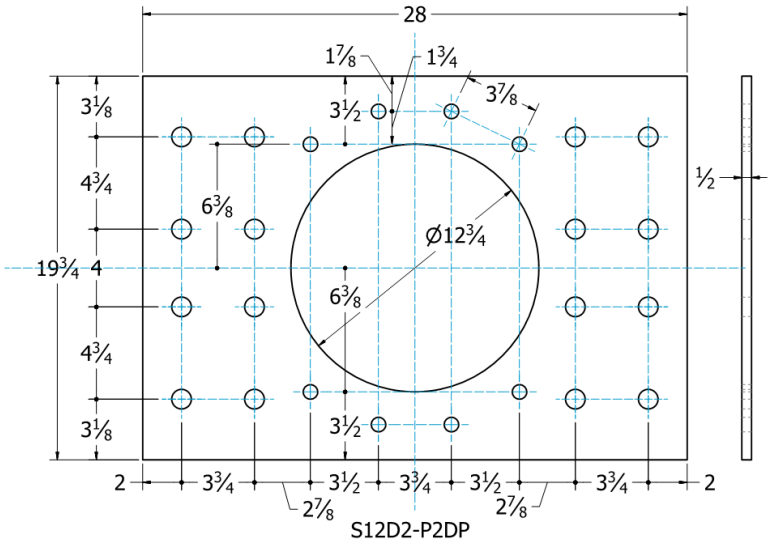

S12D2-P2DP
½ in thick plate

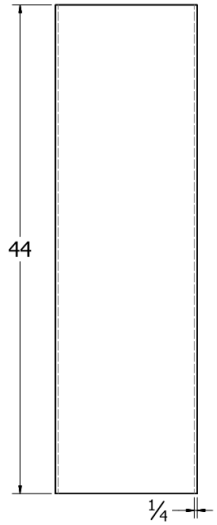

S12D2-PIPE
HSS PIPE

Parts List					
ITEM	QTY	PART NUMBER	DESCRIPTION	MATERIAL	VOLUME
8	1	S12D2-PIPE	HSS 12.75x0.250	A500 Gr. B 42 ksi	432.0
12	2	S12D2-P2DP		Steel Gr. 50	212.7

Note: 6 series of this assembly is needed.

NOTES:
1-ALL PLATES ARE GR.50 STEEL
2- HSS PIPE TO HAVE LESS THAN 55ksi YIELD STRENGTH.
3- 6 SERIES OF THIS ASSEMBLY IS NEEDED.

UNIVERSITY AT BUFFALO
206 KETTER HALL
BUFFALO, NY, 14226

Title: 12OD Shear Specimen Alternative Design No. 2

Page: 10of11	6/27/2016	STATUS: For Mnfctrng
	BY: Hadi Kenarangi	REV: 1

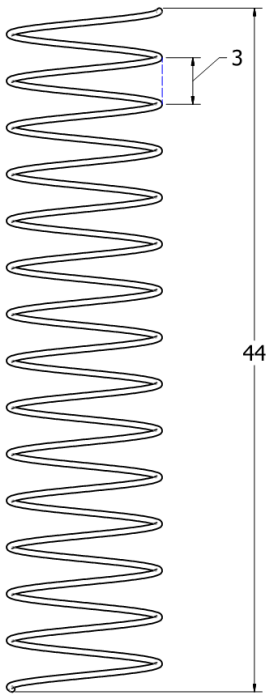

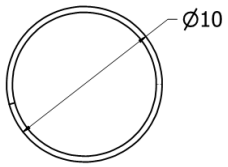

Spiral No. 1

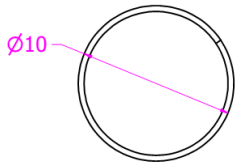

Spiral No. 2

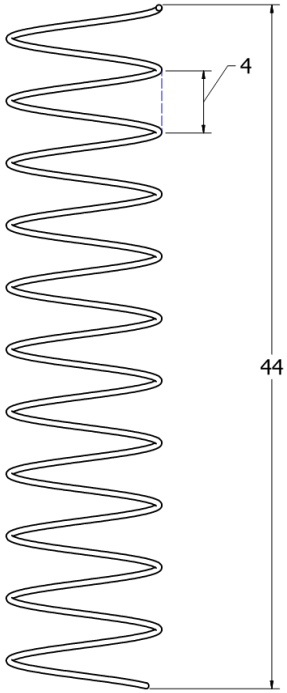

NOTES:
1-Both spirals are #3 Grade 60 rebar.
2- Longitudinal bars are #4 Grade 60 rebars.

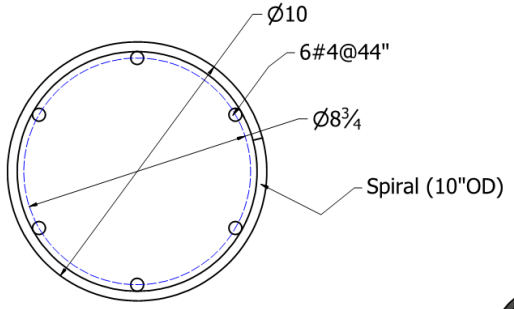

Cross Section

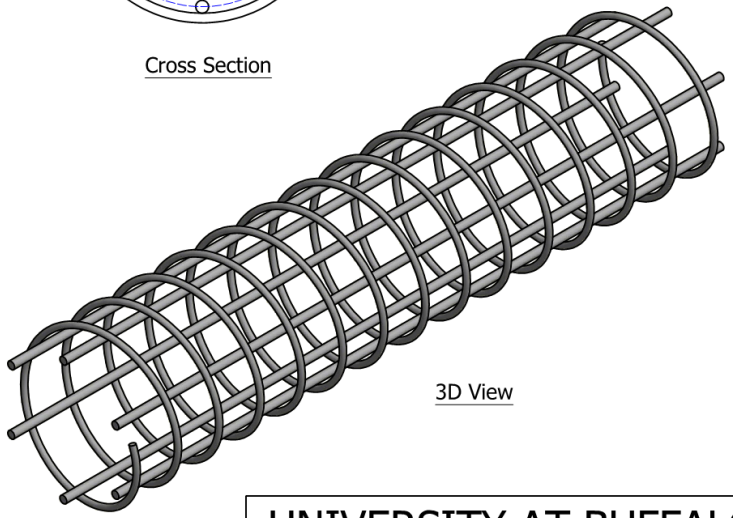

3D View

UNIVERSITY AT BUFFALO

206 KETTER HALL
BUFFALO, NY, 14226

Title: 12OD Shear Specimen Alternative Design No. 2

Page: 13of13	6/27/2016	STATUS: For Mnfctrng
	BY: Hadi Kenarangi	REV: 1

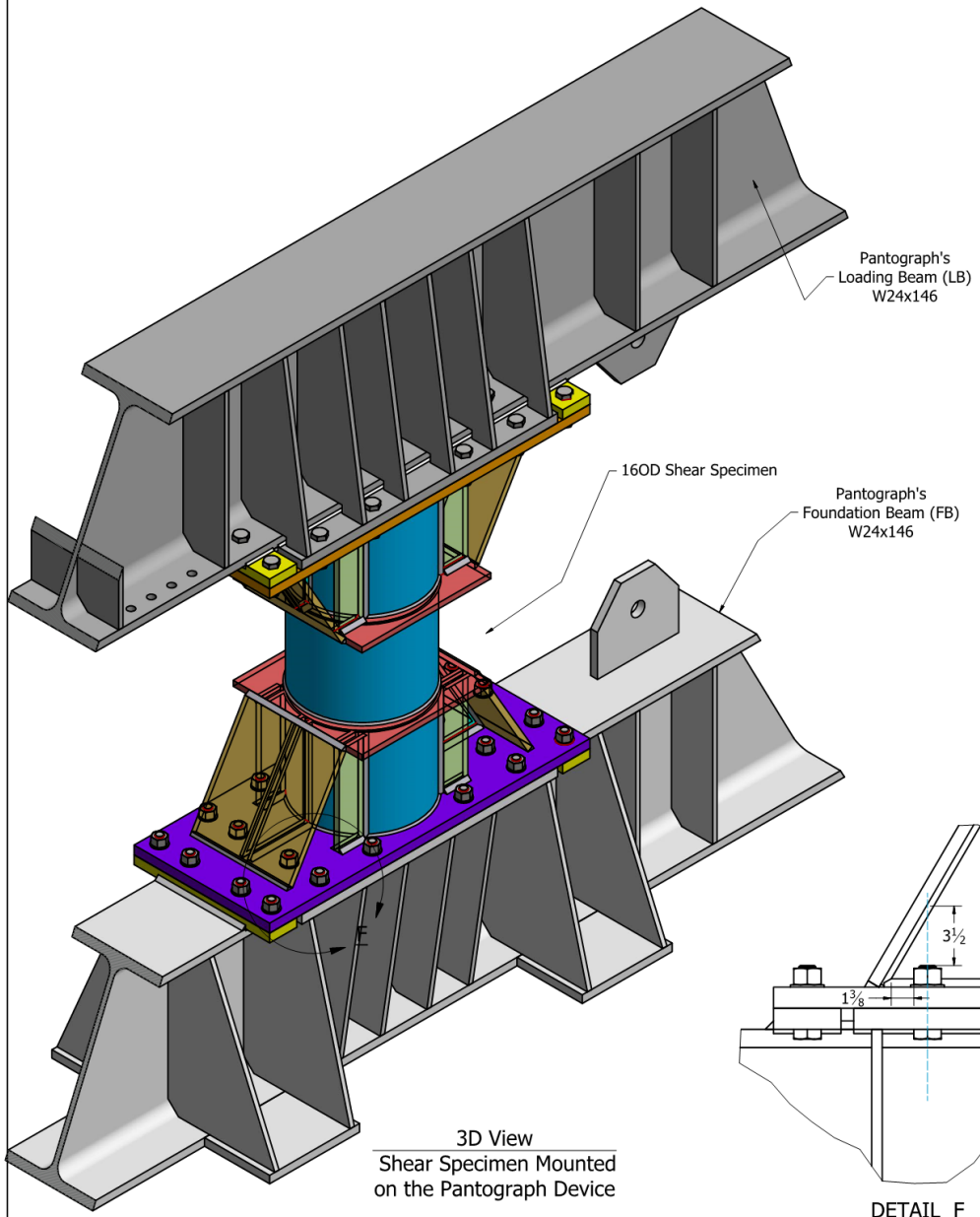

3D View
Shear Specimen Mounted
on the Pantograph Device

DETAIL F

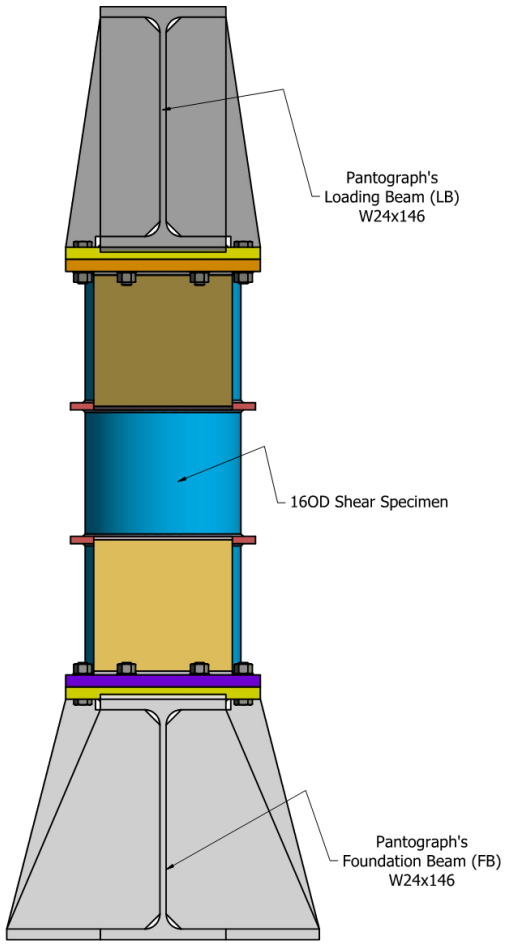

Front View

General Notes:
1- All Steel is Gr. 50.
2- HSS 16.0x0.25 is provided.
3- All bolt holes are standard holes.

UNIVERSITY AT BUFFALO 206 KETTER HALL BUFFALO, NY, 14226		
Title: 16OD Shear Specimens Design No. 2 Drawing:		
Page: 1of7	7/11/2016	STATUS: For Quoting
	BY: Hadi Kenarangi	REV: 0

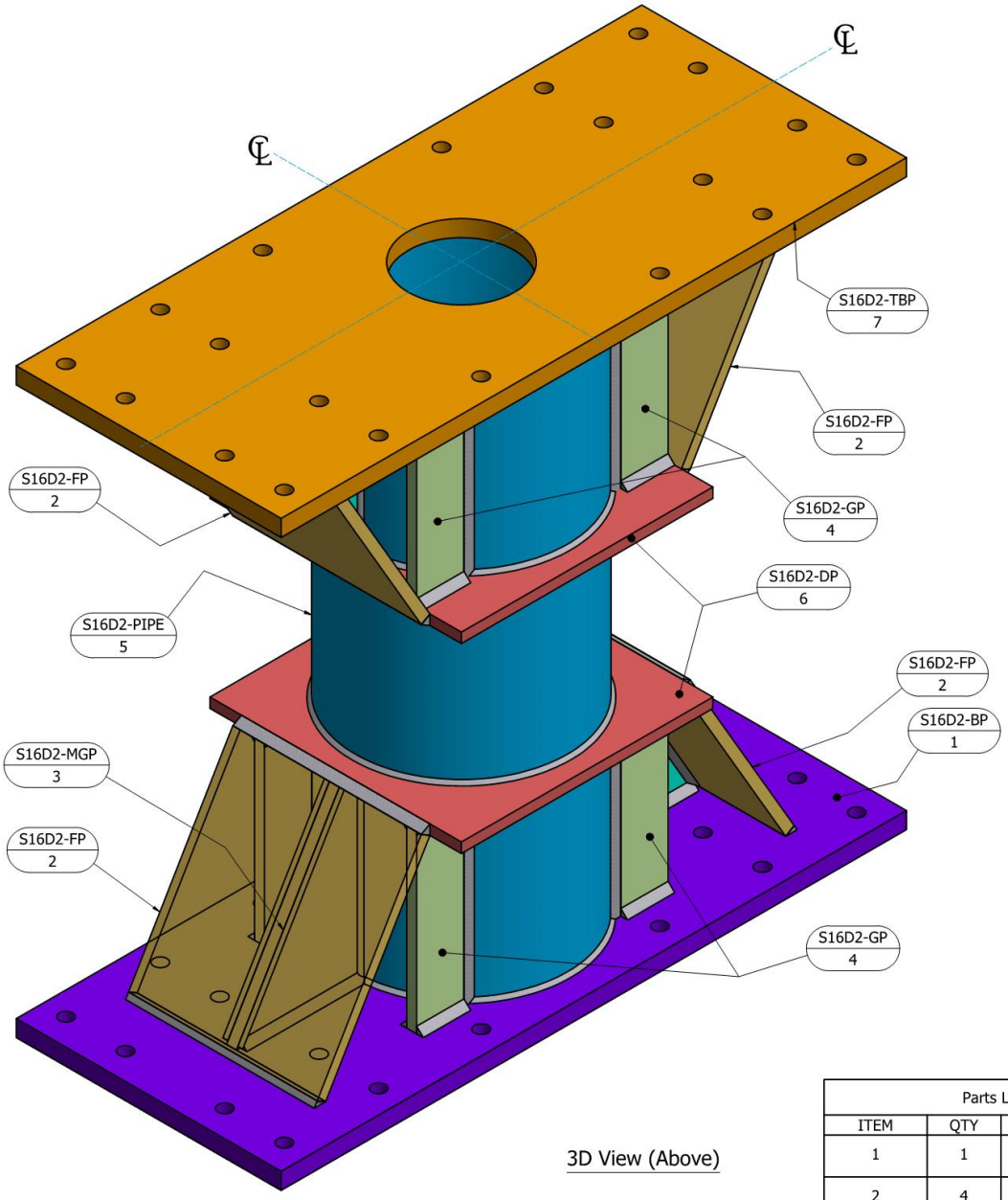

3D View (Above)

Parts List		
ITEM	QTY	PART NUMBER
1	1	S16D2-BP
2	4	S16D2-FP
3	4	S16D2-MGP
4	8	S16D2-GP
5	1	S16D2-PIPE
6	2	S16D2-DP
7	1	S16D2-TBP

UNIVERSITY AT BUFFALO
206 KETTER HALL
BUFFALO, NY, 14226

Title: 16OD Shear Specimens Design No. 2
Drawing:

Page: 2of7	7/11/2016	STATUS: For Quoting
	BY: Hadi Kenarangi	REV: 0

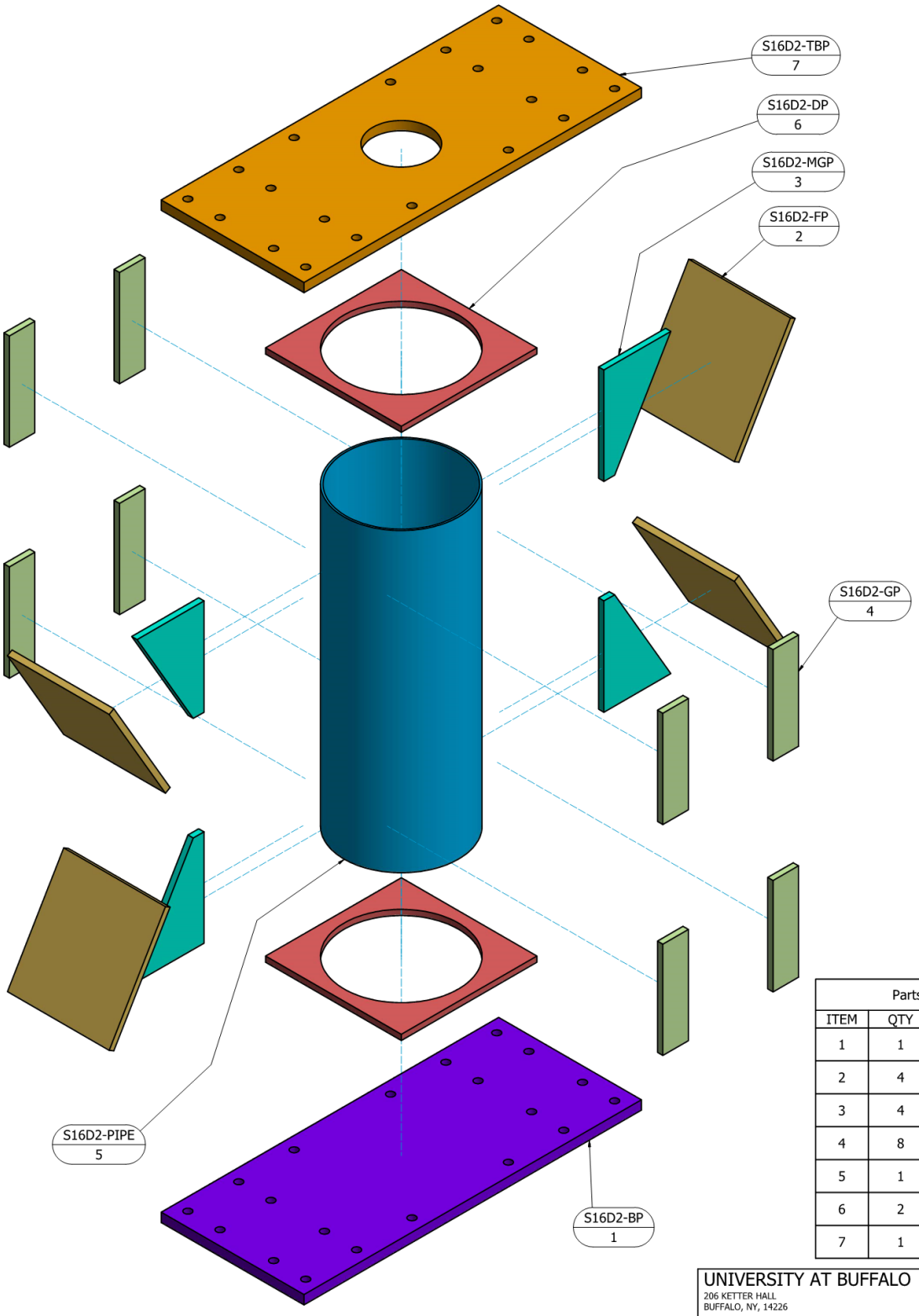

Exploded 3D View

Parts List		
ITEM	QTY	PART NUMBER
1	1	S16D2-BP
2	4	S16D2-FP
3	4	S16D2-MGP
4	8	S16D2-GP
5	1	S16D2-PIPE
6	2	S16D2-DP
7	1	S16D2-TBP

UNIVERSITY AT BUFFALO
206 KETTER HALL
BUFFALO, NY, 14226

Title: 16OD Shear Specimens Design No. 2
Drawing:

Page: 3of7	7/11/2016	STATUS: For Quoting
	BY: Hadi Kenarangi	REV: 0

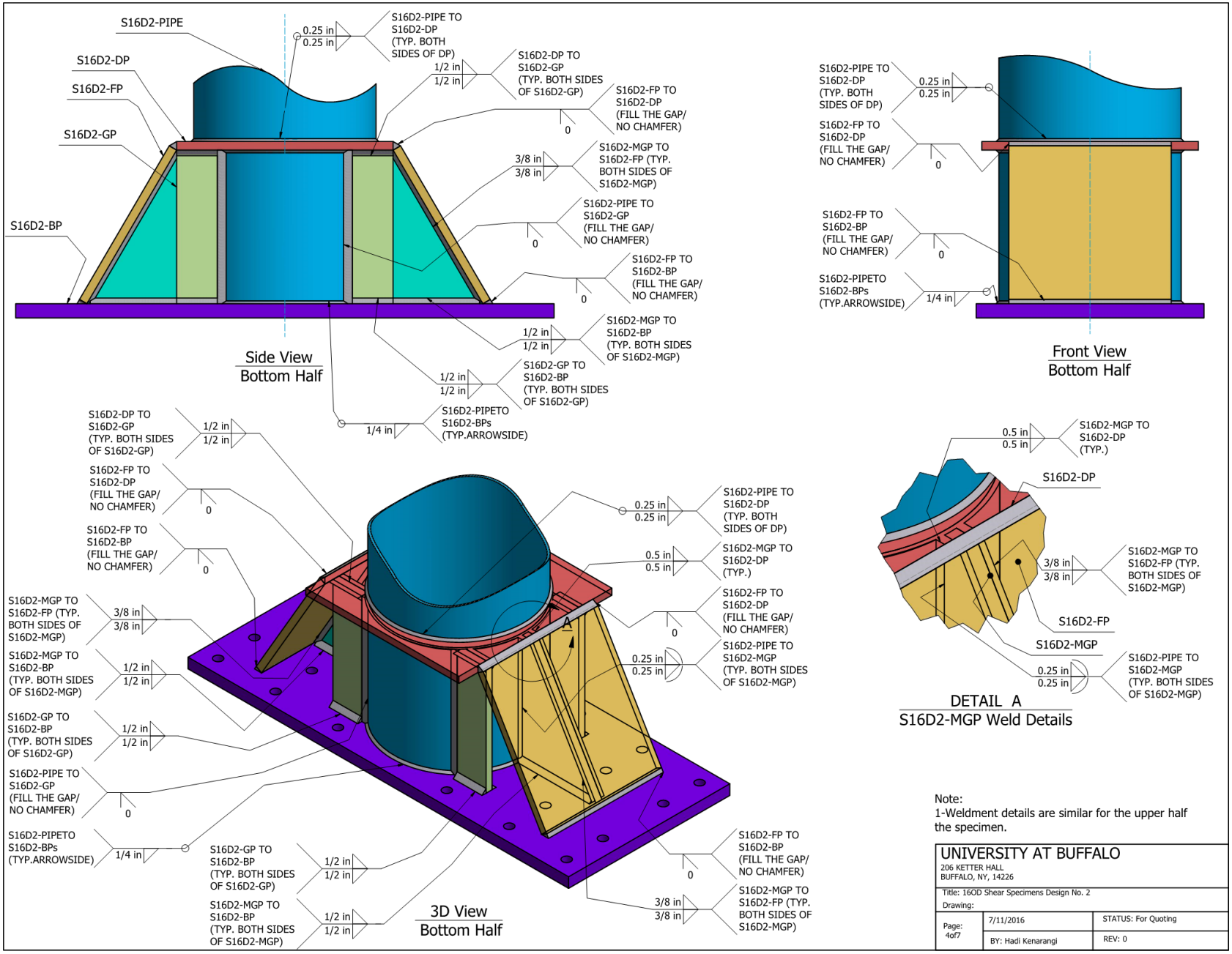
S16D2-PIPE
S16D2-DP
S16D2-FP
S16D2-GP
S16D2-BP
0.25 in
0.25 in
S16D2-PIPE TO S16D2-DP (TYP. BOTH SIDES OF DP)
1/2 in
1/2 in
S16D2-DP TO S16D2-GP (TYP. BOTH SIDES OF S16D2-GP)
0
S16D2-FP TO S16D2-DP (FILL THE GAP/ NO CHAMFER)
3/8 in
3/8 in
S16D2-MGP TO S16D2-FP (TYP. BOTH SIDES OF S16D2-MGP)
0
S16D2-PIPE TO S16D2-GP (FILL THE GAP/ NO CHAMFER)
0
S16D2-FP TO S16D2-BP (FILL THE GAP/ NO CHAMFER)
1/2 in
1/2 in
S16D2-MGP TO S16D2-BP (TYP. BOTH SIDES OF S16D2-MGP)
1/2 in
1/2 in
S16D2-GP TO S16D2-BP (TYP. BOTH SIDES OF S16D2-GP)
1/4 in
S16D2-PIPETO S16D2-BPs (TYP.ARROWSIDE)
Side View
Bottom Half
S16D2-PIPE TO S16D2-DP (TYP. BOTH SIDES OF DP)
0.25 in
0.25 in
S16D2-FP TO S16D2-DP (FILL THE GAP/ NO CHAMFER)
0
S16D2-FP TO S16D2-BP (FILL THE GAP/ NO CHAMFER)
0
S16D2-PIPETO S16D2-BPs (TYP.ARROWSIDE)
1/4 in
Front View
Bottom Half
S16D2-DP TO S16D2-GP (TYP. BOTH SIDES OF S16D2-GP)
1/2 in
1/2 in
S16D2-FP TO S16D2-DP (FILL THE GAP/ NO CHAMFER)
0
S16D2-FP TO S16D2-BP (FILL THE GAP/ NO CHAMFER)
0
S16D2-MGP TO S16D2-FP (TYP. BOTH SIDES OF S16D2-MGP)
3/8 in
3/8 in
S16D2-MGP TO S16D2-BP (TYP. BOTH SIDES OF S16D2-MGP)
1/2 in
1/2 in
S16D2-GP TO S16D2-BP (TYP. BOTH SIDES OF S16D2-GP)
1/2 in
1/2 in
S16D2-PIPETO S16D2-BPs (TYP.ARROWSIDE)
1/4 in
S16D2-PIPE TO S16D2-DP (TYP. BOTH SIDES OF DP)
0.25 in
0.25 in
S16D2-MGP TO S16D2-DP (TYP.)
0.5 in
0.5 in
S16D2-FP TO S16D2-DP (FILL THE GAP/ NO CHAMFER)
0
S16D2-PIPE TO S16D2-MGP (TYP. BOTH SIDES OF S16D2-MGP)
0.25 in
0.25 in
S16D2-FP TO S16D2-BP (FILL THE GAP/ NO CHAMFER)
0
S16D2-MGP TO S16D2-FP (TYP. BOTH SIDES OF S16D2-MGP)
3/8 in
3/8 in
A
3D View
Bottom Half
0.5 in
0.5 in
S16D2-MGP TO S16D2-DP (TYP.)
S16D2-DP
3/8 in
3/8 in
S16D2-MGP TO S16D2-FP (TYP. BOTH SIDES OF S16D2-MGP)
S16D2-FP
S16D2-MGP
0.25 in
0.25 in
S16D2-PIPE TO S16D2-MGP (TYP. BOTH SIDES OF S16D2-MGP)
DETAIL A
S16D2-MGP Weld Details
Note:
1-Weldment details are similar for the upper half the specimen.
UNIVERSITY AT BUFFALO
206 KETTER HALL
BUFFALO, NY, 14226
Title: 16OD Shear Specimens Design No. 2
Drawing:
Page: 4of7
7/11/2016
STATUS: For Quoting
BY: Hadi Kenarangi
REV: 0

M-78

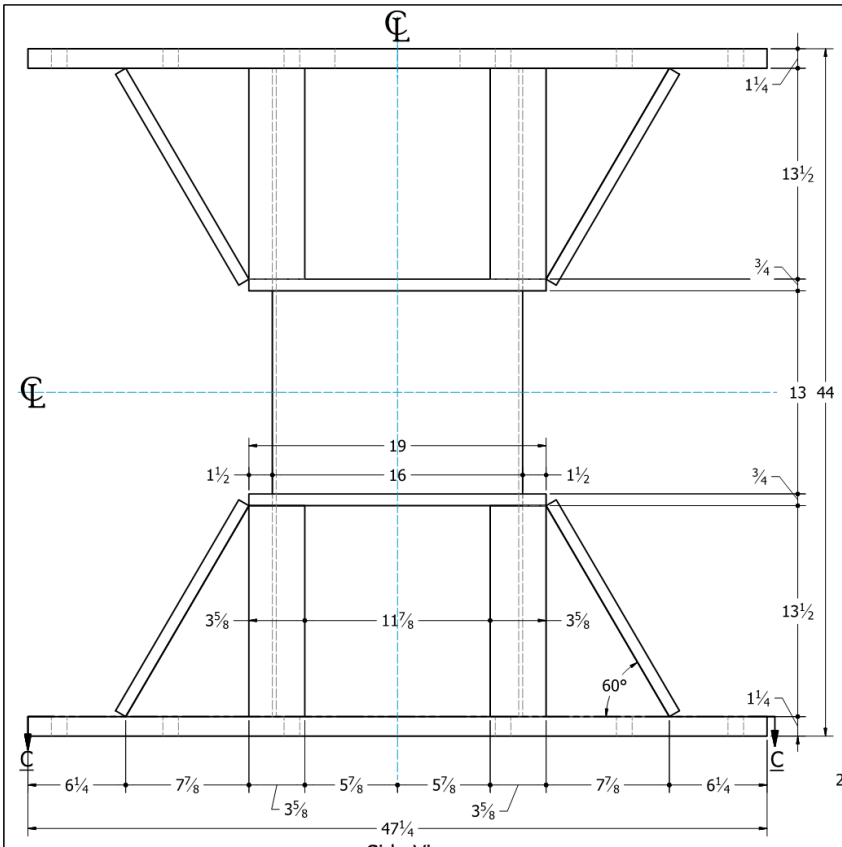

Side View

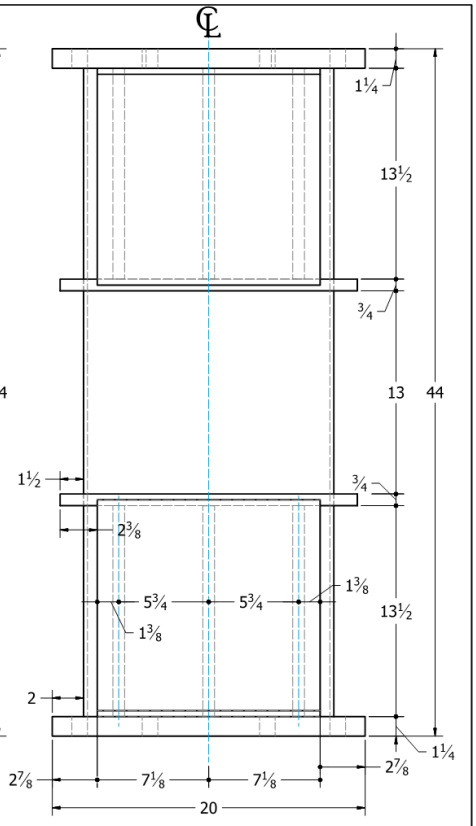

Front View

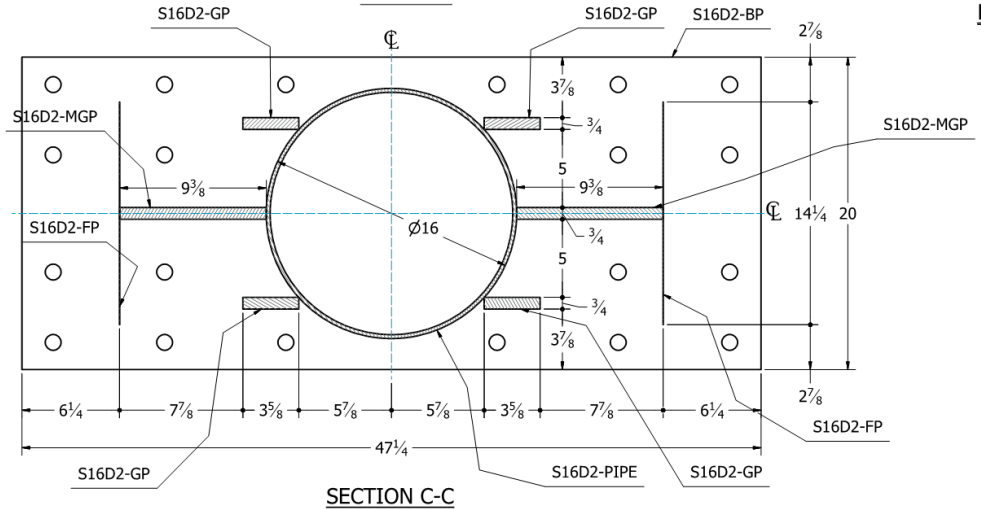

SECTION C-C

General Notes:
1- All Steel is Gr. 50.
2- HSS 16.0x0.25 is provided.
3- All bolt holes are standard holes.

UNIVERSITY AT BUFFALO 206 KETTER HALL BUFFALO, NY, 14226		
Title: 16OD Shear Specimens Design No. 2 Drawing:		
Page: 5of7	7/11/2016	STATUS: For Quoting
	BY: Hadi Kenarangi	REV: 0

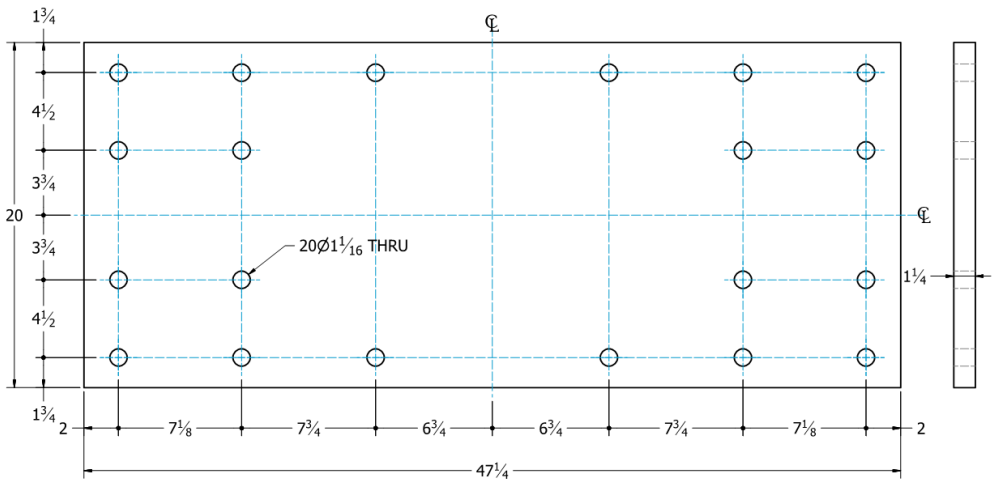

S16D2-BP
1¼ in. plate

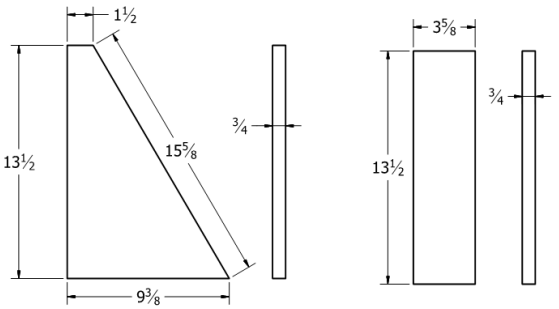

S16D2-MGP
¾ in. plate

S16D2-GP
¾ in. plate

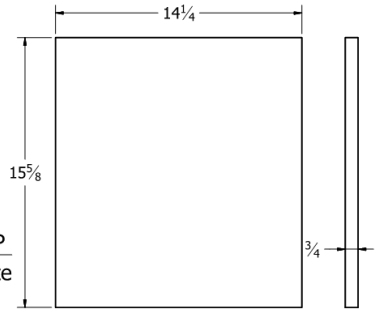

S16D2-FP
¾ in. plate

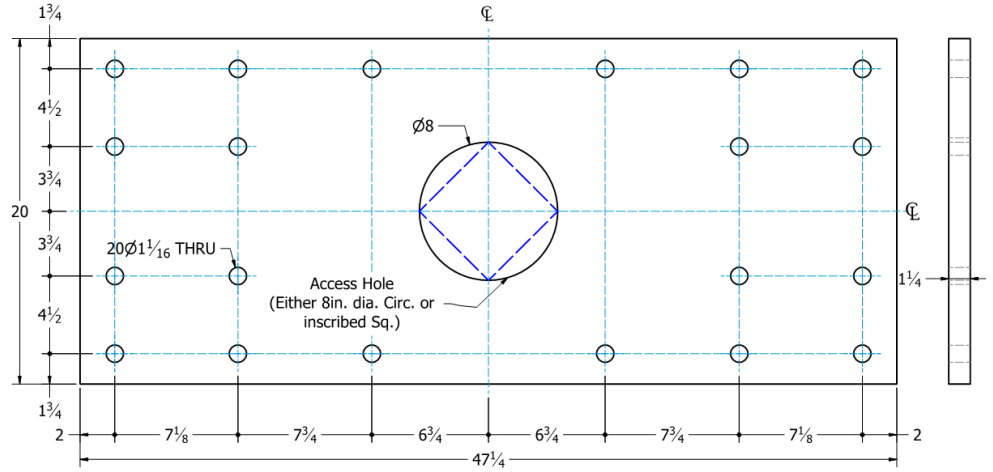

S16D2-TBP
1¼ in. plate

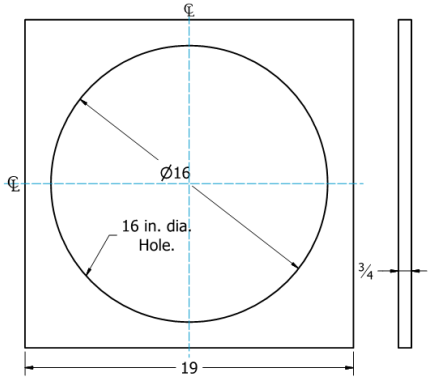

S16D2-DP
¾ in. plate

General Notes:
1- All Steel is Gr. 50.
2- HSS 16.0x0.25 is provided.
3- All bolt holes are standard holes.

UNIVERSITY AT BUFFALO 206 KETTER HALL BUFFALO, NY, 14226		
Title: 16OD Shear Specimens Design No. 2 Drawing:		
Page: 6of7	7/11/2016	STATUS: For Quoting
	BY: Hadi Kenarangi	REV: 0

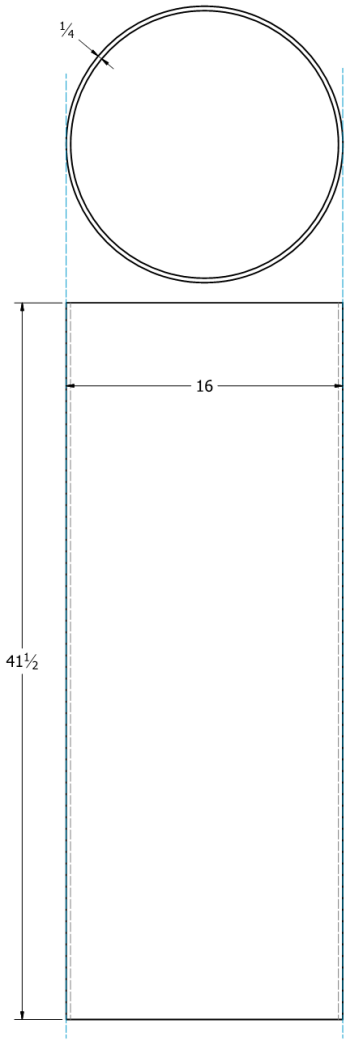

S16D2-PIPE
HSS 16x0.25

Parts List						
ITEM	QTY	PART NUMBER	DESCRIPTION	VOLUME	MATERIAL	MASS
1	1	S16D2-BP		1161.615 in^3	Gr. 50 Steel	329.899 lbmass
2	4	S16D2-FP		167.035 in^3	Gr. 50 Steel	47.438 lbmass
3	4	S16D2-MGP		55.055 in^3	Gr. 50 Steel	15.636 lbmass
4	8	S16D2-GP		36.194 in^3	Gr. 50 Steel	10.279 lbmass
5	1	S16D2-PIPE		513.356 in^3	Gr. 50 Steel	145.793 lbmass
6	2	S16D2-DP		119.954 in^3	Gr. 50 Steel	34.067 lbmass
7	1	S16D2-TBP		1098.783 in^3	Gr. 50 Steel	312.054 lbmass
					Total	1190 lbmass

General Notes:
1- All Steel is Gr. 50.
2- HSS 16.0x0.25 is provided.
3- All bolt holes are standard holes.

UNIVERSITY AT BUFFALO
206 KETTER HALL
BUFFALO, NY, 14226

Title: 16OD Shear Specimens Design No. 2
Drawing:

Page: 7of7	7/11/2016	STATUS: For Quoting
	BY: Hadi Kenarangi	REV: 0

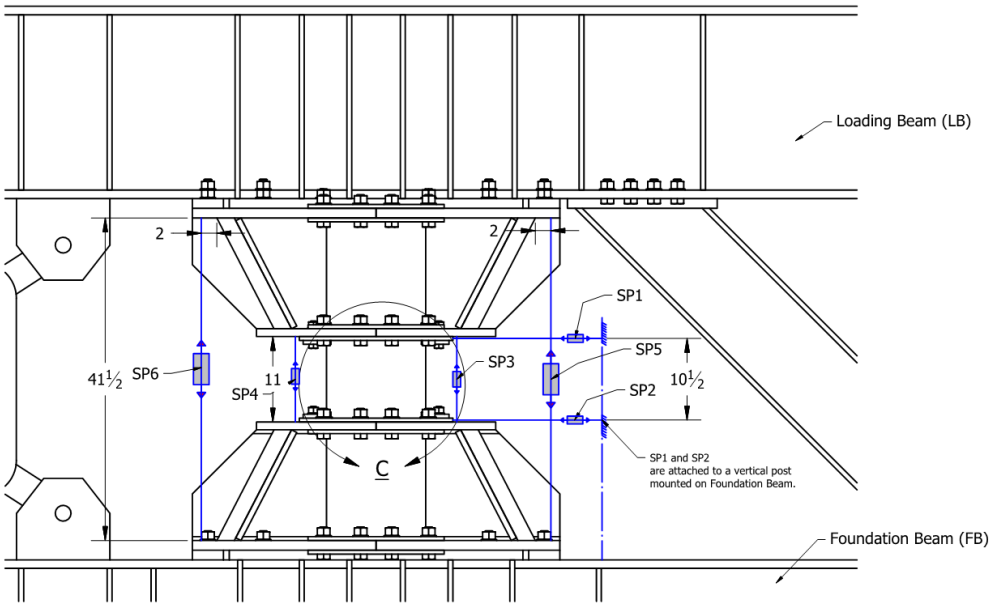

String Pots
South Elevation

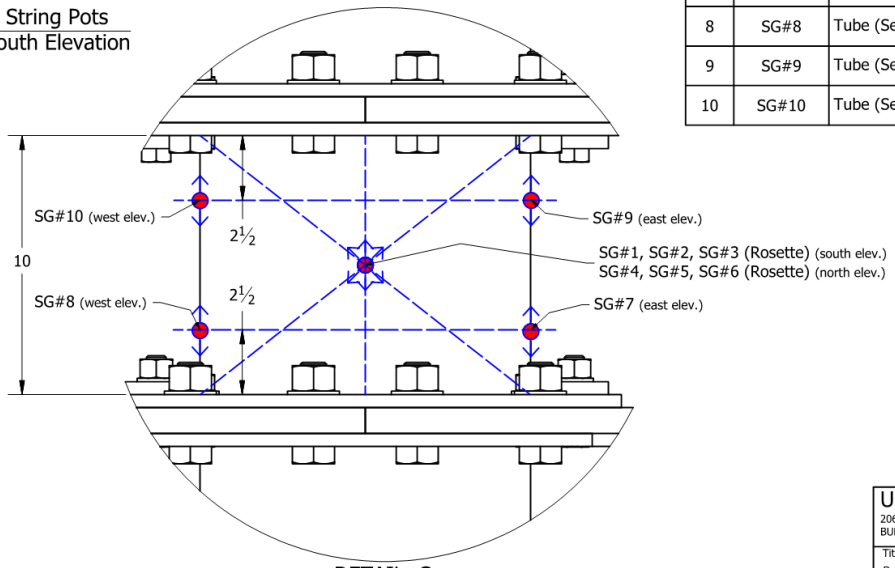

DETAIL C
Strain Guages

Table 1: String pot placement details

No.	Label	Orientation	Elevation
1	SP#1	Horizontal	East
2	SP#2	Horizontal	East
3	SP#3	Vertical	East
4	SP#4	Vertical	West
5	SP#5	Vertical	East
6	SP#6	Vertical	West

Table2: Strain gauge placement details

No.	Label	Location	Orientation	Elevation
1	SG#1	Tube (See Detail C)	45 deg.	South
2	SG#2	Tube (See Detail C)	-45 deg.	South
3	SG#3	Tube (See Detail C)	Vertical	South
4	SG#4	Tube (See Detail C)	45 deg.	North
5	SG#5	Tube (See Detail C)	-45 deg.	North
6	SG#6	Tube (See Detail C)	Vertical	North
7	SG#7	Tube (See Detail C)	Longitudinal	East
8	SG#8	Tube (See Detail C)	Longitudinal	West
9	SG#9	Tube (See Detail C)	Longitudinal	East
10	SG#10	Tube (See Detail C)	Longitudinal	West

UNIVERSITY AT BUFFALO
206 KETTER HALL
BUFFALO, NY, 14226

Title: 12OD Shear Specimens Instrumentation Plan
Drawing: String pots and Strain Gauges Details

Page: 1of3	8/30/2016	STATUS: As Built
	BY: Hadi Kenarangi	REV: 0

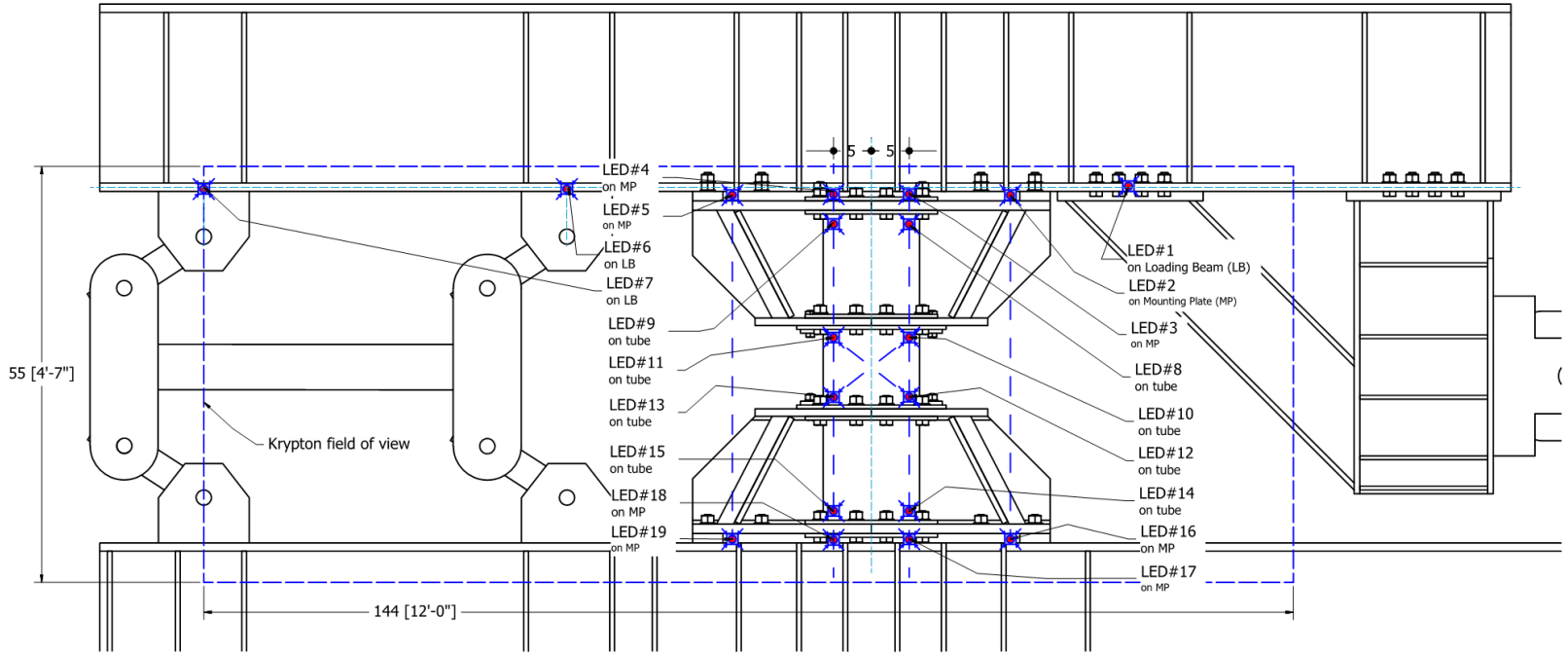

Table 3. Krypton LEDs placement details

No.	Label	Attached to	Elevation
1	LED#1	Loading beam	South
2	LED#2	Mounting plate	South
3	LED#3	Mounting plate	South
4	LED#4	Mounting plate	South
5	LED#5	Mounting plate	South
6	LED#6	Loading beam	South
7	LED#7	Loading beam	South
8	LED#8	Tube	South
9	LED#9	Tube	South
10	LED#10	Tube	South
11	LED#11	Tube	South
12	LED#12	Tube	South
13	LED#13	Tube	South
14	LED#14	Tube	South
15	LED#15	Tube	South
16	LED#16	Bot. mounting plate	South
17	LED#17	Bot. mounting plate	South
18	LED#18	Bot. mounting plate	South
19	LED#19	Bot. mounting plate	South

UNIVERSITY AT BUFFALO
206 KETTER HALL
BUFFALO, NY, 14226

Title: 12OD Shear Specimens Instrumentation Plan
Drawing: Krypton LEDs Details

Page: 2of3	8/30/2016	STATUS: As Built
	BY: Hadi Kenarangi	REV: 01